TECHNICAL TRANSACTIONS
CZASOPISMO TECHNICZNE

MECHANICS
MECHANIKA

ISSUE 1-M (5)
ZESZYT 1-M (5)

YEAR 2013 (110)
ROK 2013 (110)

WYDAWNICTWO POLITECHNIKI KRAKOWSKIEJ

TECHNICAL TRANSACTIONS | CZASOPISMO TECHNICZNE

MECHANICS | MECHANIKA

ISSUE 1-M (5) | ZESZYT 1-M (5)
YEAR 2013 (110) | ROK 2013 (110)

Pierwotną wersją każdego Czasopisma Technicznego jest wersja on-line
www.czasopismotechniczne.pl www.technicaltransactions.com

POLITECHNIKA KRAKOWSKA
WYDZIAŁ MECHANICZNY
INSTYTUT INFORMATYKI STOSOWANEJ

COMPUTER AIDED MECHANICAL ENGINEERING

Praca zbiorowa pod redakcją
Renaty Dwornickiej, Grzegorza Filo, Wojciecha Czyżyckiego,
Mariusza Domagały, Tadeusza Czyżewskiego i Pawła Lempy

Kraków 2013

TECHNICAL TRANSACTIONS | **CZASOPISMO TECHNICZNE**
MECHANICS | MECHANIKA
1-M/2013

PAWEŁ CĘPA*, EDWARD LISOWSKI**

APPLICATION OF PNEUMATIC SUCTION CUP AS A POSITIONING ELEMENT FOR THIN METAL SHEETS IN TECHNOLOGICAL PROCESSES

WYKORZYSTANIE PRZYSSAWKI PNEUMATYCZNEJ JAKO ELEMENTU POZYCJONOWANIA CIENKICH BLACH W PROCESACH TECHNOLOGICZNYCH

Abstract

In the paper an analysis of gripping thin metal sheets in technological process of stamping metal closures is presented. An object made of two suction cups and pneumatic control system of vacuum and pressure inside the suction cup was analyzed. Mathematical model contains differential equations which were solved basing on Matlab/Simulink application. Prepared model provides an opportunity to check different parameters of the system. The paper presents analysis of impact of feed pressure on the course of sucking forces.

Keywords: *pneumatic suction cup*, *modeling of pneumatic systems*, *Matlab/Simulink*

Streszczenie

W artykule podjęto zadanie analizy chwytania cienkich blach w procesie technologicznym tłoczenia zakryć koronowych. Do analizy wybrano układ składający się z dwóch przyssawek i odpowiedniego układu pneumatycznego sterującego podciśnieniem i ciśnieniem w przyssawkach. Przedstawiono model matematyczny w postaci równań różniczkowych i przeprowadzono jego analizę z wykorzystaniem pakietu Matlab/Simulink. Zbudowany model pozwala na zbadanie wpływu różnych parametrów układu. Przedstawiona analiza dotyczy wpływu ciśnienia zasilania, na przebieg wartości sił przyssania.

Słowa kluczowe: *przyssawka pneumatyczna*, *modelowanie układów pneumatycznych*, *Matalab/Simulink*

* MSc. Eng. Paweł Cępa, Can-Pack Metal Closures Sp. z o.o.
** Prof. Edward Lisowski, Institute of Applied Informatics, Faculty of Mechanical Engineering, Cracow University of Technology.

Designations

m – computational mass of element above the suction cup (metal sheet)
V – volume of suction cup chamber
x – position of metal sheet above the suction cup (measured from the bottom)
c – friction loss coefficient for suction cup material
k – centering spring stiffness coefficient for suction cup material
F – the force generated by air inside suction cup on metal sheet
G – force of gravity
d – inside diameter of the suction cup
r – split width between suction cup and metal sheet
A – active area of the suction cup
p – pressure inside suction cup chamber
p_{atm} – atmospheric pressure
Q_i – volumetric flow rate at the suction cup input
Q_o – volumetric flow rate at the split between suction cup and metal sheet
B – equivalent volumetric elastic modulus for air
N – pressure ratio of jet pump
p_s – sucking pressure
p_d – jet pump output pressure
p_i – jet pump input pressure
k_{th} – friction loss coefficient for jet pump throat
k_{en} – friction loss coefficient for jet pump throat entry
k_n – friction loss coefficient for jet pump nozzle
b – jet pump area ratio
M – volumetric flow ratio for jet pump Q_2/Q_1
Q_1 – volumetric flow rate at the jet pump input
Q_2 – volumetric flow rate of air sucked by jet pump
h – split height between suction cup and metal sheet
R_1 – suction cup inside radius
R_2 – suction cup outside radius

1. Introduction

Industrial packaging produces cans and bins are made from very thin metal sheets that are less than 0.2 mm thick. Such thin metal sheets have very low stiffness, therefore transporting and feeding to the stamping machine is very problematic. In this paper, the undertaken task is to analyze feeding system of thin metal sheets for stamping press for metal closures. The technology basis on lacquering and lithography printing before stamping process. Printing process is very accurate, the lithography have specified arrangement provide for division of metal sheet. Positioning tolerance in stamping process is less than 0.5 mm. In this case, the way in which metal sheet is grabbed influences the arrangement of the lithography. Pneumatic suction cup with absorber, which gives good distribution of pneumatic force was studied. Analysis was performed by Matlab/Simulink computer software.

2. Object of the study

General view of metal sheet gripping using pneumatic suction cup is shown in Figure 1. It is made of two suction cups consisting of sealing ring 1 and stopping bumper 2. Furthermore, in the gripping system equipment ejector 3, pneumatic valve 4 and air supply 5 can be found.

Metal sheet 6, which is ready to be feed to stamping machine is situated on positioning Table 7.

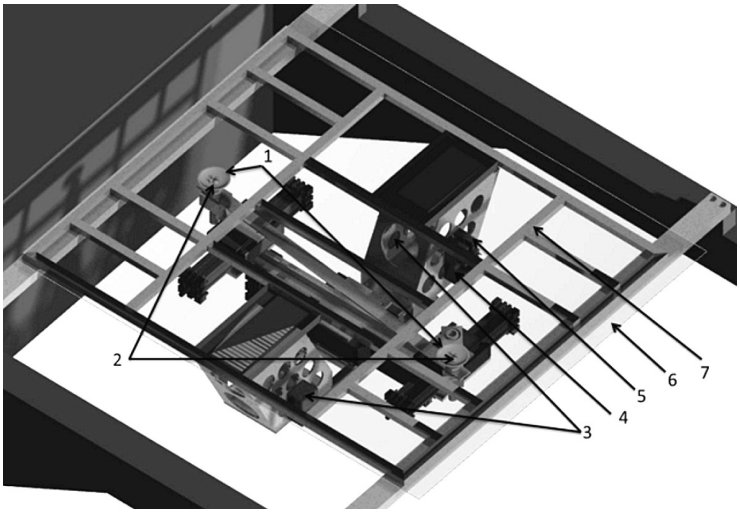

Fig. 1. Schematic diagram of gripping metal sheet using pneumatic suction cup

Rys. 1. Schemat ideowy uchwytu blachy za pomocą przyssawek pneumatycznych

Feeding process starts with taking metal sheet from a bale. In this case, air at the certain pressure is supplied to the ejector, which creates vacuum in the suction cups and at the same time sufficient lift force to grab metal sheet. At the end of positioning process metal sheet is very fast released by redirecting air stream directly to the suction cups.

3. Mathematical model

Schematic diagram of pneumatic system is shown in Figure 2. To generate vacuum the ejector with nominal nozzle value 1 mm was used. Ejector 4 is supplied from main air supplying line via pneumatic valve 3. Switching on the valve 3 produces vacuum into suction cup. Pneumatic valve 5 is responsible for switching between sucking and blow out system. Suction cup grabs metal sheet, holds it during positioning movements and then releases it. Because efficiency of the stamping machine is high, positioning and feeding cycle is very short, roughly few tenth of second, therefore time for grapping metal sheet as well as releasing has to be minimized and those times are based on the analysis performed in this paper.

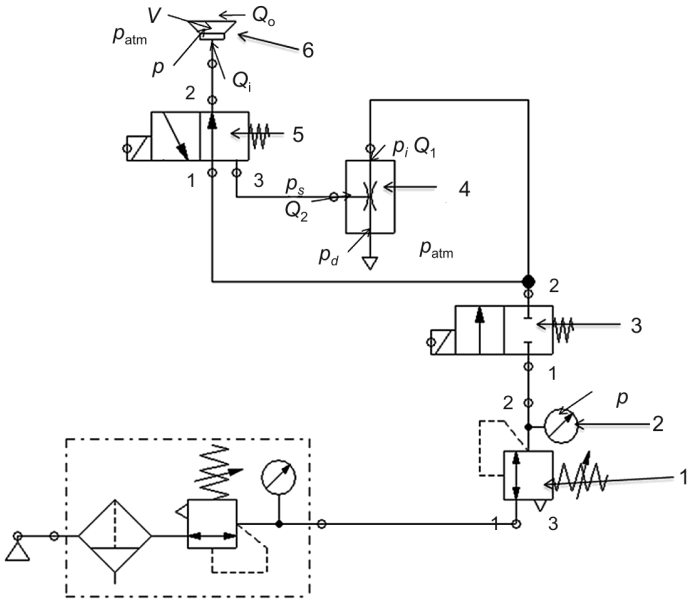

Fig. 2. Pneumatic diagram with marked system parameters

Rys. 2. Schemat pneumatyczny wraz z oznaczeniami parametrów układu

For mathematical modeling, the following assumptions were made: the system is in thermal equilibrium, elastic elements deformation is linear and the metal sheet is not deformed by air pressure. Under these assumptions, the mathematical model will constitute the differential equations for elements movement, flow rate continuity and elements characteristics.

For system modeling, model of one-degree freedom mechanical system (Fig. 3) was used. Motion equation which describes metal sheet – suction cup system:

$$m\ddot{x} = -c\dot{x} + kx + F - G \tag{1}$$

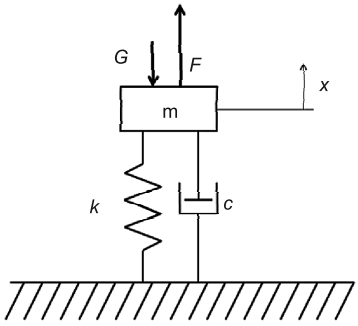

Fig. 3. Schematic diagram of one-degree freedom mechanical system

Rys. 3. Schemat układu o 1 stopniu swobody

Flow rate continuity equation inside suction cup chamber:

$$\dot{p}\frac{V}{B} = Q_i - Q_o \tag{2}$$

In Figure 4 jet pump schematic diagram is shown. The equation describing ejector [3]:

$$N(1-k_n) - 2b = M^2\left(\frac{2b^2}{1-b} - \frac{1+k_{en}}{c^2}\right) - b^2(1-k_{th})(1+M)^2 \tag{3}$$

where:

$$M = \frac{Q_2}{Q_1} \tag{4}$$

$$N = \frac{p_d - p_s}{p_i - p_d} \tag{5}$$

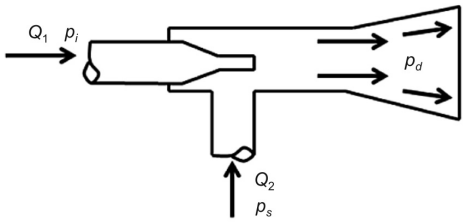

Fig. 4. Schematic diagram of jet pump with marked system parameters

Rys. 4. Schemat ideowy pompy podciśnienia wraz z oznaczonymi parametrami

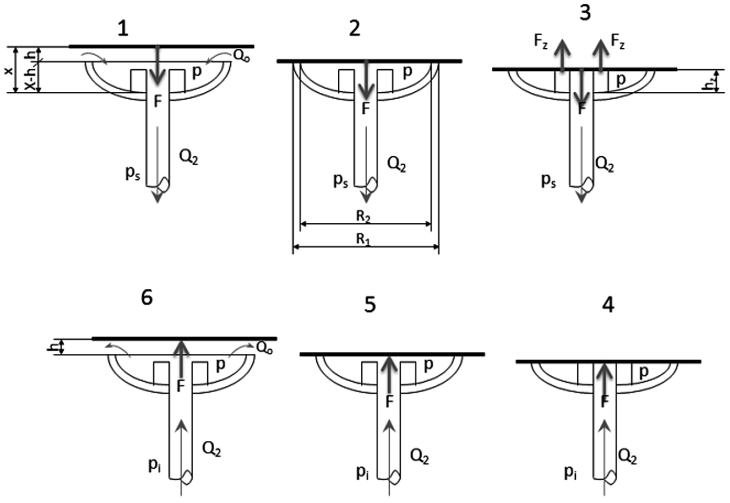

Fig. 5. Schematic diagram of metal sheet griping process

Rys. 5. Schemat układu arkusz blacha-przyssawka w procesie chwytania blachy

Before metal sheet is close enough to seal connection with the suction cup, air comes out through the interspace between metal sheet and the suction cup with height $h(x)$. In Figure 5 steps of metal sheet griping are shown: 1 – state before grab, 2 – state at the sealing moment, 3 – appropriate metal sheet grab (bottoming of the metal sheet to the absorber), 4 – direction changing from sucking to blowing, 5 – detachment of metal sheet from suction cup, 6 – metal sheet repulsion from the suction cup causes interspace $h(x)$.

Equation describes flow rate through the interspace $h(x)$ [2]:

$$Q_0 = \frac{\pi p k^3}{6\eta \ln \frac{R_1}{R_2}} \tag{6}$$

4. Simulation results

Simulation model was based on equations from 1 to 6. All equations were solved using Matlab/Simulink software. Block diagram of used equations (Fig. 6) was prepared, each block represents different parts of the system. Several simulations with unit step function flow rate input with different air pressure were made.

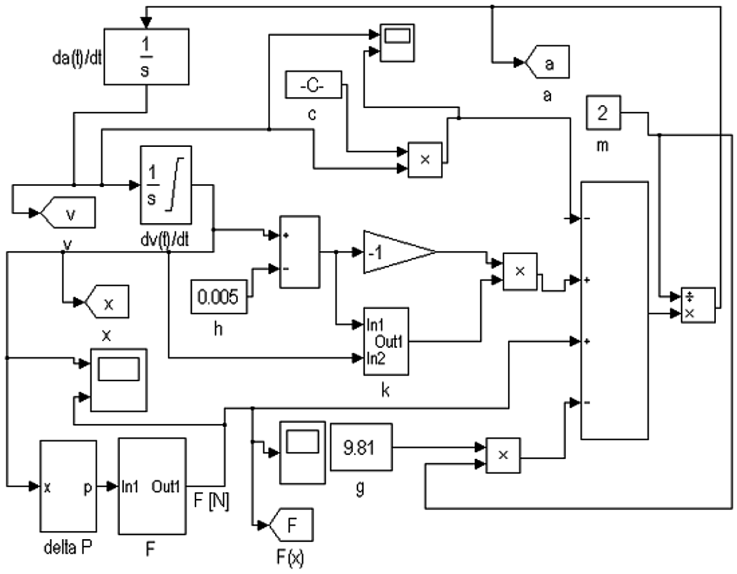

Fig. 6. Block diagram describing the suction cup (Matlab/Simulink software)

Rys. 6. Schemat blokowy opisujący przyssawkę wykonany w programie Matlab/Simulink

Simulation time was 1 [s], the system of equations was solved by fourth-order Runge-Kutta method with 0.0001 [s] time step. Simulation process was started with letting down metal sheet on suction cup. After 0.2 [s] unit step function input vacuum was generated.

It was assumed that correct position for beginning movement of metal sheet is when metal sheet touches the absorber (position x = 0.0046 [m] or lower). After positioning, switching suction to blowing takes place, it is 0.5 [s]. Blow should be sufficient for subtle convection of metal sheet above the suction cup. The result of the simulation is vertical position of the metal sheet and acting force of the pressure from the suction cup.

In the figure 7 diagram with results of the simulation for unit step function input for pressure 0.5 [MPa] is shown. It was observed that reaching maximal suction force 56.5 [N] takes place in 0.2626 [s]. Acquiring position x=0.0046 [m] (touching absorber with metal

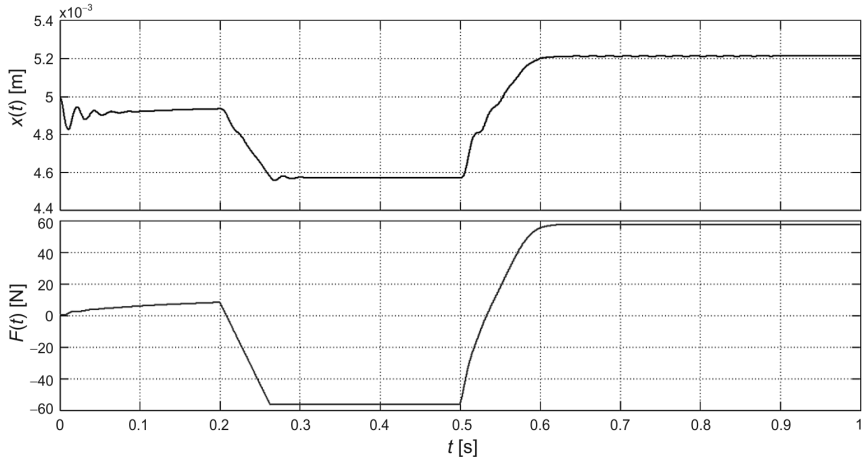

Fig. 7. Simulation results for 0.5 [MPa] pressure

Rys. 7. Wyniki symulacji przy ciśnieniu roboczym 0.5 [MPa]

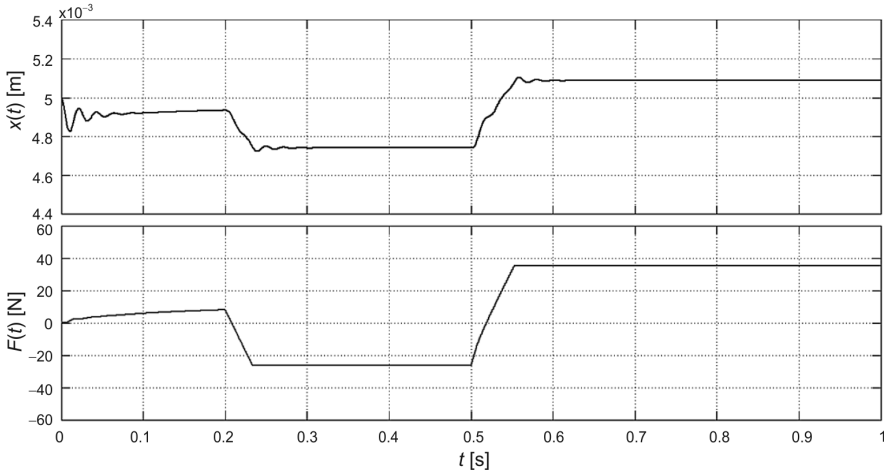

Fig. 8. Simulation results for 0.15 [MPa] pressure

Rys. 8. Wyniki symulacji przy ciśnieniu roboczym 0.15 [MPa]

sheet) takes place in 0.2587 [s], after 0.1587 [s] from the start point. Detachment of metal sheet from suction cup took place 0.5535 [s], after 0.0535 from the start point. After stabilization of position, interspace between metal sheet and the suction cup was 0.0002 [m].

Simulations for different pressures 0.4 [MPa], 0.3 [MPa], 0.2 [MPa] were performed. All of the results are close to the obtained for 0.5 [MPa] pressure. Simulations outcome proved, that for pressure lower than 0.2 [MPa] significant differences in force, time and metal sheet position can be observed (Fig.8). Vacuum generated by ejector is too low to pull metal sheet to the absorber. After switching on the vacuum pulling force 26.5 [N] in 0.2335 [s] was obtained, 0.1335 [s] after start point. Detachment of metal sheet from suction cup took place in 0.5372 [s], after 0.0372 [s] from start point. Interspace between metal sheet and the suction cup were 0.000088 [m].

5. Conclusions

Performed simulations proved that the pressures from 0.5 [MPa] to 0.2 [MPa] do not significantly affect maximal sucking force of applied suction cup. Moreover, time for starting metal sheet movement without adhesion loss does not change. It is caused by the ejector oversize comparing to the suction cup. Significant difference was observed for the pressure lower than 0.2 [MPa]. Simulation results proved that pressure 0.2 [MPa] is advantageous in context of minimal air usage and fulfilling functional requirements.

References

[1] Lisowski E., Momeni H., *CFD modeling of a jet pump with circumferential nozzles for large flow rates*, Energy Archives of Foundry Engineering, volume 3/2010, Foundry Commission of the Polish Academ of Sciences.

[2] Kwiatkowski D., *Analiza teroretyczna i doświadczalna poduszek pneumatycznycznych w zastosowaniu do podnoszenia i przemieszczana ładunków*, praca doktorska, Politechnika Krakowska, Kraków 2011.

[3] Karassik I.J., Messina J.P, Cooper P., Heald C.C., *Pump handbook*, Third Edition, McGRAW-HILL 2001.

[4] Stryczek S., *Napędy hydrostatyczne*, WNT, Warszawa 1999.

[5] Szenajch W., *Napędy i sterowanie pneumatyczne*, Wydanie trzecie zmienione, Wydawnictwo Naukowo-Techniczne, Warszawa 1992, 1997.

[6] Rahmat M.F., Sunar N.H., Najib S., Salim S., Abidin M.S.Z., Mohd Fauzi A.A., Ismail Z.H., *Review On Modeling And Controller Design In Pneumatic Actuator Control System*, International Journal On Smart Sensing And Intelligent Systems, Vol. 4, No. 4, December 2011.

TECHNICAL TRANSACTIONS | CZASOPISMO TECHNICZNE
MECHANICS | MECHANIKA
1-M/2013

PAWEŁ CĘPA*, EDWARD LISOWSKI**

INVESTIGATION OF CROWN CORK DRAWING FORCE

BADANIA PRZEBIEGU SIŁY TŁOCZENIA ZAKRYWKI KORONOWEJ

A b s t r a c t

In the paper an analysis and investigation of round metal sheet sharing force and crown cork drawing force are presented. Experimental test stand was created in order to perform analysis on sharing and drawing forces for several metal sheet thicknesses. Obtained results are sufficient for comparison of acting forces for different metal sheet thicknesses and hardness during cutting process.

Keywords: *sharing force*, *drawing force*, *experimental system*, *crown cork*

S t r e s z c z e n i e

W artykule przeprowadzono analizę oraz badania sił potrzebnych do wycinania krążka z blachy jako półproduktu do tłoczenia zakrywki koronowej oraz właściwej siły potrzebnej do wytłoczenia zakrywki. Zbudowano stanowisko badawcze oraz przeprowadzono badania przebiegu sił dla procesu cięcia i tłoczenia dla różnych grubości blach. Uzyskane wyniki pozwalają na ocenę sił w procesie cięcia dla blach o różnej grubości i wytrzymałości.

Słowa kluczowe: *siły wycinania*, *siły tłoczenia*, *stanowisko badawcze*, *zakrywka koronowa*

* MSc. Eng. Paweł Cępa, Can-Pack Metal Closures Sp. z o.o.
** Prof. PhD. Eng. Edward Lisowski, Institute of Applied Informatics, Faculty of Mechanical Engineering Cracow University of Technology.

Designations

g – thickness of the cutting material
z – number of notches
P_{max} – maximum sharing force
S – sharing surface
l – length of the cutting edge
k – coefficient depending on the clearance
R_t – shear strenght
a – pushing length
P_d – holding pressures
P_p – force necessary to pushing through the cutting die
k_p – equivalent of pushing direction
P_w – punch force
P_{id} – ideal force of deformation
P_{gn} – bending force on radius r_m
P_{tk} – friction force between punch and die
P_{tr} – friction force die radius
R_m – maximum tensile stress
β – distortion factor
D – diameter of blank
d_1 – diameter of shell
d_s – diameter of punch
μ_1 – friction coefficient between metal sheet, holder and forming die
μ_2 – friction coefficient on the forming die radius
β_0 – distortion factor

1. Introduction

One of the most common bottle metal closures in the World is crown cork. It is the simplest and the most inexpensive closure which was patented in 1890 in USA by William Painter [3]. Metal crown cork is defined precisely by standard [7] as a product in the shape of bowl with serrate side, commonly known as crown. Standard metal sheet thickness range from $g = 0.20$ to 0.26 mm, regular number of notches is $z = 21$. The seemingly simple system for bottle closure has not been significantly changed since its invention. Despite the fact, that crown cork itself is simple, large-scale production is very complex [2]. Because of that, globally not many companies produce machines for crown corks production. Starting material is metal sheet, provided in coils, the production is fully automated and consist of cutting the metal into smaller sheets, sharing blank and drawing process [1, 3]. The problem addressed in the paper was raised by Can-Pack S.A. company, which engineers took the task to improve crown cork by application of computational capabilities and new materials. In the paper the results on the acting forces determination during crown cork drawing process are presented. For the investigation, modern metal sheets with improved harness and 30% reduced thickness were applied.

2. Sharing blank and drawing process analysis

For the drawing process analysis, a model based on two drawing elements was applied [5, 6]. Such technological process has few phases: elastic-plastic, plastic flow and material crack (Fig. 1).

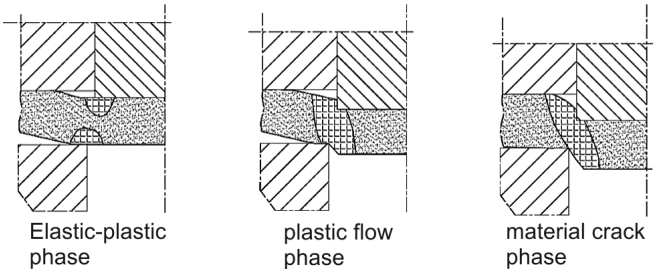

Fig. 1. Phases of drawing process

Rys. 1. Fazy procesu cięcia

During the first phase, forces acting on metal sheet are generated by approaching cutting edges and are displaced in relation to each other which causes metal sheet bulge.

Further movement of cutting edges causes decreasing of the attachment area and increasing concentration of strains and plastic deformation. As a consequence, the whole cut material is covered with the defects. It results in material flow along the braking surface and movement towards the rest of material. This leads to second phase called the flowing plastic deformation. The force in both of the mentioned phases increases progressively. The thickness of the material decreases, but the hardness rises causing the growth of sharing force to the level $P_{\max}$. The sharing stress on the material increases to the moment of achieving the critical level of particular material and losing the cohesion. The third phase of breakage is started. The material begins to part not at the leading edge, but at the appearance of the first crack or breakage in the material.

The equation for the maximum sharing force is:

$$P_{\max} = k \cdot R_t \cdot S = k \cdot R_t \cdot \sum l \tag{1}$$

where:

$S = g \sum l$ – sharing surface,

R_t – shear strenght,

$\sum l$ – length of the cutting edge,

k – coefficient depending on the clearance ($k = 1$).

The force P_p necessary for pushing the round element through the cutting die is calculated by the equation:

$$P_p = \frac{a}{g} \cdot k_p \cdot P_{\max} \tag{2}$$

where:

g – thickness of the cutting material,
a – pushing length,
k_p – equivalent of pushing direction.

The value of this equivalent is around 0.05–0.1 by pushing the element in the working direction.

Drawing causes creation of three dimension seamless shells [4]. Schematic drawing process is shown in Figure 2. Cutting punch 2 is moving down forming g – thickness of the metal sheet on forming die 3. During drawing process the collar is hold by holder 4.

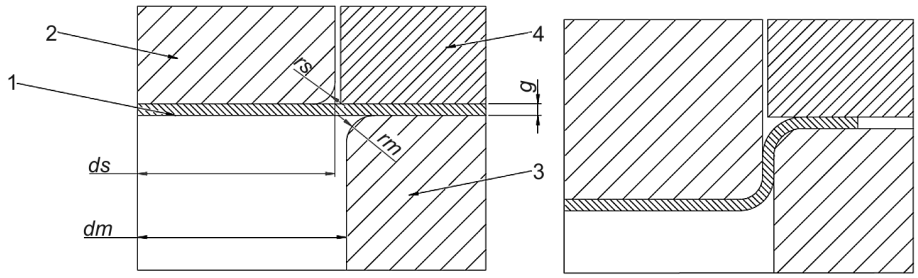

Fig. 2. Phases of drawing: a) initial and b) final

Rys. 2. Fazy wytłaczania: a) początkowa, b) końcowa

For analysis of drawing process, the punch force and blank holder pressure is necessary. The punch force needs supply the various types of work required in drawing:

$$P_w = P_{id} + P_{gn} + P_{tk} + P_{tr} \tag{3}$$

where:

P_{id} – ideal force of deformation,
P_{gn} – bending force on radius r_m,
P_{tk} – friction force between punch and die,
P_{tr} – friction force die radius.

Crown cork forming process characterizes the lack of direct holding pressure. Between metal sheet and holder some clearance occurs and it allows controlled forming process of serrate. That kind of process causes two local maximum of drawing forces. In the analysis, maximum forming force from complete process is presented. Ideal force of deformation may be calculated by the following formula:

$$P_{id} = \pi \cdot d_s \cdot g \cdot R_m \cdot \ln(\beta) \tag{4}$$

where:

β – distortion factor, $\beta = \dfrac{D}{d_1}\left[\dfrac{\text{diameter of blank}}{\text{diameter of shell}}\right]$

$$P_{gn} = \pi \cdot d_s \cdot g \cdot R_m \cdot \frac{g}{4r_m} \tag{5}$$

$$P_{id} = \frac{\pi}{2} \cdot \mu_1 \cdot d_s^2 \cdot \frac{\beta_0^2 - 1}{\beta} \cdot q \tag{6}$$

where:

μ_1 – friction coefficient between metal sheet, holder and forming die,

β_0 – distortion factor, $\beta_0 = \dfrac{D}{d_s + 2r_m}$

$$P_{tr} = \left(e^{\mu_2 \frac{\pi}{2}} - 1 \right) \cdot (P_{id} + P_{tk}) \tag{7}$$

where:

μ_2 – friction coefficient on the forming die radius.

3. Experimental system

Sharing force and drawing force on standard production machine measurement is difficult because lack of space for installation of measuring transducers. For measurements of the forces, an experimental bench was built based on inertial mechanical press (Fig. 3).

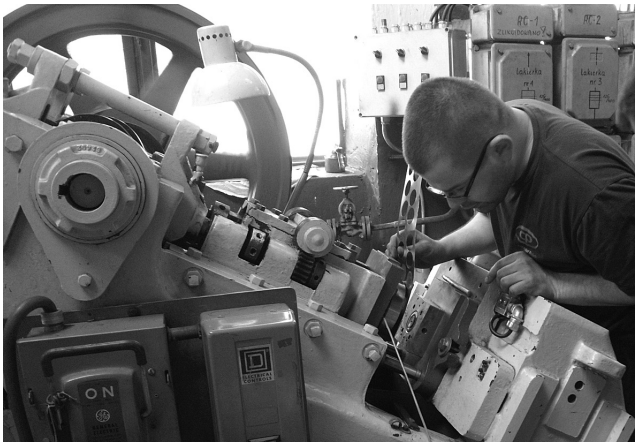

Fig. 3. View of the experimental system for measuring pressing forces

Rys. 3. Widok stanowiska badawczego do pomiaru sił tłoczenia

Sharing blank and drawing processes by building in the punch and the forming die were executed. Between the forming die and the punch force measuring transducer was installed. Construction of the punch is prepared to work as a holder with appropriate clearance. Sharing force with holding force and drawing force were independently measured. Sampling frequency was 1000 Hz. Diagram of the measuring equipment is shown in Fig. 4. The study consisted of measuring of drawing force value during the forming process.

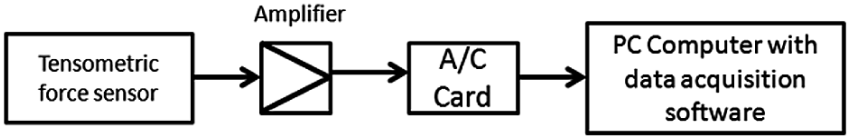

Fig. 4. Schematic diagram of the measuring equipment
Rys. 4. Schemat układu pomiarowego siły

4. Results

For drawing process, two kinds of materials were used: metal sheet with a thickness 0.21 mm and maximum tensile stress 380 MPa as well as 0.15 mm with maximum tensile stress 410 MPa. Sharing clearance was set as 0.02 mm. The measurement was performed under controlled temperature and metal closure parameters. The results obtained for sharing force of metal sheet 0.21 mm are shown in Fig. 5. Maximum value of the sharing force was 5193 N. Calculated sharing force for this kind of metal sheet was 5618 N. During the sharing force run, the plastic deformation flow can be observed. The material hardness is improved due to deformation which causes further increase of sharing force till the material breakage. As a result, the material hardness is improved significantly. Run of cutting and holding forces

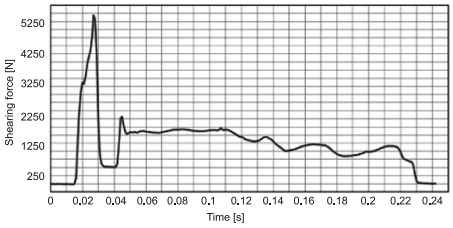

Fig. 5. Sharing and holding forces for the metal sheet 0.21 mm
Rys. 5. Przebieg siły cięcia i docisku dla blachy o grubości 0,21 mm

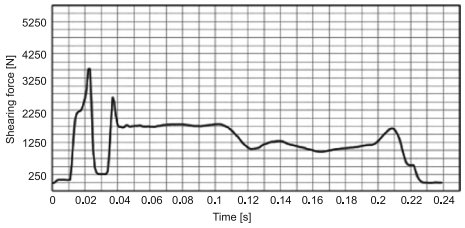

Fig. 6. Sharing and holding forces for the metal sheet 0.15mm
Rys. 6. Przebieg siły cięcia i docisku dla blachy o grubości 0,15 mm

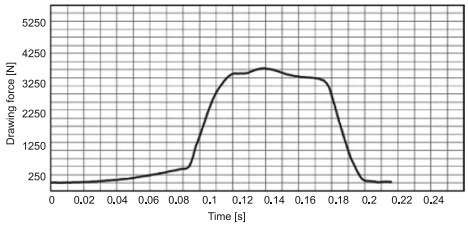

Fig. 7. Drawing force for the metal sheet 0.21 mm
Rys. 7. Przebieg siły wytłaczania dla blachy 0,21 mm

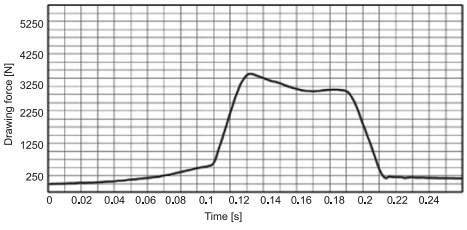

Fig. 8. Drawing force for the metal sheet 0.15 mm
Rys. 8. Przebieg siły tłoczenia dla blachy 0,15 mm

for metal sheet 0.15 mm thickness is shown in Fig. 6. Maximum value of sharing force was 3529 N, while the calculated was 4330 N. Plastic deformation flow is more pronounce for the metal sheet 0.15 mm, in addition the material hardness raised due to deformation presence. Material hardness is lower than for the metal sheet 0.21 mm.

Result of the run of drawing force for the metal sheet 0.21 mm is shown in Fig. 7. Maximum value of the forming force was 3545 N. Calculated drawing force was 3181 N. Run of forming force for metal sheet 0.15 mm is shown in Fig. 8. Maximum value of the drawing force was 3390 N, while the calculated force was 2348 N. Due to the clearance between the forming die and pressure pad, the drawing process takes place without the pre-hold. During the first phase of forming, there is no holding pressure, afterwards controlled pressing of the crown on the holder occurs. It is related to two local maximums of the drawing force. The first of them can be associated with the plastic deformation forces of forming the closures overcome. The second can be linked to pressing of the serrate and contact with the holder. Run of sharing and holding forces shows an impact of serrate on the holder (Fig. 5 and Fig. 6).

In the Table 1 calculated and measured values of forces for different material thickness are compared. Sufficient correspondence for maximum values was obtained. Obtained results provide significant knowledge on whole technological process.

Table 1

Calculated and measured values of forces for different material thickness

	Metal sheet 0,21		Metal sheet 0,15	
	Calculated value [N]	Measured value [N]	Calculated value [N]	Measured value [N]
P_{max}	5618	5193	4330	3529
P_d	50	520	71	262
P_p	1605	1600	1732	1770
P_{id}	2176		1677	
P_{gn}	469		258	
P_{tk}	0.026		0.015	
P_{tr}	535		413	
P	3181	3546	2348	3390

5. Conclusions

In the paper the analysis of sharing blank forces from the metal sheet as a material for stamping crown corks and run of the pressing forces was performed. For measurements of the forces, an experimental system was built based on inertial mechanical press and measuring transducer. The system was used for the determination of forces runs during the crown corks production process and adjustment of parameters i.e. clearance height, metal sheet holding

pressure in order to obtain proper parameters of the metal closure. The original achievement of the authors is test stand, which allows to carry out dynamic tests during the forming process of crown closures. Results can be applied for testing new materials and reducing thickness of the closures.

References

[1] Boljanovic V., *Sheet metal forming processes and die design*, Industrial Press Inc., 2004.
[2] Lisowski E., *Analiza zakrywek koronowych w systemie ABACUS*, Wydawnictwo Politechniki Krakowskiej, Kraków 2011.
[3] Painter W., *Bottle-sealing device*, Patent US468258, 1890.
[4] Domagała M., Okoński S., *Symulacja tłoczenia zakrywek koronowych*, Wydawnictwo Politechniki Krakowskiej, Kraków 2011.
[5] Stachowicz F., *Przeróbka plastyczna-laboratorium*, Oficyna Wydawnicza Politechniki Rzeszowskiej, Rzeszów 1997.
[6] Erbel S., Kuczyński K., Marciniak Z., *Obróbka plastyczna*, PWN, Warszawa 1981.
[7] PN-EN14634:2010, PN-EN14635:2010 Opakowania szklane – Główka do zamknięcia koronowego.

TECHNICAL TRANSACTIONS | CZASOPISMO TECHNICZNE
MECHANICS | MECHANIKA
1-M/2013

ARKADIUSZ CZARNUCH*, EDWARD LISOWSKI**

STUDIES OF TRUCK SEMITRAILER STABILITY DURING LOADING AND UNLOADING

BADANIA STATECZNOŚCI NACZEPY SAMOCHODU CIĘŻAROWEGO PODCZAS ZAŁADUNKU I ROZŁADUNKU

A b s t r a c t

The paper presents the effect of air suspension system on semi-trailers during loading and unloading processes while using a forklift. The mathematical model was created, which takes into account a sharp loading on the rear platform of a semi-trailer. The entry of a loaded forklift onto the rear platform of a semi-trailer causes rapid lowering of the platform, which contributes to an unstable movement of the forklift.

Keywords: *air suspension*, *semi-trailer*

S t r e s z c z e n i e

W artykule przedstawiono symulację działania pneumatycznego układu zawieszenia naczepy samochodu ciężarowego podczas załadunku i wyładunku przy wykorzystaniu wózka widłowego. Zbudowano model matematyczny dla przypadku nagłego obciążenia tylnej części naczepy to jest przy wjeździe obciążonego wózka na naczepę i badano zachowanie się układu. Wjazd obciążonego wózka na naczepę powoduje skokowe obniżenie platformy, co ma niekorzystny wpływ na stabilność jazdy wózka.

Słowa kluczowe: *układ pneumatycznego zawieszenia*, *naczepa*

* MSc. Arkadiusz Czarnuch, Wielton S.A.
** Prof. PhD. Eng. Edward Lisowski, Institute of Applied Informatics, Mechanical Faculty, Cracow University of Technology.

Nomenclature

p_S – pressure of pneumatic piston [Pa]
p_j – unitary pressure per strength [Pa/N]
p_Z – pressure in air tank [Pa]
F_S – force on airbag [N]
F_W – force on hanger bracket [N]
A_E – spring effective area [m^2]
k – air spring stiffness [N/m]
C – damping coefficient [Ns/m]
C_C – critical damping coefficient [Ns/m]
ζ – damping ratio
m – mass [kg]
m_{nr} – unsprung mass [kg]
V – volume [m^3]
V_S – volume of airbag [m3]
κ – adiabatic coefficient
ρ – density [kg/m^3]
x – displacement [m]
x_s – height of airbag working area [m]
υ_Z – velocity of air flow [m/s]
h_{tarcia} – fraction loss [m]
h_{lok} – local loss [m]
d – diameter of pipes [m]

1. Introduction

The suspension is one of the basic systems in vehicles which is responsible for safety and comfort. It is the system which connects the vehicle structure to wheels and allows for relative motion between them [1, 2, 4]. Reaction forces from the wheels are compensated and transferred to the structure of the vehicle.

There are a few types of suspension: mechanical, hydraulic and pneumatic. In pneumatic suspensions the air is a working medium. The air is characterized by low bulk elastic modulus K_s = 0.14 GPa, which means that it changes its volume under a small variation of pressure. It is an advantage for air suspensions, but in some cases it may be a disadvantage, especially while rapid loading and unloading, where large changes of force occur resulting in height movement in airbag, which consequently influences the vehicle stability. The article deals with the reaction forces appearing in suspension during loading of a semi trailer with a forklift from loading docks. Nowadays pneumatic suspension is equipped with an automatic levelling system but that system is not able to compensate rapid and abrupt load which occurs during loading with a forklift from a loading dock.

2. Statics analysis of semi-trailer platform

To analyze the statics we present a typical case of loading and unloading of a semi trailer. The forklift with cargo drives onto the rear semi trailer platform from a loading dock. It is assumed that the semi trailer platform is being levelled by the pneumatic system to the level of the loading ramp. Force distribution on semi trailer while loading is shown in Fig. 1. During driving onto the platform by the first axle of the forklift, the semi trailer is subjected to gravity forces and the rear part of platform is subjected to force F coming from the first axle of the forklift. Reaction forces are R_1 and R_2. Initially we present a simple 2D beam system supported in two points, front part as a fifth wheel of a tractor and the rear part as an assembly of suspension.

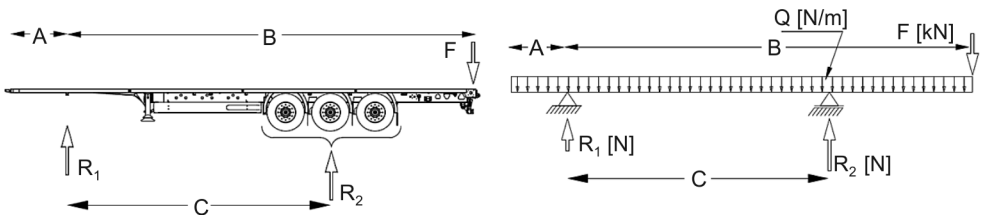

Fig. 1. Chassis of the trailer during loading and unloading

Rys. 1. Schemat podwozia naczepy siodłowej przy wjeździe wózka na platformę

3. Suspension schema

The suspension schema for one wheel is shown in Fig. 2. The system contains air spring 4, damper 3 and hanger bracket 1. In the system the characteristic values describing the suspension are: stiffness coefficient k which describes the air spring and damping coefficient C describing the damper.

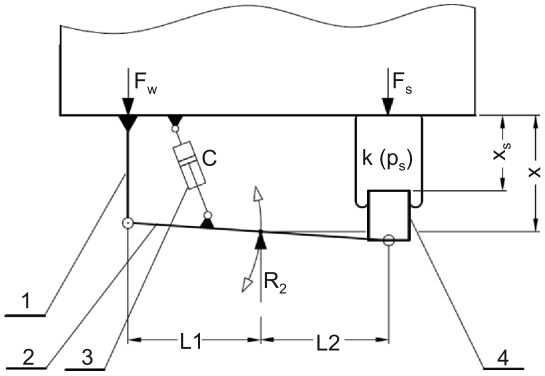

Fig. 2. Suspension model

Rys. 2. Model zawieszenia

Reaction R_2, is partially transferred to the semi trailer chassis by hanger bracket 1, force F_W, and by pneumatic air spring 4, force F_S. The kinematics and characteristic values for the suspension were determined based on the data provided by suspension and axle manufacturer SAF [3]. The X dimension describes the distance between the wheel center and the bottom of the chassis, and X_S is the height of the working area of the air spring. Relation between these values is described by the equation (1):

$$\Delta X_S = \frac{L_1}{L_1 + L_2} \cdot \Delta X \tag{1}$$

The pneumatic airbag SAF 2619V [3] was considered. The unitary pressure per 1 N of loading for airbag is:

$$p_J = 22.7 \text{ Pa/N} \tag{2}$$

Basing on the unitary pressure (2) the effective area A_E (3) was determined

$$A_E = \frac{1}{p_J} = \frac{F_S}{p_S} \tag{3}$$

The volume V_0 in the air spring relating to the initial conditions was determined based on the effective area A_E corrected by additional volume in neutral space.

$$V_O = A_E \cdot x_{SO} + \left(\left(\frac{\pi \cdot D_Z^2}{4} - A_E \right) \cdot x_{SO} \right) \tag{4}$$

where:

x_{SO} – the height of working area in the air spring related to the initial conditions.

The initial pressure in the air spring P_{S0} was determined basing on the initial volume V_0 and the initial impact force on air spring F_{S0} coming from the weight of the semi-trailer:

$$p_{S0} = \frac{F_{S0}}{A_E} \tag{5}$$

Force F_S was determined by suspension kinematics and reaction R_2 coming from the contact of the wheel with the ground:

$$F_S = \frac{L}{L + L_1} \cdot (R_2 - m_{NR}) \tag{6}$$

where:

m_{NR} – unsprung mass including tires, wheels, suspension and axle.

Force F_S was the base for the determination of the correlation between pressure in the airbag and loading of axle R_2, the correlation is described by equation (7). The pressure is designated for two airbags working on one axle. This correlation corresponds to the constant volume of the airbag and constant height from the axle to the chassis bottom:

$$p_S(R_2) = \frac{L}{2 \cdot (L + L_1)} \cdot (R_2 - m_{NR}) \cdot p_J \tag{7}$$

In the case where automatic levelling system is switched off and during manual handling, the pressure in the airbag corresponds to actual loading and during the change of loading the volume in the airbag changes. That transformation was treated as adiabatic process where $p_S \cdot V^{\kappa} = \text{const}$, the initial pressure and volume, P_{S0} and V_0, correspond to study state conditions.

$$P_S = P_{S0} \cdot \left(\frac{V_0}{V_1} \right)^K \tag{8}$$

The movement of axle in relation to the chassis was described by differential equation of motion (9):

$$m \cdot \frac{d^2x}{dt^2} + c \cdot \frac{dx}{dt} + k(p,V,x) \cdot x = F_S(t) \tag{9}$$

where:

$k(p, x) \cdot x$ – spring force of airbag,
$F_S(t)$ – force on airbag.

Value k describes the spring characteristic of the airbag and it is an increment of the force to the change of the airbag height:

$$k = \frac{dF_S}{dx} \tag{10}$$

According to (5), the stiffness coefficient k may depend upon the pressure in airbag [1]:

$$k = A_E \cdot \frac{dP_S}{dx} \tag{11}$$

These values were determined for the system where automatic leveling valve was switched off, the system was closed. The initial pressure in the airbag corresponds to unloaded semi trailer. In this case, during loading the pressure changes in airbag due to volume change, equation (8). This occurs when the platform level of a semi trailer is positioned manually to the dock level, then automatic leveling valve is switched off. The differential equation of motion (9) for the suspension system is as follows:

$$\frac{d^2x}{dt^2} = -\frac{C}{m} \cdot \frac{dx}{dt} - \frac{1}{m} \cdot \left(A_E \cdot \frac{dp_S}{dx} \right) \cdot x + \frac{1}{m} F_S(t) \tag{12}$$

The damping level C was determined using the damping ratio $\varsigma = 0.8$, which describes the relation between damping coefficient C and critical damping coefficient C_C [2]:

$$\varsigma = \frac{C}{C_C} \tag{13}$$

The critical damping coefficient is defined (14):

$$C_C = 2 \cdot \sqrt{k \cdot m} \tag{14}$$

To analyze the suspension system, where self-leveling valve is working during loading, a module which controls the movement was added to the mathematical model. The self-

leveling system works by controlling the distance between wheel center and chassis and appropriately to motion, suitable amount of air is added to or subtracted from the airbag.

It was assumed that the system is powered from an air tank, where there is constant pressure p_z. The air tank is connected with the airbags by elastic pipes of constant length and diameter. In the system there are two additional pneumatic spool valves.

In order to designate the amount of air that can be provided to the airbag, flow velocity from the air tank υ_Z was calculated by the Bernoulli's equation. The local and linear losses were taken into consideration.

$$\upsilon_Z = \sqrt{\frac{2\cdot(p_Z - p_S)}{\rho} - 2\cdot g\cdot(h_{\text{tarcia}} + h_{\text{lok}})} \tag{15}$$

Based on the flow velocity the volume flow rate was determined.

$$\dot{V}_1 = \upsilon_Z \cdot \frac{\pi \cdot d^2}{4} \tag{16}$$

To increase the stiffness coefficient of air spring, mathematically it was performed by increasing the pressure p_p per unit of time, according to adiabatic process:

$$\frac{dp_p}{dt} = p_S \cdot \left(\frac{V_1}{V_S}\right)^{\kappa} dt \tag{17}$$

4. Results

To solve the differential equation of motion (12) the Math-Lab/Simulink software was used. The initial conditions for the equation were assumed as for an unloaded semi trailer. Additional loading from the first axle of the forklift was simulated by rectangular function $R_2(t)$. The obtained displacement $X(t)$ was used to determine the temporary volume of the airbag. The pressure in the airbag was defined on the basis of the adiabatic transformation and used to determine the stiffness coefficient of the air spring. Obtained stiffness coefficients were passed to the next iteration of motion equation.

The results of the simulation are shown in Fig. 3–5. The results include the system without and with self-leveling line 1 and 2, respectively. Fig. 3 shows the motion of wheel center in time. Adequately to the change of the position the pressure and volume of the airbag is changed, as shown in Fig. 4 and 5.

Presented graphs show the system response to the rapid and abrupt load. In period 0–1 s the system is in steady state conditions, the pressure and initial volume correspond to unloaded semi-trailer including the vehicle's weight. The displacement of axle in relation to the chassis is zero. After 1 s, additional force was added to the motion equation causing the 80 mm displacement of the system.

The behavior of the system at the initial stage with and without self-leveling, after additional force is similar, in both cases the level of displacement is the same. In case 1 the respond signal of displacement changes to the level –90 mm and after 0.5 s it stabilizes to level –80 mm. In case 2 with self-leveling system signal changes also to the –90 mm but it stabilizes after 4.5 s to the initial level.

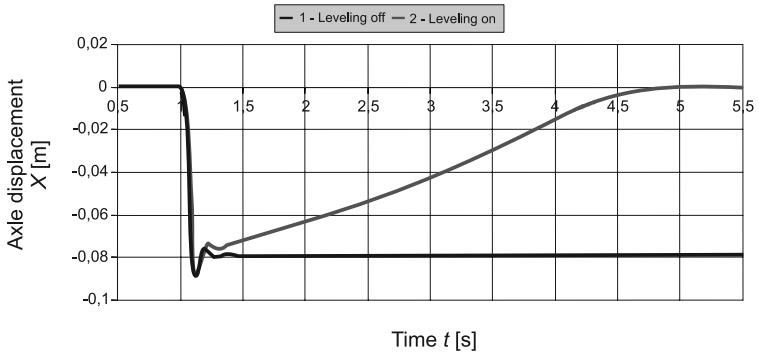

Fig. 3. Movement of axle in time

Rys. 3. Przemieszczenie osi zawieszenia w czasie

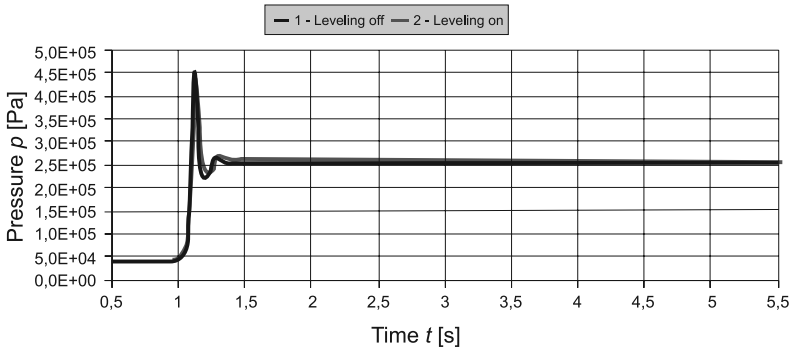

Fig. 4. Pressure in piston chamber in time

Rys. 4. Zmiana ciśnienia w siłowniku w czasie

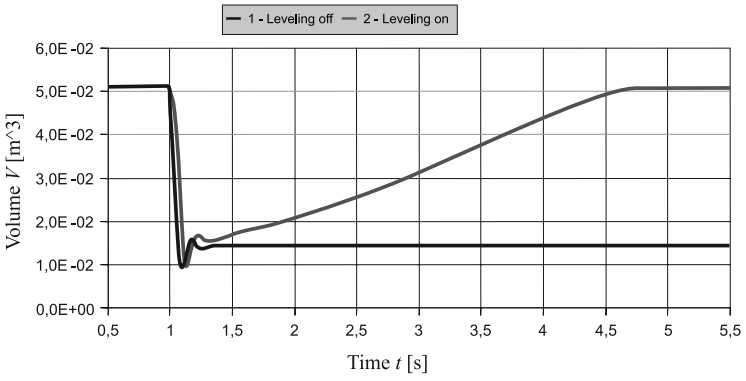

Fig. 5. Volume of piston chamber in time

Rys. 5. Zmiana objętości komory siłownika w czasie

The pressure graphs show rapid change from 0.05 MPa to 0.45 MPa in a short time of 0,15 s. The reason of this rapid change is the big difference between the initial load and the added load which increased 3,5 times. The signal stabilizes after 0,3 s and it is similar for both considered cases with and without self-levelling.

Similarly to displacement the volume signal changes. In short time, 0.3 s, volume decreases to the neutral level of 0.014 m^3. In case 2 with self-levelling, when the initial level changes, then additional amount of medium is added. The volume of airbag is changed under a constant pressure. It should be noted that the levelling system is activated following the change in displacement of 1 mm, and as a result that volume increases in the first phase.

5. Conclusions

This paper presents a theoretical simulation of air suspension behavior in the case of sudden load changes. The simulation confirms, that the air suspension is not able to compensate sudden and large load change.

The self-levelling system stabilizes displacement of the air suspension to the initial value, but it does not contribute to the reduction of displacement. The time necessary to return to the initial position is relatively long, which has an adverse effect on the stability of the semi trailer during loading and unloading.

Developed simulation of air suspension can be used for detailed analysis of the impact of different factors on the system work. The following factors mainly contribute to the unstable air suspension working during large load changes: low bulk elastic properties of air, the initial pressure is adjusted to the current load, large capacity of airbags in relation to the supply system, the neutral volume in airbag, where increased pressure does not generate vertical force on a piston, the self-levelling system does not contribute to the reduction of the displacement level.

References

[1] Nieto A.J., Morales A.L., et al., *An analytical model of pneumatic suspensions based on an experimental characterization*, Journal of Sound and Vibration, vol. 313, 2008, 290-307.
[2] Dixon J., *The Shock Absorber Handbook*, The Open University, 2008.
[3] *Design manual SAF Holland Group*, Edition 2010.
[4] Szenajch W., *Napęd i sterowanie pneumatyczne*, Wydawnictwa Naukowo-Techniczne, Warszawa 1997.
[5] Drobniak S., *Mechanika płynów*, Politechnika Częstochowska, Częstochowa 2008.

TECHNICAL TRANSACTIONS | **CZASOPISMO TECHNICZNE**
MECHANICS | MECHANIKA
1-M/2013

TADEUSZ CZYŻEWSKI*

PARALLEL COMPUTING IN KINEMATIC ANALYSIS OF HEAVY MACHINERY EQUIPMENT SYSTEM

OBLICZENIA RÓWNOLEGŁE W ANALIZIE KINEMATYKI OSPRZĘTU MASZYN ROBOCZYCH

A b s t r a c t

This paper presents a methodology to increase performance of the kinematics simulation process of heavy machinery equipment system. The proposed method is based on parallelization of calculations performed in a single simulation step. Parallelization is achieved by building application based on the OpenCL framework that allows to perform the necessary mathematical calculations using a graphics card processor. In the final part of the article were presented results of performance tests of the proposed method.

Keywords: *parallel computing*, *GPU unit*, *OpenCL*, *kinematic analysis*, *heavy machinery*

S t r e s z c z e n i e

W artykule przedstawiono metodykę zwiększania wydajności procesu symulacji kinematyki osprzętu maszyn roboczych. Zaproponowana metoda polega na zrównolegleniu obliczeń wykonywanych w ramach jednego kroku symulacyjnego. Zrównoleglanie realizowane jest poprzez zbudowanie oprogramowania opartego o szablon aplikacji OpenCL co pozwala na wykonanie niezbędnych obliczeń matematycznych za pomocą procesora karty graficznej. W końcowej części artykułu przedstawione zostały wyniki testów wydajności zaproponowanej metody.

Słowa kluczowe: *obliczenia równoległe*, *układ GPU*, *OpenCL, analiza kinematyczna*, *maszyny robocze*

* MSc. Eng. Tadeusz Czyżewski, Institute of Applied Informatics, Faculty of Mechanical Engineering, Cracow University of Technology.

1. Introduction

Designing of heavy machinery requires consideration of many aspects of the trajectory planning of particular links necessary to perform work cycle. The typical design process of heavy machinery is carried out using the 3D CAD systems. In these systems the assembly models of individual machine links are represented by solids with adequate material properties, mass, volume, etc. Between the machine links constraints are imposed. These constraints depending on the type reduce degrees of freedom to a specified number. Types of constraints are defined by the designer at the design stage. Information stored in a three-dimensional model of a modern CAD system can and should be used in the model simulations. Therefore, many CAD systems are equipped with modules enabling to conduct simulation investigations such as calculation of: kinematics, dynamics, strength, etc.

At the turn of the twentieth and twenty-first century on the hardware market appeared first graphics card equipped with a so-called GPU (*Graphics Processing Unit*). The primary purpose of these processors was to support the CPU (*Central Processing Unit*) in calculations related to the processing of 3D graphics. Over time, these systems has been used for calculations unrelated to graphics. The turning point on the way to develop a technique that allows performing general-purpose computation on GPUs (*GPGPU – General-Purpose Computing on Graphics Processor Units*) was the appearance of graphics cards equipped with programmable shader (NVIDIA GeForce 3 card series) [1,2]. The main task of shaders is to execute a short computer program written in specialized language (*shading language*), which is used to describe the properties of pixels and vertices. The syntax of this specialized language is very similar to the syntax of general-purpose programming languages such as C. Therefore, many scientific communities around the world very quickly began to experiment with writing code for a shader that implements the calculations not connected with graphics processing. As a consequence graphics card manufacturers have developed specialized platforms for the design and analysis of programs that perform calculations on GPUs. Each of these platforms is designed only for a specific manufacturer's devices. So this means that a program written for Nvidia graphics cards do not fully utilize the computing power of a computer CPU, and vice versa. This problem has been solved by the introducing in 2009 by Apple Inc. an OpenCL framework that allows to write programs implementing parallel computing on any hardware (CPU, GPU, DSP, etc.) [3].

Despite the significant growth of computing power of a hardware and capabilities of its use, CAD modules intended for simulations still do not provide parallel processing. Therefore, this article attempts to make full use of hardware computing power for parallel processing. For this purpose, an OpenCL-based application was built, which was used to conduct a series of performance tests of mathematical operations that are used in the analysis of the kinematics.

2. Simulation object

2.1. Kinematic structure

Fig. 2 presents the kinematic structure of the backhoe excavator equipment system, which was the object of research. This structure consists of a boom, arm and bucket connected to

each other and the base with revolute joints. Links and the basis connected in series form an open kinematic chain.

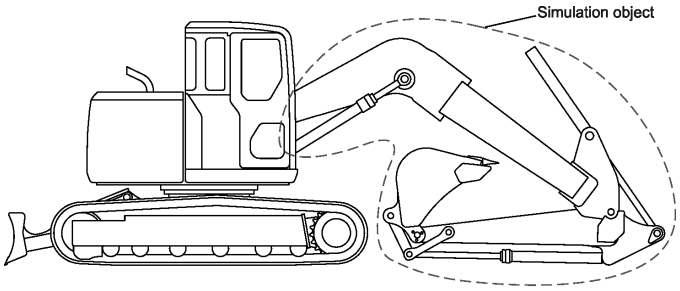

Fig. 1. Backhoe excavator with an isolated equipment system, which was the object of the simulation
Rys. 1. Koparka podsiębierna z wydzielonym osprzętem roboczym, który był obiektem symulacji

Motion of excavator links is forced by double-acting hydraulic cylinders, which together with the main kinematic chain create local kinematic loops, that was presented in Fig. 2. In order to increase bucket rotation angle, there was used a four-bar linkage mechanism, which is also a local kinematic loop. The links can be considered as a non-deformable.

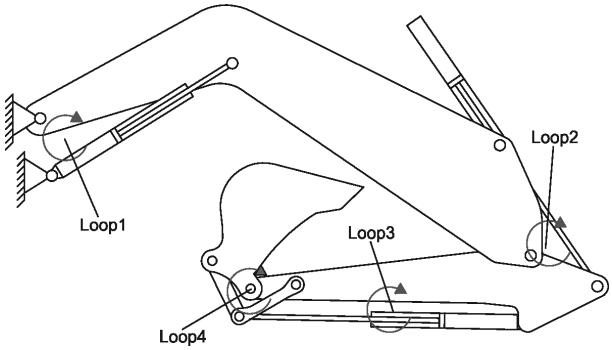

Fig. 2. Kinematic scheme of the equipment system
Rys. 2. Schemat kinematyczny osprzętu roboczego

2.2. Kinematic analysis

Kinematic analysis of the excavator equipment system can be performed by using of multibody formalism and the absolute coordinates, which describes the position and orientation of all links in every step of the simulation. In Fig. 3 are presented two links selected from the considered kinematic chain of the excavator. To each link a local reference system π is bounded. The position and orientation of any link of the excavator kinematic chain can be unequivocally defined by giving:

– vector $\boldsymbol{r}$ which specifies the position of the origin of the local reference system π of the link in global reference system π_0.

– three angles α, β, γ what describe orientation of the local reference system π of the link relative to global reference system π_0.

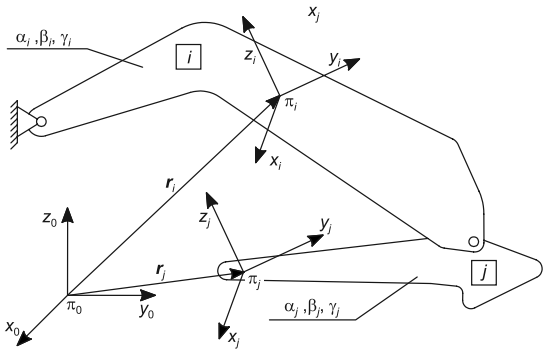

Fig. 3. Absolute coordinates

Rys. 3. Współrzędne absolutne

Thus, the absolute coordinates vector $\boldsymbol{q}_i$ of unconstrained link *i* in three dimensional space can be written as

$$\boldsymbol{q}_i = [\boldsymbol{r}_i^T, \alpha_i, \beta_i, \gamma_i]^T \tag{1}$$

where α, β, γ are the system of three Euler angles. After assuming the notation

$$\varphi_i = [\alpha_i, \beta_i, \gamma_i]^T \tag{2}$$

absolute coordinates vector $\boldsymbol{q}_i$ of unconstrained link *i* will have the following form

$$q_i = [\boldsymbol{r}_i^T, \varphi_i^T] \tag{3}$$

By using eq. (1)–(3) it is possible to write the absolute coordinates vector, which describes position and orientation of all links of backhoe excavator from Fig. 1. According to [4] the absolute coordinates vector will be as follows

$$\boldsymbol{q} = [\boldsymbol{q}_1^T, \boldsymbol{q}_2^T, \boldsymbol{q}_3^T, \boldsymbol{q}_4^T, \boldsymbol{q}_5^T, \boldsymbol{q}_6^T, \boldsymbol{q}_7^T, \boldsymbol{q}_8^T, \boldsymbol{q}_9^T, \boldsymbol{q}_{10}^T, \boldsymbol{q}_{11}^T]^T \tag{4}$$

Kinematics links between particular components of excavator is expressed by imposing on vector (4) suitable holonomic constraints in form

$$\Phi\mathrm{K} = (\boldsymbol{q}) = \boldsymbol{0} \tag{5}$$

Similar restrictions as to positions have to be applied to velocities and accelerations of excavator links. Constraints which bound the velocity vector are obtained by differentiating with respect to time equation (5)

$$\dot{\boldsymbol{\Phi}}^K(\dot{\boldsymbol{q}}, \boldsymbol{q}) = \boldsymbol{\Phi}_{\boldsymbol{q}}^K \dot{\boldsymbol{q}} = \boldsymbol{0} \tag{6}$$

where $\boldsymbol{\Phi}_{\boldsymbol{q}}^K$ is a Jacobian matrix of absolute constraints vector (4). Constraints which bind the velocity vector can be obtained by double differentiating with respect to time equation (5)

$$\ddot{\boldsymbol{\Phi}}^K(\ddot{\boldsymbol{q}},\dot{\boldsymbol{q}},\boldsymbol{q}) = \boldsymbol{\Phi}_{\boldsymbol{q}}^K\ddot{\boldsymbol{q}} = -(\boldsymbol{\Phi}_{\boldsymbol{q}}^K\dot{\boldsymbol{q}})_{\boldsymbol{q}}\dot{\boldsymbol{q}} = \boldsymbol{\Gamma}^K \tag{7}$$

For conducting kinematic analysis it is necessary to determine specific motion of the object. For this purpose there are defined additional constraint equations, which are dependent on absolute coordinates vector (4) and time. These equations are called driving constraints and are written as follows

$$\boldsymbol{\Phi}^D = (\boldsymbol{q},\, t) = \mathbf{0} \tag{8}$$

Driving constraints (8), as in the case of kinematic constraints (5), impose additional restrictions on the generalized velocities and accelerations. By differentiating twice the equation (8) with respect to time there are obtained equations of driving constraints for generalized velocities and accelerations, which take the form

$$\dot{\boldsymbol{\Phi}}^D(\dot{\boldsymbol{q}},\boldsymbol{q},t) = \boldsymbol{\Phi}_{\boldsymbol{q}}^D\dot{\boldsymbol{q}} = -\boldsymbol{\Phi}_t^D \tag{9}$$

$$\ddot{\boldsymbol{\Phi}}^D(\ddot{\boldsymbol{q}},\dot{\boldsymbol{q}},\boldsymbol{q},t) = \boldsymbol{\Phi}_{\boldsymbol{q}}^D\ddot{\boldsymbol{q}} = -(\boldsymbol{\Phi}_{\boldsymbol{q}}^D\dot{\boldsymbol{q}})_{\boldsymbol{q}}\dot{\boldsymbol{q}} - 2\boldsymbol{\Phi}_{\boldsymbol{q}t}^D\dot{\boldsymbol{q}} - \boldsymbol{\Phi}_{tt}^D = \boldsymbol{\Gamma}^D \tag{10}$$

After collecting equations (5) and (8) a system of nonlinear algebraic equations is obtained. Solution of this system gives position vector of all excavator links

$$\boldsymbol{\Phi}(\boldsymbol{q},t) = \begin{bmatrix} \boldsymbol{\Phi}^K(\boldsymbol{q}) \\ \boldsymbol{\Phi}^D(\boldsymbol{q},t) \end{bmatrix} = \mathbf{0} \tag{11}$$

Collecting equations (6) and (9), (7) and (10) give a system of linear algebraic equations. Solution of this system allows to obtain the velocity and acceleration vector of all excavator links

$$\dot{\boldsymbol{\Phi}}(\dot{\boldsymbol{q}},\boldsymbol{q},t) = \boldsymbol{\Phi}_{\boldsymbol{q}}\dot{\boldsymbol{q}} = -\boldsymbol{\Phi}_t = \begin{bmatrix} \mathbf{0} \\ -\boldsymbol{\Phi}_t^D \end{bmatrix} \tag{12}$$

$$\ddot{\boldsymbol{\Phi}}(\ddot{\boldsymbol{q}},\dot{\boldsymbol{q}},\boldsymbol{q},t) = -(\boldsymbol{\Phi}_{\boldsymbol{q}}\dot{\boldsymbol{q}})_{\boldsymbol{q}}\dot{\boldsymbol{q}} - 2\boldsymbol{\Phi}_{\boldsymbol{q}t}\dot{\boldsymbol{q}} - \boldsymbol{\Phi}_{tt} = \begin{bmatrix} -(\boldsymbol{\Phi}_{\boldsymbol{q}}^K\boldsymbol{q})_{\boldsymbol{q}}\dot{\boldsymbol{q}} \\ -(\boldsymbol{\Phi}_{\boldsymbol{q}}^D\dot{\boldsymbol{q}})_{\boldsymbol{q}}\dot{\boldsymbol{q}} - 2\boldsymbol{\Phi}_{\boldsymbol{q}t}^D\dot{\boldsymbol{q}} - \boldsymbol{\Phi}_{tt}^D \end{bmatrix} \tag{13}$$

Conducting kinematic analysis of backhoe excavator will be consist in solving system of equations (11)–(13).

3. Simulation parallelization

The basic mathematical methods in kinematic analysis based on multibody system formalism is matrix analysis. One of the most common mathematical operations in kinematic analysis is the matrix multiplication. In a single simulation step it is necessary to make tens or even hundreds of such multiplications. Depending on the size of the time step and the time interval in which the simulation is performed, the number of simulation steps may vary from a few to several hundred, and even more. Therefore, one of the key aspects that determine the efficiency of the simulation is to use a very efficient algorithm for matrix

multiplication. A good approach in this situation is to use a multi-core architecture, which enables parallelization of the matrix multiplication process.

According to [5] the mathematical definition of matrix multiplication can be written as

$$\boldsymbol{C}_{i,j} = \boldsymbol{C}_{i,j} + \sum_{k=0}^{P} \boldsymbol{A}_{i,k} \cdot \boldsymbol{B}_{k,j} \tag{14}$$

where

$$0 \le i \le N, \qquad 0 \le j \le M$$

This is shown schematically in Fig. 4. It is well known that the classical approach to matrix multiplication allows in one calculation step of designating one of the elements of the resulting. Use of OpenCL framework enables to write a special program that will be executed

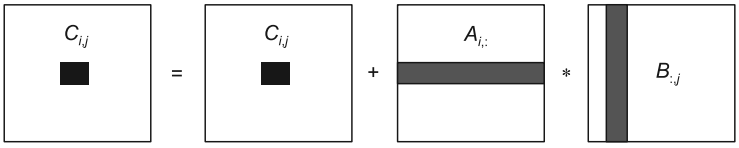

Fig. 4. Classical matrix multiplication

Rys. 4. Klasyczne mnożenie macierzy

on multiple threads of CPU or GPU. Unlike the classical approach parallel matrix multiplication allows to determine in one calculation step not only one element of the resulting matrix but the entire row or column. This was shown schematically in Fig. 5.

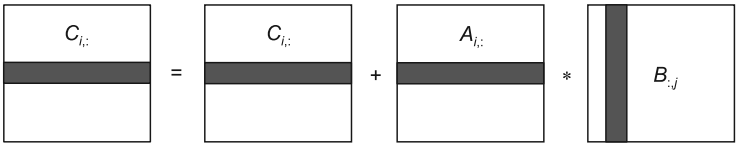

Fig. 5. Parallel matrix multiplication

Rys. 5. Równoległe mnożenie macierzy

4. Test results

Kinematic analysis of excavator equipment system shown in fig. 1 consists in solving three equations describing the position, velocity and acceleration of the entire system in time. The system of equations describing the system position is a system of nonlinear algebraic equations. To solve this system the Newton-Raphson method was used. This is an iterative method, in which one of the mathematical operations performed in a single step is to multiply the inverted Jacobian matrix of an absolute coordinates vector $\boldsymbol{q}$ with constraints imposed on these coordinates. Constraints vector is treated as a column matrix, and therefore these multiplication is simply a multiplication of two matrices. This matrix multiplication was the subject of performance test which was carried out in this article. Tests were conducted on various hardware configurations which are shown in table 1.

Table 1

Hardware configurations used in tests

Configuration symbol	Description of component	
	Processor	**Graphics card**
K1	Intel Core i7-3610QM 2.3 GHz	NVIDA GeForce GT 635M
K2	2 x Intel Xeon E5520 2.27 GHz	NVIDA GeForce GTX 285
K3	Intel Core i7-2630QM 2.0 GHz	NVIDA Quadro 3000M
K4	Intel Core i7-2670QM 2.2 GHz	NVIDIA GeForce GTX 570M

On each hardware configuration was run an OpenCL-based computer program, which performed mentioned matrix multiplication in three ways: classical approach, parallel on CPU, parallel on GPU. The test results were presented in Fig. 6. This chart shows that the largest increase of a performance compared to the classical approach has been obtained by performing parallel computations using the GPU. The resulting increase of efficiency is varying from about thirteen times in the case of K2 configuration to about fifteen times in the case of K4 configuration. The test results also show that the parallelization of matrix multiplication process using the main computer processor enables to obtain several times increase of performance. Obtained increase of efficiency is varying from about two times for configuration K3 and K4 to five times for configuration K2.

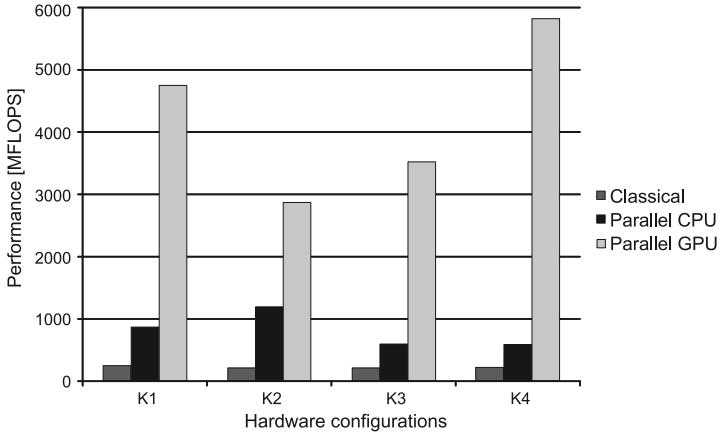

Fig. 6. Test results

Rys. 6. Wyniki testów

5. Conclusions

The article shows how the performance of mathematical operations, such as matrix multiplication, can affect the efficiency of the kinematic simulation of heavy machinery equipment system. Performed tests shown that the performance of matrix multiplication

can be repeatedly increased by parallelization of multiplication process. The best results were obtained with parallelization of the calculation process using the GPU and OpenCL framework. Obtained results leads to conclusion that the parallelization of other mathematical operations occurring in the kinematic calculations algorithm (such as matrix inversion, matrix norm determination) can further increase the efficiency of the simulation process.

References

[1] Kird B.D., Hwu W.W., *Programming massively parallel processors. A hands-on approach*, Morgan Kaufmann, Burlington 2010.

[2] Tasora A., Negrut D., Anitescu M., *GPU-Based Parallel Computing for the Simulation of Complex Multibody Systems with Unilateral and Bilateral Constraints: An Overview*, Computational Methods in Applied Sciences vol. 23, Springer, New York 2011.

[3] Munshi A., Gaster W.W., Mattson T. G., Fung J., Ginsburg D., *OpenCL programming guide*, Addision-Wesley, Boston 2012.

[4] Haug E.J., *Computer Aided Kinematics and dynamics of mechanical systems. Volume I: Basic methods*, Allyn and Bacon, Massachusetts 1989.

[5] Trefethen L.N., Bau. D., *Numerical linear algebra*, Society for Industrial and Applied Mathematics, Philadelphia 1997.

TECHNICAL TRANSACTIONS | **CZASOPISMO TECHNICZNE**
MECHANICS | MECHANIKA
1-M/2013

WOJCIECH CZYŻYCKI*

SIMULATION STUDIES OF VANE PUMP CHARACTERISTICS WITH A FUZZY CONTROLLER

BADANIA SYMULACYJNE CHARAKTERYSTYK POMPY ŁOPATKOWEJ Z REGULATOREM FLC

A b s t r a c t

This paper presents the results of simulations of vane pump static characteristics with a fuzzy controller. The controller was designed for controlling the flow rate of the vane pump. The results confirm, that the control quality is slightly better than with the PID controller, especially at low loads and rapid changes of the system load.

Keywords: *hydraulic system*, *flow control*, *fuzzy logic controller*, *vane pump*

S t r e s z c z e n i e

W artykule przedstawiono wyniki badań symulacyjnych charakterystyk statycznych pompy łopatkowej z dodatkowym regulatorem rozmytym. Regulator zaprojektowano dla sterowania wydajnością pompy łopatkowej. Uzyskane wyniki potwierdzają jakość sterowania nieco lepszą niż regulatorów typu PID zwłaszcza w zakresie małych obciążeń i szybkich zmian obciążenia układu.

Słowa kluczowe: *układ hydrauliczny*, *regulacja wydajności*, *regulator rozmyty*, *pompa łopatkowa*

* PhD. Eng. Wojciech Czyżycki, Institute of Applied Informatics, Faculty of Mechanical Engineering, Cracow University of Technology.

1. Introduction

One of the most important elements of a hydraulic system is a pump. Performance characteristics of a pump should be matched to the changes of the system needs. These capabilities, maintaining the high efficiency of the system, can be provided only by a variable pump delivery. In this area piston pumps and vane pumps are commonly used. In this paper are presented results of simulation studies of a vane pump equipped with an extra controller.

Control systems used in vane pumps do not provide maintenance of the adjustable delivery in the whole range of operating pressures coming from the system load. With the increase of the pressure, the flow rate declines as shown in Figure 1. Delivery Q is not only function of control signal k but additionally depends on pressure p in hydraulic circuit. The main reasons for the flow rate drop are: an increase of leakage in the pump and the need to power the control system using the pump. Application of eccentricity measurement system, used in solutions of companies like Bosch, Berarma or Parker does not prevent this phenomenon, because in order to maintain constant performance, information about the current real flow rate is needed. For this purpose, system for measuring the volumetric flow rate in the outlet channel of the pump must be used. Furthermore, an additional pump controller based on the control signal from the flow sensor should be applied. In order to obtain a high control accuracy and maintain ease of tuning, application of a fuzzy controller (FLC) and a PID controller to compare the control quality was proposed [1–5, 7, 8].

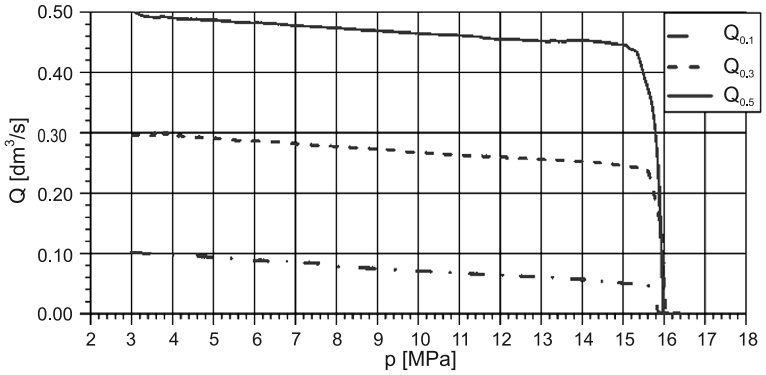

Fig. 1. Static flow rate characteristics of pump model for adjusted delivery 0.1, 0.3, 0.5 dm^3/s without additional control system

Rys. 1. Charakterystyki statyczne modelu pompy przy nastawionych wydajnościach 0.1, 0.3, 0.5 dm^3/s bez układu regulacji wydajności

2. Object of research

Model of hydraulic vane pump was built in 20sim program. Block diagrams created in this program are presented in Figure 2. The system consists of a supply unit 1, an additional supply of the load pressure control system 2, double-acting actuator with a rod on both sides 3, an inertial load of the cylinder 4, pressure control system and the pump 5, a load pressure

control system 6, direction change system of a rod movement 7. Supply block consists of: vane pump with variable displacement 8, hydraulic fluid reservoir 9, drive pump system 10 and check valve 11. The system is additionally equipped with a controller 15 (PID or fuzzy). Rod position signal comes from sensor 17. Position signal is converted to the volumetric flow rate in block 14 and transmitted to the controller 15. Block 16 generates a control signal for the system. To control the hydraulic system, a fuzzy controller (FLC) and a digital PID controller were used. Parameters of both PID and FLC were adjusted by optimizing the ratio which involved minimization of the IAE (Integral of Absolute Error) on the test model [2, 3, 6].

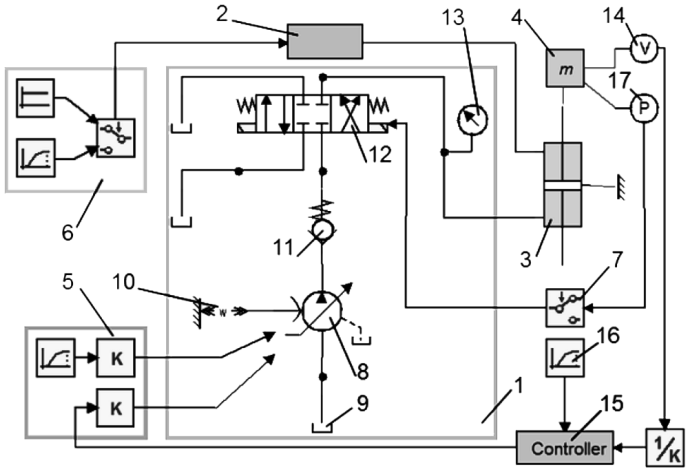

Fig. 2. Model of the system in 20-sim in the form of the block diagram
Rys. 2. Model układu w programie 20-sim w postaci blokowej

3. Development of a fuzzy logic controller

In previous studies, i.e. presented in [2], analysis of the structure of fuzzy controller based on PI controller input error e and error change Δe was carried out. In those studies, influence of the Δe on the control signal was insignificant. Furthermore, due to the large number of rules of 45, controller tuning process was very time consuming. It was observed that at low flow rates the system was characterized by a greater tendency to fall into oscillations than at the medium and high flow rates. Therefore, an alternative model of fuzzy logic with two inputs was made. In the alternative model the error change signal Δe was replaced by a flow rate signal.

At the beginning of building a fuzzification block, two input signals were adopted: a pump delivery error e and a flow rate Q. The delivery error was normalized to the range [–1, 1], while the flow rate was normalized to the range [0, 1]. In the fuzzification block, input signals were transformed into fuzzy sets using a piecewise linear membership function. The error signal was divided into seven sets, while the flow rate signal was divided into to three sets.

Diagrams of fuzzy sets of input signals are shown in Figures 3 and 4, while diagram of the output signal is presented in Figure 5.

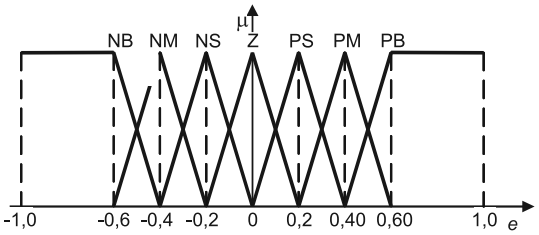

Fig. 3. Fuzzy sets of the error signal *e* of the FLC controller

Rys. 3. Rozmyte przedziały sygnału błędu *e* regulatora FLC

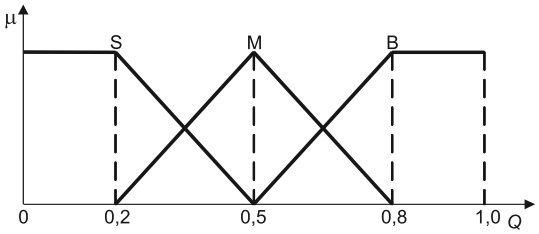

Fig. 4. Fuzzy sets of the flow rate signal *Q* of FLC controller

Rys. 4. Rozmyte przedziały sygnału wydajności *Q* regulatora FLC

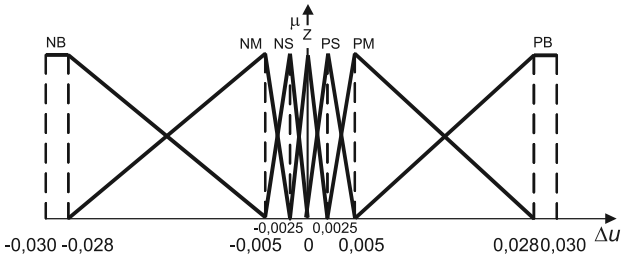

Fig. 5. Fuzzy intervals Δ*u* increase in signal of the FLC controller

Rys. 5. Rozmyte przedziały przyrostu sygnału sterującego Δ*u* regulatora FLC

4. Results of investigations

Prior to carrying out investigations, the plan of experiments was prepared. A complete plan scheme [2] was applied. Next, simulation studies of the control system performance for various values of the required flow rate at different speeds of the pressure increase were carried out. The usage of the measurement system and the controller allowed to obtain the

characteristics in which the output flow rate was maintained throughout the whole range of allowable pressures for the pump. Figures 6 and 7 show constant flow rate characteristics, which were obtained using the PID and FLC, respectively.

Presented simulation results indicate, that the application of any of tested controllers allows to obtain the pump delivery closer to the required value than in the system without the regulator. The volumetric flow rates controlled by both controllers (curves: Q_{PID}, Q_{FLC}) were maintained much closer the required value than in the system with no additional control (curve Q). Furthermore, the system with a fuzzy controller was characterized by better work at higher increase speed of the pressure in the system.

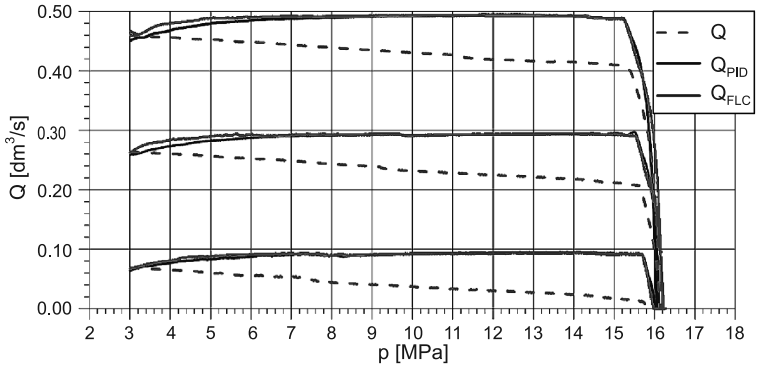

Fig. 6. Static flow rate characteristics of the pump model without the control, with PID and FLC; linear increase of the pressure at 10 MPa/s

Rys. 6. Charakterystyki stałej wydajności modelu pompy bez układu regulacji oraz z regulatorami PID i FLC; ciśnienie narastające liniowo z prędkością 10 MPa/s

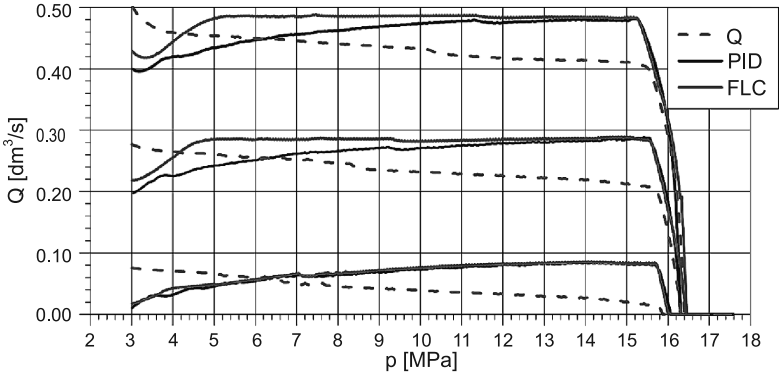

Fig. 7. Static flow rate characteristics of the pump model without the control, with PID and FLC; linear increase of the pressure at 20 MPa/s

Rys. 7. Charakterystyki stałej wydajności modelu pompy bez układu regulacji oraz z regulatorami PID i FLC; ciśnienie narastające liniowo z prędkością 20 MPa/s

5. Conclusions

Based on the obtained characteristics of vane pump, the ability to achieve improved quality control using a fuzzy controller has been demonstrated. Particularly at small and medium loads, the system with the fuzzy controller was characterized by the accurate maintenance of the required pressure value. In the case of the large load, results obtained with the FLC and the PID were similar. Additionally, it was observed during the research, that the FLC controller was characterized by increased ability to suppress the oscillations comparing to the PID.

With the ability to change the structure of the FLC input, further improvement of this controller is possible. In further studies, the behavior of the controller can be included depending on the delivery of the pump or the pressure in the system so as to improve its properties particularly for large loads.

References

[1] Czogała E., Pedrycz W., *Elementy i metody teorii zbiorów rozmytych*, PWN, Warszawa 1985.
[2] Czyżycki W., *Simulations of hydraulic system with fuzzy logic controller based on PI structure*.
[3] Czyżycki W., Lisowski E., *Badania symulacyjne układu hydraulicznego stałej mocy z regulatorem rozmytym*, XX Konferencją Naukową Problemy Rozwoju Maszyn Roboczych, Zakopane 2007.
[4] Filo G., *Pressure control in band-saw hydraulic system using the fuzzy logic*, Przegląd Mechaniczny nr 5/2009.
[5] Lisowski E., Filo G., *Pozycjonowanie ładunku podnośnikami hydraulicznymi z regulatorami w logice rozmytej*, Hydraulika i Pneumatyka, nr 1/2010, ISSN 1505-3954;
[6] Jędrzykiewicz Z., *Teoria sterowania układów jednowymiarowych*, Uczelniane Wydawnictwo Naukowo-Dydaktyczne AGH, Kraków 2002.
[7] Lachwa A., *Rozmyty świat zbiorów, liczb, relacji, faktów, reguł i decyzji*, Akademicka Oficyna Wydawnicza EXIT, Warszawa 2001.
[8] Piegat A., *Modelowanie i sterowanie rozmyte*, Akademicka Oficyna Wydawnicza EXIT, Warszawa 1999.

TECHNICAL TRANSACTIONS | **CZASOPISMO TECHNICZNE**
MECHANICS | MECHANIKA
1-M/2013

TOMASZ DĘBIŃSKI*, MIROSŁAW GŁOWACKI*

INCREASING EFFICIENCY COMPUTING OF SIMULATION ROLLING PROCESS WITH SEMI-SOLID ZONE, TESTS OF PARALLEL COMPUTING

ZWIĘKSZENIE EFEKTYWNOŚCI OBLICZEŃ PROGRAMU SYMULACJI KOMPUTEROWEJ PROCESU WALCOWANIA ZE STREFĄ PÓŁCIEKŁĄ – ZRÓWNOLEGLENIE OBLICZEŃ

Abstract

The paper deals with the speed up of a computer program, which simulates rolling of steel with semi-solid zone. The mathematical models describing the rolling process are fully three dimensional. It leads to very long computation time while the discretization of the problem is made in finite element manner. The main objectives of the contribution are optimization of the program code, as well as making of the first look at possibilities of parallel computation in application to the presented problem. The paper has proved that efficient optimization of the program code can lead to significant shortening of the computation time also with the automatic and manual parallelization. It was concluded that adaptation of the procedures and loops to rigorous requirements of the parallel compiler is strongly recommended.

Keywords: *rolling process*, *parallel computation*, *computer simulation*, *numerical models*

Streszczenie

W artykule przedstawiono metody zwiększenia efektywności programu modelującego proces walcowania stali ze strefą półciekłą. Modele matematyczne opisujące proces walcowania są w pełni trójwymiarowe, co prowadzi do bardzo długich czasów obliczeń. Dyskretyzację problemu wykonano przy użyciu metody elementów skończonych. Głównymi celami artykułu są: optymalizacja kodu programu oraz ocena możliwości zastosowania obliczeń równoległych. Przeprowadzone testy udowodniły, że optymalizacja kodu programu może doprowadzić do znacznego skrócenia czasu obliczeń, również w połączeniu z automatycznymi ręcznym zrównolegleniem. W celu efektywnego zrównoleglenia automatycznego, konieczne jest dostosowanie procedur i pętli do rygorystycznych wymogów kompilatora.

Słowa kluczowe: *walcowanie*, *strefa półciekła*, *symulacja komputerowa*, *efektywność obliczeń*, *obliczenia równoległe*

* DSc. Eng. Tomasz Dębiński, DSc. Eng. Mirosław Głowacki, prof. AGH, Department of Applied Computer Science and Modelling, Faculty of Metals Engineering and Industrial Computer Science, AGH University of Science and Technology, ZI-IF UJK Kielce.

1. Introduction

Optimization of programs was and still is very important. Despite the increasing power of computers in accordance with Moore's Law, the optimization can not be ignored. Today, it is used in most high-level languages to facilitate programming but also reduces control over the execution of processor instructions. The compilation gives different result codes dependingon the compiler and platform. For assembler, it is assumed that the execution of each instruction corresponds to one clock cycle of the processor. C and Fortran languages are higher level. One instruction no longer corresponds to one assembly instruction. Each instruction corresponds to a number of assembler instructions. Each instruction has its counterpart in the five to eight assembler instructions [1].

Software performance depends not only on the compiler but also, on coding, on decomposition of the problem into subtasks, on used structures and libraries and on system architecture. Software performance has several meanings. The most frequently used are memory and time efficiency. Memory efficiency is a way to find an algorithm that allows to solve the problem with minimal memory usage.It cannot be ignored, because in today's systems, there is a caching and paging problem that can significantly affect the speed of the program. Time performance is responsible for numerical solution of a problem in shorter time [2, 3]

The main goals of the current paper is to determine the optimal hardware platform for computer simulation of the rolling process with semi-solid zone and code optimization for best time performance and attempt of parallelization of sequential program.

2. Sequential model of rolling – thermal solution

Heat transfer is one of the main phenomena accompanying the hot rolling process, which results in formation of temperature gradients inside the deformation zone and even outside of it. In the presented model, heat flow is considered in a particular area of the specimen. The discretization process leads to selection a finite number of points inside the body. Certain temperature is attributed to each of the points (nodes). The set of all the temperature values at all given points creates a space and time dependent temperature field $T = f(x, y, z, t)$. Heat transfer models are usualy based on the solution of Fourier-Kirchhoff heat conduction equation [4, 5]. The solution is based on minimization of heat flux functional, which includes relevant boundary conditions.

$$\chi = \int_V \left\{ \frac{1}{2}\left[k_x \left(\frac{\partial T}{\partial x}\right)^2 + k_y \left(\frac{\partial T}{\partial y}\right)^2 + k_z \left(\frac{\partial T}{\partial z}\right)^2 \right] - QT \right\} \cdot dV + \int_S \left(qT + \frac{1}{2}\alpha (T - T_0)^2 \right) dS \quad (1)$$

In (1) λ_i are anisotropic heat transfer coefficients, Q – heat generation, V – control volume, S – body surface, α – heat transfer coefficient and q – heat generated by friction. In [6] one can find solution of this problem in two steps. The first one is based on the Fourier-Kirchhoff equation for steady flow of heat using the finite element method. The second step is a generalization of the resulting stationary matrix equations obtained for the steady-state

process with the help of the Galerkin residual method. In both cases the solution requires solution of anequations system represented in matrix form (2):

$$\mathbf{KT} = \mathbf{p} \tag{2}$$

where:

K – heat capacity matrix,
T – parameters vector,
p – the right hand vector.

3. Mechanical Model

Another model, the most important one for metal forming processes, is the material plastic behaviour model. In the presented approach a three dimensional rigid-plastic model of rolling process has been applied, which in the case of large plastic deformations at very high temperatures can give good results. The power functional resulting from variational formulation of the problem is non-linear in all cases and so the solution requires strong computing power. Application of finite element discretization to analysis of spatial rigid-plastic model involves processing a large number of variational parameters. Hence, the calculation requires long computation time but results in a solution which is consistent with experimental data for both simple and complex deformation zones.

The variational approach of the rolling process requires optimization of a power functional, which in general can be expressed in the form of equation (3):

$$W = W_{\sigma} + W_{\lambda} + W_{t} \tag{3}$$

where:

W_{σ} – the power of plastic deformation,
W_{λ} – the incompressibility condition (penalty power),
W_{t} – the friction power.

The deformation process of steel in semi-solid state depends on material density changes. In this case the condition of incompressibility, which is sufficient for deformation at lower temperatures, has to be replaced with a more general condition of mass conservation [7].

The application of finite element method results in case of metal forming processes in a finite set of velocity values. All of them are parameters of the deformation field. Spatial discretization allows the optimization of deformation field for a certain time step. At the same time discretization of time coordinate is necessary to perform series of time steps under the assumption of constant strain field in each step. The incremental solution of the problem has to be constructed iteratively. Each iteration involves solving linearized system which can be expressed as a matrix equation (4)

$$\mathbf{K}\boldsymbol{v} = \mathbf{f} \tag{4}$$

where:

K – the structure stiffness matrix,
v – the nodal velocity vector,
f – the right hand vector.

The process is divided into time steps. In each step (Δt) the final shape of the body is calculated from its initial shape using the velocity field resulting from optimization of the functional given by (3)

4. Code optimalization

Programs that simulate complex physical processes, using the finite element method, are always very complex numerically. The code which undergoes the penalization consists of approximately 19,000 lines. About 2000 of themlay in the critical section, which is part of the algorithm,where are located the most time-consuming calculations. For complex algorithms, where the computational time is very long, optimization is very important. May consist of the following steps: control flow analysis, data flow analysis (how to use variables in the program), optimizing transformations, improvement of the source code level (profiling, changing the algorithm), improvement of the level of indirect representation (improvement loop, calculating addresses) and finally improvements at the level of the object code (use of registers, the choice of proper instructions).

The first level of optimization involves the use of compiler options for full utilization of hardware and the second is to optimize the program code in aim to take full advantage of the speed of the algorithm. For performance tests a unit equipped with 64 Intel (R) Xeon (R) CPU E7-4830@2.13GHz, and 128GB of memory was used. Computer has the ability to work in both 64-bit and 32-bit emulation, which allows to work under any operating system compatible with the x86 architecture.

For maximum performance, compilation and calculations was made on the Linux Fedora 13 system with KVM virtual machine. Calculations were made using both32-bit and 64-bit representation for verify the increase of performance and compiler quality.

Optimization for the compiler generally allows to choice of processor and the global optimization. Global optimization includes all the development techniques such as unroll of loops, conditional statements, change of the code, queuing instructions, etc. This technique is insufficient, it depends on the code and algorithm.

The study was limited to a standard optimization options for easy comparison of their effectiveness. Three levels were used (options O1, O2, O3) containing different levels of optimization algorithms. Detailed description of a compiler one can find in the help files of the operating system [8]. The program was compiled with different optimization levels for two hardware architectures 32 and 64 bit.

In both cases, g77 compilers were used because the source code waswritten in Fortran77. In order to minimize the error, in each case the calculation was performed three times, because the computing node is located on a server cluster whichcan be loaded by other users. The results are shown in Figure 1.

The presented results show the advantage of 64-bit code. The 32-bit code was executed slower, on average about 20%.

The second stage of the work was to optimize the source code. After analysis (profiling) the 184 procedures have been found in the whole code. A major influence on the program execution time has 4 procedures, which are presented in Table 1.

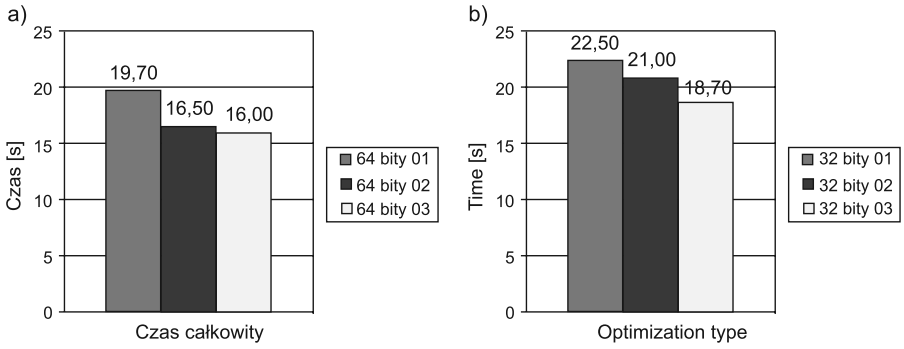

Fig. 1. Juxtaposition of computing times for 64- and 32 bit version of the program

Rys. 1. Zestawienie czasów obliczeń dla 64 bitowej (a) i 32 bitowej (b) wersji programu

Table 1

Execution time and number of calls for selected procedures

% execution time	number of calls	procedure name
37.16	4407696	b_3d
16.88	1098684	poch
13.18	492	mp11ad
5.66	2888	mp11ed
Rest	–	other

The main aim of the task is to improve performance of these procedures, which reduce the execution time for the entire program. The main applied techniques allowing the task are: the elimination of common subexpressions, use algebra rights, copy propagation, removing

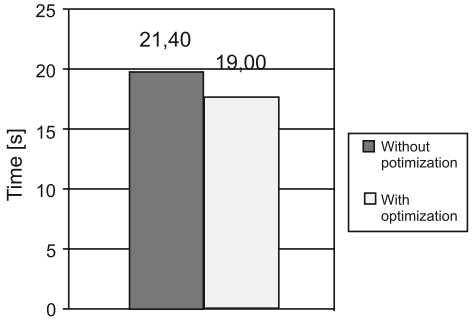

Fig. 2. Computing time before and after optimization

Rys. 2. Czas obliczeniowy przed i po optymalizacji

unused code, code movement and induction variables. After analysis of the execution time and the number of calls four procedures were selected for optimization. The calculation shows improvement of the execution time byabout 5% of the overall computation time as shown in Figure 2

It should be noticed that the calculations were performed with low level of the functional optimization.

5. Parallel computing

The most easy way leading to a parallel version of the program is to use compiler directives. Intel Fortran Compiler v 8.1 uses automatic parallelization mechanism and allows users to change the program code with the direct placement of appropriate directives in the program. The automatic parallelization requires meeting several conditions. The operation causes automatic parallelization of loops and divides code between available processors. If the considered loops contain elements of arrays then the parallel execution of instructions is possible only in case of independency of the result on the order of execution. In order to solve the task in parallel, compiler creates n threads performing the task for its own areas of control variable.

Parallel version of the loop must satisfy the following conditions: (i) the calculations in the loop does not change the same variables in the simple iteration, (ii) loop calculations do not change the variable that is used outside of the loop, (iii) the value of anarray element in the current iteration does not depend on the values of the elements from other iterations. Parallelism is not possible in the following cases: (i) DO loop is nested in another loop that is parallel, (ii) jump instructions are beyond of the scope of DO, (iii) a loop contains a call of user subroutine, (iv) the loop contains instructions for I / O and (v) the in the iteration scalar is calculated .

The program has been subjected toautomatic parallelization. The compiler has identified 22 loops which meet the above criteria. There was no increase in productivity, the difference in computation time for the calculation on a single processor can be omitted. No improvement in performance is caused by the fact that parallelization of loops which meet the criteria is not very significant, and loops are located outside the critical section. In order to meet the requirements of the compiler the need of modification of the code is required. A very important factor is the number of processors. Further studies on a larger number of processors are planned.

6. Conclusions

At this stage of the work, it is necessary to use specialized tools for program analysis (profiling) and the elimination or improvement of the code causing the greatest delays. The use of even the most basic code optimization techniques and appropriate compiler options gives good results and allows the shortening of the execution time of the program. For automatic parallelization of calculations it is necessary to adapt the procedures and loops to

requirementsof the compiler, which is the subject of further work. Because the problem is complex, a detailed analysis of the program performance is planned.

Optimization of programs implementing complex calculations, particularly working on a large amount of data is very important. Shortening the calculation time by a few percent in the context of the overall problem gives significant improvement.Performance analysis is necessary, in order to improve the time characteristics of the task.

The work has been supported by the Polish Ministry of Science and Higher Education Grant N N508 585539.

References

[1] Bulka B., Mayhew D., *Efektywne programowanie w C++*, Wydawnictwo MIKOM, Warszawa, kwiecień 2001.
[2] Gian-Paolo Musumeci D., Loukides M., *Optymalizacja systemów komputerowych*, RM 2002.
[3] Christos H. Papadimitriou, *Złożoność obliczeniowa*, Helion, 2012.
[4] Taler J., Duda P., *Direct and inverse heat transfer problems*, WNT, Warszawa 2003.
[5] Kostkowski E., *Heat flow*, Silesian Technical University, Gliwice 2000.
[6] Głowacki M., *Thermo-mechanical and microstructural model of shape rolling*, Dissertations and Monographs, Kraków 1998.
[7] Głowacki M., *Computer simulation of rolling of semi-solid steel slabs*, Proc. 15th International symposium on Plasticity & its current applications, St. Thomas, U. S. Virgin Islands, January (2009), 10–12.
[8] SUSE Limux Enterprise (http://www.suse.com/us).

TECHNICAL TRANSACTIONS | **CZASOPISMO TECHNICZNE**
MECHANICS | MECHANIKA
1-M/2013

MARIUSZ DOMAGAŁA*

SIMULATION OF CAVITATION IN JET PUMPS

SYMULACJE ZJAWISKA KAWITACJI W POMPACH STRUMIENICOWYCH

A b s t r a c t

This paper presents simulation of cavitation phenomena at jet pumps with use of CFD methods. There was also presented theoretical consideration of cavitation formation and models applied at the CFD codes. On example of liquid-jet liquid pump, which working medium is water was presented simulation of cavitation process which was conducted in Ansys CFX code. This paper also includes some selected results of simulation for fluid flow at the jet pump with consideration of cavitation process.

Keywords: *Cavitation*, *CFD*, *jet pumps*

S t r e s z c z e n i e

W artykule przedstawiono podstawy matematycznego modelowania zjawiska kawitacji, w szczególności przedstawiono modele kawitacji wykorzystywane w systemach CFD. Na przykładzie pompy strumieniowej przedstawiono symulację pracy pompy strumienicowej typu ciecz–ciecz z uwzględnieniem zjawiska kawitacji. Symulacje numeryczne przeprowadzono w systemie Ansys CFX.

Słowa kluczowe: *kawitacja*, *symulacja CFD*, *pompa strumienicowa*

* PhD. Mariusz Domagała, Institute of Applied Informatics, Mechanical Department, Cracow University of Technology.

Notations

R_b – bubble radius
p_v – vapor pressure
p – pressure of liquid surrounding the bubble
ρ – liquid density
ρ_g – vapor density
σ – surface tension
U – liquid velocity
α – vapor volume fraction
n – bubble number density
R – phase change rate
fv – vapor mass fraction
f_g – noncondesable gases
Γ – diffusion coefficient

1. Intruduction

Jet pumps particularly liquid-liquid type operation is mostly limited by cavitation process. The principle of jet pump operation is conversion of velocity energy into a pressure energy and vice versa. This may lead to that pressure drops below the level below saturation pressure of working liquid and in the consequences vapor bubbles. Such phenomena is recognized as cavitation and it is one of the parameters that limits usage of jet pumps. Cavitation is common met problems not only in jet pumps but also in a lot of engineering application. Their nature does not only disturb a flow by sudden phase changes but also is a cause of sudden wear and noise. That reasons caused the this phenomena has been a subject of studies from many years and still is. Cavitation is a complex problem on which a lot of factors may have influence. The studies presented in books of Frenkel and Skripov [1] deal with a fundamental physics of nucleation, however they were conducted on pure liquids, which engineering liquids are not. And what later studies shown the contamination as well as a aeration of working liquids have influence on cavitation process significantly. The nature of cavitation at liquid flow is a complex phenomenon and makes difficulties in modeling and simulation. There are, however, some formulas than allows to evaluate flow conditions at which cavitation may appear in jet pumps but this is only a rough estimation. Therefore, in this paper an attempt of simulation of liquid flow at Liquid Jet Liquid pump with the use of CFD method was undertaken.

2. Mathematical models of cavitation

An attempts of preparing mathematical description of cavitation has been conducted from many years. The studies presented in book [1] shows a mathematical description of cavitation and bubble dynamics. This work presents selected models of cavitation which are applied in CFD codes. Generally, tendency a flow to cavity may be defined as the cavitation number:

$$c_a = \frac{p - p_v}{0.5\rho U^2} \tag{1}$$

One of the common approach to describe bubble dynamics is The Rayleigh Plesset equation [3]:

$$R_b \frac{d^2 R_b}{dt^2} + \frac{3}{2}\left(\frac{dR_b}{dt}\right)^2 + \frac{2\sigma}{\rho R_b} = \frac{p_v - p}{\rho} \tag{2}$$

After deriving this equation, and neglecting second order terms and surface tension the equation is reduced to the following:

$$\frac{dR_b}{dt} = \sqrt{\frac{2}{3}\left(\frac{p_v - p}{\rho}\right)} \tag{3}$$

The rate of bubble volume changes is as follow:

$$\frac{dV_b}{dt} = 4\pi R_b^2 \sqrt{\frac{2}{3}\left(\frac{p_v - p}{\rho}\right)} \tag{4}$$

The rate of change bubble mass is:

$$\frac{dm_g}{dt} = 4\pi R_b^2 \rho_g \sqrt{\frac{2}{3}\left(\frac{p_v - p}{\rho}\right)} \tag{5}$$

The N_b bubbles per unit volume the volume fraction r_g is expressed by:

$$r_g = \frac{4}{3}\pi R_b^2 N_b \tag{6}$$

The total interphase mass transfer per unit volume is:

$$\dot{m}_{fg} = 3\frac{r_g \rho_g}{R_b}\sqrt{\frac{2}{3}\frac{p_v - p}{p_f}} \tag{7}$$

When including condensation this expression is as follows:

$$\dot{m}_{fg} = 3F\frac{r_g \rho_g}{R_b}\sqrt{\frac{2}{3}\frac{|p_v - p|}{p_f}\operatorname{sgn}(p_v - p)} \tag{8}$$

Vapor transport equation has the following form:

$$\frac{\partial}{\partial t}(\alpha\rho_v) + \nabla\cdot(\alpha\rho_v\vec{V}_v) = R_e - R_c \tag{9}$$

The other cavitation model, which base on full cavitation model was developed by Singhal et al. [3]. Two phase continuity equations may be presented as below. Liquid phase is described as:

$$\frac{\partial}{\partial t}[(1-\alpha)\rho] + \nabla\cdot[(1-\alpha)\rho\vec{V}] = -R \tag{10}$$

while vapor phase:

$$\frac{\partial}{\partial t}(\alpha\rho_v) + \nabla \cdot (\alpha\rho_v \vec{V}) = R \tag{11}$$

and finally mixture:

$$\frac{\partial}{\partial t}(\rho_m) + \nabla \cdot (\rho_m \vec{V}) = 0 \tag{12}$$

where:

subscript m – is a mixture phase,
v – vapor phase.

Mixture density is defined as:

$$\rho_m = \alpha\rho_v + (1-\alpha)\rho \tag{13}$$

Combining above equation gives relation between mixture density and vapor volume fraction α

$$\frac{D\rho_m}{Dt} = \frac{D\alpha}{Dt}(\rho_v - \rho) \tag{14}$$

Vapor volume fraction can be related to the bubble number density (n) and the bubble radius R_b

$$\alpha = n\left(\frac{4}{3}\pi R_b^3\right) \tag{15}$$

Using above equations leads to the evaporation rate R

$$R = 2\alpha(4\pi n)^{\frac{1}{3}} \frac{\rho_v \rho}{\rho_m} \sqrt{\frac{2}{3}\left(\frac{p_B - p}{\rho}\right)} \tag{16}$$

All terms are known except „n" wich is constant or dependent variable. The phase change expression migth be rewritten as a function of bubble radius R_b

$$R = \frac{3\alpha\rho_v \rho}{R_B \rho_m} \sqrt{\frac{2}{3}\left(\frac{p_B - p}{\rho}\right)} \tag{17}$$

Vapor mass fraction is the dependent variable in vapor transport equation:

$$\frac{\partial}{\partial t}(f_v \rho) + \nabla \cdot (f_v \rho \vec{V}_v) = \nabla \cdot (\Gamma \nabla \vec{V}_v) + R_e - R_c \tag{18}$$

Rates of mass exchange are given by:

for $p \le p_v$

$$R_e = F_{vap} \frac{\max(1.0, \sqrt{k})(1 - f_v - f_g)}{\sigma} \rho\rho_v \sqrt{\frac{2}{3}\left(\frac{p_v - p}{\rho_{ell}}\right)} \tag{19}$$

for $p > p_v$

$$R_e = F_{\text{cond}} \frac{\max(1.0, \sqrt{k}) f_v}{\sigma} \rho\rho_v \sqrt{\frac{2}{3}\left(\frac{p_v - p}{\rho}\right)} \tag{20}$$

The saturation pressure is as follows:

$$p_v = p_{\text{sat}} + 0.5(0.39k) \tag{21}$$

where F_{vap}, F_{cond} are constatns.

Another approach, which was the assumption that bubbles have the same size was proposed by Zwarat-Gerber-Belamri [2]. They assumed that interphase mass transfer per unit volume (R) is calculated used bubble density number (n) and the mass change rate of a single bubble

$$R = n\left(4\pi R_B^2 \rho_v \frac{DR_B}{Dt}\right) \tag{22}$$

After including Eq 15. we obtain:

$$R = \frac{3\alpha\rho_v}{R_B}\sqrt{\frac{2}{3}\left(\frac{p_B - p}{\rho}\right)} \tag{23}$$

$$R_e = F\frac{3\alpha\rho_v}{R_B}\sqrt{\frac{2}{3}\frac{|p_B - p|}{\rho}\text{sign}(p_B - p)} \tag{24}$$

where F is empirical coefficient.

In this model is proposed of replacing α_v with $\alpha_{\text{nuc}}(1-\alpha)$. And the final model of cavitation is as follows:

for $p \le p_v$

$$R_e = F_{vap}\frac{3\alpha_{\text{nuc}}\rho_v(1-\alpha_v)}{R_B}\sqrt{\frac{2}{3}\left(\frac{p_v - p}{\rho}\right)} \tag{25}$$

for $p > p_v$

$$R_{ec} = F_{\text{cond}}\frac{3\alpha_v\rho_v}{R_B}\sqrt{\frac{2}{3}\left(\frac{p - p_v}{\rho}\right)} \tag{26}$$

where:

α_{nuc} – is nucleation site volume fraction,
F_{vap} – evaporation coefficient,
F_{cond} – is condensation coefficient.

Another mathematical model of cavitation has been presented by Schnerr and Sauer [2]. The vapor fraction equation has the following general form:

$$\frac{\partial}{\partial t}(\alpha\rho_v) + \nabla\cdot(\alpha\rho_v\vec{V}) = \frac{\rho_v\rho}{\rho_m} \tag{27}$$

The mass source term is:

$$R = \frac{\rho_v \rho}{\rho_m} \frac{d\alpha}{dt} \tag{28}$$

Unlike mentioned previously models, the relation between vapor fraction and number of bubbles has the following form:

$$\alpha = \frac{4}{3}\pi \frac{n_b R_B^3}{1 + \frac{4}{3}\pi n_b R_B^3} \tag{29}$$

And finally the mass transfer rate is:

$$R = \frac{\rho_v \rho}{\rho_m} \alpha(1-\alpha) \frac{3}{R_B} \sqrt{\frac{2}{3}\left(\frac{p_v - p}{\rho}\right)} \tag{30}$$

while bubble radius is:

$$R_B = \left(\frac{3\alpha}{4\pi n(1-\alpha)}\right)^{\frac{1}{3}} \tag{31}$$

The final form of this model is:

When $p_v \geq p$

$$R_e = \frac{\rho_v \rho}{\rho_m} \alpha(1-\alpha) \frac{3}{R_B} \sqrt{\frac{2}{3}\left(\frac{p_v - p}{\rho}\right)} \tag{32}$$

When $p_v < p$

$$R_c = \frac{\rho_v \rho}{\rho_m} \alpha(1-\alpha) \frac{3}{R_B} \sqrt{\frac{2}{3}\left(\frac{p - p_v}{\rho}\right)} \tag{33}$$

3. CFD simulation of flow LJL pump

The object of simulation was two stage liquid jet liquid pump, which working medium is water. This pump diameter of throat is approx. 200 mm and is equipped with two annular motive nozzle. Due to the symmetry only a half of geometrical model was used. The grid which is presented in Fig. 1, it consists of tetrahedral prism layers cells and was prepared in Ansys Workbench Mesh module. Despite the pump is two stage pump for the simulation of cavitation formation only one stage was used. CFD simulation was conducted in Ansys CFX code in two stages, the first, without considering cavitation to check if there is possibility for cavitation formation at pump working conditions. The second stage was full cavitation simulation using Rayleigh Plesset model, which was presented in chapter 2. Some selected results of simulation for both stages are presented in below figures. There are presented pressure distributions, path lines as well as a distribution of volume fractions in case of cavitation simulations.

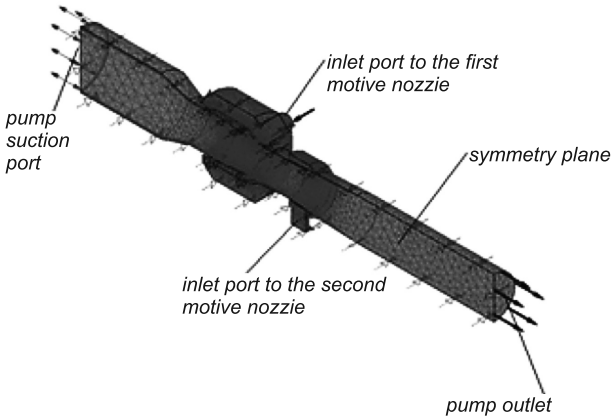

Fig. 1. CFD model of LJL pump

Rys. 1. Model CFD pompy strumienicowej

Fig. 2. Path lines of motive liquid

Rys. 2. Linie prądu wygenerowane dla strumienia napędowego

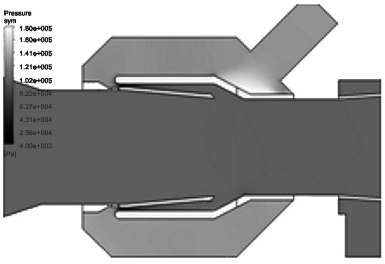

Fig. 3. Pressure distribution

Rys. 3. Rozkład ciśnienia statycznego [Pa]

Presented results for initial simulation in Figure 2 and 3 allowed to investigate the potential area where cavitation may appear. Water flowing to the motive nozzle gather velocity in the nozzle what leads to pressure drop. What was found is the biggest pressure drop was not in

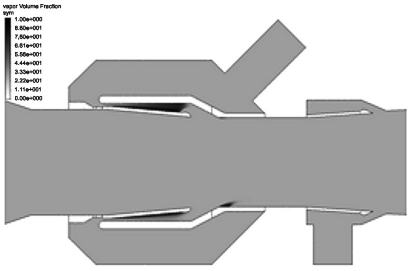

Fig. 4. Distribution of vapor fraction

Rys. 4. Rozkład fazy gazowej podczas przepływu wody

the pump throat but in the entrance to the motive nozzle. Therefore the simulation which includes cavitation models were conducted. As may be found in Figures 4 and 5 process of bubble formation begins in the area where pressure drop was observed *t* initial simulation. Figure 4 presents a distribution of vapor phase during pump operation in the symmetry plane, while Figure 5 presents the surface with vapor fraction only.

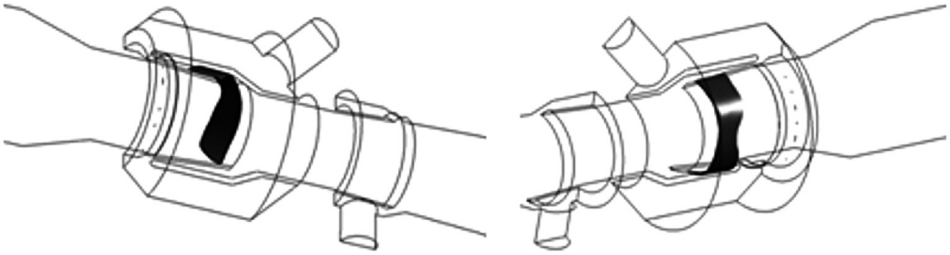

Fig. 5. Surface of vapor fraction

Rys. 5. Kształt powierzchni fazy gazowej

4. Conclusions

This paper presents a mathematical models of cavitation models which are used in CFD codes. One of such model was used in simulation of flow with cavitation at liquid jet liquid pump. There was presented selected simulation results which shown the way the cavitation may appear during water flow in the pump.

References

[1] Brennen C.E., *Cavitation and buble dynamics*, Oxford University Press, 1995.
[2] Ansys Fluent theory Guide.
[3] Ansys CFX theory Guide.
[4] Momeni H., *CFD modeling of two stage LJL pump*, praca doktorska, Krakow 2011.

TECHNICAL TRANSACTIONS | CZASOPISMO TECHNICZNE
MECHANICS | MECHANIKA
1-M/2013

IRENEUSZ DOMINIK*, RENATA DWORNICKA**

INDUSTRIAL COMPUTER PROGRAMMING ON THE BASIS OF LABORATORY STANDS

PROGRAMOWANIE KOMPUTERÓW PRZEMYSŁOWYCH W OPARCIU O STANOWISKA EDUKACYJNE

Abstract

One of the main weaknesses in the Laboratory of Distributed Control Systems at the AGH University of Science and Technology in Krakow was students' knowledge about connecting peripheral devices to industrial computers known also as PLCs. After participating in PLC laboratory course students were able to create advanced programs, control complicated mechatronic systems but they could not assemble even simple electrical circuits. It results from the fact that they worked on ready-made laboratory stands where all the electrical connections had already been set.
The paper presents the building of eight laboratory stands for learning how to connect PLC inputs and outputs as the first step before proper programming.

Keywords:PLC programming, test stands

Streszczenie

Jednym z największych braków w Laboratorium Rozproszonych Systemów Sterowania w Katedrze Automatyzacji Procesów w Akademii Górniczo-Hutniczej w Krakowie był do tej pory brak wiedzy zdobywanej przez studentów na temat podłączania elementów zewnętrznych do sterownika przemysłowego PLC. Studenci po zakończeniu zajęć laboratoryjnych potrafili tworzyć zaawansowane oprogramowanie, sterować skomplikowanymi układami mechatronicznymi, natomiast nie potrafili wykonać żadnych, nawet bardzo prostych podłączeń elektrycznych. Wynikało to z faktu, że pracowali na stanowiskach, gdzie wszystkie podłączenia elektryczne zostały wcześniej wykonane. W artykule opisano wykonanie ośmiu stanowisk dydaktycznych do nauki prawidłowego łączenia wejść i wyjść sterownika przemysłowego jako pierwszy krok przed nauką właściwego programowania. Postanowiono, że będą one służyć w przyszłości studentom do nauki zasad prawidłowego łączenia ze sobą poszczególnych elementów w nieskomplikowane układy automatyki będące bazą do ich późniejszego rozwoju.

Słowa kluczowe: programowanie sterowników przemysłowych PLC, stanowiska laboratoryjne

* PhD. Ireneusz Dominik, AGH University of Science and Technology, Faculty of Mechanical Engineering and Robotics, Department of Process Control.
** PhD. Renata Dwornicka, Institute of Applied Informatics, Faculty of Mechanics, Cracow University of Technology.

1. Introduction

The classes conducted in the Laboratory of Distributed Control Systems (LDCS) at the University of Science and Technology in Krakow are considered by our students as one of the most interesting and useful ones in their future engineer career in industry. It is a result of many years of laboratory development and gathering over thirty industrial computers operating together with different test stands. In this laboratory four subjects are taught from the first contact with PLCs to learning advanced programming. The laboratory holds a good reputation so a lot of students who are not planned to work there ask the teachers to be allowed to participate in classes outside the scope of the syllabus.

So far one of the main weaknesses was students' knowledge about connecting peripheral devices to industrial computers. After participating in PLC courses students were able to create very advanced programs, control complicated mechatronic systems e.g. control the position of photovoltaic cells, but they could not assemble even a simple electrical circuit. It results from the fact that they worked on ready-made laboratory stands, where all the electrical connections had already been set.

The topic of connecting peripheral devices was, of course, discussed during classes but as it is widely known theoretical knowledge in comparison with practical one is poorly comprehended. That is why it was decided that the described gap should be eliminated as it is described in the article.

The article presents the building of eight laboratory stands for learning how to connect PLC inputs and outputs as the first step before proper programming. It allows students not only to learn about PLC connections but also learn in practice the principles of operating different automatics devices e.g. proximity switches.

2. The conception of the laboratory stands

The preliminary analysis inclined us to integrate all peripheral devices together with an industrial computer in one closed housing. The proposed solution was chosen with respect to the students' safety because all of the 230 V power supply voltage wiring was hidden under the cover. In this way students have a possibility to touch only the safe 24 V voltage. Additionally, the housings are easy to manage during classes, as they may be connected to any PC computer or even can be used in another laboratory. As it was mentioned the main idea of the laboratory stands was educating students so the cover of the housing was prepared as a kind of interface between a user and the laboratory stand. That is why the cover was made of transparent Plexiglas with printed electrical symbols and descriptions. Panel mounting banana sockets and wires with banana plugs allow to make the connections.

Figure 1 presents the housing before electrical elements assembly. The chosen material for housing was black Plexiglas UV-proof and it was resistant to damage which may occur when used by students. Both the cover and the housing were made of 5 mm material which created a rigid construction. The housing dimensions were set bearing in mind the optimal placement of electrical connections, i.e. 24V power supply sockets next to the 24V switch. As a result, the housing of 330mm in length, 180mm in width and 60mm in height was created. The holes and cut-outs for electrical devices were also prepared in the cover.

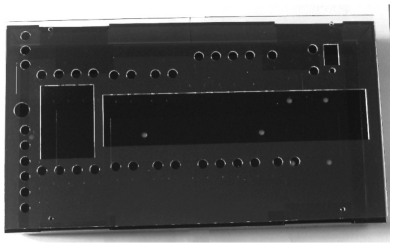

Fig. 1. The housing before electrical elements assembly
Rys. 1. Skrzynka przed montażem elementów elektrycznych

3. Devices assembly

The next step after preparing the housing fixing devices in it in a proper way. The following devices: a circuit breaker, a power supplier, a simple industrial computer (programmable relay NEED family), push buttons and a contactor were fixed to the internal

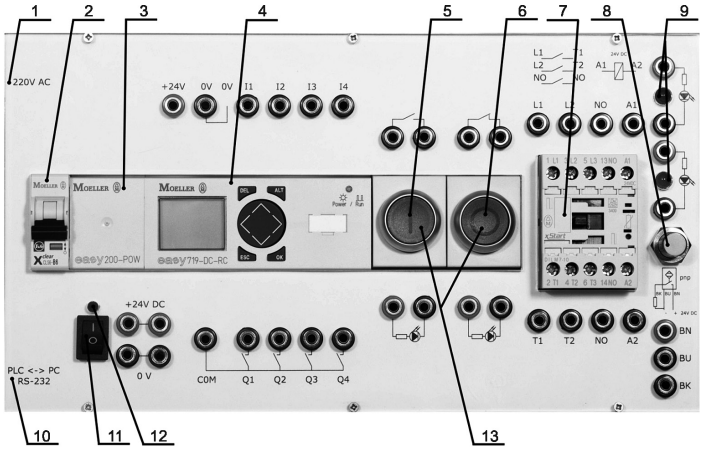

Fig. 2. The front panel of the laboratory stand: 1 – 230V AC socket , 2 – circuit breaker CLS6–B6, 3 – power supplier 24 V DC, 0.2 A, 1 phase, 4 – industrial computer (programmable relay) EASY 719-DC-RC, 5 – green push button (NO contact), 6 – red push button (NC contact), 7 – 3-phase contactor DILM 7–10, 8 – proximity sensor PR12 – 2DP, 9 – diodes LED, 10 – RS232 communication port for programming EASY device, 11 – 24 V switch, 12 –24 V power supply indicator, 13 – diodes LED built in push buttons

Rys. 2. Panel przedni stanowiska: 1 – 230 V AC gniazdo, 2 – wyłącznik nadprądowy CLS6–B6, 3 – zasilacz 24 V DC, 0.2 A, 4 – przekaźnik sterowalny EASY 719-DC-RC, 5 – przycisk zielony (NO styk), 6 – przycisk czerwony (NC styk), 7 – 3-fazowy stycznik DILM 7–10, 8 – czujnik zbliżeniowy PR12 – 2DP, 9 – diody LED, 10 – RS232 port komunikacyjny, 11 – 24 V wyłącznik, 12 – 24 V dioda zasilania, 13 – diody LED wbudowane w przyciski

DIN mounting rail. It is a metal rail of a standard type widely used for mounting industrial automatic equipment.

Other elements were fixed to the prepared cut-outs in the cover: a proximity switch with using a screw cap, 24V switch with a special construction of the switch itself (interference with the cover), a panel mounting banana socket with screw joints, and finally light-emitting LED diodes in the cover holes. The front panel of the laboratory stand is presented in Figure 2.

The front panel is arranged in a way that all connections and all descriptions are easy to comprehend and to use properly. The whole idea of the stand is to teach how to connect different devices with an industrial computer and with each other as well.

To fulfil the task the panel mounting banana sockets were connected inside the housing with all electrical connections of the available devices e.g. the industrial computer inputs (I1–I4) or green NO contact push buttons. The sockets visible for users can be connected with each other by using wires with banana plugs (Fig. 3).

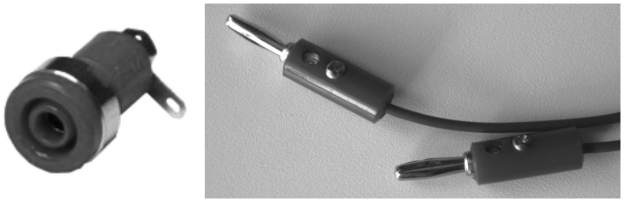

Fig. 3. The panel mounting a banana socket (left) and the wire with banana plugs (right)

Rys. 3. Gniazdo bananowe (z lewej) przewód z końcówkami bananowymi (po prawej)

4. Description of the used devices

The main part of the stand is the industrial computer. It is a digital computer which unlike general-purpose computers is designed for cooperating with the environment (industrial process) by multiple inputs and output. Also known as a Programmable Logic Controller, it is very widely used in all kinds of modern industry, wherever there is a need to control a machine or a set of machines – which is especially true with assembly lines and mass production which could not exist without PLCs [3].

In the case of the laboratory stand the industrial computer EASY 719-DC-RC made by Moeller company was used. It is a very simple type of computer and sometimes in catalogues it is classified as a programmable relay. However, nowadays differences between a programmable relay, a programmable logic controller and a more sophisticated industrial computer are vanishing and generally they are regarded as one family, very similar in operation but with different capacity.

The used EASY device presented in figure 4 consists of LCD display and keyboard so a user can program it without using a PC computer. 8 inputs (6 digital inputs and 2 analog-digital inputs) and 4 relay outputs (4 × 1 NO) are available in very small package [4].

Finally, figure 5 shows a graphical presentation of a sample task given to students where they were required to create electrical connections of a latch circuit with STOP priority – a basic connection of push buttons used widely in industry [1, 2].

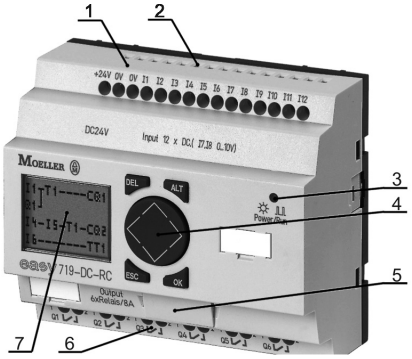

Fig. 4. The industrial computer EASY 719-DC-RC: 1 – power supply connections, 2 – inputs, 3 – power/run indicator, 4 – keyboard, 5 – communication port, 6 – outputs,7 – LCD display

Rys. 4. Komputer przemysłowy (przekaźnik programowalny) EASY 719-DC-RC: 1 – podłączenie zasilania, 2 – wejścia, 3 – diody zasilania i trybu pracy, 4 – klawiatura, 5 – port komunikacyjny, 6 – wyjścia,7 – LCD wyświetlacz

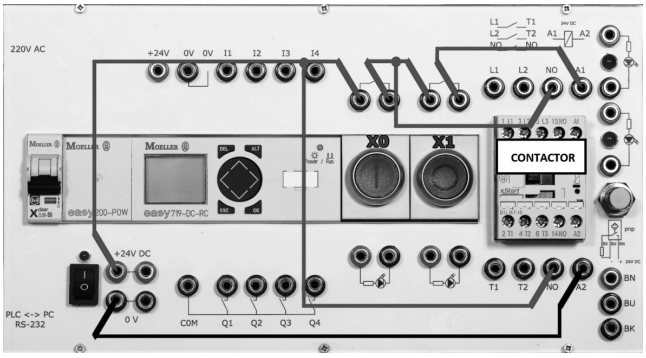

Fig. 5. The electrical connections of a latch circuit with STOP priority

Rys. 5. Elektryczne podłączenie styku z podtrzymaniem z priorytetem STOP

The tasks ranging from very simple (connect one device to the PLC) to the tasks requiring usage of twenty wires are included in the prepared instructions.

5. Conclusions

In the article the building of the laboratory stands for learning how to connect PLC inputs and outputs was presented. During the construction process two preliminary housings were designed but only the third (presented) one met the authors expectations. The maintenance of the stands was high on the priority list. That is why the cover was fixed to the housing in such a way that it is very easy to access the internal connections – it is possible to fix the broken

connection even during classes and it requires only a few minutes. The industrial safety was also very important, that is why a dangerous 230 V are beyond a user's reach.

The instructions for students were also prepared where the additional technical data about test devices together with a series of individual tasks were attached.

As the result of building described in the article test stands a student after two laboratory classes is fully prepared to connect electrical devices in their future engineering career.

References

[1] Dominik I., *PLC's programming with examples*, DELTA J.,A. JAGŁA, cop. 2011, s. 127, ISBN 978-83-62139-34-7, Kraków 2011.

[2] Flaga S., *Programowanie sterowników PLC w języku drabinkowym*, Wydaw. ResNet S.C., ISBN 83-921949-0-X, Skawina 2005.

[3] Kwaśniewski J., *Sterowniki PLC w praktyce inżynierskiej*, Legionowo, Wydawnictwo BTC, s. 344, cop. 2008.

[4] Moeller company, *Easy i MFD – Titan w praktyce. Przykłady aplikacji dla przekaźnika programowalnego easy*, Manual 2010.

TECHNICAL TRANSACTIONS | **CZASOPISMO TECHNICZNE**
MECHANICS | MECHANIKA
1-M/2013

IRENEUSZ DOMINIK*, FILIP KASZUBA*, RENATA DWORNICKA**

PROSTHESIS DESIGN DRIVEN BY ELECTROACTIVE POLYMERS

ZASTOSOWANIE POLIMERÓW ELEKTROAKTYWNYCH DO BUDOWY PROTEZ

Abstract

Applications of dielectric elastomer (DE) actuators are presented in this paper. Dielectric elastomers (a type of electroactive polymer) are one the most promising smart materials. They consist of two flexible electrodes and a dielectric film between them. After applying voltage (3–5 kV) to the electrodes, the thickness of the polymer layer lowers. Changes of the thickness can be indirectly measured , enabling the element to work as a sensor. A self-sensing and energy harvesting elements are also described. Two applications are described – an active orthosis and a force feedback device.

Keywords: *dielectric elastomers*, *electroactive polymers*, *smart materials*

Streszczenie

W artykule przedstawione są zastosowania siłowników opartych na elastomerach dielektrycznych. Materiały te są jednym z najbardziej obiecujących przedstawicieli materiałów inteligentnych, a dokładniej – polimerów elektroaktywnych. Składają się z dwu podatnych elektrod i warstwy polimerowego dielektryka pomiędzy nimi. Po przyłożeniu napięcia aktywacji (ok. 3–5 kV) zmniejsza się grubość tej warstwy. Ta zmiana grubości może być mierzona w sposób pośredni, co pozwala na pracę element jako czujnika. Opisano tryb jednoczesnej pracy siłownikowo-czujnikowej i magazynowania energii. Dwa zastosowania zostały szczegółowo opisane: aktywny wyciąg ortopedyczny palca i urządzenie do siłowego sprzężenia zwrotnego.

Słowa kluczowe: *polimery elektroaktywne*, *materiały inteligentne*, *elastomery dielektryczne*

* PhD. Ireneusz Dominik, MSc. Filip Kaszuba, AGH University of Science and Technology, Faculty of Mechanical Engineering and Robotics, Department of Process Control.
** PhD. Renata Dwornicka, Institute of Applied Informatics, Faculty of Mechanical Engineering, Cracow University of Technology.

1. Introduction

Dielectric elastomers (also called artificial muscles) are materials with a large number of potential applications, ranging from entertainment to medicine and space exploration. Intensive research is conducted worldwide to develop these materials and electroactive polymers in general. This is due to large strain (up to 380%) and very high energy density (3,4 J/g), which is unmatched by any other smart materials such as ferroelectrics and piezoelectrics [[1]].

2. Smart polymers

Applications presented in this paper are designed to utilize actuators based on dielectric elastomers, which are a type of electroactive polymers. Polymers are a large group of chemical compounds, many of which are used in everyday life [2]. So called smart polymers (or generally smart materials) have one or more properties (e.g. conductivity, dimensions, elasticity, shape, structure etc.), that can be controlled by an external stimuli such as temperature, acidity, electric or magnetic field, humidity. A smart material responds to these stimuli predictably and in a short time. The response time should be as small as possible.

Smart materials that change their dimensions in response to electrical signal (electroactive polymers, abbreviated EAP) [3] are the most interesting as far as technical applications are concerned. They can be divided into following groups, as proposed by ESNAM – European Scientific Network for Artificial Muscles [4].

- Electro active polymers
  - Ionic polymers
    - Ionic Polymer-Metal Composites
    - Ionic Polymer Gels
    - Conducting polymers
    - Carbon nanotubes
  - Dielectric polymers
    - Dielectric Elastomers
    - Electrostrictive paper
    - Liquid crystalline Polymers

EAP are commonly called artificial muscles, because of their biocompatibility and their force and energy densities similar to skeletal muscles [3, 5]. Presence of an electric field is required for electronic polymers to work, they require high actuating voltage (order of kV), with low current (μA) and do not generate voltage when actuated mechanically. Ionic electroactive polymers depend on an ion flow inside an ion-conducting polymer, require actuating voltage of max. 5 V, current approximately 100 mA. They also exhibit opposite effect – generate voltage while actuated mechanically, thus converting mechanical energy to electrical energy.

2.1. Working principle of dielectric elastomers

This is a group of smart polymers that deform under applied electric field [6]. This material consists of a thin layer of dielectric (electrical insulator) polymer and two flexible electrodes. This electrode has to be highly conductive and follow the deformation of an artificial muscle.

After inputting high voltage to the electrodes, the electric force brings the two layers closer, compressing the dielectric film (Fig. 1). Actuation pressure is described by equation 1:

$$p = \varepsilon_0 \varepsilon_r \left(\frac{U}{d} \right)^2 \tag{1}$$

where:

p – actuating pressure
ε_0 – permittivity of a vacuum
ε_r – permittivity of the elastomer
U – actuating voltage
d – thickness of the elastomer

As seen in the equation 1, actuating voltage should be as high as possible; practically it means that the actuation voltage is close to the breakdown voltage of the dielectric layer, which usually is 3–5 kV. This value is one of the biggest disadvantages of these materials. Thanks to advanced manufacturing technology, the thickness of the dielectric layer can be lowered to the order of single μm, therefore lowering the voltage to a few hundred volts [7]. Electrically, a dielectric elastomer can be described as a flexible capacitor, where flexible electrodes are its plates. A simple actuator can be constructed with widely accessible components. Insulating layers of various elastic moduli, thickness or density are commercially available and can be selected for specific purposes. Various types of stretchable electrodes are proposed, e.g. carbon black, grease, rubber, dust or glue [6].

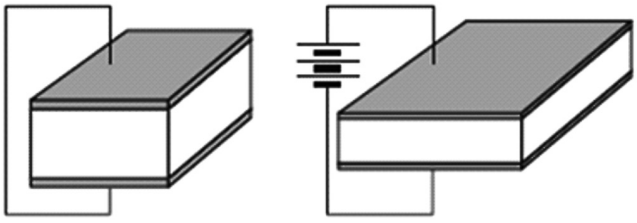

Fig. 1. Mechanical deformation of a dielectric elastomer under DC actuation voltage

Rys. 1. Mechaniczne odkształcenie elastomeru dielektrycznego pod wpływem przyłożonego napięcia

A dielectric elastomer can work in three modes – as an actuator, a sensor and an energy storage device. Sensing is possible through measurement of the capacitance of the flexible capacitor, which is inversely proportional to the distance between the plates. Applying an external force to the element moves the plates closer together. Jung et al. [8] conducted an experiment in which they designed such a system. The flexible capacitor was a part of an analog high-pass filter, and its cut-off frequency was measured. The polymer was powered by an actuating 3 kV DC signal and a 300 V peak-to-peak AC measurement signal. The measurement signal had a constant frequency of 100 Hz (lower frequencies could be cut-off by a filter). This allows the material to work as an actuator and a sensor simultaneously. Such a self-sensing element enables the integration of an actuator and a feedback loop in one element. Danfoss designed an energy storage device based on DE. Charging a stretched

polymer and relaxing it afterwards leaves some charge inside it. This energy can be stored by the element and harvested later (fig. 2). This opens various application possibilities, such as scavenging energy from the environment – this energy can be later used to power the own actuation of the element, charge batteries or power electronic devices.

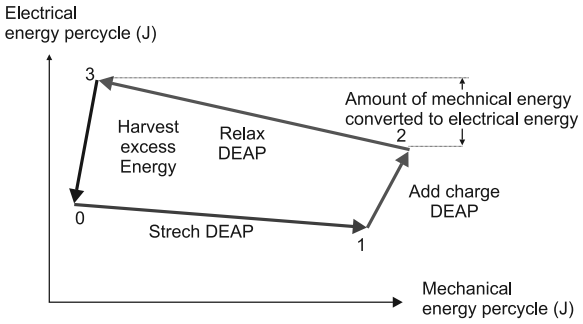

Fig. 2. Energy harvesting cycle of a dielectric elastomer [9], DEAP – dielectric electroactive polymer
Rys. 2. Cykl odzyskiwania energii elastomeru dielektrycznego [9], DEAP – elektroaktywny polimer dielektryczny

2.2. Types of actuators

An electroded dielectric film can be manufactured in large variety of shapes: stretched over a rigid frame, rolled into a scroll, formed into a tubular shape, or laminated on a flexible substrate to form unimorphs and bimorphs [10]. Each of these shapes offer different actuating possibilities, i.e. large displacement with smaller force or large force with smaller displacement. Solutions already invented to work with piezoelectric actuators can be used with DE as well.

In this paper, applications of stack actuators are presented. Stack actuators (a solution used in piezoelectric actuators) consist of several layers of dielectric elastomer, alternated by layers of conducting electrodes. It offers large linear displacements and forces, but is difficult to manufacture. Applied electrostatic field is perpendicular to the electrodes and dielectric film. Electrically it is a number of capacitors connected in parallel with opposite polarization of each layer. A more complex actuator, designed by Carpi et al. [11] consists of a two helical compliant electrodes with an elastomeric insulator interposed between. It offers better performance, but is even more difficult to fabricate. To overcome these difficulties, a folded actuator has been designed.

Dielectric polymers were used in primary research by the authors of the project. The aim of the investigation was to build a simple set to experiment on one-layer EAP actuator. An acrylic elastomer tape (VHB 4910) and graphite dust were used to build the actuator. The tape, manufactured by 3M is a very strong joining material (commonly used in construction). Such tapes exhibit the best strain, stress and energy density characteristics. Because of high elasticity it can be easily stretched in any planar direction.

In the first stage of the studies (similarly to Kofod experiment [6]) the tape was stretched 500% along the x axis, and then attached to plastic beams (Fig. 4). Then, the tapes with

five different pre-stretches (100%, 200%, 300%, 400%, 500%) were examined. When 5 kV voltage was applied, a change in the thickness and corresponding change in the area of the electrodes were observed. A prototype of a stack actuator was created by the authors.

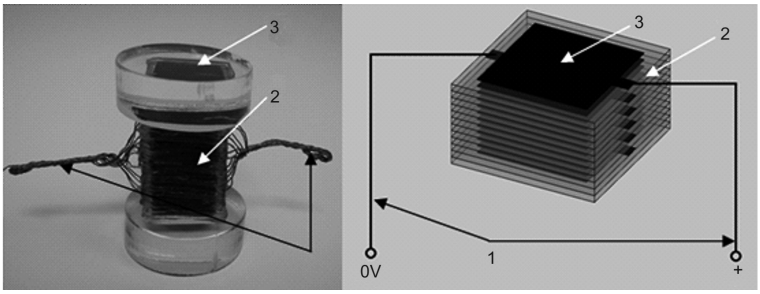

Fig. 3. Prototype of a stack actuator: 1 – electrical wiring, 2 – elastomer tape, 3 – graphite electrode
Rys. 3. Prototyp aktuatora warstwowego: 1 – druty elektryczne, 2 – taśma elastomeru, 3 – grafitowe elektrody

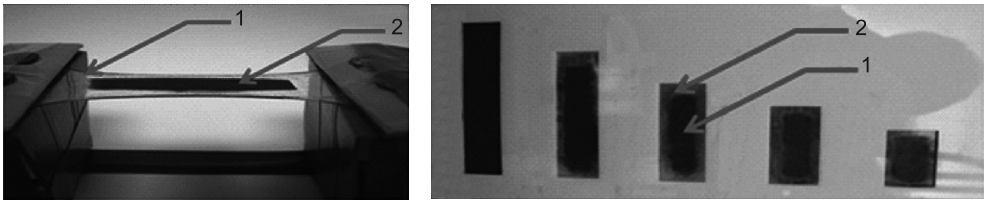

Fig. 4. Author's experiment: a single layer of pre-streched dielectric film VHB 4910 covered with graphite electrode. 1 – dielectric elastomer, 2 – graphite electrode
Rys. 4. Eksperyment Autorów: pojedyncza warstwa rozciągniętej taśmy VHB 4910 pokrytej grafitową elektrodą: 1 – dielektryczny elastomer, 2 – grafitowa elektroda

3. Applications of dielectric elastomers

A variety of technical applications of dielectric elastomers are discussed in literature. These smart polymers can be applied in biomedical sciences, robotics, mechatronics, entertainment, military, aeronautics etc. Two applications of dielectric elastomer actuators are presented in this paper as a kind of prosthesis – an active orthosis and a force feedback device. Both devices exert force on user's hand, thus the safety of the user has to be strictly considered. Dielectric elastomers can be easily used in both cases. A DE actuator is physically unable to exceed a safe value of force, also inactive actuator can still be moved freely. The only risk is associated with high actuating voltage (currently approximately 5 kV), but with carefully following safety norms, the user will be completely separated from such elements.

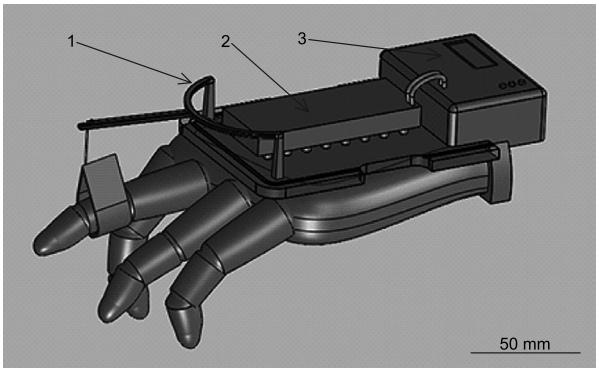

Fig. 5. CAD model of an active orthosis: 1 – interchangeable mounting element, 2 – dielectric elastomer actuator, 3 – control box
Rys. 5. Model CAD aktywnej ortezy: 1 – wewnętrzny element montażowy, 2 – aktuator z elastomeru dielektrycznego, 3 – skrzynka kontrolna

3.1. Orthosis

Orthoses are devices that accelerate the rehabilitation of damaged joints. Static and passive orthoses are most popular, but more serious injuries require active elements. These elements move the healing joint with low speeds and controllable force to prevent scarring and inflammations, while not causing pain. Currently such devices are driven by hydraulic, pneumatic of electrical actuators. All these solutions have serious disadvantages, such as complicated way of supplying power, high mass or generated noise. Dielectric elastomer actuators are lightweight, silent and do not require complicated mechanical elements such as gearboxes. High actuating voltages can be supplied by miniature DC-DC converters, enclosed in a control box (Fig. 5).

Presented solution is designed for a smaller DE actuator (Figure 5) – a lower force will be generated. It is also equipped with interchangeable mounting element (Fig. 5). This allows the device to be used with different fingers and joints, for a variety of finger lengths (e. g. for children). The force can be applied with various angles.

3.2. Force feedback device

A force feedback device is used in the manipulation of objects in a virtual reality. It usually is used as an input/output device connected to a PC. A glove with actuators is worn by a user. Whenever a virtual object is touched or grasped, the actuators do not allow a user's fingers to move further. Ideally, such a device could inform the user not only about the existence of an object, but also about its surface, shape, plasticity or temperature.

Minimum force variation that can be detected by a human's fingertip is 0.5 N, so the smallest controllable change in the generated force cannot be higher. Maximum force is restricted by user's safety – in most cases it should not exceed 30–50 N [12]. Minimum displacement registered is 2.5° angular displacement of the joint, which is approx. 1 mm of fingertip linear displacement. The sensitivity of the motion of a force feedback device should

be at least four times higher – 0.25 mm (fingertip) or 0.6° (joint). Maximum displacement varies with the size of human hands – devices with different sizes seem to be sensible. The mass of the device should be as low as possible to give a natural feeling of operation. For the same reason, the actuator should not generate force while not operating. The high power density of dielectric elastomers lowers the mass significantly. Inactive DE actuator has a 'natural feel' while handling it, and a force opposite to finger's movement can be generated to ensure the feeling of free movement. Self-sensing capabilities of dielectric elastomers can eliminate the need of using separate sensors, creating a compact and simple device.

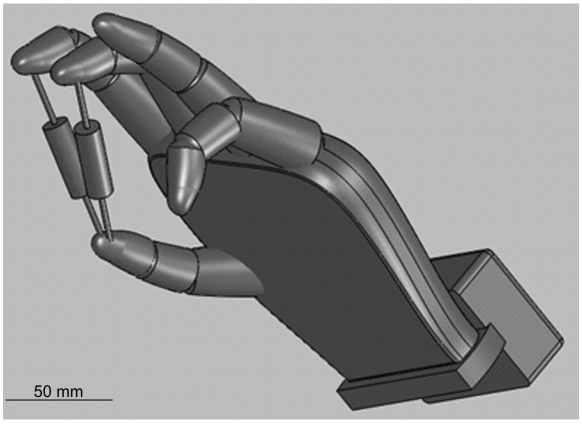

Fig. 6. Designed force feedback device

Rys. 6. Urządzenie do siłowego sprzężenia zwrotnego

Future developments could be equipped with tactile displays, which inform the user of the surface of a virtual object. Development of electroactive polymer actuators could also allow an FFD to look like a glove, with the actuators embedded in its surface.

4. Conclusions

Dielectric elastomers can be easily applied in many areas of science. Perfecting the production technology will enable the devices built with such actuators to be manufactured on large scale and compete with existing solutions. The study showed that in the area of prosthesis such as active ortheses, a DE actuator would make the devices more patient--friendly and universal. As far as force feedback devices are concerned, the presented design is much simpler than existing devices. Using polymeric materials also shows very interesting prospects for the future.

References

[1] Liu Y., Liu L., Zhang Z., Leng J., *Dielectric elastomer film actuators: characterization, experiment and analysis*, Smart Materials and Structures, vol. 18, no. 9, p. 095024, 2009 (http://stacks.iop.org/0964-1726/18/i=9/a=095024).

[2] Przychodzki W., Włochowicz A., *Fizyka Polimerów*, PWN, Warszawa 2001.

[3] Bar-Cohen Y., *Electroactive Polymer (EAP) Actuators as Artificial Muscles: Reality, Potential, and Challenges*, ser. SPIE Press Monograph. Society of Photo Optical, 2004 (http://books.google.pl/books?id=uxqgkdqE9FIC).

[4] European scientific network for artificial muscles (http://www.esnam.eu).

[5] Shahinpoor M., Bar-Cohen Y., Simpson J.O., Smith J., *Ionic polymer-metal composites (ipmcs) as biomimetic sensors, actuators and artificial muscles – a review*, Smart Materials and Structures, vol. 7, no. 6, p. R15, 1998 (http://stacks.iop.org/0964-1726/7/i=6/a=001).

[6] Kofod G., *Dielectric elastomer actuators*, Ph.D. dissertation, The Technical University of Denmark, Risø 2001.

[7] Lotz P., Matysek M., Schlaak H., *Fabrication and application of miniaturized dielectric elastomer stack actuators*, Mechatronics, IEEE/ASME Transactions on, vol. 16, no. 1, pp. 58-66, feb. 2011.

[8] Jung K., Kim K.J., Choi H.R., *A self-sensing dielectric elastomer actuator*, *S*ensors and Actuators A: Physical, vol. 143, no. 2, pp. 343-351, 2008 (http://www.sciencedirect.com/science/article/pii/S092442470700814X).

[9] Danfoss polypower (http://www.polypower.com/products/Generators).

[10] Kornbluh R.D., Pelrine R., Pei Q., Heydt, S. Stanford R., Oh S., Eckerle J., *Electroelastomers: applications of dielectric elastomer transducers for actuation, generation, and smart structures*, pp. 254-270, 2002 (http://dx.doi.org/10.1117/12.475072).

[11] Carpi F., Migliore A., Serra G., Rossi D.D., *Helical dielectric elastomer actuators*, Smart Materials and Structures, vol. 14, no. 6, p. 1210, 2005 (http://stacks.iop.org/0964-1726/14/i=6/a=014).

[12] Astin A.D., *Finger force capability: measurement and prediction using anthropometric and myoelectric measures*, Master's thesis, Virginia Polytechnic Institue and State University, Blacksburg 1999.

TECHNICAL TRANSACTIONS | **CZASOPISMO TECHNICZNE**
MECHANICS | MECHANIKA
1-M/2013

PIOTR DUDA*, ROMAN DUDA*

MODELING OF STEADY AND TRANSIENT TEMPERATURE DISTRIBUTION IN THE DEVICE FOR MEASURING THE THERMAL CONDUCTIVITY

MODELOWANIE USTALONYCH I NIEUSTALONYCH ROZKŁADÓW TEMPERATURY W APARACIE DO POMIARU WSPÓŁCZYNNIKA PRZEWODZENIA CIEPŁA

Abstract

The aim of this paper is the presentation of the method for thermal conductivity measurement and numerical modeling of temperature distribution in apparatus for measuring the thermal conductivity. Experimental studies will be carried out in transient state until the steady state heat conduction in apparatus is achieved. The calculated and measured temperature distribution will be compared. The time to steady state in apparatus for different samples will be estimated based on numerical and experimental results. The influence of the contact resistance between the sample and the measuring device will be analyzed.

Keywords: *heat conduction*, *CFD modeling*

Streszczenie

Celem artykułu jest pokazanie sposobu pomiaru współczynnika przewodzenia ciepła w ciałach stałych oraz przeprowadzenie modelowania rozkładu temperatury w przyrządzie pomiarowym. Przeprowadzone zostaną badania doświadczalne w stanach nieustalonych aż do momentu ustalenia się zjawiska przewodzenia ciepła. Przedstawione zostaną wyniki modelowania numerycznego w stanie nieustalonym. Porównane zostaną zmierzone i obliczone przebiegi temperatury. Zweryfikowany zostanie czas ustalenia się zjawiska przewodzenia ciepła w przyrządzie pomiarowym. Dodatkowo analizowany będzie wpływ oporów kontaktowych pomiędzy próbką i urządzeniem pomiarowym zarówno doświadczalnie jak i numerycznie.

Słowa kluczowe: *przewodzenie ciepła*, *modelowanie CFD*

* PhD. Eng. Piotr Duda, prof. MSc. Roman Duda, Cracow University of Technology, Department of Thermal Power Engineering, Faculty of Mechanical Engineering.

1. Measurements of thermal conductivity in solids

Heat conduction is the transfer of internal energy between directly adjoining parts of one body or different bodies [1]. In the liquids transferred is kinetic energy of atoms and molecules and in solids transferred is vibration energy of atoms in the crystal lattice and the free movement of electrons. Heat conduction takes place generally in accordance with the law of the Fourier that is saying that the transferred heat flux density is directly proportional to the temperature

$$\dot{q} = -k\frac{\partial T}{\partial x} \tag{1}$$

where:

$\dot{q}$ – the heat flux expressed in W/m^2,
k – a heat conduction coefficient in W/(m·K),
T – a temperature in °C or K,
x – a coordinate in m.

The minus sign in equation testifies to the fact that heat flows in the direction of the decreasing temperature.

The thermal conductivity of a material is a measure of the ability of the material to conduct heat. A high value for thermal conductivity indicates that the material is a good heat conductor, and a low value indicates that the material is a poor heat conductor or insulator. The thermal conductivity varies within a wide range, from 0.026 [W/(mK)] for the air to about 5000 [W/(mK)] for the graphene.

Two classes of methods exist to measure the thermal conductivity of a sample: steady--state and non-steady-state (or transient) methods.

Steady-state techniques perform a measurement when the temperature of the material measured does not change with time [2–3]. In these techniques a flat, cylindrical or spherical layer is located between the heat source of a higher temperature and the heat receiver at a lower temperature. The advantage of these methods is simple mathematics.

The disadvantages of these methods include a complex array of regulatory control and the test bench for a long time, set the heat exchange of the sample, the need to ensure perfect contact with the surface of the sample surfaces and the radiator grille and the need to ensure good thermal insulation on the other surfaces of the sample.

The transient techniques perform a measurement during the process of heating up. The advantage is that measurements can be made relatively quickly. Transient methods are usually carried out by needle probes. The disadvantage is that the mathematical analysis of the data is in general more difficult.

2. Experimental research

Apparatus used for the tests is presented in Figure 1. It consists of two sections: hot and cold. In the hot, an electric heater is mounted with a maximum power of 65 [W] (at max. voltage of 240 [V]). Heating power can be continuously reduced. Hot section is at the top of

the apparatus. It has a cylindrical shape with a diameter of 25 [mm] and is made of brass with a heat conductivity 121 [W/(mK)].

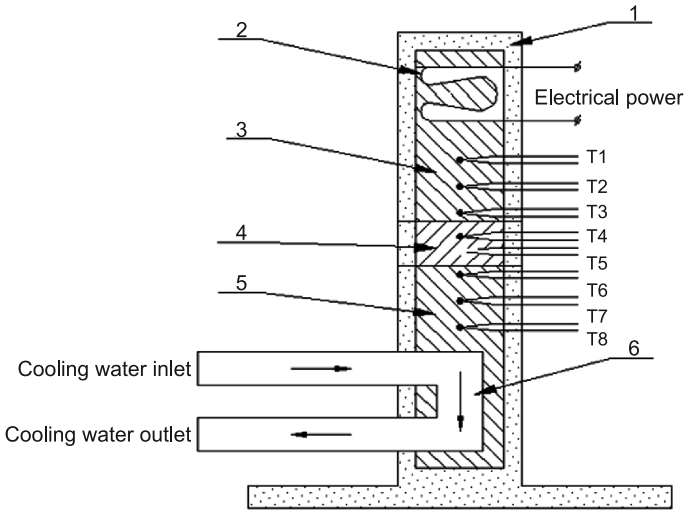

Fig. 1. Apparatus for measurement of thermal conductivity, 1 - insulation, 2 – electric heater, 3 – heating section, 4 – sample test material, 5 – cooling section, 6 – coil, T1, T2, T3, T4, T5, T6, T7, T8 – thermocouples

Rys. 1. Aparat do badań współczynnika przewodzenia ciepła; 1 – izolacja, 2 – grzałka elektryczna, 3 – sekcja grzejna, 4 – próbka materiału badanego, 5 – sekcja chłodząca, 6 – wężownica, T1, T2, T3, T4, T5, T6, T7, T8 – termopary

K type thermocouples are mounted every 15 [mm] on the surface of the heater. They are labeled T1, T2, T3. The cooling section has a cylindrical shape with a diameter of 25 [mm] and is made of the same kind of brass. This section is situated at the bottom of the apparatus. Three thermocouples are mounted with markings T6, T7, T8 on it's surface. This thermocouples are also located at 15 [mm] distance. In the cooling section, water flows through coil, where receives heat from metal area. Volume flow rate is about 1.5 [l/min]. Both sections are thermally insulated on the outer surface by plastic covers.

A test sample is mounted in the apparatus between the heating and cooling section. The samples are cylindrical with a diameter of 25 [mm] and a height of 30 [mm]. Samples are made of brass, steel and aluminum, respectively with heat conduction coefficients 121, 25, 180 [W/(mK)] according to manufacturer. A sample of brass is equipped with a two thermocouples with labels T4 T5, allowing additional verification of the temperature distribution. The surfaces of the samples that are in contact with heating and cooling sections are lubricated with grease paste to minimize contact resistance.

At the laboratory, temperature are measured in each section. The measurement is carried out since the launch of an electric heater and cooling system until the steady state heat conduction in apparatus is achieved. The contact surfaces are lubricated with grease paste and pressed. First experiment is conducted for a sample made of aluminum.

The measurement results are shown in Figure 2. For the time of 3000 [s] steady state is achieved. The temperature distribution along the height of the apparatus for the time 4000 [s] is shown in Figure 3.

The temperature distribution curve in aluminum sample is at a different angle than temperature distribution curves in heating and cooling sections. This is due to a higher

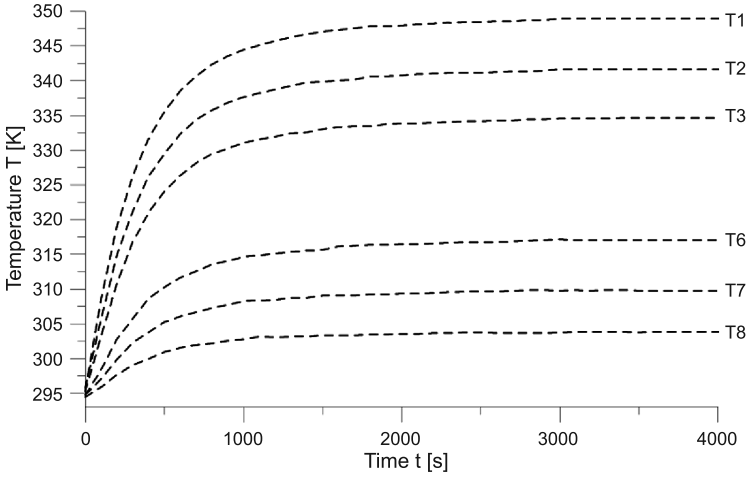

Fig. 2. Measured transient temperature at selected points in the device with inserted aluminum sample

Rys. 2. Zmierzone przebiegi temperatury w wybranych punktach w aparacie z próbką aluminiową

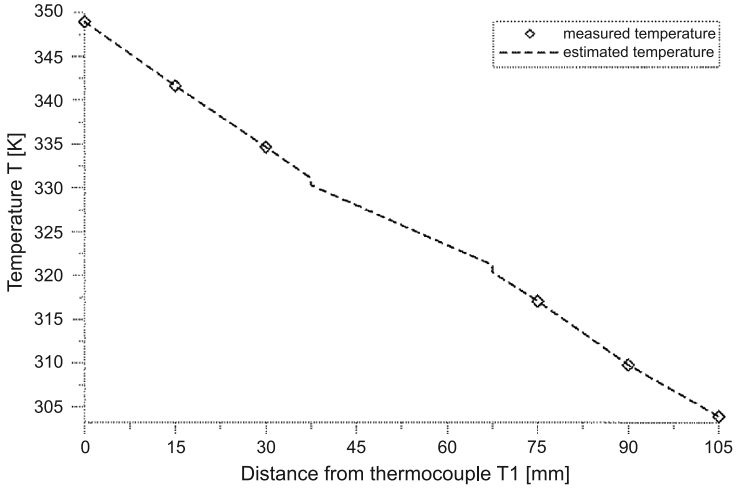

Fig. 3. Measured steady state temperature distribution in the device with inserted aluminum sample

Rys. 3. Rozkład zmierzonej ustalonej temperatury w aparacie z założoną próbką aluminiową

conductivity in aluminum than in brass. Temperature discontinuities are caused by contact resistance at the contact surfaces between the sample and cooling or heating sections. They are not higher than 0.8 [K].

Next, thermal conductivity of aluminum sample is estimated. For this purpose, the temperature of the upper and lower surfaces of the sample must be calculated. Finally, thermal conductivity can be determined from the equation (2).

$$k_{a-b} = \frac{4U\ I}{\pi D^2 \left(\frac{\Delta T_{a-b}}{\Delta x} \right)} \tag{2}$$

where:

- U – the average value of the voltage drop on the heating element [V],
- I – the average value of the heating current [A],
- D – diameter of samples and heating and cooling part of device,
- ΔT_{a-b} – the temperature difference between the upper and lower surface of the sample [K],
- Δx – thickness of the sample [m].

During the measurement the following data are observed: the current is 0.186 [A] and the voltage 160 [V] sample diameter is 25 [mm] and height 30 [mm]. Substituting these data into equation (3) the following results is obtained.

$$k_{a-b} = \frac{4 \cdot 160\,[\mathrm{V}] \cdot 0.186\,[\mathrm{A}]}{\pi \cdot (25 \cdot 10^{-3}\,[\mathrm{m}])^2 \cdot \left(\frac{10\,[\mathrm{K}]}{30 \cdot 10^{-3}\,[\mathrm{m}]} \right)} = 181.9 \left[\frac{\mathrm{W}}{\mathrm{mK}} \right] \tag{3}$$

Determined value differs from the real value of 180 [W/(mK)] for 1.04% because of temperature measurement errors and contact resistance between the sample and cooling or heating section. A much larger measurement errors of heat conductivity can occur if the measurement is carried out in transient state.

3. CFD modeling

The following part describes the numerical modeling of temperature distribution in the transient state, and steady state in the apparatus for measuring thermal conductivity [4–8].

Geometric model of the apparatus is created basing on the measured dimensions, considering its basic elements such as heating section with the resistance heater and the cooling section with water coil where the cooling water flows. This parts are made of brass with a diameter of 25 [mm] and a height of 100 [mm] each. The samples are installed between them. They are made of aluminum, stell and having the same diameter as upper and lower parts and height of 30 [mm]. Geometric model of this apparatus is shown in Figure 4. The cooling coil interferes with simplification of 3-D model into an axisymmetrical model.

The three-dimensional geometry is divided into 907467 cells, 2242059 faces, 343969 nodes. Finite elements are built from quad pave type of elements. This grid is shown in

Figure 5. Modeling is performed using the equations of balance of mass, momentum and energy. It is assumed that the flow is turbulent and the k-ε model (Viscous Standard *k*–ε, Scalable Wall Functions) is used.

After that material properties for solid and water are defined. Next flow and thermal boundary conditions are defined. At the inlet to the water coil, velocity-inlet type boundary condition is set (speed 1 [m/s], 294.65 Temperature [K]). At the water outlet of the coil, outflow type boundary condition is defined. On the surface of the heater, heat flux density (Heat Flux) is set (28000 [W/m^2]).

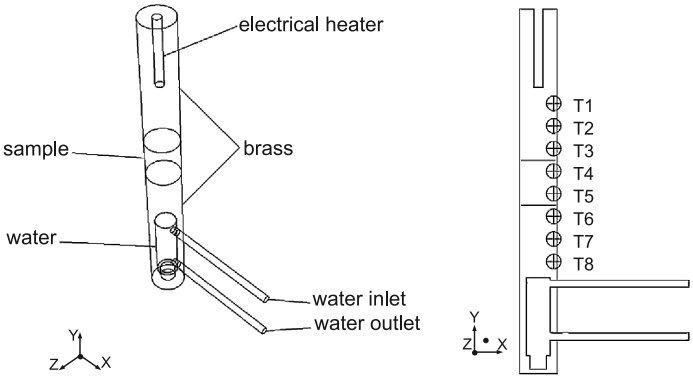

Fig. 4. Geometry of apparatus model

Rys. 4. Geometria modelu aparatu

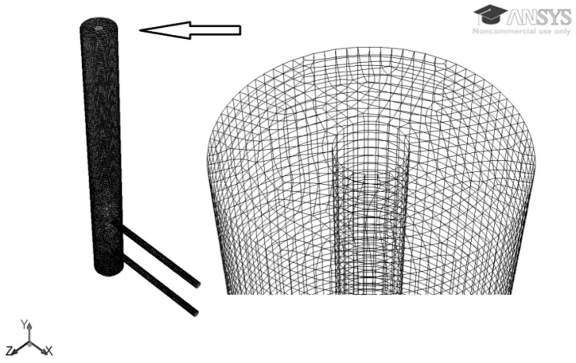

Fig. 5. Division for finite elements

Rys. 5. Podział na elementy skończone

The constant time step is set (1 [s]). Iteration starts taking the whole area parameters as at water inlet to the coil. ANSYS Fluent is used [4]. Steady state is obtained after about 3000 [s].

Figure 6 shows the calculated temperature transient at the points in the apparatus where thermocouples(T1-T8) are installed. Numerically obtained temperatures are compared with values measured at the device. The maximum error does not exceed 1.2%.

Temperature distribution along the height of the apparatus with installed aluminum sample is presented in Figure 7. Well developed and validated numerical model can be used to determine the time when steady state is achieved. This is the time at which measurements of thermal conductivity for samples can be done.

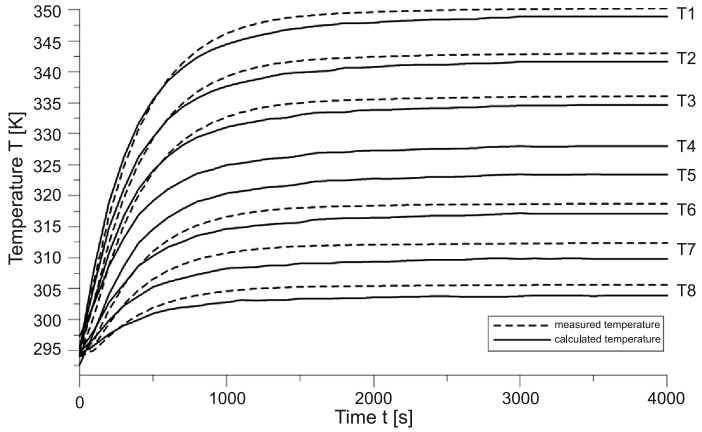

Fig. 6. Measured and calculated temperature transient at selected points in the device with inserted aluminum sample

Rys. 6. Zmierzone i obliczone przebiegi temperatury w wybranych punktach w aparacie z próbką aluminiową

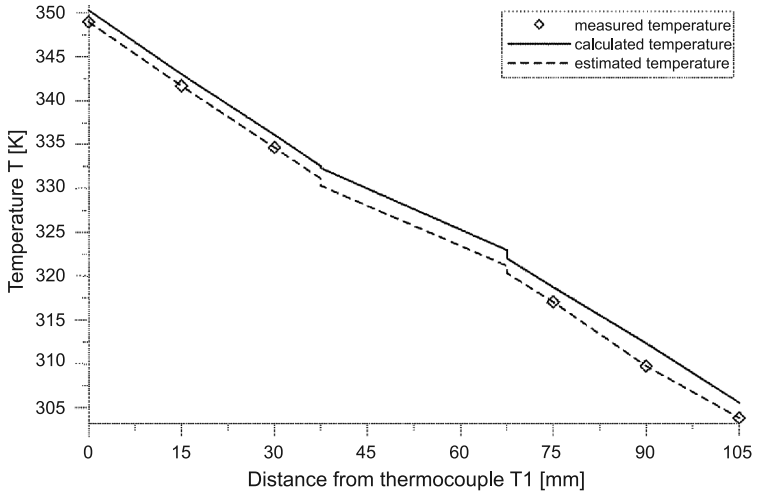

Fig. 7. Measured and calculated steady state temperature distribution in the device with inserted aluminum sample

Rys. 7. Rozkład zmierzonej i obliczonej ustalonej temperatury w aparacie z założoną próbką aluminiową

Finally numerical simulation is performed for the sample made of steel. Time when the steady state is obtained is about 5500 [s].

4. Conclusions

The apparatus for measuring thermal conductivity in solids and the method to calculate thermal conductivity were presented. Experiment was carried out and measured temperature transient at selected points in the device with inserted aluminum sample were presented. Coefficient of thermal conductivity was calculated. Determined value of conductivity differs from the real value of 180 [W/(mK)] for 1.04% because of temperature measurement errors and contact resistance between the sample and cooling or heating section.

Next, numerical model of the apparatus for measuring thermal conductivity was presented. The comparison of measured and calculated temperature transient at selected points in the device with inserted aluminum sample were presented. The maximum error between the measured and calculated values did not exceed 1.2%.

The presented numerical model calculated the time when steady state was achieved in apparatus with aluminum sample. The calculated value of 3000 [s] was validated by measurement. Additionally, the steady state time for apparatus with steel sample was determined (5500 [s]).

The knowledge of steady state time allows users for creation of an experimental plan. The measurements will not be done until the steady state heat conduction in apparatus is achieved.

Additionally, the presented numerical model allows users for contact resistance analysis. Furthermore, knowing that the temperature at any point of apparatus can not exceed 90^{o}C, the numerical model can calculate the maximum power supply.

References

[1] Fourier J.B., *Théorie analytique de la chaleur*, Paris 1822.
[2] Szydłowski H., *Pracownia fizyczna*, PWN, Warszawa 1999.
[3] Fodemski T., *Pomiary cieplne część I podstawowe pomiary cieplne*, WNT, Warszawa 2001.
[4] ANSYS® Fluent, *14.0, User manual*, ANSYS, Inc.
[5] Patankar S.V., *Numerical Heat Transfer and Fluid Flow*, Hemisphere Publishing Corporation, 1980.
[6] Taler J., Duda P., *Solving Direct and Inverse Heat Conduction Problems*, Springer-Verlag, Berlin Heidelberg 2006.
[7] Duda P., *Obliczenia cieplne i wytrzymałościowe dla wstawki temperaturowej*, Problemy Eksploatacji 79, Nr 4, Kraków 2010, 103-114.
[8] Duda P., Duda R., *Modelowanie rozkładu temperatury na stanowisku do pomiaru współczynnika przewodzenia ciepła*, Czasopismo Techniczne 2-M/2012, Kraków 2012, 81-88.

TECHNICAL TRANSACTIONS | **CZASOPISMO TECHNICZNE**
MECHANICS | MECHANIKA
1-M/2013

JAN DUDA*, JANUSZ POBOŻNIAK*

MACHINING PROCESS PLANNING IN PLM ENVIRONMENT

PROJEKTOWANIE PROCESÓW TECHNOLOGICZNYCH OBRÓBKI W ŚRODOWISKU PLM

A b s t r a c t

The paper presents the characteristics of planning actions on the stage of conceptual and detailed manufacturing process planning in an integrated PLM environment. The functionality of the available solutions is discussed in details. Based on these analysis, the directions for the future development of the machining process planning systems to increase the automation level are presented.

Keywords: *CAD/CAPP/CAM integration*, *production preparation*, *manufacturing knowledge data bases*

S t r e s z c z e n i e

Artykuł przedstawia charakterystykę działań projektowych na etapie koncepcyjnego i szczegółowego projektowania technologicznego w zintegrowanym środowisku PLM. Szczegółowo przeanalizowano funkcjonalność dostępnych rozwiązań. Bazując na tej analizie, zaproponowano kierunki dalszego rozwoju komputerowo wspomaganego rozwoju procesów technologicznych obróbki, w celu zwiększenia stopnia automatyzacji prac projektowych.

Słowa kluczowe: *integracja CAD/CAPP/CAM*, *przygotowanie produkcji*, *bazy wiedzy technologicznej*

* Prof. Jan Duda, PhD. Janusz Pobożniak, Institute of Production Engineering, Faculty of Mechanical Engineering, Cracow University of Technology.

1. Introduction

The growing competition on the market enforces the introduction of new methods and approaches both in the preparation and the realization of production processes. Competition on the market enforces several changes, including the extensive use of computer systems to shorten the development of product and production processes and the use of modern development methodologies like CE.

There is a lot of research works on modern manufacturing production preparation approaches [1, 5, 10]. A number of both Polish as well as international works on particular product lifecycle phases, as for example design [1], computer aided process planning [4, 5, 9], assembly process planning and the advanced production organization methods are available. On the other hand, the number of works characterising the use of computer systems in the particular product development phases (as for example CAD, CAPP, CAAP, DFM, DFA, CAS, etc.) and integrated design with the use of PLM applications [6, 7, 8] and modern development strategies is limited. To fill this gap, the methodology of using such systems in the manufacturing preparation phase in the Concurrent Engineering environment was developed. This papers presents the part of this methodology related to the machining process planning and discusses the functionality of the available commercial solutions. At the end, the directions for the future development are presented.

2. Integrated process and system development in PLM environment

Features of modern development strategies indicate the need for product development phase integration.

Integration and parallel execution of activities were received through the separation of the conceptual design stages, allowing for the creation of the variant solutions. Variants are then evaluated in the view of the requirements of the next development phase [5].

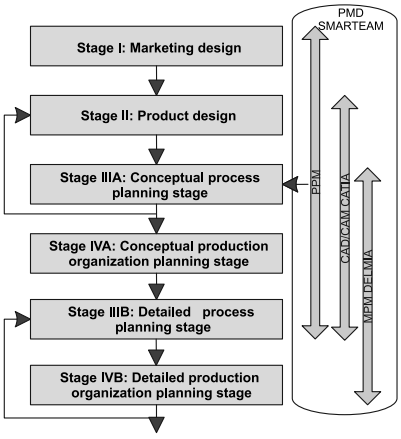

Fig. 1. Parallel execution of product development phases

Rys. 1. Równoległa realizacja faz rozwoju produktu

The integration of design and manufacturing product development suggests the separation of the following phases (Fig. 1):
– conceptual process planning phase (STAGE III A),
– detailed process planning phase (STAGE III B).

The integration of manufacturing and organizational product development suggests the separation of the following phases:
– conceptual organization process planning phase (STAGE IV A),
– detailed organizational process planning phase (STAGE IV B).

The selected variant fulfilling the established criteria is next further developed in the detail design stage (Fig. 1). The concurrent execution of selected product development phases within the scope machining process planning is presented in the following points.

3. Formal representation of machining process planning

Manufacturing process is the ordered series of discrete events occurring in the manufacturing system in relation to the product [2]. It was found, that during the manufacturing process, the product goes through several states from the initial one (raw material) to the finish state (machined product). It was also assumed that the machining process executed in manufacturing systems is described by the series of actions $\{E_0\}$ executed by the manufacturing system elements causing the discrete change of the product characteristics, from the initial state to the final state and the structure SPO describing the order of the process plan actions.

$$\text{PTO} = \{E_0\}, \text{SPO} \tag{1}$$

where:

$\{E_0\}$ – set of machining actions,
SPO – structure of machining process plan.

Based on the analysis of the machining processes, three types of actions were distinguished:
– E_{TRO} – actions changing the state of the machined part,
– E_{OPO} – actions changing the location of the object in the system (as the object the tool (N), machined part (PO) or exchangeable equipment (ZPW /ZNW) can be taken),
– E_{IDO} – actions comparing the present characteristics of the machined part with the requirements given in the manufacturing process documentation.

So:

$$\text{PTO} = \{E_{\text{TRO}}, E_{\text{OPO}}, E_{\text{IDO}}\}, \text{SPO} \tag{2}$$

Machining process planning for the given input data: production program and characteristics of the machined part:

$$\text{POW} = \{C_W, W_W, \Psi_W\} \tag{3}$$

is the creative decision process aimed to determine the shape of the raw material POP based on the technical and economical assumptions and the series of actions executed in manufacturing system, transforming the raw material POP into the machined part with the given characteristics of POW.

So, machining process planning covers:
- selection and design of the raw material,
- development of machining plan,
- development of the structure of machining process by the selection of the methods and technical means for the machining process execution,
- development of machining process documentation.

The structural elements and their order in the machining process structure depend on:
- geometry characteristics, and physical and mechanical properties of the machined part,
- dimensional and shape accuracy increasing together with the machining process realization.

The analysis of the degree of automation of computer aided process planning in the CAD/CAM and MPM ((Manufacturing Process Management) systems being the component of PLM applications is presented below.

4. Machining process planning in CAD/CAM and MPM systems

CAD/CAM and MPM systems are used for the machining process planning in PLM environment. The analysis of the machining process in PLM environment (Fig. 2) show that the level of automation is very low. Most of the planning actions still require the participation of the manufacturing engineer.

CAM system does not assist the manufacturing engineer during the raw material selection. The only available assisting function is the automatic generation of the box including the machined part. Because there is no links to the steel product database, there are just simple geometric calculations.

CAM system also does not help to select the machine tool. The machine tool selection is one of the first decisions taken by the manufacturing engineer during the machining process development. Very often, CAM system are equipped with the machine tool database and the tools for development of machine tool models. These tools allows to define the kinematics of machine tool, the range of axis movements, max. rotational and linear speed, geometry of particular machine tool elements, tool magazines, part mounting point and tool mounting point. These tasks are executed in PLM environment by MPM systems allowing to define and simulate the machining stands and systems. Nevertheless, there is no systems for selection of machine tool based on such data. These data are used only for control program simulation (Fig. 3).

In the development of machine operation contents, which covers selection of appropriate cycles, their parameters and ordering, the automatic assignment of machining cycles to recognised manufacturing features is widely used. Unfortunately, such solutions have several limitations mainly due to the limited functionality of feature recognition modules. There is no commercial solutions capable to copy with the problem of intersecting manufacturing features, i.e. features for which the common volume in 3D space is not null. As the result, the hole intersecting with the slot is recognised as two pockets, and the slot as two independent slots which influence the process of machining cycles selection. The machining selection process can be modified by the development of the simple conditions using the parameters of the recognised manufacturing feature (Fig. 4). It should be noted that there is no basic parameters important from the manufacturing process planning view.

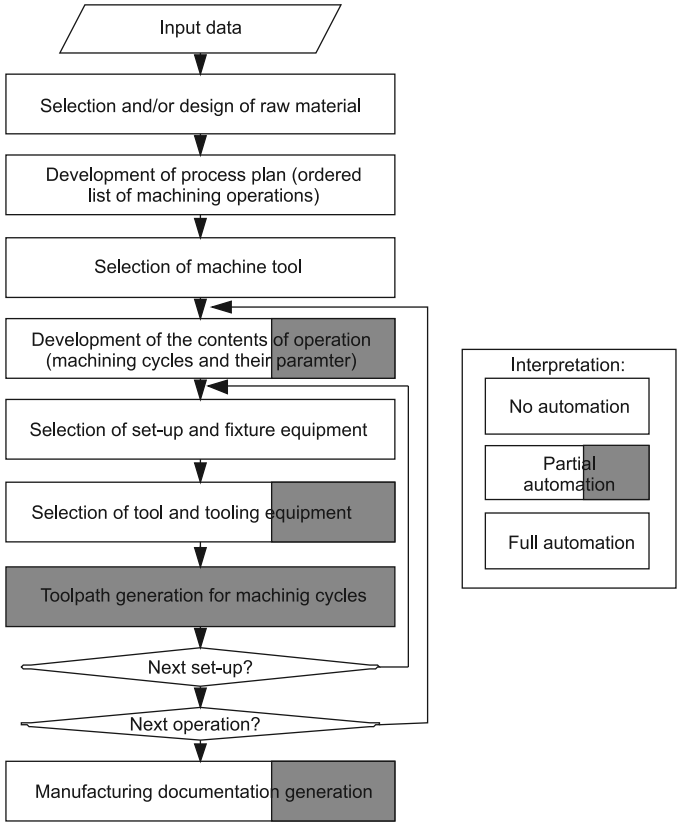

Fig. 2. Machinig process planning in CAD/CAM system - estimation of the degree of automation
Rys. 2. Przebieg projektowania procesów technologicznych obróbki w systemie CAD/CAM – ocena stopnia automatyzacji zadań składowych

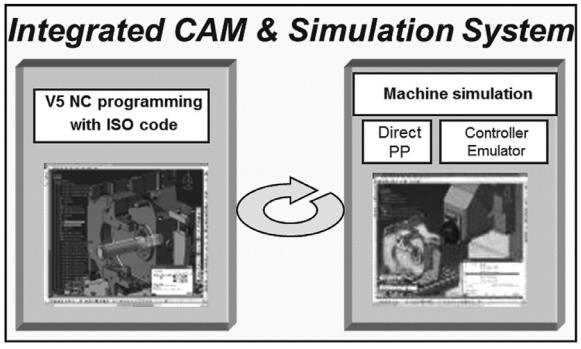

Fig. 3. Machine tool and its model for program simulation in MPM system
Rys. 3. Obrabiarka i jej model do symulacji programów w systemie MPM

For example, the pocket has no parameters describing the occurring of concave sub--profiles, requiring to the tool with the smaller diameter. No possibility to use in the selection conditions the non-geometric information of features like surface roughness or tolerance class (with some exceptions for holes) is another serious limitation. Because of this, the automatic selection of final machining cycles is not possible. Also feature recognition does not take the raw material into account. The order of machining cycles is determined base of the types of cycle, i.e. first all pocket milling cycle are executed, then drilling, reaming, etc. or the type of the tool. CAD/CAM system are not equipped with the meta-knowledge allowing to select the order of machining cycles based on the common manufacturing rules, represented for example in the form of multi-level, hierarchical decision nets [2].

Without discussion, the most important advantage of CAD/CAM system is the ability to generate the toolpaths for the defined machining cycles and their parameters. The toolpaths are generated taking onto the account the selected movement scheme and the tool dimensions. Nevertheless, the supervision of manufacturing engineer is still necessary, because CAD/CAM systems are not able to determine the appropriate approach, retract or linking motions, which results very often in the collisions between the tool and the machined part or machine tool elements.

To document the program and deliver the information necessary for its runs, the manufacturing documentation must be also developed. Not all CAM systems have such functionality. The systems having such functions are not able to save a number of important data like for example part clamping scheme in the documentation. Once more, the help of manufacturing engineer is necessary.

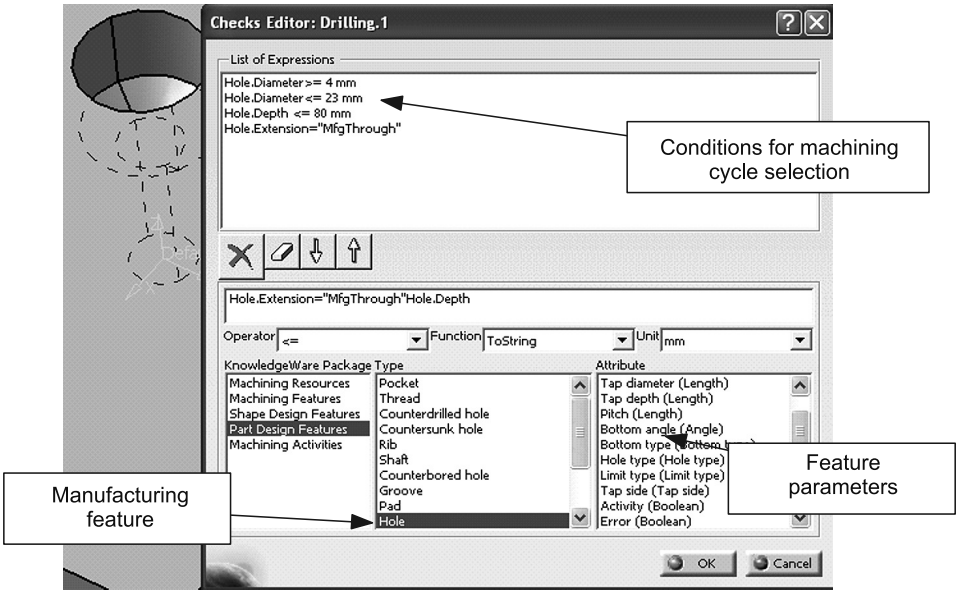

Fig. 4. The conditions for drilling cycle selection

Rys. 4. Warunki wyboru cyklu wiercenia

The increase of the functionality of the integrated systems for the process and manufacturing system development should be carried out through the development of the modules for assisting and/or automation of the particular planning tasks. The high level of integration of such systems is obtained through the use of common data model PPR (Product, Process, Resources), securing the exchange of information between the modules used in the planning actions and the development of systems based on the knowledge, using the artificial intelligence (AI) tools.

5. Conclusion – perspectives for the machining process planning automation

The analysis presented above indicate that the level of automation of CAD/CAM components of PLM applications is relatively low. The main factor deciding about the efficiency of machining process is the structure of the process plan. This function is performed by CAPP system, establishing the contents and the sequence of operations using generative and semi-generative methods. The prototype of such system is under the development in Production Engineering Institute, Cracow University of Technology. It allows for:

- storage, modification and processing of manufacturing knowledge (knowledge repositories),
- storage of characteristics of manufacturing systems in the view of manufacturing process planning,
- generation of solutions on the different degree of details.

Such system integrated with other modules of PLM application should increase the level of automation of computer aided process planning and shorten the production preparation time.

The key elements still requiring the research works are:

- development of the model of manufacturing process planning in the integrated development of the products, processes and manufacturing systems,
- development of the knowledge databases with the special attention on meta-knowledge,
- improvement of the algorithms for manufacturing feature recognition.

References

[1] Chlebus E., *Techniki komputerowe CAx w inżynierii produkcji*, Warszawa 2000.
[2] Duda J., *Wspomagane komputerowo generowanie procesu obróbki w technologii mechanicznej*, Politechnika Krakowska, Kraków 2003.
[3] Duda J., *Wspomagane komputerowo generowanie procesów wytwarzania – obecny stan i perspektywy rozwoju*, III Forum Integracyjne Polskiego Stowarzyszenia Upowszechniania Komputerowych Systemów Inżynierskich „Proca", Jedlnia 2004.
[4] Duda J., Habel J., Pobożniak J., *Repository of Knowledge for Manufacturing Process Planning*, International Conference FAIM' 2005 Bilbao, Spain 2005.
[5] Duda J., Pobożniak J., *Concurrent Development of Products, Processes and Manufacturing Systems in PLM Environment*, Management and Production Engineering Review, Production Engineering Committee of the Polish Academy of Sciences, vol. 2, No. 2.

[6] Eigner M., *Product Lifecycle Management – The Backbone for Engineering*, First International Conference, "Virtual Design and Automation", Poznań 2004.
[7] Eversheim W., Rozenfeld H., Bochtler W., Graessler R., *A Methodology for Integrated Design and Process Planning on a Concurrent Engineering Reference Model*, Annals of the CIRP 1995.
[8] Kahlert T., *From PDM to PLM – from a workgroup tool to on enterprise – wide strategy*, First International Conference, Virtual Design and Automation, Poznań 2004.
[9] Knosala R. i zespół, *Zastosowanie metod sztucznej inteligencji w inżynierii produkcji*, WNT, Warszawa 2002.
[10] Li W.D., Nee A.Y.C., *Collaborative Design and Planning for Digital Manufacturing*, Spinger 2008.
[11] Pobożniak J., *Programowanie obrabiarek CNC w systemie CATIA*, Helion 2013 (to be published).
[12] Pobożniak J., *Two stage approach to feature recognition for Computer Aided Process Planning*, Advances in Manufacturing and Science Technology, Vol. 29, 4/2005.
[13] Szatkowski K., *Przygotowanie produkcji*, Wydawnictwa Naukowe PWN, Warszawa 2008.

TECHNICAL TRANSACTIONS | **CZASOPISMO TECHNICZNE**
MECHANICS | MECHANIKA
1-M/2013

RENATA DWORNICKA*, IRENEUSZ DOMINIK**, MAREK IWANIEC**

COMPUTER-AIDED INSTRUCTION IN TEACHING BIOMEDICAL ENGINEERING STUDENTS

KOMPUTEROWE WSPOMAGANIE PROJEKTÓW W NAUCZANIU STUDENTÓW KIERUNKU INŻYNIERIA BIOMEDYCZNA

Abstract

The studies of the Biomedical Engineering faculty combine technical and humanistic elements. The biomedical engineering itself is a combination of knowledge located at the intersection of engineering, medical and biological applications. Technical universities which offer training courses on Biomedical Engineering place greater emphasis on engineering education. It is apparent, however, that the majority of students of this course are graduates of high schools with humanistic knowledge and no technical preparation. Initial teaching of technical subjects must therefore be conducted in a language and format accessible to the "non-engineers". Particularly, it is important to demonstrate and teach students the tools that will facilitate their further education.

Keywords: *engineering specialist teaching*

Streszczenie

Studenci kierunku Inżynieria biomedyczna są specyficzną grupą studencką łączącą w sobie pierwiastek techniczny i humanistyczny. Sama inżynieria biomedyczna stanowi połączenie wiedzy zlokalizowane na pograniczu nauk technicznych, medycznych i biologicznych. Uczelnie techniczne, które w ofercie kształcenia posiadają kierunek Inżynieria biomedyczna, kładą większy nacisk na kształcenie inżynierskie. Jak wykazują obserwacje, większość studentów tego kierunku to absolwenci szkół średnich z wiedzą humanistyczną bez technicznego przygotowania. Początkowe nauczanie technicznych przedmiotów musi więc być prowadzone w języku i formie przystępnej dla „nie-inżynierów". Szczególnie istotne jest zaprezentowanie i nauczenie studentów narzędzi, które ułatwią im dalszą edukację.

Słowa kluczowe: *inżynierskie nauczanie specjalistyczne*

* PhD. Eng. Renata Dwornicka, Institute of Applied Informatics, Faculty of Mechanical Engineering, Cracow University of Technology.
** PhD. Eng. Ireneusz Dominik, Prof. PhD. Eng. Marek Iwaniec, prof. AGH, University of Science and Technology, Faculty of Mechanical Engineering and Robotics, Department of Process Control.

1. Introduction

At the beginning educational programs at technical universities focused mainly on science courses. In the late 60s, and especially in the 70s, technical schools introduced the subjects beyond the science group. Firstly, foreign languages and soon after subjects of sociology, philosophy or economy were added. Broadening the engineer point of view was the main motivation. Graduate engineers should not only design and build new constructions but also find their place in society and coexist with other human beings regardless of their origins, religion or beliefs. Some of the technical universities added to their program courses on applied psychology of work, history of engineering solutions or creativity. When engineers started to take up executive positions the requirement of management and administration skills became indispensable. Thus, technical universities created new faculties of management and MBA courses in their structures. However, in spite of the changes, technical universities originally have always been dedicated to the logical minded people and as a result most of their students graduated from technical high schools.

2. The actual situation of education of engineer management staff

At present, on the labour market the shortage of engineers and technical schools graduates can be observed. According to the forecasts this situation will intensify. Because of this shortage it is easier for engineers to find a job in comparison to humanistic graduates. The media widely publicize the problem and high school graduates are more conscious about the possibility of finding future occupation in a trade profession. As a result for a few years the incline of candidates to technical studies has been noted. The survey data (prepared by the Department of Control and Supervision of Polish Ministry of Science and Education [4]) maintains that during university recruitment high school graduates chose mostly technical universities (Tab. 1). What is more: out of first five most popular universities, four were Polytechnics (Tab. 2).

Table 1

The popularity of higher education institution in 2010/2011 academic year [4]

No.	Type of the higher education institution	Number of candidates on one place
1	technical higher institutions	3.9
2	universities	3.5
3	agricultural higher institutions	3.5
4	economic higher institutions	2.8
5	physical education higher institutions	2.5
6	pedagogic higher institutions	2.5
7	state school of higher professional education	1.3

Table 2

The most popular higher education institution in 2010/2011 academic year [4]

No.	Name of the higher education institution	Number of candidates on one place
1	Warsaw University of Technology	8.6
2	Gdansk University of Technology	7.4
3	Lodz University of Technology	6.3
4	University of Warsaw	6.2
5	Poznan University of Technology	6.1

3. Bio is in vogue

In the academic community it is said that Bio is in vogue, that is Bioengineering, Biotechnology, Biomechanics, Biomaterials, Bioinformatics etc. As an instance on the Bioinformatics 5.3 candidates on one place were present in the recruitment process in 2010/2011 academic year. Similarly on the Biomedical engineering 4.8 candidates, Biotechnology 4.5 and on Bioinformatics and systems biology 3.1 [4].

Nowadays it is thought that these are domains of future. The interdisciplinary science teams are created, a lot of research are conducted and this is one of the main science major granted by European Union. As a result, in higher education the Bio-specialties ordered by the Polish government are founded. The information attracts attention of students. In Krakow Biomedical engineering can by studied at the Cracow University of Technology or at the newly created Faculty of Electrotechnics, Automatics, Informatics and Biomedical engineering at the AGH University of Science and Technology (former known as the Inter-faculty School of Biomedical Engineering founded in 2006).

In 2010 at AGH 4.8 candidates on one place were present with only four other majors with higher number (the highest – 8.4 candidates on civil engineering) [7]. The data available on the Internet page of Cracow University of Technology also indicate the popularity of the Biomedical Engineering – with 5.92 candidates on one place. It came in third place after Informatics (6.82) and Architecture (6.63) [7].

4. Student profile of the Biomedical Engineering

The candidates to the Biomedical Engineering are mainly non-technical high school graduates. At AGH they constitute almost 100% with 42% graduated from school of biological and chemical sciences and 9% from humanities (data obtain from students surveys). Similarly the situation occurs at the Cracow University of Technology. First year students have no or a little technical and science background while the standards of the Biomedical Engineering focused mainly on them [6]. The subjects of mathematics (with mathematical analysis, linear algebra and numerical methods) statistic, probability theory calculus or electrotechnics are

obligatory (Tab. 3). With most of them a student meet during the first year. It is a heavy load for humanities high school graduates.

Table 3

Basic course requirements: subjects and minimum hours course [6]

No.	Subjects	Minimum hours
1	Mathematics, statistic, probability theory calculus	120
2	Physics	60
3	Chemistry	60
4	Mechanics and strength of materials	60
5	Materials science	60
6	Electrotechnics and electronics	60

In the Internet forum a lot of interesting comments can be found:

At present I study Biomedical Engineering. How does it look like? Well, I have no life at all. I have finished humanities high school, always was very good pupil. I hoped I would manage my study somehow. After one term I am thinking about leaving it..., my psyche is no go. The biggest nightmare is informatics... [8].

...physics must be known because it is a technical major, mathematics is lectured at very high level. Additionally... mechanics... I don't recommend it for people who are interested in anatomy and biology... It is an IT-mechanical major [8].

5. Science courses for humanities

Technical universities attach importance to mathematical and informatics skills development. In their syllabuses traditional science courses were always essential. However, the methodology should be adjust to the needs of a new type of humanities high school graduates. The same student training effects should be achieved by applying the other methods e.g. simple exercises, projects, working in groups with often repeating a newly acquired knowledge.

Within the framework of informatics classes the Biomedical Engineering students have the access to educational free software. It gives them the opportunity of practicing examples from lectures and laboratories on their own. The informatics course focuses on learning the software tools which are used to efficiently enhanced preparing projects or calculations e.g. on mechanical course. Among these tools Mathcad, Maple and VBA (Visual Basic for Application) can be distinguished. The proper usage of the programs make it easier for students to deal with the other course projects only on the condition of acquiring proficiency in managing the programs. The task demanded from a teacher of humanities high school graduates is to transfer the knowledge about proper use of the programs in as accessible way as possible. During the Languages and Technics of Programming course students are learned to use the VBA environment [1–3].

During the course lectures the introduction theory is presented at the beginning. Next the students obtain some keywords (variable types, data types with their ranges, functions labels and their syntax etc.). The keywords are prepared in the form of the handy instructions. The example of MsgBox function is presented in Figures 1 and 2 (because the classes are held in Polish language the original instruction in this language is presented).

INSTRUCTION MsgBox
Syntax: *MsgBox(prompt[,buttons][,title][, helpfile,context]))*
Example: *a = MsgBox(„Treść w oknie”, vbYesNoCancel, „Tytuł okna”)*
Parameters description: – **prompt** (mandatory) – text is displayed in dialog box 1024 characters – **buttons** (optional) – expression describing number and type of buttons, icon style, default button, – **title** (optional) – text on title bar in case of lack of application name – **helpfile** (optional) – string of characters enabling using of help for window – **context** (optional) – number indicating help topic Number and type of buttons: – vbOKOnly – only button OK – vbOKCancel – button OK and Cancel – vbAbortRetryIgnore – button Abort, Retry and Ignore – vbYesNoCancel – button Yes, No and Cancel – vbYesNo – button Yes, No Style and icons: – vbCritical – vbExclamation – vbInformation – vbQuestion Buttons and icons: – vbDefaultButton1 – active first button – vbDefaultButton2 – active second button – vbDefaultButton3 – active third button – vbDefaultButton4 – active third button

Fig. 1. The handy instruction of the MsgBox function

Rys. 1. Instrukcja MsgBox

The next step during a lecture is realization simple examples common with a teacher. A PC computer with proper software is connected to a slide projector so the students can follow every step of the teacher. The first examples are additionally described in details in the slides – step by step (Fig. 3).

Lastly, the students are encouraged to active discussion about more difficult examples, where the student suggestions are immediately implemented in the program by a teacher and effects are clearly visible. The feedback created this way definitely makes the lecture more interesting and involving.

Fig. 2. The execution of the MsgBox function

Rys. 2. Styl ikony okna da instrukcji MsgBox

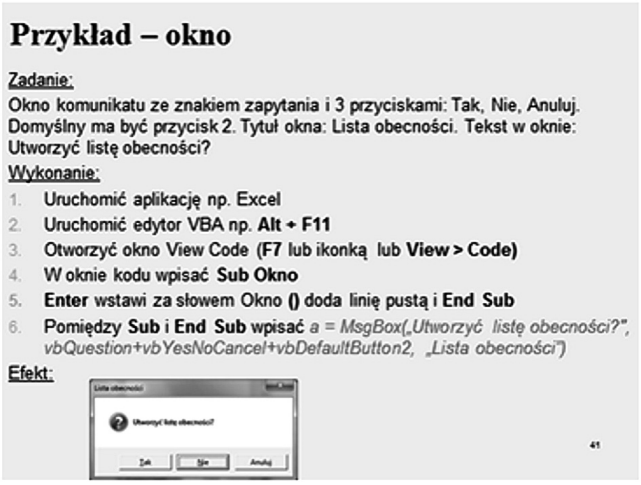

Fig. 3. The example described in details – step by step

Rys. 3. Przykład ćwiczenia z podanym schematem rozwiązania

On the other hand during project classes students work alone on the prepared tasks. However, the first steps in implementing a programming code are also presented by a teacher through a slide projector and followed by students. The fact that human beings learn mostly by eyesight increases the efficiency of the process.

6. Conclusions

One of the article co-author also graduated from a high school of biological and chemical sciences and on its own experience knows how much effort and strain required studying during the first years at the technical university. It is clear that for "non-technical" people a first contact with science courses is very demanding. In technical university syllabuses traditional science courses focus on advance mathematics and physics as well as on trade

courses as mechanics, electronics etc. are obligatory. For technic and science high school graduates the first contact is much easier because they know already the basis.

The knowledge may be transferred on many ways but the most important factor is to be accessible and comprehendible. The education success is not measured by a satisfaction of a teacher but by a satisfaction of students. It is especially true in the case of the Biomedical Engineering students who should after classes believe that studying it is not beyond their capabilities. The author's purpose was to present the proven example of such teaching.

References

[1] Walkenbach J., *Excel 2007 Bible*, ISBN-10: 0470044039/ISBN-13: 978-0470044032/Edition: PAP/CDR. 2007.

[2] Willett E.C., Cummings S., *Wiley & Sons, Incorporated, John*, Wiley & Sons, Incorporated, John 1392 pages. 2001.

[3] Łoś M., *MS Office 2000 i 2002/XP. Tworzenie własnych aplikacji w VBA*, Helion, Gliwice 2003.

[4] Department of Control and Supervision of Polish Ministry of Science and Education (http: //www.nauka.gov.pl/fileadmin/userupload/szkolnictwo/Dane statystyczne o szkolnictwie wyzszym /20220104/Wyniki rekrutacji 2010.pdf).

[5] Cracow University of Technology: 2010/2011 recritment: 2010/2011 (http://www.pk.edu.pl/ rekrutacja/index.php?option=com_content&task=view&id=178&Itemid=234).

[6] The standards of the Biomedical Engineering (http://www.nauka.gov.pl/fileadmin/user upload/16/19/16197/inzynieria biomedyczna.pdf).

[7] Zadroga A., *Oblężenie kierunków technicznych na uczelniach*, Gazeta Wyborcza 19.7.2010.

[8] The students Internet forum (http://www.uczelnie.info.pl/index.php?mod=kierunki_studiow &id=74).

TECHNICAL TRANSACTIONS | **CZASOPISMO TECHNICZNE**
MECHANICS | MECHANIKA
1-M/2013

JOANNA FABIŚ-DOMAGAŁA*

APPLICATION OF FMEA MATRIX FOR PREDICTION OF POTENTIAL FAILURES IN HYDRAULIC CYLINDER

ZASTOSOWANIE MACIERZOWEJ ANALIZY FMEA DO PRZEWIDYWANIA POTENCJALNYCH WAD SIŁOWNIKA HYDRAULICZNEGO

A b s t r a c t

This paper presents Failure Mode and Effects Analysis using relations diagrams and matrices similarity method application on the hydraulic cylinder. Functions for each hydraulic cylinder components were identified as well as a pairs for interacting components. Also potential failures were defined. Using the principle of matrices similarity the rank of hydraulic component due to performed functions has been prepared.

Keywords: *FMEA*, *analysis*, *failure*, *hydraulic cylinder*

S t r e s z c z e n i e

W artykule zaprezentowano analizę przyczyn i skutków powstawania potencjalnych wad (FMEA), dla siłownika hydraulicznego, stosując diagramy zależności oraz metodę podobieństwa macierzy. Określono funkcje dla poszczególnych elementów siłownika. Zidentyfikowano zależności zachodzące pomiędzy parami współdziałających elementów oraz ich potencjalne wady. Korzystając z zasady podobieństwa macierzy, dokonano uszeregowania elementów siłownika ze względu na realizowane funkcje.

Słowa kluczowe: *FMEA*, *analiza*, *wada*, *siłownik hydrauliczny*

* MSc. Joanna Fabiś-Domagała, Institute of Applied Informatics, Mechanical Department, Cracow University of Technology.

List of symbols

c – component of hydraulic cylinder
C – a set of hydraulic cylinder components
e – function of interacting pair
p – pairs of interacting components of hydraulic cylinder
P – a set of interacting components of hydraulic cylinder
f – failure
$\mathbf{EP}$ – matrix function-pair
$\mathbf{PF}$ – matrix pair-failure
$\mathbf{EF}$ – matrix function-failure
$\overline{\mathbf{EP}}$ – matrix function-pair created with normalized vectors
$\mathbf{EP}^T$ – transposed matrix function-pair
$\lambda_{\mathbf{PE}}$ – similarity matrix pair-function

1. Intruduction

Over the last twenty years, the drive and hydraulic control are used in many industrial branches. Among them it can be distinguished the construction industry, mining, agriculture, and aerospace, military and automotive industries. In working machinery drive systems are commonly used hydraulic cylinders that are exposed to external environment factors such as: polluted air, variable temperature and dynamic loads. Although the hydraulic cylinders belong to a group of devices with relatively uncomplicated structure are susceptible to damage and failure. Identification of defects in the early stages of its formation allows to undertake an appropriate actions and preventive measures to eliminate. Ignorance of the possible defects negatively affects the work performed by systems equipped with hydraulic cylinders. This may lead to the system malfunctioning or cause oil leaks to the environment and even a risk to use. Therefore, the methods to detect potential faults and their causes are still developed. The advantages and benefits of using qualitative methods are increasingly being noticed. One of methods that allow for the early identification of possible defects is FMEA.

The paper presents a matrix FMEA analysis to identify potential defects in the hydraulic cylinder using the method of the similarity matrix.

2. The object of investigation

The object of the research is the double action hydraulic cylinder with swivel bearing [1]. The structure of the cylinder is shown in Figure 1, where: 1 – cylinder body, 2 – piston rod, 3 – gland, 4 – piston sleeve, 5 – nut, 6 – self aligned bearing, 7 – cylinder end with self aligned bearing, 8 – piston seal, 9, 11, 12 – sealing ring, 10 – wiper ring, 13 – guide ring.

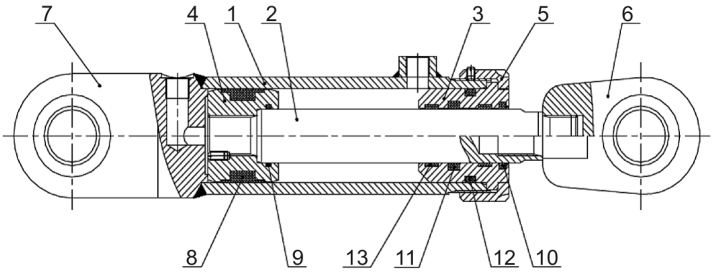

Fig. 1. Scheme of hydraulic cylinder

Rys. 1. Postać konstrukcyjna siłownika hydraulicznego

3. Input data to FMEA analysis

In order to analyze FMEA in the actuator design distinguishes ten elements (c), which may affect its improper operation. These are: cylinder body(c_1), piston sleeve (c_2), piston rod (c_3), sealing ring (c_4), piston seal (c_5), wiper ring (c_6), ring (c_7), gland (c_8) nut (c_9) and self aligned bearing (c_{10}). Among the distinguished components occurring relations that have an influence on the work of the hydraulic cylinder. Figure 2 shows a graph of dependencies that exist between the interacting components (Fig. 2).

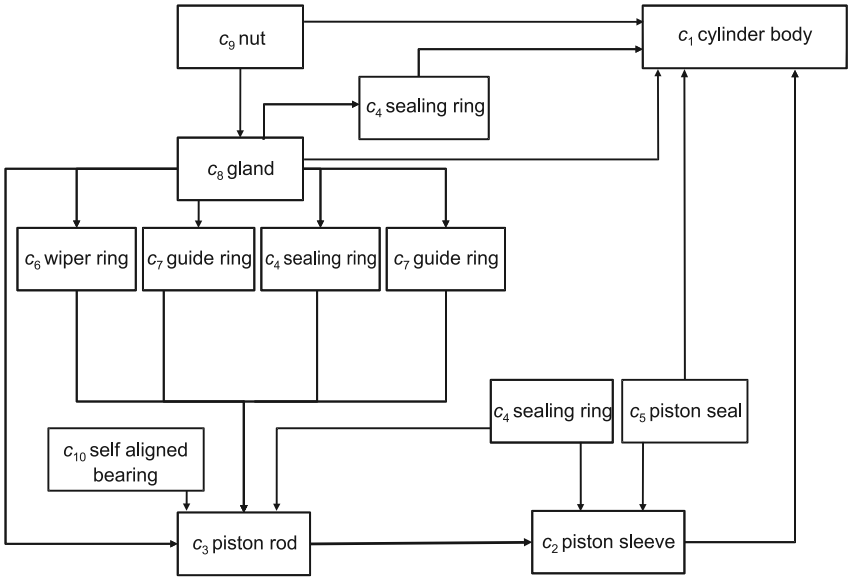

Fig. 2. Graph of relations between the interacting elements of hydraulic cylinder

Rys. 2. Graf relacji zachodzących pomiędzy współdziałającymi elementami siłownika

Using decomposition of the hydraulic cylinder and the relationship graph a seventeen pairs have been identified of interacting components. These are the following: p_1 (c_1–c_2), p_2 (c_1–c_4), p_3 (c_1–c_5), p_4 (c_1–c_8), p_5 (c_1–c_9), p_6 (c_2–c_3), p_7 (c_2–c_4), p_8 (c_2–c_5), p_9 (c_3–c_4), p_{10} (c_3–c_6), p_{11} (c_3–c_7), p_{12} (c_3–c_8), p_{13} (c_3–c_{10}), p_{14} (c_4–c_8), p_{15} (c_6–c_8), p_{16} (c_7–c_8), p_{17} (c_8–c_9). The relationships between a set of hydraulic cylinder components (C) and a set of interacting pairs (P) can be determined by relation occurring between the interacting components of the hydraulic cylinder:

$$C \subset P \tag{1}$$

For all pairs from a set P functions (e) have been specified that realizing in the hydraulic cylinder. Four functions have been identified:

- Fixing (e_1) – the correct position of the hydraulic cylinder components,
- Converting (e_2) – converting fluid pressure energy into mechanical motion straight-back, the main function of hydraulic cylinder,
- Preventing (e_3) – prevents against of dust, dirt, grains of sand, removes impurities,
- Protecting (e_4) – preventing oil leakage, seal cylinder, piston and piston rod guided in the cylinder, the lateral loads and vibration resistance.

In the next step of analysis based on the identified defects ten failures have been identified (f) for interacting pairs at hydraulic cylinder. These are: abrasive wear (f_1), crevice corrosion (f_2), fretting corrosion (f_3), seizure (f_4), fatigue friction (f_5), pitting (f_6), thermal fatigue (f_7), adhesive wear (f_8),oxidation wear (f_9), buckling (f_{10}).

4. Matrix FMEA analysis

The FMEA analysis includes creating of two diagrams of dependence. The first diagram (Table 1) shows the relationship between the pairs of interacting components (p_j) and realized functions (e_i). For each element of the matrix e_ip_j assigned value of 0 or 1. If a pair does not perform assigned function than value is 0, if the function is realized than the value is 1.

Table 1

Diagram of the relationship between functions and pairs (EP)

	p_1	p_2	p_3	p_4	p_5	p_6	p_7	p_8	p_9	p_{10}	p_{11}	p_{12}	p_{13}	p_{14}	p_{15}	p_{16}	p_{17}
e_1	1	0	0	0	1	0	0	0	0	0	0	0	1	0	0	0	1
e_2	0	0	0	0	0	1	0	0	0	0	0	0	0	0	0	0	0
e_3	0	0	0	0	0	0	0	0	0	1	0	0	0	0	1	0	0
e_4	0	1	1	1	0	0	1	1	1	0	1	1	0	1	1	1	0

The resulting graph is size [4×17], and contains 68 elements. A value of 0 has 50 elements of the matrix.

The second diagram of dependencies (Table 2) shows the relationships between interacting components (p_i) and their potential failures (f_j) defined in Chapter 2. For each pair of matrix

pf_j a value of 0 or 1 have been assigned. A value of 0 is assigned if the defect does not occur for the pair. The value of 1 if the defect occurs. The resulting matrix PF has dimensions [17×10] and has 170 elements. Over 100 elements of the matrix has a value of 0 Fragment of PF matrix [10×10] is shown below.

Table 2

Diagram of the relationship between the pair and their potential disadvantages (PF)

	f_1	f_2	f_3	f_4	f_5	f_6	f_7	f_8	f_9	f_{10}
p_1	1	0	1	1	0	1	1	1	1	0
p_2	1	0	0	1	0	0	0	0	0	0
p_3	1	0	0	0	0	0	0	0	0	0
p_4	1	0	0	1	1	0	0	0	0	0
p_5	1	1	0	0	0	0	0	0	0	0
p_6	1	1	0	0	1	1	0	0	0	0
p_7	1	0	0	1	0	0	0	1	1	0
p_8	1	0	0	0	0	0	0	0	0	0
p_9	1	0	0	1	0	0	0	0	0	0
p_{10}	1	1	0	0	0	0	0	0	0	0

In the last stage of matrix FMEA analysis, on the basis of diagrams **EP** and **PF**, using the principle of multiplication of the matrix:

$$\mathbf{EP}\ x\mathbf{PF} = \mathbf{EF} \tag{2}$$

a diagram showing the probability of failures (f) has been built, for pairs of interacting components (p) due to the function (e) performed by the pair in the hydraulic cylinder [2]. Table 3 shows the probability of occurrence of failures in the range of 0 to 11. Value 11 indicates the highest probability of failure for a given function.

Table 3

Diagram function – defect (EF)

	f_1	f_2	f_3	f_4	f_5	f_6	f_7	f_8	f_9	f_{10}
e_1	4	3	1	2	0	1	1	1	1	1
e_2	1	1	0	0	1	1	0	0	0	0
e_3	2	2	0	1	0	0	0	0	0	0
e_4	11	3	1	9	2	0	1	1	1	0

For investigated hydraulic cylinder the highest probability is for failure abrasive wear (f_1) for pairs of realizing the protecting function (e_4). These are the following pairs: p_2, p_3,

p_4, p_7, p_8, p_9, p_{11}, p_{12}, p_{14}, p_{15} and p_{16}. FMEA analysis result for abrasive wear is presented in Figure 3, where the x-axis represents function of pairs while the y-axis represents the value of the analyzed failure.

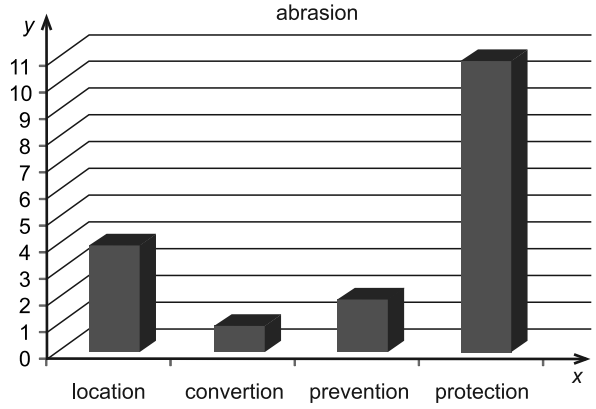

Fig. 3. Result of FMEA analysis for abrasion failure

Rys. 3. Wynik analizy FMEA dla wady zużycie ścierne

5. Application of the similarity matrix FMEA

Using the method of similarity (λ) presented in [3] it can be searched and grouped pairs of hydraulic cylinder components due to the realized functions (same or similar). These data can be used to make changes to the existing cylinder, or at the development of a new solution.

Similarity matrix $\boldsymbol{\lambda}_{\mathbf{PE}}$ (pair – component) is obtained by multiplying the transposed matrix function – pair ($\mathbf{EP}^T$) by a matrix function – pair ($\mathbf{EP}$). This matrix $\boldsymbol{\lambda}_{\mathbf{PE}}$ is a symmetric matrix described by the equation:

$$\overline{\mathbf{EP}^T} x \overline{\mathbf{EP}} = \boldsymbol{\lambda}_{\mathbf{PE}} \tag{3}$$

Matrix $\overline{\mathbf{EP}}$ is a transformed matrix $\mathbf{EP}$ described in Chapter 2. It was built with normalized vectors of a matrix – a pair (Table 4). Normalization was carried out against the columns of the matrix $\mathbf{EP}_P$.

Tabela 4

Matrix built from normalized vectors ($\overline{\mathbf{EP}}$)

	p_1	p_2	p_3	p_4	p_5	p_6	p_7	p_8	p_9	p_{10}	p_{11}	p_{12}	p_{13}	p_{14}	p_{15}	p_{16}	p_{17}
e_1	1.0	0.0	0.0	0.0	1.0	0.0	0.0	0.0	0.0	0.0	0.0	0.0	1.0	0.0	0.0	0.0	1.0
e_2	0.0	0.0	0.0	0.0	0.0	1.0	0.0	0.0	0.0	0.0	0.0	0.0	0.0	0.0	0.0	0.0	0.0
e_3	0.0	0.0	0.0	0.0	0.0	0.0	0.0	0.0	0.0	1.0	0.0	0.0	0.0	0.0	0.7	0.0	0.0
e_4	0.0	1.0	1.0	1.0	0.0	0.0	1.0	1.0	1.0	0.0	1.0	1.0	0.0	1.0	0.7	1.0	0.0

Using Equation 3, the similarity matrix $\boldsymbol{\lambda}_{PE}$ has been created. The resulting matrix with dimensions [17×17] is presented in Table 5.

Table 5

Similarity matrix pair – function ($\boldsymbol{\lambda}_{PE}$)

	p_1	p_2	p_3	p_4	p_5	p_6	p_7	p_8	p_9	p_{10}	p_{11}	p_{12}	p_{13}	p_{14}	p_{15}	p_{16}	p_{17}
p_1	×	0.0	0.0	0.0	1.0	0.0	0.0	0.0	0.0	0.0	0.0	0.0	1.0	0.0	0.0	0.0	1.0
p_2	0.0	×	1.0	1.0	0.0	0.0	1.0	1.0	1.0	0.0	1.0	1.0	0.0	1.0	0.7	1.0	0.0
p_3	0.0	1.0	×	1.0	0.0	0.0	1.0	1.0	1.0	0.0	1.0	1.0	0.0	1.0	0.7	1.0	0.0
p_4	0.0	1.0	1.0	×	0.0	0.0	1.0	1.0	1.0	0.0	1.0	1.0	0.0	1.0	0.7	1.0	0.0
p_5	1.0	0.0	0.0	0.0	×	0.0	0.0	0.0	0.0	0.0	0.0	0.0	1.0	0.0	0.0	0.0	1.0
p_6	0.0	0.0	0.0	0.0	0.0	×	0.0	0.0	0.0	0.0	0.0	0.0	0.0	0.0	0.0	0.0	0.0
p_7	0.0	1.0	1.0	1.0	0.0	0.0	×	1.0	1.0	0.0	1.0	1.0	0.0	1.0	0.7	1.0	0.0
p_8	0.0	1.0	1.0	1.0	0.0	0.0	1.0	×	1.0	0.0	1.0	1.0	0.0	1.0	0.7	1.0	0.0
p_9	0.0	1.0	1.0	1.0	0.0	0.0	1.0	1.0	×	0.0	1.0	1.0	0.0	1.0	0.7	1.0	0.0
p_{10}	0.0	0.0	0.0	0.0	0.0	0.0	0.0	0.0	0.0	×	0.0	0.0	0.0	0.0	0.7	0.0	0.0
p_{11}	0.0	1.0	1.0	1.0	0.0	0.0	1.0	1.0	1.0	0.0	×	1.0	0.0	1.0	0.7	1.0	0.0
p_{12}	0.0	1.0	1.0	1.0	0.0	0.0	1.0	1.0	1.0	0.0	1.0	×	0.0	1.0	0.7	1.0	0.0
p_{13}	1.0	0.0	0.0	0.0	1.0	0.0	0.0	0.0	0.0	0.0	0.0	0.0	×	0.0	0.0	0.0	1.0
p_{14}	0.0	1.0	1.0	1.0	0.0	0.0	1.0	1.0	1.0	0.0	1.0	1.0	0.0	×	0.7	1.0	0.0
p_{15}	0.0	0.7	0.7	0.7	0.0	0.0	0.7	0.7	0.7	0.7	0.7	0.7	0.0	0.7	×	0.7	0.0
p_{16}	0.0	1.0	1.0	1.0	0.0	0.0	1.0	1.0	1.0	0.0	1.0	1.0	0.0	1.0	0.7	×	0.0
p_{17}	1.0	0.0	0.0	0.0	1.0	0.0	0.0	0.0	0.0	0.0	0.0	0.0	1.0	0.0	0.0	0.0	×

PE similarity matrix $\boldsymbol{\lambda}_{PE}$ has values in the range 0.0 to 1.0 Each element of the matrix $\boldsymbol{\lambda}_{PEij}$ represents the similarity between pairs of components *i* and *j*. Value of 1.0 indicates the total similarity (realization of the same function) and 0.0 lack of common functions. The values on the diagonal of the matrix ($i = j$) are x (the relationship that occurs between the same pairs). Based on the PE matrix λ_{PE} a pairs of components has been grouped depending on the performed functions (Table 6).

Table 6

Grouped pairs depending on performed functions

Level	Group	Function	Pair	The similarity of the realized functions
I	1	protecting	cylinder – sealing ring	$p_3, p_4, p_7, p_8, p_9, p_{11}, p_{12}, p_{14}, p_{16}$
	2	fixing	cylinder – piston sleeve	p_5, p_{13}, p_{17}
II	3	converting	sleeve piston – psiton rod	–
	4	preventing	piston rod – wiper ring	–
		preventing	gland – wiper ring	–

Pairs were classified in two levels and four groups. To the first level belongs the first and the second group of pairs which perform the same or similar functions. These pairs are perform fixing function (including 4 pairs) and protecting function (including 10 pairs). The second level is the third and the fourth group of pairs which do not have equivalents (pairs that correspond to the carried out functions). These are the pairs which perform the converting and preventing functions.

Similarity matrix pair – function calculated for each component provides information about the possible modifications of components. It also allows to find and rank the components that perform similar functions.

6. Conclusions

The paper presents the method of similarity matrix FMEA to identify potential failures in the hydraulic cylinder. A set of pairs of interacting components (p) has been identified, for which the potential failures (f) and function (e) was determined. The using of matrices transformation allowed to obtain diagram of function-failure and detect the failure with highest probability of occurrence. Relation between failures and functions has been presented in the diagram function-failure. By the using of matrices similarity a pairs of hydraulic cylinder which perform the same functions have been classified. The calculation on matrices were performed in Mathcad software.

References

[1] Bipromasz, *Materiały informacyjne*.
[2] Stone R.B., Tumer Y., VanWie M., *The Function-Failure Design Method*, Journal of Mechanical Design, 127(3), 2005, 397-407.
[3] Roberts R.A., Stone R.B., Tumer Y., *Deriving function-failure similarity information for failure--free rotorcraft component design Method*, In ASME Design for Manufacturing Conference, 2002.
[4] Kotnis G., *Budowa i eksploatacja układów hydraulicznych w maszynach*, Wydawnictwo i Handel Książkami „KaBe", Krosno 2011.
[5] Parker Hydraulics, *Hydraulic Cylinder Troubleshooting*, Bulletin 1242/1-GB.

TECHNICAL TRANSACTIONS | **CZASOPISMO TECHNICZNE**
MECHANICS | MECHANIKA
1-M/2013

GRZEGORZ FILO*

COMPUTER MONITORING AND CONTROL SYSTEM OF A LOCAL LNG SUPPLY STATION

KOMPUTEROWY SYSTEM MONITORINGU I STEROWANIA LOKALNEJ STACJI ZASILANIA LNG

A b s t r a c t

This paper presents a proposal of computer system to support the work of local LNG supply station. The main advantages of proposed system are to increase safety and reduce the operating costs of the station. On the basis of preliminary analysis the main functional modules of the system have been distinguished. The modules include: vaporization control unit, subsystem for monitoring parameters in the cryogenic tank and installation, central database server, data visualization module, diagnostic subsystem and module for LNG supplies optimization. The system has been used for investigating a real supply station.

Keywords: *LNG*, *monitoring*, *internet application*, *software development*

S t r e s z c z e n i e

W artykule przedstawiono propozycję systemu komputerowego wspomagającego pracę lokalnej stacji zasilania LNG. Do głównych zalet wprowadzenia systemu należą zwiększenie bezpieczeństwa oraz zmniejszenie kosztów użytkowania stacji LNG. Na podstawie przeprowadzonej wstępnej analizy wyróżniono główne moduły funkcjonalne: moduł sterowania procesem parowania LNG, podsystem monitoringu parametrów w zbiorniku kriogenicznym i instalacji, centralny serwer bazy danych, moduł wizualizacji danych pomiarowych, system diagnostyki oraz moduł optymalizacji dostaw surowca. System został wykorzystany do przeprowadzenia badań rzeczywistej stacji zasilania LNG.

Słowa kluczowe: *LNG*, *monitoring*, *aplikacja internetowa*, *budowa oprogramowania*

* PhD. Grzegorz Filo, Institute of Applied Informatics, Faculty of Mechanical Engineering, Cracow University of Technology.

Denotations

t – time [s]
q, q_1, q_2 – LNG evaporation rate [kg/(m^2 s)]
k, k_1, k_2 – coefficient of evaporation [J/(m s K)]
T_s, T_1 – ambient temperature, LNG temperature [K]
ρ, ρ_1 – density [kg/m3]
ΔH_V – latent heat of evaporation [J/kg]
c_p – specific heat capacity [J/(kg K)]
α, α_s – heat dissipation factor [J/(m2 s)]
β – coefficient of cubical expansion [1/K]
ν – kinematic viscosity [m2/s]

1. Introduction

A typical LNG supply station consists of a tank where a natural gas is stored in a liquefied form. Maintenance of the gas requires temperature of minus 160 degrees Celsius, so the tank must have a construction, which minimizes heat leakage [9, 10]. Total elimination of the leakage is not possible, therefore inside of the cryogenic tank there is a liquid phase and a certain amount of a gas phase, resulting in the evaporation process [3, 4]. At low gas consumption, amount of the gas phase may be sufficient to supply the appliances. If gas consumption is higher, it is necessary to use an appropriate system of vaporizers. This approach allows to manage resource rationally, however, requires the use of two independent transmission systems with an adequate switching mechanism [2]. This mechanism can be implemented by means of automatic control, provided that the current values of parameters such as pressures, temperatures, flow rates are known. Therefore, the control system must be connected with the monitoring system. Authorized personnel of the supply station should have permanent access to the current values of the parameters using a PC computer or a mobile device with Internet access. Furthermore, the personnel must be immediately informed in case of any emergency or unusual situation. This requires access to a relational database which holds data from sensors [7]. These data will also help to optimize delivery of LNG on the basis of consumption rate in the previous time period.

Analysis of presented requirements has led to the development of a computer system that will increase safety and improve the work of a local LNG supply station.

2. Models of LNG evaporation process

Operation of a local LNG supply station is based on the LNG evaporation process. Study of LNG vaporization were carried out by many academic, research and industrial centers, among others by Kelly-Zion, Pursell, Booth and VanTilburg [8], the American Gas Association, Drake and Reid [5], Opschoor [11], Bryson [2]. On the basis of evaporation of liquid methane Zabetakis and Burgess developed a model which describes an evaporation

rate at the initial stage of the process [12]. They found that the rate is limited by the supply of heat from the environment and is given by the formula:

$$q = \frac{k}{\rho_1 \cdot \Delta H_V} \frac{T_s - T_1}{(\pi \alpha_s t)^{1/2}} \tag{1}$$

This formula is applicable only in the initial stage of evaporation, not exceeding the time of one minute after the start of the process. Double logarithmic plot of evaporation rate against time has the form similar to a straight line. LNG evaporation process has been particularly thoroughly studied by Drake and Reid [5]. They conducted a series of experiments in relation to the results obtained by the American Gas Association and Gaz de France. They demonstrated the following formula:

$$q = A_V \cdot t^{-1/2}$$

where the evaporation coefficient A_v should be determined experimentally. V.J. Clancey [6] also developed a model describing the evaporation of cryogenic liquid such as LNG. Rapid evaporation in the initial period of time has been described using the following formula (k_1 and k_2 coefficients are determined experimentally):

$$q_1 = \frac{k_1 \cdot (T_s - T_1)^2}{\Delta H_V} \tag{3}$$

while in the steady phase:

$$q_2 = \frac{k_2 \cdot (T_s - T_1)}{\Delta H_V} \tag{4}$$

Rate of the LNG evaporation process was studied by S. J. Turner. Based on the results of his research G. Opschoor formulated the following mathematical formula [6, 11]:

$$q = 0.085 \cdot k \cdot \left(\frac{g \cdot \beta \cdot \Delta T^4}{\alpha \cdot \nu} \right)^{1/2} \tag{5}$$

For the LNG, on the basis of the above equation, the following heat flux value can be obtained: $q = 2.3 \cdot 10^4$ [W/(m^{2}s)], what leads to the mass of the evaporating LNG: $m = 0.045$ [kg/(m^{2}s)]. Presented Opschoor's model was used in the development process of the LNG vaporization control unit.

3. Concept of a control and monitoring system

A typical LNG supply station contains the following components: a cryogenic tank for storing LNG, a vaporizing installation, transmission system with safety valves and installation of pressure reduction. First step of the analysis was to identify measurement points. The distinguished points are presented in Fig. 1.

As can be seen from Fig. 1, the following parameters of the LNG supply station will be subject to monitoring: P1 – LNG vapor pressure inside the cryogenic tank, VG1 – vacuum level between walls of cryogenic tank, T1, T2, T3, T4 – temperatures, respectively: at the

outlet from the tank, before and after the pressure built unit (PBU), ambient temperature, F1 – loss of LNG through the safety valve, F2 and F3 – mass flow before and after the pressure built unit (PBU), F4 – LNG consumption.

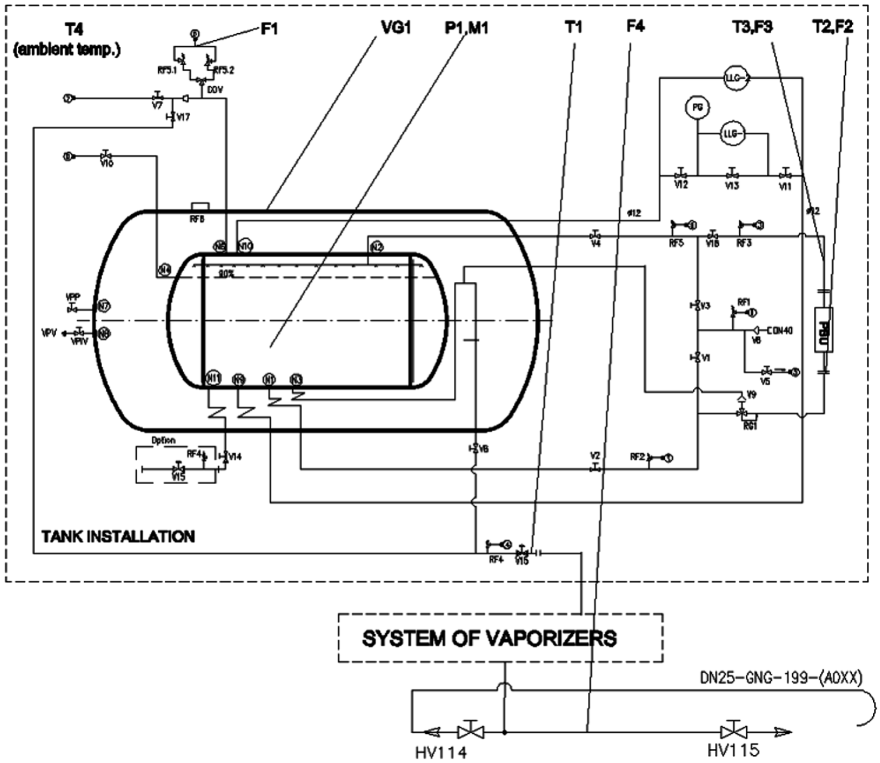

Fig. 1. Installation of a local LNG supply station with measurement points

Rys. 1. Instalacja lokalnej stacji zasilania LNG z punktami pomiarowymi

3.1. System requirements and main functionalities

Some prerequisites were taken into account at the start point of the system development. Due to the diversity of functionalities, it was decided to decompose system into modules. Individual modules have the form of desktop applications or applications running under internet browsers. Desktop applications run in Microsoft Windows system, while the internet applications are available for browsers on any operating system, including mobile devices, smartphones, tablets, PDA etc. Application for acquiring the measurement data supports typical DAQ Advantech cards. The measurement data is stored in a relational client server database Firebird.

The system should allow to acquire data from the transducers and store in a database for later processing and analysis as well as allow to control selected systems of the installation remotely by authorized personnel. The user should be able to observe time courses of

selected parameters in both numerical and graphical form. Secure remote access to data via the internet should be provided. The operator should have an access to messaging and alerting system including short text messages (SMS) and e-mails. The system should allow to optimize delivery of the LNG to the local supply station on the basis of the real-time consumption analysis.

3.2. Deployment diagram of the system

On the basis of the analysis, the following components of the system have been extracted: monitoring subsystem, relational database server, visualization and diagnostic module, control module and subsystem of the LNG delivery optimization. Fig. 2 presents relations and dependencies between individual components.

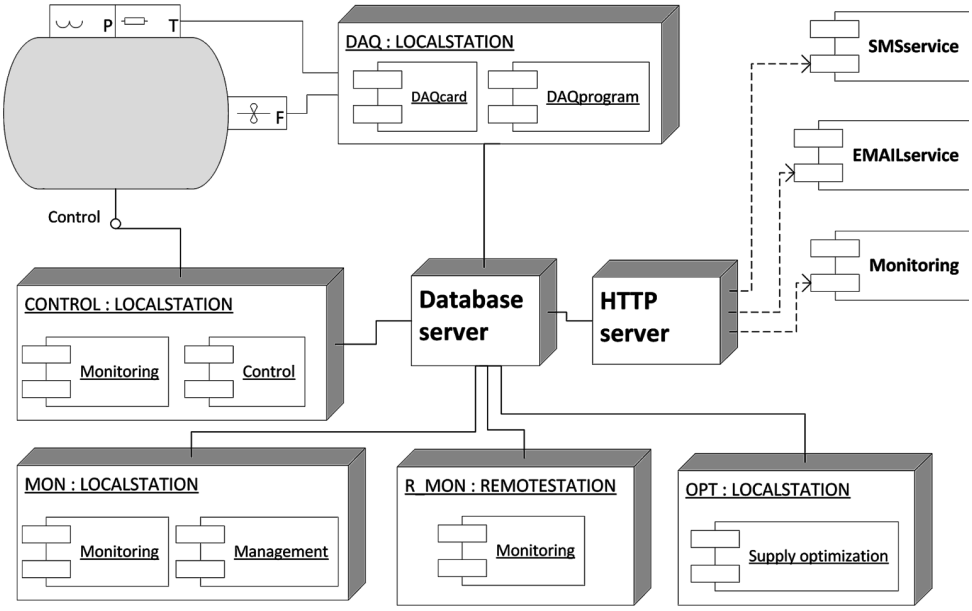

Fig. 2. Deployment diagram of the system

Rys. 2. Diagram wdrożenia systemu

As arises from Fig. 2, the monitoring subsystem includes sensors and transducers, DAQ card and a program for data acquisition implemented in a local station DAQ. Programs for management of monitoring parameters (i.e. frequency of readings from the transducers, measuring ranges, scaling parameters of the signals [1]) are implemented in local station MON. Relational database server is a central element of the system, almost all other components are connected with it. Visualization and diagnostics module can be used locally by a desktop application (local station MON) or remotely, using internet browsers (remote station R_MON*)*. Remote diagnosis includes sending messages, warning and alerts via SMS and e-mail. The control unit, for safety reasons, may be used only by authorized personnel

on local computer CONTROL. The optimal schedule for the LNG delivery is determined by a separate application which is installed locally on the OPT station.

4. Implementation and presentation of the monitoring subsystem

As a practical example of system implementation, a monitoring subsystem will be presented. Hardware diagram of the subsystem is presented in Fig. 3.

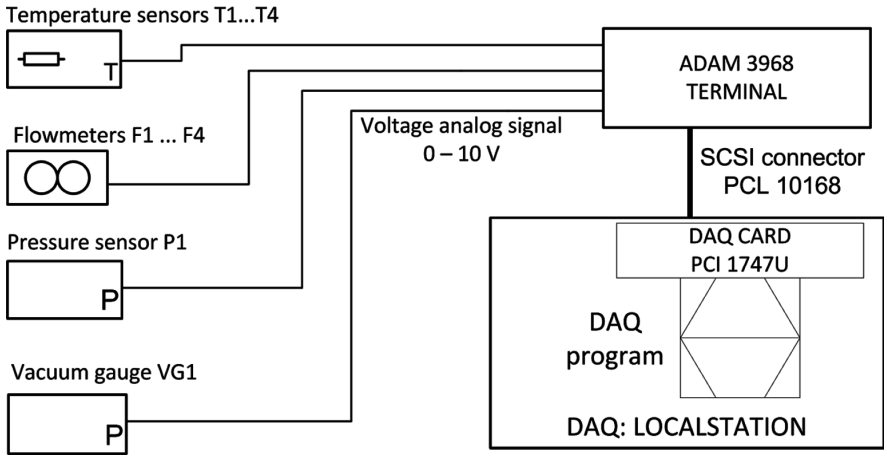

Fig. 3. Diagram of the measurement system in the monitoring module

Rys. 3. Schemat układu pomiarowego w module monitoringu

Proposed measurement system includes sensors with analog signals and a DAQ card with the A/D converters [1]. A standard SCSI connector is used for communication between the DAQ card and ADAM-3937 terminal. A DAQ program allows to acquire data and present it in a graphical form. The program was developed using C# language.

Main functionalities of the program available to a user are presented in the UML use case diagram in Fig. 4. The diagram shows the three main use cases available to the user of the program: configuring program parameters (*Config*), performing the measurement (*Measurement*) and the presenting values of the most recent measurements (*On-line presentation*). The configuration is done using the input and output settings (*I/O settings*) as paths, initialization files, output file formats, location and access parameters to the database. The configuration process also may include settings of the data acquisition card (*DAQ config*) as well as settings of the measurement channels (*Channel calibration*). Each measurement channel has an individual range, a gain coefficient and a zero-point value (*Channel calibration*). Use cases *DAQ config* and *Measurement* utilize the Advantech API interface. Furthermore, the *Measurement* uses a database connection interface. Results of the most recent measurements can be presented in a numerical format (*Numerical*) or as a function against time (*Graphical*).

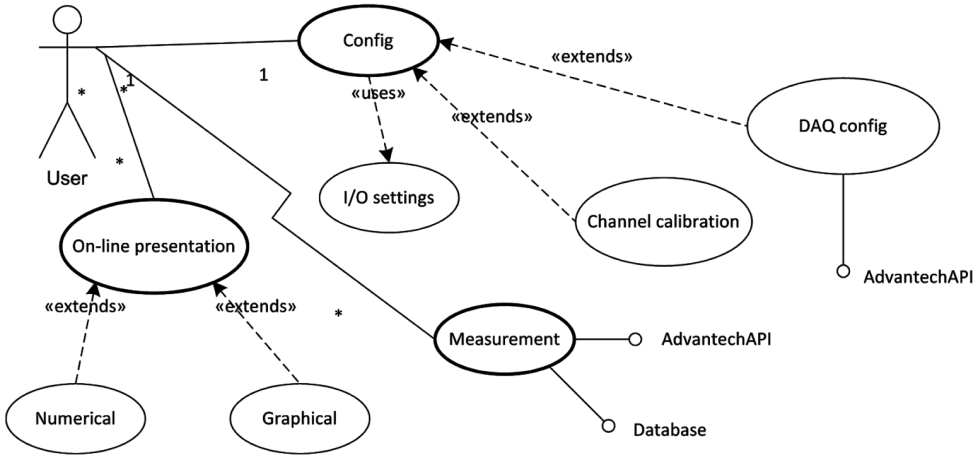

Fig. 4. Functionalities of the monitoring subsystem in the use-case diagram

Rys. 4. Funkcjonalności podsystemu monitoringu na diagramie przypadków użycia

The data acquired by the monitoring subsystem and stored in the database can be used to create plots against time of selected parameters. In Fig. 5 is presented example time chart of a pressure inside the cryogenic tank obtained during experiments.

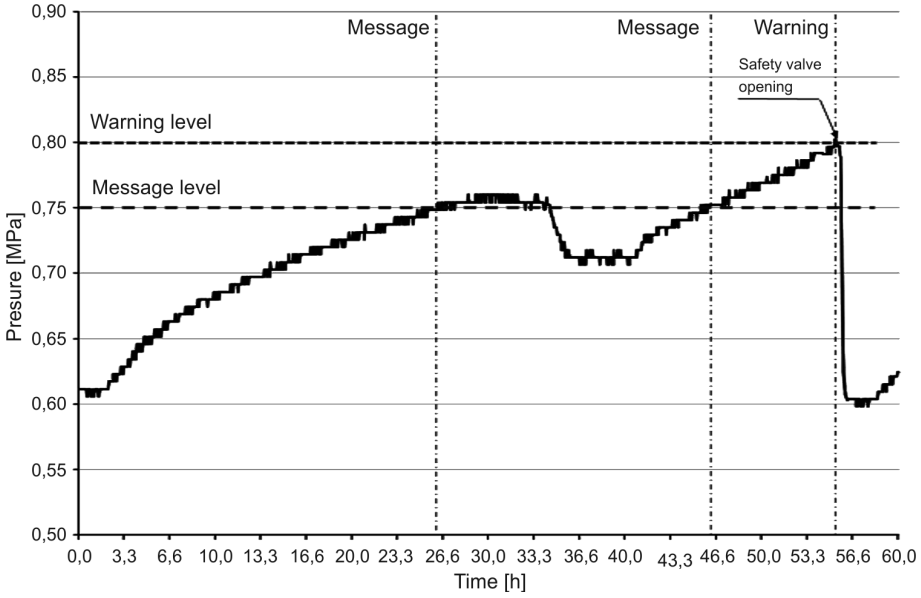

Fig. 5. Time chart of the pressure with times to send messages and warnings

Rys. 5. Przebieg ciśnienia z zaznaczonymi momentami wysyłania wiadomości i ostrzeżeń

In presented time period value of the pressure was rising from 0.61 MPa to 0.76 MPa during first 27 hours and then stabilized. At time 35.0 it started to decrease due to the increased consumption. From time 41.0 it raised again and reached the message level at time 34.0 and then warning level at time 55.5. Then the safety valve was opened, what resulted in rapid pressure drop to the value 0.6 MPa. It can be observed from the figure, that one warning and two messages were sent to the operator. The appropriate algorithm avoids sending messages when value of the pressure decreases (time points 34.0 and 56.1).

5. Conclusions

Presented system of control and monitoring of a local LNG supply station allows to significantly improve safety and reduce operational costs. The system is complex and extensive, includes several modules designed for different purposes, i.e. control, monitoring, visualization, optimization, messaging, alerting. In terms of practical applications, the monitoring subsystem was used in Chemet company for testing new generation of cryogenic tanks. Next, it is planned to implement the system in local LNG supply station in Bukowina Tatrzanska.

References

[1] Alciatore D., *Introduction to Mechatronics and Measurement Systems*, 4th edition, McGraw-Hill, 2011.

[2] Bryson W.E., *Cryogenics*, Hanser Gardner Publications, 1999.

[3] Chorowski M., *Kriogenika. Podstawy i zastosowania*, Masta, Gdańsk 2007.

[4] Czyżycki W., *Heat flow modelling on thermal insulation of cryogenic tanks using SolidWorks simulation package*, Technical Transactions, 4-M/2011/A, Issue 7, Cracow University of Technology, 2011.

[5] Drake E., Reid R., *Analysis of vapour dispersion experiments*, American Gas Association, Report on IS-3-1, ph. 2, Battelle Columbus Laboratories, 1974.

[6] Flynn T.M., *Cryogenic Engineering*, 2nd edition, Dekker 2004.

[7] Halpin T., Morgan T., *Information Modeling and Relational Databases*, 2nd edition, Morgan Kaufmann, 2008.

[8] Kelly-Zion P., Pursell Ch., et al., *Evaporation rates of pure hydrocarbon liquids under the influences of natural convection and diffusion*, International Journal of Heat and Mass Transfer, v. 52, Issues 13-14, Elsevier, 2009.

[9] Lisowski E., Czyżycki W., *Transport and storage of LNG in container tanks*, Journal of KONES Powertrain and Transport, Vol. 18, No. 3, Warsaw 2011.

[10] Łazarczyk-Głowik K., Lisowski E., *Using of SolidWorks system in design and simulation research of cryogenic tanks supports*, Technical Transactions, 4-M/2011/B, Issue 7, Cracow, 2011.

[11] Opschoor I., *Evaporation*, ch. 5 of TNO yellow book, *Methods for Calculation of Physical Effects of Escape of Dangerous Materials*, vol. III, 1978.

[12] Zabetakis M., Burgess D., *Fire and explosion hazards of LNG*, US Bureau of Mines Investigation Report no. 6099, Washington, 1962.

TECHNICAL TRANSACTIONS | **CZASOPISMO TECHNICZNE**
MECHANICS | MECHANIKA
1-M/2013

ADAM GĄSKA*, PIOTR GĄSKA*, MACIEJ GRUZA*

I++ SIMULATOR USED TO SUPPORT WORKING WITH COORDINATE MEASURING MACHINE

ZASTOSOWANIE SIMULATORA I++ DO WSPOMAGANIA PRACY NA WSPÓŁRZĘDNOŚCIOWEJ MASZYNIE POMIAROWEJ

A b s t r a c t

This paper presents examples of usage of Coordinate Measuring Machine simulator, which facilitate metrological tasks in laboratory and industrial conditions, and constitute a great convenience in Coordinate Measuring Technique learning process.

Keywords: *CMM*, *simulator*, *coordinate measurement*

S t r e s z c z e n i e

Artykuł przedstawia przykłady zastosowań symulatora Współrzędnościowej Maszyny Pomiarowej, które ułatwiają pracę metrologa w warunkach przemysłowych i laboratoryjnych oraz stanowią duże udogodnienie w procesie nauczania Współrzędnościowej Techniki Pomiarowej.

Słowa kluczowe: *WMP*, *symulator*, *pomiar współrzędnościowy*

* PhD. Eng. Adam Gąska, MSc. Eng. Piotr Gąska, MSc. Eng. Maciej Gruza, Laboratory of Coordinate Metrology, Department of Mechanical Engineering, Cracow University of Technology.

1. Introduction

The development of multimedia technology brings many benefits for both science and industry. Today, one cannot imagine, creating technical documentation using a drawing board and a pencil or writing down complex strength analysis with pen in a notebook. It happens for several reasons. Firstly, computer programs perform their tasks much faster than a human, secondly due to them, possibility of making a wrong decision can be avoided or at least limited. A perfect example of how extremely useful software can be are all kinds of simulators. Simulators are, most often, programs whose task is to restore certain phenomena or behavior of objects, using its mathematical model. In aviation an integral part of pilots training are exercises with simulator. Thanks to them pilots can face extreme situations without risking their lives. They can also practice some routine behaviours without generating costs associated with the operation of planes and fuel consumption. In engineering, as an example programs developed by Dessault Systems like Catia and Delmia can be used. Particular modules are responsible for simulating the machining process or production line simulation. Finding the optimal variant is much simpler with them, they also helps to prevent collisions and downtimes. Simulators are used in many other areas as: medicine (surgery simulations) [1], logistics [2], army, mechanical systems [3], production engineering [4]. They are also used in coordinate metrology, which is nowadays important tool in quality control of automated processes. In most of metrological programs it is possible to simulate probe head behaviour and course of the measurement path. Whereas I++ Simulator described in this article enables simulation of operation of whole measuring station based on virtual model of actual coordinate machine.

This paper presents different aspects of working with Coordinate Measuring Machines (CMM) that can be facilitated by usage of CMM simulator. Cases described in this paper are: usage of simulator for CMM programming in different conditions, the didactic use of simulator for CMM operators training and students lessons, usage of simulator combined with CMM accuracy model in order to build the software allowing determination of the best measurement strategy.

2. Coordinate Measuring Technique

In the case of the classical geometrical metrology, typical measuring devices are used to determine dimension of only one type, which in some particular situations could be used to calculate the dimensions of different type (for example, the measured lengths are used to determine the angle). In this way, however, it is difficult to measure object that has a diversified shape, often with complex dimensions. In such cases, each type of dimension should be measured individually, which in turn would lead to increase of the amount of needed tools. It can easily be noted that in a similar situation, automation of any quality control process would be, if not impossible, surely inefficient due to excessive measuring time. Coordinate Measuring Technique (CMT) based on the use of Coordinate Measuring Machines (CMM) has proved to be an excellent solution for this problem. In coordinate measuring technique, data in discrete form are collected from the surface of the measured object, and then they

are the basis for computer determination of dimensions of spatial shaped objects [5]. This technique uses the phenomenon, which for centuries has been used by artists, that is, it reduces the complex shape to the geometric primitives. CMM during the measuring process, locates the coordinates of measuring points and determines the relationship between them. On this basis, geometrical elements constituting the measured object are determined. Software cooperating with the machine, calculates information about the shape of different parts of the object using the collected coordinates (Fig. 1). It is clear that a perfect reconstruction of the measured contour is not possible because it would involve the measurement of an object in an infinite number of points. Therefore, the error of measurement performed on CMM should be understood as the difference between the actual shape of the object, and its substitute representation usually determined using Gauss least squares method. Foregoing errors can be reduced, for example by adopting appropriate measurement strategy (covering the surface of the object by equally distributed measuring points). Coordinate Measuring Technique and the related quality control process automation brings tangible benefits, such as speed and flexibility of measurement tasks.

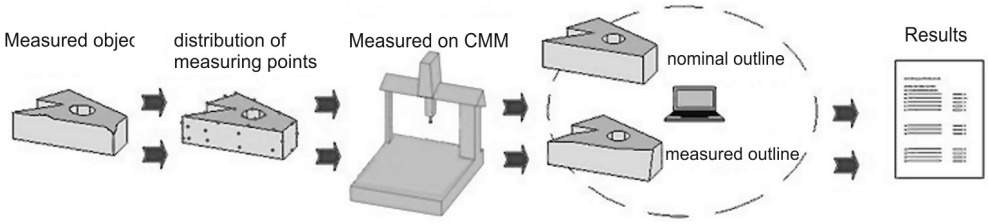

Fig. 1. The essence of coordinate metrology

Rys. 1. Istota metrologii współrzędnościowej

CMM is the most important tool in coordinate measurements. The kinematic pairs shift in mutually perpendicular directions, which determine the Cartesian axes *X*, *Y*, *Z* and define the machine measuring coordinate system. Motion between the measuring points identification system and actual measuring point on the surface of measured element is realized by sliding axle system, which movements are measured by standards of the length, and then the values are transferred to the computer and electronic control units. Gathering of measuring point coordinates is done by probe systems, contact or non-contact. This means that in the first case, the measurement is followed by the contact of the probe head with the measuring object, and in the second case, in different manner, for example using the light beam. There are several main programs which work with CMM. Geometric relationships between elements are calculated in them, they also carry out the transformations and constructions needed to determine the indirect dimensions, form errors, location and runout errors.

3. I++ Simulator used for machine programming and didactic purposes

I++ Working Group was founded in 1999, made up of representatives of various companies in the automotive industry. The main reason for the creation of the group was an attempt to unify metrology software and provide a platform for future cooperation and ideas exchange.

One of the group's achievements was the introduction of the universal protocol I++ DME, through which it is possible to communicate measuring machine with the majority of existing metrological programs. In practice, this protocol is associated with increased flexibility and machine operators independence from dedicated software, which often affords fewer opportunities, or simply is less comfortable. I++ Simulator also uses mentioned protocol making it possible to cooperate with the most common metrological programs (Quindos, PC-DMIS, Calypso, Modus).

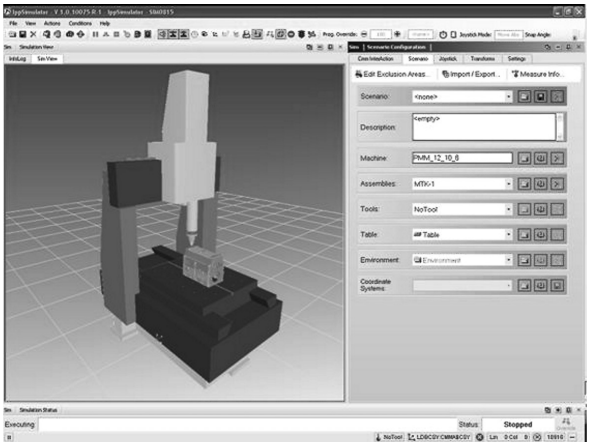

Fig. 2. CMM model loaded into the I++ Simulator

Rys. 2. Model WMP wczytany do programu I++ Simulator

At the beginning of simulation session, models of machine, magazines and probe heads with which the measurement will be carried out, have to be loaded (Fig. 2). Then functions assigned to each button of the gamepad, which is responsible for controlling the machine model, need to be defined. In the next step, the CAD model of the measured part is loaded. After turning on the metrological software, the rest of measurement is proceeded just like on the real machine.

The most convenient way to work with a simulator is using two monitors. One monitor displays the virtual model of the machine when the second one displays measurement software. For controlling the movements of the machine, the pads familiar to the controllers of game consoles are used. The control knobs are responsible for the movement of the machine model in *X*, *Y*, *Z*. Furthermore, the virtual machine can be controlled by programming it from the level of metrological applications. It is possible to simulate the measurement of both the manual and automatic mode. There is also camera control option, which allows to observe the machine movement as well as the measuring space. It helps to track the position of the object during the measurement. This makes the machine control becomes much simpler. The operator can also define custom views adapted to the needs, depending on the measurement task.

Extensive database of CMM models offered by leading companies in the industry was built-in the simulator. It is also possible to build unique model of machine using 3D modeling

software. So it can be stated, that the simulator makes it possible to simulate the activities of any existing machine. In addition, there is the option to add to the database models of styli, racks, fixing elements created by the user. The only requirement is to have a proper 3D model of the element.

The undeniable advantage of the simulator is the ability to create and test measurement programs. Although most of metrology software support off-line creation of programs, none of them gives opportunity to verify it correctness during real measurements (collisionless functioning) and thus each of the programs need to be corrected, if not written during the measurements [6]. Thanks to I++ Simulator, having the CAD model of the measured object, there is a possibility to write programs off-line, in "teaching" mode, that was not previously possible. An additional advantage is possibility of checking programs for possible collisions. This can be very useful when the measurement is difficult, for example due to the complex shape of the measured object. Obviously the program created and tested on the simulator can be implement on a real machine.

Coordinate Measuring Machines are still evolving as well as the range of their applications. Today it can be used in both nano- and large-sized measurements. Still, in some cases programming of CMM using machine itself can be difficult or almost impossible. For example, in measurements of nano elements it is a common situation when one or more dimensions are not visible to the eye. In such circumstances vision systems are used to provide zoom on probe head, measured element and their position. However, this method is cumbersome and it is leaving an operator too much space for making mistakes which can result with damage of relatively expensive stylus. I ++ simulator can be also useful when measurements are performed on a high-precision (accurate) measuring machines which work on strictly air-conditioned spaces. The presence of the operator in such room during the programming of CMM could cause an increase in temperature, which in turn could make it necessary to wait some time until conditions stabilize. Any pause during measurements is a waste of money and I ++ simulator can be very helpful in preventing it in these situations. It is used in described way in Laboratory of Coordinate Metrology (LCM) which is equipped with one of the most modern air-conditioning systems, giving the thermal stabilization at

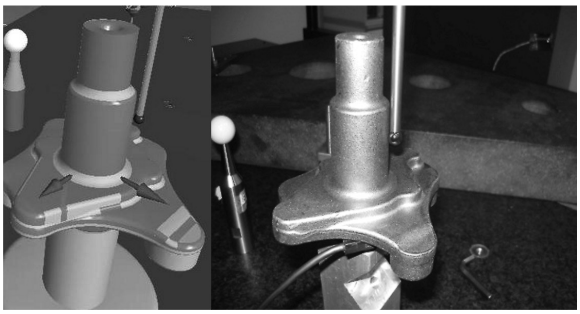

Fig. 3. Measurement programmed using I++ Simulator (left side) transferred and performed on PMM 12106 machine (right side)

Rys. 3. Pomiary zaprogramowane z wykorzystaniem programu I++ Simulator (po lewej stronie) przeniesione i uruchomione na maszynie PMM 12106 (po prawej stronie)

level of 20 ± 0,05°C. The CMM programs are written using I++ Simulator and transferred into real machine (Fig. 3). In this situation, the operator activity in close proximity to the machine can be easily reduced only to the installation of the measured workpiece on the machine table. The costs of machine downtime are also reduced in this way.

Another important aspect of the working with the I++ Simulator which is worth mentioning is its didactic potential. Performing measurements in a virtual environment is a perfect opportunity to learn techniques and strategies used in the real measurements. The system is ideal not only for didactic process at the universities but also in the training of future CMM operators, the system which forgive their possible mistakes and enables their self-correction, without having to pay for imaginable damages. At Laboratory of Coordinate Metrology the system is used at CMT lessons (Fig. 4) giving possibility to work with CMM to all students simultaneously. Before installation of this system in computer laboratory at LCM the lessons of CMM programming were more like a presentation because only one real CMM were available. Through the work on the simulator, operator has direct contact with the CMM measurements in a realistic environment. He has the ability to self-configure workplace (probe head choice - scanning or touch-trigger, styli selection depending on the subject of measurement, configuration of racks, rotary tables, systems of object mounting, etc.) and to determine procedures assigned to the specified machine. Operator learns programming with the simulation of measurement taking into account its specific characteristic of the manufacturer with the possibility of the preparation of measurement programs based on the imported CAD objects prepared in any system and stored in different formats. After the development of measurement strategy the operator has the opportunity to review the decision of the real CMM measurements and the possibility of potential corrections such as a change of stylus approach paths after a collision in the simulator.

Fig. 4. CMM simulation laboratory in Laboratory of Coordinate Metrology
Rys. 4. Laboratorium symulacji pomiarów współrzędnościowych w LMW

Working with the simulator is not limited to a system composed of CMM, the measured object and the equipment but also allows to create the environment that affects the performing of measurement. It is possible to create an entire air-conditioned room with the real machine

and its appropriate equipment with elements such as storages or rotary tables (Fig. 5). Libraries implemented in the simulator are comprehensive enough to precisely reproduce the metrology lab room. In addition, if certain specific equipment is not available it is possible to self-define the missing equipment.

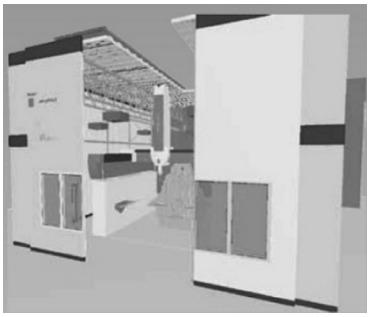

Fig. 5. Example of a real-world scenario with a large bridge CMM and air conditioned room [7]
Rys. 5. Przykład prawdziwego scenariusza z wielkogabarytową WMP w klimatyzowanym pomieszczeniu [7]

4. I++ Simulator enhanced with the CMM accuracy model

The main disadvantage of Simulator is the rudimentary system of measurement accuracy reproduction. In its present form the program does not take into an account the real machine errors and errors introduced by probe head. Variability of the results obtained from measurement simulations depends only on inaccuracy of the creation of CAD models (limited resolution with which they could be saved in digital format) and the accuracy of the point acquisition parameter, which can be defined by user.

Therefore, in Laboratory of Coordinate Metrology at Cracow University of Technology a simulation model called Virtual MC PK was created [8]. It allows to simulate errors of real machines and measuring heads at I++ Simulator. This allows to create a completely virtual measurement system, which can be used to predict the coordinate measurement accuracy and to further research the accuracy of measuring machines under the simulation conditions. Operation of model in conjunction with the I++ Simulator aims in simulation of the residual errors introduced by the kinematics of the machine and probe head errors. As an input quantities it uses the coordinates of the measuring points (simulation of residual errors of kinematic system) and its approach vectors (simulation of probe head errors). The result is the point concluding real errors of simulated machine. In this case, the results of simulated measurements will not only be the random values sampled from the range defined by the user but they will become results containing accuracy of measurements, which can be obtained during measurements performed on the real machines. Model has passed through preliminary tests in the LCM, and proved its correctness for simple measuring tasks. Software created by combining the I++ Simulator and Virtual MC PK model will allow in near future to define optimal measurement strategy and optimal location of measured detail in measuring volume, so that the best possible measurement accuracy could be achieved.

5. Conclusions

Coordinate measuring technique is now an indispensable tool of production engineering, creating a basis of quality control systems. CMMs allow quick verification of an object compliance with geometric specifications contained in the technical documentation. Due to the high measurement accuracy and a wide range of possible applications, CMMs are becoming an increasingly popular solution. In some cases, the operator interaction with the machine during its programming may be difficult. In this situation, I++ Simulator can provide invaluable assistance. Basing on results of experiments performed so far, the probability of obtaining good results in programming of micro and nano coordinate measuring machines and machines of high precision using the I++ Simulator is considerably high.

The great advantage of I++ Simulator is also its ability to connect with majority of popular metrological systems by I++ protocol. It allows to program machines using a variety of metrological software types. In addition, Simulator I++ combined with functionality of these software becomes suitable tool used to train new operators of CMM without necessity of wearing out the real machines. Laboratories equipped with I++ Simulator stations are also extremely useful at universities, during machine programming and Coordinate Measuring Technique lessons, which could be confirmed by increasing number of installations at German universities and the feedback from students who state that the CMT lessons become now really interesting and helpful.

References

[1] Kup-Sze C., Sophia S., Fu-Lai C., *A virtual training simulator for learning cataract surgery with phacoemulsification*, Computers in Biology and Medicine 39 (11), 2009, 1020-1031.

[2] Longo F., Massei M., Nicoletti L., *An application of modeling and simulation to support industrial plants design*, Int. J. Model. Simul. Sci. Comput. 03, 1240001 (2012), DOI: 10.1142/S1793962312400016.

[3] Zheng W., Zhenyu L., Jianrong T., Yun F., Changjiang W., *A virtual environment simulator for mechanical system dynamics with online interactive control*, Advances in Engineering Software 37 (10), 2006, 631-642.

[4] Klingstam, P., Gullander, P., *Overview of simulation tools for computer-aided production engineering*, Computers & Industrial Engineering 38 (2), 173, (1999), DOI: 10.1016/S0166--3615(98)00117-1.

[5] Sładek J., *Accuracy of coordinate measurement*, Cracow University of Technology, Cracow 2011.

[6] Seokyong H., Moonki Jung S., Kunwoo L., *An Analytic Method for Detecting Collisions to Develop Simulator of Coordinate Measuring Machine*, IJCC Workshop 2006 on Digital Engineering, February 08–09, 2008, Phoenix Park, South Korea.

[7] *I++ Simulator. Online simulation in the virtual laboratory* (http://www.leitz-metrology.com/i-simulator_648.htm).

[8] Sładek J., Gąska A., *Evaluation of coordinate measurement uncertainty with use of virtual machine model based on Monte Carlo method*, Measurement 45 (2012), 1564-1575, doi:10.1016/j.measurement.2012.02.020.

TECHNICAL TRANSACTIONS | **CZASOPISMO TECHNICZNE**
MECHANICS | MECHANIKA
1-M/2013

ŁUKASZ GOLA*

COMPUTER AIDED MODELING ASSEMBLY PROCESS PLAN

KOMPUTEROWO WSPOMAGANE MODELOWANIE PROCESU TECHNOLOGICZNEGO MONTAŻU

A b s t r a c t

In the Institute of Production Engineering of Cracow University of Technology carried out research in the field: design manual and robotic manufacturing systems. The paper presents computer aided modeling assembly process plan with using programs: CAD/CAM Catia v5, MS Visio 2010, MS Excel 2010). The assembly process plan is illustrated in the example of dual stage regulator.

Keywords: CAPP, assembly process plan, manufacturing system

S t r e s z c z e n i e

W Instytucie Technologii Maszyn i Automatyzacji Produkcji Politechniki Krakowskiej prowadzone są badania z zakresu projektowania ręcznych i zrobotyzowanych stanowisk i systemów wytwarzania. W artykule przedstawiono proces projektowania procesu technologicznego montażu z zastosowaniem systemów komputerowego wspomagania (system CAD/CAM Catia v5, Visio 2010, Excel 2010).

Słowa kluczowe: CAPP, proces technologiczny montażu, system wytwarzania

* PhD. Eng. Łukasz Gola, Institute of Production Engineering, Mechanical Faculty, Cracow University of Technology.

1. Introduction

Design of complex manufacturing systems (assembly manufacturing systems) is a multi--step process (design anddecision making). During this process, the basic steps are carried out:

– Prepare assumptions
– Preliminarydesign of assembly process plan
– Conceptualdesign of assebly workstations (assembly line)
– Modeling and verification

2. Prepare assumptions

The starting point of any process plan is to define product (Fig. 1) which will be mounted and next specify the production program. Characteristics of the product (the weight and size) affects for selecting appropriate manufacturing instrumentals – for example: equipment of assembly workstations, mode of transport between workstations (conveyor belt, trucks, ...). Whereas the production program determines the production cycle, which limits the duration of individual operations.

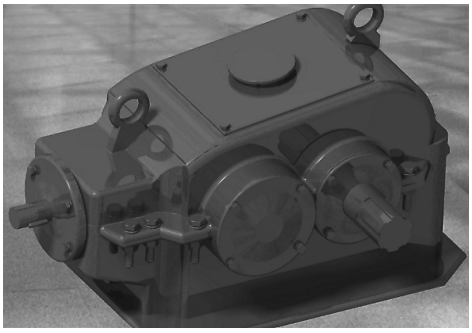

Fig. 1. Dual stage regulator
Rys. 1. Reduktor stożkowo-walcowy

Presented product (Fig 1) was modeled with using CAD/CAM Catia System (Modules: Part Design and Assembly Design).

3. Preliminary design of assembly process plan

The purpose of this step is to analyze the product structure for its possible split (assemblies and subassemblies) which can be mounted independently of each other. This process is also known as aggregation of parts. An example of a product with separate assemblies and subassemblies is shown in (Fig. 2).

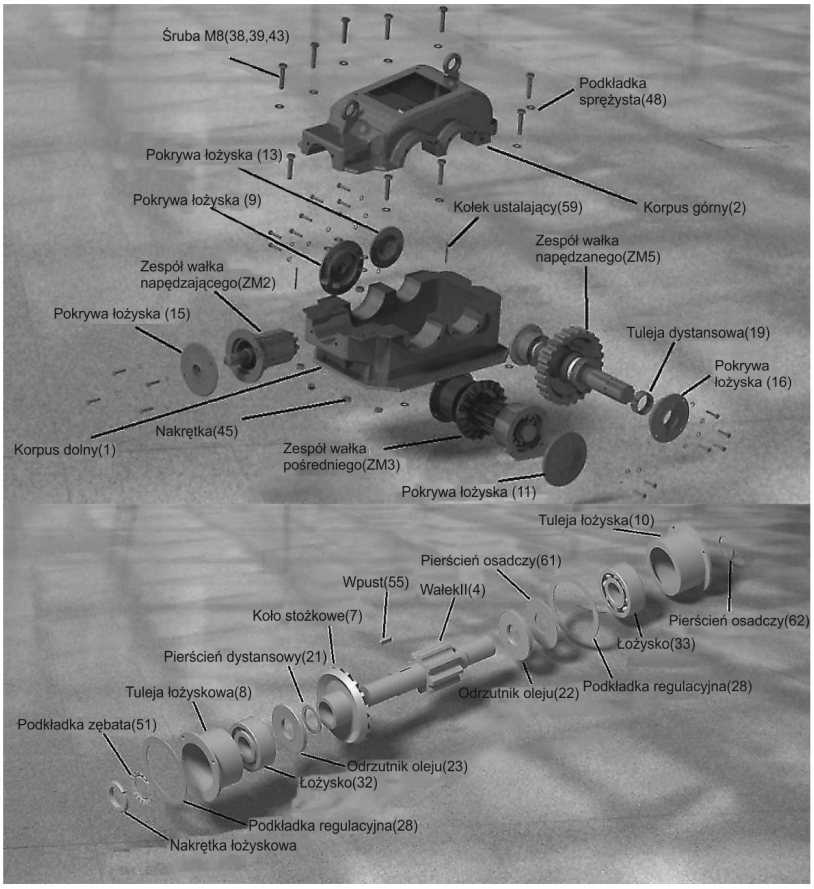

Fig. 2. Assemblies and subassemblies of dual stage regulator

Rys. 2. Zespoły i podzespoły reduktora stożkowo-walcowego

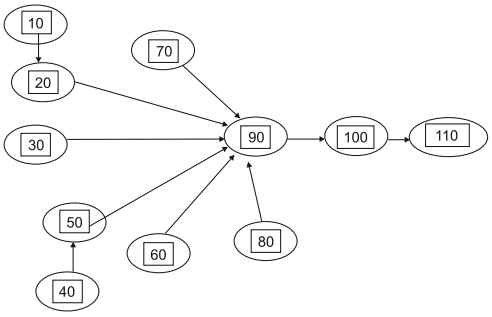

Fig. 3. Follow-graph of assembly operations

Rys. 3. Graf następstw operacji montażowych

Number of operation	Content of operations
10	Mounting subassembly drive shaft (ZM1)
20	Mounting assembly drive shaft (ZM2)
30	Mounting assembly middle shaft (ZM3)
40	Mounting subassembly middle shaft (ZM4)
50	Mounting assembly out shaft (ZM5)
60	Mounting seal of drive shaft (ZM6)
70	Mounting seal of out shaft (ZM7)
80	Mounting subassembly trunk(ZM8)
90	Mounting main assemblies (ZM9)
100	Oil charge and closing regulator (ZM10)
110	Technical control

Fig. 4. The sequence assembly

Rys. 4. Kolejność montażu

Aggregation of parts allow for the identification which assemblies and subassemblies can be mounted independently. On this basis and on the basis of follow-graph (Fig. 3) (showing the correct order of assembly), we can develop the assembly sequence (Fig. 4). The follow--graph can be very helpful in determining the sequence, especially for more complex products.

4. Conceptual design of assembly

The purpose of conceptual design is: determine the duration of the pre-planned operations, division or grouping of operations to finally get the operations of similar duration (balancing). It should also be chosen such time values, that do not exceed the production cycle. To achieve this goal we must first develop preliminary design assembly workstations (flat sketches)

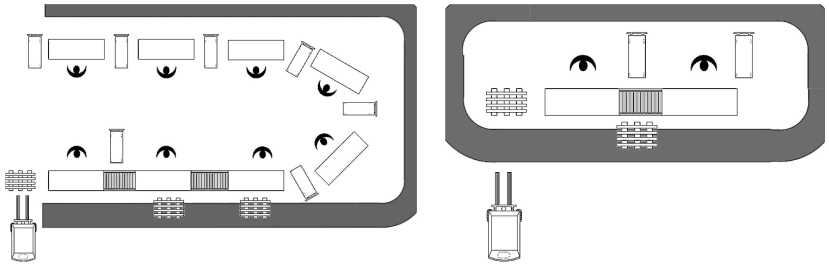

Fig. 5. Sketches of assembly workstations – MS Visio 2010

Rys. 5. Szkice stanowisk montażowych – MS Visio 2010

which include the distribution of equipment and operators (Fig. 5). A convenient computer program for the preparation of such drawings is Microsoft Visio 2010. Next then there is standardization duration of individual operations. In the case of manual work, usually the most useful method of standardization are methods: MTM1 (Fig. 6), MTM2, MOST. The choice of

method depends on the expected duration of the operation and its characteristics (standardized operation is divided into individual movements or entire sequences of operations).

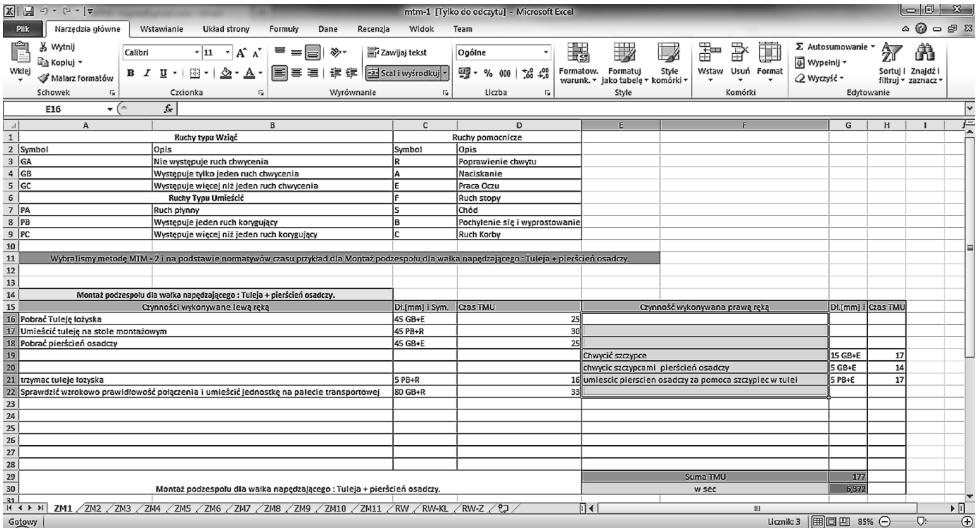

	A	B	C	D	E	F	G	H	I
1		Ruchy typu Wziąć		Ruchy pomocnicze					
2	Symbol	Opis	Symbol	Opis					
3	GA	Nie występuje ruch chwycenia	R	Poprawienie chwytu					
4	GB	Występuje tylko jeden ruch chwycenia	A	Naciskanie					
5	GC	Występuje więcej niż jeden ruch chwycenia	E	Praca Oczu					
6		Ruchy Typu Umieścić	F	Ruch stopy					
7	PA	Ruch płynny	S	Chód					
8	PB	Występuje jeden ruch korygujący	B	Pochylenie się i wyprostowanie					
9	PC	Występuje więcej niż jeden ruch korygujący	C	Ruch Korby					
10									
11	Wybraliśmy metodę MTM-2 i na podstawie normatywów czasu przykład dla Montaż podzespołu dla walka napędzającego : Tuleja + pierścień osadczy.								
12									
13									
14	Montaż podzespołu dla walka napędzającego : Tuleja + pierścień osadczy.								
15	Czynności wykonywane lewą ręką		Dł.(mm) i Sym.	Czas TMU	Czynność wykonywana prawą ręką		Dł.(mm) i	Czas TMU	
16	Pobrać Tuleję łożyska		45 GB+E	25					
17	Umieścić tuleję na stole montażowym		45 PB+R	30					
18	Pobrać pierścień osadczy		45 GB+E	25					
19					Chwycić szczypce		15 GB+E	17	
20					chwycic szczypcami pierścień osadczy		5 GB+E	14	
21	trzymac tuleje łozyska		5 PB+R	18	umiescic pierscien osadczy za pomoca szczyplec w tulei		5 PB+E	17	
22	Sprawdzić wzrokowo prawidłowość połączenia i umieścić jednostkę na palecie transportowej		80 GB+R	33					
23									
24									
25									
26									
27									
28									
29					Suma TMU		177		
30	Montaż podzespołu dla walka napędzającego : Tuleja + pierścień osadczy.				w sec		6,372		
31									

ZM1 / ZM2 / ZM3 / ZM4 / ZM5 / ZM6 / ZM7 / ZM8 / ZM9 / ZM10 / ZM11 / RW / RW-KL / RW-Z

Gotowy — Licznik: 3 — 85%

Fig. 6. Standardization of operation time – MTM-1 (Excel 2010)

Rys. 6. Standardization of operation time – MTM-1 (Excel 2010)

The next step is balancing operations. In practice often used "manual" balancing operations or heuristic methods. The best knownof these isthe methods: RPW method (Ranked Positional Weight), RRPW method (Reversed Ranked Positional Weight), Kilbridge'a and Wester'a method (K&W), matrix method of order Hoffmana, IUFF method (Immediate Update First-Fit).

Cracow University of Technology Institute of Production Engineering	Operation sheet	Name of product: Reduktor stożkowo-walcowy	Symbol: RSW	Name of assembly: ZM1		Batch
Departament	Name of operation: Mounting subassembly drive shaft		Number of operation: 10	Work-sation: SM1	Time standardization: T_{pz} [min] =30 / t_j[min] = 0,63	T [min] = 30,63

Number	Content	Mounting Devices
1	Un - conservation	Hand press
2	Put shaft (5) on the mound, inserted parallel key (56)	Brackets and mounting devices: Assembly prism
3	Set the shaft (5) in an upright position, slide flinger (26)	
4	Set the shaft (5) in an upright position, slide bearing (37) and sleeve.	Tools assembly: Sleeve
5	Visually check that the connections	Tools and measuring instruments:

Prepared	Checked	Approved	Comments

Fig. 7. Sample of operation sheet

Rys. 7. Przykładowa karta instrukcyjna

The final step in this phase is the development of technical documentation (operation sheets (Fig. 7).

5. Modeling and verification of assembly workstations

At this stage of organizational and technological preparation can now proceed to the proper design of assembly workstations. This stage includes:
- designing the structure of distribution workstations with the way transport links,
- design of individual workstations (Fig. 8; Fig. 9), developed based on early sketch of workstations,
- design equipment and transport (Fig. 10),
- assembly simulation (Fig. 11).

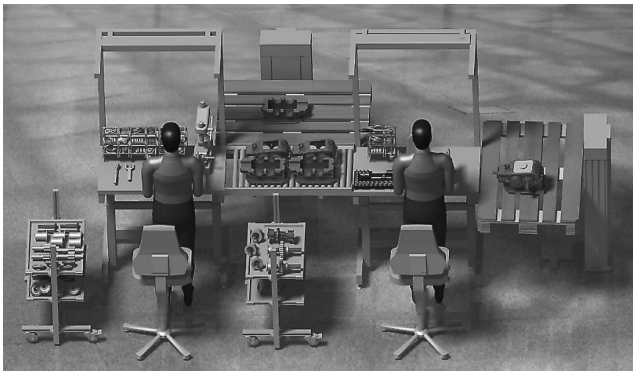

Fig. 8. Assembly workstations – CAD/CAM Catia v5
Rys. 8. Stanowiska montażowe – CAD/CAM Catia v5

Fig. 9. Assembly workstations – CAD/CAM Catia v5
Rys. 9. Stanowiska montażowe – CAD/CAM Catia v5

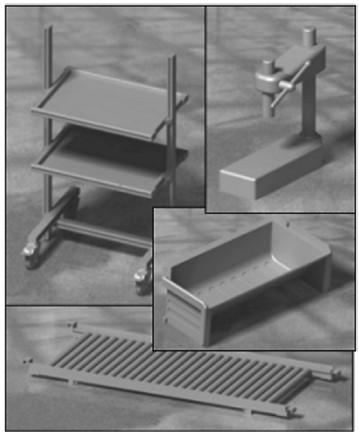

Fig. 10. Equipment of assembly workstations
Rys. 10. Wyposażenie stanowisk montażowych

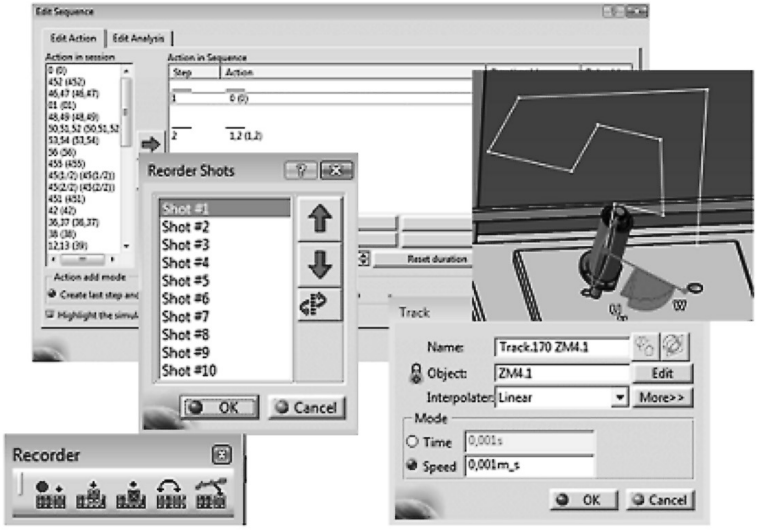

Fig. 11. Assembly simulation – Catia/Module DMU Fitting
Rys. 11. Symulacja montażu – Catia/ Module DMU Fitting

The final step, before the physical implementation of the project, is a simulation particular workstations and their evaluation due to the ergonomic requirements. System CAD/CAM Catia v5 (Fig. 12) is a tool which can be comprehensively applied to the implementation of all project activities including3D modeling of individual parts of the product, modeling workstations, modeling transport, ergonomic simulation.

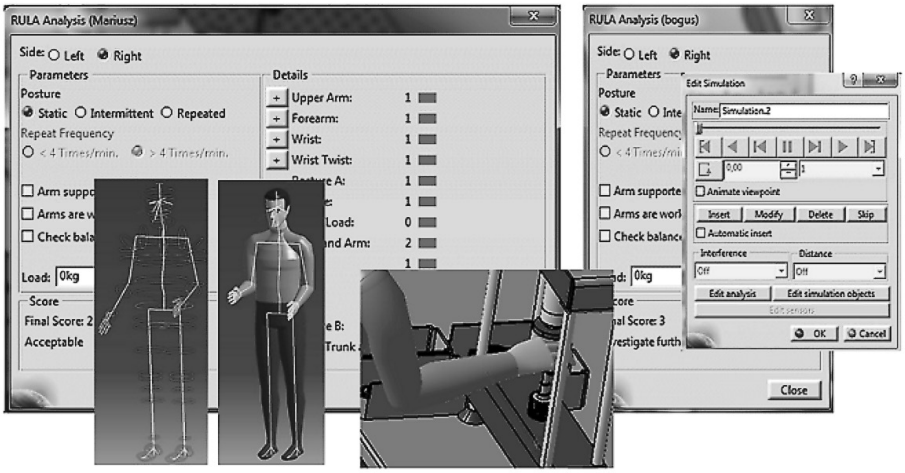

Fig. 12. Modeling ergonomics assembly workstations – Catia/Module Ergonomics

Rys. 12. Modelowanie ergonomicznych stanowisk montażowych – Catia/ Module Ergonomics

6. Conclusions

Designing of any system (assembly system) is a complex process with used in the field of knowledge: design process plans, standardization of operations, balancing operations performed in the manufacturing system, ergonomic principles. Use the tools to create a virtual 3D model of the system, allows to simulate and verify the operation of the system before it is implemented in practice. This allows to avoid a lot of errors in the construction, much lower costs and shorten the cycle time pre-production (from project to construction).

References

[1] Feld M., *Podstawy projektowania procesów technologicznych typowych części maszyn*, WNT, Warszawa 2003.

[2] Kiliński G., *Modelowanie procesu montażu i stanowiska montażu reduktora z zastosowaniem systemu CAD/CAM Catia*, praca inżynierska, Kraków 2013.

[3] Skarka W., Mazurek A., *CATIA Podstawy modelowania i zapisu konstrukcji*, Wyd. HELION, Gliwice 2005.

[4] Wyleżoł M., *CATIA v5 Modelowanie i analiza układów kinematycznych*, Wyd. HELION, Gliwice 2003.

TECHNICAL TRANSACTIONS | **CZASOPISMO TECHNICZNE**
MECHANICS | MECHANIKA
1-M/2013

ŁUKASZ GOLA*

DATABASE OF TECHNOLOGICAL CAPABILITY MANUFACTURING SYSTEM ORIENTED FOR MACHINES KINEMATICS

BAZA DANYCH MOŻLIWOŚCI TECHNOLOGICZNYCH SYSTEMU WYTWARZANIA ZORIENTOWANA NA KINEMATYKĘ OBRABIAREK

A b s t r a c t

This paper presents database of technological capability manufacturing system oriented for machines kinematics. This database is a part of CAPP (Computer Aided Process Planning) prototype system, which was built on the basis of algorithm generating multi-variant process plan. Database was implemented to Microsoft Access 2010.

Keywords: *CAPP*, *process plan*, *manufacturing system*

S t r e s z c z e n i e

W artykule przedstawiono bazę danych do zapisu możliwości technologicznych systemu wytwarzania z uwzględnieniem kinematyki obrabiarek. Baza ta jest częścią prototypu systemu CAPP (Computer Aided Process Planning) zbudowanego w oparciu o algorytm generowania wielowariantowych procesów technologicznych obróbki skrawaniem. Baza danych została zaimplementowana w MS Access 2010.

Słowa kluczowe: *CAPP*, *proces technologiczny*, *system wytwarzania*

* PhD. Eng. Łukasz Gola, Institute of Production Engineering, Faculty of Mechanical Engineering, Cracow University of Technology.

1. Introduction

Computer aided process planning systems are built with adaptation three basic methodical approaches: variant method, semi-generative method, generative method. Generative method has the most possibilities among remaining methods, particularly if it depends us on considerable to raise the automation of machining process plans. Generative method is more difficult in comparison with variant method, because generative method require to create more formal models which describes different working and objects on process planning. In Institute of Production Engineering research have brought to make algorithm generation machining process plan so far [4, 5]. The main feature of this algorithm is based on possibility choice by technologist partial solutions from admissible set on given stage.

But progress enabling realization of concurrent product development is defined requirements for computer aided process planning systems:

– the ability to projection machining process plans for wide set of typical parts of machines, the elements of component products,
– the ability to projection machining process plans with regard the fit manufacturing capabilities,
– the ability to generation of variants machining process plans with different degree of circumstantiality.

Above mentioned features were reached building generative skeletal system CAPP, which it be characterizes:

– the possibility of record, modification and manufacturing knowledge,
– the possibility of record technological profiles of manufacturing system oriented on profile realized in enterprise of productive processes, the possibility generation admissible solutions which are realized on manufacturing stations

2. Algorithm of generation multi-variant process plans

The effect of previous work carried out in Institute of Production Engineering was to develop algorithm of generation multi-variant process plans [2]. Based on the basic structure of the process plan (1), defined places where we can create variants of process plan [1, 2].

$$\mathbf{PT = [OP\text{-}operation\ [US\text{-}set\text{-}up\ [PZ\text{-}position\ [ZB\text{-}cut]]]]} \quad (1)$$

Places (where we can create variants of process plan) were the basis for the development algorithm of generation multi-variant process plan (Fig. 1).

The algorithm is carried out at different levels, including: generating operations, generating set-ups, generating positions, generating cuts. The algorithm can generate acceptable variants (possibilities of movement of individual machine components). Calculation procedures on this algorithm are based on a simple kinematics task and reverse kinematics task. Necessary data to generate acceptable variants are stored on *Database of technological capability manufacturing system oriented for machines kinematics* (Fig. 1).

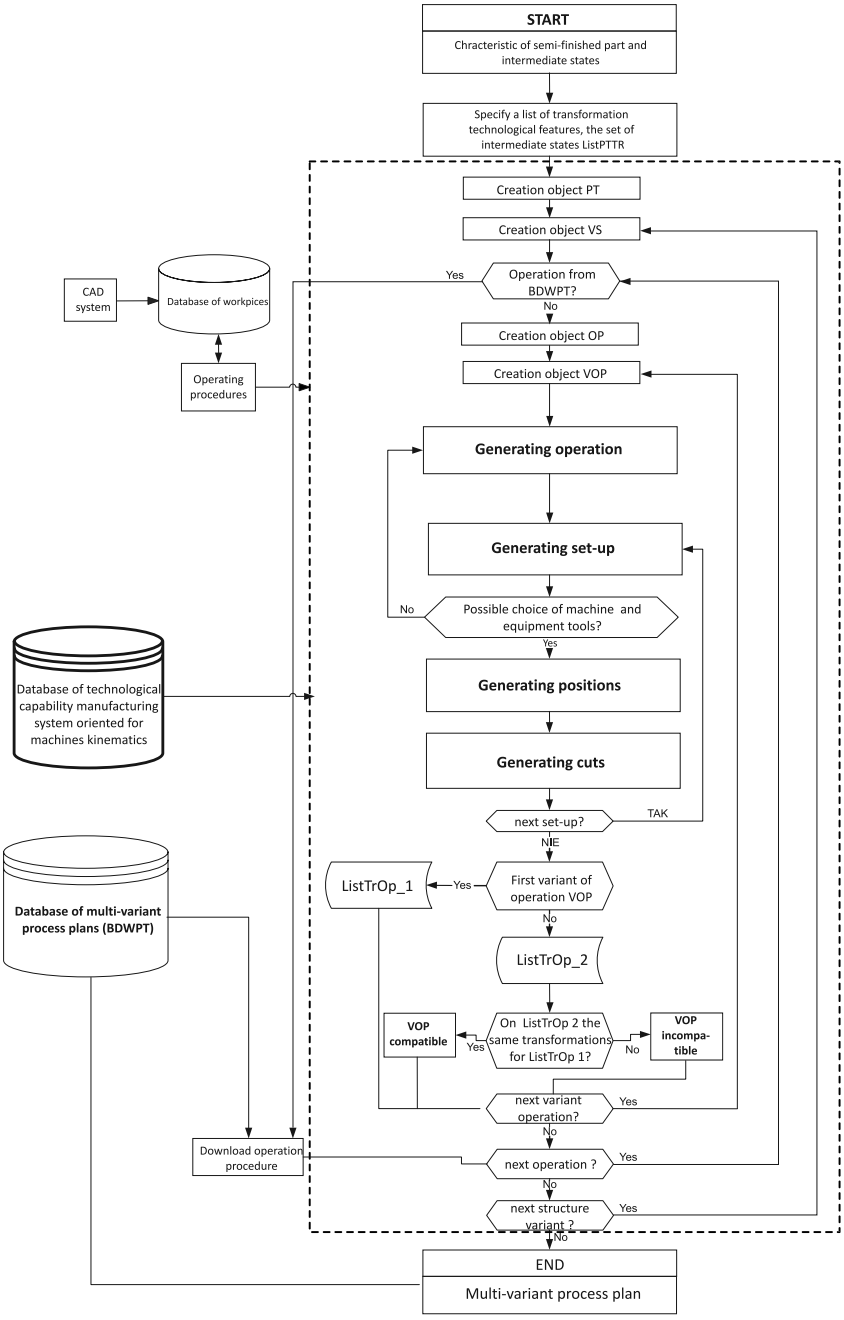

Fig. 1. Algorithm of generation multi-variant process plans

Rys. 1. Algorytm generowania wielowariantowych procesów technologicznych obróbki

3. Database of technological capability manufacturing system oriented for machines kinematics

For the purpose of generating acceptable variants of process plan, designed and built database which was named *Database of technological capability manufacturing system oriented for machines kinematics* (BDMTSWZK). The database is divided into four areas (Fig. 2):

– System resources (for example: vice, handle, jaw-chuck, cutter, drill,...),
– Technological capabilities,
– Variants of fixing W and T (workpiece and tool),
– Kinematic structures.

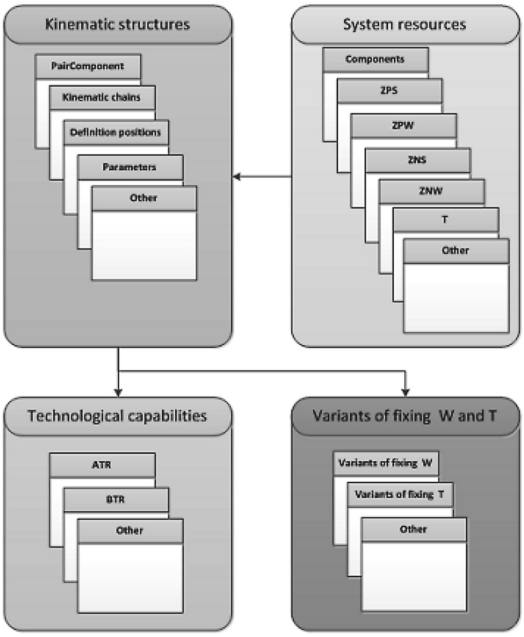

Fig. 2. BDMTSWZK – conceptual model
Rys. 2. BDMTSWZK – model koncepcyjny

This database is a modification of an earlier version developed in Institute of Production Engineering. A completely new element of the database is field *Kinematic structures*, which was designed based "method of creating a database that describes the structure of the kinematic" [3].According to this method, the definition of machine kinematics is carried out in few steps:

STEP 1

Defining a machine component objects. Component objects are saved on the *"component list"* (sample components: vice, dead centre, tailstock, spindle, ...)

STEP 2

Defining the pair of components object. For this purpose, earlier must be defined *"component list"*. Selecting object from *"component list"* we can create *"list pair components"* of machine (sample pair: cross slide – vice)

STEP 3

Defining possible to obtainment *kinematic chains*. For this purpose, earlier must be defined *"list pair components"*. Selecting from *"list pair components*" consecutive pairs, *kinematic chains* are built (sample *kinematic chain*: machine trunk – carriage – cross slide – vice – workpiece)

The (Fig. 3) shows one part of the database BDMTSWZK (*Kinematic structure*) – this is a logical data model.

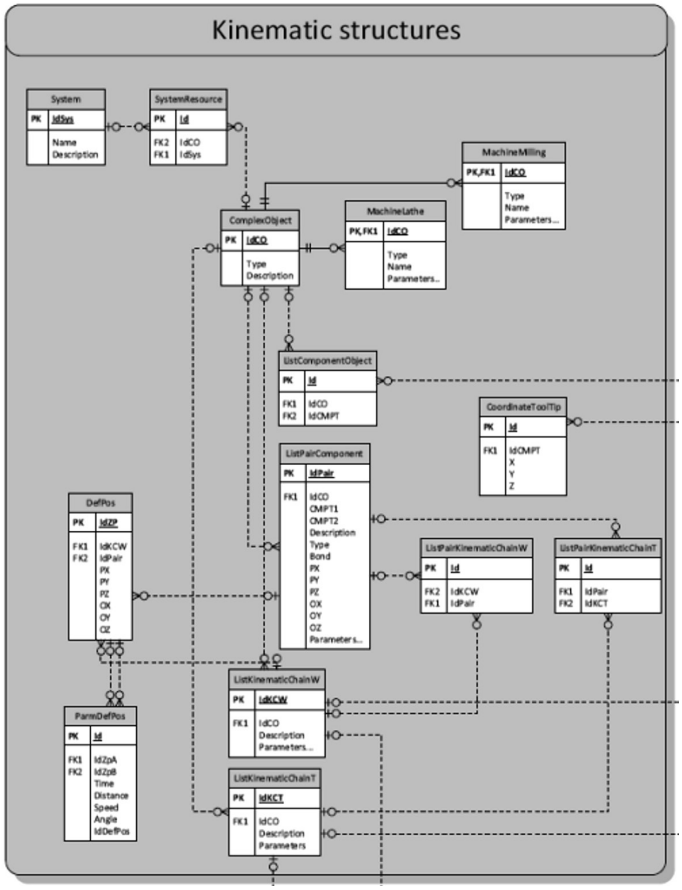

Fig. 3. Database BDMTSWZK – the logical data model (part *Kinematic structure*)

Rys. 3. Baza danych BDMTSWZK – model logiczny (część *Struktury kinematyczne*)

The figure (Fig. 4) shows a sample table *ListPairComponent.* The table identifies the kinematic pairs that may occur between objects machine components. This is the physical data model.

ListPairComponent					
Attribute name	**Domain**	**Limit**	**Kind of attribute**	**Description**	**Example**
IdPair	Char(50)	Not null	Primary key	ID kinematic pair	IdPair="P:1"
IdCO	Char(50)	Not null	Foregin Key	ID a complex object	IdCMPT="TKX:1"
IdCMPT1	Char(50)	Not null		ID 1 object component (OB1) pair	IdCMPT="ZPS:1"
IdCMPT2	Char(50)	Not null		ID 2 object component (OB2) pair	IdCMPT="ZPW:1"
Type	Char(50)			Type of pair	Typ = "przesuwna"
Bond	Char(10)			Bond type	Bond = „P,K"
PX	Decimal			Coordinates location object OB1 and OB2 along axis X	PX = „100"
PY	Decimal			Coordinates location object OB1 and OB2 along axis Y	PY = „100"
PZ	Decimal			Coordinates location object OB1 and OB2 along axis Z	PZ = „100"

Fig. 4. Sample table (*ListPairComponents*) – phisical data model

Rys. 4. Przykładowa tabela (*ListaParKomponentów*) – fizyczny model danych

4. Implementation

Database was implemented to Microsoft Access 2010. The database is filled with data of two machines: lathe machine *TKX50SN* and milling machine *Arrow500*. Data are entered using with form. Selecting another tab, the user enters data about machines, then he can builds the kinematic structure of machine.

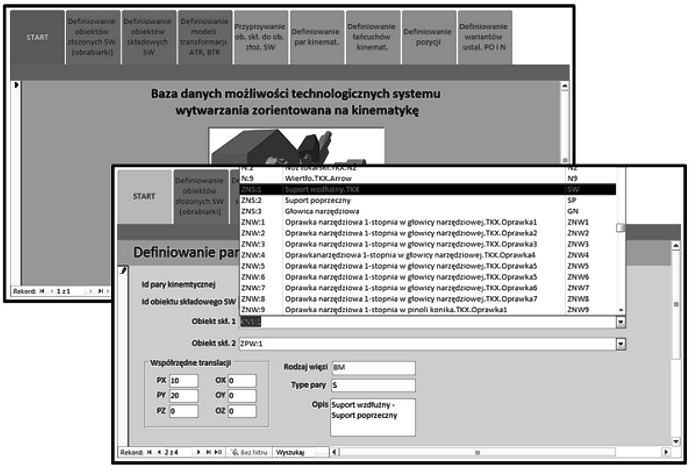

Fig. 5. Database – implementation to Microsoft Access 2010

Rys. 5. Baza danych – implementacja do Microsoft Access 2010

5. Conclusions

Presented in the article database allows to record information about the machines and kinematic structures between its components. Clearly designed form of database, cause easy and intuitive data entry. This database is an essential element of CAPP which generates multi--variant process plan. Generated variants of process plan next can be used in the construction of production schedules.

References

[1] Duda J., Habel J., Gola Ł., *Koncepcja generowania wielowariantowych procesów technologicznych obróbki*, New ways in manufacturing engineering 2008, Prešov, Slovak Republic 2008, 19-21.
[2] Gola Ł., *Wielowariantowe generowanie struktur procesów technologicznych obróbki w systemach CAPP*, praca doktorska, Kraków 2012.
[3] Habel J., *Metoda tworzenia baz danych charakterystyk i możliwości technologicznych systemów wytwarzania*, Kraków 2003.
[4] *Opracowanie założeń systemu projektującego procesy technologiczne obróbki w warunkach inżynierii równoczesnej z wykorzystaniem sztucznej inteligencji*, Projekt badawczy nr 7T07D02812 finansowany przez KBN, 1998–2000 PK.
[5] *Zasady budowy systemu projektowania i doboru oprzyrządowania przedmiotowego z wykorzystaniem metod hybrydowych*, Projekt Badawczy PB-657/T07/95/08 praca wyk. kier. prof. dr hab. inż. A. Samka, ITMiAP Politechnika Krakowska, Kraków 1995–1996.

TECHNICAL TRANSACTIONS | **CZASOPISMO TECHNICZNE**
MECHANICS | MECHANIKA
1-M/2013

ADRIAN GUMUŁA*, MIROSŁAW GŁOWACKI*

DIGITAL IMAGE ANALYSIS OF VOIDS FORMED DURING THE DEFORMATION OF STEEL SAMPLES WITH SEMI-SOLID CORE

CYFROWA ANALIZA OBRAZU DEFEKTU W POSTACI PUSTEK POWSTAŁYCH PODCZAS ODKSZTAŁCANIA PROBEK STALOWYCH Z PÓŁCIEKŁYM RDZENIEM

A b s t r a c t

In this paper the digital image analysis of voids formed during the deformation of steel samples in the GLEEBLEE 3800 physical simulator device with the semi-solid core. The presented and characterized indicators describe the shape of voids, and their relative position as qualifiers quality indicators as well as the correlation between the indicators and possible defects in the material. The paper contains the results and discussion of presented analysis.

Keywords: digital image analysis, voids, defects, semi zone.

S t r e s z c z e n i e

W artykule przedstawiono analizę obrazu pustek powstałych podczas odkształcania próbek stalowych z półciekłym rdzeniem na urządzeniu GLEEBLEE 3800. Przedstawiono oraz scharakteryzowano wskaźniki opisujące kształt pustek, oraz ich wzajemne położenie jako kwalifikatory jakości próbek. Przestawiono także korelację pomiędzy wartościami wskaźników opisowych pustek a możliwymi defektami w materiale. Praca zawiera wyniki oraz omówienie przeprowadzonej analizy.

Słowa kluczowe: cyfrowa analiza obrazu, pustki, defekty, strefa półciekła.

* MSc. Adrian Gumuła, prof. Mirosław Głowacki, Department of Applied Computer Science and Modelling, Faculty of Metals Engineering and Industrial Computer Science, AGH University of Science and Technology

1. Introduction

Measurement of properties of material structures and the quality control constructions takes in the recent years considerable attention. This is partly caused by the development of new stereological methods and benefits coming from automatic image analysis. Quantitative measurement of the microstructure has also great significance in both research and quality control as well as by determination of material properties. Optical microscopy combined with digital image recording and specialized software dedicated to automatic image analysis becomes a productive tool, which allows to acquire information within a short time. Thus, science offers increasingly better tools for structural analysis of materials and detection of resulting manufacturing defects. Presented analysis was performed on digital images formed during the deformation samples with semi-solid core on the physical simulator GLEEBLEE 3800 on the Institute for Ferrous Metallurgy in Gliwice. Although deformation process of the steel in semi-solid core state as well as continuous casting is a process that has been already a subject of series of studies, there are still problems with quality of continuously casted intermediate products. It is particularly important in case of alloyed steels casting when the steel is subjected to further processing in integrated processes of plates casting and rolling. Occurring in this respect risk of cracks can be minimized by appropriate selection of a favourable state of stress – which is not always possible – and by suitable, fine-grained microstructure of the as-cast steel. As indicated in [1] even for carbon steels the microstructure formation mechanism depends on steel chemical composition – mainly on the carbon content. Therefore, an important issue is to accomplish an appropriate quantitative analysis of substantial number of microstructure [2]. The final product (f.e cast ingots) purity strongly depends on the liquid steel flow conditions, especially in the tundish and mould. Very important are also such parameters like character and rate of heat generation in crystallizer. Both of them significantly influence segmentation and microstructure evolution, as well as stress field, material mechanical properties and defects of the ingot after solidification process. Coincidence of unfavourable stress distribution and coarse columnar crystal structure leads to cracks and shape defects of the cast strip. Therefore, it is important to develop appropriate models of solidification process and formation of internal stress. In this aspect, the computer aided analysis of material structures becomes particularly important. It can contribute to significant acceleration of research by eliminating the human factor. Moreover, the applied methods of classification based on artificial intelligence [2] allow to reduce the study effort.

The paper presents an attempt of application of digital image processing to analysis of the occurrence and distribution of voids caused by solidification process in samples which demonstrate semi-solid core. The investigation is an introduction to the analysis of a semi--solid zones in the as-cast strips, and thus may become a source of boundary conditions for the models being the basis of computer simulation of semi-solid plates. The presented results were formed with the help of an authorial, presented in [2] software dedicated to qualitative and quantitative image analysis.

2. Methodology

From the sake of occurrence and distribution of voids the analysis of as-cast steels structure is an important issue. It is a complex problem that employs both digital image processing and application of auto-expert systems and statistical methods. The schema of entire process is shown in Figure 1.

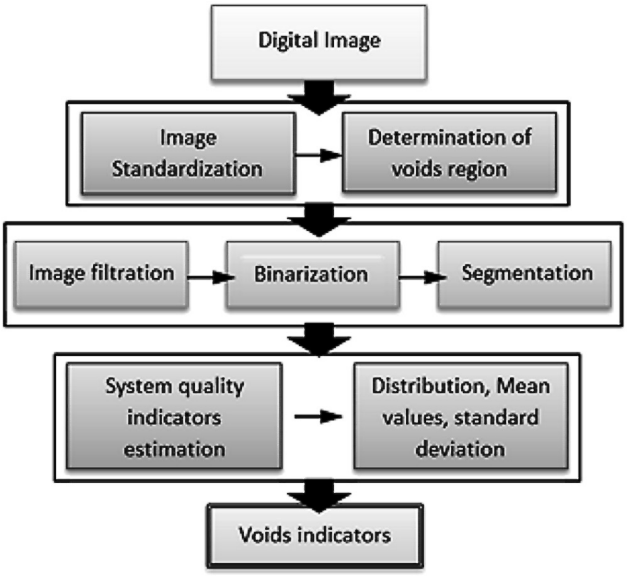

Fig. 1. The general scheme of the voids estimation and image analysis process

Rys. 1. Główny schemat procesu wyodrębnienia i analizy obrazu pustek

At the initial step the digital image is converted into a form which is most useful for further segmentation. Image scale adjustment is also taken into consideration in aim to correct even minor differences in size of analysed regions. The standardization transformations have strong impact on the final results and hence on the effectiveness of the presented solutions. The next operation is done in aim to obtain the voids occurrence polygonal region (area that includes voids). Both the operations, i.e. standardization and voids region estimation create the image preparation stage of the analysis process [2].

The subsequent and most important chain of operations is the image digital filtration consisted of three sequential operations: image filtration, binarization and segmentation. Because the presented process was performed automatically for each digital image, input parameters values of employed methods strongly depend on source images. The main goal of image filtration is both voids boundaries enhancement and minimization of the image total noise level which allows the distinction of small fragments of the image. It might have real influence on achievement of real final result [5]. The image filtration is consisted with several transformations like: removal the non-flat background illumination, contrast enhancement

and median filtration in order to remove image artefacts and false voids. The sequent operation is called binarization. The essence of this transformation is the extracting of voids from the image and rejecting its rest as useless for further analysis. The Otsu auto binarization method is employed to calculate the correct threshold level. The method provides the best results in comparison to the other approaches (minimum histogram variance, entropy, *k*-means). In addition the ultimate erosion points are estimated and serve as reference points for the system of quantity indicators. The final image filtration method is called segmentation. This operation divides image into the list of subgroups, i.e. list of voids groups. The conjunction of the entire image filtration methods have the strongest impact on finial results of the analysis [6].

The list of voids images serves as an input data to the next phase of analysis called segments descriptors estimation. At this stage a segments descriptors shape estimation is executed for each individual void. Its results are parameters representing shapes of individual segments and theirs mutual correlation. To evaluate the quality of samples with semi solid core the authors have taken into consideration following parameters that were used to calculate the system quality indicators:

A. The average void equivalent diameter and diameter standard deviation:

$$D_{eq} = \sqrt{4\pi / Area;\ D_{eq}} = \frac{1}{N}\sum_{i=1}^{N} D_{eq}^{i} \tag{1}$$

B. Standard deviation of voids orientation:

$$\sigma_{\alpha} = \frac{1}{N}\sqrt{\sum_{i=1}^{N}(\bar{\alpha} - \alpha_i)}; \quad \text{where} \quad \alpha = \tan^{-1}\frac{K + \sqrt{K^2 + 4M_{xy}^2}}{2M_{xy}} \tag{2}$$

C. The number of voids per unit length:

$$N_L = \sqrt{\left(\frac{N_{OX}}{L_X}\right)^2 + \left(\frac{N_{OY}}{L_Y}\right)} \tag{3}$$

D. The average distance between voids (calculated in specific distance from centre):

$$L_i^O = \frac{1}{N_R}\sum_{i=0}^{R} L_i \tag{4}$$

E. The volume fraction level of voids:

$$V_V = \frac{V_{\text{voids}}}{V_{\text{region}}} \tag{5}$$

Where symbols in equations (1) to (6) denote:

- M_{ij} – moment invariants calculated in ij directions,
- N – the number of voids,
- N_R – the number of grains located inside the circle of radius R,
- N_{OX} – the number of voids located over a segment of length L_X in X direction,

V_{voids} – the volume occupied by voids,
V_{region} – the volume of analysed region.

Each individual parameter indicates the most common value and the range of occurrence. The average void equivalent diameter represents the most common void size and the standard deviation represents the range of occurrence of various sizes. In addition at the description estimation stage the histogram of occurrences is calculated. It serves as a supplementary information parameter concerning the voids distribution. The parameter histograms can be a source of second step of voids segmentation leading to the shape factor, but the authors did not take this issue into consideration, because in the presented case it has not been required. Voids orientation coefficient and theirs standard deviations as well as the distribution histogram indicate the privileged orientation of voids – both global and local. It also shows the potential directions of defects formation in casted steels. The number of voids per unit length together with average voids equivalent diameters show how specific voids sizes form local clusters. If the local cluster is situated near the material surface the risk of material cracking significantly increases. The parameter describing the distance between voids (calculated in the specific distance, relative to each void centre) with assistance of its histogram and variation parameter show the tendency to form a single local cluster of voids. The distance between voids is calculated on basis of reference points acquired at the ultimate erosion image filtration stage. The last parameter being under consideration of the current study is called voids volume fraction level. This value is scaled to aim image magnification and voids occurrences region and plays role of standard volume invariant. Volume fraction of voids represents the ratio of voids volume to total region volume and describes the state of volumetric defects of a sample after solidification process. The fallowing indicators were used to estimate system quality (tested sample quality): formability of local clusters, cluster type, privileged voids orientation, volumetric defects state. Methods of determining above indicators as well as theirs values are shown in Tables 1–4.

Table 1

Formability of local voids cluster indicator

$\overline{D}_{eq}$ [mm]	L_i^O [mm]	Formability of local clusters
Low	Low	Medium or High
Low	High	None or Low
High	Low	Very High
High	High	Medium

Table 2

Cluster types indicator

$\overline{D}_{eq}$ [mm]	N_L [mm^{-1}]	Cluster type
Low	Low	Local cluster with small sizes voids
Low	High	No cluster or local cluster with scattered voids
High	Low	Local cluster, potential location of material failure
High	High	No cluster

Table 3

Indicator describing privileged voids orientation occurrence

σ_α [°]	Privileged voids orientation occurrence
Low	High
Medium	Medium
High	Low

Table 4

Indicator of the volume state of defects in the form of voids

V_V [%]	Volumetric defects state
Low (< 0.2%)	Insignificant
Medium (0.2%–1.0%)	Possible sample
High (> 1.0%)	Faulty sample

3. Results

Figure 2 shows the pre-processed image of longitudinal cross section of a sample, which was previously used in the study of strain-stress relationship at very high temperature. The mechanical properties of semi-solid steel were investigated using physical GLEEBLE 3800 simulator in the Institute for Ferrous Metallurgy in Gliwice Poland.

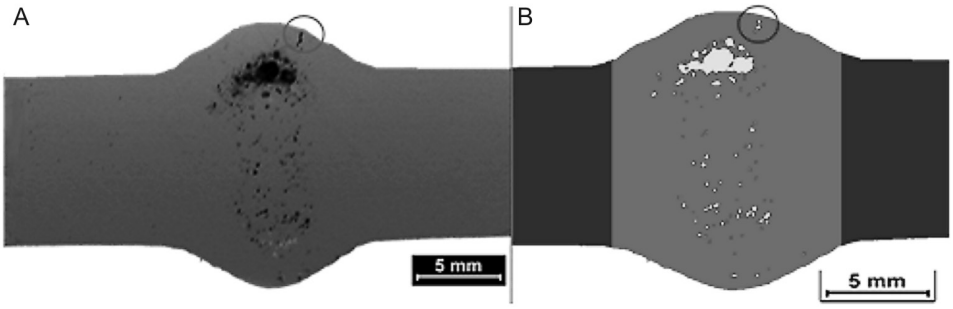

Fig. 2. A non-etched sample deformed at 1460°C using GLEEBLE 3800 physical simulator with marked surface crack: A – original, B – voids region marked (the red colour highlights the analysed area, the light blue colour emphasizes unclosed voids)

Rys. 2. Obraz próbki nietrawionej otrzymanej na symulatorze fizycznym GLEEBLE 3800 w temperaturze 1460°C z zaznaczonym powierzchniowym pęknięciem: A – obraz wyjściowy, B – obszar z uwidocznionymi pustkami (kolor niebieski – oznaczone niezamknięte pustki, kolor czerwony – osnowa – metal

The presented in figure 2 shape of the sample central part is a result of its deformation in final stage of solidification process [3, 4]. The quantitative analysis were performed to estimate

parameters used in the system quality indicators based on equations (1) to (5) as shown in table 5. In the figure 2 two separated voids clusters are seen. The largest and occupying the most space cluster is located near the material surface and could emerge in case of high compressive force during the testing in the GLEEBLE equipment. Moreover, the figure demonstrates the specific privileged orientations. The second cluster with significantly lower average equivalent diameters and greater value of average distance coefficient is located below the centre of the tested sample. In addition the surface perforation crack (marked with blue circle on images A and B) can be identified and with high probability will cause material failure at this region during further sample deformation. Assessment of visualized morphology of voids and sparse regions allow better analysis of the material properties and its resistance to cracking. The exemplary result of the analysis is collected in Table 5 and Table 6.

Table 5

The values of quality indicators taken for the digital analysis of the image shown in Figure 2

$\overline{D}_{eq}$ [mm]	α [°]	N_L [mm^{-1}]	L_i^O [mm]	V_V [*100%]
0.24	8.6	0.19	1.08	1.2

Table 6

The results of the analysis of the deformed sample included into a of quality indicators

Clusters Formability	Cluster type	Occurrence of privileged orientation	Volumetric defects state
High	Local cluster, potential location of material failure	Low	Faulty sample

Quality indicators analysis of the steel sample presented in this paper with semi-solid core after deformation process shows that there is high cluster formability indicator and the local clusters are constructed with large voids. This type of cluster may cause material damage during further deformation and forming parameters of the steel sample process should be considered risks subjected and chanced. The privileged orientation is not found in the tested sample.

4. Conclusions

The voids analysis method presented in this paper provides good descriptive characteristics of sample defects state as well as gives expert-system-like results. The applied indicators are computed very quick in fully automated process from input image to the received results. The most critical operations in chain of subsequent transformations are both standardization and segmentation. Theses transformations have strong impact on the recognition results and hence on the effectiveness of the presented analysis. It is necessary to focus in the nearest future to perform method optimization and selection of the segmentation methods that not only detect local defect clusters but also estimate the most critical and favourable locations of defect

formation. This paper presents the results from the prototype application of digital image processing to analysis of the occurrence and distribution of voids caused by solidification process in samples which demonstrate semi-solid core.

The work has been supported by the Polish Ministry of Science and Higher Education Grant N N508 585539.

References

[1] Tsuchiya S., *Elucidation of formation mechanism of γ grain structures in as-cast and semi-solid carbon steels including viscosity behaviour of the semi-solid steel*, PhD Thesis, AGH, Kraków 2012.
[2] Gumuła A., Dębiński T., Głowacki M., *Automatic approach to microstructural image recognition and analysis*, Steel research Int, spec.ed., 2012, 1331-1334.
[3] Głowacki M., *Inverse Analysis Applied to Mushy Steel Rheological Properties Testing Using Hybrid Numerical-Analytical Model*, In: Numerical Modeling InTech Publisher, 2012, 278-302.
[4] Głowacki M., Hojny M., *Investigation of Mushy Steel Rheological Properties at Temperatures Close to Solidus Level*, In: Polish Metallurgy 2006–2012 in Time of the Worldwide Economic Crisis Publishing House Akapit, 2010, 193-212.
[5] Russ J.C., *The image processing handbook – sixth edition*, Taylor and Francis Group, 2011.
[6] Szala J., *Selected problems of quantitative metallography*, Ivo Schindler & Eugeniusz Hadasik, Deformation behavior and properties of selected metallic materials, 2007, 29-54.

TECHNICAL TRANSACTIONS | **CZASOPISMO TECHNICZNE**
MECHANICS | MECHANIKA
1-M/2013

JACEK HABEL*

THE IDEA OF MACHINING PROCESS PLANNING WITH ALTERNATIVE ROUTES IN FORM OF NON-CYCLIC GRAPH FOR CAPP IMPLEMENTATION

PLANOWANIE PROCESÓW TECHNOLOGICZNYCH OBRÓBKI Z ZAPISEM WARIANTÓW W FORMIE GRAFÓW NIECYKLICZNYCH DLA POTRZEB CAPP

A b s t r a c t

The paper presents the formal method of recording the alternatives of machining process plan. This method based on levels distinguished in hierarchical structure of process, where alternatives can be created. The algorithm for linking intermediate states of workpiece was developed. It enables to change series of linear processes into one network of alternative plans in the form of non-cyclic graph.

Keywords: *CAPP*, *alternative process plans*

S t r e s z c z e n i e

W artykule przedstawiono metodę zapisu wielowariantowych procesów technologicznych dla obróbki skrawaniem. Podstawą tego zapisu było wydzielenie poziomów, na których w hierarchicznej strukturze procesu mogą powstawać warianty. Następnie opracowano algorytm łączenia stanów pośrednich, dzięki któremu z początkowo liniowych wariantów procesów tworzona jest sieć wariantów w postaci grafu niecyklicznego.

Słowa kluczowe: *CAPP*, *wariantowe procesy technologiczne*

* PhD. Eng. Jacek Habel, Institute of Production Engineering, Faculty of Mechanical Engineering, Cracow University of Technology.

1. Introduction

Nowadays planning and production management is still difficult. Competitive market forces to verify all possible methods which lead to shorten product cycle time and reduce manufacturing cost. From the production management point of view, among the product life--cycle, there is one critical stage: manufacturing process planning, which have considerable influence on making the cycle time shorter. One of encouraging directions to extend flexibility of this stages relies on adding decision alternatives.

Manufacturing process planning can be aided by CAPP (Computer Aided Process Planinng) systems [2]. Previous implementations of CAPP were focused on single process plan creation method e.g. with manufacturing knowledge utilization [1]. Next generation of CAPP systems were focused on generation process alternatives [9, 12], what gives decision flexibility. Nowadays researches are going to use CAPP as a tool, which can be a data source to solve more complex problems. Many examples of integration of process planning and e.g. scheduling can be found [10, 11].

The main goal of this paper is to find out the possible alternatives in machining processes and its structure recording type. The idea of process alternative is still not fully defined. Moreover there is the problem how to record the structure of process alternatives?

2. Characteristic of CAPP system implementation

Manufacturing process planning can be supported by many CAx systems [2]. At that stage we have to separate assembly and any other manufacturing methods (e.g. machining). This paper will take into consideration only machining methods as an assumption. Including that assumption we can find in literature many examples which describe CAPP systems implementation [1, 9, 13].

The CAPP system is a tool used to create the process plan. It could aim at different manufacturing methods, but typical application is to aim at machining process planning [1, 9]. In that case, an input information is a workpiece data. This data can be entered into CAPP system manually or can be retrieved from CAD system (based on e.g. feature recognition procedures) [9, 10]. The machining process plan, recorded and presented in different forms, is the output from CAPP.

The CAPP system implementation depends on the selected method. Following methods can be distinguished [2]: variant, generative and semi-generative.

The *TechPlan CAPP* system is an example of using the semi-generative method. TechPlan system was developed at Production Engineering Institute on Cracow University of Technology. Authors developed the architecture of semi-generative CAPP system [3, 5]. Key features of the developed system are: (i) manufacturing knowledge divided into: (a) *production knowledge* (decision rules representation) which defines conditions to apply machining method, (b) *classification knowledge* (tree representation) which allows to features recognition and (c) *control knowledge* (hierarchical decision networks and frames representation) which defines process route alternatives as a process template [3, 6]; (ii) the EXSYS expert system shell used to store production knowledge and allow to the

exchange of data between other modules; (iii) control mechanism of decision making with backward reasoning [3]; (iv) object oriented and feature based formal workpiece (part and its intermediate states) representation with automated procedures of feature recognition and translation from CAD [6,8]; (v) formal description of manufacturing activities which allows to define manufacturing capabilities of resources [4]; (vi) database of manufacturing system capabilities and resources [4, 7].

The TechPlan CAPP system runs in three stages [3]: (i) the workpiece type recognition; (ii) generation of blank design and intermediate states of workpiece using reverse method; (iii) detailed generation of machining operation's properties.

At the first stage, based on classification knowledge, the system recognizes the type of workpiece. This stage is significant, because in semi-generative method, the different knowledge templates are created for different workpiece types (part families).

At the second stage, based on control knowledge, what in fact is a general template of process plan for given set of similar workpieces (e.g. shafts), and production knowledge, the possible alternatives of intermediate states of workpiece and alternatives of final blank design are generated.

The last stage is a generation of manufacturing process alternatives. The main rule is to utilise intermediate states of workpiece generated at second stage and try to find (using three sources: workpiece feature oriented database, database of manufacturing system capabilities and manufacturing knowledge recorded in expert system) all possible alternatives. It is possible thanks to, defined before, manufacturing activities stored in database of the manufacturing system capabilities [4, 7].

3. Representation of machining process structure

Manufacturing process can be, in general, described as follow. Given *part*, which has to be machined from selected (or designed) *blank* (semi-finished product or raw material), is passing through successive stages of that process. As a result, the *ready part* (final product), which fulfills quality requirements, is processed. The *workpiece*, passing through the process, is changing its *state* (Fig. 1), what will be named as *intermediate state of workpiece features* S_f, where f is an index of intermediate state and $f = 0 \ldots F$, where F is the highest number of recorded S_f. There are two special states: *initial state* S_0, given by blank design and *final state* S_F, given by ready part drawing.

To perform manufacturing process, for each stage, selected *manufacturing resources R* are required. In typical manufacturing system environment (based on cells and work stations), resources R can be defined as a set of *processing resources RP* and *part flow resources RF*:

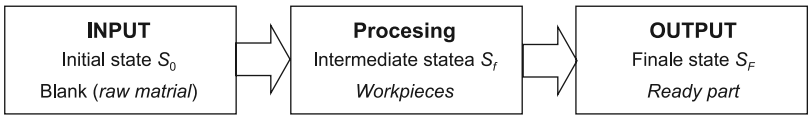

Fig. 1. General model of manufacturing process and intermediate states of workpiece

Rys. 1. Ogólny model procesu wytwarzania i stanów pośrednich przedmiotu obrabianego

$R = \{RP, RF\}$. Processing resources can be defined as a set of *machine tools* (metal-working machines) *RM,* and a set of *exchangeable equipment RE*: $RP = \{RM, RE\}$. In machining operation the following RE types can be utilized: *work holding devices RW* (e.g. three-jaw chucks, dead or live centers, face drivers, etc.) and *cutting tools* with tooling system (together form a *tool assembly*) *RT*, which can be defined as a set: $RE = \{RW, RT\}$.

Machining process plan MP combines all needed activities to change the blank into ready part. That defines main function of machining process as intended change of workpiece characteristics, starting from initial state S_0, passing through intermediate states S_f, and finally reaches the state of ready part S_F. Because it is a discrete process, the following manufacturing process components can be distinguished: (i) *machining operation MO*, which is performed on single workstation *RM* on a single workpiece or batch without interruption; (ii) *workpiece setup SU*, which concerns the fixing type with *RW*, understood by applying clamping forces to the workpiece to ensure the stability of its position during the machining (position of a workpiece can be changed only by unclamping and reclamping it again); (iii) *machining cut MC*, which is the main element of machining operation, performed by the same resources *RT* and with unchanged cutting parameters. These components create the *hierarchical structure*, where above component can consist of a set of below components, with one-to--many relation. It is assumed also that each parent component of that hierarchy can has a set of child components with different number of members.

Formally it can be noted as follow. Each *i*-th part *PT* has at least one machining process plan *MP*. The *i* is an index of part, and $i = 1\ldots N$, where the *N* is the total number of recorded *PT*. By definition the machining process consist of machining operations. In general: $MP_i = \{MO_1^i, MO_2^i, \ldots, MO_j^i\}$, where each *i*-th machining process consist of a set of machining operations MO_j^i. The *j* is an index of machining operation in *i*-th process plan and the *J* is the total number of recorded MO_j^i. Important to notice is possibility to define different *J* number of operations for each *i*-th process.

Then each machining operation MO_j^i can consist of a set of workpiece setups SU_k^{ij}: $MO_j^i = \{SU_1^{ij}, SU_2^{ij}, \ldots, SU_K^{ij}\}$. The *k* is an index of workpiece setup, where the *K* is the total number of recorded SU_k^{ij} in MO_j^i.

Finally, in each setup SU_k^{ij} can be performed a set of machining cuts MC_l^{ijk}: $SU_k^{ij} = \{MC_1^{ijk}, MC_2^{ijk}, \ldots, MC_L^{ijk}\}$. The *l* is an index of machining cut, where the *L* is the total number of recorded MC_l^{ijk} in SU_k^{ij}.

4. Possibilities of machining process alternatives creation

Omitting the creation process plan method, the question is how to create alternatives of manufacturing process plan? The most important is an idea of *intermediate states of workpiece*. The intermediate state S_f of workpiece defines the state of all workpiece features.

The state of workpiece feature can be defined as a set of: dimensions, shape type, surface quality and physicochemical properties. Because the intermediate state can be reached by implementing different machining methods, it causes possibility to create some alternatives.

To create *machining process plan alternatives MPA*, it is needed to distinguish places where that alternatives can be defined. From the theoretical point of view, alternatives can be found on each level of machining process hierarchy. The structure of MP depends on the following factors: (i) possessed manufacturing resources RP and their capabilities; (ii) manufacturing knowledge of the process engineer or CAPP; (iii) production size and selected type of blank.

At that stage following assumption has to be made: set of resources RP of manufacturing system and their capabilities are known. It means that process engineer, based on his experience and manufacturing knowledge (or control mechanism of CAPP system), can change the structure of MP only by selecting different machine tools route (with different number of operations in MP) or by selecting another type of blank. Based on such rule, the machining process alternatives MPA can be created.

In general, the five levels of *alternatives* can be defined: **level 1** of MP structure, where each *MPA* has a different set of machining operations MO; **level 2** of MO structure, where alternatives *MOA* can be created by selecting other machine tool RM or by changing MO internal structure on lower levels, what causes a difference in implementation, number of used resources RE, time and cost; **level 3** of SU structure, where alternatives *SUA* can represent different alternatives of workpiece setup by using different exchangeable equipment RW to clamp workpiece and it causes division of machining operation on different number of setups; **level 4** of MC sequence *MCS* in given SU, what is the most complex. There are two reasons to create MCS alternatives: (i) SUA defines different number of MC in each, (ii) in given *SUA* is possible to change or optimize the sequence of machining cuts MCS; **level 5** of MC implementation, where each MCA can be realized by using different tool type RT (e.g. solid, brazed or indexable tool) and each MCA can be realized by applying different cutting parameters.

From the shop floor control point of view only first two levels are important to take for further consideration. But typical structure of MP is not sufficient and must be changed. The main reason is the difference in interpretation of operation.

By definition machining operation is connected with only one workstation (machine tool), but there is possibility to change position of workpiece by changing setup SU. To realize this other resources RF are needed (e.g. robot). Moreover it makes necessary to stop machine tool and e.g. change some RE or upload new NC program. Taking this into consideration, the new definition of machining operation has to be established. It will be called *machining activity*.

Machining activity MA is an ordered set of basic activities (e.g. machining cuts) realized in one machining operation MO and one setup SU on given machine tool RM. MA has own NC program. For that assumptions, the new definition of operation as machining activity was adopted. Moreover the new way of operation identification and *MPA* recording was developed.

Each part PT_i can has a set of machining process alternatives MPA_v^i (with different route and set of machining operations): $PT_i = \{MPA_1^i, MPA_2^i, \ldots, MPA_V^i\}$. The v is an index of machining process alternative MPA and the V is a total number of recorded MPA_v^i.

Then each MPA_v^i can consist of a set of machining activities MA, but each can be defined as a set of its alternatives. To simplify the model naming, these alternatives will be further called as *operation alternative* OA_{rw}^{vijk}: $MA_{jk}^{vi} = \{OA_{r1}^{vijk}, OA_2^{vijk}, \ldots, OA_{rW}^{vijk}\}$. The w is an index of operation alternative OA and the W is a total number of recorded alternatives OA_{rw}^{vijk}. Moreover each operation alternative OA can be defined as 8-tuple:

$$OA_{rw}^{vijk}(MPA_v^i, PT_i, MO_j^i, SU_k^{ij}, RP_r, TP, CP, NC) \tag{1}$$

In (1) additional parameters are defined: *TP* – standard time of part processing; *CP* – processing cost; *NC* – identifier of NC code file to upload to the machine tool control system. First five elements are defining the place of OA in MPA hierarchical structure. Figure 2 presents all used indexes to identify the operation alternative OA.

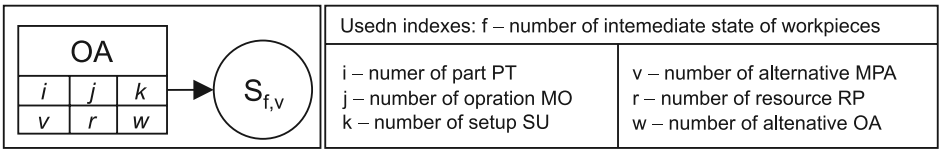

Fig. 2. Indexes of operation alternative OA identification

Rys. 2. Oznaczenia identyfikujące wariant operacji OA

5. Example of recording machining process alternatives

As mentioned before, the typical structure of machining process has hierarchical form. This representation is inconvenient for process plan generation and also for further analysis (from the algorithmic point of view). Moreover in that representation, hierarchical tree is made of nodes, which represent different process elements (operation, cut etc.) on different levels of this hierarchy. It is also not consistent.

The new way of process representation, which remove above weaknesses, was developed. First of all, the structure of alternative process will be recorded as a network in form of non-cyclic graph. Secondly, what is the most important here, nodes will represent intermediate states S_f of workpiece and edges will represent operation alternatives *OA*.

To verify the *MPA* recording structure, series of testing examples was introduced. Because the TechPlan system possess manufacturing knowledge only for rotational parts, only for that kind of parts was verified. Also tests were limited to defined set of manufacturing system resources RP (12 different machine tools RM, with minimum two different standard RE).

For selected part (id: shaft_01) the following alternative process plan was designed. The process has two initial states S_0, because this shaft can be processed from rolled bar or forging. Then there were 3 different routes created (2 for rolled bar and 1 for forging). For example route 1 (for rolled bar blank type) has following six operations: (i) cutting off, (ii) facing and centering, (iii) rough turning, (iv) medium turning, (v) milling and (vi) grinding. In each route different setups in machining operations were added. Finally 6 different linear

routes of MPA were created (with total 37 different OA), what defines set of alternatives: $PT_1 = \{MPA_1^1, MPA_2^1, MPA_3^1, MPA_4^1, MPA_5^1, MPA_6^1\}$.

Figure 3 presents linear alternatives for selected shaft01. Each alternative process plan MPA has its internal structure of operation alternatives OA, where each MPA has different number of operations and setups. Each operation OA has assigned needed recourses RP. This can be written: $MPA_4^1 = \{OA_{1.1}^{4111}, OA_{7.1}^{4121}, OA_{17.1}^{4131}, OA_{16.1}^{4141}, OA_{18.1}^{4151}, OA_{22.1}^{4161}\}$, and it is only one example of alternative route number 4.

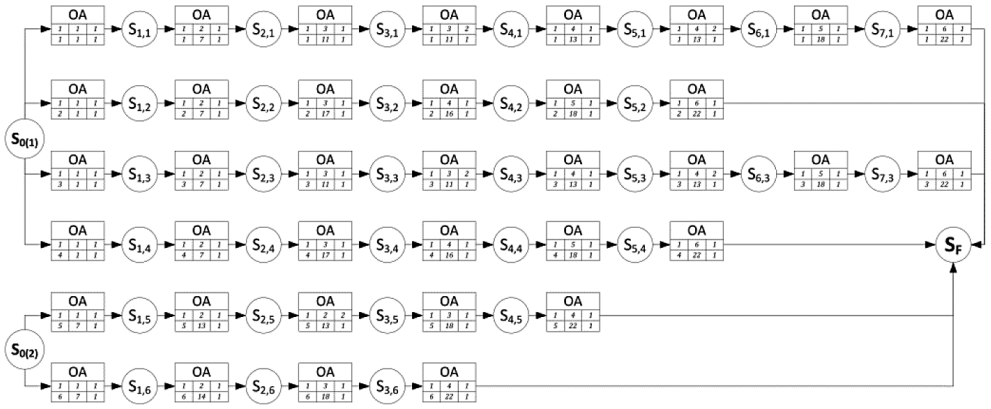

Fig. 3. Linear machining process plan alternatives – an example

Rys. 3. Liniowe warianty procesu technologicznego obróbki – przykład

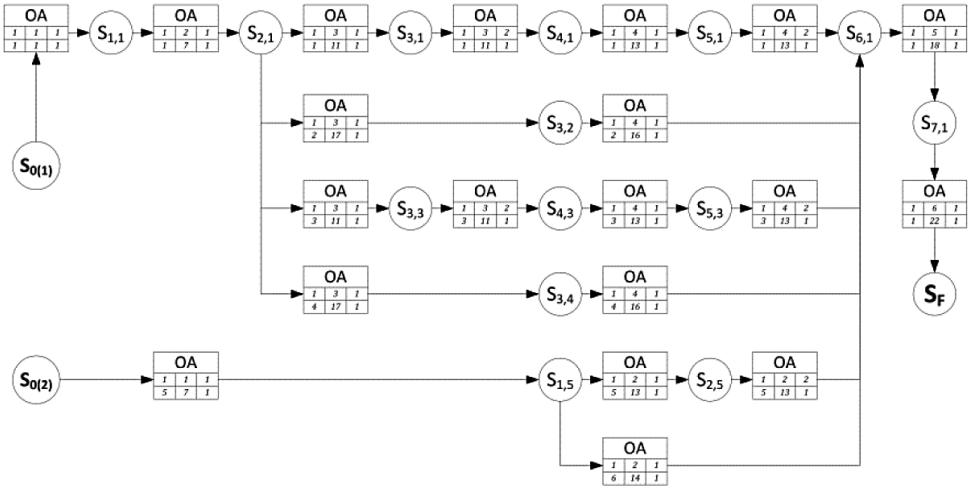

Fig. 4. Nonlinear machining process plan alternatives as a non-cyclic graph

Rys. 4. Nieliniowy wariantowy proces technologiczny obróbki w postaci grafu niecyklicznego

Important to notice is that each OA changes the intermediate state of workpiece S_f. That means, even when we start with different input states S_0 (blanks), there is possibility that some of S_f states are the same. Because the S_f states are represented as a set of parameters, it is possible to built procedure to compare S_f states, what was made. The applied procedure was comparing, generated operation alternatives OA and S_f states. If some are the same, algorithm links them and final number of OA and S_f is smaller than at the beginning. That procedure creates non-linear process plan as a non-cyclic graph of operation alternatives.

6. Conclusions

The representation of machining process plan with alternative routes in form of non--cyclic graph was worked out. The most important idea was to define the intermediate states of workpiece. This approach gives possibility to record all alternative routes of machining process plan in one non-cyclic graph, where node represents intermediate state of workpiece and transition represents operation alternative. Moreover the formal description of machining process plan alternatives MPA was also worked out. Based on this notation the logical structure ERD of database was also developed. The next step will be integration with CAPP TechPlan system. The worked out representation gives many possibilities to utilization, like the integration with online shop floor control system. Moreover, based on generated alternatives can be applied optimization procedure to find the best process route based on given criteria.

References

[1] Chang T.Ch., *Expert Process Planning for Manufacturing*, Addison-Wesley Publishing Company, USA 1990.

[2] Chryssolouris G., *Manufacturing systems, theory and practice*, Springer-Verlag, USA 1992.

[3] Duda J., Habel J., Pobożniak J., *Control mechanism of expert system with representation of knowledge in the form of hierarchical decision nets*, Proceedings of 12th International Conference on Applications of Artificial Intelligence in Engineering, AIENG XII, Wessex Institute of Technology UK, Capri, Italy, July 1997.

[4] Duda J., Habel J., Kwatera M., Samek A., *Data Base with open architecture for defining Manufacture System Capabilities*, Proceedings of the 9th FAIM International Conference, Tilburg, Nederlands 1999.

[5] Duda J., *Semigenerative System for Manufacturing Process Planning*, Proceedings of the 10th FAIM International Conference, University of Maryland, USA, Vol. 2, 2000, 1007-1016.

[6] Duda J., Habel J., Pobożniak J., *Repository of Knowledge for Manufacturing Process Planning*, Proceedings of the 15th FAIM International Conference, Deusto University Bilbao, Spain 2005, 171-178.

[7] Habel J., *The Idea of Integrated Manufacturing Process Planning System*, Proceedings of 16th FAIM International Conference, University of Limerick, Irland, June 2006, 185-192.

[8] Pobożniak J., *Integration of CAD and Generative CAPP Based on Feature Technology*, Proceedings of the 3rd International Symposium on Intelligent Manufacturing Systems, Turkey 2001.

[9] Sormaz D.N., Khoshnevis B., *Generation of alternative process plans in integrated manufacturing systems*, Journal of Intelligent Manufacturing, vol. 14, 2003, 509-526.
[10] Sormaz D.N., Arumugam J., Harihara R.S., Patel C., Neerukonda N., *Integration of product design, process planning, scheduling and FMS control using XML data representation*, Journal of Robotics and Computer-Integrated Manufacturing, vol. 26, 2010, 583-595.
[11] Tan W., Khoshnevis B., *Integration of process planning and schedulling – a review*, Journal of Intelligent Manufacturing, vol. 11, 2000, 51-63.
[12] Yang Y.N., Parsaei H.R., Leep H.R., *A prototype of a feature-based multiple-alternative process planning system with scheduling verification*, Journal of Computers & Industrial Engineering, vol. 39, 2001, 109-124.

TECHNICAL TRANSACTIONS | **CZASOPISMO TECHNICZNE**
MECHANICS | MECHANIKA
1-M/2013

DAVID HLAVÁČEK*

METHODS OF DUCTED FAN AIRCRAFT PROPULSION UNIT NOISE PREDICTION

METODY PROGNOZOWANIA HAŁASU JEDNOSTKI NAPĘDOWEJ KANAŁOWEGO WENTYLATORA LOTNICZEGO

Abstract

The UL-39 ultra-light aircraft which is being developed by the Department of Aerospace Engineering, Faculty of Mechanical Engineering, Czech Technical University in Prague, is equipped with an unconventional ducted fan propulsion unit. This paper deals with identifying noise sources of this propulsion unit and easily applicable ways of predicting its noise level. At the end, a few potential noise-suppressing design improvements are presented.

Keywords: *UL-39*, *ducted fan propulsion unit*, *rotor-stator interaction noise*, *rotor-alone noise*, *cold air jet noise*, *flow passage noise*

Streszczenie

UL-39 to ultra lekki samolot, który został skonstruowany w Instytucie Inżynierii Lotnictwa, na Wydziale Mechanicznym Czeskiego Uniwersytetu Technicznego w Pradze. Został on wyposażony w niekonwencjonalny wentylator kanałowy jednostki napędowej. W artykule autor zaprezentował metody identyfikacji źródeł hałasu badanej jednostki napędowej oraz łatwe w zastosowaniu metody przewidywania poziomu generowanego hałasu. Zostały również przedstawione propozycje zmian konstrukcyjnych redukujących hałas.

Słowa kluczowe: *UL-39*, *jednostka napędowa wentylatora kanałowego*, *hałas rotor-stator*, *hałas zimnego strumienia powietrza*, *hałas przepływu*

* Eng. David Hlaváček, Department of Aerospace Engineering, Faculty of Mechanical Engineering, Czech Technical University in Prague.

List of symbols

a – speed of sound [m·s^{-1}]
$c_{D,R}$ – rotor blade drag coefficient [1]
c_R, c_S – rotor and stator blade chord length [mm]
D – sound attenuation [dB]
d – flow passage diameter [mm]
f – frequency [Hz]
F_y – lift force [N]
K – nozzle experimental constant [1]
L_p, L_W – noise pressure level, noise power level [dB]
Ma – Mach number [1]
p – pressure, acoustic pressure [Pa]
R_T – parameter respecting the Reynolds number (Goody) [1]
r – radial coordinate [mm]
S – flow passage area [m^2]
$S(\omega)$ – stator blade transversal response function [1]
$T(\omega)$ – stator blade longitudinal response function [1]
U, U_e – incident flow and rotor blade relative velocities [m·s^{-1}]
v – flow passage velocity, nozzle exit velocity [m·s^{-1}]
W – acoustic power [W]
z_R – rotor blade number [1]
α_∞ – angle of attack [°]
δ – boundary layer thickness [mm]
ν – kinematic viscosity [m·s^{-1}]
ρ – density [kg·m^{-3}]
τ – shear stress [N·mm^{-2}]
Φ – acoustic pressure spectral density [Pa·s]
Ω – rotor angular frequency [s^{-1}]
ω – reduced angular frequency [s^{-1}]
Subscripts:
i – incident acoustic pressure
t – transferred acoustic pressure
p, s – blade pressure side, suction side
R, S – rotor, stator
w – relative flow velocity
0 – wake
∞ – undisturbed flow

1. Introduction

The ducted fan propulsion unit of the UL-39 aircraft (see Fig. 1) which consists of an axial fan of stator-arrangement driven by a piston engine, is encountering difficulties with noise during its experimental operation. Beside the noise generated by the piston engine, tone

noise generated by the fan is present in the perceived acoustic spectrum. Therefore, during its future operation, the UL-39 aircraft may not fulfil the requirements concerning noise given by legislature. With these issues in mind, a new fan will be designed which will take into account the necessity of reducing noise while being capable to improve the aircraft flight performance at the same time.

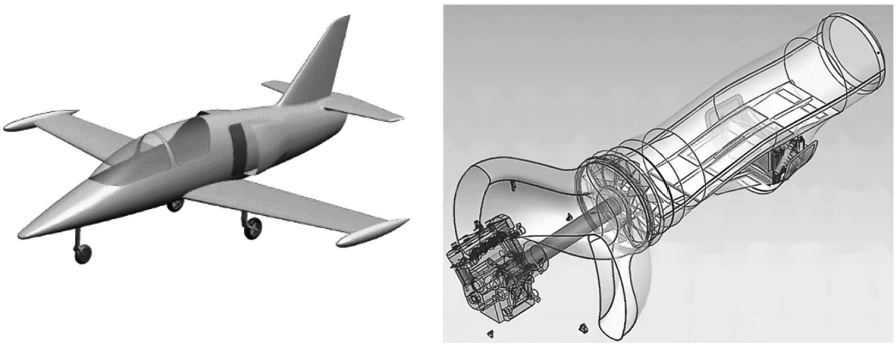

Fig. 1. The UL-39 and its ducted fan propulsion unit
Rys. 1. UL-39 i jednostka napędowa jego wentylatora kanałowego

In this paper, the noise sources of the propulsion unit will be identified and discussed. For each respective source, methods of computational estimation of noise level will be presented. In the final chapter, potential noise-suppressing design improvements will be briefly mentioned.

Beside the noise generated by the piston engine, four basic noise sources can be identified in the UL-39 propulsion unit – the rotor-stator interaction, the rotor alone, turbulent flow inside the flow passages and the cold air jet flowing from the exit nozzle. The cold air jet noise is not included in this paper since the nozzle will primarily be optimized for the best flight performance.

2. Rotor-stator interaction noise prediction

The rotor-stator interaction generates tonal noise with a so-called blade-passing frequency which is caused by wakes behind one blade cascade interfering with another cascade placed downstream. The downstream blades generate instationary lift from which the tonal noise comes. Methods of rotor-stator interaction noise prediction and suppression which can be applied to the UL-39 ducted fan propulsion unit were first used in turbofan engine fan design and development. Therefore, the rotor-stator configuration is only taken into account in the studies referred to. During the future development of the UL-39 propulsion unit, advantages and disadvantages of the respective fan configurations will be thoroughly discussed and the most suitable solution chosen.

The in stationary lift force generated by the stator blade cascade under the influence of incident wakes from rotor blades placed upstream and the resulting noise power level can be computed according to [2].

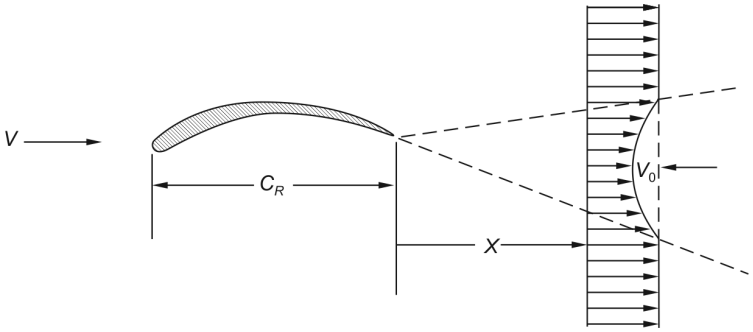

Fig. 2. Model of the rotor wake velocity defect [2]
Rys. 2. Model wadliwego śladu strumieniowego rotora [2]

In this technical memorandum, different equations for computing the wake velocity defect are presented and compared. With different constants, the following relationship is used:

$$\frac{v_0}{v_\infty} \sim \frac{\sqrt{c_{D,R}}}{\sqrt{\frac{x}{c_R}}} \tag{1}$$

The response of the stator blades to the instationary pressure changes caused by the rotor wakes can be expressed using two experimentally determined functions based on the fundamentals of instationary aerodynamics, $S(\omega)$ and $T(\omega)$. These complex functions are related to transversal and longitudinal response of the stator blades, respectively (see Fig. 3). The functions $S(\omega)$ and $T(\omega)$ depend on the so-called reduced angular frequency. The change of lift force is then computed as follows:

$$\Delta F_y \sim S(\omega) - \alpha_\infty T(\omega); \quad \omega = \frac{\pi c_s z_R \Omega}{c_{a,s}} \tag{2}$$

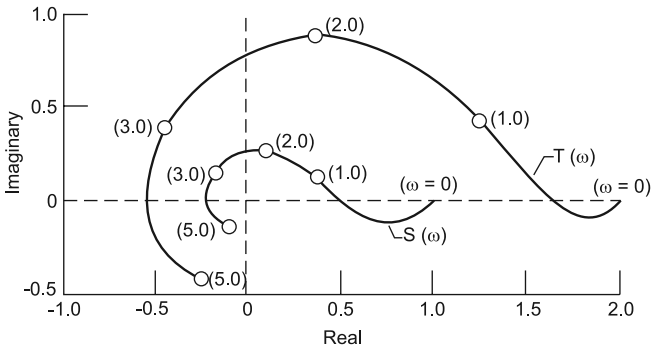

Fig. 3. Transversal and longitudinal blade response functions [2]
Rys. 3. Wzdłużna i poprzeczna funkcja odpowiedzi dla ostrza

Using this computation, no absolute noise level can be determined. However, the current fan and the new one can be compared with each other since the noise power level difference can be calculated.

$$\Delta L_W = 20 \log \frac{\Delta F_{y,2}}{\Delta F_{y,1}} \tag{3}$$

It should be noted that the above-mentioned method is not numerically precise since the equations it incorporates were derived considering a flat and isolated air foil (not installed in a cascade). Regardless of that, it can still be used for comparing the currently-used fan to a new one.

A more sophisticated method of rotor-stator interaction noise prediction is presented in [7]. In opposition to the previous method, it is already based on a blade cascade, not an isolated air foil. Moreover, the cascades are assumed to be placed in a cylindrical duct of infinite length. The coordinate system used by this method is shown in Fig. 4. The wakes behind the air foils placed upstream which generate can be modelled using various functions, including hyperbolic functions or Gaussian distribution. Recommendations concerning the wake models are presented in [8].

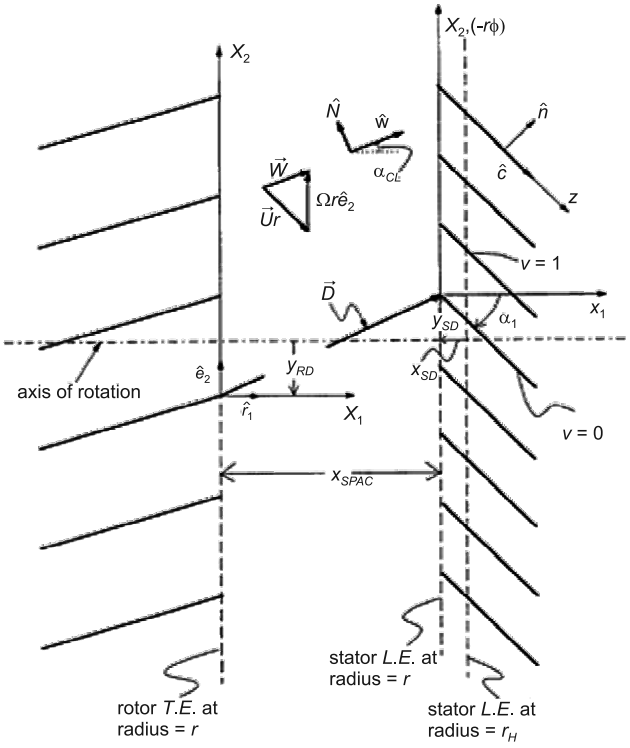

Fig. 4. Model of rotor and stator blade cascades presented in [7]

Rys. 4. Model łopatek kaskadowych wirnika i stojana [7]

Using this method, the acoustic pressure field inside a cylindrical fan duct can be computed as well as noise power level generated by the fan. Since this method involves using sophisticated mathematical operations, such as Green functions or integral equations, it comes as a computer program called *V072* created by the NASA. This program is distributed via the Internet [14] on request.

3. Flow passage noise prediction

Inside the flow passages of the ducted fan, broadband noise is generated by turbulent air flow. This type of noise can be suppressed by applying acoustic liners along the duct walls (which will be described below) or by reflecting the forward-radiating noise back downstream by the stator inlet guide vane (if present).

A method of quantifying the attenuation by the inlet guide vane can be found in [12]. It is based on using the longitudinal and transversal stator blade response functions, $S(\omega)$ and $T(\omega)$, already mentioned above. The calculation is to be made in elementary cylindrical layers of the fan inlet guide vane. The vane is modelled as a cascade of flat air foils. The incident acoustic wave is assumed to be planar. A part of the incident wave (its acoustic pressure is denoted p_i) passes through the blade cascade (p_t) while the other part is reflected. The ratio of acoustic pressures of the transmitted and incident waves is a function:

$$\frac{p_t}{p_i} = f(Ma_w, \alpha, \vartheta) \tag{4}$$

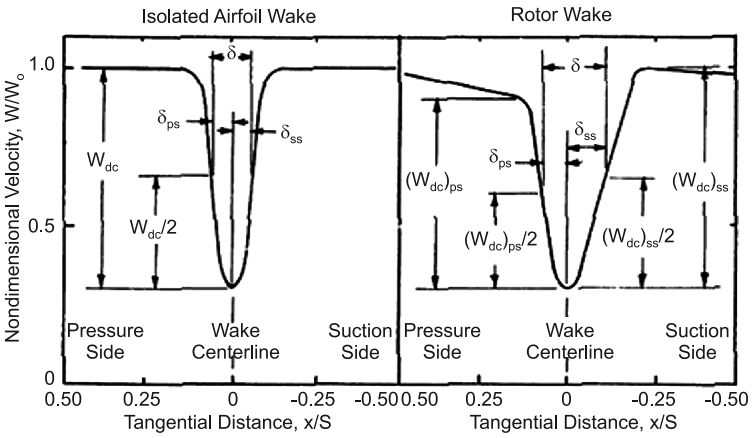

Fig. 5. Examples of wake models presented in [8]

Rys. 5. Przykłady modeli łopatek [8]

In this equation, Ma_w means the relative velocity Mach number, α is the angle between the acoustic wave direction and the blades and θ is the angle between the blades and the axis of rotation (as shown in Fig. 6). The resulting sound attenuation can be calculated as follows:

$$D = \frac{\int_d^D \left(\frac{p_t}{p_i}\right)^2 \left(\frac{\partial F_y}{\partial t}\right)^2 \frac{1}{r}\,\mathrm{d}r}{\int_d^D \left(\frac{\partial F_y}{\partial t}\right)^2 \frac{1}{r}\,\mathrm{d}r} \tag{5}$$

The lift force time derivative can be computed using the functions $S(\omega)$ and $T(\omega)$, Mach numbers of various velocities, the blade drag coefficient and their chord length (described in [12]). The acoustic pressure ratio is determined by calculating a system of partial differential equations. This calculation is described step by step in [6].

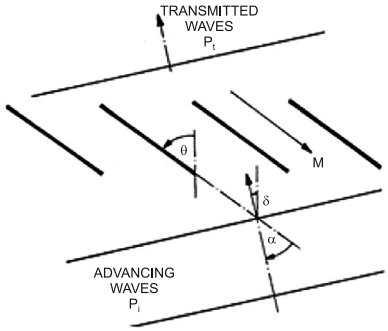

Fig. 6. The method of inlet guide vane attenuation [12]

Rys. 6. Schemat wlotu prowadzącego łopatki [12]

4. Rotor-alone noise prediction

As can be seen from the physical nature of the problem, the noise produced by the rotor itself is caused by a multitude of factors and it is not easy to predict. Not only does the rotor generate noise by its presence (and rotation) in a turbulent mean flow. It can also ingest flow instabilities from upstream or boundary layers separated from the duct walls, both of which contribute to the noise generation by locally increasing the turbulence intensity.

A prediction method concerning the acoustic pressure spectral density on the surface of the rotor blades is described in [13]. The spectral density can be determined from the following integral:

$$\Phi_{p,R} = \frac{z_R c_R}{4\pi f^2} \int_0^R U^2(r)[\Phi_{p,p}(r,f) + \Phi_{p,s}(r,f)]\,\mathrm{d}r \tag{6}$$

The functions denoted $\Phi_{p,p}$ and $\Phi_{p,s}$ (acoustic pressure spectral densities on the pressure and suction side of the blades, respectively) can be determined both experimentally and computationally. The experimental evaluation of these functions is also described in [13] and involves using a miniature microphone placed inside a rotor blade close to its trailing edge (on both the pressure side and the suction side, consecutively).

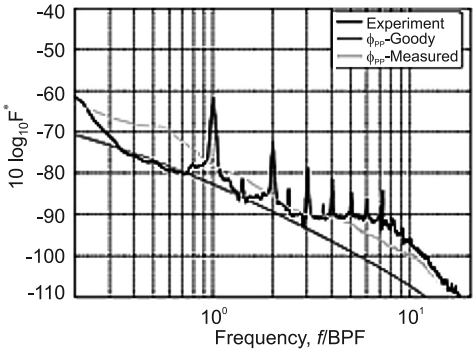

Fig. 7. Comparison of spectral acoustic densities determined by Goody model and experiment [13]
Rys. 7. Porównanie gęstości akustycznej spektralnej określonej przez model Goody'ego oraz wyznaczonej doświadczalnie

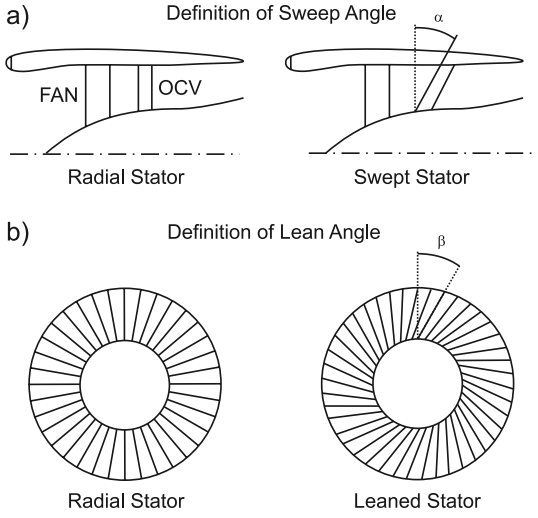

Fig. 8. The swept and leaned stator concept [4]
Rys. 8. Koncepcja omiatania i pochylania się statora [4]

The computational determination of these functions is relatively easy and incorporates a model of a dependence of the spectral acoustic density on reduced frequency − the Goody model. The Goody model is defined by the relationship:

$$\frac{\Phi_p(\omega)U_e}{\tau^2\delta} = \frac{3\omega^2}{(\omega^{0.75}+0.5)^{3.7}+(1.1R_T^{-0.57}\omega)^7} \tag{7}$$

in which $\omega = 2\pi f\delta/U_e$ stands for the reduced frequency, δ denotes the boundary layer thickness (can be determined from the wake model shown in Fig. 5), U_e is the relative velocity of the incident flow, τ is the blade surface shear stress which can be calculated with the use of

various boundary layer models, and R_T is a parameter respecting the Reynolds criterion. It can be calculated from the relation: $R_T = 0.11 \cdot (U_e \vartheta/\nu)^{0.75}$, in which, according to [13]: $\vartheta = \delta/11.6$. These relationships are valid for both the pressure side and the suction side of the blades. In [13], this model is compared to the experiment and it is stated that, for most cases, the results of both methods coincide to a satisfying extent (one of the results of this comparison is shown in Fig. 7).

It is clear that the Goody model can be very helpful during preliminary fan design stages for comparing the currently-used fan to a new one in terms of rotor noise as well as determining the key design parameters which may help decrease this type of noise.

5. Applicable design improvements of the propulsion unit

5.1. Rotor-stator interaction noise

In [2], the following methods are presented:

1. Increasing the gap between the rotor and stator. By doubling its length, a noise power level suppression of 2 dB can be achieved.
2. Lengthening the stator blades' chords. A longer chord means more wavelengths of the incident acoustic pressure waves acting on the stator blades. The incident and reflected waves can interfere and thus reduce the acoustic pressure.

Optimizing the rotor speed or reducing the rotor blade drag coefficient are other possibilities.

In [4] and [5], another noise suppression method is presented which is called the *swept and leaned stator* (see Fig. 8). The fundamental idea of this concept is increasing the number of incident wakes from the rotor blades acting on each stator blade (by leaning the stator blades) and diversifying the phase angle of these wakes at the same time (by sweeping the blades) which means that if a stator blade is swept, the pressure waves generated by wakes in different places along the radial coordinate hit it at each at a different time. The effect of the swept and leaned stator can be easily simulated using the model presented in [7].

5.2. Flow passage turbulent flow noise

The turbulent flow noise, can be efficiently suppressed by applying acoustic liners. Different types of acoustic liners used in aircraft propulsion are described in [3]. Two types of liners are distinguished – locally and non-locally-acting ones.

Locally-acting liners consist of a perforated sheet, a honeycomb core, and a solid back plate. Their denomination comes from the fact that they don't allow the acoustic waves to radiate in the direction parallel to their surface. Their working principle is that of a Helmholtz resonator.

The locally-acting liners are, as already suggested, designed to absorb acoustic waves in a relatively narrow bandwidth of approx. one octave (which corresponds to the fan tone noise, for example). Non-locally-acting acoustic liners contain porous materials instead of honeycombs. They can absorb acoustic waves within a bandwidth of more than three octaves. When applying acoustic liners to the propulsion unit if the UL-39 aircraft, the following issues are to be taken into account:

1. The complicated nature of interaction between the locally-acting acoustic liners and the surrounding flow field prevents any simple mathematical prediction method from being applicable. However, the liners must be tuned very precisely in order to act at the frequencies needed. The fitted design of these liners would be so complicated as to require extensive research capacities. This already restricts the use of acoustic liners in the UL-39 propulsion unit to non-locally-acting ones.
2. By using acoustic liners, the weight of the aircraft would increase considerably. Moreover, the longitudinal stability conditions of the aircraft would change.

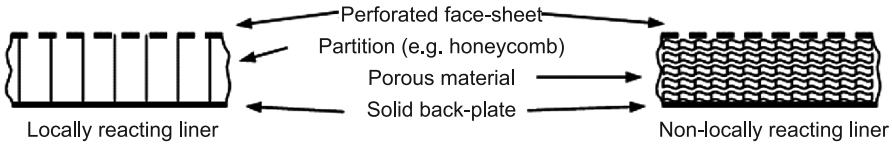

Fig. 9. Two types of acoustic liners as described in [3]
Rys. 9. Dwa przykłady linii akustycznej opisane w [3]

5.3. Rotor-alone noise

One useful method of rotor noise suppression is discussed in [1]. It is based on using so-called tip platform extensions at the tips of the rotor blades. The fundamental idea of this improvement is reducing the generation of tip leakage vortices by preventing the air from flowing from the pressure side to the suction side of the blades to a certain extent. The vortices generated by the tip leakage flow cause instationarities and turbulent momentum transfer in the flow which produces noise and induces aerodynamic losses inside the fan stage. As stated in [1], the use of tip platform extensions at the rotor blades reduces the rotor noise, widens the range of high fan efficiencies and increases its thrust.

6. Conclusions

All of the computational methods presented in this paper are relatively easy to apply and will be, of course, used during the design process. As for the noise-suppressing design improvements, one of the potentially most effective and, at the same time, easiest methods is increasing the length of stator blades and the rotor-stator gap. Sweeping and leaning the stator of the fan will be applied preferably as well. After performing the measurements needed, using rotor tip platform extensions or roughening the inner surface of the exit nozzle is also possible.

The goal of all the computational and design measures introduced in this paper is safely adhering to the limits given by the noise legislature while maintaining sufficient properties in terms of flight dynamics of the aircraft.

References

[1] Aktürk, Ali – Camci, Cengiz., *Axial Flow Fan Tip Leakage Flow Control Using Tip Platform Extensions*, In: Transactions of the ASME, Vol. 132, May 2010.

[2] Dittmar James H., *Methods for Reducing Blade Passing Frequency Noise Generated by Rotor--wake-Stator Interaction*, Technical Memorandum, Washington: NASA, 1972, 31 s., Report No. NASA TM-X 2669.

[3] Elnady Tamer., *Modelling and Characterization of Perforates in Lined Ducts and Mufflers*, Doctoral Thesis. Stockholm: KTH, Department of Aeronautical and Vehicle Engineering, 2004, Supervised by Hans Bodén.

[4] Envia Edmane – Nallasamy M., *Design Selection and Analysis of a Swept and Leaned Stator Concept*, Technical Memorandum, Cleveland: NASA, 1998, 23 s., Report No. NASA TM-1998-208662.

[5] Envia, Edmane, *Fan Noise Reduction: An Overview*, Technical Memorandum, Cleveland: NASA, 2001, Report No. NASA TM-2001-210699.

[6] Kaji S. – Okazaki T., *Propagation of Sound Waves Through a Blade Row: I. Analysis Basedd on the Semi-actuator Disk Theory*, Journal of Sound and Vibration, Vol. 11, Issue 3, Mar 1970, Elsevier, 1970, ISSN 0022-460X.

[7] Meyer Harold D. – Envia Edmane, *Aeroacoustic Analysis of Turbofan Noise Generation*, Final Contractor Report, 73 s., Cleveland: NASA, 1996. Report No. NASA CR-4175.

[8] Majjigi, R. K. – Gliebe, P.R., *Development of a Rotor Wake/Vortex Model. Volume I – Final Technical Report*, Final Contractor Report, Washington: NASA, 1984, 156 s., Report No. NASA CR 174849.

[9] Nový Richard, Hluk a chvění, Vydání 3, př. Praha: ČVUT, 2009, 400 s., ISBN 978-80-01-04347-9.

[10] Parrott, Tony L – Jones, Michael G – Watson, Willie R., *Status of Duct Liner Technology for Application to Aircraft Engine Nacelles*, Conference Paper. Minneapolis: Noise-Con, 2005.

[11] Pernet, David F., *Experimental Noise Investigation of Model Nozzles. Technical Report*, Wright--Patterson Air Force Base: Air Force Aero Propulsion Laboratory, 1964, 126 s., Report No. AFAPL-TR-64-138.

[12] Schwartz Ira R., Nagamatsu Henry T., Warren C., *Aeroacoustics: Fan Noise and Control; Duct Acoustics; Rotor Noise*, Technical Papers from AIAA 2nd Aero-Acoustics Conference. New York: AIAA, Cambridge: MIT Press, 1976, 634 s., ISBN 0-915928-09-4.

[13] Stephens, David B. – Morris, Scott C., *Measurements and Modeling of the Self Noise of a Low--speed Ducted Rotor*. In: Aeroacoustics volume 10, number 5&6, 2011.

[14] *Glenn Research Center – Acoustics Branch Fan Tone Noise Support Home*, 2012 (http: //www.grc.nasa.gov/WWW/Acoustics/analysis/support/fantone.htm).

TECHNICAL TRANSACTIONS | **CZASOPISMO TECHNICZNE**
MECHANICS | MECHANIKA
1-M/2013

MARCIN HOJNY*

BASICS OF THE NEW MULTISCALE METHODOLOGY 3D OF MECHANICAL PROPERTIES PREDICTION AT EXTRA-HIGH TEMPERATURES

PODSTAWY WIELOSKALOWEJ METODOLOGII 3D WYZNACZANIA WŁAŚCIWOŚCI MECHANICZNYCH W EKSTRA WYSOKICH TEMPERATURACH

A b s t r a c t

The paper presents example results leading to develop multiscale 3D methodology of mechanical properties prediction for steel deformed in the temperature range close to solidus line. Conducted experiments and simulations confirms the need to seek new methods to obtain precise characteristics in the context of detailed computer simulations.

Keywords: *physical simulation*, *finite element method*, *extra-high temperatures*

S t r e s z c z e n i e

W artykule przedstawiono wyniki prac zmierzających do opracowania wieloskalowej metodologii 3D wyznaczania własności mechanicznych stali odkształcanej w zakresach temperatur bliskich linii solidus. Przeprowadzone badania eksperymentalne i symulacyjne potwierdzają konieczność poszukiwania nowych metod w celu otrzymania precyzyjniejszych charakterystyk materiałowych w kontekście dokładniejszych symulacji komputerowych.

Słowa kluczowe: *symulacja fizyczna*, *metoda elementów skończonych*, *wysokie temperatury*

* PhD. Marcin Hojny, AGH University of Science and Technology, Faculty of Metals Engineering and Industrial Computer Science.

1. Introduction

In the recent two decades, researchers have paid much attention to semi-solid forming (SSF). The reason of being under attention is higher production rate and lower energy consumption rather than conventional forming processes. The mathematical and experimental modelling of mushy steel deformation is an innovative topic regarding the very high temperature range deformation processes. Tracing the related papers published in the past 10–15 years, one can find many papers regarding experimental results [1] and modelling [2, 3] for non-ferrous metals tests, but the papers deal mainly with tixotrophy.

The first results regarding steel deformation at extra high temperature were presented in the past few years [4–7]. The situation is caused by the very high level of steel liquidus and solidus temperatures in comparison with non-ferrous metals. The deformation tests for non-ferrous metals are much easier. Thixoforming or semi-solid metal forming offers many advantages in comparison with casting and conventional forging. However, because of the high-melting temperature and other related difficulties, there is relatively less amount of experimental data and investigations available on steels. The work [4] provide the basic deformation characteristics of stainless steel under semi-solid state, which was affected by the change in morphologies of microstructure at elevated temperature. Microstructural evolution and flow stress of semi-solid type 304 stainless steel using strain-induced melt activation method was investigated, and different morphologies of microstructure of type 304 steel was observed at different forming temperatures in the semi-solid state.

Hot compression tests for varied combination of deformation rate and deformation temperature around solidus temperature were conducted to obtain flow stress curves of type 304 stainless steel for two different semi-solid states and solid state. Flow stress curves around solidus temperature exhibit abrupt change according to the change in morphologies of microstructure, which was related to the phase change from delta-ferrite/austenite to liquid/delta-ferrite via liquid/delta-ferrite/austenite. The characteristics of deformation in two semi-solid states of type 304 stainless steel were discussed referring the change in flow stress and micrographs of quenched microstructure obtained by the experiments. The rising abilities of thermo-mechanical simulators such as a Gleeble® or Zwick Z250 machine enable steel sample testing at extra high temperatures. The material behaviour in temperature range above the solidus line is strongly temperature-dependent [8]. There are a few characteristic temperature values near the solidus line. The nil strength temperature (NST) is the temperature in which material strength drops to zero while the steel is being heated above the solidus temperature. Another temperature associated with NST is the strength recovery temperature (SRT), which is specified during cooling. At this temperature the material regains strength greater than 0.5 N/mm2. Nil ductility temperature (NDT) represents the temperature at which the heated material loses its ductility. The ductility recovery temperature (DRT) is the temperature at which the ductility of the material (characterized by reduction of area) reaches 5% while it is being cooled. Above this temperature the plastic deformation, which is specific for traditional processes like rolling, is not allowed at any stress tensor configuration. Very important for plastic behaviour is the material's density. It varies with temperature and depends on the cooling rate. The solidification process causes non-uniform density distribution in the controlled volume. There are three main factors causing density changes: solid phase

formation, thermal shrinkage and liquid phase flow inside the mushy zone. The density plays an important role in both mechanical and thermal solutions. Strain-stress relationship is extremely important and has crucial influence on the metal flow path. Special methods are usually applied for testing steel behaviour of steel in semi-solid state. An example method of strain-stress curve computation for steel in tixotropic state is presented in [6]. Keeping temperature constant during the whole experiment procedure is difficult. There are also some additional difficulties with interpretation of measurement results in case of samples with central mushy zone, which consist of dendritic skeleton of solid phase surrounding liquid phase. The solid phase may be subjected to the plastic deformation while liquid phase can flow through the porous solid phase. Lack of good methods of semi-solid steel simulation and significant inhomogeneity in strain distribution in the deformation zone lead to weak accuracy of the resulting stress field. On the other hand, the strain-stress curves, necessary for the mechanical model, can be constructed only on basis of a series of experiments conducted on physical simulators [8].

2. Extra-High Temperature Solutions Platform

The Extra-High Temperature Solutions Platform (EHTS Platform) has been developed in order to support modelling of plastic deformation of materials at very high temperature levels (Fig. 1).

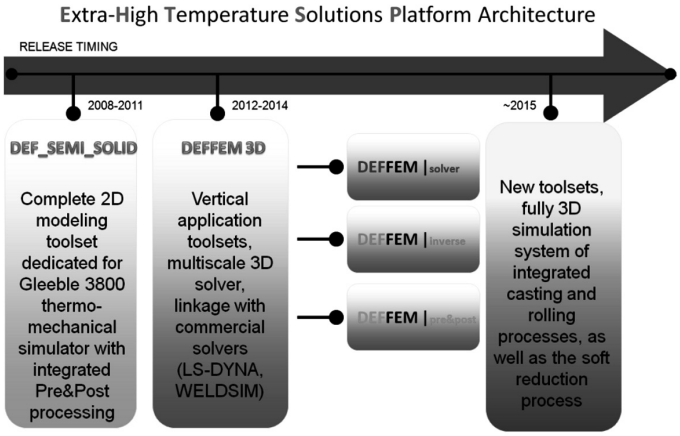

Fig. 1. Architecture of extra-high temperature solutions platform

Rys. 1. Architektura platformy obliczeń wysokotemperaturowych

The solutions platform consists of two independent tools: ***Def_Semi_Solid v.5.0*** – complete 2D modelling toolset dedicated for Gleeble® 3800 thermo-mechanical simulator with integrated Pre&Postprocessor and ***DEFFEM 3D*** – vertical application toolset including three modules: DEFFEM solver (still in development) full three dimensional multiscale thermo-mechanical solver for new methodology purposes, DEFFEM inverse and DEFFEM

pre&postprocessor. The last two modules was tested in real industrial tests during modelling of TIG welding process of Inconel super alloy. Those modules supported of boundary condition identification as well as strain-stress curves based on industrial results of welding process. More details concerning modelling of TIG welding process with DEFFEM inverse module support can be found in [9].

In the current work experimental part was supported by using Def_Semi_Solid v.5.0 toolset. The main advantage of the main thermo-mechanical solver is the analytical form of mass conservation condition. The solution prevents usual unintentional specimen volume loss caused by numerical errors. Due to concurrent solidification and deformation the material is unstable. It results in strong inhomogeneity of strain distribution and difficulties in interpretation of results of deformation tests. Hence, the application of smart simulation system based on hybrid numerical-analytical model and inverse analysis is strongly recommended. The analytical part of the model was motivated by volume loss caused by numerical errors. In case of deformation of mushy materials the loss is comparable to volume changes related to the physical phenomenon of density evolution. Thus, the process requires solution with very accurate fulfillment of mass conservation condition. Because the numerical form of the condition is not satisfactory an analytical solution of the problem was proposed and a hybrid model was developed, avoiding problems with unintentional specimen volume changes, which is very important for modelling of thermal-mechanical behaviour of mushy steel. More details concerning mathematical model can be found in [10, 11].

3. Theoretical background of the new multiscale methodology – example results

The experimental work was done in Institute for Ferrous Metallurgy in Gliwice, Poland using Gleeble® 3800 thermo-mechanical simulator. The steel used for the experiments was the C45 grade steel with 0.45% carbon content. In all cases, experiments were performed according to the following schedule: initial stage: sample preparation divided into several sub stages (e.g. thermocouple assembly, die selection); stage 2: melting procedure; stage 3: deformation process. It is good practice to test materials in isothermal conditions [11]. Unfortunately, this is not possible for semi-solid steel. Nevertheless, the condition should be as close to isothermal as possible due to the very high sensitivity of material rheology to even small variations of temperature. The basic reason for uneven temperature distribution inside the sample body on the Gleeble® simulator is the contact with cold/warm copper handles [11]. The estimated liquidus and solidus temperature levels of the investigated steel are: 1495°C and 1410°C, respectively. Thermal solution of the theoretical model has crucial influence on simulation results, since the temperature has strong effect on remaining parameters. The resistance sample heating and contact of the sample with cooper handles cause non-uniform distribution of temperature inside heated material, especially along the sample. The semi-solid conditions in central parts of the sample cause even greater temperature gradient due to latent transformation heat. Such non-uniform temperature distribution is the source of significant differences in the microstructure and hence in material rheological properties.

During the experiments samples were heated to 1430°C and after maintaining at constant temperature were cooled down to the required deformation temperature. The

temperature distribution model requires solutions of Fourier-Kirchhoff's equation. One of its parameters is the rate of heat generation (or consumption) due to different physical phenomena accompanying the deformation i.e.: phase transformation, plastic work done and – in case of electric heating – electric current flow. The last one is usually not known because the Gleeble® equipment uses an adaptive procedure for resistive heating controlled by temperature instead of current flow. Hence, the actual heat generated by direct current flow (in fact the rate of heat generation Q) which is required for the theoretical model, has to be calculated using inverse procedure. In this case the objective function (F) was again defined as a norm of discrepancies between calculated (T_c) and measured (T_m) temperatures at a checkpoint (steering thermocouple position: TC4 in Fig. 2).

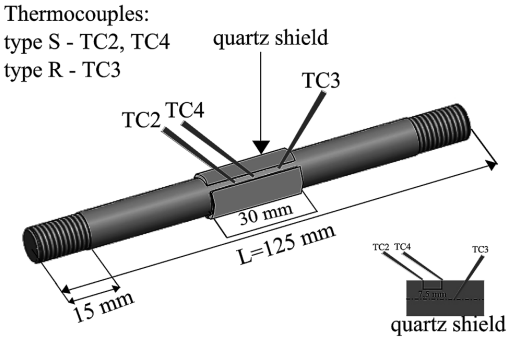

Fig. 2. Samples used for the experiments. TC2, TC3 and TC4 thermocouples
Rys. 2. Schemat próbki wraz z rozmieszczeniem termoelementów TC2,TC3,TC4

In the final stage of physical test the temperature difference between core (TC3 thermocouple position) of the sample and the surface (TC4 thermocouple position) can be significant. In all cases the core temperature was higher than surface temperature. Difference between these two was around 30°C for cold handle and about 40°C for hot handle (handle with short contact zone) for tests at 1380°C. The numerical simulation results are in agreement with results obtained during experiments. Fig. 3 presents the temperature distributions in the

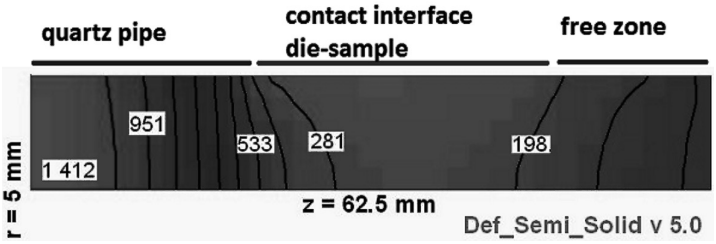

Fig. 3. Distribution of temperature in the cross section of sample tested at temperature 1380°C right before deformation (variant with cold handle)
Rys. 3. Rozkład temperatury na przekroju próbki dla próby realizowanej w temperaturze 1380°C (wariant dla uchwytów zimnych)

cross section of sample tested at 1380°C right before deformation (variant with cold handle). One can observe major temperature gradient between die-sample contact surface. However, difference between experimental and theoretical core temperatures for cold handles was only 2°C (calculated core temperature was equal to 1412°C and measured one was equal to 1410°C.)

The micro and macrostructure of the tested samples were investigated as well. Fig. 4 shows macrostructure of the central part/ transitory zone/boundary of cross-sections of samples right before deformation and calculated core temperature (measurement of the core temperature is not always possible). Liquid phase particles were observed in the central part of the sample. Experimental and numerical results can be compared taking into consideration the temperature gradient within the sample. This shows that the mathematical model of resistance heating is consistent with the experimental data.

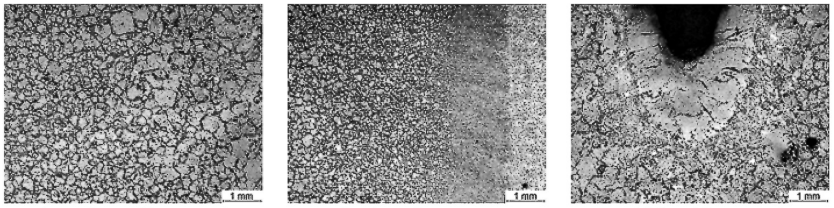

Fig. 4. Macrostructure of the sample central/transitory zone/boundary part right before deformation. Variant with cold handle. Magnification: 10×

Rys. 4. Makrostruktura rdzenia/strefy przejściowej/brzegu próbki tuż przed procesem odkształcenia. (wariant dla uchwytów zimnych). Powiększenie: 10×

Compression tests were performed, according to the methodology described detailed in [11]. The old version of steel examination methodology, denoted as variant no. 1, was based on both tension and compression tests. The temperature range was divided into two sub-ranges: lower – below NDT – and higher – above this temperature. The usual experimental procedure based on tensile tests, which is valid for cold and low-level hot deformation was applied for the lower temperature range. The resulting yield curves were described by modified Voce formula using approximation of experimental data.

A special technique of testing was developed for temperatures higher than NDT due to several serious experimental problems. The deformation process has been divided into two main stages. The first one – a very small preliminary compression and the second one – the ultimate compression. The preliminary deformation was designed to eliminate clearances in the testing equipment. The coefficients of the Voce formula were calculated using inverse solutions. This was the only acceptable method due to strong strain inhomogeneity of semi-sold steel. This approach allowed to compute strain-stress curves depending on only one additional parameter – the temperature. The newly modified developed methodology (denoted as variant no. 2) allows the computation of curves depending on both temperature and strain rate. The tension has been replaced by compression and the Voce formula was replaced by more adequate equation. During experiments die displacement, force and temperature

changes in the deformation zone were recorded. The computer simulations were performed in order to obtain optimal process parameters. All series of tests and computer simulations were done using long contact zone between samples and simulator jaws (cold handle). The deformation zone had the initial height of 62.5 mm. The sample diameter was 10 mm. The samples were melted at 1430°C, and then cooled to deformation temperature. During the tests each sample was subjected to 10 mm reduction of height. Results of each test were used for inverse analysis to compute yield stress curve parameters. In Fig. 5 strain-stress curves at several strain rate levels for temperature 1380°C as well as comparison between calculated and measured forces, are shown (for methodology variant no. 2). Comparison between the calculated and measured loads showing quite good agreement.

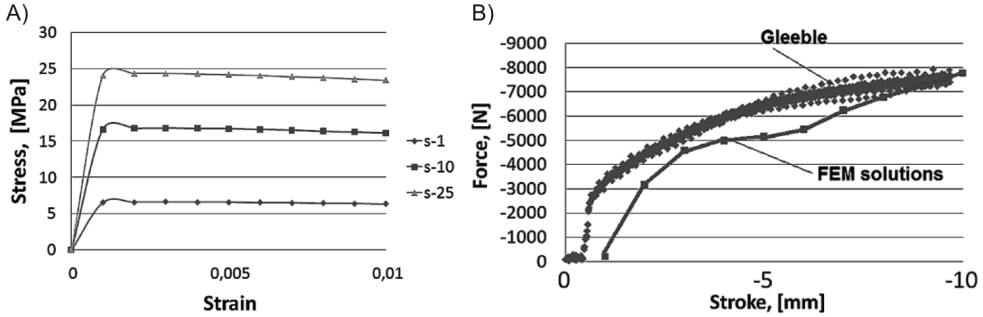

Fig. 5. A) Stress-strain curves at several strain rate levels for temperature 1380°C, B) Comparison between measured and predicted loads at temperature 1380°C

Rys. 5. A) Krzywe umocnienia dla temperatury 1380°C i trzech prędkości odkształcenia, B) Porównanie przebiegu sił zmierzonych i obliczonych dla próby w temperaturze 1380°C

Calculated and experimental shapes of the sample allow a rough verification of methodology. For verification two comparative criteria were used: comparison between the maximum measured and calculated diameters of the sample and comparison between the measured and calculated lengths of the deformation zone. The mean error for earlier methodology (variant no. 1) is greater than its equivalent for methodology denoted as a variant no. 2. The main reason for that is the lack of strain rate dependency of yield stress relationships in case of variant no. 1. Considering the strain rate as a parameter of the flow curve one can obtain more accurate results for extra high temperature range.

4. Conclusions

The investigations presented in the current paper has shown, that temperature distribution inside the controlled semi-solid volume is strongly heterogeneous and non-uniform. Axial--symmetrical model does not take into account all the physical phenomena accompanying the deformation. Finally, the error of the predicted strain-stress curves can still be improved. The proposed solution of the presented problem is application of both fully three-dimensional solution and more adequate solidification model taking into consideration evolution of forming steel microstructure. Therefore, the study of multiscale modelling of mechanical properties is the main target of the future work. Contrary to the current model the new approach should

allow to better capture the physical principles of semi-solid steel deformation in micro-scale. Additionally, the methodology should allow to transfer the characteristics of the material behaviour between the micro- and macro-scale. As a consequence the final results should be more precise and accurate.

The project has been supported by the Polish National Science Centre, Decision number: DEC-2011/03/D/ST8/04041

References

[1] Kopp R., Choi J., Neudenberger D., *Simple compression test and simulation of an Sn–15% Pb alloy in the semi-solid state*, J. Mater. Proc. Technol., vol. 135, 2003, 317-323.
[2] Modigell M., Pape L., Hufschmidt M., *The rheological behaviour of metallic suspensions*, Steel Research Int., vol. 75, 2004, 506-512.
[3] Hufschmidt M., Modigell M., Petera J., *Two-phase simulations as a development tool for thixoforming processes*, Steel Research Int., vol. 75, 2004, 513-518.
[4] Jing Y.L., Sumio S., Jun Y., *Microstructural evolution and flow stress of semi-solid type 304 stainless steel*, J. Mater. Proc. Technol., vol. 161, 2005, 396-406.
[5] Jin S.D., Hwan O.K., *Phase-field modelling of the thermo-mechanical properties of carbon steels*, Acta Materialia, vol. 50, 2002, 2259-2268.
[6] Seol D.J., Won Y.M., Yeo T., Oh K.H., Park J.K., Yim C.H., *High temperature deformation behaviour of carbon steel in the austenite and ferrite regions*, ISIJ Int., vol. 39, 1999, 91-98.
[7] Shimahara H., Baadjou R., Kopp R., Hirt G., *Investigation of flow behaviour and microstructure on X210CrW12 steel in semi-solid state*, Proc. 9th Conf. Semi-solid Alloys and Composites, Solid State Phenomena, vol. 116-117, 2006, 189-192.
[8] Hojny M., Głowacki M., *Computer modelling of deformation of steel samples with mushy zone*, Steel Research Int., vol. 79, 2008, 868-874.
[9] Hojny M., *Thermo-mechanical model of a TIG welding process for the aircraft industry*, Archives of Metallurgy and Materials, 2013 (in press).
[10] Hojny M., Głowacki M., *The physical and computer modeling of plastic deformation of low carbon steel in semi-solid state*, Journal of Engineering Materials and Technology, vol. 131, 2009, 041003.1-041003.7.
[11] Hojny M., Głowacki M., *Modeling of strain-stress relationship for carbon steel deformed at temperature exceeding hot rolling range*, Journal of Engineering Materials and Technology, vol. 133, 2011, 021008.1-021008.7.

TECHNICAL TRANSACTIONS | **CZASOPISMO TECHNICZNE**
MECHANICS | MECHANIKA
1-M/2013

KAMILA JAGOSZ*, KRZYSZTOF LALIK*

HUMAN ENDOPROSTHESIS DESIGN USING FINITE ELEMENT METHOD AND RAPID PROTOTYPING

PROJEKTOWANIE ENDOPROTEZY PRZY POMOCY METODY ELEMENTÓW SKOŃCZONYCH I SZYBKIEGO PROTOTYPOWANIA

A b s t r a c t

The paper presents the application of the Finite Element Method (FEM) in the analysis of the stress state in artificial hip prosthesis. A virtual model of hip prosthesis was made using computer aided design systems (CAD). A better construction of this component was developed in combination with numerical analysis. Virtual model allows manufacturing the real workpiece using Rapid Prototyping technology. The article describes also the hardware and software--aspects of the RP technology.

Keywords: *CAD systems*, *Finite Element Method*, *Rapid Prototyping*

S t r e s z c z e n i e

W artykule przedstawiono wykorzystanie metody elementów skończonych w analizie stanu naprężeń w endoprotezie stawu biodrowego. Za pomocą programów komputerowo wspomagających projektowanie (CAD) stworzono wirtualny model endoprotezy, co w połączeniu z analizą numeryczną pozwoliło na opracowanie lepszej konstrukcji elementu. Wirtualny model pozwolił na stworzenie modelu rzeczywistego dzięki wykorzystaniu technologii Rapid prototyping. W artykule zostały opisane także sprzętowe oraz softwarowe aspekty technologii szybkiego prototypowania.

Słowa kluczowe: *Systemy CAD*, *Metoda elementów skończonych*, *Rapid Prototyping*

* Jagosz Kamila, MSc. Krzysztof Lalik, AGH University of Science and Technology, Faculty of Mechanical Engineering and Robotics, Department of Process Control.

1. Introduction

The civilization progress has caused a significant prolongation of human life. The problems so far not present occur with aging of the population and with change of human life mode. Some of them are a variety of defects and degenerative diseases of the human skeleton system. The hip joint is one of the most perishable elements of this system. Sedentary lifestyle and low physical activity will exacerbate this situation in future. Medicine is able for a long time to help patients with degeneration of the hip joint using artificial prosthesis. The mechanical and materials engineering comes also with help. Very intensive research on new materials and constructions of the implants are carried out currently. Modern engineering and biomechanics are trying to develop the shape of the prosthesis as close as possible to the shape of the bone marrow cavity. It would allow for uniform stress distribution in prosthesis by matching it to the natural shape of the marrow cavity. Even stress transmission will result in longer hip prosthesis exploitation. It would prevent the bone osteolysis, which is the process, which due to the bone dissolving and resorption is causing bone loss.

According to official statistics about 6000 hip implantation surgeries are performed in Poland per year. Unofficial data are saying about demand even five times greater. In addition, the life of the already implanted hip joint prosthesis is 7 to 15 years, depending on its type and on the condition of the patient bone tissue. As a result, apart from people waiting for their first implantation surgery, there are also people in line waiting for reimplantation surgery. In addition, all secondary implantation surgeries are much more expensive and time consuming. The implant materials are not the cheapest. Computer-aided design can be useful for elimination all of those problems. CAD systems allow to reduce the costs of prototyping and of endurance tests of prostheses. Creation of optimal implant shape is possible using analysis based on Finite Element Method. This will reduce the size of the prosthesis, and thus reduce the consumption of expensive material. Smaller size of the prosthesis will also reduce the size of the surgical intervention in human body. It will allow for a quick return to health and will improve patients comfort.

2. Finite Element Method modeling

The prosthesis model was made in CAD system in two versions. The first version (Fig. 1a) presents the prosthesis model immediately after the surgery, when the prosthesis in attached only by two bolt screws. The second model (Fig. 1b) presents the endoprosthesis, which is conjoined with the bone marrow cavity. The difference between the models lies in the mounting conditions and explains the importance of a good prosthesis fit to the shape of the bone marrow cavity.

The model was designed based on standard ISO 7206-4:1995, which defines basic parameters and range of some dimensions of the endoprosthesis. The change suggested by the authors is located in section between the head and the mandrel of the model. This shape is different from the shape proposed by the standard. Preliminary simulations showed that the greatest stress is located in this area. Suggested change in cross-section area will result in a large increase in cross-section moment of inertia I. The results of numerical simulation

using Finite Element Method are shown in Figure2a for the model immediately after the surgery, and in Figure 2b for the model of the prosthesis conjoined with the bone marrow cavity. Detailed image of stress distribution in fixing bond for the first model is shown in Figure 3. The solid element was used for numerical computation.

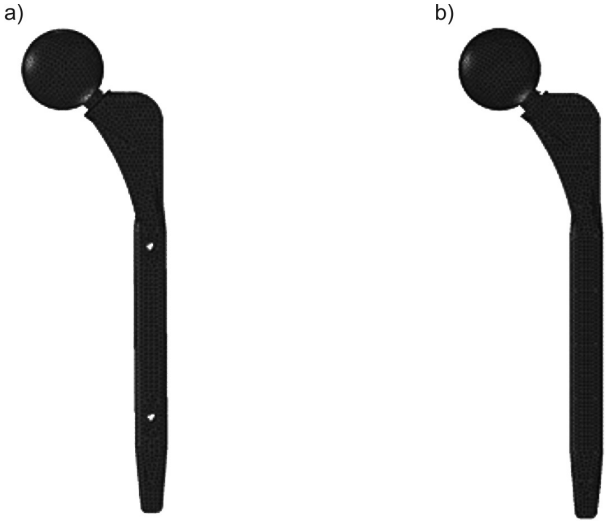

Fig. 1. 3D model of human hip joint endoprosthesis performed in SolidWorks 2011
Rys. 1. Model 3D endoprotezy ludzkiego stawu biodrowego wykonany w programie SolidWorks 2011

The stress around upper hole increase significantly for the model with two fixing bolts. The boundary conditions are changed after conjoining with the marrow cavity. It reduces significantly the stresses in the prosthesis. The stress concentration in the top of mandrel is still noticeable despite of the modification in construction between the head and the mandrel of the prosthesis. The "a priori" modification of this section is not possible, since it depends on the patient bone degeneration condition. However, the shape of the mandrel branching can be individually developed after medical consultation for the patient.

The analysis was performed assuming an isotropic material, and it is assumed that the material behavior is linear and consistent with Hooke's law. In addition, it was assumed that the change in the stiffness of the material due to the load may be excluded because of the small displacements. The judgments on the element could not be based only on the basis of data provided by even most accurate numerical analysis. Those information can be used only in conjunction with experimental data. Operational tests are necessary for the verification of the final design. CAD programs with additional packages for numerical analysis can be useful to decrease the time required to obtain the final product by reducing, but not eliminating the tests. Authors suggest therefore to performance from the virtual model a real prototype in the form of a ready foundry pattern made from model obtained from Rapid Prototyping technology.

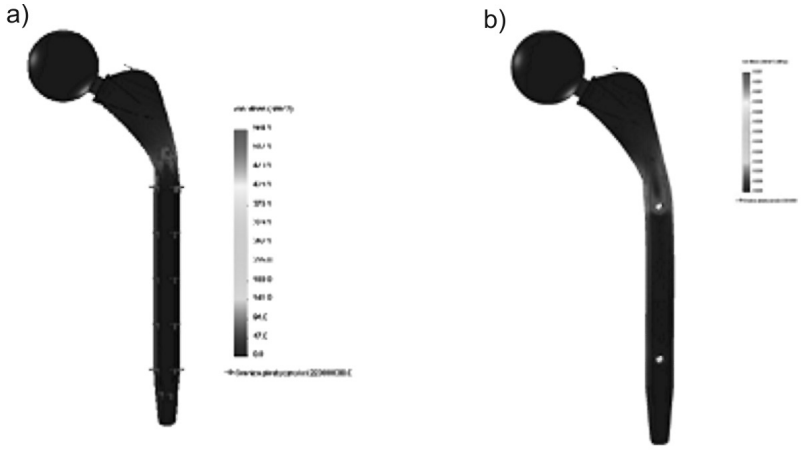

Fig. 2. Distribution of stresses in the hip joint endoprothesis for different kinds of boundary conditions

Rys. 2. Rozkład naprężeń w endoprotezie stawu biodrowego dla różnych warunków brzegowych

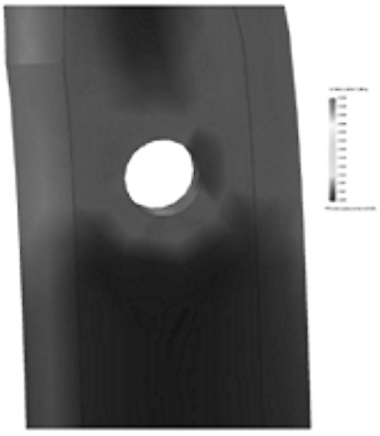

Fig. 3. Detailed image of stress distribution in fixing bond

Rys. 3. Szczegółowy obraz rozkładu naprężeń w węźle mocującym

3. Virtual i Rapid Prototyping

Virtual prototyping is a technology based on virtual model testing, which allows modeling and simulation with realistic visualization. The work starts with the construction of geometrical models of designed products, and then the computer simulations are carried out. The designer is able in this way to determine whether will meet all criteria and requirements, for example – ergonomic criteria. A model observation in virtual reality allows engineers to

perceive many construction errors. Virtual prototyping of all aspects of the newly created products plays a crucial role in fast realization of the best designed product or process. Additionally, due to the fact that design is a process which has almost no limits, the VP technology allows the designer to analyze various types of solutions and enables fast and not expensive prototyping of new, often unconventional projects. It reduces also the time needed to product final market arrival, improves the quality, as well as helps to reduce the cost of its development. [1]

Virtual prototyping technique allows to transition from concept, through design in CAD system and various stages of the construction, up to virtual testing of final product. It allows approving for production a built structure, tested complete in the virtual world, using easy available engineering software. [3, 5, 7]

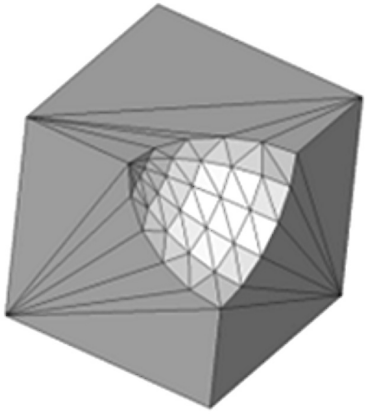

Fig. 4. 3D model surface saved in STL format [2]

Rys. 4. Powierzchnia modelu 3D zapisana w formacie STL [2]

Independently of the used method, rapid prototyping starts with creation of a 3D virtual model of the new structure in any available CAD system.[6]. In the next step, the model is transformed in the numerical process into RP appropriate data. In practice, it means converting of a 3D model to STL format (Standard Triangulation Language). This format is

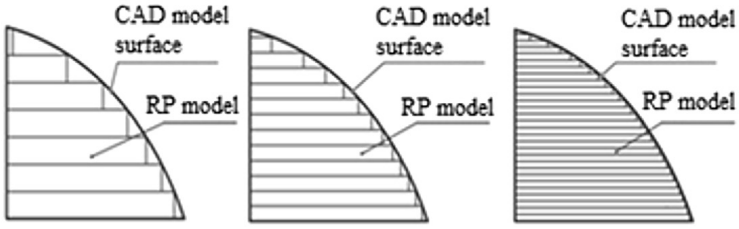

Fig. 5. Influence of film thickness for the model surface finish [*2*]

Rys. 5. Wpływ grubości warstwy na wykończenie powierzchni modelu [2]

an informal language of the RP technology. STL is a triangular surface mesh definedas a set of vertices, edges and triangles [4]. They are connected with each other in such a way that each edge as well vertex is common for at least two adjoining triangle in according to vertex--to-vertex rule. In other words, the grid of triangles represents approximately model surfaces described in STL format (Fig. 4.).

The next step after creating a triangle model mesh is the transversal slitting to even thin layers (XY plane) [8, 9]. The thickness of the layers depends on the accuracy which a designer wants to get and as well on the type of used RP method (Fig. 5.).

The model prepared in this way is sent to machine, which is a 3D RepRap printer, and a prototype of the designed item is formed.

4. Production of the prototype

Foundry model of the human hip joint endoprosthesis was manufactured using a 3D RepRap printer, designed in Department of Process Control UST AGH (Fig. 6).

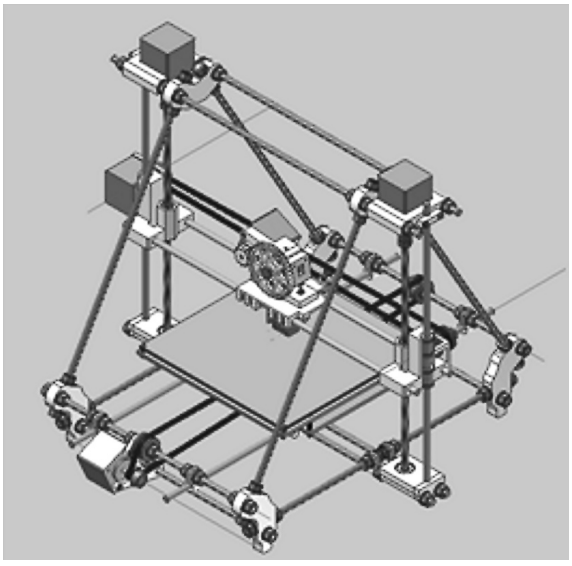

Fig. 6. The assembly of the 3D RepRap printer

Rys. 6. Rysunek złożeniowy drukarki 3D typu RepRap

Basic parameters of the print can be entered using the Slic3r – it is a dedicated software for the 3D printers. They are fundamental to the quality of the prints. Couple printouts for different printing configuration parameters are presented in Figure 7 The left prosthesis was performed with 40% fill density and layer thickness of 1 mm. Its manufacture time was about 6 minutes. The left prosthesis was performed with 100% fill density and layer thickness of 0.3 mm. Its. The execution time was 1 hour and 12 minutes.

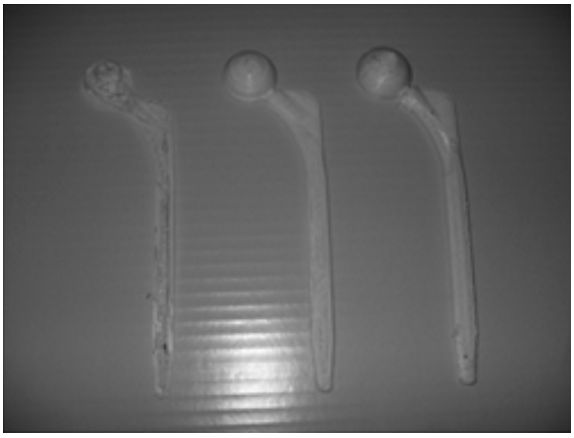

Fig. 7. Human hip joint endoprosthesis printout for various configurations of printing parameters
Rys. 7. Widok modeli endoprotezy stawu biodrowego w zależności od konfiguracji parametrów drukowania

Subsequent steps of foundry model production are showed in Figure 8. There are possibilities to print the hip joint endoprosthesis foundry model together with casting gating system, which would accelerate even more the production of the final metal structure.

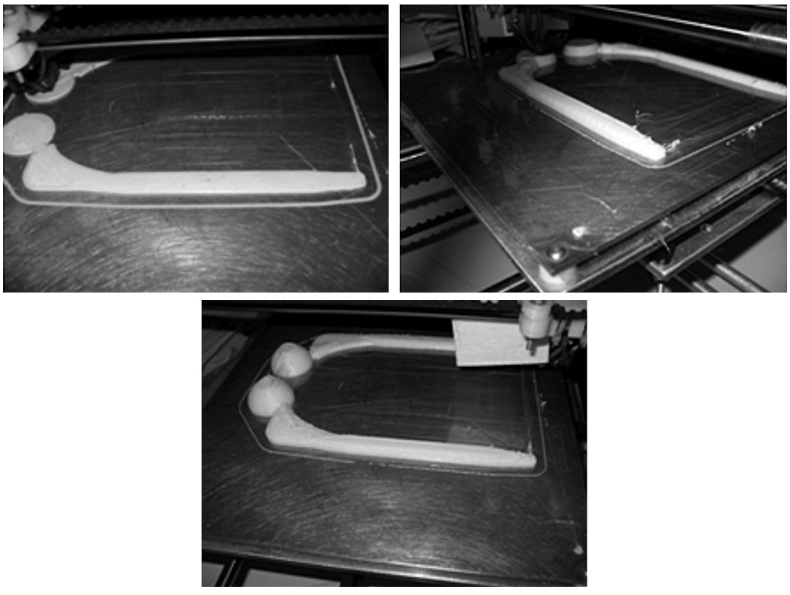

Fig. 8. The next stages of human hip joint endoprosthesis production using Rapid Prototyping technology
Rys. 8. Kolejne stadia wytwarzania endoprotezy stawu biodrowego w technologii RP

5. Conclusions

Prosthetic arthroplasty is a major surgical intervention, but in this moment, a good long term alternative solution simply does not exist. The price of hip joint prosthesis implantation is about 8 thousand dollars.. According to official data, extension of the life of hip bone endoprosthesis only for one year would result in saving over 70 million dollars per year at the current demand in Poland. However, the demand will rise. Constant improvement and development in design of implant has therefore a great importance.

This paper presents the application of CAD systems in virtual designing of the shape of the hip joint endoprosthesis. Application of the Finite Element Method (FEM) allows to show the distribution of stresses in prosthesis and thus, to virtual redesign of its shape reducing their concentration. The real casting model can be also performed using specialized software. It would help in experimental confirmation of the numerical analysis results.

Computer-aided system allows reducing the cost of manufacturing and testing of prototypes, which significantly affects the price, quality and durability of the final product. This provides to significantly enhance of patient comfort after hip joint prosthetic arthroplasty.

References

[1] Bubicz M., *Cyfrowe czy jednak fizyczne*, *Projektowanie i Konstrukcje inżynierskie*, 1(01)/2007, 2007, 27-30.

[2] Sitek M., Sacha M., *Projekt Wieloosiowego urządzenia drukującego przestrzennie do szybkiego prototypowania*, KAP AGH, 2012.

[3] Bubicz M., *„Drukowanie"...nożem?*, Przegląd współczesnych technologii szybkiego prototypowania cz. I, *CADblog.pl*, 1(11)/2010, 2010, 26-32.

[4] Bubicz M., *Raport: szybkie prototypowanie. Przegląd dostępnych rozwiązań...*, Projektowanie i Konstrukcje inżynierskie, 4(07)/2008, 2008, 27-30.

[5] Budzik G., Budzik W., Magniszewski M., Pająk D., *Metody szybkiego prototypowania*, Stal, numer 1/2011, 2011, 78-80.

[6] Budzik G., Pacana J., Sobolak M., *Obróbka i przygotowanie danych pod potrzeby urządzeń szybkiego prototypowania*, Rzeszów, Oficyna Wydawnicza Politechniki Rzeszowskiej, 2009.

[7] Budzik G., Skoczylas L., *Znaczenie i przebieg inżynierii odwrotnej w procesie przygotowania produkcji*, Ekonomika i Organizacja Przedsiębiorstwa, 9(704)/2008, 2008, 38-40.

[8] Gebhardt A., *Rapid Prototyping*, Monachium, Carl Hanser Verlag 2003.

[9] Grochowiak A., *Rapid prototyping i rapid tooling*, CADCAM Forum, 7/2000, 2000, 23-30.

TECHNICAL TRANSACTIONS | CZASOPISMO TECHNICZNE
MECHANICS | MECHANIKA
1-M/2013

ZDZISŁAW JUDA*,TOMASZ NABAGŁO*, PAWEŁ OCŁOŃ**,
BOHDAN WĘGLOWSKI**, MARIUSZ KRAWCZYK***

POWER EFFICIENCY MANAGEMENT OF PHOTOVOLTAIC ENERGY SOURCE BASED ON MPPT ALGORITHM

ZARZĄDZANIE SPRAWNOŚCIĄ ENERGETYCZNĄ FOTOWOLTAICZNEGO ŹRÓDŁA ENERGII Z UŻYCIEM ALGORYTMU MPPT

Abstract

In the paper energy supply system based on photovoltaic (PV) arrays was described. Also models of a single PV cell and a voltage boost converter were described. The boost converter was used for holding an appropriate work state of the PV arrays associated with its maximum power point level in various work conditions associated with irradiance level and the arrays temperature. Finally, comparison of two strategies of voltage level control in PV arrays system was put forward. These strategies were used to attain the maximum power point, and to define the work conditions, in which described control algorithms are the most effective.

Keywords: *photo-voltaic arrays*, *Maximum Power Point Tracking (MPPT) algorithm*, *Perturb & Observe (P&O) algorithm*

Streszczenie

W artykule opisano system zasilania z wykorzystaniem baterii ogniw fotowoltaicznych. Przedstawiono model ogniwa fotowoltaicznego oraz przekształtnika podwyższającego napięcie. Przekształtnik ten zastosowano do utrzymywania właściwego stanu pracy związanego z maksymalną mocą osiąganą przez ogniwa w określonych warunkach pracy związanych z nasłonecznieniem i temperaturą ogniw. Przedstawiono porównanie dwu podstawowych strategii sterowania poziomem napięcia w układzie ogniw w celu uzyskania maksymalnego punktu pracy wraz z warunkami, w jakich opisane algorytmy sterowania są najskuteczniejsze.

Słowa kluczowe: *ogniwa fotowoltaiczne*, *algorytm MPPT*, *algorytm P&O*

* PhD. Eng. Zdzisław Juda, PhD. Eng. Tomasz Nabagło, Institute of Automobiles and Internal Combustion Engines, Faculty of Mechanical Engineering, Cracow University of Technology.
** MSc. Paweł Ocłoń, PhD. Eng. Bohdan Węglowski, prof. PK, Department of Thermal Power Engineering, Faculty of Mechanical Engineering, Cracow University of Technology.
*** MSc. Mariusz Krawczyk, Institute of Applied Informatics, Faculty of Mechanical Engineering, Cracow University of Technology.

1. Introduction

During energetic crisis, people have to search alternative sources of the electrical power. The most popular of all available energy sources, which could be easily transformed to electrical energy, is energy of the Sun. The Sun gives us a huge amount of it, as heat energy and light. Especially the light can be transformed to electrical energy with photovoltaic (PV) cells. These cells nowadays can reach, in the best case, efficiency on the level of 30%, but most of them do not exceed 20%. This barrier is associated with technological limitations, but PV cells as a research object appears to be more complicated than could be seen in superficial observation. It can be noticed on power-voltage and current-voltage characteristics. On the first of them one can observe maximum power point. This point is dependent to electrical current and voltage in the PV circuit system, as also to temperature of the cells. For these reason, the authors have chosen way to efficiency improvement through Maximum Power Point Tracking (MPPT) algorithm.

2. Literature analysis for finding MPPT algorithm solutions

To investigate MPPT algorithm solutions, an appropriate model was needed. This model should be simplified to decrease a simulation time. This simple model is based on equivalent circuit of PV cell and also on equations, which describes PV cell properties [1].

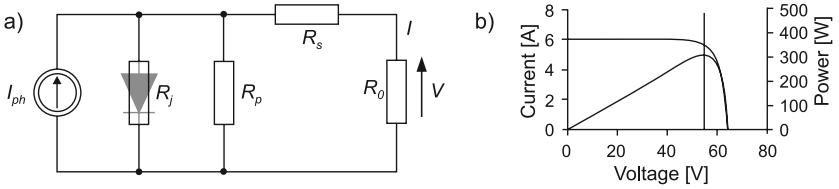

Fig. 1. Equivalent circuit of PV cell (a), PV cell characteristics (b)

Rys. 1. Obwód równoważny dla ogniwa fotowoltaicznego (a), charakterystyki ogniwa (b)

In equivalent circuit (Fig. 1a) I_{ph} represents current directly produced in PV process. R_j is the p-n junction impedance. R_p, R_s and R_0 represent consequently parallel resistance, series resistance and load resistance. Voltage drop on this resistance equals V. The current I in PV cell output is described by equation (1), but its component current I_{ph} is described by equation (2). These equations shows, that produced energy is also temperature-dependent value. These phenomena can be observed also on power-voltage characteristics [2], based on current-voltage dependence of a photodiode [3]. Due to the sign convention of the positive and negative power, its shape is the same as inverted characteristics of photodiode (Fig. 1b).

$$I = I_{ph} - I_{rs} \cdot e^{\left(\frac{q}{kTA}\frac{V}{n_s}\right)} - 1 \tag{1}$$

$$I_{ph} = [I_{scr} + k_i(T - T_T)] \cdot \frac{s}{10} \tag{2}$$

where:

I_{ph} – photocurrent,
I_{rs} – reverse saturation current,
I_{scr} – cell short-circuit current at reference temperature and radiation,
q – charge of an electron,
k – Boltzmann's constant,
k_i – short-circuit current temperature coefficient,
T – cell temperature,
T_r – cell reference temperature,
A – coefficient of cell deviation from ideal p-n junction characteristics,
n_s – number of cells connected in series,
S – irradiance in kW/m^2.

Based on these circuits and equations, a cell array was constructed where the cells are connected in series. Finally these series arrays were connected in parallel in full model named PV array.

3. Structure of the system

The PV array model was used in more complex model with MPPT algorithm control system (Fig. 2). In this system, so called Boost Converter was used. This converter lets control the voltage on the PV array and through this variable it lets hold maximum power point of the system. As a load of the electrical system a simple resistance was used. The below model consist of three main elements. First is above described PV array, second is the boost converter and third is a controller based on MPPT algorithm.

3.1. Boost converter

Because the cell voltage varies with temperature and irradiance, it is necessary to use the boost converter. The purpose of the boost converter is processing voltage from photovoltaic cells array to that adopted for the inverter input voltage level, in accordance with the MPPT algorithm. Boost converter is used in the system for regulation of PV array voltage to hold maximum power point position on power-voltage characteristics through changing irradiance and temperature conditions (Fig. 3). These characteristics are taken for PV cells SunPower SPR-305-WHT connected in configuration: 5 series modules per string and 66 in parallel connection. The boost converter consist of an inductor, which accumulate energy, IGBT transistor, which work as a switch, controlled by Pulse Width Modulation (PWM) element, and diode, which conducts current in one direction, as also capacitor connected in parallel to the load resistance [2] (Fig. 4). In photovoltaic applications boost converter is working typically in continuous coil current flow. Part of the input energy is transferred to the RC circuit via diode during transistor conduction and part of the energy is stored in a coil magnetic field. During open state of the transistor, this stored energy is transferred to the output RC circuit. This action is the basis for increasing the converter output voltage [4].

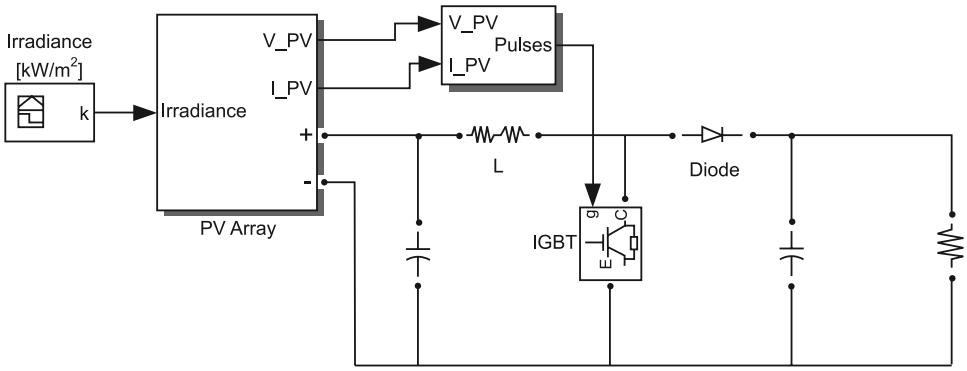

Fig. 2. PV array circuit with MPPT algorithm control in resistance load conditions

Rys. 2. Bateria ogniw PV ze sterowaniem algorytmem MPPT w warunkach obciążenia rezystancją

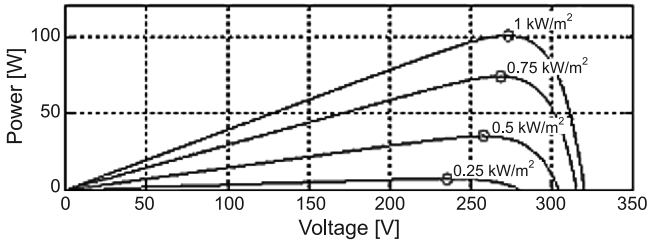

Fig. 3. Set of power-voltage characteristics of PV array for various irradiance conditions

Rys. 3. Bateria ogniw PV ze sterowaniem algorytmem MPPT w warunkach obciążenia rezystancją

During proper work of the boost converter output voltage is greater than input voltage. Relation between these two voltages is expressed in equation (3) [2].

$$V_{out} = \frac{1}{1-D} \cdot V_{in} \tag{3}$$

where:

D – duty cycle.

V_{in}, V_{out} – respectively input and output voltage.

After transformation of equation (3), appropriate duty cycle can be calculated according equation (4) to hold correct voltage for control strategy realization. In this equation an assumption that $V_{out} = V_{ref}$ should be taken.

$$D = 1 - \frac{V_{in}}{V_{ref}} \tag{4}$$

If the transistor is in the ON state, the coil current increases, and if the transistor is in the OFF state, the coil current decreases. This causes the output voltage ripple. The ripple should be in the range of up to 2% due to the correct operation of the inverter.

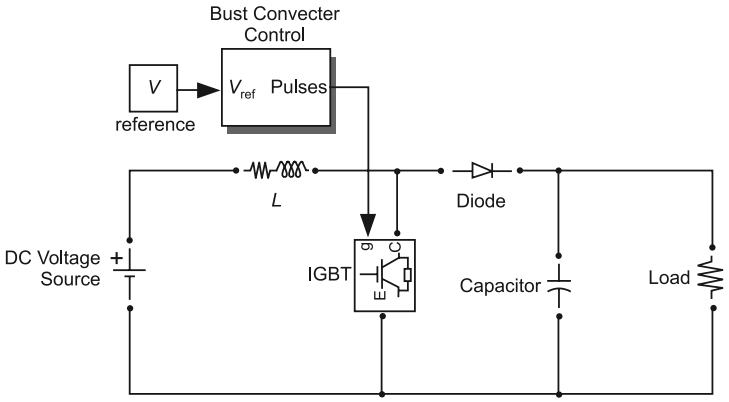

Fig. 4. Boost converter system

Rys. 4. Układ przekształtnika podwyższającego napięcie

Allowable ripple defined as the ratio of output voltage fluctuations and V_{out} are described in the following equation.

$$\frac{\Delta V_{out}}{V_{out}} = \frac{D}{R \cdot f \cdot C} \tag{5}$$

where:

R – load resistance in Ω,
C – boost converter capacitance in F,
f – boost converter frequency in Hz.

For the assumed limit for ripple and frequency, the value of boost converter capacitance C can be determined. Transfer of energy from the lower voltage DC source to a higher voltage DC source by a pulse boost converter is a high conversion efficiency [5] method (typically above 90%). Minimum values for L and C of boost converter depend on the extent of variation Duty Cycle D, load value R and the operating frequency of the system f.

3.2. MPPT Controller

The main aim of MPPT strategy is to hold maximum power point during work of the PV array system. As can be noticed in figure 3 this point depends to irradiance level [6]. It depends also to temperature. The easiest way to find this maximum power point is to observe behavior of the power level. The clue information is if power value decreasing or increasing, during increasing or decreasing voltage value. Based on this information, very simple strategy can be described. Shape of power-voltage characteristics is always similar and can be described with relations enclosed in section 2. Therefore, dependence that when voltage increases and power also increases shows that we are on the left side from maximum power point of voltage-power characteristics (Fig. 3). If voltage decreases but power increases, it is obvious that we are on the right side on the characteristics. Based on this information, the MPPT algorithm was constructed. The algorithm is presented in the Figure 5.

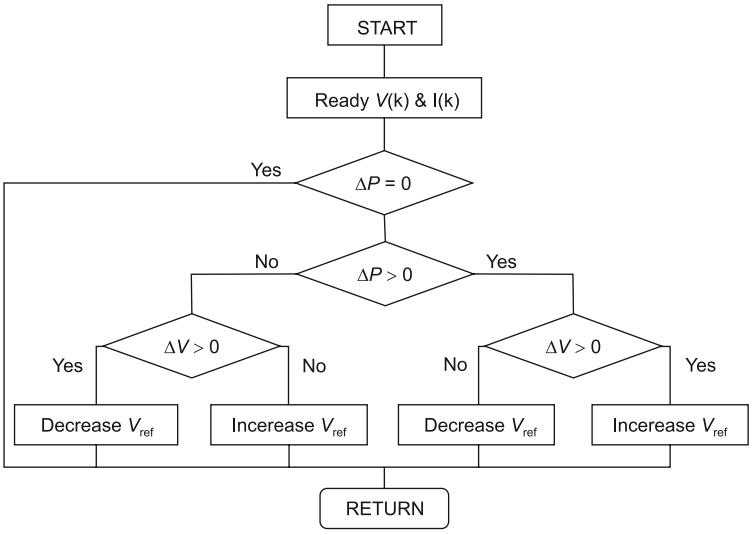

Fig. 5. MPPT algorithm
Rys. 5. Algorytm MPPT

During its work power level and voltage of the PV system oscillates around maximum power point. This main idea of MPPT was developed but only in small range. For example in MPPT algorithm known as Perturb and Observe algorithm, perturbation coefficient is introduced. It decides about step size of the voltage changing during maximum power point searching process.

4. Simulation and results comparison

During simulation process the authors used various irradiance levels to observe full range of power levels. Range of irradiance level enclosed between 0.25 and 1 kW/m^2 (Fig. 6). This changing character simulates character of illumination during normal work of PV arrays when irradiance is changing due to clouds movement. In this simulation two MPPT algorithms were used for power level maximization. Results were introduced in the figure 7, which encloses power level during 3 seconds simulation. This is power produced by PV array system. The first presented algorithm is associated with general MPPT algorithm strategy and its results are represented with blue line. Second algorithm is associated with P&O strategy and its results are represented with green line. Last one, red line represents result for the PV system without control.

During results comparison, the authors calculated coefficients of produced power in comparison to the uncontrolled PV system. This no dimensional coefficient was calculated with equation (6).

$$c_x = \frac{\int P_{\text{controlled}}}{P_{\text{uncontrolled}}} \tag{6}$$

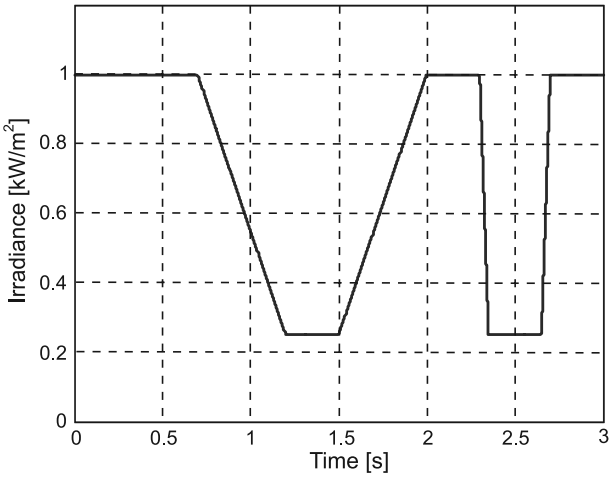

Fig. 6. Various irradiance levels

Rys. 6. Zmienny poziom napromieniowania

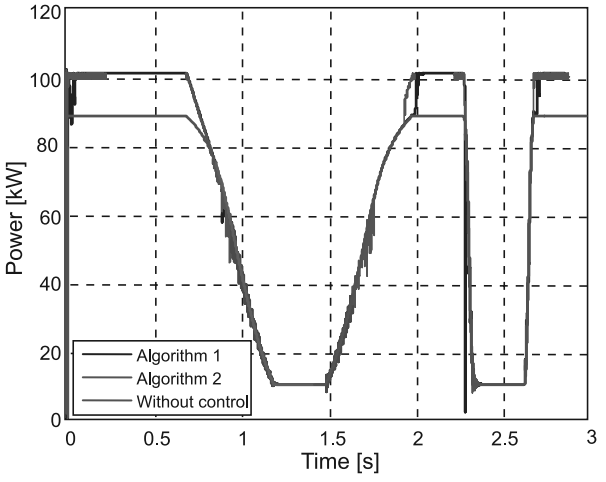

Fig. 7. Level of power produced by PV array

Rys. 7. Poziom mocy produkowanej przez baterię PV

The c_x coefficient for the first algorithm equals 1.0841 and for the second algorithm equals 1.0854. Differences appears to be very small, but range of input radiation is wide, than when we observe time-traces from figure 7, we can notice that differences between these coefficient can be extremely big in range of irradiance between 0.8 and 1 kW/m^2. This means, that these algorithms can be very effective in higher radiation conditions. In above mentioned range also differences between effects of first and second algorithm can be significant. In this comparison P&O algorithm appears to be more effective than traditional MPPT algorithm.

5. Conclusions

As it was said in previous section both presented control algorithms can be very effective in higher radiation conditions, but in lower radiation conditions they could be turned off. It could suggest that these algorithms are not effective or even useless, but it is not true. We have to remember that most of the PV arrays systems works in conditions of higher irradiance and where irradiance is too low the system is turned off. This strategy is especially applied in a solution which cooperates with AC electrical grid, where surplus of produced energy can be send to this grid. In the context of the protection of the Earth from global warming, the use of renewable energy sources is appropriate and cost effective. The use of photovoltaic solar systems leads to improved energy balance in accordance with the requirements of climate. In addition, the pulse energy conversion methods are characterized by high efficiency, aided by the use of algorithms for maximum power point tracking MPPT.

The paper is a part of TEWI platform project: tewi.p.lodz.pl

References

[1] Hussein K.H., Muta I., *Maximum Photovoltaic Power Tracking: An Algorithm for Rapidly Changing Atmospheric Conditions*, IEEE Proceedings on Generation, Translation and Disturbation, Vol. 142, No. 1, 1995, 59-64.

[2] Alsadi S., Alsayid B., *Maximum Power Point Tracking Simulation for Photovoltaic Systems Using Perturb and Observe Algorithm*, Internal Journal of Engineering and Innovative Technology, Vol. 2, Issue 6, 2012, 80-85.

[3] Salmi T., Bouzguenda M., Gastli A., Masmoudi A., *MATLAB/Simulink Based Modelling of Solar Photovoltaic Cell*, International Journal of Renewable Energy Research, Vol. 2, No. 2, 2012.

[4] Wilamowski B.M., Irwin J.D., *Power Electronics and Motor Drives*, CRC Press, ISBN 1439802858/9781439802854, 2011.

[5] *Efficiency in Electricity Generation*, Union of the Electricity Industry – EURELECTRIC, Boulevard de l'Impératrice, 66 – B-1000 Brussels, July 2003.

[6] Hohm D.H., Ropp M.E., *Comparative Study of Maximum Power Point Tracking Algorithms*, Progress in Photovoltaics: Research and Applications, 11, 2003, 47-62.

TECHNICAL TRANSACTIONS | **CZASOPISMO TECHNICZNE**
MECHANICS | MECHANIKA
1-M/2013

MARIUSZ KRAWCZYK*

PROPORTIONAL FLOW CONTROLLER MODEL IN MATLAB-SIMULINK

MODEL PROPORCJONALNEGO REGULATORA PRZEPŁYWU W MATLAB-SIMULINK

A b s t r a c t

This paper presents a method of creating a model of proportional flow control in Matlab-Simulink. A mathematical model of the controller and power supply system where the regulator is running. Model in Simulink is a block diagram. The individual blocks represent components of the hydraulic system.

Keywords: *simulations*, *mathematical model*, *flow control*, *Matlab Simulink*

S t r e s z c z e n i e

W artykule przedstawiono metodę budowy modelu proporcjonalnego regulatora przepływu w programie Matlab-Simulink. Przedstawiono model matematyczny regulatora oraz układu zasilacza w którym pracuje ten regulator. Model w programie Simulink ma postać schematu blokowego. Poszczególne bloki reprezentują elementy układu hydraulicznego.

Słowa kluczowe: *symulacje*, *model matematyczny*, *regulator przepływu*, *Matlab Simulink*

* MSc. Eng. Mariusz Krawczyk, Institute of Applied Informatics, Faculty of Mechanical Engineering, Cracow University of Technology.

1. Introduction

Hydraulic system components – including hydraulic valves – are still intensive development. This development includes both distributors, logical elements, pumps and proportional valves. Commonly used microprocessor control improves the characteristics of proportional elements those components while increasing their range. Hydraulic systems built with them, gain new uses and new features in many cases. This paper discussed issues of creating of a simulation model of proportional flow control.

2. Object of research

The object of research is proportional electronically controlled flow control scheme which presented in Fig 1. Consists of of items such as: 1 – solenoid, 2 – body, 3 – bushing, 4 – piston, 5 – displacement transducer, 6 – pin magnet, 7 – spring. The controller consists of a throttle section and section differential. Working fluid flows from port A to port B is suppressed by the throttle slot formed f_A of the sleeve 3 and the body 2. The volumetric fluid flow rate is proportional to the current the electromagnet 1.

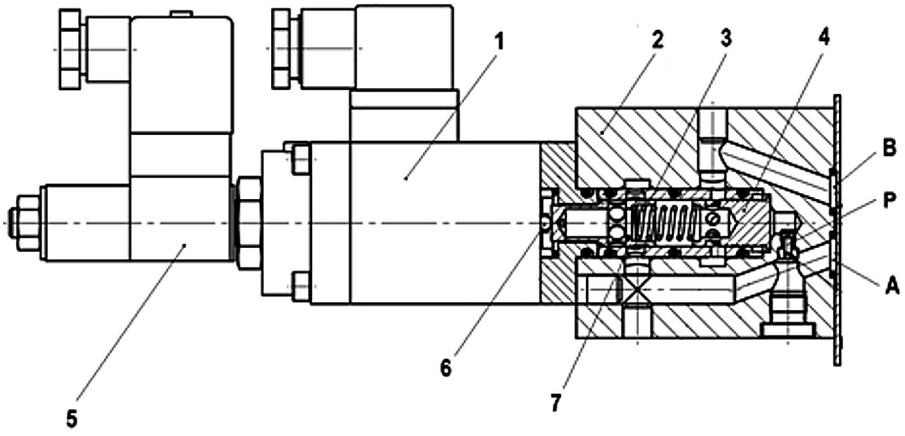

Fig. 1. Diagram of two-way proportional flow control

Rys. 1. Schemat dwudrogowego proporcjonalnego regulatora przepływu

To flow controller appeared working fluid flow slot open stuffing box f_A. We achieve this by giving an appropriate voltage on electromagnet clamps resulting in the 6 pin coming out of the solenoid moves the sleeve 3, which opens the throttle gap. Working fluid flowing in the canal flows through the slot B f_B formed on the edge of the piston 4 and body 2. Gap size f_B specifies the location of the piston 4, which is based on the forces acting on it. On the one hand, it is mainly the sum of the forces: spring 7 and the hydrostatic force flowing liquid, on the other hand liquid hydrostatic force acting on the opposite side of the piston 4, affecting channel P. Moving the plunger through the influence on the position of the spring 7 of the

sleeve 3, which is controlled by encoder. Change the position of the sleeve 3 are adjusted by electronic control system by amending the solenoid voltage. This situation continues until you establish a balance of power between the elements of the flow. In the case of fluid pressure changes following re-establish the balance of forces. As a result, the volumetric flow through the flow control is set by the operator and is independent of the level of pressure of the working medium.

2.1. Mathematical model

For the mathematical description of the equations have been used for the balance of forces, torque, expenses, continous flow, logic and geometrical relationships. The analysis includes mathematical model of the controller and power supply system model which consists of: 1 – electric motor, 2 – hydraulic pump with fixed delivery, 3 – relief valve, 4 – Proportional flow controller, 5 – supply line, 6 – throttle valve, 7 – pressure gauge and pressure transducer, 8 – flowmeter.

Adopted the following simplifying assumptions: the system work in thermal equilibrium state, the system external no leakage, the pump pulse was omitted and the phenomenon of wave, springs in valves have linear characteristics, deformability omitted bodies, individual sections of power lines has become a equivalent bulk modulus of elasticity, ignored liquid flow resistance in the channels of the valves and conduits.

Figure 2 shows the general scheme system.

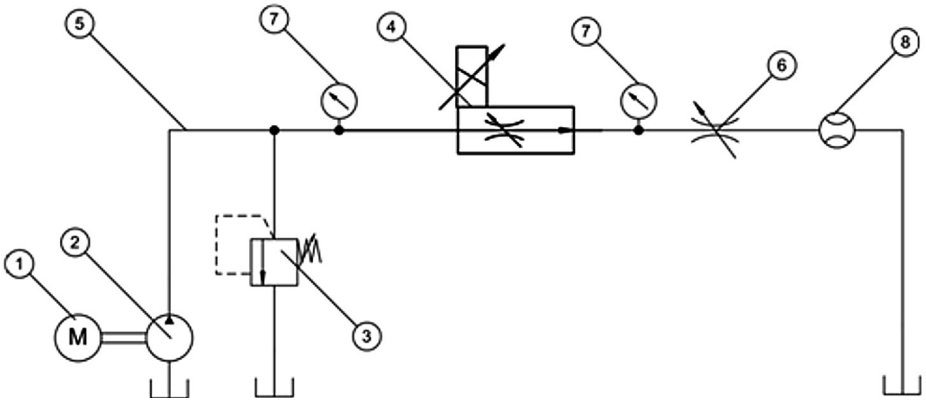

Fig. 2. General diagram of the power supply system and flow controller

Rys. 2. Schemat ogólny układu zasilacza wraz z regulatorem przepływu

Hydraulic pump

Basic parameters pump operation is volumetric flow rate Q_p and pump output pressure p_2. With appropriate simplifying assumptions described pump model

$$Q_p = q_p \frac{\omega_p}{2\pi} \eta_{vp} \tag{1}$$

where:

q_p – Performance Unit,
ω_p – angular velocity of the shaft pump,
η_{vp} – pump volumetric efficiency.

Power supply line

Liquid flows into the controller with constant flow rates of Q_R Q_p pump intensity, the supply line V_z volume and bulk modulus of elasticity substitute B_z. Flow balance equation can be described by the equation

$$\frac{dp_z}{dt} = (Q_p - Q_R - Q_{zp})\frac{B_z}{V_z} \tag{2}$$

where:

p_z – pressure in the supply line,
Q_{zp} – volumetric flow rate through the overflow valve.

Flow controller

In Figure 3. shows a simplified diagram of the modeled flow controller which sets out elements such as: 1 – slider, 2 – piston, 3 – pin electromagnet, 4 – slot inlet, 5 – chamber of the regulator, 6 – channel 7 – slot outlet, 8 – spring.

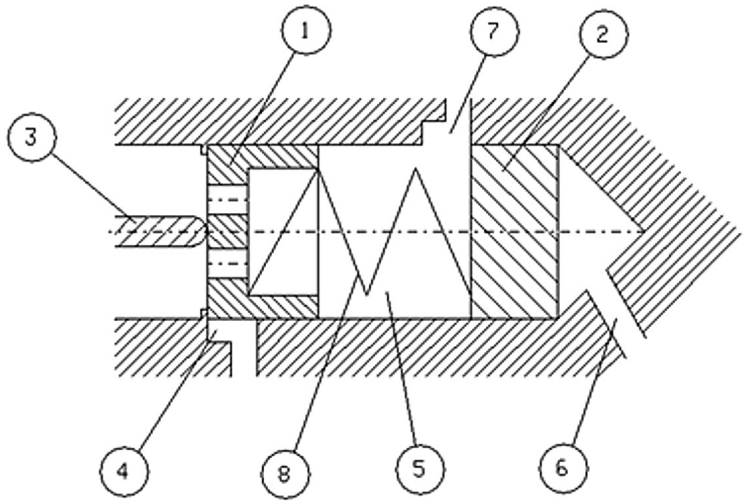

Fig. 3. Simplified schematic of the flow controller
Rys. 3. Uproszczony schemat regulatora przepływu

The volumetric flow rate passing through the gap 4 we calculate using the formula

$$Q_R = \mu_A S_A \sqrt{\frac{2(p_z - p_{S1})}{\rho}} \tag{3}$$

where:

μ_A – gap aspect ratio of,
S_A – cross sectional area gap 4,
p_z – pressure in the supply line,
p_{S1} – pressure in the flow controller chamber,
ρ – density of the liquid.

Pressure in the flow controller

The pressure in the valve chamber p_{S1} describes of liquid flow balance, taking into account the compressibility

$$\frac{dp_{S1}}{dt} = (Q_R - Q_{S1})\frac{B_z}{V_{S1}(x_s)} \tag{4}$$

where:

$V_{S1}(x_s)$ – valve chamber volume as a function of slider is moved.

Flow controller slider and piston

On the slider m_s with a mass controller work force:

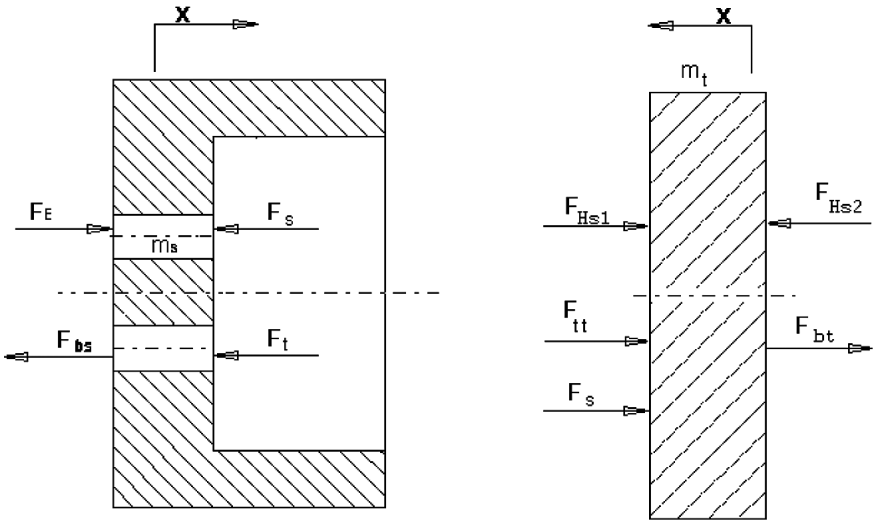

Fig. 4. Forces acting on the slider and piston controller
Rys. 4. Siły działające na suwak oraz tłoczek regulatora

Forces acting on the slider

Force of inertia

$$F_{bs} = m_s \frac{d^2 x_s}{dt^2} \tag{5}$$

where:

m_s – mass of the slider,

x_s – moving the slider.

Viscous friction force

$$F_t = f_s \frac{dx_s}{dt} \tag{6}$$

where:

f_s – coefficient of resistance to motion.

The spring force

$$F_s = c(x_s + x_w + x_t) \tag{7}$$

where:

c – spring constant,

x_w – initial deflection,

x_t – piston displacement.

Because the same pressure acts on both sides of the slider H_{s1} hydrostatic force is balanced and does not affect system balance of forces.

Forces acting on the piston

Force of inertia

$$F_{bt} = m_t \frac{d^2 x_t}{dt^2} \tag{8}$$

where:

m_s – mass of the piston

Viscous friction force

$$F_{tt} = f_s \frac{dx_t}{dt} \tag{9}$$

The spring force

$$F_s = c\,(x_s + x_w + x_c) \tag{10}$$

Hydrostatic forces

$$F_{Hs1} = p_{S1} S_t \tag{11}$$

$$F_{Hs2} = p_z S_t \tag{12}$$

where:

S_t – surface area of the piston,

p_{s1} – pressure in the valve,

p_z – supply line pressure.

3. Model in Matlab-Simulink

Set of equations are equations (1)–(12). To solve the equations used in the program MATLAB / Simulink. For this purpose was built block diagram which is shown in Figure 5.

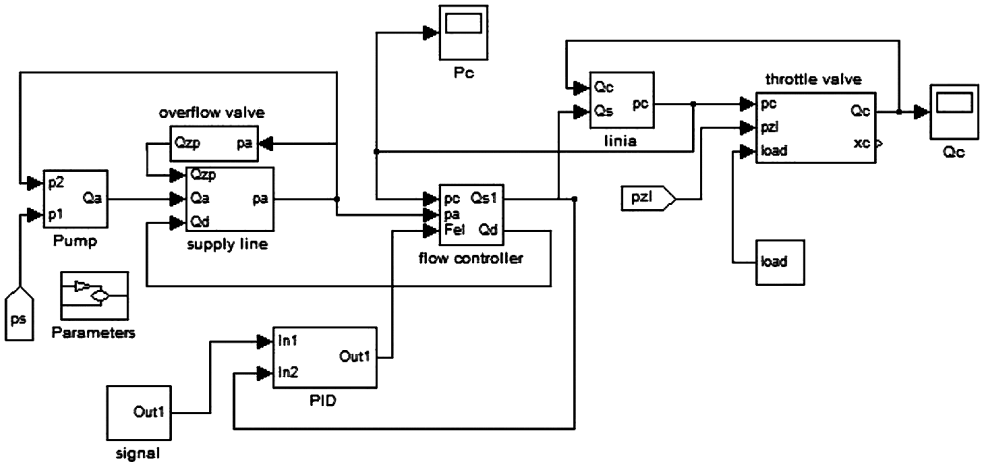

Fig. 5. Block diagram of the hydraulic system was built in Matlab - Simulink

Rys. 5. Schemat blokowy układu hydraulicznego zbudowany w Matlab-Simulink

The construction scheme uses the convention that the individual sub-blocks represent system components. In this way it is possible to easy modification and extension of system of additional elements. Figure 6 shows a simulation result in the initial stage of pump start-up until the determination of the conditions of pressure and flow.

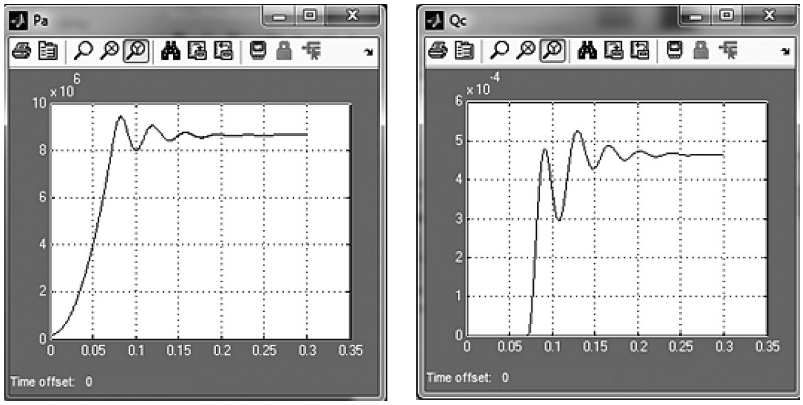

Fig. 6. Sparkline pressure p_a on input to the flow controller and course of the volumetric flow rate Q_c

Rys. 6. Wykres przebiegu ciśnienia p_a na wejściu do regulatora przepływu oraz przebieg objętościowego natężenia przepływu Q_c

4. Conclusions

The model allows the simulation and testing of an item in a variety of configurations. Possible to use it to search for better controller of geometric parameters increase the precision control. The next step is to verify the real model of the hydraulic system, and selection of parameters of the PID controller to improve the characteristics of the valve.

Reference

[1] Lisowski E., Filo G., *Zastosowanie logiki rozmytej do sterowania proporcjonalnym zaworem przelewowym*, Przegląd Mechaniczny nr 1/2002.
[2] Filo G., Lisowski E., *Pozycjonowanie siłownika hydraulicznego przy zastosowaniu regulatorów cyfrowych*, Przegląd Mechaniczny nr 1/2006.
[3] Lisowski E., Filo G., *Pozycjonowanie ładunku podnośnikami hydraulicznymi z regulatorami w logice rozmytej*, Hydraulika i Pneumatyka, nr 1/2010.
[4] Brandys P., *Modelowanie synchronizatora przepływu w układzie napędowym z siłownikami hydraulicznymi*, praca doktorska, Politechnika Krakowska, Kraków 2002.

TECHNICAL TRANSACTIONS | **CZASOPISMO TECHNICZNE**
MECHANICS | MECHANIKA
1-M/2013

ARTUR KROWIAK*

DETERMINATION OF THE WEIGHTING COEFFICIENTS FOR DIFFERENTIAL QUADRATURE METHOD BASED ON SPLINE INTERPOLATION

WYZNACZANIE WSPÓŁCZYNNIKÓW WAGOWYCH W METODZIE KWADRATÓR RÓŻNICZKOWYCH BAZUJĄCEJ NA FUNKCJACH SKLEJANYCH

A b s t r a c t

The paper deals with the methodology of the determination of the weighting coefficients for differential quadrature method based on spline interpolation. Appropriate formulas are derived and two practical approaches to determine mentioned coefficients are proposed, one – pure numeric, the other that uses symbolic-numeric programming. Both approaches are analyzed on account of efficiency, conditioning of the problem and easiness of the implementation.

Keywords: *differential quadrature method*, *spline interpolation*, *weighting coefficients*

S t r e s z c z e n i e

W artykule omówiono metodykę wyznaczania współczynników wagowych dla metody kwadratur różniczkowych bazującej na interpolacji funkcjami sklejanymi. Wyprowadzono związki na wspomniane współczynniki oraz zaproponowano dwa sposoby praktycznej realizacji tego zagadnienia, jeden – czysto numeryczny, drugi – wykorzystujący programowanie symboliczno-numeryczne. Oba sposoby przeanalizowano pod kątem efektywności obliczeń, uwarunkowania zagadnienia oraz łatwości implementacji.

Słowa kluczowe: *metoda kwadratur różniczkowych*, *funkcje sklejane*, *współczynniki wagowe*

* PhD. Eng. Artur Krowiak, Institute of Applied Informatics, Faculty of Mechanical Engineering, Cracow University of Technology.

1. Introduction

The differential quadrature method (DQM) is an efficient numerical tool for solving differential equations. One can achieve very accurate results of the considered problem with a little computational effort. The DQM is characterized by simple formulation, which allows to implement even complex mathematical problems without having much programming skills. These features make the method very useful in solving various scientific or engineering problems [1].

The main idea of the DQM is to descritize spatial derivatives in the governing equation by a linear weighted sum of all function values $f(x_i)$ from the domain, which can be put as

$$\frac{d^r f(x)}{dx^r}|_{x=x_i} = \sum_{j=1}^{N} a_j^{(r)}(x_i) f(x_j) = \sum_{j=1}^{N} a_{ij}^{(r)} f_j \quad i = 1,...,N \tag{1}$$

where N denotes the number of nodes x_i and $a_{ij}^{(r)}$ are the weighting coefficients for the rth order derivative. In such a way the differential equation and associated boundary or initial conditions can be written in the form of algebraic equations. The key stage of the method is to determine the weighting coefficients. To this end some algebraic expressions, based on the Lagrange interpolation formula, have been derived [2, 3]. This approach turns out to be very efficient since no system of equations has to be solved to obtain these coefficients. However, the use of these coefficients to problem discretization may lead to an unstable solution, especially in dynamics problems [4, 5]. To overcome this drawback, the spline interpolation has been introduced instead of Lagrange polynomial [6]. In this approach the function sought is approximated in the following way

$$f(x) \approx \{s_i(x),\ x \in [x_i, x_{i+1}],\ \ i = 1,...,N-1 \tag{2}$$

where the $s_i(x)$ spline segment of n-th degree is defined by the formula

$$s_i(x) = \sum_{j=0}^{n} c_{ij}(x - x_i)^j \tag{3}$$

In Equation (3) c_{ij} denotes the spline coefficients, which are calculated using the interpolation conditions (4) as well as derivative continuity conditions (5) and the so called natural end conditions.

$$s_i(x_i) = f_i\,,\ \ s_i(x_{i+1}) = f_{i+1}\,,\ \ i = 1,\ldots,N-1 \tag{4}$$

$$s_i^{(k)}(x_{i+1}) = s_{i+1}^{(k)}(x_{i+1}),\ \ i = 1,\ldots,N-2,\ \ k = 1,\ldots,n-1 \tag{5}$$

$$s_1^{(k)}(x_1) = 0,\ s_{N-1}^{(k)}(x_N) = 0,\ \ k = \frac{n+1}{2},\ldots,n-1 \tag{6}$$

Although one can use an odd or even degree of the spline function, the formulas presented in this paper are limited to odd spline degrees. Similar formulas can be easily derived for an even spline degree.

In the present paper the details of the calculation of the weighting coefficients for spline-based DQM are presented. Two algorithms are shown and compared with respect to their efficiency, conditioning of the problem and easiness of the implementation.

2. Weighting coefficients

Spline coefficients from Equation are linear combinations of the function sought

$$c_{ij} = \sum_{k=1}^{N} C_{ijk} \cdot f_k , \quad i = 1,...,N-1, j = 0,...,n \tag{7}$$

where the values of C_{ijk} depend on the node distribution. In order to obtain the weighting coefficients for the DQM, an appropriate order derivative of the interpolation function (2) has to be calculated and evaluated at each node of the domain, what can be expressed by the formula

$$f^{(r)}(x_i) \approx \left\{ s_i^{(r)}(x_i),\ i = 1,\ldots,N-1, s_{N-1}^{(r)}(x_N) \right\} \tag{8}$$

where

$$s_i^{(r)}(x_i) = c_{ir} \cdot r! , \quad i = 1,...,N-1, \quad s_{N-1}^{(r)}(x_N) = \sum_{j=r}^{n} \left(c_{N-1\,j} \cdot (x_N - x_{N-1})^{j-r} \cdot \frac{j!}{(j-r)!} \right) \tag{9}$$

Introducing Equation (7) into Equation (9), after simple algebraic transformations one obtains

$$\begin{aligned} s_i^{(r)}(x_i) &= \sum_{k=1}^{N} \left[C_{irk} \cdot r! \right] f_k , \quad i = 1,...,N-1, \\ s_{N-1}^{(r)}(x_N) &= \sum_{k=1}^{N} \left[\sum_{j=r}^{n} \left(C_{N-1\,jk} \cdot (x_N - x_{N-1})^{j-r} \cdot \frac{j!}{(j-r)!} \right) \right] f_k \end{aligned} \tag{10}$$

Comparing Equation (10) with the main formula of the DQM (1) it is easy to notice that the expressions enclosed in square brackets are the weighting coefficients for the DQM based on spline interpolation

$$\begin{aligned} a_{ik}^{(r)} &= C_{irk} \cdot r!, \quad i = 1,...,N-1,\ k = 1,...,N \\ a_{Nk}^{(r)} &= \sum_{j=r}^{n} \left(C_{N-1\,jk} \cdot (x_N - x_{N-1})^{j-r} \cdot \frac{j!}{(j-r)!} \right), \quad k = 1,...,N \end{aligned} \tag{11}$$

Due to the assumed approximation (2), the determination of the weighting coefficients is possible, when the coefficients C_{ijk} are computed. Unfortunately, this process requires to solve the system of equations mentioned in section 1 what is an inconvenience compared to classical DQM. However, this inconvenience is compensated by more versatility of the method based on spline functions.

3. Practical approaches to determining the weighting coefficients

In order to compute the weighting coefficients given by Equation (11) the set of equations for coefficients C_{ijk} has to be formulated and solved. Two approaches are proposed to this end.

3.1. Numeric approach

Introducing Equation (7) into interpolation conditions (4) and comparing the terms standing next to the appropriate values of f_i one obtains

$$\begin{aligned} &C_{i0k} = \delta_{ik}, \quad i = 1,...,N-1,\ k = 1,...,N \\ &\sum_{j=0}^{n} C_{ijk} \cdot (x_{i+1} - x_i)^j = \delta_{ik-1}, \quad i = 1,...,N-1,\ k = 1,...,N \end{aligned} \tag{12}$$

where δ_{ik} is the Kronecker symbol.

Taking into account Equation (7) in derivative continuity conditions (5), the following equations can be derived

$$\sum_{j=r}^{n} C_{ijk} \cdot (x_{i+1} - x_i)^{j-r} \cdot \frac{j!}{(j-r)!} = r! \cdot C_{i+1rk}, \quad i = 1,...,N-2,\ k = 1,...,N, r = 1,...,n-1 \tag{13}$$

To complete the set of equations, expression (7) should be introduced into the natural end conditions (6), what yields

$$\begin{aligned} &C_{1rk} = 0, \quad r = \frac{n+1}{2},...,n-1,\ k = 1,...,N \\ &\sum_{j=r}^{n} C_{N-1jk} \cdot (x_N - x_{N-1})^{j-r} \cdot \frac{j!}{(j-r)!} = 0, \quad r = \frac{n+1}{2},...,n-1,\ k = 1,...,N \end{aligned} \tag{14}$$

Expressions (12)–(14) constitute the system of $NE = (N-1) \cdot (n+1) \cdot N$ equations for C_{ijk}. Once this system is solved, the weighting coefficients can be computed using formula(11). Although this system is characterized by a sparse matrix and some coefficients C_{ijk} in (12)–(14) are directly defined, the solution of the system can be troublesome due to weak conditioning. This problem is illustrated in Fig. 1. To overcome the inconvenience, another approach that takes advantage of symbolic-numeric programing is proposed.

3.2. Symbolic-numeric approach

This approach requires the following steps:

- Definition of the interpolation conditions as well as derivative continuity conditions and the end conditions (4)–(6), where unknown function values f_i are noted as symbols.
- Solution of the defined set of equations for the interpolation coefficients c_{ij}. The coefficients obtained are in the form of symbolic-numeric terms given by (7).
- Determination of the numeric values C_{ijk} in expression (7) by separating these numbers from appropriate symbols f_i. This step is easy to implement using some tools provided by Computer Algebra Systems (CAS).

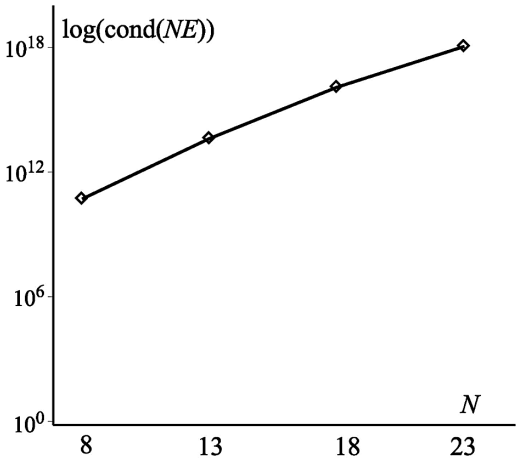

Fig. 1. Condition number of the system of equations (spline degree $n = 9$) versus number of nodes
Rys. 1. Wskaźnik uwarunkowania układu równań (stopień funkcji sklejanej $n = 9$) w zależności od liczby węzłów

Once the C_{ijk} coefficients are obtained, the weighting coefficients can be computed using formula (11). It is well known that the symbolic manipulations are less efficient than numeric ones, but the algorithm presented above requires far fewer equations to solve then the approach described in section 2.1. Moreover, the possibilities of using exact arithmetic provided by CAS eliminate the ill-conditioning problem that arises in the pure numeric approach. Therefore the algorithm presented here seems to be a more convenient way to determine the weighting coefficients for the DQM based on spline interpolation.

3.3. Some notes on efficiency

In order to show the efficiency of the algorithms presented in the previous subsections some numerical experiments have been carried out. The algorithms have been implemented in the Maple programming language. The reason of the choice of this environment is the broad possibilities of the symbolic and numeric manipulations. The CPU (AMD Phenom II X4 810, 2.6 GHz) time of the computation of the C_{ijk} coefficients, which are crucial for the calculation of the weighting coefficients $a_{ij}^{(r)}$, has been determined. The results are presented in Table 1.

Results in table 1 indicate that the symbolic-numeric approach is quite good alternative for the determination of the weighting coefficients for the DQM based on spline functions. When the system of equations is large enough, this algorithm works faster than the pure numeric one. The reason lies in the fact that this algorithm requires far fewer equations to solve then pure numeric one. Moreover, as mentioned earlier the use of the exact arithmetic in the symbolic-numeric approach overcomes the problem of the ill-conditioning that arises during pure numeric computations.

Table 1

CPU time of the computation of the C_{ijk} coefficients

Spline degree (n), Number of nodes (N)	CPU Time [s]	
	Numeric approach	Symbolic-numeric approach
$n = 7$		
$N = 8$	0.078	0.156
$N = 13$	0.577	0.500
$N = 18$	3.541	0.936
$n = 9$		
$N = 8$	0.125	0.234
$N = 13$	1.076	0.827
$N = 18$	6.630	2.574
$n = 11$		
$N = 8$	0.156	0.327
$N = 13$	1.638	1.498
$N = 18$	11.060	4.274

4. Conclusions

The DQM based on spline interpolation is an alternative to the classical DQM, especially in the case of dynamics problems, where the latter is not a reliable tool due to its instability. In the paper two algorithms to determine the weighting coefficients for spline-based DQM have been presented. The discussion on the efficiency and simplicity of these approaches has been carried out. One can conclude that the symbolic-numeric algorithm is better way to determine of the weighting coefficients than pure numeric one.

References

[1] Bert C.W., Malik M., *Differential quadrature method in computational mechanics*, Applied Mechanics Review, 49, 1996, 1-28.

[2] Shu C., Richards B.E., *Application of generalized differential quadrature to solve two-dimensional incompressible Nanier-Stokes equations*, International Journal for Numerical Methods in Fluids, 15**,** 1992, 791-798.

[3] Shu C., *Differential quadrature and its application in engineering*, Springer-Verlag, London, 2000.

[4] Krowiak A., *The application of the differential quadrature method based on a piecewise polynomial to the vibration analysis of geometrically nonlinear beams*, Computer Assisted Mechanics and Engineering Sciences, 15, 2008, 1-13.

[5] Zong Z., *A variable order approach to improve differential quadrature accuracy in dynamic analysis*, Journal of Sound and Vibration, 266, 2003, 307-323.

[6] Krowiak A., *Symbolic computing in spline-based differential quadrature method*, Communications in Numerical Methods in Engineering, 22, 2006, 1097-1107.

TECHNICAL TRANSACTIONS | CZASOPISMO TECHNICZNE
MECHANICS | MECHANIKA
1-M/2013

JANUSZ KWAŚNIEWSKI*, IRENEUSZ DOMINIK*, KRZYSZTOF LALIK*

REAL-TIME SYSTEM BASED ON FPGA APPLIED TO SELF-EXCITED ACOUSTICAL SYSTEM FOR STRESS CHANGE MEASUREMENT

SYSTEM CZASU RZECZYWISTEGO OPARTY O FPGA ZASTOSOWANY W SAMOWZBUDNYM AKUSTYCZNYM SYSTEMIE POMIAROWYM DO POMIARU ZMIAN NAPRĘŻEŃ

Abstract

In the paper the real-time system based on FPGA applied to control the delay time in feedback loop of the Self-excited Acoustical System is presented. The system can be used for stress change measurement in elastic constructions. Stress changes manifest themselves in small but detectable variations of resonance frequency. This phenomenon can be used to indirect measure stress changes in the material. In the article the limits of the measurement system which occurred during research on the analogue version of the system were eliminated by applying FPGA technology.

Keywords: real-time computing, field-programmable gate array, computer supported experiment

Streszczenie

W artykule przedstawiono wykorzystanie systemów czasu rzeczywistego i układów FPGA do sterowania opóźnieniem pętli sprzężenia zwrotnego w Samowzbudnym Systemie Akustycznym do pomiaru zmian naprężeń w konstrukcjach sprężystych. Zjawisko to może zostać użyte do pośredniego pomiaru naprężeń w konstrukcjach. W artykule wskazano ograniczenia układu pomiarowego, które zostały wyeliminowane dzięki zastosowaniu systemów czasu rzeczywistego oraz układów FPGA.

Słowa kluczowe: systemy czasu rzeczywistego, układy FPGA, komputerowe systemy nadzoru

* Prof. Janusz Kwaśniewski, PhD. Ireneusz Dominik, MSc. Krzysztof Lalik, AGH University of Science and Technology, Faculty of Mechanical Engineering and Robotics, Department of Process Control.

1. Introduction

The autooscillator also known as the auto-oscillating system is generally introduced as dynamical system capable of performing oscillations. The autooscillation, which appears in the system, is a kind of a non-damped oscillation in a non-linear dynamical system, whose amplitude and frequency can remain constant during a long period of time and are largely independent of the initial conditions. According the soviet physicist A.A. Andronov theory amplitude and frequency are determined by the properties of the system itself [14].

The autooscillators are quite common in practice. The simple non-linear mechanical systems can hold a particular frequency. A good example is the music instrument: reed woodwinds, which gives a constant frequency sound with a wind flowing round.

At the Department of Process Control at AGH University of Science and Technology the Self-excited Acoustical System (SAS), which is a kind of the autooscillator, was developed [1]. The essence of the SAS system is to use a vibration exciter and vibration receiver placed on a sample at a distance with a positive feedback, which causes the excitation of the system. Stress changes manifest themselves in small but detectable variations of resonance frequency (autooscillator frequency). As a parallel to reed woodwinds a sample under load examined by the SAS system changes its length thus the system resonance frequency. This phenomenon can be used to indirect measure stress changes in the material [2, 3].

Non-synchronous autooscillators set the frequency near the resonance frequency of a system [4, 8]. Due to a piezoelectric shaker application the high proper vibration forms are observed. In order to synchronize an autooscillator to the lower forms an additional controlled delay in the SAS feedback loop can be implemented. During a numerous experiments it was deduced that for the high proper vibration forms resulting in the high oscillation frequency of the SAS system it is impossible to use the general purpose operation systems. The problem was solved by working in the Real-Time Operating System (RTOS) implemented in the Field Programmable Gate Array (FPGA) platform.

In the article the principles and basic parameters of the SAS system are described. The used computer methods with reference to the created control application are also explained. The relationship between individual components of the real-time system is also described. The focus is put on influence of the controlled delay in the feedback loop on resonance frequency of the SAS system.

2. Preliminary research

The scheme of the Self-excited Acoustical System is presented in Figure 1. It can be divided into three main parts: electrical, mechanical and software. The mechanical part consists of a sample under examination, fasten points, a base. The electrical part consist of a shaker (vibration exciter E) and accelerometer (vibration receiver R) placed on a sample at a distance. Together with a conditioner, a power amplifier and the RTOS system the positive feedback loop is created.

The software part focuses on implementing the RTOS on FPGA platform. The data acquisition by the measurement card and especially the implementation of the additional controlled delay in the feedback loop are the main parts of the software.

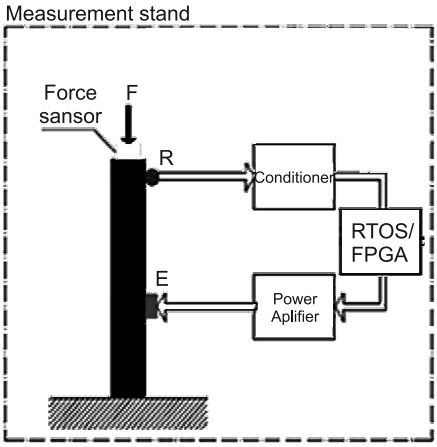

Fig. 1. The scheme of the Self-excited Acoustical System, where *E* – exciter, *R* – receiver, *F* – applied force

Rys. 1. Schemat Samowzbudnego Systemu Akustycznego, gdzie *E* – wzbudnik, *R* – odbiornik, *F* – przyłożona siła

According to the theory proposed in [1] and [5] for the design SAS system the following relationship may be delivered:

$$\frac{\Delta f}{f_0} = -\frac{\Delta\tau}{\tau_0} - \frac{\tau_E}{\tau_0}\frac{\Delta f_E}{f_0} - \frac{\tau_R}{\tau_0}\frac{\Delta f_R}{f_0} - \frac{\tau_{\text{comp}}}{\tau_0} \tag{1}$$

where:

f_0 and τ_0 – are the frequency and delay for preliminary load of the sample,
f_E and τ_E – are the frequency and delay for exciter – amplifier connection,
f_R and τ_R – are the frequency and delay for receiver – conditioner connection,
τ_{comp} – a controlled delay of the feedback (part of software in RTOS).

It is proved that increasing any of the delays (in Eq. 1) can decrease the resonance frequency of the autooscillator (Eq. 2). Thus the frequency of the whole system is decreased. It enables usage of the longer window functions in the Fourier analysis and as a result it improves measurement accuracy [6, 7].

$$f_0 = \frac{m}{\sum \tau_{0i}} \tag{2}$$

where m is a integer number, which is estimated as number of wavelengths λ on a distance l: $m \approx l/\lambda$.

Figure 2 presents the results of applying two types of the exciter to the SAS system. The upper piezoelectric exciter has time response of 500 ns while the lower electro-acoustic exciter of 50 μs. In both cases the main idea of the SAS system can be observed: the resonance frequency of the system is changing in accordance to the compressive force applied to the sample.

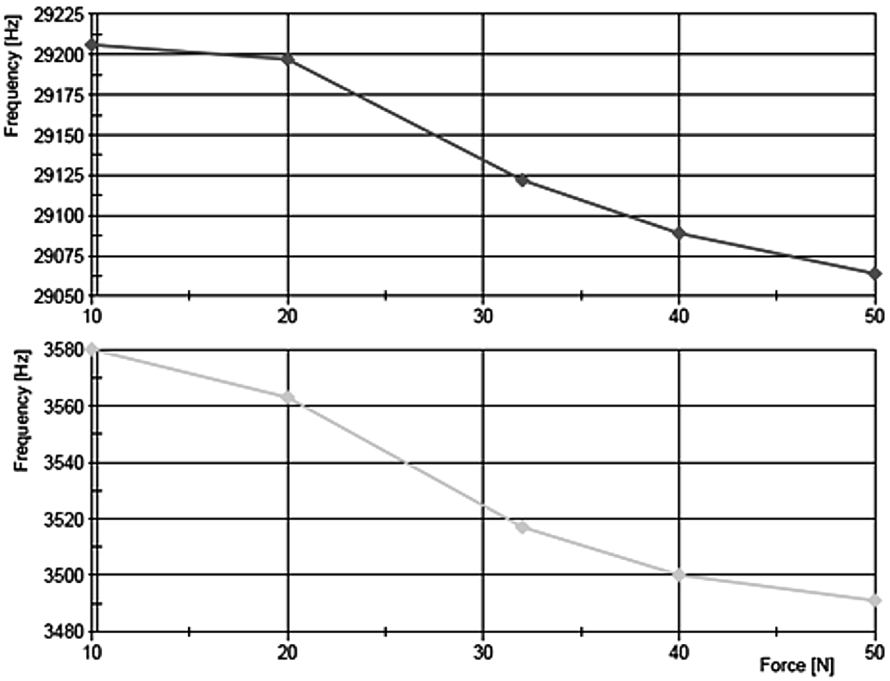

Fig. 2. The dependence between the autooscillator resonance frequency and the load force of the sample for the piezoelectric exciter (above) and the electro-acoustic exciter (below)
Rys. 2. Zależność pomiędzy częstotliwością autooscylatora i siłą obciążającą badana belkę dla wzbudnika piezoelektrycznego (góra) i wzbudnika elektroakustycznego (dół)

The results indicate that using the slow electro-acoustic exciter decreased the system frequency which allows the SAS system work properly without the powerful specialized hardware. On the other hand the bigger delay time in the system the narrowed pass band – in the case of some high frequency constructions the SAS system may not work properly. That is why the best solution seems to be usage of the fast piezoelectric exciter with the controlled delay in the feedback loop implemented in FPGA platform.

3. Real time operating systems

An Embedded System is usually a computerized system integrated with a bigger system. Embedded systems are associated with the concept of real - time operations. A real-time operation is an operation of the unit, which is dependent on the time of its execution. It results in a constant competition between the two systems: external (environmental) and internal (real time device). In order to keep pace with the environment, in which the unit works, there are special criteria for limiting the development time for RTOS. This limitation and a system repeatability to fulfill those restrictions is the basis for quality assessment of the real time operating system [9].

Real time operating system is able to execute the program reliably, even with its specific requirements for the synchronization and coordination. The special operating system –RTOS is a key to build a real time unit. The Authors used a dedicated real-time system built in the LabVIEW environment to control the SAS system delay duration in the feedback loop. Unfortunately, the built in real-time systems have the software frequency limitation. The restriction for LabVIEW amounts to 1 kHz [10]. For this reason, it was necessary to use a FPGA system additionally.

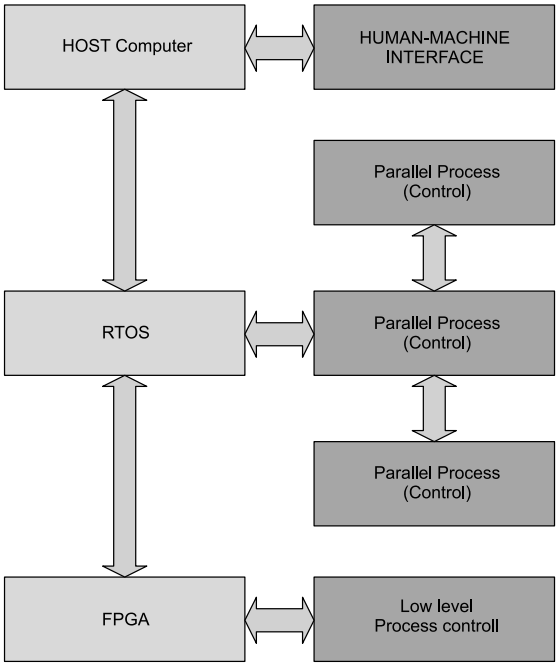

Fig. 3. The communication architecture: HOST/RTOS/FPGA

Rys. 3. Architektura komunikacyjna HOST/RTOS/FPGA

Figure 3 shows a popular architecture, which can be used as a starting point for the most control and monitoring applications. The host program provides the user interface based on the system events so the operator has access to the built-in system and can interact with it [11]. A real-time operating system performs the high level control while the FPGA system is engaged in the low-level control.

4. FPGA systems

For the system designer FPGAs (Field Programmable Gate Array) performs the same function as dedicated built-in systems, which are constructed for the implementation of the defined tasks. The difference between them lies in the fact that FPGAs may be reprogrammed

many times after their design and installation in a target circuit. Thus FPGAs are the excellent tool for building real time embedded systems [12, 13].

The system architecture shown in Figure 3 consists of each device processes and data communication paths. Processes are represented by gray blocks. Target hardware devices, which execute those processes are marked as yellow blocks. Data communication paths are represented as white arrows. Major tasks of the designed software are shown in Figure 4.

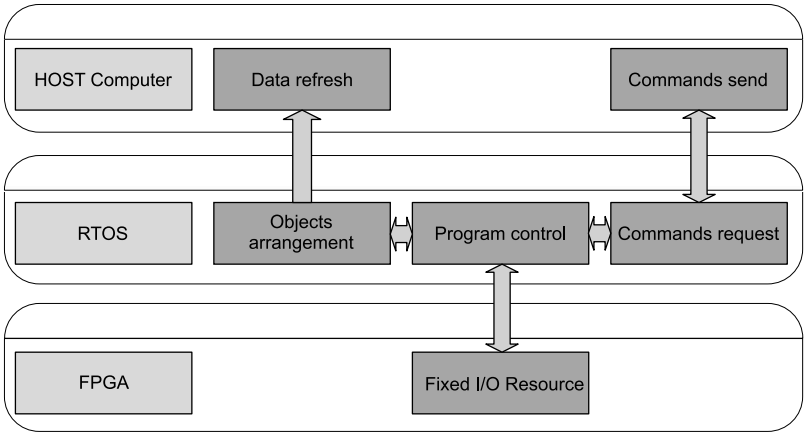

Fig. 4. The basic tasks of the control architecture components: HOST/RTOS/FPGA

Rys. 4. Podstawowe zadania komponentów architektury HOST/RTOS/FPGA

The LabVIEW Interface mode enables the physical adaptation of the FPGA, including programming of a real time processor. It allows achieving the performance that typically required a dedicated hardware. An exemplary FPGA process for delay duration control of the Self-excited Acoustical System is shown in Figure 5.

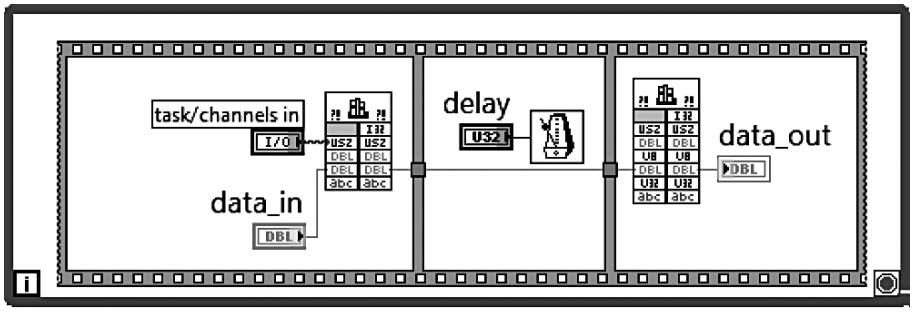

Fig. 5. FPGA process for delay duration control

Rys. 5. Proces FPGA ze sterowalnym opóźnieniem

By default FPGA communicates with I/O modules automatically. It provides a deterministic I/O field for a real time processing. The system allows a real-time control program to access

I/O with the jitter shorter than 500ns. FPGA can be also directly programmed in order to further customization and improvement of the system. The valid circuit diagram for the communication between RTOS and FPGA is shown in Figure 6.

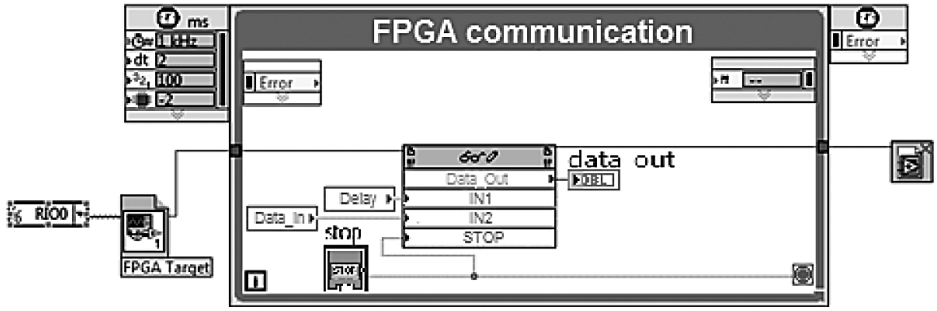

Fig. 6. The FPGA-RTOS communication program diagram

Rys. 6. Program odpowiedzialny za komunikację z układem FPGA

5. Conclusions

This paper presents the real-time system based on FPGA applied to control the delay duration in feedback loop of the Self-excited Acoustical System for stress change measurement.

The computer-aided system is highly flexible, which is achieved at the programming level. The application of the real-time operating system and the field programmable gate arrays allowed completing the control system. It allows to determine the delay duration of the feedback loop in SAS system. The FPGA technology gave the possibility of interference in the acoustic signals that go beyond the human ear audibility.

The main task of FPGA implementation to the SAS system was fulfilled – the user can control the feedback delay time and thus reduce the measurement system sampling frequency. As a result the level of the hardware requirements is lowered – there is no need to use very expensive high frequency shakers and advanced measurement systems.

In the further system development phase variety of filters will be applied and tested using LabVIEW and FPGAs. The whole set of filters, starting from classic and ending with advanced filters, based on artificial neural networks will be considered. The embedded filter will select a frequency bandwidth. It allows the system to eliminate any possible frequency shift resulting from the changes in the form of vibration in the tested material under load.

References

[1] Kwaśniewski J., Dominik I., Konieczny J., Lalik K., Sakeb A., *Application of self-excited acoustical system for stress changes measurement in sandstone bar*, Journal of Theoretical and Applied Mechanics ; ISSN 1429-2955, 2011, vol. 49, no. 4.

[2] Bobrowski Z., Chmiel J., Dorobczyński L., Kravtsov Y.A., *Ultrasonic system for monitoring stress changes and deformations in the ship hull*, EXPLO SHIP, ISSN 0209-2069, 2004.
[3] Bogusz W., Engel Z., Giergiel. J., *Drgania i szumy*, Wydawnictwo Geologiczne, Warszawa 1974.
[4] Deputat J., Mackiewicz S., Szelążek J., *Problemy i techniki nieniszczących badań materiałów – wybrane wykłady*, GAMMA, 2007.
[5] Kwaśniewski J., Dominik I., Konieczny J., Kravtsov Y., Sakeb A., *Experimental system for stress measurement in rock. 9th Conference on Active noise and vibration control methods*, Kraków––Zakopane, Poland, May 24–27, 2009.
[6] Gordienko V., Aleksandr D., Konovalov A., Kurochkin N., Putivskii Y., Panchenko V., Ul'yanov A., *Autodyne effect in the presence of laser-induced hydrodynamic flows and its use in identification of the type of biotissue in the course of its destruction*, Quantum electronic, Volume 26, Number 10, 1996.
[7] Chen Ch., *Ultrasonic & Advanced Methods For Nondestructive Testing & Material Characterization*, ISBN-10: 9812704094World Scientific Publishing; 1 edition, 2007.
[8] Washer G.A., Green R.E., Pond Jr. R.B., *Velocity Constants for Ultrasonic Stress Measurement in Prestressing Tendons*, Federal Highway Administration NDE Validation Center, 6300 Georgetown Pike, McLean, VA 22101, USA.
[9] Barszcz T., Randall R.B., *Application of spectral kurtosis for detection of a tooth crack in the planetary gear of a wind turbine*, Mechanical Systems and Signal Processing; ISSN 0888-3270, 2009, vol. 23.
[10] Jamro E., Cioch W., *Digital signal acquisition and processing in FPGAs*, Przegląd Elektrotechniczny = Electrical Review, ISSN 0033-2097, 2009.
[11] Jamro E., Wiatr K., *Dynamic constant coefficient convolvers implemented in FPGAs*, Field--Programmable Logic and Applications: reconfigurable computing is going mainstream: 12th international conference, FPL 2002: Montpellier, France, September 2–4, 2002.
[12] Jamro E., *FPGA implementation of high speed diagnostic systems*, Polish Journal of Environmental Studies, ISSN 1230-1485, 2007, vol. 16, no. 4B.
[13] Penczek A., Stala R., Stawiarski Ł., Szarek M., *Hardware-in-the-Loop FPGA-based simulations of switch-mode converters for research and educational purposes*, Przegląd Elektrotechniczny, ISSN 0033-2097, 2011, R. 87, nr 11.
[14] Abraham R., Marsden J.E., *Foundations of mechanics*, Benjamin/Cummings (1978) MR0515141 (http://www.ams.org/mathscinet-getitem?mr=0515141) Zbl 0393.70001 (http: //www.zentralblattmath.org/zbmath/search/?q=an%3A0393.70001).

TECHNICAL TRANSACTIONS | **CZASOPISMO TECHNICZNE**
MECHANICS | MECHANIKA
1-M/2013

WALDEMAR KWAŚNY*, PAWEŁ NUCKOWSKI*, TYMOTEUSZ JUNG*,
ZBIGNIEW RDZAWSKI*, WOJCIECH GŁUCHOWSKI*

EFFECT OF PLASTIC DEFORMATION ON THE STRUCTURE AND TEXTURE OF CUSN6 ALLOY

WPŁYW INTENSYWNEGO ODKSZTAŁCENIA PLASTYCZNEGO NA STRUKTURĘ I TEKSTURĘ STOPU CUSN6

Abstract

This paper presents the results of study in the structure and texture CuSn6 alloy deformed in the RCS (repetitive corrugation and straightening) process. Investigated the influence of process parameters on the above property. The obtained results were correlated with the results of the alloy subjected to cold rolling.

Keywords: *Copper alloys*, *Plastic deformation*, *structure and texture*, *X-ray analysis*, *EBSD analysis*

Streszczenie

W artykule przedstawiono wyniki badań struktury oraz tekstury stopu CuSn6 odkształconego w procesie RCS (cykliczne gięcie i prostowanie). Określono wpływ parametrów procesu na wyżej wymienione własności. Uzyskane rezultaty skorelowano z wynikami badań stopu poddanego walcowaniu na zimno.

Słowa kluczowe: *stopy miedzi*, *odkształcenie plastyczne, struktura i tekstury*, *analiza rentgenowska*, *badania EBSD.*

* Prof. Waldemar Kwaśny, MSc. Paweł Nuckowski, MSc. Tymoteusz Jung, prof. Zbigniew Rdzawski, PhD. Wojciech Głuchowski, Institute of Engineering Materials and Biomaterials, Faculty of Mechanical Engineering, Silesian University of Technology, Gliwice.

1. Introduction

In response to still increasing requirements of modern engineering materials, more research is moving towards the development of the materials with finest microstructure, known as ultra-fine-grained materials that will have improved properties compared to currently known materials. In the group of methods used to modify the properties of the materials, in order to obtain a microstructure of the smallest particle size (10 to 1,000 nm) can be featured SPD method (Severe Plastic Deformation). SPD method belongs to a group of plastic treatment method consists in intensive plastic deformation, which is not intended to change shape, but the development of requested mechanical properties of the metal by the ultrafine of microstructure. One of the recently developed techniques of SPD is a cyclic process of repetitive corrugation and straightening plates, called RCS [2, 4, 5].

2. The course of study

2.1. Material to studied

The studied material consisted non annealed tape of CuSn6 alloy, initial strengthening state (z4), cold-rolled in 8 cycles and the tape subjected to intensive plastic deformation using the RCS method (repetitive corrugation and straightening) in 8 and 13 cycles [4, 5]. The chemical composition of the test material are presented in Table 1.

Table 1

CuSn6 chemical composition (PN-92/H-87050) (%wag.)

Material	Tin	Zinc	Phosphorus	Nickel	Lead	Iron	Other	Copper
CuSn6	5.5–7	0.3	0.01–0.35	0.3	0.05	0.1	0.2	reszta

2.2. Studied methodology

X-ray diffraction studies samples were analyzed on the PANalytical X'Pert PRO diffraction system, using filtered radiation from the lamp with copper anode. X-ray phase analysis was conducted in the Bragg-Brentano geometry using *X'* celerator strip detector. Stress measurements were made of samples analyzed with sin2ψ technique using Stress X'Pert Plus software. Crystallite size was determined by using Sherrera method. In order to determine the texture is made of four pole figures for each of the studied samples. Then set the orientation distribution function (FRO) [1]. In the FRO analysis was applied ADC method using iterative operator. Calculations was made using the Tex Labo 3.0 [3]. EBSD analysis was conducted in Zeiss supra 35 scanning electron microscopy equipped with acamera and software for acquisition and analysis of backscattered electrons.

3. The results

The results of *X*-ray phase analysis showed, regardless of the deformation process, CuSn phase in the studied materials (Fig. 1). Stress Measurement in the two directions shown that after classic rolling the material were compressive stresses. Material after deformation

in the RCS process were a compressive stress in the direction of the rolling direction and the tensile stress in the cross direction to the rolling direction independent of the number of cycles (Fig. 2). Table 2 shows the obtained measurement values and the results of stress measurement and crystallite size analyzed strip. Figure 3 shows the change in position of the reflex (311) CuSn phase as a function of ψ (deformed material in the RCS in 13 cycles).

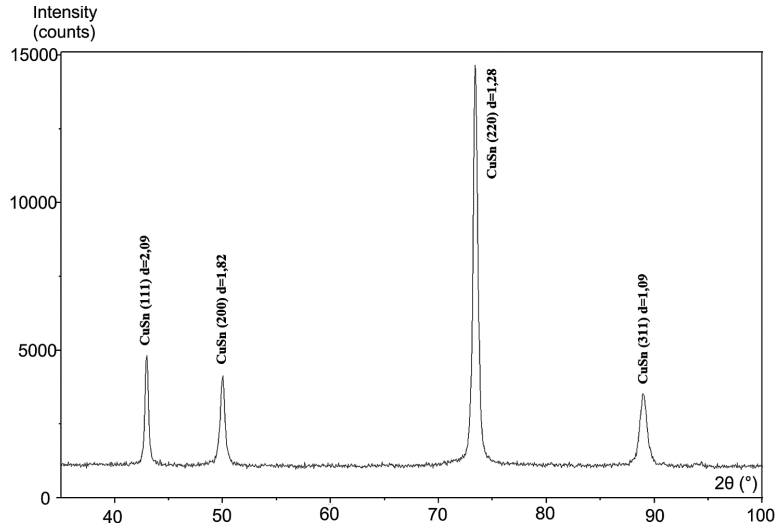

Fig. 1. Diffraction pattern of CuSn6 alloy strip rolled in 8 cycles

Rys. 1. Dyfraktogram taśmy stopu CuSn6 walcowanej w 8 przepustach

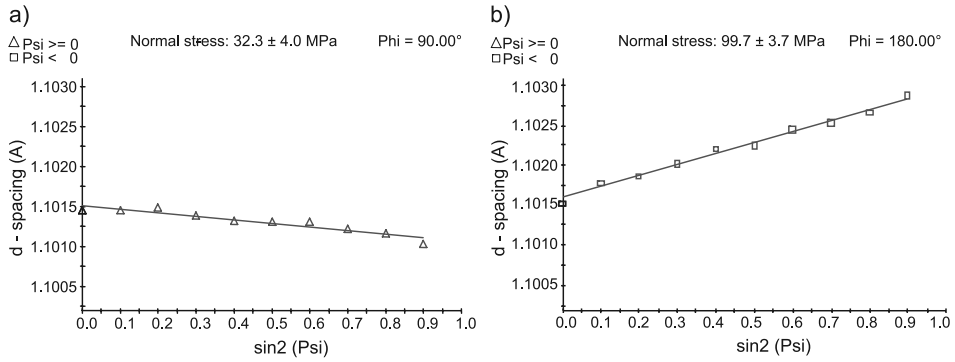

Fig. 2. Stress measurement results in the direction of: a) the rolling direction and b) the cross direction to the rolling direction (CuSn6 alloy strip after deformation in RCS process in 13 cycles, the dependence of d spacings sin2ψ function , peak (311))

Rys. 2. Wyniki pomiaru naprężeń w kierunku: a) równoległym do kierunku walcowania oraz b) w kierunku prostopadłym do kierunku walcowania (taśma stopu CuSn6 po odkształceniu metodą RCS w 13 przepustach, zależność wartości odległości międzypłaszczyznowej d w funkcji sin2 ψ, refleks (311))

Table 2

Summary results of the stress and the crystallite size measurements

Type of the treatment process	Stress results in the direction of the rolling direction [MPa]	Stress results in the cross direction to the rolling direction [MPa]	Crystallite size [nm]
CuSn6 alloy strip classic rolled in 8 cycles	–138.9 ± 6.1	–161,2 ± 7,9	35,1
CuSn6 alloy strip deformation in the RCS process in 8 cycles	–9.2 ± 10.4	115,2 ± 9,3	19,5
CuSn6 alloy strip deformation in the RCS process in 13 cycles	–32.3 ± 4.0	99,7 ± 3,7	20,9

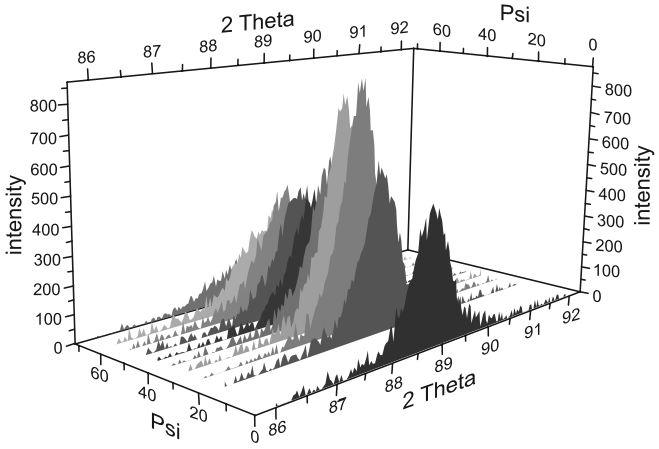

Fig. 3. Changes in the peak position (311) phase CuSn w sin2 ψ function (CuSn$_6$ alloy strip deformation in the RCS process in 13 cycles)

Rys. 3. Zmiany położenia refleksu (311) fazy CuSn w funkcji ψ (taśma CuSn6 odkształcona metodą RCS w 13 przepustach)

In order to determine the texture of studied materials were determinated experimental pole figures by the reflectance method (Fig. 4a). Figure 5 presented FRO and figure 4b – calculated complete pole figures. FRO analysis revealed the presence of several components of texture. Classic rolled conducive to formation of Brass texture component – {011} <211> faded in the direction of Goss texture component – {011} <100>. Deformation of the material by RCS process causes changes in the shares of the above texture components. Table 3 presented the results of texture analysis of studied samples.

EBSD analysis made it possible to obtain the orientation distribution maps, distribution of grains map and qualitative map with plotted boundaries of grain (Fig. 6).

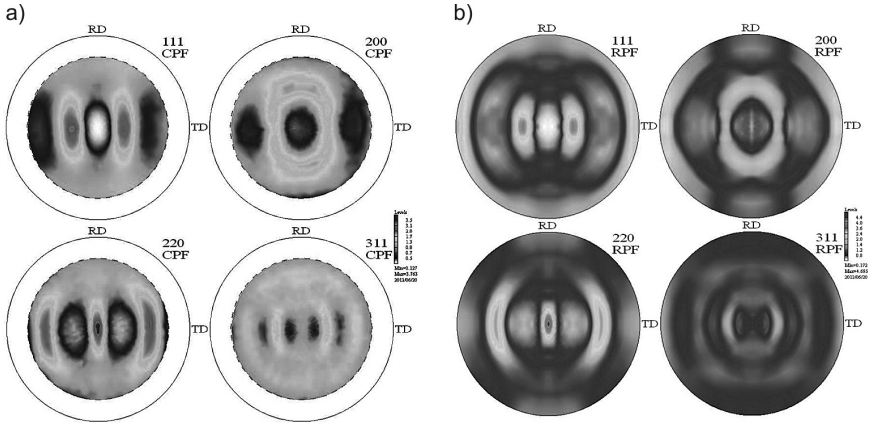

Fig. 4. a) Experimentally determined pole figures $CuSn_6$ alloy strip classic rolled in 8 cycles. b) calculated complete pole figures $CuSn_6$ alloy strip classic rolled in 8 cycles

Rys. 4. a) Wyznaczone eksperymentalnie figury biegunowe taśmy stopu CuSn6 walcowanej klasycznie w 8 przepustach, b) obliczone pełne figury biegunowe taśmy stopu CuSn6 walcowanej klasycznie w 8 przepustach

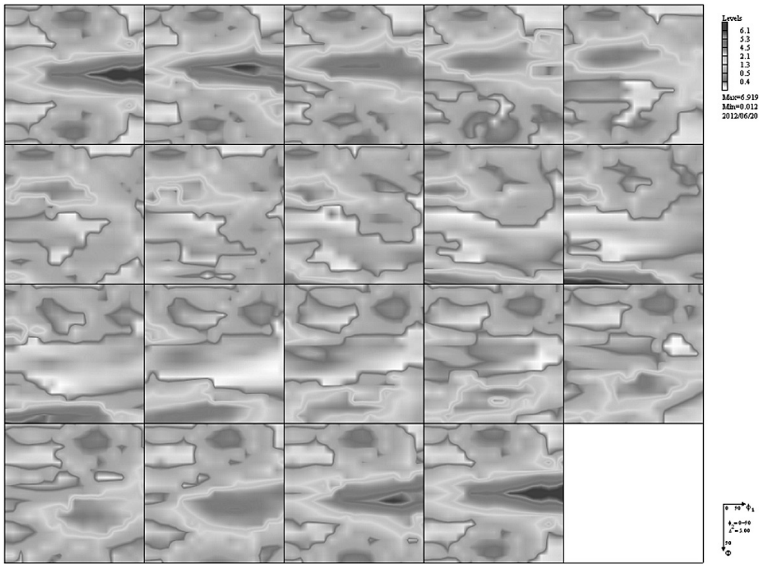

Fig. 5. Orientation distribution function $CuSn_6$ alloy strip classic rolled in 8 cycles

Rys. 5. Funkcja rozkładu orientacji taśmy stopu CuSn6 walcowanej klasycznie w 8 przepustach

From the study it can be concluded, that the RCS process did not affect significantly to average grain size, but changed the nature of the grain boundaries turning their proportions relative to classic rolled material. That means the deformations of this type form the low-

angle edge boundaries in the workpiece material. In the structure of RCS deformed material number of twins and some grains elongated along was observed.

Table 3

Summary results of texture measurements

Type of the treatment process	Share of texture brass component [%]	Share of texture Goss component [%]	Share of texture random component [%]
CuSn6 alloy strip classic rolled in 8 cycles	33	17	50
CuSn6 alloy strip deformation in the RCS process in 8 cycles	40	4	56
CuSn6 alloy strip deformation in the RCS process in 13 cycles	44	2	54

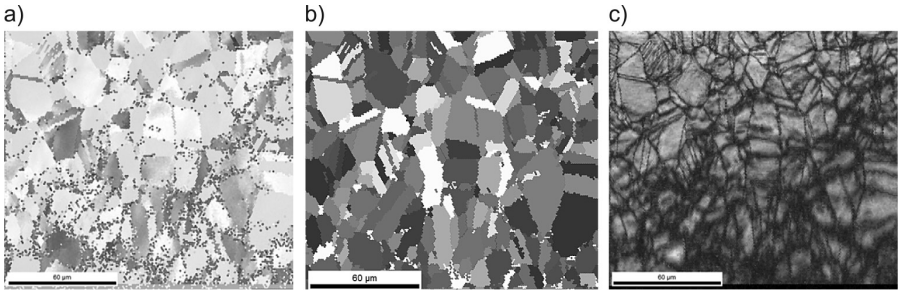

Rys. 6. EBSD analysis results of $CuSn_6$ alloy strip classic rolled in 8 cycles: a) orientation distribution maps, b) distribution of grains map, c) boundaries of grain map – kolor niebieski – kąt > 15°, kolor czerwony – kąt > 2°

Rys. 6. Wyniki badań EBSD taśmy CuSn6 walcowanej klasycznie w 8 przepustach: a) mapa rozkładu orientacji, b) mapa rozkładu ziaren, c) mapa rozkładu granic ziaren – kolor niebieski – kąt >15º, kolor czerwony – kąt > 2º

4. Conclusions

Based on the experimental results were the following conclusions:

1. Texture analysis showd, that CuSn6 alloy deformation in RCS process increase the share of Brass component, and reduces the share of Goss component compared to classic rolled.
2. EBSD analysis showd, that RCS proces has impact to microstructure modification through visible grain elongation in the direction of the deformation proces, that resulting twins are formed and affect to low-angle edge boundaries compared to classic rolled material.

3. Crystallite size measurement by sherrer method confirm the presence of nano-scale structures in the studied materials after deformation by RCS process.
4. Stress measurment was occured compressive stress after classic rolled process, while in stips after deformation in the RCS process were a compressive stress in the direction of the rolling direction and the tensile stress in the cross direction to the rolling direction.

References

[1] Kwaśny W., *Predicting properties of PVD and CVD coatings based on fractal quantities describing their surface*, Journal of Achievements in Materials and Manufacturing Engineering, Vol. 37, Issues 2, 2009, 125-192.
[2] Lisiecki A., *Laser welding of titanium alloy Ti6Al4V using a disk laser*, MTM virtual journal, Issue 7/2012, 53-56.
[3] Pawlik K., *Determination of the Orientation Distribution Function from Pole Figures In Arbitrarily Defined Cells*, Physica Status Solidi (b) 134 (1986), 477-483.
[4] Głuchowski W., Stobrawa J., Rdzawski Z., *Microstructure refinement of selected copper alloys processed by SPD method*, Archives of Materials Science Engineering, vol. 47, issue 2, February 2011, 103-109.
[5] Głuchowski W., Stobrawa J., Rdzawski Z., Malec W., *Microstructure and properties of CuNi2Si1 alloy processed by continuous RCS method*, Archives of Materials Science Engineering, vol. 37, issue 2, February 2009.

TECHNICAL TRANSACTIONS | CZASOPISMO TECHNICZNE
MECHANICS | MECHANIKA
1-M/2013

DOMINIK KWIATKOWSKI*, EDWARD LISOWSKI*

MINIMIZING OF AIR CONSUMPTION FOR THE AIR CUSHION WITH MULTIPLE OUTLET NOZZLES

MINIMALIZACJA ZUŻYCIA POWIETRZA DLA PODUSZKI PNEUMATYCZNEJ Z WIELOMA DYSZAMI WYLOTOWYMI

A b s t r a c t

The paper presents the results of research on minimizing the air consumption of the air cushions used to move the transport platform. This kind of transport becomes more popular in industry. It is applied especially to move heavy machinery and equipment in factories with hardened floors. The working medium is air. This system has many advantages but it is characterized by high air consumption. The paper takes the issues of searching solutions to minimizing the air consumption. To perform the computational analysis a mathematical model was defined. Simulations were performed by using Maple software.

Keywords: *air cushion*, *air consumption*, *minimizing*, *Maple*

S t r e s z c z e n i e

W artykule przedstawiono analizę, której celem jest minimalizacja zużycia powietrza przez poduszki pneumatyczne stosowane w platformach transportowych. W tym transporcie wykorzystuje się jako czynnik roboczy powietrze, które przepływa przez poduszki powodując unoszenie ładunku. System ten ma wiele cech korzystnych, charakteryzuje go jednak znaczne zużycie powietrza. W referacie podjęto zadanie polegające na poszukiwaniu rozwiązań umożliwiających minimalizację zużycia powietrza. Do tego celu zbudowano model matematyczny oraz przeprowadzono obliczenia symulacyjne za pomocą programu Maple.

Słowa kluczowe: *poduszka pneumatyczna*, *zużycie powietrza*, *minimalizacja*, *Maple*

* MSc. Dominik Kwiatkowski, Prof. PhD. Eng. Edward Lisowski, Institute of Applied Informatics, Faculty of Mechanical Engineering, Cracow University of Technology.

Denotations

A – length of the carrying plate [m]
B – height of the carrying plate [m]
F_o – force from a load [kg]
R_1, R_2 – external and internal radius of the surface cooperating with the floor [m]
p_o – ambient pressure [MPa]
T – ambient temperature [K]
p_1 – inlet pressure [MPa]
p_{zas} – supply pressure [MPa]
p_2, p_3 – pressure in air chambers [MPa]
V_2,V_3 – volume in air chambers [m^3]
h_f – height of the air slit [m]
h_p – height of lifting [m]
A_i – cross sectional area of the nozzle [m]
v_i – average air flow velocity [m/s]
μ_i – discharge coefficient [–]
d_i – diameter of the nozzle [m]
ρ_i – air density for given cross sections [kg/ m^3]
ρ_p – ambient air density [kg/ m^3]
φ – velocity coefficient [–]
κ – adiabatic index [–]
η – dynamic viscosity [Pa·s]
R – universal gas constant [J/kgK]
Q_i – volumetric flow rate [m^3/s]
i – parameter depends on the number of nozzles [–]
a – number of nozzles [–]
x_i – decision variable [–]
$\hat{a}_i$ – optimal point [–]
Φ – set of acceptable solutions [–]

1. Introduction

In the industrial plants, there is a need to transport heavy loads and also locate different types of machines. For this purpose are used expensive lifting devices such as cranes, winches, forklifts, etc. Current production halls being built using new technologies ensure the high quality surfaces, which are horizontal and smooth. These are excellent conditions for the transportation systems using the air cushions. The air cushion is a structurally simple mechanism that is characterized by a small height, so it is easily to slip it under the devices [1, 2]. The air flow under the air cushion causes the formation of air film, which reduces friction for the floor surface to a value close to zero, so people can move the load, which weight is more than few tons using strength of muscles (Fig. 1) [11].

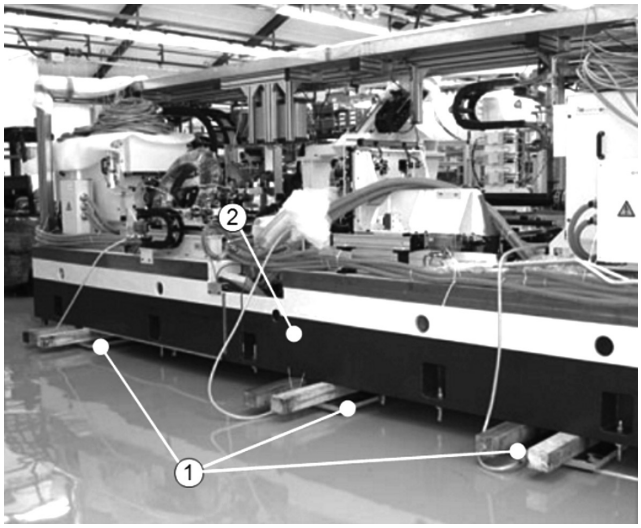

Fig. 1. An Installation weighing 30 tons moved easily on air cushions: 1 – air cushion, 2 – cargo
Rys. 1. Instalacja o masie 30 ton przesuwana na poduszkach pneumatycznych: 1 – poduszka pneumatyczna, 2 – ładunek

2. Determination of the volume flow rate

To determine the volumetric flow rate in the air cushion a mathematical model was created. The mathematical model was constructed using a simplified model of the air cushion as shown in Fig. 2. The air cushion is built with an internal 4 and an external 7 flexible torus. Torus is fixed to the carrying plate 1 where a supply collector 6 is made. The throttle nozzle 2 is installed to the plate 1. The air flows through the collector 6 to a volume V_2 in the torus further by the throttle nozzle 2 to a volume V_3 and next by the slit created between rigid surface 9 and the cushion torus 7. The air cushion is described by the physical and geometrical parameters as shown in the schema of air cushion (Fig. 2).

In the air cushion beyond the main outlet nozzle 2 and the lower chamber exist additional nozzles 3. These are arranged on the lower surface of the cushion 7 uniformly on a circle of a certain radius R_d.

With the assumption of the flow continuity and steady state, the volume flow rate in individual points of the air cushion can be expressed by formulas (1)–(5). The flow rate through the supply collector nozzle has been described by equation:

$$Q_1 = \mu_1 \cdot A_1 \cdot v_1 = \frac{\mu_1 \cdot \pi \cdot d_1^2}{4} \cdot \sqrt{\frac{2}{\rho_p} \cdot (p_{zas} - p_1)} \tag{1}$$

where:

μ_1 – discharge coefficient,
A_1 – cross sectional area of the nozzle,

v_1 – average air flow velocity,
d_2 – diameter of the nozzle,
ρ_p – ambient air density,
p_1 – inlet pressure,
p_3 – pressure in air chamber.

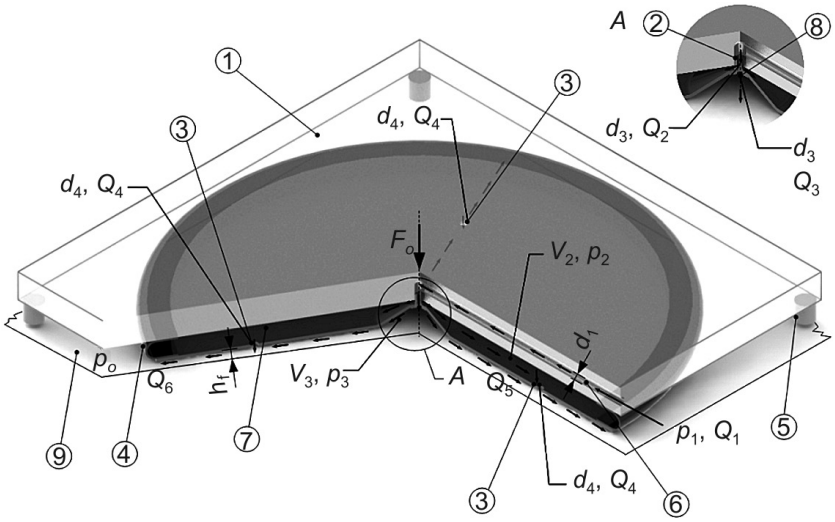

Fig. 2. Model of the air cushion with multi-nozzle air outflow: 1 – carrying plate, 2, 3 – nozzles, 4 –side surface of the air chamber, 5 – bracket, 6 – supply collector, 7 – cushion bearing surface, 8 – fixing plate, 9 – rigid surface

Rys. 2. Model poduszki pneumatycznej z wieloma dyszami: 1 – płyta nośna, 2, 3 – dysze, 4 – powierzchnia boczna komory powietrznej, 5 – podpora, 6 – kanał zasilający, 7 – powierzchnia nośna poduszki, 8 – płytka mocująca, 9 – podłoże

The volumetric flow rate through the nozzles respectively to the side chamber and the lower chamber were expressed by the following equations:

$$Q_2 = \mu_2 \cdot A_2 \cdot v_2 = \frac{\varphi \cdot \mu_2 \cdot \pi \cdot d_2^2}{4} \cdot \sqrt{v_1^2 + \frac{2 \cdot \kappa}{\kappa - 1} \cdot \left(\frac{p_1}{\rho_1} - \frac{p_2}{\rho_2} \right)} \tag{2}$$

$$Q_3 = \mu_3 \cdot A_3 \cdot v_3 = \frac{\varphi \cdot \mu_3 \cdot \pi \cdot d_3^2}{4} \cdot \sqrt{v_1^2 + \frac{2 \cdot \kappa}{\kappa - 1} \cdot \left(\frac{p_1}{\rho_1} - \frac{p_3}{\rho_3} \right)} = Q_5 \tag{3}$$

The volumetric flow rate each of the nozzles placed in the surface cooperating with the floor of the side chamber with assumption of the load uniformity and the symmetry of system:

$$Q_4 = \mu_4 \cdot A_4 \cdot v_4 = \frac{\mu_4 \cdot \pi \cdot d_4^2}{4} \cdot \sqrt{\frac{2}{\rho_2} \cdot (p_2 - p_3)} \tag{4}$$

The total volumetric flow rate through the slit between the cushion and the rigid surface:

$$Q_6 = Q_5 + a \cdot Q_4 = \frac{\pi \cdot p_3}{6 \cdot \eta \cdot \ln\left(\frac{R_1}{R_2}\right)} \cdot h_f^3 \tag{5}$$

where:

a – number of nozzles,
h_f – height of the air slit,
p_3 – pressure in air chamber,
η – dynamic viscosity,
R_1, R_2 – external and internal radius of the surface cooperating with the floor.

3. Minimizing of the air consumption

To determine the minimum value of volumetric flow rate correlation (6) [7] was defined:

$$\hat{a} \in \Phi = \underset{s \in \Phi}{\wedge} Q(x) \geq Q(\hat{a}) \tag{6}$$

where:

x_i – decision variable,
$\hat{a}_i$ – optimal point,
Q – volumetric flow rate,
Φ – set of acceptable solutions.

The decision variables are assigned to the geometrical and physical parameters of the air cushion with restrictions:

- $x_1 = R_1$ for $x_{1A} \leq R_1 \leq x_{1B}$ [m] where R_1 is the external radius of the torus cooperating with the floor.
- $x_2 = R_2$ for $x_{2A} \leq R_2 \leq x_{2B}$ [m] where R_2 is the internal radius of the torus cooperating with the floor.
- $x_3 = p_1$ for $x_{3A} \leq p_1 \leq x_{3B}$ [Pa] where p_1 is the inlet pressure.
- $x_4 = a$ for $x_{4A} \leq a \leq x_{4B}$ [–] where a is the number of nozzles.
- $x_5 = d_4$ for $x_{5A} \leq d_4 \leq x_{5B}$ [m] where d_4 is the diameter of the nozzle.
- $x_6 = h_f$ for $x_{6A} \leq h_f \leq x_{6B}$ [m] where h_f is slit height.

The minimization was performed by using Maple software. For minimizing problem Maple used linear programming and modified Newton method. Adopting minimum of objective function $Q_6(x_1 \ldots x_6)$ gives problem solution. Data adopted for the analysis:

$$T = 298.15\,[\mathrm{K}];\ \eta = 1.79 \cdot 10^{-5}\,[\mathrm{Pa \cdot s}];\ R = 287.05\left[\frac{\mathrm{J}}{\mathrm{kg \cdot K}}\right];\ \mu_4 = 0.05\,[-];\ \mu_5 = 0.4\,[-];$$

$$p_2 = 0.71 \cdot 10^5\,[\mathrm{Pa}];\ p_3 = 0.69 \cdot 10^5\,[\mathrm{Pa}];\ x_{1A} = 0.22\,[\mathrm{m}];\ x_{1B} = 0.3\,[\mathrm{m}];\ x_{2A} = 0.1\,[\mathrm{m}];$$

$$x_{2B} = 0.2\,[\mathrm{m}];\ x_{3A} = 1 \cdot 10^5\,[\mathrm{Pa}];\ x_{3B} = 3 \cdot 10^5\,[\mathrm{Pa}];\ x_{4A} = 0\,[-];\ x_{4B} = 20\,[-];$$

$$x_{5A} = 0.005\,[\text{m}];\ x_{5B} = 0.01\,[\text{m}];\ x_{6A} = 0.5 \cdot 10^{-4}\,[\text{m}];\ x_{6B} = 1 \cdot 10^{-4}\,[\text{m}]$$

For minimization task by using Maple software NLPSolve function was applied. Definition of that function is shown in Fig. 3.

Optimization[*NLPSolve*](Q_6,
$R_1 = 0.22 \,..0.3$,
$R_2 = 0.1 \,..0.2$,
$p_1 = 1 \cdot 10^5 \,..3 \cdot 10^5$,
$a = 0 \,..20$,
$d_4 = 0.005 \,..0.01$,
$h_f = 0.50 \cdot 10^{-4} \,..1 \cdot 10^{-4}$,
initialpoint = [$R_1 = 0.27$, $R_2 = 0.15$, $p_1 = 200000$, $d_4 = 0.08$, $h_f = 0.75 \cdot 10^{-4}$, $a = 10$],
assume = *nonnegative*, *method* = *modifiednewton*).

Fig. 3. The definition of NLPSolve function in the optimization task by using the Maple software
Rys. 3. Definicja zadania optymalizacji za pomocą funkcji NLPSolve w programie Maple

4. Conclusions

Analysis of the air cushion parameters affecting to the air consumption was performed. It was found that parameters have a significant impact on air consumption. As a result of

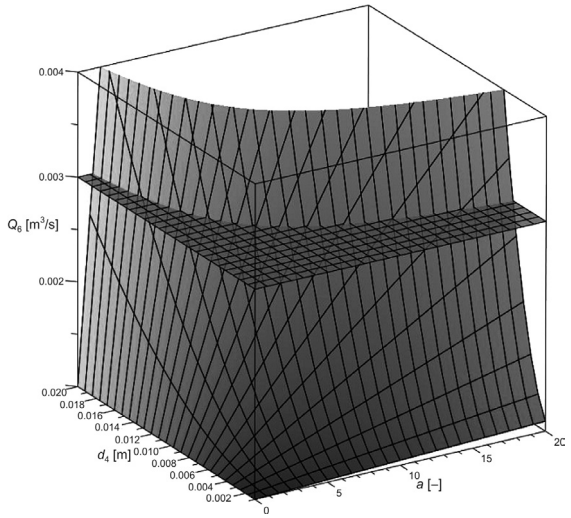

Fig. 4. The volumetric flow rate at the outlet Q_6 [m^3/s] dependence of nozzle's number a [–] and nozzle's diameter d_4 [m]
Rys. 4. Zależność objętościowego natężenia przepływu na wylocie Q_6 [m^3/s] od ilości dysz a [–] oraz średnicy dyszy d_4 [m]

minimization Q_6 = 0.0004 [m^3/s] was obtained for the following values of the decision variables: R_1 = 0.3 [m]; R_2 = 0.1 [m]; h_f = 0.5·10^{-4} [m]; d_4 = 0.01 [m]; p_1 = 1·10^5 [Pa]; a = 0 [–]. The results of the decision variables are on the limits of sets. The minimization including six decision variables showed that in addition to the significant impact of R_1 and R_2 to the needs of air consumption important are the inlet pressure p_1, height of the air slit h_f, diameter of outlet nozzle d_4 and number of nozzles a. After the adoption of x_1, x_2, x_3, x_6 as constant values the influence of diameter of outlet nozzle d_4 and number of nozzles a for air consumption can be determined. Adopted data: R_1 = 0.24 [m]; R_2 = 0.16 [m]; h_f = 0.5·10^{-4} [m]; p_1 = 26·10^5 [Pa]. In Fig. 4 the volumetric flow rate at the outlet Q_6 in dependence of diameter of outlet nozzle d_4 and number of nozzles a is shown. The vertical surface shows the case when mass of load is equal to m = 252 [kg] with a supply pressure p_1 = 0.26 [MPa]. The best solution is for the minimum of d_4 and a, where Q_6 = 0.001[m^3/s].

References

[1] Lisowski E., Filo G., *Pressure control in air cushions of the mobile platform*, Journal of KONES Powertrain and Transport, Vol. 18, No. 2, Warszawa 2011, 261.

[2] Lisowski E., Kwiatkowski D., *Określenie podstawowych parametrów systemu pneumatycznego platformy transportowej na poduszkach pneumatycznych*, Przegląd Mechaniczny, no 2/12, Warszawa 2012, 45-48.

[3] Hebda M., Wachał A., *Trybologia*, Wydawnictwa Naukowo-Techniczne, Warszawa 1980.

[4] Wołkow J.,Dindorf R., *Teoria i Obliczenia układów pneumatycznych*, Wydawnictwo PK, Kraków 1995.

[5] Praca zbiorowa pod red. Tyrlika T., *Laboratorium napędów i sterowania, hydraulicznego i pneumatycznego*, Wydawnictwo PŚk, 1998.

[6] Yun L., Bliault A., *Theory and design of air cushion craft*, Butterworth-Heinemann, Oxford 2000.

[7] Osiński Z., Wróbel J., *Teoria konstrukcji*, Wydawnictwo Naukowe PWN, Warszawa 1995.

[8] Krowiak A., *Maple. Podręcznik*, Helion, Gliwice 2012.

[9] Messina A., Giannoccaro N., Gentile A., *Experimenting and modeling the dynamics of pneumatic actuators controlled by the pulse width modulation (PWM) technique*, Mechatronics, vol. 15, issue 7, Elsevier 2005, 859-881.

[10] Moon J.-H., Lee B.-G., *Modeling and sensitivity analysis of a pneumatic vibration isolation system with two air chambers*, Mechanism and Machine Theory, vol. 45, issue 12, Elsevier 2010, 1828-1850.

[11] Luftkissentechnik GbR (http://www.luftkissen-transportsysteme.biz).

TECHNICAL TRANSACTIONS | **CZASOPISMO TECHNICZNE**
MECHANICS | MECHANIKA
1-M/2013

PAWEŁ LEMPA*, EDWARD LISOWSKI*

GENETIC ALGORITHM IN OPTIMIZATION OF CYCLOID PUMP

ALGORYTM GENETYCZNY W OPTYMALIZACJI POMPY CYKLOIDALNEJ

A b s t r a c t

The paper presents a method of optimizing the geometry of a cycloid positive displacement pump using genetic algorithm. This allowed for increasing its delivery and efficiency and reduce pulsation.

Keywords: *optimization positive displacement pump genetic algorithms*

S t r e s z c z e n i e

W artykule przedstawiono metodę optymalizacji geometrii pompy wyporowej cykloidalnej z wykorzystaniem algorytmu genetycznego. Pozwoliło to na zwiększenie jej wydajności i sprawności oraz obniżenie pulsacji.

Słowa kluczowe: *optymalizacja pompa wyporowa algorytm genetyczny*

* MSc. Eng. Paweł Lempa, Prof. Eng. Edward Lisowski, Institute of Applied Informatics, Faculty of Mechanical Engineering, Cracow University of Technology.

1. Introduction

The paper presents the task of optimizing the displacement gear pump with three teeth. Due to the small number of teeth is obtained discharge and suction chamber with large volume. This allows on the one hand, to obtain a high delivery in a unitary pump with small dimensions, on the other hand a low sensitivity of the pump parameters for the pumped medium and the contamination contained in pump. Selection of geometric parameters is essential for pump parameters. To help select solution optimization task can be formulated. The paper presents own software that using a genetic algorithm [1,2,6,7] which by API interface is connected to the CAD system [8,9], and can automatically generate 3D models and perform multi-criteria optimization for gear pump [5].

2. Cycloid gear wheel with three teeth

Gear wheels of cycloidal profile are designed using whole cycloid curves arcs and have the form as on figure 1.

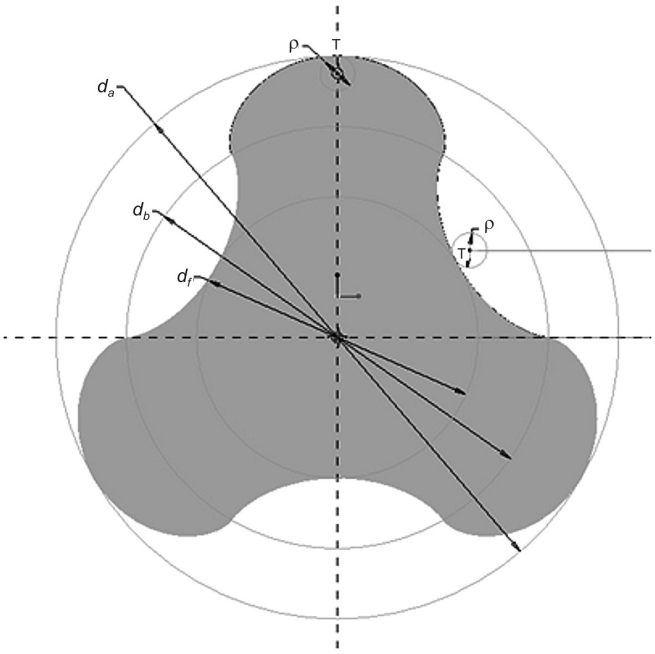

Fig. 1. Gear wheel with cycloidal profile

Rys. 1. Koło zębate o profilu cykloidalnym

The tooth profile is created by rolling in a circle with a diameter d_b of a circle of radius ρ_h, on the inner side, resulting in that a point M which lies on that circle creates an arc

of ordinary hypocycloid. From the outside circle of radius ρ_e rolls creating an arc of ordinary Hypocycloid. However, at the point *P*, which is located on the diameter d_b of the two arcs [3, 10]. Ratio of base circle d_b and radius ρ rolling circle must be:

$$\frac{d_b}{\rho} = 4z \tag{1}$$

Length of the pitch circle is:

$$m = 4\rho \tag{2}$$

Pitch circle divides tooth on the head with a height h_a and foot with a height h_f, according to the relationship:

$$h_a = h_f = 2\rho \tag{3}$$

Formulas for determining the diameter of addendum circle d_a and the diameter of root circle d_f have form:

$$d_a = d + 2h_a = 4\rho z + 4\rho = 4\rho\ (z + 1) \tag{4}$$

$$d_f = d - 2h_f = 4\rho z - 4\rho = 4\rho\ (z - 1) \tag{5}$$

3. Optimization of pump parameters

Optimization of pumps can be carried out taking into account the different objective functions. In the case of positive displacement pumps it may be getting the biggest pump delivery or the total efficiency, minimalize pulsation or cost of manufacture product, getting higher operating pressure, etc. The most common approach known in the literature rely on formulating one objective with a fixed range of decision variables [4, 11], which facilitates the solution of the problem. However, it appears that higher effects are obtainable using a multiobjective optimization [7, 11]. As the objectives of optimizing for the analyzed pump in this article were selected: maximum unitary delivery, maximum pump delivery, minimum of pulsation and the total efficiency. Mathematical relations for these functions can be determined from the following relations [3]:

Geometric dependencies of the positive displacement pump

Geometrical relations are as the following formulas:

– Unitary delivery:

$$Q_u = \frac{bm^2}{8}[2(z_1 + 1)^2 - 2z^2 - 2] \tag{6}$$

where:

Q_u – unitary delivery,
b – gearwheel width,
m – module,
z – number of teeth.

– Theoretical delivery[3]:

$$Q_t = \frac{\pi b m^2}{4}[2(z+1)^2 - 2z^2 - 1] \tag{7}$$

where:

Q_t – theoretical delivery.

– Pulsation:

$$\delta = \frac{2\frac{z^2}{R^2}\sin 2\frac{\pi R}{2z}}{2\left(\frac{z}{2}+1\right)^2 - \frac{z^2}{2} - \frac{z^2}{R^2}\left(1+\frac{z}{\pi R}\sin\frac{\pi R}{z}\right)} \tag{8}$$

where:

δ – pulsation,

R – tooth shape factor

The efficiency of the pump

Parameters related to the operation of the pump are: working pressure, fluid parameters and above all, the total pump efficiency, which is defined as the product of the volumetric, mechanical and hydraulic efficiency [3, 4]. Total efficiency η_c is defined as the quotient of output power P_{out} to the power input P_{in} or can be calculated as the product of the volumetric efficiency η_v and hydraulic-mechanical efficiency η_{hm}.

$$\eta_c = \frac{P_{out}}{P_{in}} = \eta_v \eta_{hm} \tag{9}$$

Volumetric efficiency is defined as the quotient of real delivery Q_r to a theoretical:

$$\eta_v = \frac{Q_r}{Q_t} = \frac{Q_t - \Delta Q}{Q_t} = 1 - \frac{\Delta Q}{Q_t} \tag{10}$$

where:

ΔQ – volumetric losses.

$$\Delta Q = Q_\mu + Q_\varsigma \tag{11}$$

where:

Q_u – losses associated with viscosity of the liquid,

Q_ς – losses associated with the density of the liquid.

$$Q_u = c_\mu \frac{p}{2\pi\mu_d} q \tag{12}$$

where:

μ_d – dynamic viscosity of liquid,

c_μ – loss coefficient associated with the viscosity, depending on the unitary delivery.

$$Q_\varsigma = c_r \sqrt{\frac{2p}{\varsigma}} \sqrt[3]{q^2} \tag{13}$$

where:

ς – density of the liquid,

c_r – loss coefficient associated with the density, depending on the type and size of the slots, and the unitary delivery.

Substituting relations (11), (12), (13) for (10) receives a formula which defines the volumetric efficiency:

$$\eta_v = 1 - c_\mu \frac{p}{2\pi\mu_d n} - c_r \frac{1}{n}\sqrt{\frac{2p}{\varsigma}}\sqrt[3]{q-1} \tag{14}$$

Hydraulic-mechanical efficiency is defined as the quotient of the theoretical moment M_t on the pump shaft to the actual moment M_r:

$$\eta_{hm} = \frac{M_t}{M_r} = \frac{M_t}{M_t + \Delta M} \tag{15}$$

where:

ΔM – a moment of loss.

$$M = M_v + M_\varsigma + M_\mathrm{p} \tag{16}$$

where:

M_v – moment of losses associated with the resistances caused by the friction of viscous liquids,

M_ς – moment of losses associated with the density of the working medium,

M_p – moment of losses associated with the mechanical losses dependent on the working pressure of the pump.

These moments can be calculated from the following formulas [3]:

$$M_v = c_v \mu_d n q \tag{17}$$

$$M_\varsigma = c_\varsigma \frac{n^2}{4\pi}\sqrt[3]{q^5} \tag{18}$$

$$M_p = c_p \frac{pq}{2\pi} \tag{19}$$

where:

c_v – proportionality coefficient,

c_ς – ensity coefficient,

c_p – pressure coefficient.

Substituting dependeces (17), (18), (19) and (16) for (15)receives a formula defining the hydraulic-mechanical efficiency:

$$\eta_{hm} = \frac{1}{1 + c_v 2\pi \frac{\mu_d n}{p} + c_p \frac{\varsigma n^2}{2\pi}\sqrt[3]{q^2 + c_p}} \tag{20}$$

Substituting the formula for volumetric efficiency (14) and model of the hydraulic--mechanical efficiency (20) we get the following formula on the total efficiency:

$$\eta_c = \frac{1 - c_\mu \frac{p}{2\pi\mu_d n} - c_r \frac{1}{n}\sqrt{\frac{2p}{\varsigma}}\sqrt[3]{q-1}}{1 + c_v 2\pi \frac{\mu_d n}{p} + c_\varsigma \frac{\varsigma n^2}{2p}\sqrt[3]{q^2} + c_p} \tag{21}$$

The objective function

On basis of formulas (6), (7), (8), (21) constituting mathematical model of the pump was built four objective functions . The following notation were prepared: f_1 – function of the unitary delivery (22), f_2 – function of the theoretical delivery (23), f_3 – function of the pulsation, for it is used inverse function (24) (for compatibility with other functions, i.e. maximum f_3 means the minimum pulsation), f_4 – function of the total efficiency (25).

$$f_1 = f_1\,(q\,(b, r_w, r_t)) \tag{22}$$

$$f_2 = f_2\,(Q_t(x, y, z, b)) \tag{23}$$

$$f_3 = f_3\,(\delta(z, y, z, b)) \tag{24}$$

$$f_4 = f_4\,(\eta_c\,(Q_{ew}, p, \mu_d, \varsigma)) \tag{25}$$

For the defined objective function multi-criteria optimization problem can be written as [11]:

$$f = \max\,(w_1 \cdot f_1 + w_2 \cdot f_2 + w_3\,(-1)\,f_3 + w_4 f_4) \tag{26}$$

4. The simulation studies

Calculations were carried out for various variants of the pump design.

To carry out the calculations a hydraulic oil with the following specifications was selected: dynamic viscosity of liquid u_k=41 mm^2/s, liquid density ς = 840 kg/m^3, and the number of teeth equal to 3.

Decision variables x_i:

– height tooth coefficient y $\quad x_{1\min} < x_1 < x_{1\max}$
– gearwheel width b $\quad x_{2\min} < x_2 < x_{2\max}$
– the pumping pressure p $\quad x_{3\min} < x_3 < x_{3\max}$

The range of values of the decision variables are shown in Table 1.

Table 1

The Range of the decision variables

x_i	x_i min	x_i max	units
×1	0.6	1.2	–
×2	30	50	mm
×3	1.2	2.5	MPa

For optimization using a genetic algorithm the following parameters were selected:
- The type of representation: floating point
- Crossover: 2-point, with a probability: 0.9
- The probability of mutation: 0.1
- The size of population: 20
- The number of algorithm iterations: 2000

The greatest effect of the conducted optimization was reduction of the pump pulsation by 47.2%, total efficiency improved by 9.2%, unitary delivery improved by 2.9% and theoretical delivery improved by 2.8%. This effect is presented in Figure 2.

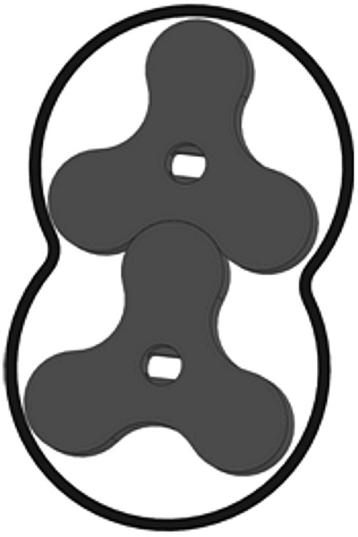

Fig. 2. Gear wheels after optimization
Rys. 2. Koła zębate po optymalizacji

5. Conclusions

This paper presents the problem of multi-criteria optimization displacement pump design using a genetic algorithm. To optimize pump was used known in the literature mathematical models describing the basic properties of the pump, such as unitary delivery, pump delivery, pulsation and the total efficiency. As the object of the investigations the standard model of the positive displacement pump used in industry was selected. On pump was conducted simulation studies looking for better solutions to reduce pulsation and increase unitary delivery, pump delivery and total efficiency. A software Creo (Pro/Engineer) was used for the purpose of construction of the gear geometry. Own software with the use genetic algorithm was developed for the optimization. The developed software proved to be an effective tool in the search for better solutions, which improved pump parameters in particular significantly reduce the pulsation.

References

[1] Fleming P.J., Zalzala A.M.S., *Genetic algorithms in engineering systems*, The Institution of Electrical Engineers, London 1997.

[2] Goldberg D., *Algorytmy genetyczne i ich zastosowanie*, Wydawnictwa Naukowo-Techniczne, Warszawa 2003.

[3] Kollek W., *Pompy zębate – konstrukcja i eksploatacja*, Zakład Narodowy im. Ossolińskich, Wrocław 1996.

[4] Kollek W., Palczak E., *Optymalizacja elementów układów hydraulicznych*, Zakład Narodowy im. Ossolińskich, Wrocław 1994.

[5] Lisowski E., *Automatyzacja i integracja zadań projektowania. Z przykładami dla systemu Pro/Engineer Wildfire*, Kraków 2007.

[6] Michalewicz Z., *Algorytmy genetyczne + struktury danych = programy ewolucyjne*, Wydawnictwa Naukowo-Techniczne, Warszawa 2003.

[7] Pieczara J., *Algorytmy genetyczne w mechanice konstrukcji*, Uczelniane Wydawnictwo Naukowo-Dydaktyczne AGH, Kraków 2004.

[8] Parametric Technology Corporation, *Getting Started with Creo® Parametric TOOLKI 2.0*, 2012.

[9] Parametric Technology Corporation, *Creo® Parametric TOOLKIT 2.0 Release Notes*, 2012.

[10] Stryczek J., *Koła zębate maszyn hydraulicznych*, Oficyna Wydawnicza Politechniki Wrocławskiej, Wrocław 2007.

[11] Tarnowski W., *Podstawy projektowania technicznego*, Wydawnictwa Naukowo-Techniczne, Warszawa 1997.

TECHNICAL TRANSACTIONS | **CZASOPISMO TECHNICZNE**
MECHANICS | MECHANIKA
1-M/2013

FILIP LISOWSKI*

APPLICATION OF FINITE ELEMENT METHOD IN THE OPTIMAL DESIGN OF THE NUT WITH A GROOVE IN THE END-FACE

ZASTOSOWANIE METODY ELEMENTÓW SKOŃCZONYCH W OPTYMALNYM PROJEKTOWNIU NAKRĘTKI Z ROWKIEM W POWIERZCHNI CZOŁOWEJ

A b s t r a c t

The paper presents an application of finite element method in the optimal design of the nut with a groove in the end-face. There were described issues of the load distribution and FEM modeling of threaded connections. The optimization problem was formulated with the aim of obtaining the uniform load distribution on the bolt's thread depending on the geometry of nut.

Keywords: *nut with a groove in the end-face*, *parametric optimization*, *finite element method*

S t r e s z c z e n i e

W artykule przedstawiono zastosowanie metody elementów skończonych w optymalnym projektowaniu nakrętki z rowkiem w powierzchni czołowej. Opisano zagadnienia rozkładu obciążenia na gwincie w połączeniu śrubowym oraz modelowania MES połączeń gwintowych. Sformułowano zadanie optymalizacyjne, którego celem jest uzyskanie równomiernego rozkładu obciążenia na gwincie śruby w zależności od geometrii nakrętki.

Słowa kluczowe: *nakrętka z rowkiem z powierzchni czołowej*, *optymalizacja parametryczna*, *metoda elementów skończonych*

* MSc. Filip Lisowski, Institute of Machine Design, Faculty of Mechanical Engineering, Cracow University of Technology.

Denotations

$q(z)$ – expenditure of axial load in bolted joint [N]
F – axial load in bolted joint [N]
m – height of the thread [mm]
z – coordinate of the thread height [mm]
k – factor given by equation (2)
e – factor given by equation (3)
C – dimensionless coefficient dependent on the size of thread
σ_{HMH} – Huber-Mises-Hencky reduced stress [MPa]
σ_{HMH}^{d2} – Huber-Mises-Hencky reduced stress on $d2$ diameter [MPa]
$\Delta\sigma_{HMH}^{d2}$ – average standard deviation of σ_{HMH}^{d2}
σ_{HMH}^{d2ave} – average Huber-Mises-Hencky reduced stress on $d2$ diameter for n cooperating coils of thread
C_{press} – contact pressure on thread [MPa]
C_{press}^{all} – allowable contact pressure for chosen material [MPa]
A_B, A_N – cross-sectional areas of bolt and nut [mm^2]
E_B, E_N – modulus of elasticity (Young modulus) of bolt and nut [MPa]
d – outside diameter of bolt [mm]
$d2$ – average diameter of thread [mm]
Q – objective function
pp_i – design variables [mm]
n – number of cooperating coils of thread
Re – yield stress
Rm – tensile strength

1. Introduction

Inspiration for this study was the report on durability analysis and variant optimization of the bolted joint Tr85×4 in the injection molder UT 440T. Researches were developed at Cracow University of Technology under the guidance of professor A.P. Zieliński. In the analyzed bolted joint the nut with supporting ring was applied. The aim of researches was to eliminate the cracking of a bolt at the first carrying coils of thread. The goal was achieved within the proper design of the nut and the supporting ring, which provided more uniform load distribution along bolt's thread.

Researches described in this paper consider the designing of the nut with a groove in the end-face subjected to the similar load conditions. The main advantages of such a nut are the uniform load distribution in axial direction and the reduction of the load on the most loaded coils of thread. The goal of the paper was to optimize the geometry of such a nut in order to obtain the uniform load distribution on the thread and therefore increase the fatigue strength of the bolt.

In the recent years some issues related to the fatigue failure, load distribution and bearing capacity of bolted joints were developed by: [1–4]. Some basic information about the nut with a groove in the end-face is also described in [5] and [6].

2. Load distribution on the thread

The nature of thread's load is complex. Axial force that tightens the screw causes bending and shear stresses in the bolt. Furthermore, contact pressure affects the thread's surface. This pressure can reach significant values even while the axial force is relatively small. Strength of the bolted joint depends on these loads. Stress concentration in the roots of thread can result in shearing the bolt. On the other hand, high contact pressure can hasten the wear of the thread surface. The analytical computational model of bolted connection based on the thin plate theory is presented in [7]. According to that model, for a typical bolted joint where the bolt is stretched and the nut is compressed, the load distribution along thread is described by equation (1).

$$q(z) = \frac{kF}{\sinh km} \cosh k(m - z) \tag{1}$$

$$k^2 = \frac{e}{C} \tag{2}$$

$$e = \frac{1}{E_B A_B} + \frac{1}{E_N A_N} \tag{3}$$

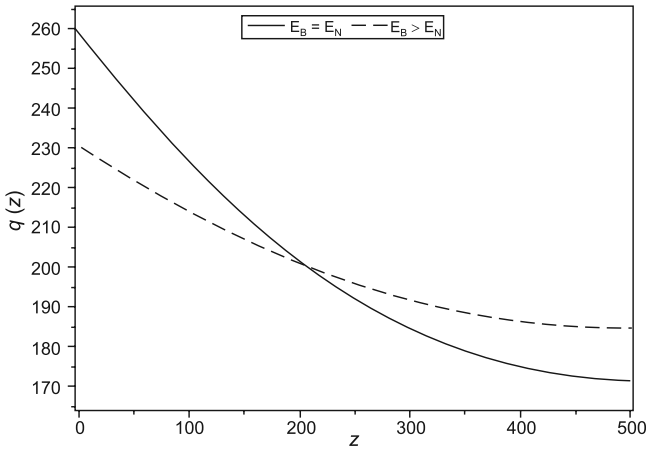

Fig. 1. Load distribution along the thread for $F = 100$ [kN], $C = 0{,}1$: a) $E_B = E_N = 2{,}11 \cdot 10^5$ [MPa], b) $E_B = 2{,}11 \cdot 10^5$ [MPa], $E_N = 0{,}7 \cdot 10^5$ [MPa]

Rys. 1. Rozkład obciążenia na gwincie $F = 100$[kN], $C = 0{,}1$: a) $E_B = E_N = 2{,}11 \cdot 10^5$ [MPa], b) $E_B = 2{,}11 \cdot 10^5$ [MPa], $E_N = 0{,}7 \cdot 10^5$ [MPa]

3. Finite element model of bolted joint

In the numerical analysis of bolted connections the 3D model is usually simplified as 2D axisymmetric model. However, two contact forces, which are orthogonal to the axial direction, cannot be calculated from axysymetric analysis, because they balance each other. To determine their values 3D analysis is required. Previous researches show that those two forces are only a small fraction of the total applied load and can be omitted for the load distribution analysis.

The helical effect on the load distribution was studied by [10] and also by [11]. It was concluded that the helix angle can be neglected therefore the axysymmetric model can give a good estimation of the load distribution. At the same it was shown that 2D model gives slightly higher values of loads than 3D model.

4. Optimization of the nut with a groove in the end-face

To perform the optimization problem 2D axisymmetric finite element model of the bolted joint Tr85×4 was built (Fig. 2). Plane82 elements available in ANSYS software were used. Between threads of the bolt and the nut contact elements Conta172 and Target169 were defined. The coefficient of friction in the plane of model was set to $\mu = 0.1$. The radius of the root of thread was modeled by proper size of finite element as described by [12] which resulted in a reduction of the optimization time. To the surface of the bolt's core the load F=110[kN] was applied. Both for the bolt and the nut steel 42CrMo4 (EN 10083-1) with tensile strength $Rm = 1030$ [MPa], yield stress $Re = 880$ [MPa] and allowable contact pressure $C_{press}^{all} = 344\,[\mathrm{MPa}]$ was chosen. Young modulus of the bolt and the nut $E_B = E_N = 2{,}11 \cdot 10^5$ [MPa] and Poisson ratio $\nu = 0.3$ were accepted. The geometry of a groove in the nut's end-face was parameterized as shown in Fig.3. Parametric optimization was performed by applying of ANSYS software as described by [13].

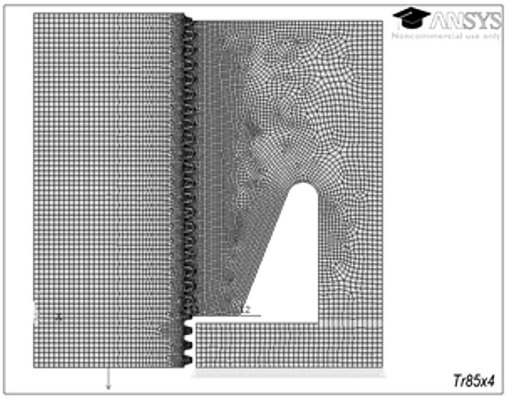

Fig. 2. Axisymmetric finite element model of bolted joint Tr85×4 with boundary conditions

Rys. 2. Osiowosymetryczny model MES połączenia śrubowego Tr85×4 z warunkami brzegowymi

4.1. Objective function

As an objective function average deviation of reduced stress on average diameter of bolted connection was accepted (eq. 4). Minimization of this function results in the more uniform load distribution and relieving the mostly loaded regions of thread.

$$Q(pp) = \Delta\sigma_{HMH}^{d2} = \sqrt{\frac{\sum_{i=1}^{n}(\sigma_{HMH_i}^{d2} - \sigma_{HMH}^{d2ave})^2}{n-1}} \tag{4}$$

$$Q(pp) \rightarrow \min \tag{5}$$

where:

Q – objective function,

$\Delta\sigma_{HMH}^{d2}$ – average standard deviation of σ_{HMH}^{d2},

σ_{HMH}^{d2ave} – average Huber-Mises-Hencky reduced stress on diameter *d2* for all cooperating coils of thread,

n – number of cooperating coils of thread

4.2. Design variables and state variables

For the optimization process five of six parameters were chosen as design variables (*pp*1, *pp*2, *pp*3, *pp*4, *pp*5). Height of the nut was accepted due to respect the restriction of contact pressure and was accepted as constant for all starting points.

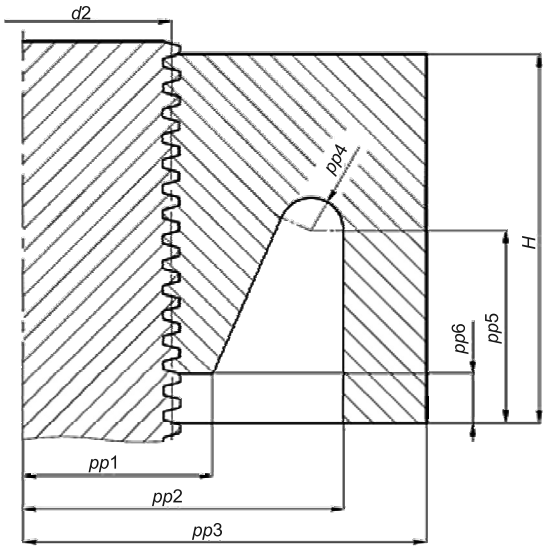

Fig. 3. Design variables and dimensions of the nut with a groove in the end-face

Rys. 3. Zmienne decyzyjne oraz wymiary nakrętki z rowkiem w powierzchni czołowej

Restrictions assumed for designed and state variables as well as starting points depending on bolt diameter summarized Table 1. The estimation of starting point's dimensions was partially based on the information included in [5] and drawings given by [9].

Table 1

Design and state variables with restrictions and optimization starting points

Design variables	***Sp*1**	***Sp*2**	***Sp*3**	**Restrictions**
$pp1$	$0.65 \cdot d$	$0.65 \cdot d$	$0.65 \cdot d$	$d < pp1 < pp2 - pp$
$pp2$	$0.9 \cdot d$	$0.9 \cdot d$	$0.8 \cdot d$	$pp1 + 2 \cdot pp4 < pp2 < pp3$
$pp3$	$1.2 \cdot d$	$1.2 \cdot d$	$1.3 \cdot d$	$pp2 < pp3 < 1.6 \cdot d$
$pp4$	$0.05 \cdot d$	$0.05 \cdot d$	$0.1 \cdot d$	$0.05 \cdot d < pp4 < pp2 - pp1$
$pp5$	$0.4 \cdot d$	d	$0.7 \cdot d$	$0.4 \cdot d < pp5 < 0.9 \cdot H$
State variables				
$pp6$	$0.05 \cdot d$	$0.05 \cdot d$	$0.05 \cdot d$	–
H	$1.69 \cdot d$	$1.69 \cdot d$	$1.69 \cdot d$	–
C_{press}	–	–	–	$C_{press} < C_{press}^{all}$
σ_{HMH}	–	–	–	$\sigma_{HMH} < Re$

4.3. Results and discussion

In the Fig. 4 values of function Q resulted from optimization with starting points $Sp1$, $Sp2$, $Sp3$ were compared with values for the full nut and the reference nut with dimension of the groove proposed in [5].

Table 2

Design and state variables for the best optimization result (SP3)

$pp1$	$0.62 \cdot d$
$pp2$	$0.87 \cdot d$
$pp3$	$1.23 \cdot d$
$pp4$	$0.05 \cdot d$
$pp5$	$0.86 \cdot d$
$pp6$	$0.05 \cdot d$
H	$1.69 \cdot d$
C_{press}	297 MPa
σ_{HMH}	618 MPa
Q	4,1

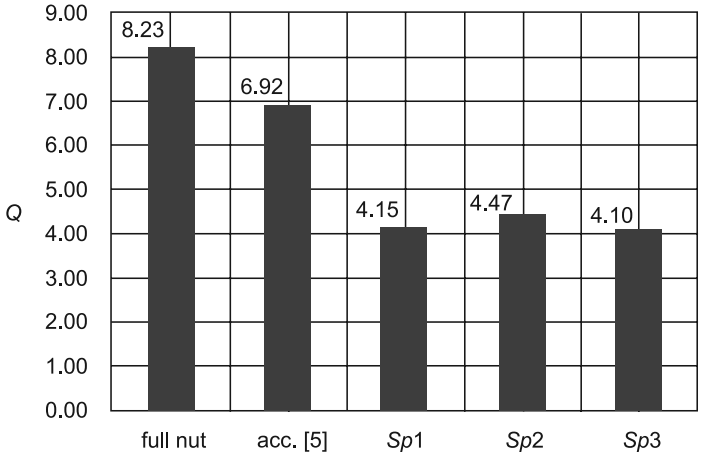

Fig. 4. Objective function after optimization with starting points in comparison with full and reference nut acc. [5]

Rys. 4. Funkcja Q po optymalizacji dla punktów startowych oraz nakrętki pełnej i odniesienia wg [5]

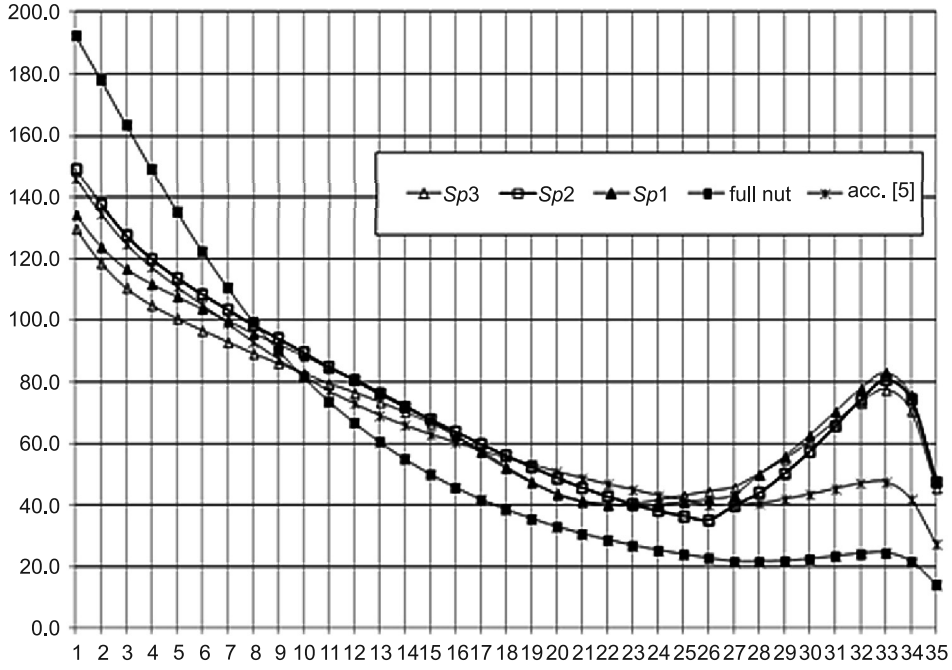

Fig. 5. Distribution of reduced stress σ_{HMH}^{d2} on coils of thread

Rys. 5. Rozkład obciążenia zredukowanego σ_{HMH}^{d2} na zwojach gwintu

The best result of optimization was obtained for starting point *Sp*3. Decrease of objective function in relation to the full nut was about 50%, decrease of maximum contact pressure 16% and decrease of the maximum of reduced stress about 61%. In comparison with the nut with a groove in the end-face according [5] decrease of objective function was close to 41%, decrease of maximum contact pressure 13% and decrease of maximum reduced stress about 9%.

5. Conclusions

Application of finite element method with optimization procedure in the designing of the nut with a groove in the end-face resulted in the improving of the load distribution in bolted joint and in the decreasing of maximum contact pressure on the thread. Presented approach shows that application of the optimization procedure in the designing of bolted joints allows to obtain significant improvement of the load distribution on thread and therefore can increase the fatigue strength of the bolt.

References

[1] Libin Z., Fengrui L., Jianyu Z., *3D Numerical simulation and fatigue life prediction of high strength threaded bolt*, Key Engineering Materials, 2010, Vols. 417–418, 855-888.

[2] Knes M., Glodž S., Kramberger J., *Fatigue assessment of piston rod threaded end*, Engineering Failure Analysis, Vol. 16, 2009, 1977-1982.

[3] Honarmandi P., Zu J. W., Behdinan K., *Elasto–plastic fatigue life improvement of bolted joints and introducing FBI method*, Mechanics Based Design of Structures and Machines, Vol. 33, 2005, 311-330.

[4] Pai N.G., Hess D.P., *Three–dimensional finite element analysis of threaded fasteners loosening due to dynamic shear load*, Engineering Failure Analysis, Vol. 9, 2002, 383-402.

[5] Dobrovolsky K., Zablonsky S., Mak S., Radchik A., Erlikh L., *Machine Elements*, Mir Publishers, Moscow 1968.

[6] Orłow P.I, *Osnowy konstruirowainja*, Maszinoctroenie, Moscow 1977.

[7] Dietrich M., *Podstawy konstrukcji maszyn*, WNT, Warszawa 1995.

[8] Skoć A., Spałek J., *Podstawy konstrukcji maszyn T.I*, WNT, Warszawa 2006.

[9] Szewczyk K., *Połączenia gwintowe*, PWN, Warszawa 1991.

[10] Chen J.-J., Shin Y.-S., *A study of the helical effect on the thread connection by three dimensional finite element analysis*, Nuclear Engineering and Design, Vol. 191, 1999, 109-116.

[11] OHIO CAE INC., *Three-dimensional modeling of a bolted connection* (http://www.ohiocae.com/bolt.htm).

[12] Lisowski F., *FEM modelling of structures with serial notches*, Czasopismo Techniczne, Politechnika Krakowska, 4M/2011/B, 2011, 341-348.

[13] Stadnicki J., *Teoria i praktyka rozwiązywania zadań optymalizacji z przykładami zastosowań technicznych*, WNT, Warszawa 2006.

TECHNICAL TRANSACTIONS | **CZASOPISMO TECHNICZNE**
MECHANICS | MECHANIKA
1-M/2013

SEBASTIAN MAZUR*, RYSZARD DINDORF*, PIOTR WOŚ*

REMOTE CONTROL OF THE ELECTRO-PNEUMATIC SERVO DRIVE USING BIOSIGNALS

ZDALNE STEROWANIE SERWONAPĘDU ELEKTROPNEUMATYCZNEGO ZA POMOCĄ BIOSYGNAŁÓW

Abstract

Machines and devices control can be held using keyboard, joystick, touch interface, gesture recognition interface or speech. Completely different control form is biosignals use, such as electromyogram, electrooculogram or electroencephalogram. In the article presented the controller construction of electro-pneumatic servo drive, which control is backed up by biosignals generated by activity patterns in muscles, brain and eye.

Keywords: *wireless network*, *biosignals*, *electro-pneumatic servo drive*

Streszczenie

Sterowanie maszyn i urządzeń może odbywać się za pomocą klawiatury, joysticka, interfejsu dotykowego, interfejsu rozpoznawania gestów czy też mowy. Zupełnie odmienną formą sterowania jest wykorzystanie biosygnałów takich jak elektromiogram, elektrookulogram czy też elektroencefalogram. W artykule przedstawiono budowę sterownika serwonapędu elektropneumatycznego, którego sterowanie wsparte jest biosygnałami.

Słowa kluczowe: *sieci bezprzewodowe*, *biosygnały*, *serwonapęd elektropneumatyczny*

* Prof. PhD. Eng. Ryszard Dindorf, MSc. Eng. Sebastian Mazur, PhD. Eng. Piotr Woś, Chair of Mechatronics Devices, Faculty of Mechatronics and Machine Building, Kielce University of Technology.

1. Introduction

Remote control of machines and devices contributes to significantly safety increase of their service, since operator doesn't have to be directly at operated machine. One way to implement remote control is the use of radio waves, which are commonly used in wireless computer networks. These networks at the turn of the last few years gained more popularity. Constant their development causes that they are faster, safer, more reliable and due to easiness of installation becomes increasingly common in the industry [1].

Operator communication with the machine can be held using keyboard, joystick, touch interface, gesture recognition interface or speech, which additionally can be backed up by biopotentials, such as electromyogram, electrooculogram or electroencephalogram. These biosignals measured by electrodes placed on operator head it is possible to use to speed up the reaction to appearing incidents.

For the purposes to present possibility of using wireless network WiFi and biosignals in electro-pneumatic servo drive control a laboratory position was built and written communication application between the operator and servomechanism.

2. Communication in computer networks

The information exchange between network devices is held according to closely of defined principles called protocols. Their task is to define the format and structure of sent message, ways of information and errors exchange as well as to establish and finish connections. Protocols don't usually describe how to carry determined function out, therefore implementation of given protocol is independent from specific technology.

Network communications interacts with many different protocols, which forms a connected group of protocols presented as the stack (see Fig.1) [2]. There are two basic models of the network. Model TCP/IP (protocol model) and OSI model (reference model).

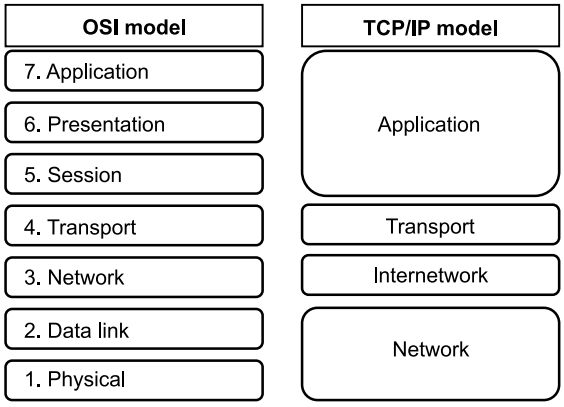

Fig. 1. OSI model and TCP/IP model

Rys. 1. Model odniesienia i model protokołów

Model TCP/IP is regarded as the model of Internet network. It defines four layers responsible for correct communication network. Access layer to the network is responsible for control of physical devices and media forming the network. Internet layer determines the best route of packages in the network, however transport layer deals with the communication between different devices in different networks. The last (application layer) presents as well as reads data from the user. OSI model consisting of seven layers provides a list of functions and services, which may occur in every layer, by what has a significant participation in the development of other protocols [2], [3].

Communication process takes place in two directions. Sending data to network consist on passing information from the application layer to access layer in network, however receipt data is an opposite process.

2.1. Wireless communication

In the access layer to network of the TCP/IP model it is possible to distinguish three types of media transmission, which connect the terminal equipment and provide data transmission between them. These are metal cables (copper), fibre-optic cables and wireless communication. Due to easy access to the medium transmission as well as easiness of structure and networks expansions based on wireless medium communication is more widely used in the communication. One of popular access wireless methods to the computer network is WLAN (Wireless Local Area Network). These networks are in accordance with the 802.11 group of standards, which describes rules for the first and second layer OSI model. Frequency range of the radio waves used by the standard doesn't require the concession; therefore it is possible to use this standard without special licenses. In the first standard version, transmission underwent in 2.4 GHz band and in infrared at wavelength from 850 nm to 950 nm. However, the infrared didn't entertain due to numerous restrictions of this transmission type. Currently also 5 GHz band is used.

2.2. Network protocols

Exchange of data fragments via network between determined terminal devices takes place through Internet layers in addressing, encapsulation, routing and decapsulation of transmitted data process. Commonly used protocol in the network layer is Internet Protocol, in 4 version as well as 6 newest version, which is successively implemented. Moreover, in the network layer implement are protocols such as: IPX (Internetwork Packet Exchange), Apple Talk or connectionless service CLNS/DECNet network.

IP protocol is a connectionless protocol; therefore communication with its use is fast and flexible. Unfortunately information exchange can be unreliable, since protocol doesn't assure that packages will reach the addressee, will be in the correct order, won't be fragmented or doubled. Reliability transmission task is held on layers of the high level in network model.

2.3. Transport protocols

Transport layer task is to provide simultaneous work in multiple different applications by placing in one transmission channel of messages parts from different applications. This task is performed in the segmentation and multiplexing data process.

Depending on requirements which are put to transmit data, two basic transmission protocols are distinguished: TCP and UDP. The TCP Protocol is a protocol which guarantees reliable provision of data to the recipient by tracking transmitted data, receipt confirmation of data and repetition of lost data. It is interconnection protocol, what means that before transmitted data by the network, connection is established between the communicating devices. Second protocol which is simpler under construction is UDP protocol. This protocol above all performs less function from TCP. It is a protocol faster than TCP, doesn't require confirmations as well as doesn't provide lost data for the retransmission, by which doesn't ensure reliability. It's characterized by a small additional data mark-up. As for applying mentioned protocols, where reliability of the data transmission is required the TCP protocol is applied. In case of less sensitive data, where applications are tolerant to loss of small data amounts, UDP protocol is applied [2, 4, 5].

2.4. Application

An application layer is responsible for providing interface between the user of network device and data network. In this layer it is possible to distinguish two types of the software: applications and services. Services of the application layer are usually transparent for the user and are responsible for connecting the application with network and sending data. Application provides interface for the user, reads and presents data as well as initiates the process of data transmission by network.

Protocols of the application layer define the way of data exchange between applications and services, which are started on devices participating in the communication. They carry it out by determining the type and format of exchanged message as well as by determining the way of sending and receiving message. In this layer a different types of protocols function, defined by standards as well as data formats. Telnet can be an example of the application, service and protocol, which is an interface for user (application), program supporting connections for the transmission files (service) and interchange standard of network communications (protocol) [2].

3. Biosignals

Biosignals source can be bioelectric signals, bioresistances, bioaccoustic, biomechanical and biochemical. Measuring impedance tissue during microelectricities transmission it is possible to obtain bioresistances signals, which are a source of information about structure and tissue composition. Using bioaccoustic signals it is possible to obtain information about phenomenon, such as blood flow in vessels or heart. Measuring movement or pressure biomechanical it is possible to obtain biomechanical signals, however biochemical signal source is a measurement on living tissues or laboratory samples. Bioelectric signals are generated by nerve cells or muscle and are often used for examinations in medicine. Most commonly potentials used are electromyogram (EMG), electrooculogram (EOG) and electroencephalogram (EEG). Electromyogram uses electrical signals originating from working muscles, electrooculogram it's a record of appearing tension course, between front

(positive) and back (negative) eyeball pole, and electroencephalogram records electric activity of the brain [7]. Table 1 shows the frequency and amplitude of the biosignals [8].

Table 1

Frequency and amplitude of the biosignals

Type	Frequency (Hz)	Amplitude
EMG	0.01–15000	strongly dependent on the activity of muscle < 10 μV – 100 mV
EOG	0.1–50	< 1 μV – 10 mV
EEG	0.01–150	< 1 μV – 1 mV

4. Controller of the electro-pneumatic servo drive

The controller of servomechanism was built based on the ALIX.1D microcomputer board, module for data acquisition MicroDAQ USB-1208FS, WiFi Ubiquiti XR2 card as well as biosignals reader NIA – Neural Impulse Actuator (Fig. 2).

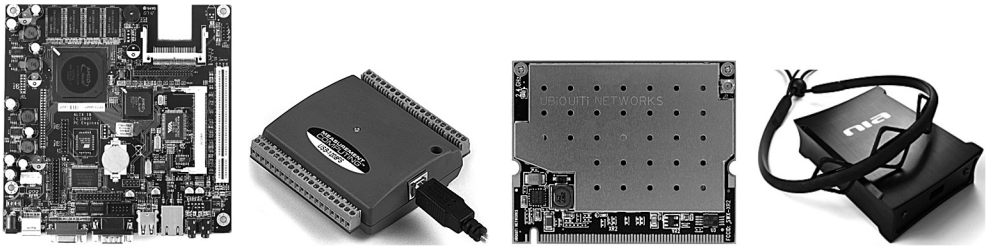

Fig. 2. Elements used for the controller construction. From left: ALIX 1D microcomputer board, module of the acquisition data MicroDAQ USB-1208FS, wireless card Ubiquiti XR2, Neural Impulse Actuator – biosignals reader

Rys. 2. Elementy wykorzystane do budowy sterownika. Od lewej: płyta mikrokomputera ALIX 1D, moduł akwizycji danych MicroDAQ USB-1208FS, karta bezprzewodowa Ubiquiti XR2, Neural Impulse Actuator – czytnik biosygnałów

Microcomputer board ALIX.1D is equipped with AMD Geode 500 MHz processor and 256 MB memory RAM. Powered with voltage 12 V and characterized by small conscription of the electricity, row of 0.4 to 0.5 A. The task of board is to connect wireless card, input output port and application for the controller. On the memory card was installed operating system Windows XP, because equipping board meets the minimal requirements for system as well as in this system doesn't have problems with detection installed additional devices and with drivers to it [6].

As input/output port for the driver was chosen module for the data acquisition MicroDAQ USB-1208FS. This system has 4 analog inputs in the symmetrical system about resolution

of 12 bits and 8 inputs in the asymmetrical system about resolution of 11 bits. In the asymmetrical system is a possibility of voltage measurement ±10 V, while in the symmetric system ±20 V. For generation output signals are available 2 analog outputs about resolutions of 12 bits. Output voltage range amounts to 0–4.096 V at maximum load current 15 mA. This module is connected to the driver board by USB interface.

Communication with the operator computer is ensured by Ubiquiti XR2 card. The card is equipped with connector MMCX, which provides better connection card – pigtail than popular in miniPCI cards UFL connectors. Card supports standard 802.11b and 802.11g, has a high output power (26 dB) and receiver sensitivity up to -95 dB. Depending on used aerial inside the premises it is possible to obtain up to 200 m, however on the open area about 50 km.

For the driver communication with operator were written two applications: one for controller and second for operator. The application of controller performs role of the service. Its task is to adjust the actuator position as well as to listen and wait for connection on chosen port from the operator. In case of connection detection the service starts to collect (set position value) and send data (current position value). When operator finishes the connection, application again turns into the state of listening and waiting. Application operator task is to collect data from the user and their presentation as well as control signals process from the biosignals reader.

Biosignals reader has own application, which can be configure so that based on determined biopotentials values the appropriate control signals were generated, e.g. pressing bottom on the keyboard. In program it is possible to exploit three biopotentials: electromyogram, electrooculogram and electroencephalogram, which use Alpha and Beta waves. Biosignals are measured using three electrodes located on elastic band, which are placed on operator's forehead.

Controller program and for the operator were written using LabVIEW software, which allows to write program using protocols, such as TCP, UDP, Bluetooth or IrDA [6]. Due to ensuring small delays during data transmission, UDP was chosen as the transport protocol. For communication created are two connections: one to send the set value of actuator location and second to send current value of actuator location.

The controller role is to receive from operator by wireless network the actuator set point and to make appropriate adjustment position values process based on measured current value of the actuator location.

On the test-stand was used rodless pneumatic actuator of the Festo Company, magnetostrictional position converter of the Balluff Company, which is used to measurement current value of the actuator location and proportioned valve 5/3 of the Festo Company (Fig. 3). Signal coming from the converter position is a voltage signal from the scope 0–10 V, however the control signal for valve is a voltage about 0–10 V values. Module for data acquisition it is possible to measure voltage ±20 V, however the maximum voltage which can be generate is 4.096 V. Therefore, in the controller preamplifier is applied, built on LM358 system. It's operational amplifier system of the rail-to-rail type. This type of amplifier was applied due to asymmetrical supply controller voltage, which amounts +24 V. In order to match the microcomputer supply voltage, which amounts 12 V, a converter impulse LM2576 was used.

Controller based on measured and set value establishes the actuator position. For position adjuster of the actuator location a popular PID regulator was applied, which setting was conducted by Ziegler-Nichols method.

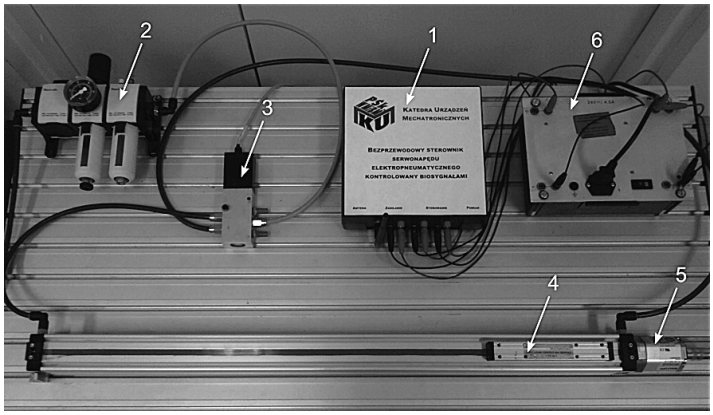

Fig. 3. Test-stand: 1 – Wireless controller of the servomechanism, 2 – Air preparation unit, 3 – Valve, 4 – Actuator, 5 – Location converter, 6 – Power supply
Rys. 3. Stanowisko badawcze: 1 – bezprzewodowy sterownik serwomechanizmu, 2 – zespół przygotowania powietrza, 3 – zawór, 4 – siłownik, 5 – przetwornik położenia, 6 – zasilanie

5. Results

On the laboratory position studied the wireless network use in servomechanism electro-pneumatic control as well as biosignals application in the control process. In experiment used all available biosignals from the application level: muscle tension measurement, eyeball movement measurement as well as Alpha and Beta waves. To determined signal levels, they were assigned to simulation pressing appropriate buttons on the keyboard: Page Up – increase actuator position value, Page Down – reduce actuator position value, End – press emergency stop button. As a result of conducted experiments stated that electromyogram signals use, e.g. through adjustment of the pressure tongue strength to palate or clenching teeth with bigger or smaller strength gives the best effects to generate control signal. Unfortunately during examinations it was very hard to precisely determine the demanded actuator position. Remaining biosignals, due to difficulty of appropriate level obtaining, didn't allow for simple determining the actuator position. As a result of conducted experiment in the laboratory position obtained characterizations of the servomechanism electro-pneumatic work, which were presented on Fig. 4.

It results from the analysis of above graphs that there is a delay between set signal value and actuator position. This delay is implemented by acquisition data module, since it results from the analysis program action that the most time take to generate voltage by the system. The second reason of acquisition data module delays is that communication with module takes place via USB interface, which isn't a real time interface.

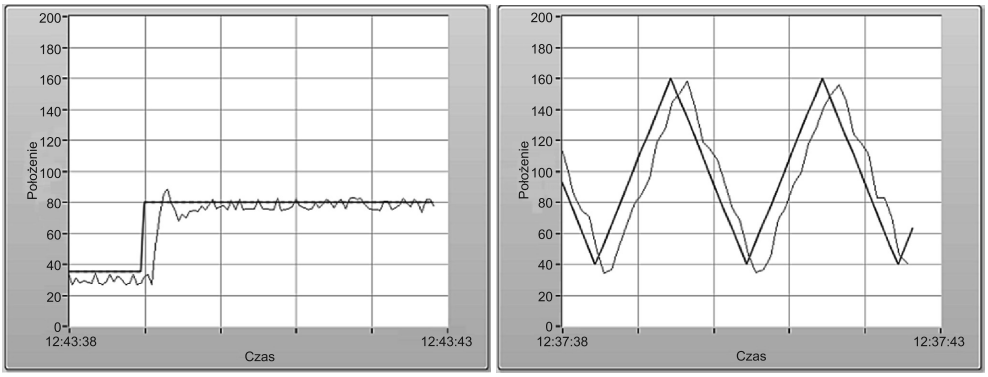

Fig. 4. Manual and automatic control of the electro-pneumatic servo drive

Rys. 4. Sterowanie ręczne i automatyczne serwonapędu elektropneumatycznego

In spite of the fact that defect in the studied controller is impose of delays between the control and read signal, what disqualifies it as the adjuster, it is possible to use it for simple control of the servo drive in systems not-requiring big precision and in places dangerous to very operator of the servomechanism.

6. Conclusions

Wireless communication in spite of its limitations, such as susceptibility to disruptions or delays in transmission gives us great possibilities of use where it isn't possible to apply cable networks. Wireless control can significantly improve security of the operator as well as reduce structure costs of the network infrastructure. Conducted simulations in the laboratory position confirm that it is possible to use the wireless computer network WiFi without obstacles to communication of the operator with the remote device. Examinations also confirm that in the process it is possible to use control biosignals of different types. Although a precise determination of the actuator position was difficult, this type of control can be used in accelerating operator response on the existing reaction. An example can be pressing the emergency device stop button.

References

[1] Główny Urząd Statystyczny, *Wykorzystanie technologii informacyjno-(tele)komunikacyjnych w przedsiębiorstwach i gospodarstwach domowych w 2011 r*., 2012.

[2] Mark A. Dye i inni, *Network Fundamentals, CCNA Exploration Companion Guide*, Cisco Press, 2007.

[3] Meyer D., *TCP/IP versus OSI*, Journals & Magazines, Vol. 9, 1990, 16-19.

[4] *RFC 793 – Transmission Control Protocol*.

[5] *RFC 768 – User Datagram Protocol*.

[6] Mazur S., Dindorf R., Woś P., *Wireless communication system in the control electro-pneumatic servodrive*, Pneumatyka nr 2, 2012, 46-51.
[7] Mandeep Singh, *Introduction to Biomedical Instrumentation,* PHI Learning Private Limited, ISBN 978-81-203-4163-0, 2010.
[8] Ndubuisi J. Ekekwe, *Reconfigurable application-specific instrumentation and control integrated systems*, The Johns Hopkins University, ISBN 978-11-091-3054-6, 2009.

TECHNICAL TRANSACTIONS | **CZASOPISMO TECHNICZNE**
MECHANICS | MECHANIKA
1-M/2013

PRZEMYSŁAW MŁYNARCZYK*

CFD ANALYSIS OF THE IMPULSE FLOW DAMPING BY THE SPECIALLY SHAPED NOZZLE

ANALIZA CFD TŁUMIENIA IMPULSU PRZEPŁYWU PRZEZ DYSZĘ SPECJALNEGO KSZTAŁTU

A b s t r a c t

The vibrations and noise caused by pressure pulsations are one of the major problems in volumetric compressors manifolds. There is still no easy solution for this problem. Passive damping of those pulsations is possible using specially shaped nozzle placed in place of the straight tube. Experimental analysis of the pressure pulsations damping caused by a nozzle is possible however only some arbitrary chosen nozzle shapes can be investigated. The analysis of damping of the impulse flow by the nozzle using CFD simulation is more general and gives the possibility to estimate the nozzle influence on the pulsating flow in theoretical way, so many different shapes can be investigated. In this paper examples of impulse flow damping factors for three different nozzles have been shown.

Keywords: *CFD simulations*, *Pressure pulsations damping*

S t r e s z c z e n i e

Wibracje i hałas powodowane pulsacjami ciśnienia są jednym z głównych problemów pojawiających się przy eksploatacji układów sprężonego powietrza. Wciąż nie ma prostego rozwiązania dla tego typu problemów. Pasywne tłumienie tych pulsacji można osiągnąć wykorzystując dysze o specjalnym kształcie. Artykuł prezentuje próbę symulacji impulsu jednostkowego poprzez trzy typy elementów tłumiących oraz opisuje wpływ kształtu elementu na pulsacje ciśnienia występujące w układzie.

Słowa kluczowe: *symulacje CFD*, *Pulsacje ciśnienia*

* MSc. Eng. Przemysław Młynarczyk, Institute of Thermal and Process Engineering, Faculty of Mechanical Engineering, Cracow University of Technology.

Nomenclature

ξ – damping factor
ω – natural frequency of the system
τ_0 – response time
T – period

1. Introduction

The main problem, addressed by this article, is the possibility of pressure pulsations attenuation in the compressors manifold system. Periodic work flow of the volumetric compressors cause the pressure and mass flow pulsations. The pressure pulsations attenuation in the volumetric compressor manifolds is one of the major design problems both in small refrigerating compressor units due to noise, but also in high capacity volumetric compressors due to vibrations caused by pulsations [1]. Development of the design is, among other things, a result of advances in computer modelling, computational fluid dynamics allows to get answers to questions on how to optimize constructions. This brings up the need to analyse the phenomena of pulsation wave propagation and it's damping. In the smaller compressors we can't use large muffling systems- the one way to suppress pressure pulsations is to install choking elements at the start of the compressor outflow pipe. This attenuates the pulsations but also increases the compression power. So the optimisation is required.

Computer simulation may be used to investigate the influence of different muffler types on pressure pulsations [7, 8]. CFD simulations have become also a working tool for designers and maintenance engineers [2–5]. There are several approaches such as generalised Helmholtz method based on CFD simulations, 2D transfer matrix [6] etc. In this paper simplified analysis of one most important parameter resulting from CFD calculations is shown.

2. Compressor pressure pulsations

Pressure pulsations frequency result from the compressor forced flow, what means that first basic harmonic results from multiplying number of revolutions and amount of volumes extruded during one rotation of the drive shaft. Therefore, the strongest excitation comes from one cylinder, single-acting reciprocating compressor. Extorting is still not critical and sufficient to evaluate the propagation of pressure pulsation. Depending on the system configuration, harmonic waves of pressure pulsations can strengthen or weaken each other. In the system occurs a lot of phenomena such as: wave reflections, interference of reflected waves, pulsation damping, thus all of the phenomena associated with the internal acoustics. A pulsating gas stream significantly influences the functioning of the entire compressor manifold, especially affected in a negative way to the compressor systems. Pressure pulse waves, carry a significant acoustic energy which is a system energy loss, but in the special case in the compressor dynamic charge it can be positively used. The main problems which pressure pulsations cause are [3, 4]:

– System vibrations and sometimes even mechanical damage.
– Aerodynamic and mechanical noise.
– Reduction in displacement chamber filling with wrong pressure phase in the suction cycle.
– Resonance with the work of the valves causing them to wear faster.
– Problems with the operation of the associated equipment, for example: flow meters, pressure gauges etc.

Author performed a series of experiments, using various of choking elements to decrease pressure pulsations. After the experiment, according to the results, author choose three different shapes to use in the computational simulations.

3. Muffling elements

Passive damping pressure pulsations is possible using specially shaped nozzle placed in place of the straight tube. Experimental analysis of the pressure pulsations damping caused by a nozzle is possible however only some arbitrary chosen nozzle shapes can be investigated. Author made a series of measurements for different nozzle shapes.

The three different shapes, which was chosen after this measurements, is venturi orifice with inner diameter ϕ15, venturi nozzle with inner diameter ϕ15 and hyperboloidal nozzle with inner diameter ϕ20. Simulations was performed for the pipe with this three types of choking elements and, obviously, for the empty system pipe.

3.1. Venturi orifice

Ventouri orifice ϕ15 is the longest element used in the simulation, as the geometrical dimension as shown in Figure 1a. The data obtained during the experiment shows that this element damped pressure pulsations well, with not much loss in the system fluid flow rate.

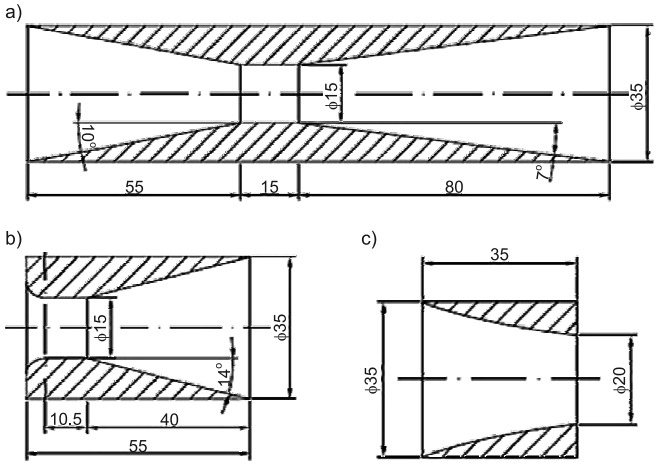

Fig. 1. Shape and main dimensions of the a) venturi orifice, b) venturi nozzle, c) hiperboloidal nozzle
Rys. 1. Kształt i podstawowe wymiary a) zwężki venturiego, b) dyszy venturiego, c) dyszy hiperboloidalnej

3.2. Venturi nozzle

Venturi nozzle ϕ15, from data obtained in the experiment, is characterized by very similar parameters of pressure pulsations damping and flow rate like venturi orifice. Shape of this element is harder to made, however the advantage of this solution is the smaller dimensions which is important in the small compressors systems.

3.3. Hyperboloidal nozzle

The last choking element is hyperboloidal nozzle ϕ20. Experiment shows that this type of choking elements haven't big influence on pressure pulsations. Furthermore, this nozzle have very complicated geometry which is expensive to produce.

4. Simulations results

Computational simulations were performed in the Ansys Fluent environment. The most common approach in analysis of the phenomenon of pressure pulsation is the use of the ideal gas equation of state.

To the simulation were used density-based, transient model, with using energy equations and inviscid fluid model which was chosen as ideal gas. As impulse, which had represented dirac pulse at the pipe inlet in the first time step, was chosen mass flow impulse with a value of 0.1 kg/s. The end of pipe was declared as open pressure outlet. As the velocity of wave propagation is dependent on the temperature, for both, inlet total temperature and outlet backflow total temperature has been declared the same as the environment temperature and it is 350 K. Size of the grid elements was assumed for every one example individually, but as default minimum cell size was chosen 1mm, which gives a grid density of around 1 cell per mm^2. There was used a default Fluent grid type for this type of simulations. According to the cell size and transient time model, time stepping method has been chosen fixed with duration of time step equal to $2 \cdot e^{-6}$ s. To gain desirable simulation time 0.01s was needed 5000 time steps. In the model definition also declared axisymmetric calculations, so geometry used in the simulations was only the profile of nozzle shape in the tube. Convergence of every time step solutions was usually achieved around 60–70 iterations step, with declaration of 100 maximum iterations per time step. For every simulations, geometry of the whole pipe had length 327,3 mm and all elements were placed 5 mm behind pipe inlet. In the Figure 2. are shown results of pressure contours for two elements (venturi orifice and hyperboloidal nozzle).

In the Figure 2. are shown pressure contours in two different elements but in the same time: after 1000 and 4000 time steps. There is visible clear difference in the process of propagation of the pressure pulsations. It could be said, that in hyperboloidal nozzle there is a spatial pressure propagation while in the venturi orifice it looks like a one-dimensional propagation.

In the Figure 3. Is presented attenuation of the pressure pulsations (in the pascal unit) in the impulse flow in four choking elements. Graphs shows pressure value at the pipe outflow. To present how the pressure pulsations are suppressed, on the graphs in Figure 3. are drawn damping characteristic curves. They are characterized by the equation [1, 3]:

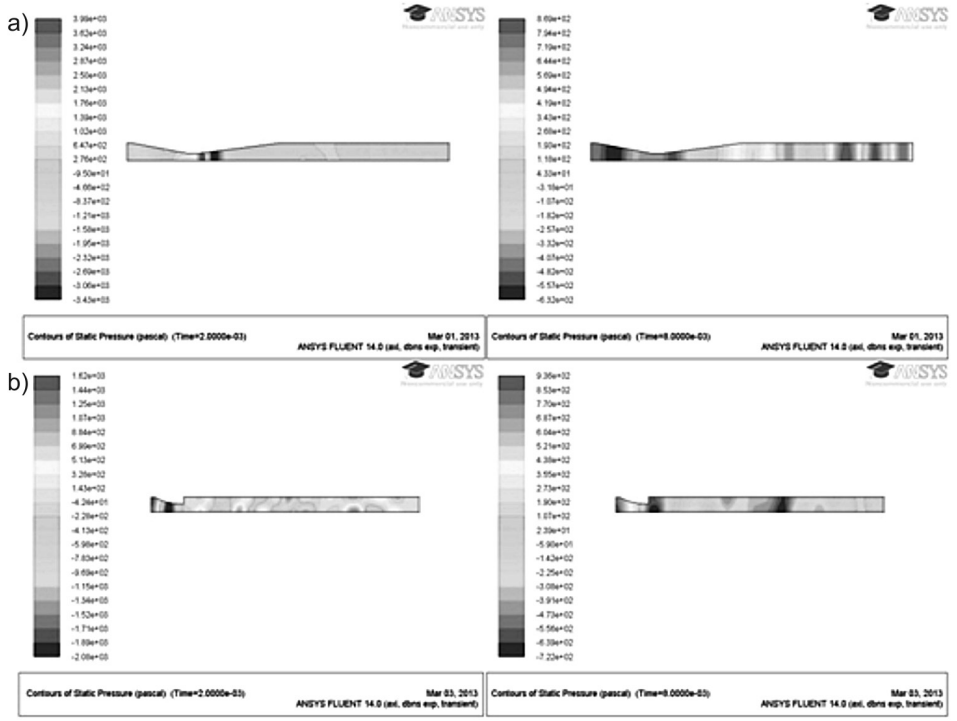

Fig. 2. Pressure map in 0.002 (left) and 0.008 (right) second: a) venturi orifice, b) hyperboloidal nozzle

Rys. 2. Mapa rozkładu ciśnienia w 0.002 (z lewej) oraz 0.008 (z prawej) sekundzie: a) zwężki venturiego, b) dyszy hiperboloidalnej

$$y(\tau) = A_0 \cdot e^{-B(\tau-\tau_0)} \tag{1}$$

where:

$$B = \xi\omega \tag{2}$$

where omega is:

$$\omega = \frac{2\pi}{T} \tag{3}$$

Period of every pressure pulsations is known. It can be taken from the graphs or simulations results table.

In the present case author could manipulate the B value to obtain attenuation curves, by matching them to the pressure pulsation signal. When the value of the exponent of damping characteristic equation is known, and the natural frequency of the system is known, we can deduce from equation (3) the damping coefficient ξ. Damping factor and exponent of the damping characteristic equation for every simulations are shown in the Table 1.

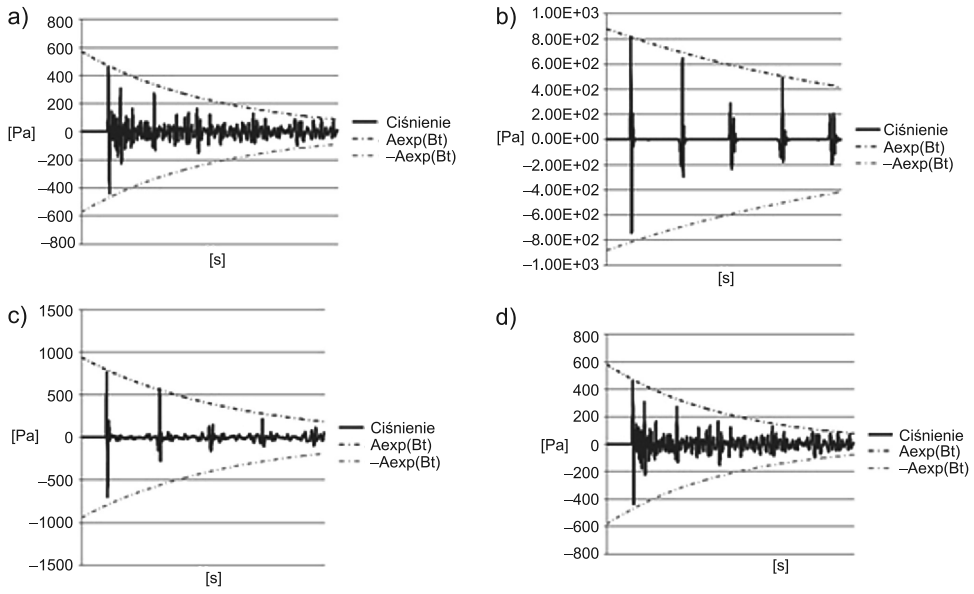

Fig. 3. Pressure pulsations graphs with damping characteristic curves for: a) hyperboloidal nozzle, b) empty pipe, c) venturi orifice, d) venturi nozzle

Rys. 3. Pulsacje ciśnienia z krzywymi charakterystyki tłumienia dla: a) dyszy hiperboloidalnej, b) pustej rury, c)zwężki venturiego, c)dyszy venturiego

Table 1

Value of the exponent of the damping characteristic equation *B* and the damping coefficient ξ

Element	ξ	*B*
Venturi orifice φ15	–0.056	–195
Venturi nozzle φ15	–0.057	–242
Hyperboloidal nozzle φ20	–0.053	–225
Empty pipe	–0.025	–90

The simulation result obtained damping coefficients at a similar level. As it can be noticed damping in the empty pipe is much smaller than in the other elements, which looks natural and correct. Results for two venturi choking elements looks good, because damping percent for this types of mufflers with the same diameter obtained very close to each other also in the experiment. However, if we look at the results of the experiment the ξ coefficient for hyperboloidal nozzle is too close to the other two elements with smaller inner diameter.

5. Conclusions

The main problem in conducting simulations is the discretization and selection of the calculation method. Especially, for hyperboloidal element, the most difficult problem was to precise design the shape of the nozzle, and then make the appropriate discretization of this element. Anyhow the presented calculations shows that the impulse flow propagation through the choking element may by an interesting and simple tool to assess the possibility to utilise specially designed nozzle shape for pressure pulsation attenuation. The experimental investigation carried by the author are not included here due to the space limits and subject of the paper, but there is a correlation between the experimental results and calculated results presented in this paper.

References

[1] Advanced Reciprocating Compression Technology (Arct) Final Report SwRI® Project No. 18.11052 DOE Award No. DE-FC26-04NT42269 Reporting Period: October 1, 2004 – September 30, 2005.

[2] Cyklis P., *Advanced techniques for pressure pulsations modeling in volumetric compressor manifolds*, J. Vib. Acoust., Volume 132, Issue 6, December 2010.

[3] Cyklis P., Hendla R., *Influence of real gas model on the simulation of pressure pulsation in the reciprocating compressor manifolds*, Archieves of thermodynamics, Vol. 26(2005), No. 3, 21-35.

[4] Cyklis P., *Symulacja procesów termodynamicznych w sprężarkach wyporowych i ich instalacjach*, Politechnika Krakowska, Kraków 2008.

[5] Kantor R., *Analiza oddziaływania odolejacza sprężarki wyporowej w instalacji w warunkach przepływu ustalonego i pulsującego za pomocą symulacji CFD*, praca doktorska, Politechnika Krakowska, 2004.

[6] Ma Y.-C. and Min O.-K., *Pressure calculation in a compressor cylinder by a modified new Helmholtz modeling*, Journal of Sound and Vibration 243, 2001.

[7] Zhaoyu H., Weikang J., *Analysis of source models for two-dimensional acoustic systems using the transfer matrix method*, Journal of Sound and Vibration 306, 2007.

[8] Zhou W., Kim J., *Formulation of four poles of three-dimensional acoustic systems from pressure response functions with special attention to source modeling*, Journal of Sound and Vibration 219, 1999.

TECHNICAL TRANSACTIONS | **CZASOPISMO TECHNICZNE**
MECHANICS | MECHANIKA
1-M/2013

HASSAN MOMENI*

RAPID PROTOTYPING OF AED TRAINING DEVICE COVER

WYKORZYSTANIE METODY SZYBKIEGO PROTOTYPOWANIA NA PRZYKŁADZIE OBUDOWY DEFIBRYLATORA TRENINGOWEGO

A b s t r a c t

This paper presents the utilization of Rapid Prototype technology in industrial design. On example of cover for AED training device there was presented in what way the prototype is made. Cad model created in PTC/Creo is ready to be printed using any of available RP technology.

Keywords: *Rapid Prototyping*, *CAD*

S t r e s z c z e n i e

W artykule przedstawiono podstawowe rodzaje technologii szybkiego prototypowania oraz ich zastosowania w przemyśle. Na przykładzie obudowy urządzenia treningowego automatycznego defibrylatora pokazano sposób budowy modelu CAD oraz jego wykorzystanie w procesie przygotowania prototypu wykonanego w technologii FDM.

Słowa kluczowe: *szybkie prototypowanie*, *CAD*

* PhD. Hassan Momeni, Institute of Machine and Maritime Technology, Bergen University College.

1. Introduction

In the late 70's the first 3D printing devices where made to produce prototypes. 3D printing started with a desire to print 3D-modelles, in the same way as text and picture printers work. The first printers that were produced were large and extremely expensive. Today you can get 3D printers for different costs. This depends on the quality of the printer and the material it produces. 3D printing is currently used for making various prototypes, this can be anything from new part of a car or material savings for soda bottles. It is estimated that there are approximately 120 printing devices in Norway with a cost of more than 200 000 NOK. The main buyers are often architects, engineering firms and designers. Although most of the printers are used to produce prototypes, there is a roughly 25% usage of making retail products. This will increase as the technologies are getting better and prices on 3D printers decrease. Benefits with 3D printing is that you have almost unlimited possibilities of making whatever you want and for a low cost. All you need is 3D drawing program, a printer and materials. Figure 1 displays were 3D printing is used in different industries. Figure 1 displays were 3D printing is used in different industries.

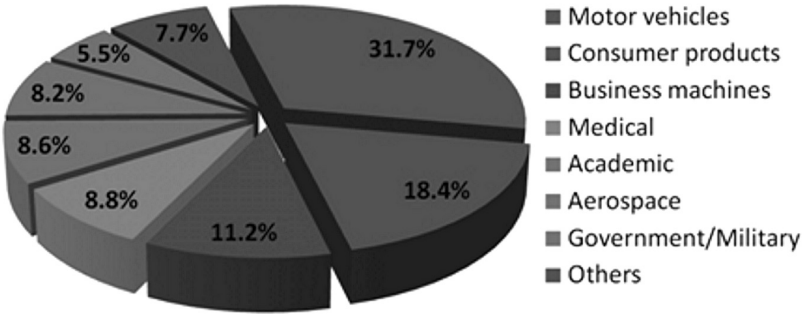

Fig. 1. Marked shares for 3D printing [1]

Rys. 1. Wykorzystanie technologii szybkiego prototypowania [1]

2. RP Technologies

3D printing, also known as rapid prototyping or rapid production is a technology based on text and picture printers. Text printers use only two axes, *X* and *Y* in a coordinate system. 3D printers use the same principles as a text printer, but it can also print in several layers in Z-axe direction. Today rapid prototyping machines have a limited size of the final product, the height extends to about 50 cm at the maximum height for the average printer. This will increase with evolving technology. Printers used today can create devices in different materials and colors. Everything from cheap printers that prints in plastic to expensive machines that prints in diverse metal alloys. Common for all the printers are that the printing is slow, normal operation speed is 20–28 mm per hour. This will vary, and it depends on quality of the product.

Table 1

Some types of technologies for 3D printing [2]

Type	Technologies	Materials
Extrusion	Fused deposition modeling (FDM)	Thermoplastics (e.g. PLA, ABS), eutectic metals, edible materials
Granular	Direct metal laser sintering (DMLS)	Almost any metal alloy
	Electron beam melting (EBM)	Titanium alloys
	Selective heat sintering (SHS)	Thermoplastic powder
	Selective laser sintering (SLS)	Thermoplastics, metal powders, ceramic powders
	Powder bed and inkjet head 3d printing, Plaster-based 3D printing (PP)	Plaster
Laminated	Laminated object manufacturing (LOM)	Paper, metal foil, plastic film
Light polymerised	Stereolithography (SLA)	photopolymer
	Digital Light Processing (DLP)	liquid resin

3D printing technology commonly used today are:

1. Monomer liquid
   The simplest of the professional models can make plastic models within a cube of 17×23×20 cm. The principle is that you pull the model up from a bath with a monomer liquid which flows on to a slim layer on top of a glass plate. It is affected by UV-light making the liquid polymerized. When a layer is completed, the bottom plate will move 1 mm in the Z-direction and the next layer can be produced.
2. Polymer powder
   This technology using polymer powder gives porous products. This type of printing allows for multiple color combinations when you add dye. In order to harden the polymer, it can be brushed or immersed in a binder. The binding liquid is epoxy or cyanoacrylate.
3. Selective Laser Melting (SLM)
   These types of printing machine use almost the same principle as the Monomer liquid technology. For each layer that is printed, metal powder is melted with a laser. This procedure will repeat itself, until it is finished [3].

3D printing technology is today on the way forward. Future researchers believe that people no longer will buy finished products in stores, but rather create/print products themselves. Researcher Dave Evans believes rapid production machines will revolutionize the current production technology. “A few years into the future, humans will be able to create everything from artificial organs to foods”, he believes.

He also believes that there may be an industrial revolution in terms of how 3D printers produce units. There is another type of production preparation for building up layer by layer. This is very different compared to the production we have today, where we have to remove materials with the help of milling and drilling machines.

3. CAD model of AED training device

A practical using of Rapid Prototyping method was presented on example of AED training device cover. Before the prototype was prepared a CAD model was created. It was prepared in PTC/Creo software. Below figure presents the main dimensions of the cover, while complete model of the cover is presented in Fig. 3.

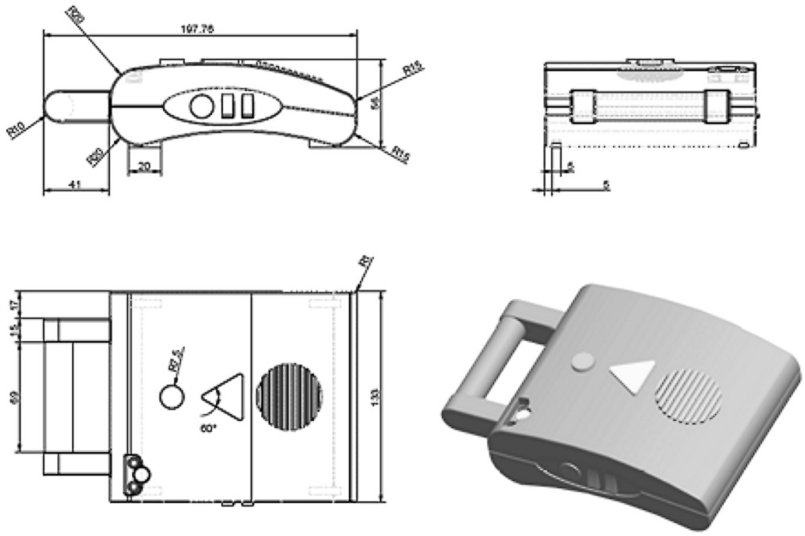

Fig. 2. Main dimensions of AED cover

Rys. 2. Główne wymiary obudowy defibrylatora

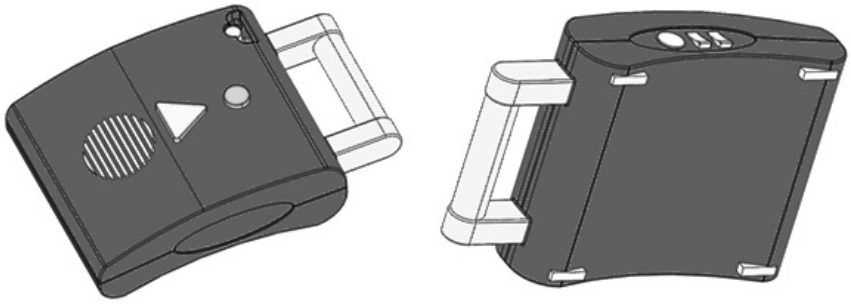

Fig. 3. Complete CAD model of AED cover

Rys. 3. Model obudowy defibrylatora

Presented CAD model was later used for preparing model in .stl format file and creating input data in appropriate software to Rapid Prototyping machine. Prepared prototype by the use of FDM technology is shown on below picture.

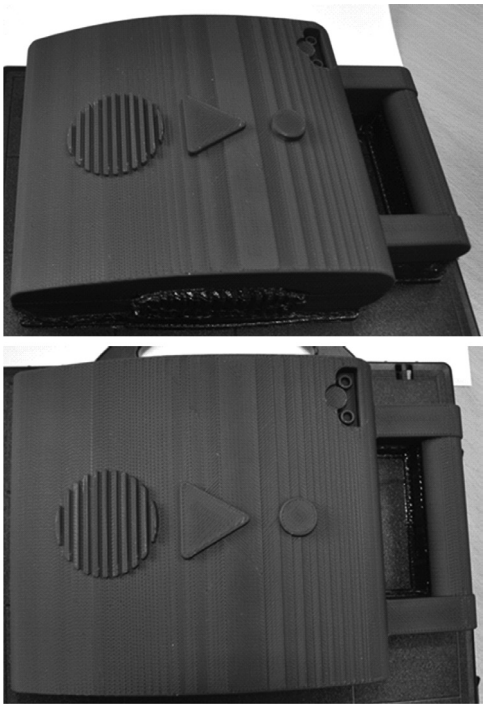

Fig. 4. FDM prototype of AED cover

Rys. 4. Prototyp obudowy defibrylatora wykonany w technologi FDM

4. Conclusions

Combining CAD systems and Rapid Prototyping technology allows to prepare prototype in reasonable time and cost. It also allows for testing various solution before product goes to final production and eliminate potential errors. Rapid Prototyping methods are still developing and allows to achieve better and better quality, but even now, allows to conducting test which were not available yet few years ago.

References

[1] Rapid prototyping worldwide by Zureks (http://upload.wikimedia.org/wikipedia/commons/0/0b/Rapid_prototyping_worldwide_by_Zureks.png).
[2] 3D printing (http://en.wikipedia.org/wiki/3D_printing#cite_note-21).
[3] Teknisk Ukeblad nr.01/10. JAN 2013
[4] PTC (http://ptc.com).

TECHNICAL TRANSACTIONS | CZASOPISMO TECHNICZNE
MECHANICS | MECHANIKA
1-M/2013

ARTUR OLSZAK*, ELŻBIETA ZIĄBSKA**, ZBIGNIEW KĘSY**

COMPUTER-AIDED DESIGN OF INDUSTRIAL INSTALLATIONS

PROJEKTOWANIE INSTALACJI PRZEMYSŁOWYCH Z WYKORZYSTANIEM PROGRAMÓW KOMPUTEROWYCH

A b s t r a c t

The paper concerns the design of industrial installations using computer programs. It also contains a description of problems that must be solved by a constructor who designs industrial installations, their components and characteristics at different stages of industrial design.

Keywords: *Computer-aided design*, *industrial installations*

S t r e s z c z e n i e

Artykuł dotyczy projektowania instalacji przemysłowych z wykorzystaniem programów komputerowych i zawiera opis problemów jakie musi rozwiązać konstruktor projektujący instalacje przemysłowe i ich elementy oraz charakterystykę poszczególnych etapów projektowania instalacji przemysłowych.

Słowa kluczowe: *komputerowe wspomaganie projektowania*, *instalacje przemysłowe*

* PhD. Artur Olszak, Fertilizer Research Institute.
** MSc. Elzbieta Ziąbska, PhD. Zbigniew Kęsy, Institute of Applied Mechanics and Power Engineering, Faculty of Mechanical Engineering, Kazimierz Pulaski University of Technology and Humanities in Radom.

1. Introduction

Industrial installation design is a complex process and requires a solution of many problems, mainly mechanical ones but also electrical and those connected with the assembly, construction, control and measurement. Calculating individual components, the industrial designer needs to know not only the rules of construction, but also many regulations and standards that allow to carry out the correct calculations. The complete engineering design of an industrial installation contains the descriptive and executive documentation that includes many areas, so avoiding mistakes is very difficult. Therefore, different kinds of CAD computer software are helpful for the design and strength calculations.

2. Design stages

2.1. Design data

The basic source of data in order to begin the design work is a technical project, including the process design. The process design involves the detailed data describing the technology of manufacturing or processing products. The final product may be a finished product or a product intended for further processing. The whole process is presented in the form of diagrams, for example the so-called P & ID diagram as well as the descriptive part. From the designer's point of view, the process design includes basic information enabling to start the design work for the respective areas, such as machine, apparatus and device specifications, guidelines for selection of materials for components, data for the design of piping, fittings, guidelines for electrical, control and measurement projects. In addition, the process project includes the design data sheets necessary for the design of new devices as well as the layout drawing. On the basis of the process project, the data and the detailed design of industry installation for different areas can be carried out [1, 2].

2.2. Mechanical aspects of industrial installation design

When a technologist chooses equipment to carry out the process, he usually chooses standard solutions available on the market. However, it is not always possible to find the optimal size and efficiency of the available device. Therefore, some of the devices should be designed and manufactured in accordance with the data contained in the data sheet. It consists of a descriptive part that includes the process data and work parameters of a device as well as the data for the technical execution of the project, such as calculation parameters, size and markings of nozzles, the sketch with the overall dimensions and the location of each nozzle, the material data, anti–corrosion protection guidelines or guidelines for the foundation of the device and thermal insulation.The main parameters taken into account by the manufacturer are pressure and temperature of the manufacturing process. On the basis of these parameters, the constructor's task is to design a device and create the technical documentation. The new device should meet the technological specifications, endurance and safety, so the construction of a new apparatus or device requires knowledge not only of the typical design solutions and methods of strength calculations but also regulations and standards [3].

After having been designed and made, the installations must undergo inspection, that will guarantee safe operation. It particularly relates to devices with high pressure and temperature or when corrosive or explosive chemicals are processed. The design and implementation of such devices is supervised by such departments as the Office of Technical Inspection (UDT). Procedures and requirements which the designer should follow while preparing the documentation are contained in the regulations and specifications of UDT [4] and in Directive 97/23/EC concerning pressure equipment [5]. Common standards for the installation design have not been established yet, so, for example, in Sweden, the United States, Britain and Germany there are different standards, requirements and design guidelines.

2.3. Aspects of assembly of industrial installation design

The project of the assembly includes the detailed guidelines for installation of devices, appliances, fittings and other components included in the industrial installation. The proper assembly ensures the proper operation of the installation. The individual components of it are mounted on steel structures or foundations and are connected by pipelines. Pipelines ensure a product flow between the individual devices according to the technological process. The pipeline documentation is an important part of the assembly area as pipelines are exposed to high pressure, temperature and toxicity of the product flowing therein. The technical documentation and strength calculations of pipelines are subjected to the requirements of standards and regulations. The technical project of a pipeline contains the descriptive section with guidelines for implementing, installation, testing, and isometric drawing showing the route of the pipeline as well as the detailed specification of materials, a list of the components of the pipeline, a guideline for anti–corrosion protection and other requirements.

2.4. Construction aspects of industrial installation design

The technical project of the installation includes projects of foundations, buildings (e.g warehouses, social rooms), supporting steel structures, platforms for equipment maintenance, motorways, access roads, etc. The constructor's task is to place individual system components in accordance with the guidelines. He should also take into account where to situate equipment of control cabinet and the foundation of pipelines. The building technology project includes the guidelines for the execution and acceptance of individual work, strength calculations and specifications of various elements of a building or steel structure, guidelines for anti-corrosion protection of steel and concrete elements

2.5. Electrical aspects of industrial installation design

The project scope includes the diagrams of electrical installations that provide power to individual devices and lighting diagrams of essential elements of installations, buildings and access roads.

2.6. Control and measurement aspects of industrial installations

Control and measurement equipment is used in every industrial installation in order to ensure control of the technological process. The control and measurement project includes

measurement, control and regulation diagrams, lists of equipment, control and measurement cabinet foundations including material specifications and descriptions of the construction, operation and measurement devices. The parameters that are supposed to be controlled, include, among others: pressure, temperature, flow, and level of refrigerant in the tank.

3. Computer-aided design programs

Visual Vessel Design program, developed by the Norwegian company Ohm Tech A/S [6, 7] is used for design and calculation of industrial installation elements. The assistant and aid function as well as the included manual help and facilitate the design. This program allows to use several design standards, such as European (EN 13445) and American (ASME VIII Division 1), UK (PD550), Swedish (TKN), and Norwegian (TBK2). It includes computational models that allow for the structure of typical industrial elements: heat exchangers, columns, tanks, etc. The constructor can use such materials and standard parts as bolts, flanges, gaskets, pipes, forgings, plates, foundation bolts, according to various European and international standards. The designer can generate a design documentation in the form of assembly drawings of a device and engineering drawings of its individual elements. Drawings can be exported to other CAD systems by means of files: .dxf and .dwg. Progress visualization of the project enables successive element joining and checking their position and dimensions in the modules: 2D and 3D. The program validates the data entered by the designer considering the limits resulting from construction and geometric solutions as well as regulations and standards. In addition, Visual Vessel Design program generates the general report, which lists the performed calculations, record of changes, calculation parameters, warnings, and information about errors that occur in the project, nozzle specification, a list of the components and materials that have been used, as well as the percentage level of the material usage (in the form of a graph). This information facilitates the analysis of existing stresses and allow for the optimal design of the device. AutoCAD P & ID software constitutes a part of a software suite for designing industrial installations by Autodesk. This program allows to create, modify, and manage piping diagrams and measuring equipment. The program includes a library of industry-standard symbols (PIP, ISA, JIS and ISO/DIN). A scanning tool enables the detection of errors connected with the position of elements relative to each other. The software allows to create reports and descriptions. The data can be exported to tables in drawings and to other programs, such as Microsoft Excel [8, 9].

AutoCAD Plant 3D is an application destined for industrial installation design. In this program, there is a direct exchange of basic data between the 3D model, piping diagrams and control and measuring equipment, as well as isometric and orthogonal drawings. This guarantees the control of data entry news and design changes. The program enables the design based on standard parts catalogs, such as: ANSI, ASME (B16) and DIN/ISO. It is also possible to use the extensive database of catalogs and the additional equipment library. This information is helpful for the design of pipelines and supporting constructions. Functions of AutoCAD Plant 3D application enables to lay out pipelines routes, the edition of the pipe line and its components and determine the method of joint. Isometric, orthogonal drawings can be easily generated from the 3D model [8, 9].

Autodesk Revit Structure application is used for the industrial design. This program, designed for 3D modelling enables cooperation with Auto CAD Plant 3D program. It is equipped with special tools necessary to design, analyze, and document the design, which significantly improves the coordination of projects from several fields and cooperation among designers. It also has options how to minimize designer's errors. AutoCAD Structural Detailing is an application in which the way of part construction and efficient creation of drawings is considered [8, 9].

AutoCAD and Autodesk Inventor are programs for the overall design and preparation of technical documentation. With broad capabilities, they are quite commonly used by designers. Additionally, Autodesk Inventor enables 3D modelling of plant equipment. Thanks to special features, the import of three-dimensional models from Autodesk Inventor to AutoCAD PLANT 3D program and combining them with piping models is possible [8, 9].

Autodesk Navisworks software enables a complex assessment of the installation validity check. It is possible to simulate movement within the model approximation, maximizing, shifting, rotation, etc., using advanced navigation tools. Through these capabilities, you can avoid potential problems before the installation construction. The software can detect errors of the installation component position and easily correct them [8, 9].

4. Examples of computer-aided industrial installation element design

4.1. Heat exchangers

Heat exchangers are important parts of industrial installations. There are several types and varieties of heat exchangers [10–12]. In the standard BN-68-2250-01 [13] heat exchangers are divided into: shell and tube shell-and-tube, and plate heat exchangers. Each of these heat

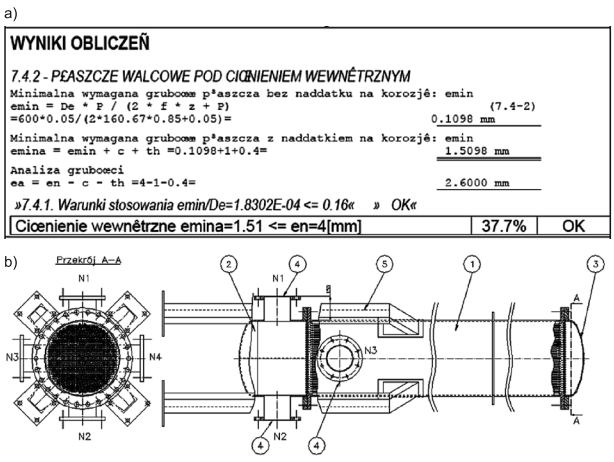

Fig. 1. Stell-and-tube heat exchanger: a – fragment of calculations, b – design solution: 1 – shell, 2 – upper head, 3 – lower head, 4 – nozzles, 5 – legs

Rys. 1. Wymiennik ciepła płaszczowo-rurowy: a – fragment obliczeń, b – rozwiązanie konstrukcyjne: 1 – płaszcz, 2 – głowica przednia, 3 – głowica tylna, 4 – króćce, 5 – nogi

exchangers can have a different structure. The most common ones are shell-and-tube heat exchangers. An example of heat exchanger shell calculations made on the basis of Visual Vessel Design program has been shown in Figure 1a whereas in Figure 1b there is the design solution, prepared in accordance with AutoCAD program [14, 15].

In accordance with the standards specified by TEMA [16] the shell–and–tube heat exchanger can be divided into three main components: the shell jacket and the heads: front head and rear head. Each of these elements can have an individual design solution according to the needs.

4.2. Tanks

Tanks constitute a different group of industrial installation components. In general, they are divided into horizontal and vertical tanks. A typical design of the tank, made by means of using AutoCAD, is shown in Figure 2.

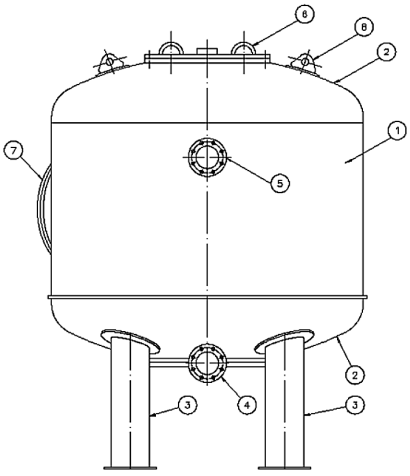

Fig. 2. Tank construction: 1 – shell, 2 – elliptical bottom, 3 – legs, 4, 5 – nozzles, 6, 7 – manhole, 8 – lifting lugs

Rys. 2. Konstrukcja zbiornika: 1 – płaszcz, 2 – dno wyoblone, 3 – nogi, 4, 5 – króćce, 6, 7 – właz, 8 – uchwyty

The tank consists of a shell 1, made of a tube or sheet of plate. Shell elliptical bottoms 2 are welded to the shell 1, closing the tank space. Additional elements welded to the upper and lower shell cover are legs 3 and lifting lugs 8. Besides typical technological nozzles 4 and 5, the tanks should have manholes 6, 7 that enable the internal audit, cleaning, tests and tank repair [14, 15].

4.3. Pipelines

Besides heat exchangers and tanks, towers, separators, pumps etc. are basic components of industrial installations [1–3]. All these components are connected to each other, according

to the diagram, by means of pipelines. The basic elements pipelines are made of are: pipes, flanges, reducing pipes, tees tee-connections, etc.

Figure 3 shows a fragment of the 3D pipeline technical documentation made by means of the Inventor program.

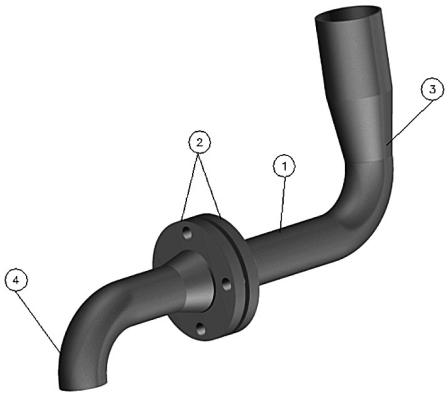

Fig. 3. Pipeline design: 1 – pipe, 2 – flanges, 3 – reducing pipe, 4 – elbow
Rys. 3. Konstrukcja rurociągu: 1 – rura, 2 – kołnierze, 3 – zwężka, 4 – kolano

Fittings that satisfy technological and safety functions are mounted in both the components and pipelines. The fittings include: valves (isolation, throttle, safety), bolts and measurement and control equipment. There are mechanical and thermal loads in the fittings and thus it must be selected according to its guidelines included in designed standards in order to ensure not only the implementation of tasks resulting from the ongoing process, but also for safety [14, 15].

5. Conclusions

Designing industrial installations is a great challenge for designers. Variety of issues arising in many areas require a lot of designer's experience and the proper coordination of a project preparation. The use of CAD software for design significantly improves the quality of projects and accelerates the time of their execution. A designer can use the library of ready-made elements, and add new ones if needed. Making changes in the design and review of documentation is done in an easy way. It is possible to check systematically if there are no errors in the project, which reduces the costs of modification during the construction. An important advantage of the CAD software is the ability to present a 3D installation model system, particularly during the evaluation of the project installation correctness.

References

[1] Pikoń J., *Aparatura chemiczna*, Państwowe Wydawnictwo Naukowe, Warszawa 1983.
[2] Pikoń J., *Podstawy konstrukcji aparatury chemicznej*, Część I i II, Państwowe Wydawnictwo Naukowe, Warszawa 1979.

[3] Wilczewski T., *Pomoce projektowe z podstaw maszynoznawstwa chemicznego*, Wydawnictwo Politechniki Gdańskiej, Gdańsk 2008.
[4] Warunki Urzędu Dozoru Technicznego WUDT/UC/2003 Urządzenia Ciśnieniowe, Wydanie I, Warszawa 2003.
[5] Dyrektywa Parlamentu Europejskiego 97/23/WE w sprawie zbliżenia przepisów prawnych państw członkowskich dotyczących urządzeń ciśnieniowych, 1997.
[6] Materiały firmy Ohm Tech A/S.
[7] OHMTech (www.ohmtech.no).
[8] Broszury firmy Autodesk.
[9] Autodesk (www.autodesk.com).
[10] Kalinowski E., *Przekazywanie ciepła i wymienniki*, OWPW, Wrocław 1995.
[11] Rubik M., *Chłodnictwo*, PWN, Warszawa 1979.
[12] Kuppan T., *Heat exchanger design handbook*, Marcel Dekker, Inc, United States of America, 2000.
[13] BN-68-2250–01 Wymienniki ciepła. Podział oznaczenia i klasyfikacja.
[14] Olszak A., Kęsy Z., Kęsy A., *Problematyka projektowania i wytwarzania instalacji przemysłowych*, Mechanik, nr 1, 2012, s. 31, na załączonej płycie CD.
[15] Olszak A, Kęsy Z., *Obliczanie wymienników ciepła z wykorzystaniem specjalistycznych programów komputerowych*, Mechanik. nr 12, 2011, s. 987, na załączonej płycie CD.
[16] Tubular Exchanger Manufacturers Association (www.tema.org).

TECHNICAL TRANSACTIONS | **CZASOPISMO TECHNICZNE**
MECHANICS | MECHANIKA
1-M/2013

ANDRZEJ OPALIŃSKI*, WOJCIECH TUREK*, MIROSŁAW GŁOWACKI*

INFORMATION MONITORING BASED ON WEB RESOURCES

MONITORING INFORMACJI W OPARCIU O ZASOBY SIECI WEB

A b s t r a c t

The paper summarizes the system for WEB resources monitoring based on defined query. Experiment compares results returned by the proposed system to those provided by Google Search and Google Alert services. Results indicate that the system could be solid base for development and tests of pattern detection and information retrieval mechanism, while providing more data than Google solutions. Drawback of system and further development plans are also presented.

Keywords: *crawling*, *WEB monitoring*, *information retrieval*

S t r e s z c z e n i e

W artykule przedstawiono architekturę systemu monitorującego zasoby sieci WEB pod kątem zdefiniowanego zapytania. Wyniki działania systemu porównano z prowadzonym w tym samym czasie monitoringiem za pomocą mechanizmów oferowanych przez Google. Rezultaty wskazują, że system może być przydatną bazą do badania mechanizmów wykrywania wzorców i wyszukiwania informacji, udostępniając więcej danych w porównaniu do mechanizmów Googla. Wykazano też niedoskonałości aktualnej wersji systemu wynikające ze specyfiki źródeł danych i zaproponowano kierunki jego rozwoju.

Słowa kluczowe: *crawling*, *monitoring Internetu*, *wyszukiwanie informacji*

* MSc. Eng. Andrzej Opaliński, PhD. Eng. Wojciech Turek, Prof. Eng. Mirosław Głowacki, Department of Applied Computer Science and Modelling, Faculty of Metals Engineering and Industrial Computer Science, AGH University of Science and Technology.

1. Introduction

The growth of the World Wide Web, which has been observed over last years, has resulted in the greatest base of electronic data. It is even hard to estimate real size of the Web. The WorldWideWebSize.com portal claims that the most popular search services index more than 50 billion Web pages [1]. In 2008 Google published an information, that the indexer found 1 trillion unique addresses [2]. These estimates definitely do not show the real size of the Web because the indexers deliberately ignore particular fragments, like content generators, link farms or pages with illegal content.

The features of the Web pose huge challenges for searching systems. The size itself creates significant scalability and performance issues. What is more, it is very hard to acquire information about a content which is really looked for by an user and detect pages containing information needed by an user.

WEB crawling in information retrieval domain is well described issue, spread along with the Internet development. Numerous summarized surveys were made in this topic [3,4]. Many researchers described information retrieval related problems, and presented their own solutions to deal with it. Pandey used agent-based system to solve the problem of crawling order [5], Manku et.al. focused on finding and eliminating duplicates in crawl process [6], and Broder et.al. proposed efficient mechanism for url caching in this research area [7].

Mostly due to the scale problem, there are still many unresolved aspects in this area. Publicly available Web search services offer access to very simple and fast ways of finding pages. This method of finding information in the Web is used every day by each Internet user. However, several significant drawbacks and limitations of the approach do exist. Firstly, if several pages contain all specified words, ordering of results is imposed by the search engine. Sorting is typically based on webpage's popularity. This feature connected with the limit in the number of found pages, results in inability of finding some pages. Secondly, the query language is typically very simple. It is impossible to express advanced patters concerning sentences or use of synonyms. It is even impossible to describe clearly the rules specifying letters casing, distance between words or words ordering. Thirdly, low frequency of crawling causes outdated results. The searchers often find pages which contain different content than expected or no longer existing one.

These limitations encourage researchers to continue work on different ways of finding valuable information in the Web. The subject of focused crawling has received significant attention over the last few years. The idea of a crawler which can select pages relevant to a specified topic [8] has been implemented using various techniques [9, 10]. Most obvious application of a focused crawler is a topic-specific search service, which can provide more accurate results.

Use of index-based search engines can successfully direct a user to potentially interesting Web sites. However, when the content of the Web sites changes fast and the information must be detected as soon as possible after it is published, indexing-based methods becomes insufficient. When a user knows where to look for results, but it is impossible to watch the Web sites continuously, a different approach to the problem of searching the Web is needed.

A lot of proprietary tools is offered for WEB crawling purposes. Even Microsoft released this kind of software, called FAST Search Web crawler, as a part of Share Point Server 2010

[11]. There are also a few open sources solutions, compared by Girardi [12]. One of the most popular is Heritix [13] and Websphinx [14]. Those tools allows to crawl and collect data from specified domains, but scalability and more advanced modifications are the drawbacks. Many companies offers such services, returning just a results, based on requested query. Of course such a services are not free of charge, and providers does not present an algorithm of their solutions. There is also one common free service of this type – Google Alert [15]. It offers query monitoring and returns results as a link sent by an email.

In this paper, a system for crawling and monitoring selected fragments of the Web is presented. It provides a service, which can monitor precisely specified fragments of the Web and actively report when a particular pattern is found in newly-published content. Possible applications of the system include monitoring auctions services or job advertisements. It can also be used by law enforcement services for detecting illegal content quickly.

Monitoring of Polish Internet resources for query "shale gas energetics" is presented as an experiment. Results returned by proposed system are compared to the results provided by Google Search Engine and Google Alert service for the same time and query.

2. The architecture of the presented system

The architecture of the system is inspired by a Java-based general purpose Web crawler with indexer presented in [16, 17]. The system can be deployed in three different ways. The less hardware-expensive version is to deploy the system on single PC computer, where all components are running on the machine. This configuration uses particular settings, that significantly limit required system resources and can be used only for monitoring several small Web domains. The second version is a sever based deployment, where a MySQL database server and an JBoss application server are executed on a powerful machine. In this configuration several users can use the same server. Tests showed that a single server can process around 100 000 Web pages every hour. The most robust configuration is based on cluster of servers. It could be used to monitor large data sources, because the performance of processing in this configuration can be easily increased by adding new servers to the cluster.

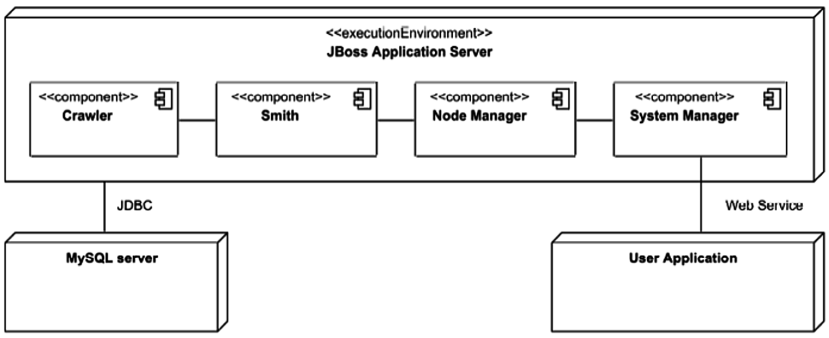

Fig. 1. Abstract architecture of the Web Monitoring System

Rys. 1. Architektura systemu monitoringu informacji w oparciu o dane z sieci WEB

The abstract architecture of the system, which consists all main components is presented in Figure 1. The Crawler component is a single processing thread. It contains a queue of URLs to download and analyze. It is responsible for performing all operations needed to process a Web Page – details on processing algorithms will be presented in the next section. The most important result of the processing is URLs detection – the URLs are returned to the Smith Component. The Client application uses provided Web Service interface. While running configured on cluster of servers The Smith component controls multiple Crawler threads. It starts specified number of Crawlers, manages URLs queues, receives found URLs and communicates with the Node Manager. When running in cluster-based configuration each node used by a system has a single Node Manager which is responsible for communication with global System Manager. The System Manager is responsible for controlling nodes. It collects and distributes found URLs, performs distributed search and provides access to management interface of every node. It also provides a Web Service interface for clients of the system.

3. Resources Processing Algorithm

The most important part of the system is implemented by the Crawler component. It performs processing of Web pages content downloaded from the Internet. A diagram of steps performed by the Crawler is shown in Figure 2. The process of crawling is controlled by the Manager, which keeps a queue of URLs to process. All URLs found by the node are stored in the Urls database. The Manager continuously executes the processing sequence, that consists of the following steps:

– Resource downloading, which results in HTML source stored in a memory buffer,
– HTML parsing by the Lexer and the document model building,
– Changes detection algorithm, avoid storing already processed webpages,
– Content processing by various plugins.

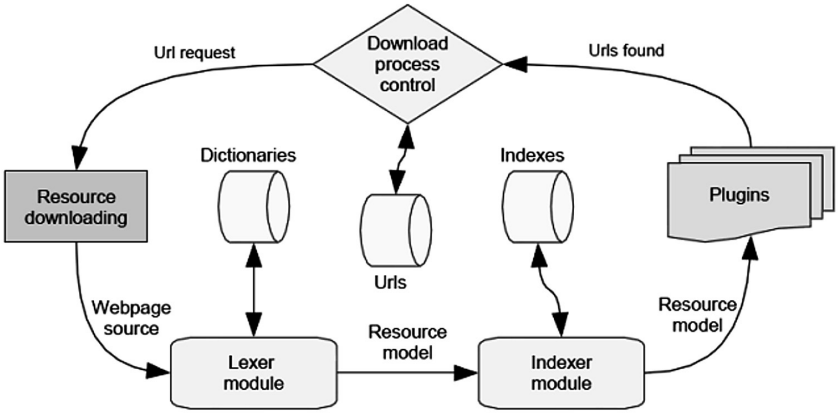

Fig. 2. Processing performed by a single crawler component

Rys. 2. Proces przetwarzania pojedynczego crawlera

This sequence is being executed by every single URL which appears on the list of the Manager. The following sections provide more details on the processing algorithms.

3.1. Parsing and Resource Model Building

The Lexer converts HTML source into a resource model. The model represents a tree structure built of segments. Each segment represents a selected structural element of a Web page (tables, paragraphs and lists). Segment can contains other segments, or can be leaf--segment, containing lists of words, special characters and HTML tags. Each element of the HTML source is converted to an element of the tree structure or to a token. There are three basic types of tokens: words, tags and special characters and each token has its unique identifier. The content of each leaf segment is converted into a list of identifiers, making following processing very efficient.

The dictionary of words is a very large data structure. Average Web page contains several thousand words, however typically very few are new words. Nevertheless, the size of the words dictionary can reach millions of entries after a few days of crawling. Therefore the implementation uses large in-memory caches based on hash maps to make the word-to--identifier conversion as fast as possible.

3.2. Changes Detection Algorithm and Content Processing

The changes detection algorithm is based on hash codes calculated for analyzed content. The hash code for a segment containing is calculated using tokens' ids based on the idea used by Java String class implementation. The hash codes are calculated for every leaf segment. If the hash code has been found in any previous processing of the same Web page, the segment is considered unchanged and is not processed any further.

To determine what values of hash codes have been already processed, the Content cache database is used. It stores all hash codes of leaf segments found in the page content. Leaf segments that are considered new or modified, are processed by all enabled plugins.

There is one plugin which is mandatory for proper functioning of the system. The URL detector plugin must be enabled for continuation crawling process. It finds URLs in the content of provided segments, searching for anchor HTML tags. The pattern detection plugin used in the presented version of the system is based on the list of optional words, and required match threshold. A segment will match the pattern if the number of specified words found in the segment exceeds the threshold. This plugin can also use stems instead of words. Other efficient methods for patterns detection could be applied by implementing further plugins. This mechanism provide much more flexibility than the query languages provided by the most popular publicly available search services.

4. Experiments and evaluation

To test the presented system an experiment was performed. The monitored query was "shale gas energetics" and it was applied to the Google Search and and Google Alert services. As a source for the proposed system, there were selected 7 websites of the Google Results list,

with highest rank by Alexa web metric [18]. It tends to be the most popular and dynamically changing its content, while it's expected to be the best source for an experiment. Results of the test, which lasted for 70 hours are presented in Table 1.

Table 1

Number of results returned by systems

Domains	Presented system				Google				
	distinct urls	urls with content changes	content related	content related after 9 hours	Google Search	"site:"	"site:"+ duplic.	total count	Google Alert
1	680	1001	47	26	43	564	601	2010	2
2	619	4072	1165	871	11	523	603	3300	2
3	3402	4748	82	28	10	408	607	9660	0
4	3414	4411	21	11	7	632	684	37100	0
5	9268	24556	343	186	11	612	650	10500	1
6	59	82	1	0	6	305	333	1900	0
7	1	1	0	0	4	77	86	77	0

Domains: 1 – serwisy.gazetaprawna.pl, 2 – gazownictwo.wnp.pl, 3 – wyborcza.biz, 4 – forsal.pl, 5 – cire.pl, 6 – egospodarka.pl, 7 – energetyka.pl

Selected domains were crawled by presented system every 6 hours, with the average single crawl time about 30 minutes. Match pattern threshold was set to 2 of 3 words. Results of total crawl period for exemplary domain are presented in Figure 3. Over 90% of results are collected after first crawl process. A logarithmic scale has to be apllied to present the results. Table 1 contains results corresponding to each domain. Values in columns represents: 1 – domain ID, 2 – total number of distinct URLs containing pattern, 3 – total number of URLs, including changing content, 4 – number of webpages with HTML title related to the query, 5 – number of URLs including results after 9th hour of the test – that is comparable to the Google Alert service results. Values in columns corresponding to Google part of table are: 7 – number of urls from domain returned by default Google Search, 8 – number of results with "domain:" option set (results just from specified domain), 9 – "domain:" option including duplicates, 10 – declared number of results, 11 – number of results returned by Google Alert service.

There are some interesting observations, that could be concluded by examination of those results. At first, the number of results returned by default Google Search is just a minor part (1–7%) of results from entire domain – obtained by "site". Most default Google Search results are links from static domains – only 15% comes from news portals, and only 11% comes from domain that are later sources for Google Alerts. Google Search engine has never returned more than 684 result links. It reported up to 37100 total results, but did not returned links to the remaining part of results. Google Alert service returned just 6 results during the experiment duration. It correspond to more than 1000 results returned by the system presented in this article. Vast number of results is an effect of trivial content changes algorithm, vulnerable to a dynamic add-keyword-tags systems, which are applied with common keywords, that was a part of our query.

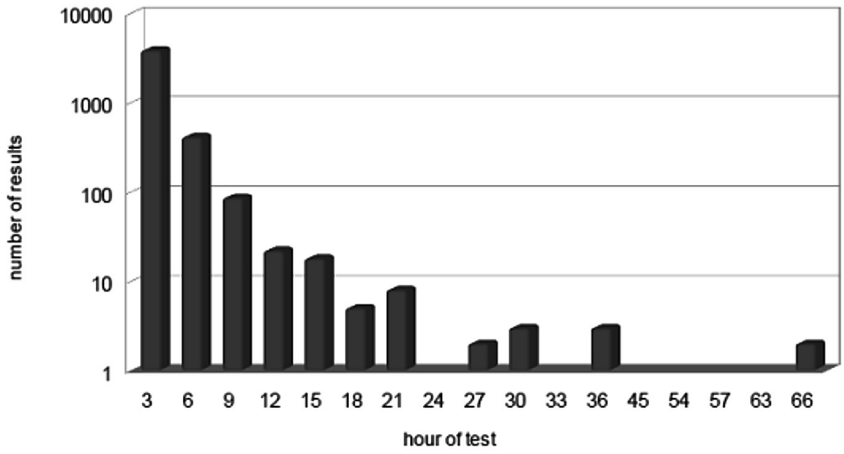

Fig. 3. Results number for forsal.pl domain
Rys. 3. Liczba rezultatów w dla domeny forsal.pl

5. Conclusions and Further Work

The results of the tests highlighted presented system weaknesses and benefits. First is the consequence of trivial content change detection algorithm – high rate of false positive results number, based on tag-keywords html segments. It is very susceptible applied to popular keywords. Advanced methods of content meaning recognition are also required for application in information retrieval domain. Although the benefits of proposed architecture are undeniable. It provides convenient base to testing and development algorithms for pattern detection and information retrieval. It could be adopted to particular user needs, by specifying advanced detection algorithm and provide large amount of data for further processing. It grants an independence comparing to the usage of Google services, where user has very limited influence of returned results. Also scalability is a great advantage, as the system could be configured to be launch as low-cost or cluster-based configuration.

Where Google services are useful in simple and general use cases, presented system gives the potential to by much more flexible and adaptable in more advanced purposes.

Further research should account implementing advanced techniques of subject detection and dynamic tagging independence. Also methods for defining advanced content patterns should be developed. The possibility of defining semantic meaning of the content or similarity to a given text, rather than specifying a list of words, would be very useful.

References

[1] Kunder M., *WorldWideWebSize.com*, 12.2012.
[2] Alpert J., Hajaj N., *We knew the web was big...* (http://tinyurl.com/crzays7–25.07.2008).

[3] Croft, W.B., Metzler D., Strohman T., *Search engines: Information retrieval in practice*, Addison-Wesley 2010.
[4] Kobayashi M., Takeda K., *Information retrieval on the web*, ACM Computing Surveys (CSUR), 32(2), 2000, 144-173.
[5] Pandey S.K., Mishra R.B., *Intelligent Web mining model to enhance knowledge discovery on the Web*, In Parallel and Distributed Computing, Applications and Technologies, 2006. PDCAT'06. Seventh International Conference on, 339-343, IEEE.
[6] Manku G.S., Jain A. & Das Sarma A., *Detecting near-duplicates for web crawling*, In Proceedings of the 16th international conference on WWW, 141-150, ACM, 2007.
[7] Broder A.Z., Najork M., Wiener J.L., *Efficient URL caching for world wide web crawling*, In Proc. of the 12th international conf. on WWW, 679-689, ACM, 2003.
[8] Menczer F., Belew R.K., *Adaptive Information Agents in Distributed Textual Environments*, Proc. of the 2nd Int. Conf. on Autonomous Agents, ACM, 1998, 157-164.
[9] Dong H., Hussain F.K., Chang E., *State of the Art in Semantic Focused Crawlers*, Computational Science and Its Applications, Seoul, Korea, 2009, 910-924.
[10] Dorosz K., Korzycki M., *Latent Semantic Analysis Evaluation of Conceptual Dependency Driven Focused Crawling*, Multimedia Communications, Services and Security, 5th International Conference, MCSS 2012, Krakow 2012, 77-84.
[11] *Crawling Web content with the FAST Search Web crawler*, MS SharePoint library (http://technet.microsoft.com/en-us/library/ff383271%28v=office.14%29.aspx).
[12] Mohr G., Stack M., Rnitovic I., Avery D., Kimpton M., *Introduction to heritrix*, In 4th International Web Archiving Workshop, 2004.
[13] Miller R., *Websphinx, a personal, customizable web crawler* (http://www. cs. cmu. edu/~ rcm/websphinx – 2011-02-12).
[14] Girardi C., Ricca, F., Tonella, P., *Web crawlers compared*, International Journal of Web Information Systems, 2(2), 2006, 85-94.
[15] *Getting Started Guide – What are Google Alerts?* (http://tinyurl.com/csr4z3b).
[16] Turek W., Opaliński A., Kisiel-Dorohinicki M., *Extensible Web Crawler – Towards Multimedia Material Analysis*, Multimedia Communications, Services and Security, 4th International Conference, MCSS 2011, Krakow 2011, 183-190.
[17] Wilaszek K., Wójcik T., Opaliński A., Turek W., *Internet Identity Analysis and Similarities Detection*, MCSS 2012, Krakow 2012, 369-379.
[18] Alexa – provider of global web metrics (http://www.alexa.com – 01.2013).

TECHNICAL TRANSACTIONS | CZASOPISMO TECHNICZNE
MECHANICS | MECHANIKA
1-M/2013

KAROL OSOWSKI*, MARCIN MIGUS**, ANDRZEJ KĘSY*

EXPERT SYSTEM FOR SUPPORTING THE PROCESS OF HYDRODYNAMIC TORQUE CONVERTER CONSTRUCTION

SYSTEM EKSPERTOWY WSPOMAGAJĄCY PROCES KONSTRUOWANIA PRZEKŁADNI HYDROKINETYCZNEJ

A b s t r a c t

This paper presents an advisory expert system to assist the process of constructing the hydrodynamic torque converter. The system has been constructed using program Delphi 7 Enterprise in Object Pascal. The system includes three types of means of transport, a car, a rail bus and a working machine.

Keywords: *expert systems*, *computer aided design*, *hydrodynamic torque converter*

S t r e s z c z e n i e

W artykule przedstawiono doradczy system ekspertowy wspomagający proces konstruowania przekładni hydrokinetycznej. System zbudowano z użyciem programu *Delphi 7 Enterprise* w języku *Object Pascal*. W systemie tym uwzględniono trzy rodzaje środków transportu, w którym przekładnia hydrokinetyczna pracuje: samochód osobowy, autobus szynowy i maszynę roboczą.

Słowa kluczowe: *systemy ekspertowe*, *komputerowe wspomaganie konstrukcji*, *przekładnia hydrokinetyczna*

* MSc. Karol Osowski, prof. PhD. Eng. Andrzej Kęsy Institute of Applied Mechanics and Energetics, Faculty of Mechanical Engineering , Kazimierz Pulaski University of Technology and Humanities in Radom.

** PhD. Eng. Marcin Migus, The State School of Higher Education in Sandomierz.

Symbols

η_{75} – economic range of operation
η^* – maximum efficiency
χ_p – computational durability
$\lambda_{M,i}$ – moment coefficient
α_1, α_2 – damping factor for pump and turbine impellers
S – execution cost
g – metal consumption factor
i_{d0} – dynamic transmission ratio
n_p – idle gear loss coefficient
i_M – coefficient of torque limit
$\lambda_{A,i}$ – coefficient of axial force
i_ω – coefficient of speed reduction
p – permeability
X – coefficient of stiffness performance
β_{11} – blade angle at the entrance of the pump impeller
β_{12} – blade angle at the exit of the pump impeller
β_{21} – blade angle at the entrance of the turbine impeller
β_{22} – blade angle at the exit of the turbine impeller
β_{31} – blade angle at the entrance of the stator impeller
β_{32} – blade angle at the exit of the stator impeller
r_{12} – radius of the average line at the exit to the pump impeller
r_{21} – radius of the average line at the entrance to the turbine impeller
r_{22} – radius of the average line at the exit to the turbine impeller
J_1, J_2 – moments of inertia of the input shaft
c_1, c_2 – stiffness of the input shaft
l_2 – length of the average line

1. Introduction

A hydrodynamic transmission system (HTS) is a part of the propulsion system in the ground transportation using the kinetic energy of the working fluid. No permanent connection between the input shaft and the output shaft causes no shock loads transferred from the working tool to the propulsion system. The main advantage of the HTS is shifting in relation to the applied load. Furthermore, it effectively reduces the dynamic load and damping vibration, thus highly increasing the durability of the propulsion system [1]. One of the major disadvantages of the HTS is low maximum efficiency and narrow range of high efficiency as a function of the speed ratio. The basic element of a HTS consists of an hydrodynamic sub-assembly which includes: torque converters, clutch or brake. The most complicated component in the design is the hydrodynamic torque converter (HTC) which is composed of three impellers: pump, turbine and the stator as it is shown in Figure 1.

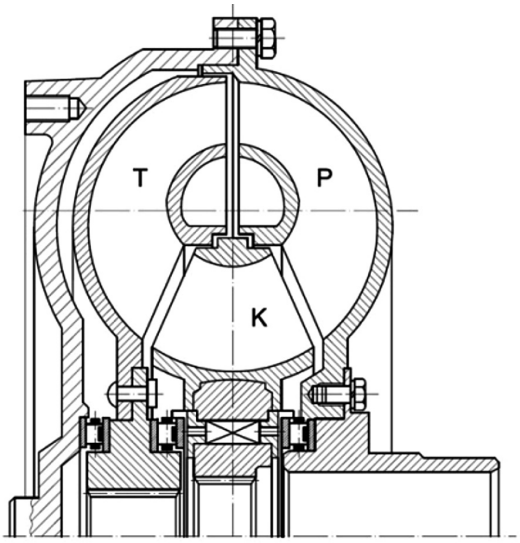

Fig. 1. Construction of the hydrodynamic torque converter [2]: *P* – pump impeller, *T* – turbine impeller, *K* – stator impeller
Rys. 1. Budowa przekładni hydrokinetycznej [2]: *P* – koło łopatkowe pompy, *T* – koło łopatkowe turbiny, *K* – koło łopatkowe kierownicy

The impellers consist of blades that with together the housing create the work area for the working fluid.

The introduction of modern low-speed engines using alternative fuels, the requirement of exhaust emissions reduction and the increase of the efficiency of the propulsion system reducing fuel consumption means that the torque converter design process is very current and important. Too low accuracy of existing mathematical models results in a large discrepancy between the requirements and the resulting characteristics of the HTC. The failure to comply with the prescribed requirements results in the deterioration of the characteristics of the propulsion system and forms of economic losses.

The development of the methodology supporting the process of constructing the HTC by using expert system can resolve the existing problems of the construction. The benefits of using this solution can include not only economic aspects in the form of increasing the efficiency, but also the optimal choice of torque converter for a given mode of transport.

Expert systems are complex computer programs that use knowledge derived from subject matter experts sources. They consist of three main components: the interface, inference engine and a knowledge base. Such systems are increasingly being used in the design and operation of machines and equipment. They can be divided into advisory, diagnostic and decision-making systems. Are widely used in supporting the construction process advisory systems [3], their main task is to solve a problem using the knowledge contained within the database.

This paper presents an advisory system for supporting the process of design the HTC.

2. Advisory expert system to assist in the process of designing a hydrodynamic torque converter

The presented system in the paper the which support the design of a HTC is an advisory expert system software based on the collected data [4]. The system has been developed using *Delphi 7 Enerprise* software with the help of object-oriented programming language – *Object Pascal*. The result of the working system is the choice of the optimum design solution for the design of a HTC. Solving the decision-making problems in the system is done by selecting:
– optimal torque converter evaluation index for the predefined means of transport,
– optimal design parameters having an impact on the rate of the highest evaluation,
– field variation of the optimal design parameters.

The diagram of the system in the form of a decision tree is shown in Figure 2.

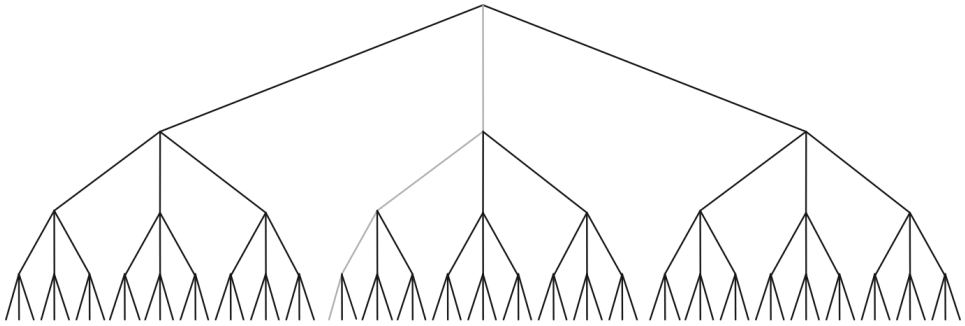

Fig. 2. A decision tree system supporting the process of designing a hydrodynamic torque converter
Rys. 2. Drzewo decyzyjne systemu wspomagającego proces konstruowania przekładni hydrokinetycznej

The selection of the optimal values of the assessment indicators, construction parameters and their ranges of variation have been implemented for a passenger car, a rail bus and a working machine.

A knowledge base of the advisory expert system to support the process of designing the hydrodynamic torque converter has been developed on the basis of domain subject matter experts opinions and professional literature in the field of HTS such as: scholarly articles, books, standards, patents. The knowledge base includes:
– assessment indicator impact on a means of transport,
– the impact of construction parameters on the assessment indicators,
– ranges of the construction parameters variability.

The knowledge base has been divided into various sources of data provenance. The data obtained during the point assessment method as well as the data from books, articles, JCR and standards [5] has been implemented. The data coming from various literature sources has been divided into experimental and theoretical ones. In addition, arbitrary coefficients of confidence have been introduced for all the data. A division of the knowledge base fragment is shown in Figure 3.

SYEXP2

```
{MASZYNA ROBOCZA}
  Procedure Dane1m;{Dane dla etamax - maszyna robocza}
 begin
  ocenaeksperta:= 161; maxpunktow:=180;
  wksiazkach:=3; wartykulachJCR:=7; winnych:=9;
  eksperymentalne:=10; teoretyczne:=9;
  u1:=0.9; u2:=0.9; u3:=0.9;
 end;
  Procedure Dane2m;{Dane dla id0max - maszyna robocza}
 begin
  ocenaeksperta:= 178; maxpunktow:=180;
  wksiazkach:=4; wartykulachJCR:=6; winnych:=2;
  eksperymentalne:= 10; teoretyczne:=2;
  u1:=1; u2:=1; u3:=0.9;
 end;
```

Fig. 3. A division of the knowledge base fragment

Rys. 3. Podział fragmentu bazy wiedzy

The inference engine retrieves data from a knowledge base with some weights. The value of "1" is assigned to the data coming from the books, the value of "0.8" to the articles of the JCR and the value of "0.5" to other literature sources.

3. Indicators assessment and design parameters

Completely different working conditions of ground transportation cause that the propulsion system is subjected to different types of resistance, and hence there are various types of loads. The HTC design requires the determination of the requirements for a given means of transport, including the expected load, or cooperation with the propulsion system. To ensure the optimal design the following requirements kinematic, dynamic, productive, economical and exploitation ones should be taken into account in order to ensure the optimal design. Assessment indicators have been introduced to check if HTC meets the requirements and to assess the impact of design parameters on the design process [2, 5]. When selecting a HTC for a given means of transport which operates in very specific conditions, the assessment indicator is to achieve its optimal value.

Assessment indicators chosen for the HTC which have been subjected to the expert point assessment method [5–7] have been selected they are affected by a large number of construction parameters: η_{75}, η^*, χ_p, $\lambda_{M,i}$, α_1, α_2, S, g, i_{d0}, n_p, i_M, $\lambda_{A,i}$, i_ω, p, X. Next the indicators have been evaluated by subject – matter experts. The level of validity of the assessment indicators for a given means of transport using the point assessment method [5] has been evaluated by experts. The indicators have been assessed on the scale 0 to 180. The results are shown in Table 1.

For each means of transport three assessment indicators with most points have been selected and they have been implemented to the knowledge base of the advisory expert system.

In order to obtain optimum values of the HTC assessment indicators is the structural parameters directly affecting the assessment indicators must be changed. Design parameters with greatest impact on the assessment indicators evaluated by means of the assessed using point assessment expert method [4, 6], have been selected. They are: β_{22}, β_{32}, β_{12}, r_{12}, J_1, r_{21}, r_{22}, J_2, β_{21}, β_{11}, c_1, c_2, β_{31}, l_2.

Table 1

Assessment indicator impact on a selected means of transport

	Passenger car	Rail bus	Working machine
η_{75}	148	176	164
η^*	158	158	174
χ_p	134	98	78
$\lambda_{M,i}$	88	122	112
α_1, α_2	111	95	100
S	82	68	75
g	123	114	102
i_{d0}	172	148	56
n_p	48	68	126
i_M	92	75	93
$\lambda_{A,i}$	116	46	69
i_ω	77	123	112
p	58	88	148
X	66	48	96

The parameters were subjected to subject matter experts evaluation. The experts assessed the impact of various design parameters on the indicators [5] by using the point assessment method. The parameters were assessed on 0 to 180 points scale. The results are shown in Table 2.

Three design parameters with the highest score have been selected and implemented to the knowledge base of the advisory expert system.

The ranges of design indicator variability have been selected on the base of current HTC construction and they have been evaluated by subject matter experts on 0 to 180 scale. The results are shown in Table 3.

Table 2

Design parameters impact on the indicators of the hydrodynamic torque converter

	η_{75}	η^*	i_{d0}	p
β_{22}	168	162	128	118
β_{32}	172	143	166	122
β_{12}	162	140	149	136
r_{12}	112	98	85	75
J_1	88	48	102	98
r_{21}	78	66	59	66
r_{22}	67	104	100	88
J_2	74	62	84	60
β_{21}	166	122	116	162
β_{11}	168	138	141	144
c_1	112	110	66	78
c_2	88	90	110	94
β_{31}	175	144	170	128
l_2	66	50	65	70

Table 3

Ranges of design of parameter variability

	Range I	Range II	Range III		Range I	Range II	Range III
β_{22}	129–139	139–148	148–160	β_{21}	30–45	45–50	50–75
Rating	122	164	125	Rating	149	88	138
β_{32}	20–30	30–40	40–50	β_{11}	90–102	102–114	114–130
Rating	158	98	48	Rating	111	166	102
β_{12}	75–100	100–125	125–150	β_{31}	70–92	92–114	114–140
Rating	74	148	134	Rating	66	165	78

4. The result of the system performance

The optimal design solution suggested by the described expert system for the HTC is following:

– for a passenger car – assessment index p and the construction parameter β_{12} (75º – 100º),
– for rail bus assessment index i_{d0} and the construction parameter β_{12} (125º – 150º),
– for a working machine – evaluation index $\eta*$ and the construction parameter β_{32} (20º – 30º).

5. Conclusions

1. The expert system for each means of transport chooses the assessment indicator which is to achieve the max. The process is carried out by choosing the design parameter and the variability range of this parameter.
2. Inference system is based on the data contained in the knowledge base.
3. The knowledge base is separated from the rest of the program, which allows for continuous modification and the data completion.

References

[1] Kęsy A., Kęsy Z., *Damping Characteristics of a Transmission System with a Hydrodynamic Torque Converter*, J. of Sound and Vibration, 16/3, 1993.
[2] Kęsy A., *Modele bryłowe w konstrukcji podzespołów hydrokinetycznych*, Wydawnictwo Politechniki Radomskiej, Radom 2012.
[3] Pokojski J., *Systemy doradcze w projektowaniu maszyn*, WNT, Warszawa 2005.
[4] Osowski K., Migus M., Kęsy A., *Assumptions for Expert System Creation to Assess Durability of Hydrodynamic Transmission System*, The XIIth International Scientific IFToMM Conference "Tribology and Reliability", Sankt Petersburg 24–26 October 2012, CD, 2012.
[5] Stesin S.P., *Optymalizacja parametrów hydrodynamicznych przewodów maszyn budowlanych i drogowych*, *Budowa maszyn,* Moskwa 1996 (tłum. autor z cyrylicy).
[6] Kęsy A., *Numeryczna identyfikacja i optymalizacja napędów hydrokinetycznych środków transport*u, Wydawnictwo Politechniki Radomskiej, Radom 2004.
[7] Kęsy Z., Kęsy A., Madeja J., *Identyfication of Hydrodynamic Torque Converter Controlled by Physical Properties of Working Fluid*, Int. Conference „Modern Practice In Stress and Vibration Analysis", Dublin 1997.

TECHNICAL TRANSACTIONS | **CZASOPISMO TECHNICZNE**
MECHANICS | MECHANIKA
1-M/2013

RAFAŁ PALEJ*

CUBICALLY CONVERGENT METHOD FOR SOLVING A STANDARD BOUNDARY VALUE PROBLEM

SZEŚCIENNIE ZBIEŻNA METODA ROZWIĄZYWANIA STANDARDOWEGO ZAGADNIENIA BRZEGOWEGO

Abstract

The paper presents a cubically convergent method for solving a standard boundary value problem consisting of n coupled first-order differential equations and n boundary conditions. The idea of the presented method is based on the shooting method using the expansion of the desired function into Taylor's series including second-order derivatives. Effective use of the iteration formula requires introduction of sensitivity functions and their derivatives. In each iteration, the initial problem, composed of $n(1+n_1+n_1^2)$ first-order differential equations, must be solved, where n_1 signifies the number of unknown parameters. The convergence of the presented method has been illustrated on an example.

Keywords: *shooting method, sensitivity functions*, *derivatives of sensitivity functions*, *cubic convergence*

Streszczenie

W artykule przestawiono sześciennie zbieżną metodę rozwiązywania standardowego zagadnienia brzegowego składającego się z n sprzężonych równań różniczkowych pierwszego rzędu i n warunków brzegowych. Idea prezentowanej metody oparta jest na metodzie strzałów wykorzystującej rozwinięcie poszukiwanych funkcji w szereg Taylora uwzględniający pochodne drugiego rzędu. Efektywne skorzystanie ze wzoru iteracyjnego wymaga wprowadzenia funkcji wrażliwości i ich pochodnych. W każdej iteracji należy rozwiązać zagadnienie początkowe składające się z $n(1+n_1+n_1^2)$ równań różniczkowych pierwszego rzędu, gdzie n_1 oznacza liczbę nieznanych parametrów. Zbieżność prezentowanej metody zilustrowano na przykładzie.

Słowa kluczowe: *metoda strzałów*, *funkcje wrażliwości*, *pochodne funkcji wrażliwości*, *zbieżność sześcienna*

* Prof. Rafał Palej, Institute of Applied Informatics, Faculty of Mechanical Engineering, Cracow University of Technology.

1. Introduction

A standard two-point boundary value problem consists of n coupled first-order ordinary differential equations as well as n_1 boundary conditions at one end of the domain and a remaining set of boundary conditions at the other end. There are two classes of numerical methods for solving such a problem: the shooting method and the relaxation methods [1]. The shooting method usually implements a quadratically convergent Newton-Raphson method. Faster convergence can be obtained by taking into account the second-order derivatives in the Taylor's expansion. Proceeding in this way, however, leads to obtaining a set of non-linear equations due to the unknown parameters. The non-linear equations may be "made linear" with the use of the Newton-Raphson solution while the cubic convergence of the iteration process is retained. This approach may be used for iterational solving the set of non--linear algebraic equations [2]. In order to use the iteration formula effectively, we need to introduce not only the sensitivity functions [3] but their derivatives as well. The description of the presented method depends on the manner of the formulation the boundary conditions. The paper presents a situation when each desired function has an imposed boundary condition only at one end of the domain.

2. Formulation of the problem

We shall analyze a boundary value problem defined by a set of n first-order differential equations in the following form:

$$\frac{dy_i}{dx} = f_i(x, y_1, \ldots, y_n), \quad i = 1, \ldots, n \tag{1}$$

For the sake of simplification of the subsequent notation, let us assume that each function $y_i(x)$ has the imposed boundary condition only at one end of the domain. We shall also assume that the number of conditions imposed at the initial point of the domain is at least equal to the number of conditions at the final point. Let us number the desired functions in such a way that the lowest indicators are ascribed to the functions that have the imposed boundary conditions at the final point, i.e.

$$y_i(b) = y_{ib}, \qquad i = 1, \ldots, n_1 \tag{2}$$

and then the functions with indicators greater than n_1 will have the imposed boundary conditions at the initial point

$$y_i(a) = y_{ia}, \qquad i = n_1 + 1, \ldots, n \tag{3}$$

In order to replace the boundary value problem with the initial value problem, we need to complete conditions (3) by introducing n_1 unknown parameters.

$$y_i(a) = p, \qquad i = 1, \ldots, n_1 \tag{4}$$

The desired solutions will now be the functions of the variable x and parameters p_i, i.e.

$$y_i = y_i(x, p_1, \ldots, p_{n_i}), \quad i = 1, \ldots, n \tag{5}$$

We want to find such values of parameters p_i that would enable the initial value problem to fulfil the boundary conditions with the prescribed accuracy (2).

3. The method of finding the solution

We shall expand the functions y_i = 1, …, n_1 into the Taylor's series around the trial values of parameters $p_i^{(1)}$, $i = 1,\ldots,n_1$ for $x = b$, including the expressions containing second derivatives. The connection between the value of the i-th function at point $\mathbf{p}^{(2)}$ and the values of the said function and its derivatives at point $\mathbf{p}^{(1)}$ – signifying the first approximation of the unknown parameters, is provided by the Taylor's formula

$$y_i(b,\mathbf{p}^{(2)}) = y_i(b,\mathbf{p}^{(1)}) + \nabla y_i^T(b,\mathbf{p}^{(1)})\mathbf{h}^{(1)} + \frac{1}{2}\mathbf{h}^{(1)T}\mathbf{H}_i(b,\mathbf{p}^{(1)})\mathbf{h}^{(1)} + \ldots, \quad i = 1,\ldots,n_1 \tag{6}$$

where $\mathbf{h}^{(1)} = \mathbf{p}^{(2)} - \mathbf{p}^{(1)}$ while $\nabla y_i^T(b,\mathbf{p}^{(1)})$ and $\mathbf{H}_i(b, \mathbf{p}^{(1)})$ signify the gradient and the hessian of the i-th function.

Relation (6) may also be expressed for all n_1 functions simultaneously in the following form:

$$\mathbf{y}(b,\mathbf{p}^{(2)}) \simeq \mathbf{y}(b,\mathbf{p}^{(1)}) + \mathbf{J}(b,\mathbf{p}^{(1)})\mathbf{h}^{(1)} + \frac{1}{2}\begin{bmatrix} \mathbf{h}^{(1)T}\mathbf{H}_1(b,\mathbf{p}^{(1)})\mathbf{h}^{(1)} \\ \mathbf{h}^{(1)T}\mathbf{H}_2(b,\mathbf{p}^{(1)})\mathbf{h}^{(1)} \\ \vdots \\ \mathbf{h}^{(1)T}\mathbf{H}_{n_1}(b,\mathbf{p}^{(1)})\mathbf{h}^{(1)} \end{bmatrix} \tag{7}$$

where $\mathbf{J}(b, \mathbf{p}^{(1)})$ signifies the Jacobian matrix of function y_i, i = 1, …, n_1.

Looking for vector $\mathbf{h}^{(1)}$, for which $\mathbf{y}(b, \mathbf{p}^{(2)}) = \mathbf{y}_b$, where $\mathbf{y}_b = [y_{1b}, y_{2b}, \ldots, y_{n_1 b}]^T$, we will obtain a non-linear set of equations for the coordinates of vector $\mathbf{p}^{(2)}$ in the form:

$$\mathbf{y}(b,\mathbf{p}^{(1)}) + \mathbf{J}(b,\mathbf{p}^{(1)})\mathbf{h}^{(1)} + \frac{1}{2}\begin{bmatrix} \mathbf{h}^{(1)T}\mathbf{H}_1(b,\mathbf{p}^{(1)})\mathbf{h}^{(1)} \\ \mathbf{h}^{(1)T}\mathbf{H}_2(b,\mathbf{p}^{(1)})\mathbf{h}^{(1)} \\ \vdots \\ \mathbf{h}^{(1)T}\mathbf{H}_{n_1}(b,\mathbf{p}^{(1)})\mathbf{h}^{(1)} \end{bmatrix} = \mathbf{y}_b \tag{8}$$

In the Newton-Raphson method based on the Taylor's formula including only the first derivatives, vector $\mathbf{h}^{(1)}$ is described with the following formula:

$$\mathbf{h}^{(1)} = -\mathbf{J}^{-1}(b, \mathbf{p}^{(1)})\,(\mathbf{y}(b, \mathbf{p}^{(1)}) - \mathbf{y}_b) \tag{9}$$

Substituting expression (9) into the third term of equation (8) we shall obtain

$$\mathbf{y}(b, \mathbf{p}^{(1)}) + \mathbf{J}(b, \mathbf{p}^{(1)})\mathbf{h}^{(1)} + \mathbf{r}(b, \mathbf{p}^{(1)}) = \mathbf{y}_b \tag{10}$$

where vector $\mathbf{r}(b, \mathbf{p}^{(1)})$ is built in the following way:

$$\mathbf{r}(b,\mathbf{p}^{(1)}) = \frac{1}{2}\begin{bmatrix} (\mathbf{y}(b,\mathbf{p}^{(1)})-\mathbf{y}_b)^T\mathbf{J}^{-T}(b,\mathbf{p}^{(1)})\mathbf{H}_1(b,\mathbf{p}^{(1)})\mathbf{J}^{-1}(b,\mathbf{p}^{(1)})(\mathbf{y}(b,\mathbf{p}^{(1)})-\mathbf{y}_b) \\ (\mathbf{y}(b,\mathbf{p}^{(1)})-\mathbf{y}_b)^T\mathbf{J}^{-T}(b,\mathbf{p}^{(1)})\mathbf{H}_2(b,\mathbf{p}^{(1)})\mathbf{J}^{-1}(b,\mathbf{p}^{(1)})(\mathbf{y}(b,\mathbf{p}^{(1)})-\mathbf{y}_b) \\ \vdots \\ (\mathbf{y}(b,\mathbf{p}^{(1)})-\mathbf{y}_b)^T\mathbf{J}^{-T}(b,\mathbf{p}^{(1)})\mathbf{H}_{n_1}(b,\mathbf{p}^{(1)})\mathbf{J}^{-1}(b,\mathbf{p}^{(1)})(\mathbf{y}(b,\mathbf{p}^{(1)})-\mathbf{y}_b) \end{bmatrix} \tag{11}$$

Solving equation (10) with respect to $\mathbf{h}^{(1)}$ we shall obtain the following iteration formula:

$$\mathbf{p}^{(k+1)} = \mathbf{p}^{(k)} - \mathbf{J}^{-1}(b,\mathbf{p}^{(k)})(\mathbf{y}(b,\mathbf{p}^{(k)}) - \mathbf{y}_b + \mathbf{r}(b,\mathbf{p}^{(k)})), \quad k = 1,2,\ldots \tag{12}$$

In order to be able to use formula (12), it is necessary to know the derivatives determining the Jacobian matrix $\mathbf{J}(b,\ \mathbf{p}^{(1)})$ and the Hessian matrices $\mathbf{H}_i\,(b,\ \mathbf{p}^{(1)})$, $i = 1, \ldots, n_1$. To this end we shall differentiate differential equations (1) with respect to individual parameters $p_j, j = 1, \ldots, n_1$.

$$\frac{\partial}{\partial p_j}\left(\frac{dy_i}{dx}\right) = \sum_{k=1}^{n}\frac{\partial f_i}{\partial y_k}\frac{\partial y_k}{\partial p_j}, \quad i = 1,\ldots,n, \quad j = 1,\ldots,n_1 \tag{13}$$

Defining the derivative sensitivity functions with the following formulas

$$g_{kj} = \frac{\partial y_k}{\partial p_j}, \quad k = 1,\ldots,n, \quad j = 1,\ldots,n_1 \tag{14}$$

we shall express equations (13) in the following form

$$\frac{dg_{ij}}{dx} = \sum_{k=1}^{n}\frac{\partial f_i}{\partial y_k}g_{kj}, \quad i = 1,\ldots,n, \quad j = 1,\ldots,n_1 \tag{15}$$

The initial conditions for the sensitivity function will be determined on the basis of formulas (3), (4) and (14)

$$g_{ij}(a) = \frac{\partial y_i(a)}{\partial p_j} = \delta_{ij}, \quad i = 1,\ldots,n, \quad j = 1,\ldots,n_1 \tag{16}$$

where δ_{ij} signifies the Kronecker symbol.

In order to determine the elements of the Hessian matrix, we shall differentiate differential equations (15) with respect to individual parameters p_r, $r = 1, \ldots, n_1$

$$\frac{\partial}{\partial p_r}\left(\frac{dg_{ij}}{dx}\right) = \sum_{k=1}^{n}\left[\sum_{q=1}^{n}\frac{\partial}{\partial y_q}\left(\frac{\partial f_i}{\partial y_k}\right)\frac{\partial y_q}{\partial p_r}g_{kj} + \frac{\partial f_i}{\partial y_k}\frac{\partial g_{kj}}{\partial p_r}\right], i = 1,\ldots,n,\ j = 1,\ldots n_1, r = 1,\ldots,n_1 \tag{17}$$

Defining the sensitivity functions derivatives with the following formulas

$$h_{jr}^{(k)} = \frac{\partial g_{kj}}{\partial p_r} = \frac{\partial^2 y_k}{\partial p_j \partial p_r}, \quad k = 1,\ldots,n, \quad j = 1,\ldots,n_1, r = 1,\ldots,n_1 \tag{18}$$

we shall express equations (17) in the following form

$$\frac{dh_{jr}^{(i)}}{dx}=\sum_{k=1}^{n}\left[\sum_{q=1}^{n}\frac{\partial}{\partial y_q}\left(\frac{\partial f_i}{\partial y_k}\right)g_{qr}g_{kj}+\frac{\partial f_i}{\partial y_k}h_{jr}^{(k)}\right],\quad i=1,\ldots,n,\quad j=1,\ldots,n_1,\quad r=1,\ldots,n_1 \tag{19}$$

The initial conditions for the sensitivity function will be determined on the basis of formulas (16) and (18)

$$h_{jr}^{(i)}(a)=\frac{\partial g_{ij}(a)}{\partial p_r}=0,\quad i=1,\ldots,n,\quad j=1,\ldots,n_1,\quad r=1,\ldots,n_1 \tag{20}$$

Finally, in each iteration we must solve the initial problem consisting of $n(1+n_1+n_1^2)$ equations (1), (15) and (19) and the same number of initial conditions determined by relations (3), (4), (16) and (20). Functions g_{ij} and $h_{jr}^{(i)}$ of indicator i less than or equal to n_1 compose the Jacobian matrix and the Hessian matrices respectively. The remaining functions appear only in differential equations (15) and (19).

4. Numerical example

Let us consider the boundary value problem in the following form

$$y''=\frac{1}{2}\frac{2(1+(y')^2)^{\frac{3}{2}}-(y')^2-1}{1.1-y},\quad \begin{cases} y(0)=0 \\ y'(1)=1 \end{cases}$$

The above problem may be formulated with the use of a set of first-order equations in the form ($y_2 = y$)

$$\begin{cases} \dfrac{dy_1}{dx}=\dfrac{1}{2}\dfrac{2(1+(y_1)^2)^{\frac{3}{2}}}{1.1-y_2} \\ \dfrac{dy_2}{dx}=y_1 \end{cases},\quad \begin{cases} y_1(1)=1 \\ y_2(0)=0 \end{cases}$$

In the problem under consideration we have: $n = 2$, $n_1 = 1$. The initial problem that must be solved in each iteration consists of 6 first order differential equations

$$\frac{dy_1}{dx}=\frac{1}{2}\frac{2(1+(y_1)^2)^{\frac{3}{2}}-(y_1)^2-1}{1.1-y_2}$$

$$\frac{dy_2}{dx}=y_1$$

$$\frac{dg_{11}}{dx}=\frac{\partial f_1}{\partial y_1}g_{11}+\frac{\partial f_1}{\partial y_2}g_{21}$$

$$\frac{dg_{21}}{dx}=\frac{\partial f_2}{\partial y_1}g_{11}+\frac{\partial f_2}{\partial y_2}g_{21}$$

$$\frac{dh_{11}^{(1)}}{dx} = \frac{\partial^2 f_1}{\partial y_1^2} g_{11}^2 + 2\frac{\partial^2 f_1}{\partial y_1 \partial y_2} g_{21} g_{11} + \frac{\partial^2 f_1}{\partial y_2^2} g_{21}^2 + \frac{\partial f_1}{\partial y_1} h_{11}^{(1)} + \frac{\partial f_1}{\partial y_2} h_{11}^{(2)}$$

$$\frac{dh_{11}^{(2)}}{dx} = \frac{\partial^2 f_2}{\partial y_1^2} g_{11}^2 + 2\frac{\partial^2 f_2}{\partial y_1 \partial y_2} g_{21} g_{11} + \frac{\partial^2 f_2}{\partial y_2^2} g_{21}^2 + \frac{\partial f_2}{\partial y_1} h_{11}^{(2)} + \frac{\partial f_2}{\partial y_2} h_{11}^{(2)}$$

and 6 initial conditions

$$y_1(0) = p, \quad y_2(0) = 0, \quad g_{11}(0) = 1, \quad g_{21}(0) = 0, \quad h_{11}^{(1)}(0) = 0, \quad h_{11}^{(2)}(0) = 0$$

Iteration formula (12) will now adopt the form corresponding to one of the Halley's method variants [4]

$$p_{k+1} = p_k - \frac{2(y_1(b, p_k) - y_{1b}) g_{11}(b, p_k)^2 + (y_1(b, p_k) - y_{1b})^2 h_{11}^{(1)}(b, p_k)}{2 g_{11}(b, p_k)^3}, \quad k = 1, 2, \ldots$$

Adopting $h_{11}^{(1)}(b, p_k) = 0$ in the above iteration formula and taking into consideration the first 4 differential equations and 4 initial conditions we shall obtain Newton's approach characterized by quadratic convergence. The results of calculations for the quadratically convergent and cubically convergent methods have been presented in Table 1; in both approaches the parameter value $p_1 = 0$ has been adopted as the initial value.

Table 1

The convergence of presented method and Newton-Raphson method

Iterations	Parameter p values ($p_1 = 0$)	
	Newton-Raphson method	Cubically convergent method
1	0.**1**674150636	0.**1**029115260
2	0.**13**24421677	0.**115**7670195
3	0.**11**73361567	0.**1158044384**
4	0.**1158**168118	
5	0.**1158044**392	
6	0.**1158044384**	

As we can see, the number of significant figures in subsequent approximations triples if we use the presented method, while with the use of the Newton-Raphson approach it only doubles.

5. Conclusions

The method presented in the work requires that we know the Jacobian and Hessian matrices for functions with imposed boundary conditions at the final point of the domain. Replacing the boundary value problem with the initial value problem results in the increase

of the number of differential equations from n to $n(1+n_1+n_1^2)$, with $n \cdot n_1$ of them pertaining to sensitivity function $g_{ij}(x)$ and $h_{jr}^{(i)}(x)$. pertaining to the derivatives of sensitivity function $h_{jr}^{(i)}(x)$. The definition of the above-mentioned matrices and formulation of the iteration formula and additional differential equations can be done in a simple way with the use of software for symbolic computation. The Newton-Raphson approach does not require knowledge of the Hessian matrix, hence the number of equations in the initial value problem is $n \cdot n_1^2$ less than in the approach presented in the work. The presented method may also be used to solve the boundary value problem in which some of the functions have boundary conditions imposed at both ends of the domain.

References

[1] Press W.H., Teukolsky S.A., Vetterling B.F., *Numerical Recipes. The Art of Scientific Computing*, third ed. Cambridge University Press, New York 2007.

[2] Palej R., *Cubically convergent method for nonlinear equation systems*, Czasopismo Techniczne 4-M/2011/B, Wydawnictwo PK, Kraków 2011.

[3] Rao S.S., *Applied Numerical Methods for Engineers and Scientists*, Prentice Hall, New Jersey 2002.

[4] Dahlquist G., Björck Å., *Numerical Methods in Scientific Computing*, Volume I, SIAM, Philadelphia 2008.

TECHNICAL TRANSACTIONS | **CZASOPISMO TECHNICZNE**
MECHANICS | MECHANIKA
1-M/2013

RAFAŁ PETRYNIAK*

EDGE PRESERVING TECHNIQUES IN IMAGE NOISE REMOVAL PROCESS

TECHNIKI USUWANIA SZUMU Z OBRAZU MINIMALIZUJĄCE STRATĘ OSTROŚCI GRANIC MIĘDZY OBIEKTAMI

A b s t r a c t

The paper describes how to prepare dynamic graphic filters, which main goal is to remove noise from an image and also to preserve information on edges between objects. These types of filters are able to focus on operations inside objects, and at the same time weaken the process at objects borders.

Keywords: *image noise removal*, *graphic filter*, *edge detection*, *adaptive methods*

S t r e s z c z e n i e

W artykule przedstawiono metody dynamicznego konstruowania filtrów graficznych, których głównym zadaniem jest usuwanie szumu z obrazu, przy jednoczesnym zachowaniu informacji o krawędziach między obiektami. Tego typu filtry potrafią samodzielnie wzmacniać swoje działanie wewnątrz obiektów i jednocześnie osłabić je na ich granicach.

Słowa kluczowe: *usuwanie szumu z obrazu*, *filtry graficzne*, *detekcja krawędzi*, *metody adaptacyjne przetwarzania obrazu*

* PhD. Eng. Rafał Petryniak, Institute of Applied Informatics, Faculty of Mechanical Engineering, Cracow University of Technology.

1. Introduction

The quality of the input image is one of the most important factors that influences the image analysis process. The preferred quality shall reproduce the actual structure of the existing objects. Unfortunately, many factors affect the result of image capturing process, so it is difficult to achieve the perfect data. Simple examples of quality reduction are poor image sharpness and accompanying noise.

In the design phase of an algorithm, we need to take care of the algorithm performance objectives. For instance, we do not want the algorithm to destroy the image information, which might be important for us. Applying of dynamic methods for filter construction allows us to process the image fragments step by step.

2. Filters based on point neighbourhood

One of the simplest methods of noise removal from an image is to use the filter which is based on the local neighbourhood of each point. This approach requires the simplified assumption that point and its closest surrounding belong to the same object. So the points shall have similar values or the values should change gradually. Based on that, a value that differs significantly from the other is considered to be affected by an external factor (like noise) and should be modified. Taking an average value of surrounding points is a popular technique. Two types of average values are usually used:

- ***Arithmetic mean*** – smoothes the image by setting the point with the mean value of its neighbourhood.
- ***Median*** – does not introduce new values to the image, but choose the central value from the neighbourhood.

3. Linear image smoothing based on the Gaussian function

When we use the arithmetic mean in a filtering process, all points from neighbourhood are treated in the same way. Applying of arithmetic mean to remove a noise may lead to much smoothing, and to loosing of some important data regarding object edges (Fig. 1c). To minimize this effect, we may apply the *weighted mean*, which distinguish the points nearest to the central one from the further located. *Gaussian function* may help us to choose the weights.

$$G(x,y) = \frac{1}{2\pi\sigma} e^{\frac{x^2+y^2}{2\sigma^2}} \tag{1}$$

where:

x – distance from the X axis,
y – distance from the Y axis,
σ – standard deviation of normal distribution (*sigma*).

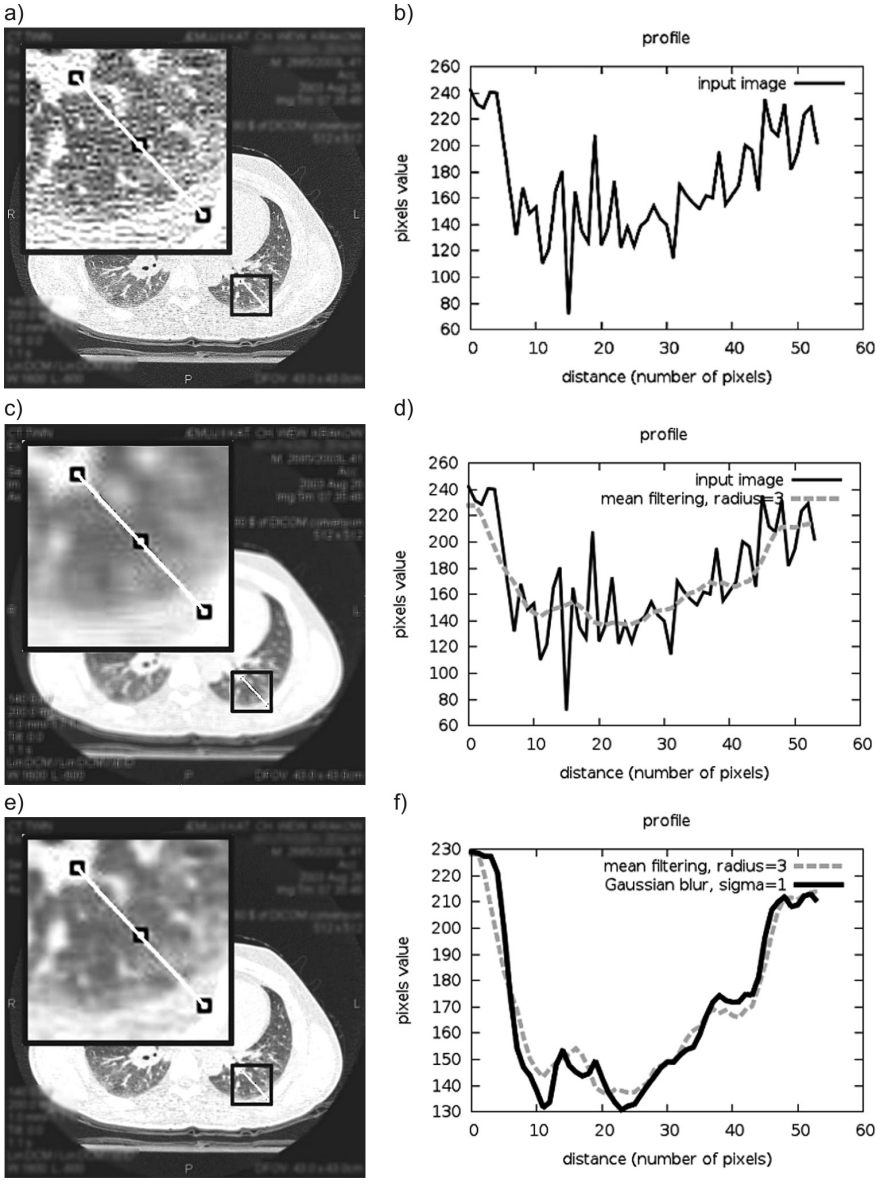

Fig. 1. The results of linear smoothing filters for a example tomographic image of the chest: (a) original image, (c) mean filtering, (e) Gaussian blur. The right column shows the profiles of the pixels values for the selected line

Rys. 1. Wyniki działania liniowych filtrów wygładzających dla przykładowego obrazu tomograficznego klatki piersiowej: (a) obraz oryginalny, (c) filtracja uśredniająca o promieniu = 3, (e) filtracja Gaussa o wartości sigma = 1. W prawej kolumnie przedstawiono profile wartości pikseli dla wybranej linii

4. Non-linear image smoothing based on the Gaussian function

Gaussian smoothing helps to keep the object edges, however, it still treats all points in the same way. This is typical for linear filters. To improve the process, we might want to modify it in a way that it takes into account the localization of the point – whether it is in the middle of the object, or close to the edge. Then the smoothing process shall focus on similar fragments on the image, and not on the edges.

One of the first publications in this area was paper about *Perona-Malik model* [1]. The authors introduced a variable *g*, which decides on smoothing level, based on *E* value – estimator for edges. For *E* estimator the authors suggested to use gradient operator.

$$E(x, y) = \| \nabla u(x, y) \| \tag{2}$$

In the mentioned paper, there were described also two functions *g*, that influence the smoothing level.

$$g_1(E) = \exp\left(-\left(\frac{E}{K} \right)^2 \right) \tag{3}$$

$$g_2(E) = \frac{1}{1 + \left(\frac{E}{K} \right)^2} \tag{4}$$

Additional parameter $K > 0$ represents the minimal value required to decide if a point belongs to the edge or not. *K* may be considered as difference of pixel value between the edge and its surrounding. This parameter may be set by the user or may depend on the histogram of image noise [1].

Comparing with previously described linear filters, the *Perona-Malik model* operates on the points from the nearest neighbourhood (filter radius = 1), and not on the wide neighbourhood. To manipulate with the level of smoothing, it is recommended to run the filter several times on the image (this is an iterative approach).

The algorithm results are presented on Figure 2. Selected image fragment was zoomed out (Fig. 2a) and its profile (pixel values) was put on chart (Fig. 2b). The image profiles of *Perona-Malik model* and *Gaussian function* were compered and shown on Fig. 2b. Although both profiles look similar, we can see differences in edge areas. With *Perona-Malik model* we observe bigger values changes in these areas, whereas *Gaussian filter* provides smoother values. Additionally, we can notice that edges on the Figure 2a are sharpen than on Figure 1a. The noise removal process seems to clean up the image.

In *Perona-Malik model* edge estimator *E* may be the thin throat. If we use a local gradient for *E* calculation, it may happen that a point may be classified to an edge, and not to the body of an object, and such areas will not be smoothed. High noise may influence the local gradient method significantly and may change the results. To mitigate the noise influence, in the paper [2] there was proposed additional step with ***model regularization***. For this purpose the linear filter can be selected (*Gaussian function* is recommended), which smoothes the biggest value changes. On such filtered image the value of *E* will not be much influenced by local noise, and *Perona-Malik model* will provide better results.

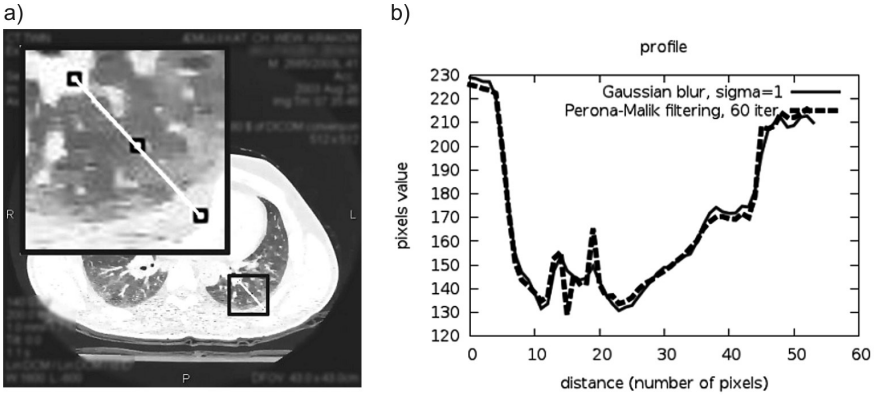

Fig. 2. The results of the non-linear image blur filter based on the *Perona-Malik model*: (a) result image after filtering (60 iterations), (b) profile of the selected line compared to blurred image profile of Gaussian function

Rys. 2. Wyniki działania nieliniowego filtru rozmycia obrazu opartego o *model Perona-Malik*: (a) obraz po filtracji (60 iteracji), (b) profil wartości dla wybranej linii porównany z profilem obrazu po rozmyciu funkcją Gaussa

Regularization is performed only once before first calculation of estimator E, in order not to lose too much data on edges.

5. Summary of the practical aspects of non-linear filtering methods usage

Non-linear filtering method described above may give better results than linear methods, like mean filter or *Gaussian blur*. However, in some cases it is not the perfect solution. Main weakness is the time needed for calculation due to iterative approach [3]. For instance, to reach the results on Figure 2a, 60 iterations for the whole image were performed. It is much more effort, than for other popular filters like mean or median, which need to be performed only once for each point. Additional issue with the non-linear filters is to define the optimal number of iterations.

Generally, the algorithm is not much influenced by small changes in number of iterations. Nevertheless, for a person using this method rarely, it might be not obvious what number of iterations shall be applied – 30, 60, or 120 iterations. Another issue is with the popularization of the non-linear algorithms. It is very likely, that we will not have them implemented in our daily used tools. The implementation of these methods is more difficult, than the implementation of linear methods.

If described weaknesses (calculation time, defining number of iterations, implementation effort) are uncomfortable, then a simpler non-linear method may be applied – *median*, already mentioned in this paper. It also has some drawbacks (possible change of object geometry due to smoothing of sharp edges or thin lines [4]), however it may give results good enough. If we look at the Figure 3a, we can see that edges are still sharp. The profile was presented on Figure 3b.

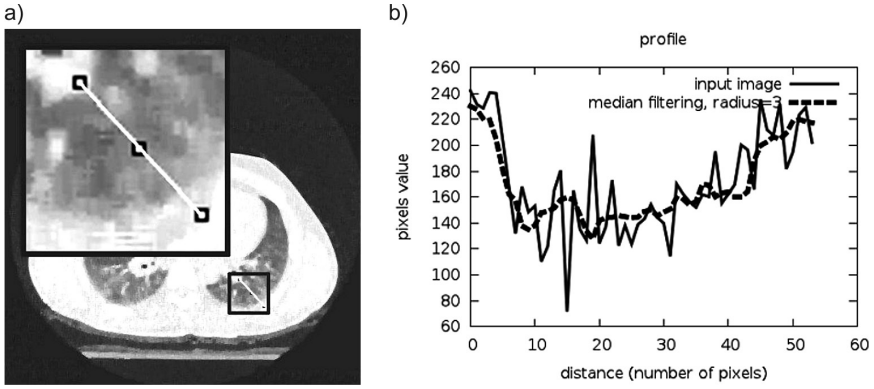

Fig. 3. The results of the median filter: (a) image after filtration, (b) profile of the selected line
Rys. 3. Wyniki działania filtru medianowego: (a) obraz po filtracji, (b) profil wartości dla wybranej linii

In opposite to the mean filter, removal of extreme values, does cause much smoothing and allows to keep edges of objects (Figure 4). Despite the fact that both filters – mean and median works good in areas of pixel values shocks, it seems that *Perona-Malik filter* profile suits better with original image profile in areas where two objects are connected (Figure 5).

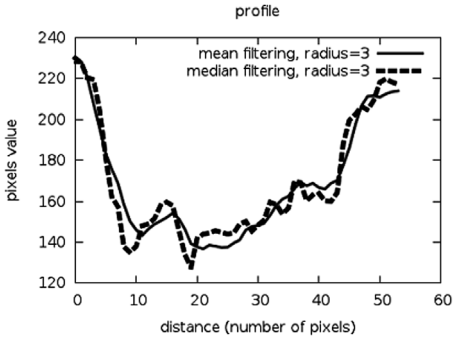

Fig. 4. Comparison of mean filter profile (Figure 3.1c) with a median (Figure 3.3a)
Rys. 4. Porównanie profilu filtracji średnią arytmetyczną (rys. 3.1c) z medianą (rys. 3.3a)

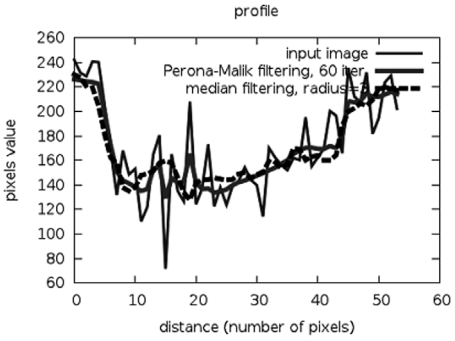

Fig. 5. Comparison of median filtering profile (Figure 3.3a) and Perona-Malik filtration (Figure 3.2a) to the original image (Figure 3.1a)
Rys. 5. Porównanie profilu filtracji medianowej (rys. 3.3a) i filtracji Perona-Malik (rys. 3.2a) z obrazem oryginalnym (rys. 3.1a)

6. Conclusions

Presented in this paper non-linear image filters are suitable for images with high noise. Applying popular linear image filters, like arithmetic mean or *Gaussian filter*, in such cases may cause too much smoothing of object edges, which may lead to failures in further image analysis process.

References

[1] Perona P., Malik J., *Scale-space and edge detection using anisotropic diffusion*, IEEE Transactions on Pattern Analysis and Machine Intelligence, 12(7):629–639, July 1990.

[2] Catte F., Lions P. L., Morel J.M., Coll T., *Image selective smoothing and edge detection by nonlinear diffusion*, SIAM Journal on Numerical Analysis, 29(1):182–193, 1992.

[3] Jabłoński B., *Filtracja obrazów i trajektorii przestrzennych za pomocą równań różniczkowych cząstkowych*, EXIT, 2008.

[4] Russ J.C., *The Image Processing Handbook*, Taylor and Francis, Inc., London, UK, edition 5, September 2006.

TECHNICAL TRANSACTIONS | **CZASOPISMO TECHNICZNE**
MECHANICS | MECHANIKA
1-M/2013

JACEK PIETRASZEK*, ANETA GĄDEK-MOSZCZAK*

THE CONCEPT OF THE VARIANCE ESTIMATION FOR THE NEURAL NETWORK APPROXIMATOR BY JACKKNIFE SUBSAMPLING

KONCEPCJA ESTYMACJI WARIANCJI APROKSYMATORA NEURONOWEGO ZA POMOCĄ PODPRÓBKOWANIA JACKKNIFE

A b s t r a c t

The estimation of a variance for a semi-parametric neural network model variance for geometric properties of sintered metal will be done on the basis of jackknife subsampling method. Calculation results are of great practical significance because it will be possible to use proposed approach in similar microscale modelling. The proposed approach is simple and has many advantages if model identification procedure is computational expensive.

Keywords: *jackknife variance estimation*, *statistical methods*, *image analysis*, *error estimate*, *metal powder sintering*

S t r e s z c z e n i e

W artykule przedstawiono estymację wariancji półparametrycznego modelu neuronowego cech geometrycznych spieku metali przeprowadzoną za pomocą metody podpróbkowania *jackknife*. Obliczone wyniki są cenne z uwagi na możliwość zastosowania proponowanego podejścia do analogicznych zagadnień modelowania w mikroskali.

Słowa kluczowe: *estymator wariancji jackknife*, *metody statystyczne*, *analiza obrazu*, *estymacja błędu*, *spiekanie proszków metali*

* PhD. Jacek Pietraszek, PhD. Aneta Gądek-Moszczak, Institute of Applied Informatics, Faculty of Mechanical Engineering, Cracow University of Technology.

1. Introduction

1.1. Geometrical properties of 2D images of sintered metals

The ferritic-austenitic stainless steel was obtained by sintering the mixture of ferritic stainless steel AISI 434L powders with different amount of additions: Mn, Ni and Si. Effects of additions on quality of sintered products were studied [1]. Microscopic geometrical properties of porosity formulate one of the quality assessment criterion. In porous materials the character of the pore structure strongly effects on its mechanical properties. The microscopic structure of sintered samples was investigated by computer image analysis methods [2]. The obtained 2D optical image was processed by specialized software for image analysis [3]. The quantitative properties of pores were identified, among others pores area and circularity ratio. These properties were non-homogeneous and thus an empirical cumulative distribution and a histogram were their appropriate descriptions. For the evaluation of sinter produced with a variety of additions, there is necessary to create models for simulating the distributions of geometric properties including estimation of some measures of uncertainty e.g. variance.

1.2. Modelling

The empirical cumulative distribution function is stepwise and the histogram has little smoothness. For sintering simulation purposes, it is appropriate to create a smooth model of empirical cumulative distribution function with confidence bands [4, 5]. Unavoidable setting uncertainties of compacting and sintering lead to dispersion of obtained sinters characteristics. Reducing dispersion would be possible using replications i.e. compacting and sintering in the same setting nominal conditions. Replicated compacting and sintering, however, introduce into the experiment additional block factors associated with individual systematic differences in mixing additives, compacting and sintering, even at the same nominal settings. Identification of block factors impact would require a significant increase in the number of completed samples, metallographic specimens and analyses [6]. Instead, it is possible to use methods based on controlled perturbations of obtained model and analyse the impact of disturbances on the modelled output. The most promising non-parametric models do not allow to examine these effects with analytical methods, as is used in the classical perturbation theory [7, 8].

1.3. Jackknife method

Nonparametric and semi-parametric models have not imposed a priori regression formula [9]. The formula structure is adaptively data driven what allows much better fit prediction to the raw data. It should be noted that, contrary to commonly named, non-parametric models have parameters. In most cases, the identification of non-parametric models (neural networks, NPMEL, FEM) is computationally very expensive, so it is advisable to seek the most cost-effective use of the procedures for the identification of such models. In the absence of known in advance function formula, it is not possible to determine probability distributions of output variables and their confidence bands by analytical methods.

Numerical determination of such distributions is possible by using Monte Carlo methods [10–12]. The use of most frequently encountered bootstrap method [13], allowing to obtain

the whole probability distribution of the output, would require multiple (from a few hundred to several thousand times) identifications of the auxiliary parametric models, which can be very expensive computationally. If the uncertainty assessment would be limited to estimates of variance, it will allows to implement jackknife subsampling procedure [14], which requires the use of a relatively small and acceptable (from a few to tens of times) number of non--parametric identification of auxiliary models. Simultaneously, the knowledge of the variance enables fully reliable estimate searched uncertainty.

2. Materials and methods

2.1. Sintered sample [1]

The water atomized powder AISI 434L of Höganäs Corporation [15] was used as a base powder. The additions were manganese powder, silicon powder and nickel powder. The four blends were prepared, but in this article, data collected for the sample 434 L+14% Mn are analysed.

2.2. Image analysis

The images of the sample 2D structure was acquired by Olympus camera model DP-25 coupled with Nikon microscope model Eclipse E400 and PC computer system. The images were analysed by algorithm written in environment of ADCIS Aphelion software [3] and pores were detected and quantified.

2.3. Neural network model

The basic model is an artificial neural network with feed-forward multi-layer architecture [16]. This network has single input and single output:

$$y = F(x, \beta_i, f_j) \tag{1}$$

where:

x – pore size,
y – predicted quantile corresponding to the size of a pore,
β_i – i-th weight of neural network synapse,
f_j – activation function of j-th neuron.

This basic model was identified (learned) by Statsoft Statistica program with Automatic Neural Network module. The best topology and activation functions were selected automatically by the program. Sub-sampling models were identified (learned) by Statsoft Statistica program with Automatic Neural Network module, but only synapses weight were selected while the topology and activation functions were the same as in the basic model.

2.4. Jackknife variance estimator for nonlinear regression

Statistic is a function of data selected according to some principle e.g. likelihood, sufficiency etc. Such statistic, prior to data collection, is a random quantity having probability distribution called the *sampling distribution*. The sampling distribution of a statistic depend

on the underlying population and therefore is unknown. The *jackknife* is a method for estimating the sampling distribution of a statistic and its characteristic. The comprehensive elaborate is available at Shao and Tu [14]. The general nonlinear model of feed forward neural network has the following formula (eq. 2):

$$y_i = f(x_i, \beta) + \varepsilon_i, \qquad i = 1, \ldots, n \tag{2}$$

where:

- β – q-vector of unknown parameters (weights and biases in neural networks),
- f – known function nonlinear in β,
- x_i – p-vectors,
- ε_i – random errors with $E(\varepsilon_i|x_i) = 0$.

Pairs (y_i, x_i) are i.i.d. with a finite second moment. Typical estimators of weights and biases β in neural network regression problems are obtained in supervised approach. The estimators $\hat{\beta}_{LS}$ are taken as least squares estimator (eq. 3)

$$L_n(\hat{\beta}_{LS}) = \min L_n(\gamma), \quad \gamma \in B \tag{3}$$

where B is a set of all possible values of β and criterion L_n is of formula (eq. 4):

$$L_n(\gamma) = \frac{1}{2}\sum_{i=1}^{n}[y_i - f(x_i, \gamma)]^2 \tag{4}$$

If the parameter of interest ϑ is defined as a given function g of parameters β (eq. 5):

$$\vartheta = g(\beta) \tag{5}$$

then the LSE estimator of ϑ is (eq. 6):

$$\hat{\vartheta}_{LS} = g(\hat{\beta}_{LS}) \tag{6}$$

and jackknife variance estimator of $\hat{\vartheta}_{LS}$ is (eq. 7):

$$\upsilon_{\text{JACK}} = \frac{n-1}{n}\sum_{i=1}^{n}\left(\hat{\vartheta}_{LS,i} - \frac{1}{n}\sum_{j=1}^{n}\hat{\vartheta}_{LS,j}\right)^2 \tag{7}$$

The values $\hat{\vartheta}_{LS,i}$ are based on $\hat{\beta}_{LS,j}$, being the LSE of β obtained after deleting the i-th pair (y_i, x_i). Now, if g is defined as f at arbitrary x i.e. (eq. 8):

$$g(\beta) = f(x, \beta) \tag{8}$$

then ϑ is mean value of f at x. With this assumption, $\hat{\vartheta}_{LS}$ and υ_{JACK} are jackknife estimators of the mean and the variance of the function f at arbitrary x (eq. 9):

$$\begin{aligned} E(\hat{\vartheta}_{LS}) &\xrightarrow[n\to\infty]{} E(y\,|\,x) \\ E(\upsilon_{\text{JACK}}) &\xrightarrow[n\to\infty]{} \text{var}(y\,|\,x) \end{aligned} \tag{9}$$

Now, evaluating estimators $\hat{\vartheta}_{LS}$ and υ_{JACK} at any arbitrary x, the mean and variance can be estimated. These estimators are used in the rest of the article.

2.5. General idea of simulation

The general outline of the workflow consists from the following 8 stages: (1) pre--processing of raw data from image analysis; (2) identification of the basic neural network model for the whole sample; (3) evaluating predictions from the basic neural network model; (4) decomposing of data into sub-samples; (5) identification of auxiliary neural networks models for sub-samples; (6) evaluating predictions from the auxiliary neural network models; (7) *jackknife* processing of the predictions from sub-samples models; (8) analysis of results.

2.6. Computational software

Image analysis was performed using ADCIS Aphelion package [3]. Numerical simulations were performed using PTC Mathcad version 15 [17]. Statistical analysis and significance tests were performed using Statsoft Statistica package [18].

3. Results

3.1. Raw data

The raw data obtained from the image analysis contain 17800 records. There were detected many pixelization artefacts associated with small objects below 32 pixel size. They were trimmed out with threshold of 32 pixels and data records were reduced to the number of 4544. Data were very irregular with lacks in many area sizes. The direct processing on this records is futile due to these irregularities generating only noise and smooth approximation is desirable. Next, area of pores were classified into 9 classes presented in Tab. 1. Class boundaries are arranged densely in these places, where the curvature is greater.

Table 1

Distribution of pores area frequency

Pore area [pixels]	32	43	62	93	123	188	265	634	2931
Number of pores with area less or equal	0	1000	2000	3000	3500	4000	4250	4500	4544

3.2. Neural models

The best fitted neural network model for pores area was topology 1-2-1 with *logistic* function for hidden layer and logistic function for output neuron. This topology was fixed as well as activation functions and subsample's identifications were processed. Predictions of full sample (basic) model, jackknife variance estimator and associated standard deviations are presented in Tab. 2.

Table 2

Neural network predictions and jackknife variance estimators for pores area frequency

Area	Measure	Full sample prediction	Residual	v_{jack}	$stdev_{jack}$
32	0	1142	1142	1585782	1260
43	1000	1315	315	1141451	1065
62	2000	1817	–183	385877	616
93	3000	2922	–78	846047	919
123	3500	3657	157	365754	602
188	4000	4207	207	23522	153
265	4250	4347	97	29215	171
634	4500	4405	–95	51505	227
2931	4544	4406	–138	46381	216

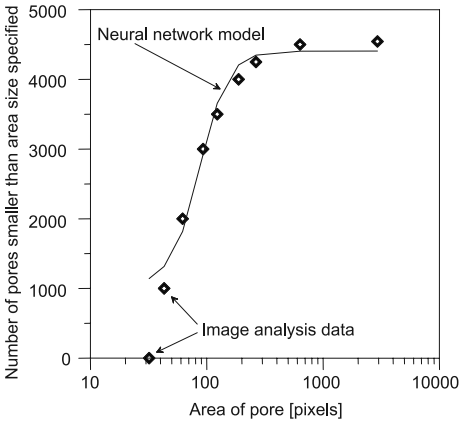

Fig. 1. The comparison of image analysis data and neural network model for distribution of pores area

Rys. 1. Porównanie rozkładów powierzchni porów dla danych z analizy obrazu oraz modelu neuronowego

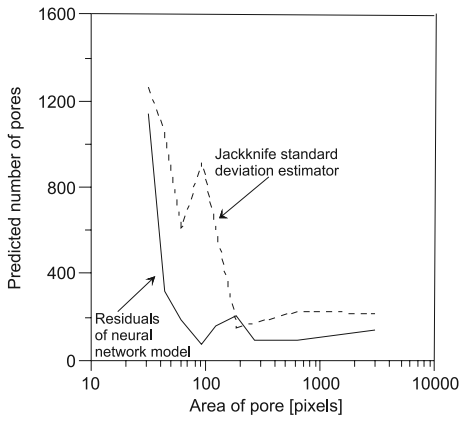

Fig. 2. The comparison of residuals and jackknife standard deviation estimator

Rys. 2. Porównanie wartości resztowych modelu neuronowego oraz odchylenia standardowego *jackknife*

Residuals may be treated as normally distributed (Kolmogorov test gives *p-value* = = 0.142). The comparison of image analysis data and neural network is presented on Fig. 1. The log scale for horizontal axis was selected due to saturation effects which make linear axis unreadable. The comparison of residuals and jackknife standard deviation estimator is presented on Fig. 2.

4. Discussion of the results

Neural network model approximates distribution of pores area continuously as expected. Model shows large errors at the left bound (for small pores). It does not reach the exact zero value but predicts the value of 1142 (see Fig. 1). This behaviour is reflected in both: residual values and an estimator of standard deviation predicted using *jackknife* method (Fig. 2). Estimator generally behaves in a similar way as real residual values of the model, but in one place (at pore size of 100) shows a sharp local spike, which looks like a slightly phase-shifted reflection of the smaller jump in the residuals. Such behaviour requires more study to determine whether it is associated with a specific model and data set, or is it the behaviour of the *jackknife* procedure interfering with a neural network model.

5. Conclusions

Metallographic studies were performed with sintered powder of stainless steel AISI 434L. Cumulative distribution of frequencies of the pore area were modelled by a neural network approximator and such approach produced a smooth waveform. The subsampling *jackknife* approach was used to estimate a variance and standard deviation of predicted values. Satisfactory results were achieved. This argues for the wider use of this methods with nonparametric approximator in the context of materials science.

References

[1] Sekuła M., *Sintering process analysis for modified powders of stainless steel AISI 434L*, Ph.D. Thesis., Cracow University of Technology, Kraków 2006.

[2] Wojnar L., *Image Analysis: Applications in Materials Engineering*, CRC Press, Boca Raton, 1998.

[3] Aphelion v 4.1.1., ADCIS, Saint-Contest, France 2012.

[4] *Springer Handbook of Engineering Statistics*, Springer, London 2006.

[5] Heinz S., *Mathematical Modeling*, Springer, Heidelberg 2011.

[6] Hinkelman K., Kempthorne O., *Design and Analysis of Experiments. Volume 2: Advanced Experimental Design*, John Wiley & Sons, Hoboken, NJ, USA 2005.

[7] Muralidhar K., Sarathy R., *A theoretical basis for perturbation methods*, Stat Comput 13, 2003, 329.

[8] Muralidhar K., Sarathy R., *An enhanced data perturbation approach for small data sets*, Decision Sci 36, 2005, 513.

[9] Horowitz J.L., *Semiparametric Models*, in *Handbook of Computational Statistics*, Gentle J.E., Härdle W.K., Mori Y. (eds.), Springer, Berlin Heidelberg, 2012, 597-618.

[10] Liu J.S., *Monte Carlo Strategies in Scientific Computing*, Springer Science+Business Media, LLC, New York 2008.

[11] Robert C.P., Casella G., *Monte Carlo Statistical Methods*, Second Edition, Springer Science+Business Media, LLC, New York 2004.

[12] Rubinstein R.Y., Kroese D.P., *Simulation and the Monte Carlo Method*, John Wiley & Sons, Hoboken, NJ, USA 2008.

[13] Mammern E., Nandi S., *Bootstrap and resampling, in Handbook of Computational Statistics*, Gentle J.E., Härdle W.K., Mori Y. (eds.), Springer, Heidelberg 2012
[14] Shao J., Tu D., *The Jackknife and Bootstrap*, Springer, New York 1995.
[15] *Höganäs Handbook for sintered components*, Höganäs AB.
[16] Samarasinghe S., *Neural Network for Applied Sciences and Engineering*, Taylor & Francis Group, LLC, Boca Raton, FL, USA 2007.
[17] Mathcad version 15, Parametric Technology Corporation, 140 Kendrick Street, Needham, MA 02494, USA, 2010.
[18] STATISTICA (data analysis software system), version 10., StatSoft, Inc., Tulsa, OK, USA 2011.

TECHNICAL TRANSACTIONS | **CZASOPISMO TECHNICZNE**
MECHANICS | MECHANIKA
1-M/2013

JACEK PIETRASZEK*, MACIEJ KOŁOMYCKI*, ELŻBIETA KOCYŁOWSKA**

THE IMPACT OF CUDA TECHNOLOGY ON THE EFFICIENCY OF BLENDER RENDERER PROGRAM

OCENA WPŁYWU TECHNOLOGII CUDA NA WYDAJNOŚĆ PROGRAMU RENDERUJĄCEGO BLENDER

A b s t r a c t

The paper summarizes the quantity assessment of GPU processing and supporting CUDA technology on the efficiency of BLENDER rendering program.

Keywords: *CUDA*, *GPU*, *orthogonal design*, *design of experiment*, *BLENDER*

S t r e s z c z e n i e

W artykule przedstawiono ilościową ocenę wpływu zastosowania przetwarzania GPU i wspierającej to technologii CUDA na wydajność programu renderującego BLENDER.

Słowa kluczowe: *CUDA*, *GPU*, *plany ortogonalne*, *planowanie doświadczeń*, *BLENDER*

* PhD. Jacek Pietraszek, MSc. Maciej Kołomycki, Institute of Applied Informatics, Faculty of Mechanical Engineering, Cracow University of Technology.
** BA. Elżbieta Kocyłowska, Faculty of Interior Design, Academy of Fine Arts in Kraków.

1. Introduction

1.1. Rendering

In the last years the intense development of computer technologies had a strong influence on widening the possibilities offered by programs that are used to create photorealistic scenes, and that increased the hardware requirements even more.

The last step in creating computer graphics is the process of rendering. It is based on the analysis of the three-dimensional model or scene, which later on creates a two-dimensional (static or animated) outcome image. The module used in the process is called a rendering engine.

The development of 3D graphics reaches back to 1960, when W. Fetter, a designer working for Boeing Corp., generated very first orthographic images of a human silhouette using a computer and created the "computer graphics" term [1]. In 1963 I.E. Sutherland has proposed a system for interactive image generation, a computer screen called sketchpad in his doctoral thesis work [2, 3]. First three-dimensional wireframes were built from simple geometric shapes, which made it possible to view the model from all angles. HSR (hidden surface removal) algorithm, which allowed creation images of full solids, was created by Sutherlands' co-workers: D.C. Evans, C. Wylie, G.W. Romney and A. Erdahl [4].

With the development of technology, the next obstacle that computer graphics had to face, was the realism of obtained images. Improving the complexity of a scene without undue increase in geometry complexity – and at the same time, memory usage – became possible thanks to the introduction of increased number of polygons. It allowed for the formal complication of the mesh, but because of the simplified shadow system, the smoothness created with the increased polygon count was lost with a sufficiently close camera.

New shading model was created by H. Gouraud later on [5]. The algorithm was based on calculating the normal vector of every vertex in the model (in order to determine the angle of incidence of the light beam), calculating the colour of pixels of the vertices and linearly interpolating the values between them. Thanks to that, the obtained effect is smoother. The only flaws are still visible at the edges and with the way the light source is reflected on the model surface. The concept introduced by Gouraud was developed by B.T. Phong, whose algorithm [6] interpolates vectors normal to surface elements of the face and then determines the colours of each pixel. It allows us to obtain a very smooth surface, but the main problem is the increased time of image processing. In 1978 J.F. Blinn proposed the disturbed surface geometry [7]. Addition of a special black and white texture allowed to define which pixels had a perturbed normal, and that in turn allowed for to simulate the look of realistic objects in a much more precise way. Bump mapping [8] is still used in many media such as games or animations. Its development is displacement mapping [9], where both the pixel and the normal are transformed. With the development of the method, a technique called normal mapping was created. The problem of fading of surface details by the edges returned, as well as the usage of the processor and the memory increased. The solution to the problem was implementing a data structure, which created an illusion of a very complicated model, without further complication of its geometry. Innovations in the domain of computer technologies, starting from 1960, changed the way of thinking about computer modelling, which lead to the creation of new techniques and trends in its usage.

The level of rendering realism is described using lots of parameters, the most important which are:

– shading – the correlation of the colour and brightness of the object with the light,
– shadows and soft shadows – the way the light is blocked by the object's surface,
– reflection and refraction – the reflection and refraction of light by the object,
– graphic, optic transparency and opacity – the way the light is transmitted by a object,
– translucency – light scattering by objects,
– indirect illumination and caustics – the light reflected from other objects and focused as defined by material properties,
– texture mapping and bump mapping – giving the model material texture and unevenness.

The level of render realism is based on preforming very complex and labour-intensive calculations. For many years it was the main impulse in developing the graphics processor cards. It led to implementation, by NVIDIA Company, of multicore compute unified device architecture (CUDA).

1.2. CUDA computing technology

CUDA (compute unified device architecture) is a specific architecture of graphics processing units proposed and implemented in 2006 by NVIDIA Company [9]. The main advantage is the two-way communication with the program that is used within the memory of the main host and the ability to send a GP GPU (General-Purpose computing on Graphics Processing Units) program to the card's memory, where it will be used by its multi-core processor organized as a hierarchical symmetric structure. The number of cores varies from hundreds to thousands and the size of card's memory from several MiB to several GiB. GP GPU cores in CUDA architecture are equipped in a set of general computing programming instructions. It distinguishes it from existing solutions, in which only subsets of specialized commands for graphics processing were available.

A typical program using CUDA architecture is built from several pieces that are executed either on the main CPU (Control Processing Unit), or the GPU card's processor [10]. NVIDIA provides a C language compiler separating the code into two groups of instructions – for the CPU and GPU – during compilation. The code for CPU is a typical ANSI C code. The one used for GPU is extended by keywords identifying parallel data processing functions called kernels and functions associated with these data structures. Due to the high labour intensity of creating programs this way, tools that provide automatic identification of code fragments suitable for parallelization were developed. The leading role is played by the family of compilers distributed by The Portland Group for FORTRAN, C and C++ languages [11].

The modern multipurpose CPU processor contains at most a dozen cores that allow concurrent execution of instructions. The buffer memory blocks (called cache) and predictive blocks are complex. They enable concurrent execution of successive instructions within the same core on the basis of their compliance tracking. The case is different in the GPU processors since they contain from several dozen to thousands of cores working concurrently with the simultaneous sharing of resources such as memory and registers. The buffer memories in GPU processors are small, since their main purpose is to avoid collisions when

accessing shared memory, and not to store data. Processing on a single core is sequential and hyper-threading is not used. Improved performance is obtained not by the sophisticated configuration of pipeline instruction execution, but through multiplication of execution units.

The critical point for the performance of the programs that use GP GPU is the data transfer from the main computer memory to the card memory, and the other way around. In the worst case scenario it can cause the resultant performance of the entire program to be lower than just being limited to CPU processor, despite great efficiency of the card. It imposes large data structure organization and algorithm selection requirements, in order to minimize such transfers.

2. Materials and methods

2.1. Blender program

Blender is a program to model and render three-dimensional images and animations. It was created in 1995 by NeoGeo Company, and was developed further by Blender Foundation. It's available on different system platforms. The performance tests were made using 2.66a version for MS Windows 7 system.

2.2. Equipment and system environment

The rendering process was made on 3 CPU variants: 1 core × 3600 MHz, 2 cores × 2800 MHz and 8 cores × 3600 MHz. 4 NVIDIA GPU cards were used: GT440, GTX560Ti, 635MGT, GTX680. Due to availability of hardware, the measurements were carried out in 6 combinations CPU vs. GPU (Tab. 1)

Table 1

Combinations of hardware CPU vs. GPU

ID	CPU	GPU
1	1 core × 3600 MHz	–
2	1 core × 3600 MHz	680GTX
3	8 cores × 3600 MHz	–
4	8 cores × 3600 MHz	680GTX
5	8 cores × 3600 MHz	440GT
6	2 cores × 2800 MHz	635MGT

2.3. Methods of analysis

Result analysis was carried out according to the methodology of the design of experiment (DoE) [12]. Calculations were made using STATISTICA [13] and Minitab [14] software.

The object of study was treated as a two-input two-level full factorial. The directly measured value was the time of rendering. Due to the fact that this is a volume measured at the ratio scale (according to the Stevens classification of measurement scales [15]) directly

applying regression would lead to nonphysical results: negative times. For this reason, the initial data pre-processing conversion was performed by using mapping that transferred positive time values into unlimited range of natural logarithms of the rendering time.

The final analysis model was the following formula:

$$\ln(t_{ij}) = \mu + CPU_i + GPU_j + CPU \times GPU_{ij} \quad (1)$$

where:

μ – the average logarithm of rendering time,
CPU_i – the effect associated with *i*-th CPU variant,
GPU_j – the effect associated with *j*-th GPU variant,
$CPU \times GPU_{ij}$ – the effect associated with interaction between CPU and GPU.

This approach prevents the obtaining of non-physical values, yet allows the assessment of mean effects of the introduction of multi-core CPU and GPU cards.

2.4. Rendered scene

The object of rendering was the 3D scene consisting of 3 cups and a teapot (Fig. 1). The metallic, reflective surface of all four elements was a defining characteristic, while the background was a simple, smooth white surface. The whole scene was illuminated with 3 point light sources. The new rendering engine called Cycles Renderer, which is developed now by Blender Foundation, was used in the experiment.

The characteristic properties of the file were:

– samples set to 1000,
– light bounces set to: min. 0 and max.4,
– performance tiles set to 256 × 256 size.

Fig. 1. Rendered scene used in the efficiency test

Rys. 1. Kreowana sceneria zastosowana w teście wydajności

3. Results

Efficiency tests that involved rendering the test scene (Fig. 1) with different hardware settings were conducted. The obtained operation times are compared in the table (Tab.2) and shown on the graph (Fig. 2).

Table 2

Obtained Times of rendering process of the test scene

ID	Time, hh:min:sec
1	01:33:08
2	00:02:26
3	00:16:49
4	00:02:22
5	00:08:47
6	00:12:09

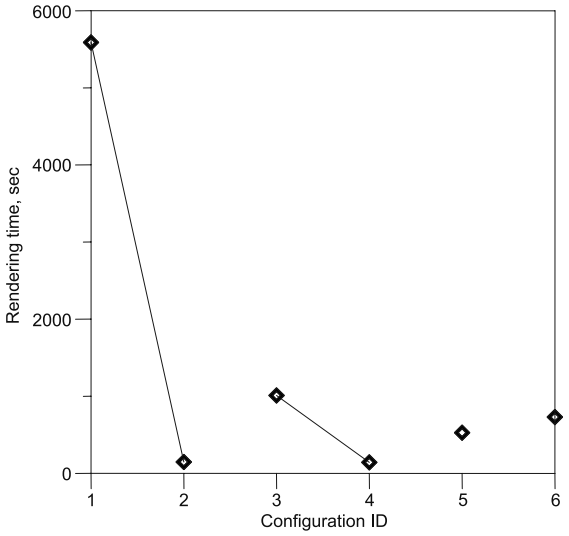

Fig. 2. Obtained test scene render time

Rys. 2. Czasy renderowania scenerii testowej

4. Result analysis

Particularly important information was obtained from the combination that used 680GTX card, because it exhausted all possible combinations of CPU and GPU. The application of DoE method to the results tied with configurations 1, 2, 3 and 4 gave a possibility to determine the main effects and the interaction effect (Tab. 3). It's important to remember that the shown effect values refer to the logarithmic scale.

The average main effects shown in Fig. 3 clearly indicate that a more significant time gain is obtained by using a GPU card than by increasing the number of cores in CPU processor.

Relatively significant interaction effect – at a level of the value of main CPU – has an antagonistic character. In practice, it means that simultaneous increase of the number of CPU cores and implementation of a GPU card has no technical and economic sense for this rendering software. Most probably it stems from the fact that the Blender software in

GP GPU mode does not enable CPU processor multithreading, and in turn its multicore capabilities have little impact. It can be clearly seen with the measured render times (ID 2 and 4, Tab. 2). The difference is only 4.5 s.

Table 3

Effect of the linear model with two-way interaction

Factor	Effect
const	6,37354
CPU	–0,87137
GPU	–2,79779
CPU × GPU	0,84062

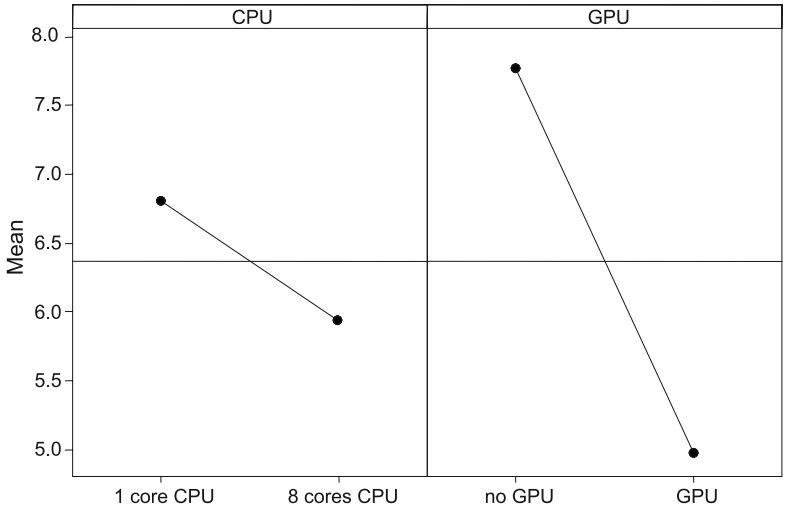

Fig. 3. Average main effects CPU and GPU (left axis – natural logarithm of rendering time)

Rys. 3. Średnie efekty główne CPU I GPU (oś lewa – logarytm naturalny czasu renderowania)

5. Conclusions

This paper presents a quantitative assessment of the impact of CUDA technology in application performance in the Blender rendering program. The selected test scene measurements were performed using a full-factorial design plan divalent. Also - for the two variants of hardware configurations - were measured for comparative purposes. The results of the measurements were analysed according to the methodology of experiment planning. Developed analysis indicates a much larger performance boost obtained from the use of GPU processor cards than from an increase in the number of CPU cores. Also it demonstrated futility, in case of Blender, of simultaneous implementation of multi-core CPU with a GPU card.

References

[1] Fetter W., *Computer Graphics*, Proceedings of the First Boston Architectural Center Conference, Boston MA, Dec. 5, 1964, 34-36.

[2] Sutherland I.E., *Sketchpad: A man-machine graphical communication system*, Ph.D. thesis, MIT Lincoln Laboratory Technical Report #296, January 1963.

[3] Sutherland I.E., Sproull R.F., Schumacker R.A., *A Characterization of Ten Hidden-Surface Algorithms*, ACM Computing Surveys 6 (1), 1974, 1-55.

[4] Wylie C., Romney G.W., Evans D.C., Erdahl A., *Halftone Perspective Drawings by Computer*, Proceedings of AFIPS FJCC, Vol. 31, 1967, 1-49.

[5] Gouraud H., *Continuous shading of curved surfaces*, IEEE Transactions on Computers C–20 (6), 1971, 623-629.

[6] Phong B.T., *Illumination for computer generated pictures*, Communications of ACM 18 (6), 1975, 311-317.

[7] Blinn J.F., *Simulation of Wrinkled Surfaces*, ACM SIGGRAPH Computer Graphics 12 (3), 1978, 286-292.

[8] Max, N.L., Becker, B.G., *Bump shading for volume textures*, IEEE Computer Graphics and Applications 14 (4), 1994, 18-20.

[9] *NVIDIA unleashes CUDA technology*, Computer Graphics World 29 (12), 2006, 4-4.

[10] Sanders J., Kandrot E., *CUDA by Example: an Introduction to General-Purpose GPU Programming*, NVIDIA Corp., Boston 2011.

[11] *PGI Fortran and C/C++ for 64-bit x64 processor-based systems Version 13.3*, The Portland Group, Inc., Two Centerpointe Drive, Suite 320, Lake Oswego, Oregon 9703.

[12] Montgomery D.C., *Design and analysis of experiments*, John Wiley & Sons, New York 1997.

[13] Statsoft, Inc., *STATISTICA (data analysis software system), version 10* (www.statsoft.com – 2011).

[14] Minitab, Inc., *Minitab, version 16* (www.minitab.com – 2012).

[15] Stevens S.S., *On the theory of scales of measurements*, Science 103, 1946, 677-680.

TECHNICAL TRANSACTIONS | **CZASOPISMO TECHNICZNE**
MECHANICS | MECHANIKA
1-M/2013

ROBERT PŁATEK*, ŁUKASZ MATYSIAK*, MICHAŁ BANAŚ*

eRAMZES – A NEW WEB-BASED TOOL FOR REACTIVE MOULDING SIMULATIONS

eRAMZES – NOWE NARZĘDZIE DLA SYMULACJI FORMOWANIA REAKTYWNEGO

Abstract

This paper describes a unique multiphysics simulation tool allowing one to analyse and optimize the reactive moulding process used for the production of epoxy resin based electrical insulation in many power products. The presented methodology offers fully automated numerical computations of the mentioned process excluding the requirement for high knowledge and experience of the tool end-user in the area of computer simulations.

Keywords: *reactive moulding*, *computational fluid dynamics*, *finite element method*, *automated meshing*, *Web-based computations*

Streszczenie

W artykule przedstawiono unikalne narzędzie do multifizycznych symulacji pozwalające na analizę i optymalizację procesu formowania reaktywnego używanego do produkcji żywicznej izolacji elektrycznej w wielu produktach elektroenergetycznych. Przedstawiona metodologia oferuje w pełni zautomatyzowane obliczenia numeryczne wspomnianego procesu wykluczając konieczność posiadania przez użytkownika narzędzia dogłębnej wiedzy i doświadczenia w dziedzinie symulacji komputerowych.

Słowa kluczowe: *formowanie reaktywne*, *obliczeniowa mechanika płynów*, *metoda elementów skończonych*, *automatyczna dyskretyzacja*, *obliczenia zdalne*

* MSc. Eng. Robert Płatek, MSc. Eng. Łukasz Matysiak, MSc. Eng. Michał Banaś, ABB Corporate Research, Krakow.

1. Introduction

APG (Automated Pressure Gelation) process is one of the leading reactive moulding technologies [1] used in the production of many epoxy resin insulated power products. This is a complex multistep process presented schematically in Fig. 1. Due to the mentioned complexity, it was proposed to use advanced computer simulations in order to detect technological problems such as premature gelation, undesired weld-line locations, air traps or cracks [2, 3] even prior to the mould manufacturing.

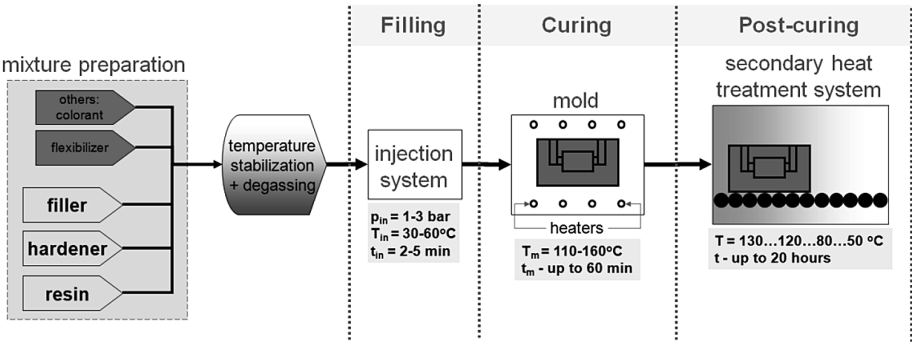

Fig. 1. Stages of reactive moulding manufacturing process

Rys. 1. Poszczególne etapy w procesie formowania reaktywnego

In the traditional approach to the analysis of the reactive moulding process [4] all design stages are executed manually by engineers utilizing different autonomous computer programs that are not directly linked to each other. These operations are time-consuming and require from the user a specialized expertise in many areas connected with numerical modelling. As a consequence, a new Web-based and automated tool linking several state of the art numerical software, called eRAMZES, has been developed to give engineers an online and, hence, unlimited access to advanced reactive moulding simulations [5, 6, 7]. This opened totally new horizons for the analysis and optimization of the products manufactured in reactive moulding technology.

2. Mathematical modelling of the reactive moulding process

The complexity of the reactive moulding process is presented in Fig. 2 illustrating phenomena taking place during all stages involved in APG technology, i.e. filling, curing and post-curing. Each phenomenon is reflected in an appropriate mathematical model implemented in the developed simulation tool. In the case of CFD (Computational Fluid Dynamics) analysis one have to deal not only with numerically unstable multiphase flow calculations, but also with the kinetics of curing reaction and conjugate heat transfer. Additionally, because of the dynamics of the chemical reaction and complexity of the resulting thermal effect, an accurate modelling of the stresses and deformations during mechanical analysis is not an easy task.

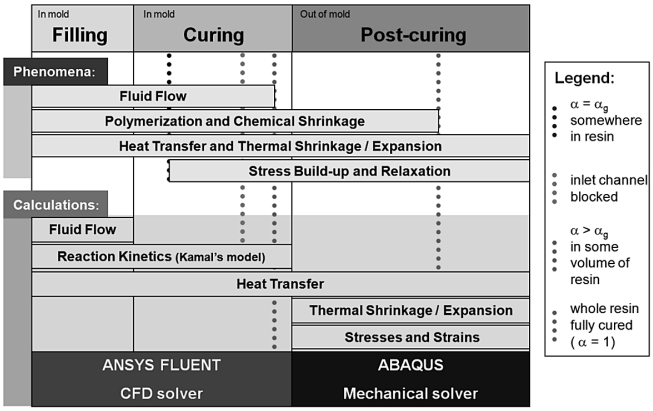

Fig. 2. Mathematical modelling of the reactive moulding manufacturing technology

Rys. 2. Modelowanie matematyczne technologii wytwarzania formowania reaktywnego

2.1. CFD simulations

The transient calculations of the filling and curing stage of APG process are performed in CFD commercial software ANSYS Fluent. For this purpose the standard set of governing equations including continuity equation, Navier-Stokes equation and energy equation is applied [8].

Due to the presence of two different fluids during the mould filling stage (epoxy resin and air) VOF (Volume of Fluid) method is used to predict accurately the location of the interface between both phases. In the VOF approach the volume fraction of resin a in each cell is solved from the conservation equation:

$$\frac{\partial a}{\partial t} + \nabla \cdot (au) = 0 \tag{1}$$

where:

t – time,

u – the velocity of fluid.

The nature of the reactive moulding process causes that it is important to monitor the course of polymerization reaction of thermosetting epoxy resin. For this purpose curing kinetics model in the form of Kamal-Sourour equation is applied [9] and implemented in ANSYS FLUENT by using User Defined Function and User Defined Scalar functionalities [8]. According to this model the value of degree of curing α at time t is defined as:

$$\alpha = \frac{H(t)}{H_{\Sigma}} \tag{2}$$

where:

$H(t)$ – the heat of reaction released until time t,

H_{Σ} – the total heat of reaction.

The progress of the curing phenomenon is linked to the mass conservation and, thus, the degree of curing α is governed by its own un-steady state conservation equation:

$$\frac{\partial(\rho\alpha)}{\partial t} + \nabla \cdot (\rho u \alpha) = S_a \tag{3}$$

In the equation (3), S_a is the source term of degree of curing calculated according to the mentioned Kamal-Sourour model and used to determine the source term of energy equation resulting from the exothermic curing reaction $S_T = S_a H_\Sigma$. S_a is expressed by the equation:

$$S_a = \rho\left[A_1 e\left(\frac{-E_1}{RT}\right) + A_2 e\left(\frac{-E_2}{RT}\right)\alpha^m \right](1-\alpha)^n \tag{4}$$

where:

m, n – the model constants,
A_1, A_2 – the pre-exponential factors,
E_1, E_2 – the activation energies,
R – the universal gas constant,
T – the absolute temperature.

It is worth stressing that all parameters of Kamal-Sourour model mentioned above and the total heat of exothermic reaction are determined experimentally (usually by using Differential Scanning Calorimetric technique) and their values are characteristic for each epoxy resin.

2.2. Mechanical simulations

The structural results are obtained in a transient and coupled thermal and stress analyses conducted sequentially. In the first step the effects related to the heat transfer are determined and then chemically driven deformations are calculated. Finally, this leads to the definition of the strains and stresses as a function of the process time.

The chemical shrinkage model was developed based on the assumption that the total strain increment $\Delta\varepsilon^{\text{Total}}$ (in each time-step) can be expressed as a sum of mechanical $\Delta\varepsilon^{\text{Mechanical}}$ and thermal $\Delta\varepsilon^{\text{Thermal}}$ components:

$$\Delta\varepsilon^{\text{Total}} = \Delta\varepsilon^{\text{Mechanical}} + \Delta\varepsilon^{\text{Thermal}} \tag{5}$$

ABAQUS software allows defining thermal component by applying a user-defined subroutine. This component covers both chemical and thermal effects influencing the material density:

$$\Delta\varepsilon^{\text{Thermal}} = \sqrt[3]{\frac{\rho}{\rho'}} - 1 \tag{6}$$

where:

ρ' – actual density,
ρ – the value of density from the previous time-step.

It is worth stressing that in order to realize that stage of calculations it was necessary to apply the dependence of temperature and degree of curing on density. This correlation was derived based on the experimental measurements. More information about the modelling of epoxy resin shrinkage can be found in [10].

3. Web-based tool for automated reactive moulding simulations

3.1. The architecture of eRAMZES tool

The eRAMZES tool is controlled by a dedicated multifunctional Web platform linking a number of applications (commercial and developed) interacting between each other. The general workflow of eRAMZES tool is presented schematically in Fig. 3. One can notice that engineer is obliged only to define the geometrical model and process parameters, while the remaining computational steps are executed in an automated manner.

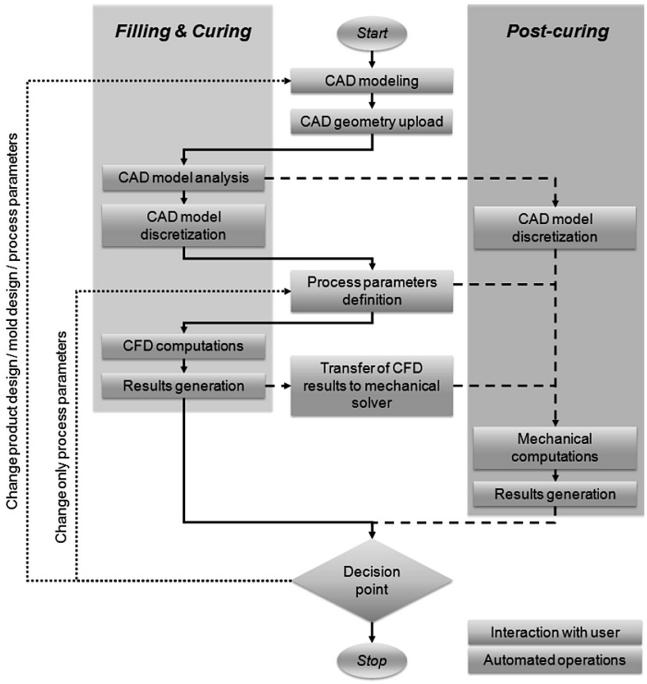

Fig. 3. The principle of working of the eRAMZES tool

Rys. 3. Podstawy działania narzędzia eRAMZES

3.2. CAD model and discretization

The very first step of the analysis that must be taken by user is CAD modelling. Engineer decides at this stage about the geometrical components, their features and possible simplifications, which will be taken into consideration during computations. In the consecutive step the prepared geometry is loaded into eRAMZES by the mentioned Web platform. Next, the CAD geometry is analysed automatically to detect parts included in the model and the gathered data is used further during the meshing and solving operations.

Next stage is geometry discretization which was recognized as one of the most challenging part of the tool development, mainly due to high complexity and diversity of the products

manufactured in APG technology. In the proposed approach all operations done on geometry are executed automatically by using dedicated scripts giving commands to the meshing software (HyperMesh and ABAQUS for CFD and mechanical module respectively). In this way the CAD geometry is imported, modified if needed, discretized and exported to solvers. The geometry of an exemplary product (current transformer) analysed by using eRAMZES tool is presented in Fig. 4.

Fig. 4. Geometry of current transformer (left) and its discretization in ABAQUS (right)
Rys. 4. Geometria transformatora (po lewej) oraz jego dyskretyzacja (po prawej)

3.3. Process parameters definition and computations

Definition of the process parameters is another step of the reactive moulding analysis with the eRAMZES tool that requires input from the user side. The Web application uses information gathered during the CAD model analysis and creates dynamically a dedicated Website allowing user to enter all parameters required to configure the simulation. At this stage both the process parameters (e.g. mould filling time, mould heating temperature etc.), material properties, materials assignment to product parts and, finally, basic numerical parameters related to structural computations are selected and then sent automatically to solvers.

Processing is the subsequent fully automated stage of the simulation procedure, executed in a batch mode by using scripts generated automatically and individually for each simulation case. At this stage the CAD model analysed by the tool and the process parameters provided by user in the previous steps are read into processors.

The solver configuration requires the choice of mathematical models used in the reactive moulding simulation (both built-in models like e.g. turbulence model, flow model etc. as well as additionally implemented models like curing kinetics model) and the definition of numerical parameters ensuring reliable and accurate solution of these models. In the consecutive step the transient numerical computations for filling and curing stage are conducted in ANSYS FLUENT and, once done, results are generated and exported.

The computations can be continued if user decides to include the post-curing simulation. In such case temperature results obtained for the end of curing stage are translated by using dedicated in-house developed software [10] and transferred to the mechanical solver ABAQUS to constitute the starting point for post-curing computations.

It is worth noticing that the solution convergence is monitored and controlled automatically, what was recognized as one of the biggest challenges during the tool development as well.

3.4. Results visualization

The simulation results are processed in a batch-mode in ANSYS CFD-Post and built-in ABAQUS post-processor. For this purpose master macros, recorded for each post-processor individually, are executed for each simulation case making the results visualization process automated and repeatable irrespective of the product under consideration. The obtained results are presented to user in different forms like movies, pictures and charts (see Fig. 5) via the Website or as a printable PDF document.

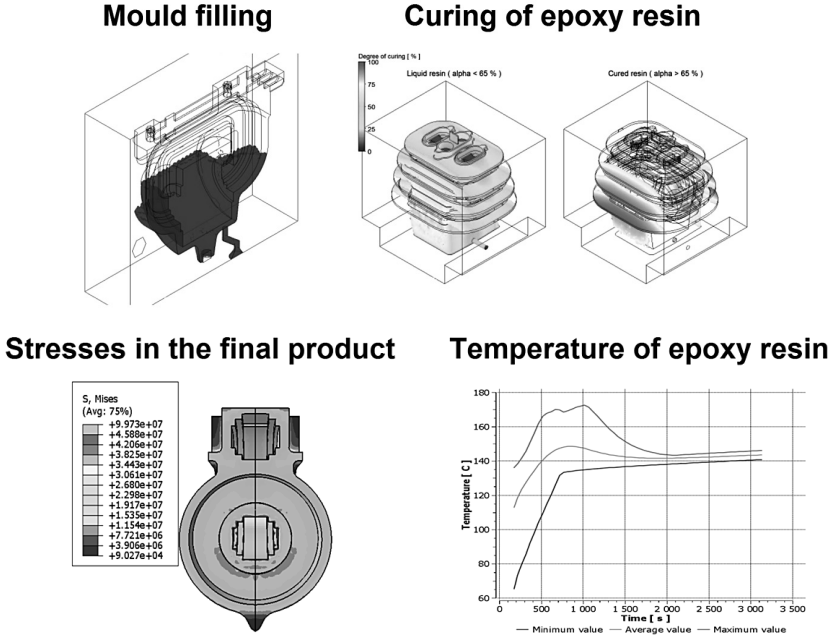

Fig. 5. Exemplary results of eRAMZES computations

Rys. 5. Przykład wizualizacji wyników obliczeń eRAMZES

The developed way of results visualization allows users to observe in details the course of the reactive moulding process and to capture effects inside the mould and product, which cannot be detected in a normal production process or in an experimental way. This includes information about the flow pattern of epoxy resin during the filling stage, distribution of temperature in time during all process stages, distribution of degree of curing in time during the filling and the curing stage, distribution of deformations, stresses and strains during the post-curing stage. The acquired knowledge is then used by engineer to decide whether further process and product optimization is needed or not.

4. Conclusions

The presented novel Web-based tool combining CFD and mechanical simulations can be successfully utilized both for the design of new and optimization of the existing products manufactured in the reactive moulding technology. The tool allow users to observe the influence of changes in the product and/or mould design as well as in the configuration of the process parameters without any interference on the real production process. This was achieved by high quality simulation results presenting details about the process course.

The described automation of the meshing and solving operations executed during CFD and mechanical computations allowed one to shorten significantly the total computational time and to eliminate the requirement for high user knowledge and experience in the field of numerical simulations. Among the other eRAMZES advantages one can notice its user--friendliness, unlimited online access to the tool and the repeatability of the simulation process resulting in manual-error resistance.

All aspects mentioned above lead, on the one hand, to shorter development time of new products manufactured in the reactive moulding technology and, on the second hand, to improved quality of the epoxy based components. Moreover, the presented approach can be adapted to provide the possibility to analyse also other manufacturing processes.

References

[1] Sekula R., Saj P., Nowak T., Kaczmarek K., *3-D Modeling of Reactive Moulding Processes: From Tool Development to Industrial Application*, Advances in Polymer Technology, 22 (1), 2003, 42-55.

[2] Macosko C.W., *RIM. Fundamentals of Reaction Injection Molding*, Hanser Gardner Publications, New York 1989.

[3] Grindling J., Gehrig M., *Introduction to FEM Based Computer Simulation to Assist Molding and Casting Processes*, Electrical Manufacturing and Coil Winding Conference, 1998, 327-333.

[4] Sekula R., Saj P., Nowak T., Kaczmarek K., *3D Computer Simulations of Thermosetting Materials Molding*, SGI Users' Conference, Krakow 2000.

[5] Rajca R., Matysiak L., Banas M., Sekula R., *A Novel Simulation Approach for Analyzing Reactive Molding Process*, International Journal of Mathematics and Computers In Simulation, 4 (4), 2010, 99-106.

[6] Rajca R., Matysiak L., Banas M., Sekula R., *Industrial Application of a new CFD Simulation Approach*, 25th European Conference on Modelling and Simulation, Krakow 2011, 374-380.

[7] Matysiak L., Platek R., Banas M., Sekula R., *eRAMZES – Novel Approach for Simulation of Reactive Molding Process*, 26th European Conference on Modelling and Simulation, Koblenz 2012, 128-135.

[8] ANSYS Help, ANSYS Inc., 2010.

[9] Kamal M.R., Sourour S., *Kinetics and Thermal Characterization of Thermoset Resin*, Polymer Engineering and Science, 13 (1), 1973, 59-64.

[10] Isotalo P., Bednarowski D., Nowak T., *Reactive Molding Process Modeling: Structural Analysis of Thermoset Insulated Electrical Components*, International Journal of Materials and Product Technology, 20 (4), 2004, 239-253.

TECHNICAL TRANSACTIONS | **CZASOPISMO TECHNICZNE**
MECHANICS | MECHANIKA
1-M/2013

JANUSZ POBOŻNIAK*

THE USE OF STEP-NC (ISO 14649) FOR THE INTEGRATION OF CAD/CAM/CNC CHAIN

ZASTOSOWANIE STANDARDU STEP-NC (ISO 14649) W INTEGRACJI ŁAŃCUCHA CAD/CAM/CNC

A b s t r a c t

The paper presents the information flow between CAD/CAM/CNC systems when using the CNC machine tool programming language based on ISO 6983. Next, the data structure of the new programming standard STEP-NC, defined in ISO 14649, is presented. The information flow for this new standard is also discussed. The results of analysis show how this standard can be used for the increase of the automation of CNC machine tool programming.

Keywords: *STEP*, *STEP-NC*, *process planning*, *CAD/CAPP/CAM/CNC*

S t r e s z c z e n i e

W artykule przeanalizowano przepływ informacji pomiędzy systemami CAD/CAM/CNC przy korzystaniu z języka programowania obrabiarek CNC opartego na normie ISO 6983. Następnie scharakteryzowano strukturę danych w nowym standardzie programowania OSN STEP-NC, zdefiniowanym w normie ISO 14649 i również przeprowadzono dla tego standardu analizę przepływu informacji. Uzyskane wyniki analizy wskazują, w jaki sposób można wykorzystać ten standard do dalszej automatyzacji programowania obrabiarek sterowanych numerycznie.

Słowa kluczowe: *STEP*, *STEP-NC*, *projektowanie procesów*, *CAD/CAPP/CAM/CNC*

* PhD. Janusz Pobożniak, Production Engineering Institute, Faculty of Mechanical Engineering, Cracow University of Technology.

1. Information flow in the CAD/CAM/CNC for machine tool programming language based on ISO 6983

CNC machine tool programming language defined in ISO 6983 [6] is still widely used despite the fact, the it was not fundamentally changed since more than 50 years. Generally speaking, the ISO 6983 control program contains (only) three basic groups of information:

- data about the required position of the tool relative to the machined part (for example G00 – linear interpolation in rapid travel, G02 – clockwise circular interpolation),
- data about the relation between the tool and part during the material removal (for example S960 – cutting speed of 960 m/min, F160 – feedrate of 160 mm/min),
- data controlling the auxiliary functions (like M03 – spindle clockwise rotation, M08 – coolant flow on).

The main purpose of ISO 6983 language is to describe the tool trajectory and not the machining tasks for the part. Now, the model created in CAD system is usually used by the CAM system for machining tool programming. The nowadays CAM systems are very advanced [8, 10]. They analyse the part not on the level of the basic geometric primitives like points and lines, but on the level of the elements useful from the manufacturing point of view, i.e. machining features [7]. Slot, open pocket, closed pocket or counterbored hole can be given as examples. CAM systems are able to automatically select the appropriate machining cycles for the automatically recognised manufacturing features. During the CNC program development, the manufacturing engineer can use the sophisticated databases of the cutting tools. Before execution of the program on the real machine tool, it can be simulated using the model of this machine tool. Unfortunately, the ISO 6983 program, containing mainly G and M functions does not include all the information about the machined part, manufacturing features, defined machining cycles or the manufacturing recourses. All machining cycles, as for example deep hole drilling cycle or pocket milling cycles are transformed into the series of elementary motions. It is not possible to make the reverse transformation, i.e. to convert the elementary motions into the machining cycles. As the results, ISO 6983 program does not include the structure created in CAM system and it is not possible to make any changes, even the simplest one, as the change of the cutting depth. So, the decision taken during the program development can not be later changed on the stage of the program trial runs, because the high-level information is transformed into the elementary movement of the controlled axes.

All the part information modelled in CAD system, and then enhanced by the manufacturing data describing the machining processes and the manufacturing equipment are significantly reduced when sending to CNC system (Fig. 1).

Also the information about the cutting tools selected for the machining is lost. CAM systems allow to select tool bodies, cutting inserts as well as tool holders. Not only geometric parameters can be defined, but also 3D models can be used. Very often, the cutting tool manufactures offers such 3D models, as for example Sandvik Coromant. These exact models allow to exactly check the amount of materials still remaining on the part, the amount of material removed due to programming errors or the find all collisions between the tools and part. In ISO 6983 program, the tool is represented only by number. The machine tool operator must have the additional documentation to start the production. This proofs once again the

lack of information in ISO 6983 programs. The program processed by postprocessor is tailored for the given combination of machine tool/CNC control system and thus looses its flexibility. This is due to the fact, the modern machine tools have a lot of functions not covered by ISO 6983. To use the full functionality of the machine tools, the manufactures introduce own addresses as well as preparatory and auxiliary functions. Although such solution is efficient, it blocks the flexibility and restricts the area of the use of the program.

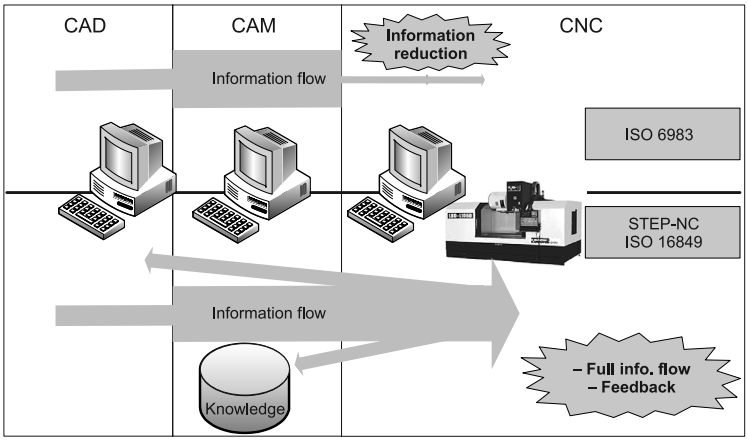

Fig. 1. Comparison of CNC machine tool programming with ISO 6983 and STEP-NC

Rys. 1. Porównanie programowania OSN wg normy ISO 6983 i normy STEP-NC

The other problem is the number of postprocessor, resulting from the rich set of CNC control systems available on the market. The primary concern of every persons starting the work with new CAM system is to find the appropriate postprocessor. The modification of ISO 6983 language introduced by CNC control system manufactures resulted in the hundreds of its dialects. Because the CAM system producers can not deliver the postprocessors to all control systems, the postprocessors are created on its own using CAM system tools or delivered on demand by specialized companies. One thing is sure, it does not simplify the operation of the manufacturing department.

Summarizing, the main disadvantage of ISO 6983 control program is the reduction of information available in CAM system, lack of cooperation with CAD/CAM and unidirectional flow of information. Usually, it is not possible to change the destination of the ISO 6983 program developed for the particular machine tool. ISO 6983 program is definitively the link breaking the CAD/CAM/CNC chain.

2. ISO 14649 standard (STEP-NC)

STEP, the Standard for the Exchange of Product Model Data (ISO 10303) is a complete and the unambiguous product data description throughout its life cycle [1]. STEP-NC is the application of STEP into the CNC machine tool programming. Unlike the ISO 6983 standard

describing the tool motions relative to the part and informing "how to make" that part, STEP--NC standard informs "what to do", describes the sequence of machining cycles, tool path style, the required accuracy and the tools. The STEP-NC concept uses the manufacturing features.

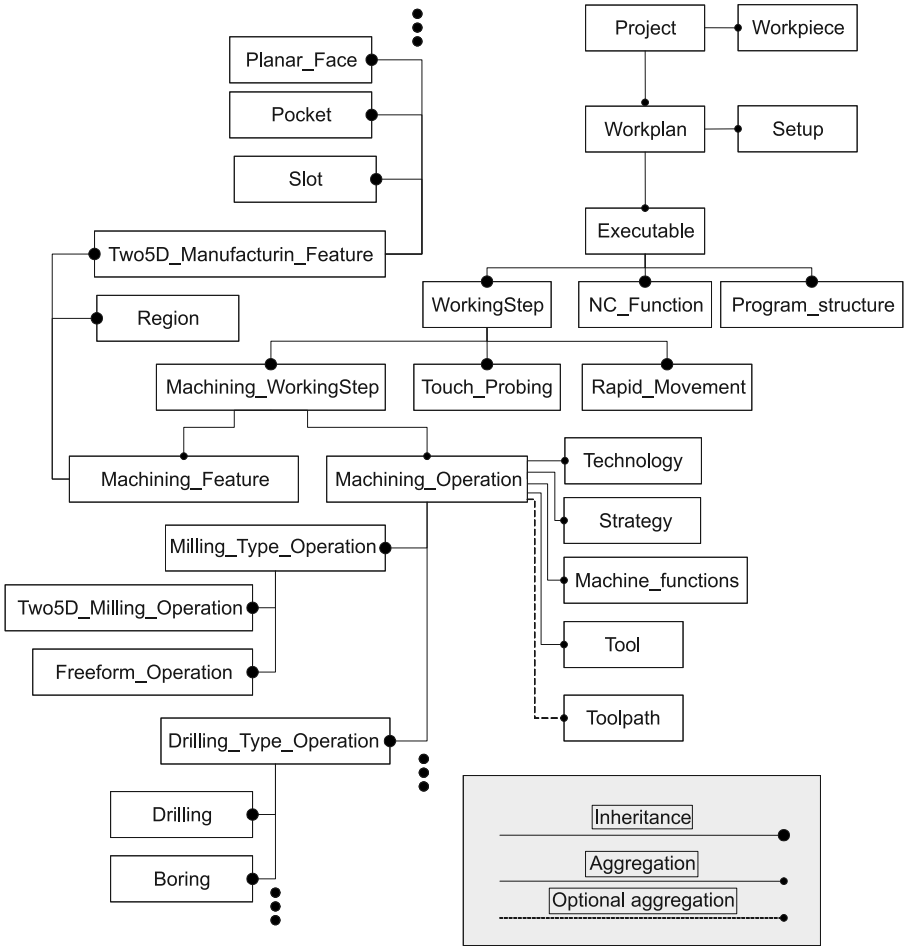

Fig. 2. The simplified view of STEP-NC data structure

Rys. 2. Poglądowy model danych standardu STEP-NC

Fig. 2. presents the simplified, object data model of STEP-NC. The inheritance, aggregation and optional aggregation relations should be noted on this scheme. The top element is Project object. This object has assigned the data about the project owner, versions, status and machined part information. Apart from the basic information like material or tolerance class, also the complete B-Rep representation of the machine part can be optionally stored. This is the option, as the part is described using manufacturing features. The Workplan is assigned to

Project. Then the Setup is assigned to Workplan. The list of so called Executables representing the machine tool activities is also assigned to the workplan. The inheritance relations distinguish three types of executables, namely working steps (WorkingStep), auxiliary NC functions (NC_Function, activity of machine tool does not moving the interpolated axis, as conditional stop, program stop, etc.) and control structure (Program_structure) deciding about the execution of executables based on the state of given conditions. Program_structure object allows for example to run executables in parallel. This is important in case of multipath machine tools. The WorkingStep blocks are the basic elements of STEP-NC standards. They describe the actions using the numerical controlled axes of machine tools. The can represent rapid linear movement (Rapid_Movement), measuring cycles (Touch_Probing) or machining blocks (Machining_WorkingStep) removing the material from the part. In the later case, WorkingStep define the relations between manufacturing feature (Machining_Feature) and its machining cycle (Machining_Operation). If the particular machining feature requires more than one machining cycle, the workplan has appropriate number of machining blocks (one for each machining cycle).

Each machining cycle has assigned the objects representing cutting parameters (Technology), machining strategy (Strategy), the state of the auxiliary machine tool functions (Machine_functions) and the optional toolpath (Toolpath). Technology object can represent such information like feed, cutting speed, spindle rotational speed, spindle synchronization, disable of feed and speed override, etc. Strategy object can represent such information like feed reduction on the beginning of the cutting movement, selection of conventional/climbing milling, distance between paths, etc. Machine_functions object is used to turn on the coolant, set the cooling fluid pressure system, start the chip removal, etc.

Object representing the tool contains the information about the tool holder, the list of cutting inserts, the total length of tool assembly, etc. The information about the material and the tool life management data are assigned to cutting insert objects. Despite this information, it seems that the B-Rep representation of the tool, with the categorization into cutting and non-cutting parts is missing. Of course, such B-Rep models can be created but will be stored outside of the STEP-NC file. This will increase the self documentary advantages of this format. The optional toolpath can be assigned to Machinining_operation object. The program send to CNC control system does not include the toolpath, it is generated by the procedures of CNC control system, based on the information about the machining tasks included in this STEP-NC file. Nevertheless, in the interim period, to facilitate the introduction of this new standard, CAM system can store the explicit tool path. This releases CNC from its generation.

The objects representing the machining cycles are categorized based on the machining method. Each machining method is the subject of the separate STEP-NC standard part. Now the standard parts for milling [4] and turning [5] are available. Within the milling, the milling and drilling cycles are distinguished. Milling cycles are divided into the 2.5D machining cycles requiring the simultaneous interpolation of two numerical controlled axes and the surface milling cycles requiring the simultaneous interpolation of at least 3 axes.

Manufacturing feature is assigned to each Machining_WorkingStep. Two groups of features were distinguished. The first is related to the freeform surfaces (Region), while the second to 2.5D machining features. The representation of the manufacturing feature is similar to common solutions [9].

3. Information flow in the CAD/CAM/CNC chain for machine tool programming language based on STEP-NC

Because STEP-NC does not describe "how to do" (as ISO 6983 programming language), but "what to do", CNC control systems can intelligently optimize the control program. They decide alone how to convert machining task into the movement of the numerical controlled axes. The way of machining can be changed "online" by the CNC control system, using the real-time feedback information. The introduced changes can be sent back to CAM system and stored in the library of standard machining processes for further reuse. This creates the mechanism for update and expansion of the manufacturing knowledge used by CAM system. Bidirectional communication with STEP-NC does not break the continuity of CAM/CNC chain. Furthermore, the same mechanism can be used to sent back the changes introduced by the machine tool operator (Fig. 1).

STEP-NC includes the full description of the machining task. There is a lot of information about the cutting tool available, not only the short mysterious word like T0101. The file contains also the description of the machined part. This includes not only the geometry definition, but also all manufacturing information like shape and location tolerances or the material hardness. Optional, also the definition of the raw material can be added, depending on the conformance class. STEP-NC program taken from the repository after several months can by analyzed (of course using software) and no additional documentation is needed.

The complete part description in STEP-NC standard is one of the most important attributes of this solution as it allows to further automate CNC machine tool programming. The lack of such description in computer readable form was one of the reasons blocking the entrance to the next level of CAM system automation. Having such information, CAM system can offer additional, new functions, releasing the time of the manufacturing engineers. The use of manufacturing feature oriented product data representation can be given as the example. Based on such feature representation of product data, including the non-geometry information like tolerances and material properties, advanced CAM systems can automatically select the appropriate machining cycles and establish their order. They can use the manufacturing knowledge databases also based on these features. Additionally, the experiences gathered during the actual machining, as the received surface quality, can be directly stored in the manufacturing knowledge database, for example as facts in the form "machining parameters – machining cycle – feature geometry". These facts can be used during the generation of the next CNC machining programs. This guarantees the direct integration of CAM/CNC systems.

Summarizing, STEP-NC integrates CAD/CAM/CNC chain and allows to create the feedback loop to upstream systems.

4. Conclusions

There is a number of obstacles blocking the implementation of STEP-NC in industry: the costs of the investment in this new technology, lack of commercial CNC systems based on STEP-NC and proved in industry environment, as well as reluctance of the people used to

employ the traditional approaches. Nevertheless, taking into the account the functionality of STEP-NC, especially related to CAD/CAM/CNC integration, no reduction of information to downstream systems as well as feedback loop, it seems that this is the solution of the future. The complete set of information about the CNC machine tool programming task and the working environment, including the feature based part description and the tool database can be used for the further automation of CNC machine tool programming. The author used the presented analysis of STEP-NC and its functionality as the base for the continuation of works related to the automation of manufacturing production preparation, using the STEP-NC as one of the basic elements.

References

[1] ISO 10303-1:1994 Industrial automation systems and integration – Product data representation and exchange – Part 1: Overview and fundamental principles, 1994.

[2] ISO 10303-203:2011 Industrial automation systems and integration – Product data representation and exchange – Part 203: Application protocol: Configuration controlled 3D design of mechanical parts and assemblies, 2011.

[3] ISO 14649-10. 2004. Industrial automation systems and integration – Physical device control – Data model for computerized numerical controllers – Part 10: General process data, 2004.

[4] ISO 14649-11:2004 Industrial automation systems and integration – Physical device control – Data model for computerized numerical controllers – Part 11: Process data for milling, 2004.

[5] ISO 14649-12:2005 Industrial automation systems and integration – Physical device control – Data model for computerized numerical controllers – Part 12: Process data for turning, 2005.

[6] ISO 6983-1:2009 Numerical Control of Machines – Program Format and Definition of Address Words – Part 1: Data Format for Positioning, Line Motion and Contouring Control Systems, 2009.

[7] Nikiel G., *Wymiana danych geometrycznych w komputerowo wspomaganym projektowaniu i wytwarzaniu*, Mechanik, No. 2/2010, 2010, 125-127.

[8] Pobożniak J., *Programowanie obrabiarek sterowanych numerycznie w systemie CAD/CAM Catia*, Helion, 2013 (w przygotowaniu do druku).

[9] Pobożniak J., *Two stage approach to feature recognition for Computer Aided Process Planning*, Advances in Manufacturing and Science Technology, Vol. 29, No. 4, 2005, 33-43.

[10] Stryczek R., Pytlak B., *Elastyczne programowanie obrabiarek*, Wydawnictwo Naukowe PWN, Warszawa 2011.

TECHNICAL TRANSACTIONS | **CZASOPISMO TECHNICZNE**
MECHANICS | MECHANIKA
1-M/2013

JANUSZ RAJDA*, EDWARD LISOWSKI**

ANALYSIS OF SWITCHING TIME FOR PILOT OPERATED DIRECTIONAL CONTROL VALVE

ANALIZA CZASU PRZESTEROWANIA ROZDZIELACZA STEROWANEGO POŚREDNIO

Abstract

The paper presents an analysis of switching time for pilot operated directional control valve [1–3] in a typical hydraulic system, in which the actuator is a hydraulic cylinder. A mathematical model has been built which contains equations of motion for the valve and actuator components, the balance of fluid flow, flow through the gap, and the principle of conservation of momentum and the flow curves of pressure relief valves [6, 8]. The system of equations is solved by fourth--order Runge-Kutta method. A survey to find minimal switching time has been conducted [4]. Positive overlap value, the coefficient of its movement resistance and control pressure value have significant impact on the switching time in the tested valve.

Keywords: *modeling of hydraulic systems*, *spool type directional control valve*

Streszczenie

W artykule przedstawiono analizę czasu przesterowania suwakowego rozdzielacza pośredniego działania [1–3] w typowym układzie hydraulicznym, w którym elementem wykonawczym jest siłownik hydrauliczny. Zbudowano model matematyczny zawierający równania ruchu elementów zaworu i siłownika, bilansu przepływu cieczy, przepływu przez szczelinę i zasady zachowania pędu oraz charakterystyki zaworów przelewowych [6, 8]. Układ równań rozwiązano metodą zmiennokrokową Runge-Kutty 4 rzędu. Przeprowadzono badania polegające na poszukiwaniu najkrótszego czasu przesterowania [4]. Istotny wpływ na czas przesterowania w badanym rozdzielaczu ma wartość dodatniego przekrycia suwaka, współczynnik oporów jego ruchu oraz wartość ciśnienia sterownia.

Słowa kluczowe: *modelowanie układów hydraulicznych*, *rozdzielacz hydrauliczny suwakowy*

* MSc. Eng. Janusz Rajda, Ponar Wadowice S.A.
** Prof. Eng. Edward Lisowski, Institute of Applied Informatics, Faculty of Mechanical Engineering, Cracow University of Technology.

Designations

m_s, m_t – computational mass of directional control valve spool (or cylinder rod and piston) respectively, plus the mass of retainer, spring and volume mass of attached liquid
V_i – the volume of the *i*-th line of the hydraulic system
B_i – equivalent volumetric elastic modulus for *i*-th line of the hydraulic system
Q_i – volumetric flow rate at the input for *i*-th line of the hydraulic system
Q_p – pump volumetric efficiency
p_i – pressure at *i*-th line of the hydraulic system
p_{z1} – cracking pressure for pressure relief valve at the system input
dp_{z1} – excess of cracking pressure for relief valve at the system input
p_{z2} – cracking pressure for pressure relief valve at the cylinder output
dp_{z2} – excess of cracking pressure for pressure relief valve at the cylinder output
α_s, α_t – kinematic coefficient of friction for the valve spool (or cylinder rod and piston)
c – centering spring stiffness coefficient for directional control valve
F_{ss0} – centering spring preload force for directional control valve
F_{ss} – centering spring force for directional control valve
F_{ts}, F_{tt} – kinematic friction force of directional control valve (or cylinder rod and piston)
x_1 – coordinate of the spool position (from the neutral position)
F_{hs} – control pressure force acting on the surface of the valve spool
A_s – active area of the valve spool affected by pressure p_1
F_{ht} – resultant pressure force acting on the surface of the piston/piston rod
F_{ds} – resultant hydrodynamic force acting on the spool of directional control valve,
x_2 – coordinate of position of the cylinder piston/piston rod (from the maximum extended position)
v_2 – speed of movement of the piston/piston rod
S_1 – sectional area of the piston rod
S_k – active cross-sectional area on the side of the cylinder piston rod
S_s – width of the flow gap at the valve spool
S_k – minimum cross section of stream at the valve channel
x_{p1} – overlap value for the valve spool
μ_1 – liquid outflow coefficient
ρ – fluid density
α_i – fluid inlet/outlet angle for *i*-th control edge
v_{Qi} – fluid flow speed at the *i*-th control edge

1. Introduction

Control of working movements at the machinery or equipment with hydraulic drive is usually carried out by means of directional control valves, usually spool type [1, 2]. Start or change of direction of the working movement is caused by the spool shift. Therefore, switching of the directional control valve is forcing the system, so switching time is important in the valve operation. By changing the switching time, we can change time constants for

the whole hydraulic system [11]. In industrial applications, there are many solutions to allow forcing of hydraulic directional control valves, for example in the form of slots cut in the spool, proportional spool position control by a given course, etc. [5, 7, 10, 12]. All of these solutions increase the time constant of the directional control valve, which usually has a positive effect on the elimination of hydraulic hammer and pressure excess at start of the system. However, in some applications of directional control valves, such as safety devices, in order to obtain a rapid response of the machinery or equipment, the switching time should be as short as possible [9]. In this paper, the task undertaken is to determine parameters associated with the spool which affect the speed of the opening of flow path at the valve. The study has been conducted using the hydraulic pilot operated directional control valve type WEH22E [13].

2. Object of the study

General view of the directional control valve is shown in Fig. 1. It is built of the main body 1, the spool 2, the retainers 3 and the centering spools 4 , the covers 5 forming the pressure chambers 6 and 7 and the pilot valve 8. Switching the valve is caused by the fluid under pressure provided into the chamber 6 (or 7) and the simultaneous relief of the opposite chamber 7 (or 6). As a result of the force of the fluid pressure, the spool overcoming the force of the spring , motion resistance and hydrodynamic force, moves toward the extreme position forming different configuration of connections.

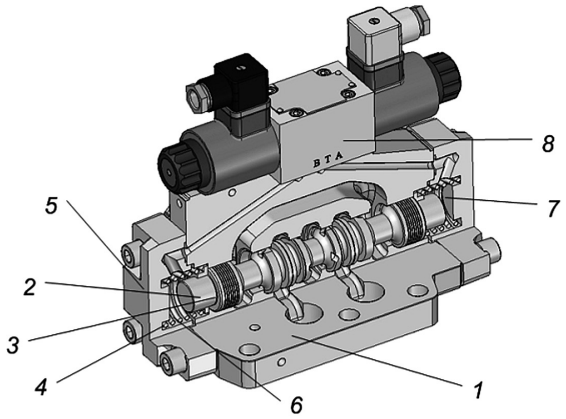

Fig. 1. Schematic structure of directional control valve WEH22E
Rys. 1. Schemat budowy rozdzielacza WEH22E

3. Mathematical model

Operation of directional control valve WEH22E has been examined in the hydraulic system, the schematic diagram of which is shown in Figure 2. Hydraulic cylinder 4 is assumed to be working element. The system is supplied by a fixed displacement pump of

capacity Q_p. The pump is connected with a hydraulic directional control valve by means of the conduit with volume V_1 and pressure p_1. This line is characterized by constant volumetric elastic modulus B_1. At the output of the directional control valve and the inlet of the hydraulic line having a volume V_2 and equivalent volumetric elastic modulus B_2, flow is Q_1. Pressure in this line is p_2. The liquid of flow rate Q_2 flows into the hydraulic cylinder and flows out of flow rate Q_3 to the hydraulic line V_3 with an equivalent volumetric elastic module B_3. In this line, there is pressure p_3. The cylinder load is simulated by means of pressure relief valve 6. On energizing the solenoid 3, pilot valve 1 gives pressure into control chamber of the spool initiating the process of moving the spool and allowing the flow of fluid in the system. It is assumed that the system is in thermal equilibrium, and the mass of the liquid is concentrated in specific points of the system, that is, the valve spool, the individual sections of the line and the rod (and the piston) of the cylinder. The pressure in the drain line is omitted. Under these assumptions, the mathematical model will constitute the differential equations for the valve spool movement and cylinder piston rod movement, equations of flow continuity and the principle of conservation of momentum as well as equations of flow through the slot and performance curves of pressure relief valves.

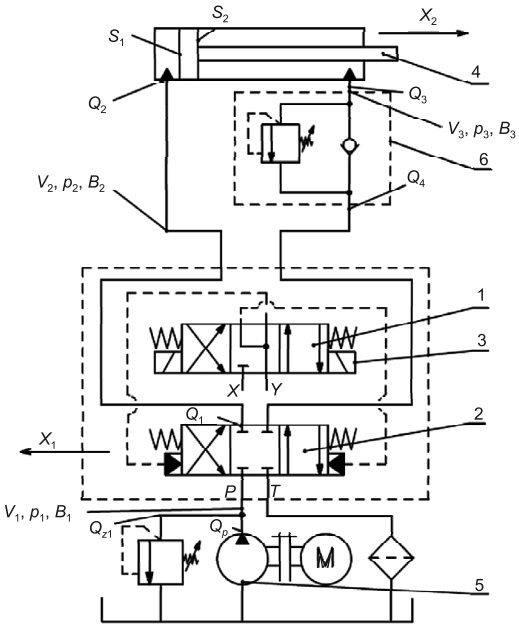

Fig. 2. Hydraulic diagram with the marked system parameters

Rys. 2. Schemat hydrauliczny wraz z oznaczeniami parametrów układu

Equations of the forces acting on the spool of directional control valve:

$$m_s \frac{d^2 x_1}{dt^2} + F_{ts} + F_{ss} + F_{ds} = F_{hs} \tag{1}$$

Equation of the cylinder piston rod motion:

$$m_t \frac{d^2 x_2}{dt^2} + F_{tt} = F_{ht} \tag{2}$$

Flow balance equation for volume V_1:

$$Q_p - Q_1 - Q_{z1} = \frac{V_1}{B_1} \frac{dp_1}{dt} \tag{3}$$

Flow balance equation for volume V_2:

$$Q_1 - Q_2 = \frac{(V_2 + S_1 \cdot x_2)}{B_2} \frac{dp_2}{dt} \tag{4}$$

Flow balance equation for volume V_3:

$$Q_3 - Q_4 = \frac{(V_3 - S_2 \cdot x_2)}{B_3} \frac{dp_3}{dt} \tag{5}$$

Volumetric flow rate Q_2 and Q_3 can be determined from the relation:

$$Q_3 = S_2 \cdot v_2, \quad Q_2 = S_1 \cdot v_2 \tag{6}$$

Volumetric flow rate through the slot Q_1 can be determined:

$$Q_1 = \mu_1 \cdot S_s(x_1) \cdot \sqrt{\frac{2 \cdot (p_1 - p_2)}{\rho}} \tag{7}$$

Function $S_s(x_1)$ is determined on the base of measurements on 3D model and approximated by the function:

$$\begin{aligned} &S_s(x_1) = a_1 \cdot (x_1 - x_{p1}) + a_2 \cdot (x_1 - x_{p1})^2 \quad \text{for} \quad S_s < S_k \\ &S_s = S_k \quad \text{for} \quad S_s \geq S_k \\ &S_s = 0 \quad \text{for} \quad x_1 < x_{p1} \end{aligned} \tag{8}$$

Volumetric flow rate Q_4 can be determined from the valve performance curve and describe by the relation:

$$\begin{aligned} Q_4 = k_4 \cdot (p_3 + dp_{z2}) \quad \text{for} \quad p_3 > p_{z2} \\ Q_4 = 0 \quad \text{for} \quad p_3 \leq p_{z2} \end{aligned} \tag{9}$$

Volumetric flow rate Q_{z1} can be determined from the valve performance curve and describe by the relation:

$$\begin{aligned} Q_{z1} = k_{z1} \cdot (p_1 + dp_{z1}) \quad \text{for} \quad p_1 > p_{z1} \\ Q_{z1} = 0 \quad \textit{for} \quad p_1 \leq p_{z1} \end{aligned} \tag{10}$$

Spring force F_{ss} can be determined from the relation:

$$F_{ss} = F_{ss0} + c \cdot x_1 \tag{11}$$

Viscous friction force of the spool F_{ts} and piston rod F_{tt} can be determined from the relation:

$$F_{tt} = \alpha_t \cdot x_2, \quad F_{ts} = \alpha_s \cdot x_1 \tag{12}$$

Forces from control pressure acting on the spool F_{hs} and cylinder piston rod F_{ht} can be determined from the relation:

$$F_{ht} = A_1 \cdot p_2 - A_2 \cdot p_3, \quad F_{hs} = A_a \cdot p_1 \tag{13}$$

The resultant value of hydrodynamic forces acting on the valve spool can be calculated from the relation (Figure 3):

$$F_{hd1} = \rho \cdot [Q_1(v_{Q1}\cos\alpha_1 - v_{Q2}\cos\alpha_2) - Q_4(v_{Q4}\cos\alpha_4 - v_{Q5}\cos\alpha_5)] \tag{14}$$

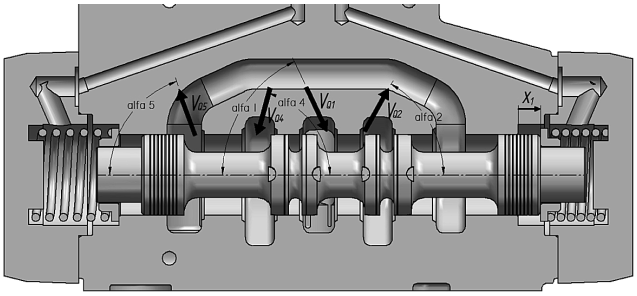

Fig. 3. Inlet and outlet angle of fluid stream on control edges

Rys. 3. Kąt wlotu i wylotu strugi cieczy na krawędziach sterujących

4. Test results

In order to determine the time for full opening of the directional control valve, system of equations (1) to (14) is resolved, using the data from technical information of the directional control valve WEH22E. It was assumed that the control pressure (X) is obtained from the main supply line of the system (P). Moreover, the figures are taken for the cylinder: diameter D = 100 mm, d_t = 56 mm and stroke 1000 mm. Forcing at the input is pump with constant flow Q_p = 480 dm^3/min. Example response of the spool to step forcing for standard value of positive spool overlap (x_{p1} = 5 mm) and reduced overlap (x_{p1} = 0.5 mm) are shown in Fig. 4. Fig. 5 and 6 show respectively pressure course in the volume V_1 and piston rod velocities v_2. As follows from the courses, the lower value of overlap parameter (x_{p1} = 0.5 mm), the valve spool moves a little more slowly to the end position. This is due to a lower pressure during the start-up of the system (Fig. 5). Reducing the spool overlap value, however, results in earlier opening of the flow ways and the piston rod faster begins to move, as is shown in Fig. 6.

Reduction of the directional control valve overlap allows to reduce the response time of the valve in the initial phase of its operation. In the final stage, speed of the spool movement decreases due to the pressure drop at pressure line, from where control pressure is taken. Excessive reduction of the spool overlap value will result in increased internal leakage. The study for various combination of parameters have shown that in addition to reducing the spool overlap value, reduction of spool movement resistance and increase of control pressure have a significant impact on minimizing the switching time.

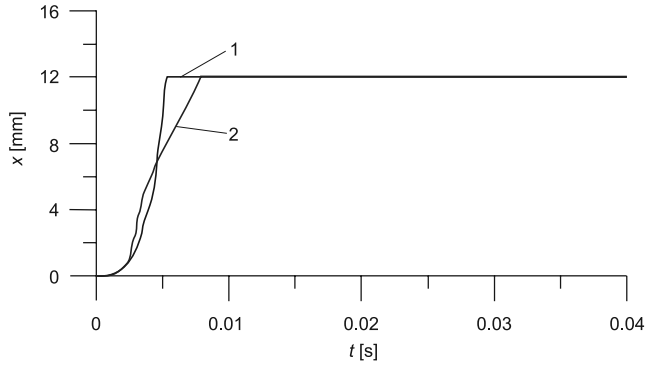

Fig. 4. Spool valve movement as a response to step forcing

Rys. 4. Przemieszczenie suwaka rozdzielacza jako odpowiedź na wymuszenie skokowe

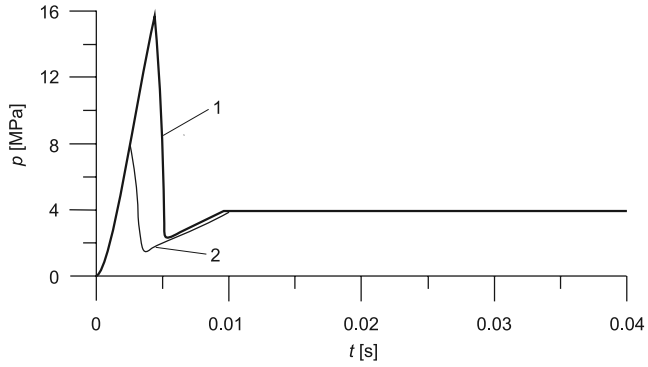

Fig. 5. Pressure course at the system inlet

Rys. 5. Przebieg ciśnienia na wejściu do układu

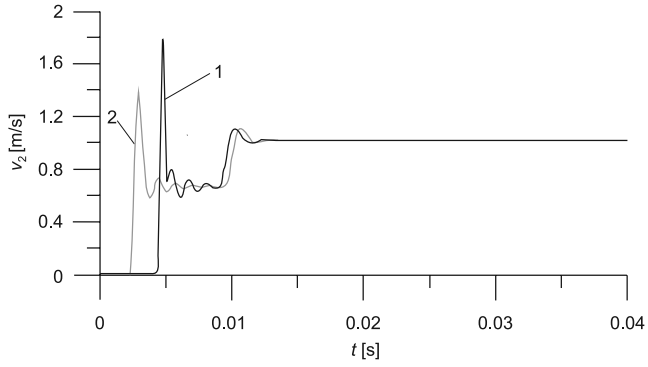

Fig. 6. Velocity course for the cylinder piston rod

Rys. 6. Przebieg prędkości tłoczyska siłownika

References

[1] Amirante R., Moscatelli P.G., Catalano L.A., *Evaluation of the flow forces on a direct (single stage) proportional by means of a computational fluid dynamic analysis*, Energy Conversion and Management 48, 2007, 942-953.

[2] Amirante R., Del Vescovo G., Lippolis A., *Evaluation of the flow forces on an open centre directional control valve by means of a computational fluid dynamic analysis*, Energy Conversion and Management 47, 2006, 1748-1760.

[3] Lisowski E., Domagała M., *Determination of static characteristic of direct acting relief valve*, Proceedings of the 1st international conference on computational methods in fluid power technology, Melbourne 2003, 211-220.

[4] Lisowski E., Domagała M., *Optimization hydraulic components using fluid-solid interaction simulation*, Proceedings of 4th FPNI-PhD Symposium, Florida-Sarassota 2006, 151-159.

[5] Lisowski E., Filo G., *Zastosowanie logiki rozmytej do sterowania proporcjonalnym zaworem przelewowym*, Przegląd Mechaniczny, nr 1/2002.

[6] Momeni H., Lisowski E., *CFD analysis of pilot operated relief valve*, Proceedings of 5th FP -NI-PhD Symposium, Kraków 2008, 493-500.

[7] Stryczek S., *Napędy hydrostatyczne*, WNT, Warszawa 1999.

[8] Lisowski E., Rajda J., *Modelowanie CFD przepływu przez zespół zaworów*, Konferencja „Napędy i sterowania hydrauliczne i pneumatyczne", Wrocław 2012.

[9] Renn J.C., Kao T.C., *Application of CFD to design a power-saving hydraulic directional two-land-four-way-valve*, Proceedings of the 1st international conference on computational methods in fluid power technology, Melbourne 2003, 26-28.

[10] Standard ISO 4401-08-07-0-94.

[11] Manring N.D., *Modeling Spool-Valve Flow Forces*, University of Missouri at Columbia, 2004, ASME International Mechanical Engineering Congress and Exposition, Anaheim, USA, 2004.

[12] Osiecki A., *Napęd i sterowanie hydrauliczne maszyn. Teoria obliczenia układu*, Wydawnictwo Politechniki Gdańskiej, Gdańsk 1981.

[13] Catalogue: Ponar Wadowice. Directional spool valve, WK 460 110, 04.2001.

TECHNICAL TRANSACTIONS | **CZASOPISMO TECHNICZNE**
MECHANICS | MECHANIKA
1-M/2013

JANUSZ RAJDA*, EDWARD LISOWSKI**

FLOW FORCES ACTING ON THE SPOOL OF DIRECTIONAL CONTROL VALVE

ODDZIAŁYWANIE PRZEPŁYWAJĄCEJ STRUGI NA SUWAK ROZDZIELACZA HYDRAULICZNEGO

A b s t r a c t

This paper presents a method with the use of CFD analysis for calculating the forces acting on the spool during the flow of working liquid stream through the electro-hydraulic pilot operated directional control valve. The liquid stream flowing through the directional valve causes hydrodynamic response according to the principle of conservation of momentum. Liquid pressure acting on the spool surface affects the forces balance of valve spool as well. An object of the research is the pilot operated directional control valve WEH22 type with flow rate up to 450 dm^3/min. For the analysis ANSYS/Fluent software was used.

Keywords: *CFD modelling*, *directional control valve*, *Fluent/Ansys*

S t r e s z c z e n i e

W artykule przedstawiono metodę obliczania sił powstających na skutek oddziaływania strumienia przepływającej cieczy na suwak rozdzielacza z wykorzystaniem analizy CFD. Obiektem badań jest rozdzielacz hydrauliczny sterowany pośrednio elektrohydraulicznie. Struga przepływająca przez rozdzielacz hydrauliczny zgodnie z zasadą zachowania pędu wywołuje reakcję hydrodynamiczną. Również ciśnienie cieczy, działając na powierzchnię suwaka wpływa na bilans sił działających na suwak rozdzielacza. W artykule przedstawiono analizę sił związanych z przepływem dla rozdzielacza hydraulicznego typu WEH22 dla przepływu w zakresie do 450 dm^3/min. Do analizy zastosowano program ANSYS/FLUENT.

Słowa kluczowe: *modelowanie CFD*, *rozdzielacz hydrauliczny*, *Fluent/Ansys*

* MSc. Janusz Rajda, Ponar Wadowice.
** Prof. DSc. PhD. Edward Lisowski, Institute of Applied Informatics, Cracow University of Technology.

1. Introduction

Development of hydraulic machine drive is connected with the development of its individual elements. The main aim of development of hydraulic components is to increase their parameters, including the range of flow and working pressure [1, 4]. Increasing the flow and pressure result in an increase of forces acting on the valve spool. It may happen that at high flow rate, the increase of flow forces affects adversely the total balance of forces acting on the spool and thus interferes with the correct operation of the valve [4, 5]. This paper presents a method for calculating the forces connected with the flow of working liquid with the use of ANSYS/Fluent software.

2. Object of the research

An object of the research is a popular type of hydraulic directional control valve WEH22 produced by several manufacturers [7]. It is designated for hydraulic systems in which pressure does not exceed 35 MPa, and flow rate is up to 450 dm^3/min. Design of the directional control valve WEH22 type is shown in figure 1. The valve consists of the main body (1) with the valve spool (2) and the pilot valve (4). The pilot valve is controlled by the solenoids (5) with manual override buttons (6). When one of electromagnets is energized the pilot valve causes the spool (2) in the main body to move to the extreme position and it allows the flow from port P to A and from B to T (or P to B and A to T). The paper presents the analysis of flow from P to A (P-A) and B to T ports (B-T) as representing the basic flow path for this directional valve.

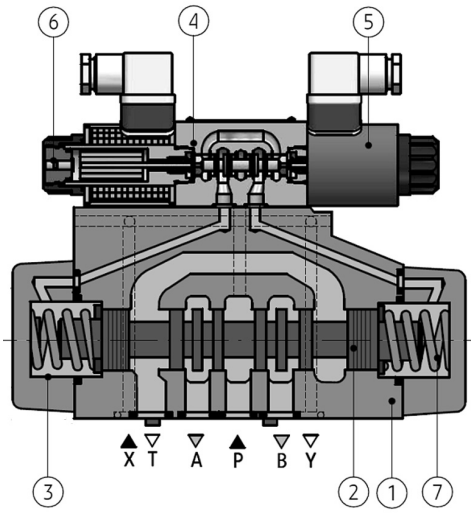

Fig. 1. Design of directional control valve WEH22J type

Rys. 1. Budowa rozdzielacza hydraulicznego typu WEH22J

3. Discrete model of flow paths

3D models of the body and spool created in Solid Edge for technical documentation are used to built stream geometry. For this purpose, 3D models of the body and spool are loaded to the CREO software. The surfaces are copied from these 3D models and irrelevant components of non-geometric nature of the channel surface are remove. Then solids are created using the CREO Solidify command. For these components the logical operations are performed which give as a result geometric model of the streams. FEM mesh and flow models are made using ANSYS/Fluent software. The individual flow path have a different geometric structure and different flow paths within the valve body. Figure 2 shows the discrete model of P-A flow path and in figure 3 model of B-T path. These models are made using the advanced features of the grid compaction. In the areas of complex geometry the grid is properly compacted. The model for P-A path includes 358 800 cells and 121 081 nodes and for B-T path 1 917 405 cells and 414 778 nodes.

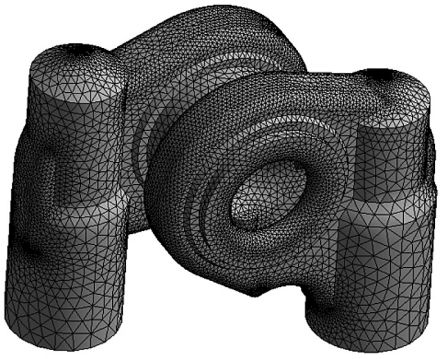

Fig. 2. Mesh of P-A flow path
Rys. 2. Siatka MES drogi przepływowej P-A

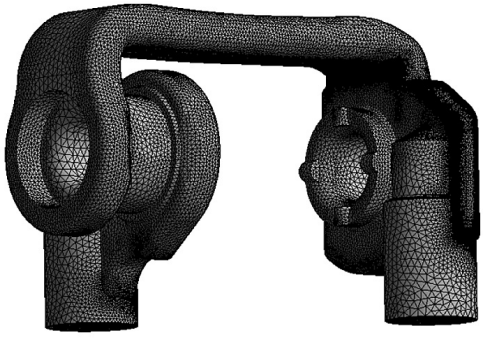

Fig. 3. Mesh of B-T flow path
Rys. 3. Siatka MES drogi przepływowej B-T

4. CFD model

In order to perform the analysis flow kind must be determined. Due to the fact that at the directional control valve there are no conditions for the formation of laminar flow, turbulent flow pattern was assumed to simulate flow. The ANSYS/FLUENT [6] program allows to choose from a variety of models available including: *k*-epsilon, K-Omega and Reynolds. In the case of flow through the directional control valve *k*-epsilon model works well enough due to the fact that in the valve there are no conditions for the formation of laminar flow [2, 3]. Thus, for the simulation study turbulence model *k*-epsilon was chosen. The kinetic energy of the turbulence and dissipation factor are computed from the following equations [1]:

$$\frac{\partial}{\partial t}(\rho k)+\frac{\partial}{\partial x_i}(\rho k u_i)=\frac{\partial}{\partial x_j}\left(\alpha_k \mu_{eff}\frac{\partial k}{\partial x_j}\right)+G_k+G_b-\rho\varepsilon-Y_M \tag{2}$$

$$\frac{\partial}{\partial t}(\rho \varepsilon)+\frac{\partial}{\partial x_i}(\rho \varepsilon u_i)=\frac{\partial}{\partial x_j}\left(\alpha_\varepsilon \mu_{eff}\frac{\partial \varepsilon}{\partial x_j}\right)+C_{1\varepsilon}(G_k+C_{3\varepsilon}G_b)-C_{2\varepsilon}\rho\frac{\varepsilon^2}{k} \tag{3}$$

In these equations G_k represents the increase in the kinetic energy of turbulence caused by gradient of average velocities. G_b is the energy generated by the phenomenon of buoyancy. Y_m is the energy associated with the compressibility of liquids, $C_{1\varepsilon}$, $C_{2\varepsilon}$ and $C_{3\varepsilon}$ are constants of the model, s_k , s_ε are Prandtl's numbers, respectively.

Turbulent viscosity, m_t, is calculated as follows:

$$\mu_t=\rho C_\mu\frac{k^2}{\varepsilon} \tag{4}$$

where model constants [1]: $C_{1\varepsilon}$ = 1.44, $C_{2\varepsilon}$ = 1.92, C_m = 0.09, s_k = 1.0, s_ε = 1.3.

To carry out the calculation in ANSYS Fluent program after generating grid, boundary conditions in *Setup* module of the program must be defined. In the option *Boundary Conditions* as inlet velocity magnitude normal to boundary is assumed. Value Velocity magnitude is introduced as input parameter to *Workbench*. As outlet condition outlet pressure is taken. Value *k* and *epsilon* are introduced as intensity and length scale. Using model *Results* of ANSYS Fluent program, with the command *Calculators* and *Expressions* to *Workbench* there are introduced as parameters F_x, F_y and F_z forces acting on the valve spool. In the module *Expressions* the following variables specified by *Calculators* are defined:

- force_x()@spool – force in X axial direction (axis along port),
- force_y()@spool – force in Y axial direction (axis along the spool),
- force_z()@spool – force in Z axial direction (axis normal to port),
- ave(Pressure)@a_inlet – average pressure at the inlet to the flow path.

5. Results of calculations

The P-A flow path

The results of the CFD analysis provide information about the values of hydraulic forces, as well as the distribution of flow velocity and pressure in the analysed flow paths. Figure 4

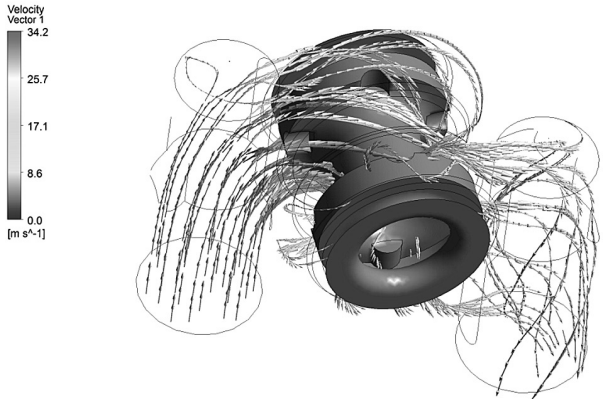

Fig. 4. Velocity vectors on the stream lines for P-A flow path

Rys. 4. Wektory prędkości na liniach prądu dla drogi przepływowej P-A

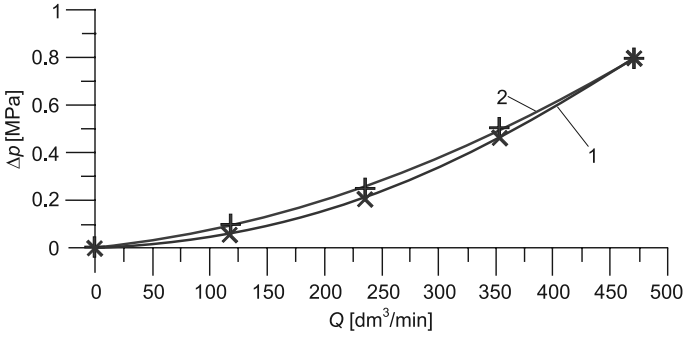

Fig. 5. Pressure loss for flow path P-A

Rys. 5. Straty ciśnienia dla drogi przepływowej P-A

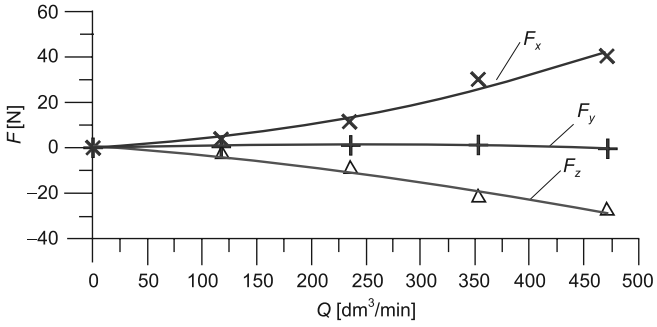

Fig. 6. F_x,F_y,F_z forces acting on the spool for P-A flow path

Rys. 6. Siły F_x, F_y, F_z działające na suwak dla przepływowej P-A

shows distribution of the velocity on streamline acting on the walls for Q = 450 [dm^3/min]. for P-A flow path and the spool surface which the stream flows around. Figure 5 – curve 1 – shows the pressure drop during the flow while Figure 6 shows the relation of forces F_x, F_y, F_z acting on the spool. Figure 5 – curve 2 – shows the pressure losses took from the manufacturer's catalog [7]. As can be seen from this figure, the catalogue data (received from test bench) are consistent with the ones obtained from the CFD analysis. The following force values are estimated for Q = 450 dm^3/min.: F_x = 40 [N], F_y = –0.8 [N], F_z = –28 [N]. Thus, F_y axial force obtains the lowest value, and F_x axial force obtains the highest value. This result informs us that the influence of flow is very small on balance force acting on the spool.

B-T flow path

Similarly, the analysis for B-T flow path is conducted. For this flow path Figure 7 shows velocity vectors on the stream lines and an outline of the spool surface flown around by the stream of liquid.

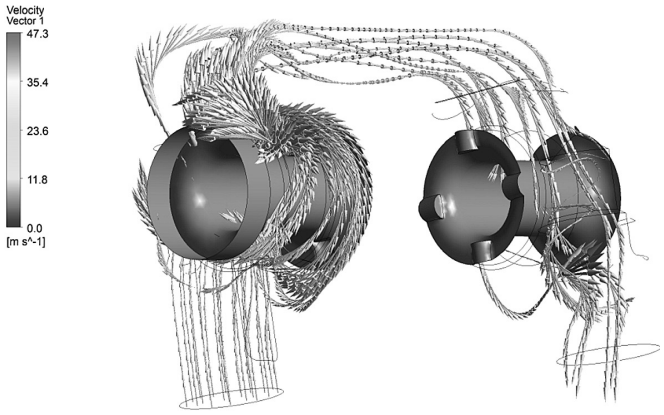

Fig. 7. Velocity vectors on the stream lines for B-T flow path

Rys. 7. Wektory prędkości na liniach prądu dla drogi przepływowej B-T

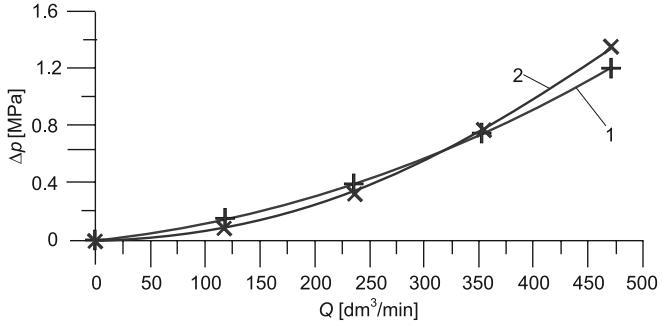

Fig. 8. Pressure losses for B-T flow path

Rys. 8. Straty ciśnienia dla drogi przepływowej B-T

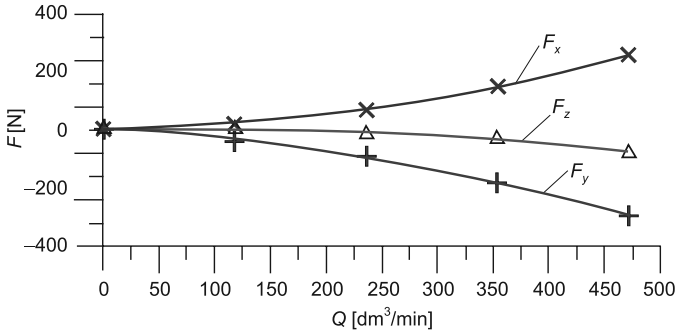

Fig. 9. F_x, F_y, F_z forces acting on the spool for B-T flow path

Rys. 9. Siły F_x, F_y, F_z działające na suwak dla przepływowej B-T

Figure 8 shows the comparison of pressure losses during the flow through the path obtained from CFD calculations and catalogue data. Figure 9 shows the change of F_x, F_y, F_z forces acting on the spool. This flow path is more complicated. Stream of liquid on its way flows the spool around twice and the velocity vectors change its direction several times. The forces which arise at the flow through this path are several times larger than those of P-A path. The following force values are estimated for Q = 450 [dm^3/min]: F_x = 252 [N], F_y = –99 [N], F_z = –83 [N]. Thus, F_y axial force obtains the highest value, and F_z axial force obtains the lowest value. This result informs us that the influence of flow on balance force acting on spool is very high.

6. Conclusions

The paper considers the issue of determination of the forces acting on the valve spool of directional control valve derived from the liquid stream. The analysis concerns the hydraulic directional control valve of flow range up to 450 [dm^3/min]. The article shows that the forces derived from the stream interaction can obtain high values interfering the valve operation. By shaping the geometry of the flow paths, the negative effects can be minimized. With several flow paths in the body, this task may be difficult. Using CFD method research can be conducted to seek compromise solutions.

References

[1] Launder B.E., Spalding D.B., *The Numerical Computation of Turbulent Flows. Computer Methods in Applied Mechanics and Engineering*, no. 3, 1974, 269-289.

[2] Lisowski E., Domagala M., *Determination of static characteristic of direct acting relief valve*, Proceedings of the 1st international conference on computational methods in fluid power technology, Melbourne 2003, 211-220.

[3] Lisowski E., Rajda J., *CFD analysis of pressure loss during flow by hydraulic directional control valve constructed from logic valves*, Energy Conversion and Management 65, 2013, 285-291.

[4] Renn J-C., Kao T-C., *Application of CFD to design a power-saving hydraulic directional two--land-four-way-valve*, Proceedings of the 1st international conference on computational methods in fluid power technology, Melbourne 2003, 26-28.
[5] Del Vescovo G., Lippolis A., *Three-dimensional analysis of flow forces on directional control valves*, International Journal of Fluid Power, 4(2), 2003.
[6] *ANSYS/Fluent Inc. 13.0 users guide*; 2011.
[7] Catalogue *Directional spool valve type WEH22 electrically operated*, Ponar Wadowice, WK 491 800 01.2013.

TECHNICAL TRANSACTIONS | **CZASOPISMO TECHNICZNE**
MECHANICS | MECHANIKA
1-M/2013

ANDRZEJ SKOWRONEK*

EVALUATING THE INFLUENCE OF GENERATION METHODS ON THE QUALITY OF THE SMART DESIGNS OF EXPERIMENT

OCENA WPŁYWU METOD GENEROWANIA NA JAKOŚĆ ELASTYCZNYCH PLANÓW EKSPERYMENTU

Abstract

This paper presents results of computer simulation made to evaluate how the quality of the smart designs of experiment depends on the methods of generating. The quality of smart designs was evaluated by comparing the known values of special testing functions simulating the real research object and approximated values predicted by neural networks trained with the sets based on smart designs of experiment. The results suggest the possibility of significant reducing the number of experiments runs using studied smart designs.

Keywords: *smart design of experiment*, *experimental research*, *neural approximation*

Streszczenie

Artykuł przedstawia wyniki symulacji komputerowej, której celem było dokonanie oceny wpływu metody generowania elastycznych planów eksperymentu na ich jakość. Jakość planów oceniana była na podstawie porównania znanych wartości funkcji testowych symulujących rzeczywisty obiekt badań i wartości aproksymowanych zwracanych przez sieć neuronową uczoną z wykorzystaniem zbiorów danych opartych na analizowanych planach. Wyniki sugerują możliwość znacznej redukcji rozmiaru potencjalnych badań eksperymentalnych planowanych z wykorzystaniem analizowanych planów elastycznych.

Słowa kluczowe: *elastyczny plan eksperymentu*, *badania eksperymentalne*, *aproksymacja neuronowa*

* PhD. Eng. Andrzej Skowronek, Institute of Applied Informatics, Faculty of Mechanical Engineering, Cracow University of Technology.

1. Introduction

Experimental research play in many areas of science a key role in obtaining the knowledge and information. Using techniques offered by theory of experiment you can support conducting experimental research, especially when it is necessary to limit the time of experiment or cost. In the theory of experiment there are used various types of experimental designs. The type of design depends largely on the specific purpose of research ([1, 2, 3]), which could be for instance looking for unknown object's function, verification how inputs effect output and looking for extremes of object's function. Application the experimental designs with special techniques for analysis of experiment's results can often facilitate reducing the size of the experiment (number of runs, observations, etc.) and obtaining relevant information from research, without reducing their quality ([4, 5]). In addition to the undoubted benefits of using traditional designs of experiment (reducing the number of experiment's runs, reducing time and cost of research), you can also see some negative effects in case of conducting experiment according to them. The researcher can not change number of design's units, number of inputs' levels and has to carry out the experiment strictly according to used design. A quite different approach to the concept of planning the experiment enable smart designs of experiments ([6]) which allow the researcher to set the number of design's units and number of inputs' levels.

2. Smart designs of experiment

Smart designs of experiment are generated in a dedicated computer application. Creating of smart design consists of the following steps [7]:

- defining characteristics of the design: number of inputs (factors), number of designs units, number of inputs levels
- generating of inputs' levels according to chosen method
- generating of sets of inputs factors levels
- generating of set of all possible designs' units by permuting all inputs levels
- completing the design by selecting from the set of all possible design's units only fulfilling the special condition
- equipartitional analysis to evaluate quality of design (quality means regular and equipartitional distribution of design's units in inputs space).

Smart designs are generated basing on three important principles: adaptation, randomness and equipartition ([6, 7]). The first principle means the possibility of adjusting the design's characterisctics to the conditions of the experiment and characteristics of the analyzed object, what was discussed above. The second principle means that smart designs are created in non-deterministic way: both generation of inputs levels and selection of designs units are conducted using pseudo-random numbers. However, there are some limitations put on the random way of generation of design's units:

- using a parameter called "important difference" (Δx), a minimal permissible distance between currently generated value and existing values of each input factor levels (Fig. 1),
- a parameter called "minimal Euclid's distance" (*esmin*) – it is Euclid's distance to the nearest "neighbour-unit" in the inputs space, calculated for each design's unit, each unit must fulfill the condition: es ≥ esmin (Fig. 2).

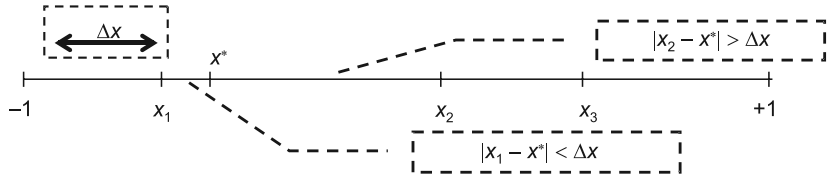

Fig. 1. Value x^* doesn't pass the important difference condition test and will be removed

Rys. 1. Wartość x^* nie spełnia kryterium różnicy istotnej i zostanie usunięta

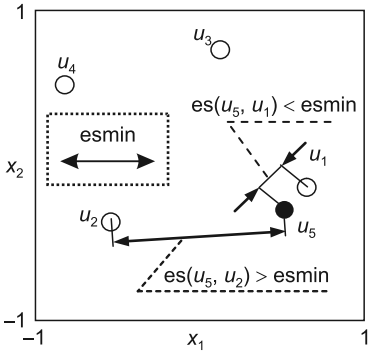

Fig. 2. Unit u_5 fails the es ≥ esmin condition test $es(u_5, u_1) < esmin$ and will be removed

Rys. 2. Układ u_5 nie spełnia warunku es ≥ esmin i zostanie usunięty

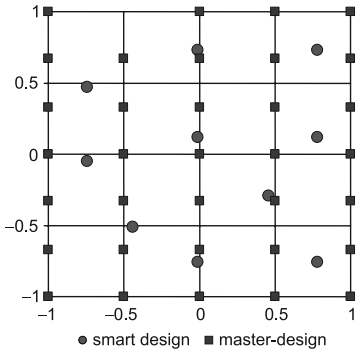

Fig. 3. 2-inputs master-design and smart design

Rys. 3. Plan wzorcowy o 2 wielkościach wejściowych i plan elastyczny

The conceptions of both described above parameters are based on a conception of Euclid's distance and they use the fact that a set of experimental design units in the space of inputs is equivalent to the set of points in orthogonal coordinate system and the combinations of inputs' levels (which make up units of designs) are equivalent to points coordinates. The Δx and *esmin* parameters support equipartition of the designs units in the inputs space. If there are no other assumptions designs units should cover regularly the whole inputs space (the third rule). To estimate the regularity of the distribution of the designs units it is used the method of the equipartitional analysis (EPA, [6]). The analysed (created) experimental design is compared with the master-design which units are distributed perfectly regularly in the inputs space ([6, 7], Fig. 3). The master-designs have the same numbers of inputs as the analysed designs, the same number of various inputs levels but the number of design's units is often significant higher and equal to the product of numbers of all inputs levels. However, the levels of master-design are calculated for each input by dividing the length of input range by the number of input levels (Fig. 3). For each unit of the master-design you can evaluate the Euclid's distance to the nearest unit of the analysed design. Next you can evaluate for such a collection (called equipartitional set) a lot of statistical parameters (for example descriptive statistics) or make one of the statistical tests (for example goodness of fit test, see: [8]). Each

of them could be an equipartition criterion in this analysis. In this paper there were used two parameters: maximal (*e1max*) and mean (*e1mean*) value of equipartitional set. The *e1mean* parameter describes the central tendency of equipartitional set and the *e1max* parameter gives information if there are some huge empty areas in the input space (without designs units), what is important taking into consideration the assumption that the designs units should cover the whole inputs space. The dependence between the both equipartitional analysis parameters and the designs quality (quality means equipartition, perfect regularity of the designs units in the inputs space) was verified and described in [7]. The conclusion was: the less value of equipartitional parameter the more regular distribution of design's units in inputs space.

There are actually three ways to generate the inputs' levels ([9]). In the first method ("Z" method) inputs levels are generated as pseudo-random values from the normalized range [–1, 1] and checked if they pass the important difference condition. If a value fail the test, it is removed and the next one is generated to reach the right amount. In "R" method levels of inputs are calculated by dividing the inputs ranges by the demanded numbers of inputs levels. The smallest level is calculated as the minimum of input's range and the biggest (last) level is calculated as maximum of input's range. In the R2-method the idea of levels calculating is that each level should be the center point of equal areas of influence. The first and the last levels are not equal to minimum and maximum of input range (Tab.1).

Table 1

Examples of levels in R and R2 methods

Method	Values used in case of 5 levels				
R	–1	–0.5	0	0.5	1
R2	–0.8	–0.4	0	0,4	0.8

The smart designs generator in the current version has implemented functionalities that support selecting the optimal values of important generation's parameters – important difference (Δx, used in Z-method of levels generating) and minimal Euclid's distance (*esmin*, used to ensure high regularity and equipartition of design's units in the inputs' space). In the previous versions of generator researcher must set it by himself. If he doesn't know well the principles of functioning the smart designs generator and doesn't have some intuition or experience in designs generating process it is likely that the generated design won't be optimal – designs units won't cover equally the whole inputs space. In a case of setting to small values of generation parameters equipartition decreases or it is not possible to get experimental design with the assumed number of units otherwise.

If inputs levels are generated with Z-method, the initial value of Δx is calculated as:

$$\Delta x = \frac{r}{n_k} \tag{1}$$

where:

r – a length of inputs range [–1..1],

n_k – a number of levels for each of 1..k inputs.

If it is not possible to generate all the levels, the initial value is reduced by 10% and the process of levels generating starts again to obtain the demanded number of inputs levels.

The *esmin* parameter is calculated similar to Δx parameter. The initial value is calculated according to the formula:

$$esmin = \sqrt{\sum_{j=k}^{i} \frac{r}{k_j}} \cdot \left(2 - \frac{u}{\prod_{j=1}^{i} k_j} \right) \tag{2}$$

where:

r – means length of inputs range, which is usually normalized to [–1, 1],
k_j – means number of levels for j-input,
u – means number of designs units,
i – means number of inputs,
$j = 1..i$.

The next step is generating series of designs fulfilling the *esmin* condition. If at least one design can be created, *esmin* value is automatically increased and new designs are generated again. If any design is created, *esmin* value is automatically decreased and designs are generated again. In the case of increasing *esmin* value, if the new generated design has a better quality than the previous, *esmin* value is increased again and new designs are generated once again. If the new generated design has worse quality than the previous, new design is not generated again and the previous (with better quality) design is saved. In the case of decreasing *esmin* value, if at least one new design can be generated, new designs are not generated again. If any new design can be generated, *esmin* value is automatically decreased again and new designs are generated once again.

The better quality design is selected basing on equipartitional parameters *e1max* and *e1mean*. The lower values of these parameters means better design's quality (more regular distribution of unit, equally and without excessive concentration in the inputs' space). However, it is a question which of to applied parameters is more important. The answer is not easy and could depend on the researcher's preferences or conditions of the conducted experiment. In this research the design is selected as having the better quality if one of two conditions selected by the generator's user is true:

– either both of parameters *e1max* and *e1mean* have the lower values than the best previous,
– or *e1max* parameter is lower than 95% the best previous and *e1sr* parameter is lower than 105% the previous best.

The second condition could be applied if the generator's user prefers especially *e1max* parameter, which is calculated as a maximal value of equipartitonal set and can be interpreted as an indicator of big areas in the input's space without any design's unit.

The smart designs of experiment are multiple-generated ([7]). The reason is application of pseudo-random numbers in algorithm of designs generating. Designs generated with the same seed of pseudo-random number generator, the same parameters of generation (Δx, method of inputs levels generating, *esmin*) and the same design's characteristic (number of inputs, number of inputs levels, number of design's units) will be identical. But if you change the seed value or just if you try to generate it next time even with the same generation parameters,

they could be different and the difference of design's quality could be sometimes significant. To avoid such a problem it seems to be necessary to generate several designs and choose one basing on EPA-parameters (*e1max* and *e1mean)*. That is the idea of multi-generated smart designs of experiment. The researcher can set pseudo-random number generator seed value by oneself or can generate it basing on real-time clock. To generate identical design again you need only know its seed value. The researcher can select the EPA-parameter which he prefers to choose the best design. Each design generating is repeated up to 20 times to get 10 designs.

3. Computer simulation

To evaluate quality of the smart designs of experiment it was carried out a computer simulation. In the simulation instead of using the real object of research, the special test functions were used. It was generated a series of smart designs with 2 inputs, 15 units (cases) and inputs' levels calculated according to Z, R and R2 methods. In the simulation two testing functions were used to simulate the real research object: SumOfSquare function (first function of De Jong's, Eq. 3) and Rosenbrock's function (2. function of De Jong's, Eq. 4) [10].

$$f(x1, x2) = (1 - x1)^2 + 100 \cdot (x2 - x1^2)^2 \tag{3}$$

$$f(x1, x2) = x1^2 + x2^2 \tag{4}$$

The real values of testing functions were compared to approximated values. Approximation was conducted with application of neural networks. The learning sets were built basing on values of testing functions calculated for each smart design unit. Additionally as a base of learning set was used 2-inputs 5-levels design (called "K"), generated according to R-method but with 25 units, created as all possible unique combinations of both inputs levels. The approximated values were calculated by the trained neural networks as predicted for a special 121-elemnents testing set (all unique combinations of values {–1, –0.9, …, 1}). The differences between real and approximated values were saved as approximation errors sets. Basing on error sets various statistics were calculated: maximal value of errors set, average value, standard deviation of errors set, correlation coefficient between the testing function values and approximated values.

4. Results of simulation

Results of simulation for all generation methods (Z, R, R2 for 15 units and K for 25 units) show Tab. 2 (for SumOfSquare function) and Tab. 3 (for Rosenbrock's function). Both testing functions were normalized to the range [0, 1], so for example the value 0.37 of the maximal error obtained in case of method "Z" of inputs levels generation means 37% difference between the real and approximated values for one of testing cases. Analyzing the maximal errors you can notice big differences between values obtained for three methods used to generate inputs' levels. The best results for 15-units designs were observed for "R" method and it is confirmed by the other statistics. As you can see, for the Rosenbrock's function there are generally generated larger errors than for SumOfSquare function. It is

important, that the errors statistics for "R" method are not significantly worse than those obtained for "K" method, despite the size of training set was 15 units instead of 25, what means a serious reduction of runs in conducted experiment and possibly reduction in cost of experiment.

Table 2

Statistics calculated for approximation error sets for SumOfSquare function

	Z	R	R2	K
maximal error	0,37	0,13	0,50	0,15
average error	0,06	0,03	0,12	0,02

Table 3

Statistics calculated for approximation error sets for Rosenbrock's function

	Z	R	R2	K
maximal error	0,50	0,24	0,30	0,24
average error	0,10	0,07	0,05	0,03

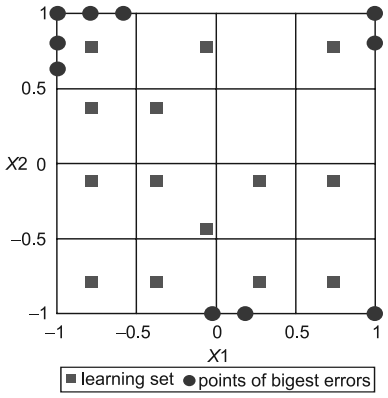

Fig. 4. Places of 10 biggest errors and learning set for SumOfSquare function

Rys 4. Miejsca położenia 10 największych błędów i zbiór uczący dla funkcji SumOfSquare

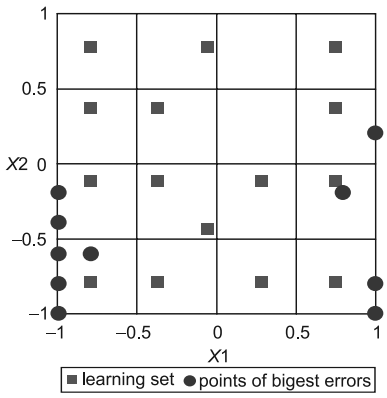

Fig. 5. Places of 10 biggest errors and learning set for Rosenbrock's function

Rys. 5. Miejsca położenia 10 największych błędów i zbiór uczący dla funkcji Rosenbrocka

Fig. 4 and 5 show learning set and the places of the 10 biggest errors – differences between real and approximated values evaluated for the testing set for "Z" method and both testing function. The conclusions after analyzing points of 10 biggest errors are that they are noticed in the edges of inputs range. Two reasons of the fact are possible. The first reason could be a lack of close "learning data points" what could have an influence on approximated values errors. The second cause could be strong increasing or decreasing of testing function's values in the area of the significant errors.

5. Conclusions

Among the analyzed three methods of generating the inputs levels especially "R" method is high recommended because the obtained approximation errors were not significantly worse than obtained for "K" method. It is important especially if we want to limit cost or time of experiment by reducing the number of experiment's runs. The difference in number of design's units which were bases of training set in neural approximation in the simulation was 40 percent. Advantageous feature of "R" method seems to be that the designs units are distributed very regular in inputs space and some of them are placed on the edges of inputs' ranges, what could be important if the research object's function is a varied and unpredictable shape in that area. The simulation was conducted for smart designs of experiment with two inputs, five levels of each input and 15 units. However, the procedures of generating and analysis smart designs are universal for all designs' characteristics, so the conclusions are true for cases of another number of inputs, levels or design's units and can be used in a broad area of engineering if you need to conduct an experimental research. The quality of smart design's of experiment was evaluated basing on neural approximation errors. The neural networks were created and learn according to the same default procedures and it was assumed that it does not have a significant influence on the results.

References

[1] Polański Z., *Design of experiment*, PWN, Warsaw 1984.

[2] Montgomery C., *Design and Analysis of Experiments*, 8th edition, John Wiley & Sons, 2012.

[3] Hinkelmann K., Kempthorne O., *Design and Analysis of Experiments, Volume 1, Introduction to Experimental Design*, 2nd Edition, John Wiley and Sons, 2008.

[4] Hinkelmann K., Kempthorne O., *Design and Analysis of Experiments, Volume 2, Advanced Experimental Design*, John Wiley and Sons, 2005.

[5] Goos P., Jones B., *Optimal Design of Experiments: A Case Study Approach*, Wiley 2011.

[6] Polański Z., *Empirical research – methodology and computer support* (in Contemporary metrology, editor J. Barzykowski), WNT, Warsaw 2004.

[7] Skowronek A., *A method of self-adaptation calculating the value of the smart designs of experiment generation's parameter*, Polish Journal of Environmental Studies, Vol. 18, No. 3B, 2009.

[8] Johnson R.A., Bhattacharyya G.K., *Statistics: Principles and Methods*, 2th Edition, John Wiley and Sons, 2010.

[9] Skowronek A., *The smart designs of experiment generated with circular inputs's ranges*, Conference Proceeding of Engineering & Education 2009, Białka Tatrzańska, 4–6 November 2009, Problems Of Modern Techniques In Engineering And Education, 2009.

[10] Pohlheim H., *Examples of objective functions* (http://www.geatbx.com/download/GEATbx_ObjFunExpl_v38.pdf – 25.02.13).

TECHNICAL TRANSACTIONS | **CZASOPISMO TECHNICZNE**
MECHANICS | MECHANIKA
1-M/2013

JOLANTA STACHARSKA-TARGOSZ*

REGULATION OF FLOW RATE GENERATED BY CROSS FLOW FAN WITH USE OF INTERNAL VANE. EXPERIMENTAL AND NUMERICAL RESULTS

REGULACJA STRUMIENIA OBJĘTOŚCI WYTWARZANEGO PRZEZ WENTYLATOR POPRZECZNY. WYNIKI EKSPERYMENTALNE I NUMERYCZNE

Abstract

In this paper the problem of volumetric flow rate regulation is considered. The change of angular position of an element mounted axially inside of the cross flow fan impeller creates different aerodynamic performances: $\psi_t = f(\varphi)$, $\psi_s = f(\varphi)$ at the same rotational speed and in consequence the qualitative diversification of fan operation is obtained. It gives possibility to use a cross flow fan for several applications depending on an actual requirement respecting to volumetric flow rate or pressure coefficient. The shape of inner element as well as its angular position have an important influence on the flow structures so a method of volumetric flow rate control without necessity of rotational speed change is proposed. This way of cross flow fan flow rate control, commonly made with use of frequency converter, seems to be more effective for reduction of an energy consumption and gives an evident economic advantage.

Keywords: *cross flow fan*, *volumetric flow rate control*, *internal vane*

Streszczenie

W artykule rozpatrywany jest problem regulacji strumienia objętości. Zmiana kątowego położenia elementu zamontowanego osiowo w wirniku wentylatora poprzecznego powoduje uzyskanie różnych charakterystyk aerodynamicznych: $\psi_t = f(\varphi)$, $\psi_s = f(\varphi)$ przy tej samej częstości obrotów i w konsekwencji jakościową dywersyfikację działania wentylatora. Stwarza to możliwość szerszego zastosowania wentylatora poprzecznego w zależności od aktualnych wymagań dotyczących wielkości strumienia objętości i ciśnienia. Kształt wewnętrznego elementu oraz kątowego położenia maja istotny wpływ na strukturę przepływu stąd zaproponowano metodę kontroli wielkości strumienia objętości bez konieczności zmiany częstości obrotów. Ten sposób regulacji strumienia objętości, zwykle wykonywanego przy użyciu przetwornicy częstotliwości, wydaje się bardziej efektywnym w redukcji zużycia energii i ekonomicznie korzystnym.

Słowa kluczowe: *wentylator poprzeczny*, *regulacja strumienia objętości*, *łopatka wewnętrzna*

* Prof. PhD. Eng. Jolanta Stacharska-Targosz, Institute of Thermal and Process Engineering, Faculty of Mechanical Engineering, Cracow University of Technology.

Nomenclature

D – impeller diameter [m]
L – impeller length [m]
n – rotational speed [s^{-1}]
Δp – pressure [Pa]
u – circumferential velocity [m s^{-1}]
$\dot{V}$ – volumetric flow rate [m^3 s^{-1}]
α – angular position of vane
ρ – fluid density [kg m^{-3}]
φ – $\dfrac{\dot{V}}{D_2 \cdot L \cdot u_2}$ – flow rate coefficient [–]
ψ – $\dfrac{2 \cdot \Delta p}{\rho \cdot u_2^2}$ – pressure coefficient [–]

indexes:
s – static
t – total
2 – outer

1. Introduction

The fan dimensional or dimensionless performances may undergo a change as a result of control process. The aim of control is to fulfill the requirements of varying in time resistance of network or productivity at possible high efficiency. It can be obtained using the different ways of timing gear control in the fan or in its drive. Fan control is usually realized by change of an impeller rotational speed as well as varying of setting in motion impeller blades or mounting the guide vanes (axial and radial fans), and not only one curve but the curve families are obtained covering the wider range of fan operation.

Fans operate at varying conditions established by received networks described by resistance-drag- curves or at constant volumetric flow rate ($\dot{V} = \text{const}$) as well as at constant total pressure ($\Delta p_t = \text{const}$) so it is necessary to provide an acceptable efficiency in the whole range of fan control.

The range of volumetric flow rate control (RVFRC) is defined as a ratio of difference between maximal and minimal values of volumetric flow rate to maximal value of volumetric flow rate at the known (prescribed) resistance curve.

The most popular way for changing volumetric flow rate is use of frequency converters. Increase of the rotational speed of impeller causes enlargement of volumetric flow rate, but in some cases so high values are not required like for example in the air conditioning systems or drying rooms. There are more useful rather uniform velocity distributions in the discharge region of fan than high values of volumetric flow rate as it can be seen in hospital operating room where some parts specially near an operating table requires the laminar flow of very clean air [1].

2. Cross flow fan with internal vane

The cross flow fan sometimes called tangential fan or peripheral fan belongs to a unique type of turbo-machine with completely different operation from axial or centrifugal fans.

It consists of a long impeller with forward curved blades and casing which let the air cross twice a blading creating two steps of compression. Geometric design of fan casing (identified as a rear wall, vortex wall and ends-walls) has an important influence on the operating conditions and sometimes is difficult to parameterize. Usually the area of internal flow inside of cross flow fan has been divided into three regions: inlet, interior of impeller and outlet. The most interesting but complicated to mathematical as well as to physical description is impeller interior divided into two regions: eccentric vortex region, called the recirculation region, characterized by closed streamlines, and throughflow region, a main asymmetrical flow.

The complexity of flow conditions: the unsteady and highly turbulent nature of twice accelerated fluid, cyclic and variable working conditions of blades as well as the continuous crossing of the main eccentric vortex by the blading are the reasons of a lack of generally accepted method for cross flow fan design.

The change of operating parameters of a cross flow fan could be realized by mounting immobile or mobile elements, having different shape and localization, in inlet or outlet region of fan as well as inside of the impeller. The immobile one- or multi- blades guide vanes in shape assuring the uniform stream velocity distribution at outflow from the first stage and at inflow on the second stage of impeller were presented in papers [2, 3].

The results of experimental and theoretical methods to perform quantitative and qualitative estimation of the flow structures and flow phenomena for different shapes of inner rotated vane were published in [4]. Investigations of several models having different impeller diameters or lengths and different shapes of casing have created possibility to observe some relationships between geometric parameters and its influence on flow structure as well as on cross flow fan performances.

3. Influence of internal vane angular position on volumetric flow rate – qualitative results obtained from water visualization

Flow visualization, carried out in water tank with the tracers in form of 2 mm diameter polystyrene balls allowed for a quantitative estimation of some flow phenomena effected on flow structure inside the cross flow fan. Using different shapes of an internal vane and changing their angular positions one could observe an important influence on flow structure. In the case of so called “moonlike” vane mounted inside of cross flow fan constructed with symmetric shape of inflow and outflow parts of spiral casing the fluid stream has changed its flow direction about 180º at the constant impeller rotational speed. So the reverse flow resulted from casing symmetry and an adequate angular position of internal vane has occurred. This phenomena could be applied in ventilating systems where for very quick the change of air in room (flow of air stream inside or outside) has been realized by change of angular position of vane located inside of a cross flow fan operating with the same rotational

speed (no necessity to use converter, more electric power or using another type of fan). The angular position of "drop-like" vane orders the inflow on blading in suction region, creates two streams on both sides of vane forming the throughflow, which takes full advantage of length of discharge arc flowing into the outlet region of cross flow fan. In this region the velocity of flow has the highest values in comparison to other angular positions (detected by the length of flow lines of tracers) what is the synonymous with the greatest flow rate. Analyzing the flow structures for the different angular positions of vane it has been observed that the flow rate can be easy regulated using an internal element mounted axially inside of impeller [4].

4. Quantitative results of flat plate vane influence on volumetric flow rate

The best qualitative and quantitative results have been obtained for rotated internal vane in the shape of flat plate. The influence of an angular position of vane on the flow rate has been analyzed on the basis of dimensionless performances: total ψ_t and static ψ_s pressure coefficients in function of flow coefficient φ.

Cross flow fan with casing profiled in its part of outlet in form adapted to co-operation with a heat exchanger had the basic dimensions: outer diameter of impeller D_2 = 60 mm and length L = 180 mm. Analyzing curves $\psi_t = f(\varphi)$ and $\psi_s = f(\varphi)$ presented in Fig, 1a, b, three different ranges of cross flow fan operation determined by the ranges of vane angular position change are observed.

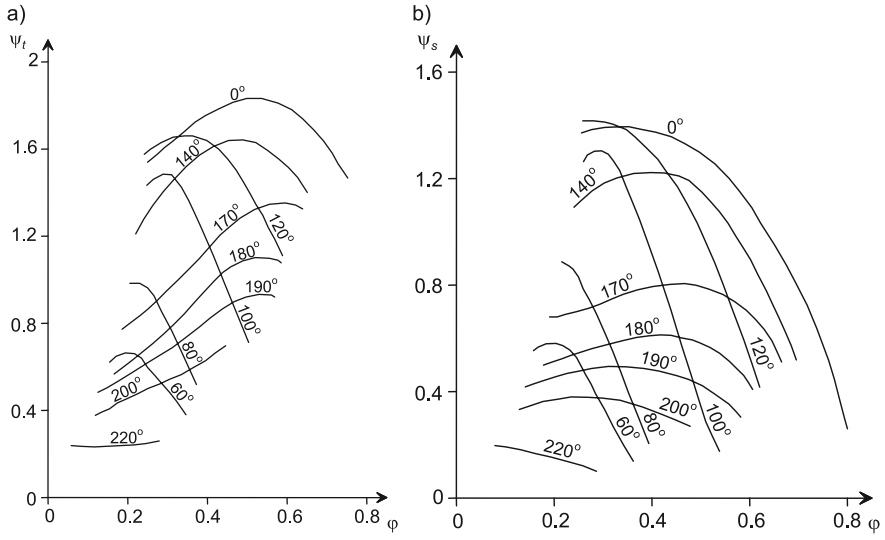

Fig. 1. Total (a) and static (b) pressure coefficients versus flow coefficient for different angular position of internal vane, n = 37.5 s^{-1}

Rys. 1. Wskaźniki spiętrzenia całkowitego(a) i statycznego (b) w funkcji wskaźnika przepływu dla różnych położeń kątowych elementu wewnętrznego, n = 37.5 s^{-1}

In the first range $\alpha = 60^o–120^o$ the relatively great increase of total and static pressure coefficients is observed in rather small changes of flow coefficient values – steep curves. The second range of $\alpha = 140^o–220^o$ characterized by more flat runs of curves shows that flow rate varies in the widest range of values. In the third range $\alpha = 320^o–360^o$ (0^o) the highest values of total and static pressure coefficient were obtained and only a treble increase in flow coefficient. The influence of angular position α on the values of dimensionless coefficients and in consequence on different aerodynamic performances obtained for one model of cross flow fan at constant rotational speed n =37.5 s^{-1} are presented in Table 1.

Table 1

Variation in dimensionless coefficients values at different ranges of α

Range of α	Multiplicity of ψ_t	Multiplicity of ψ_s	Multiplicity of φ	Notes
60º–120º	~4	14	~3	steep curves
140º–220º	5	12	**10**	flat curves
320º–360º	1.5	9	3	stable performances

The complex comparison between the flow rate coefficients obtained for angular positions of internal vane: $\alpha = 210^o$ and $\alpha = 350^o$ is very difficult to make because some of total and static pressure coefficients are located in different ranges of values, Fig. 2.

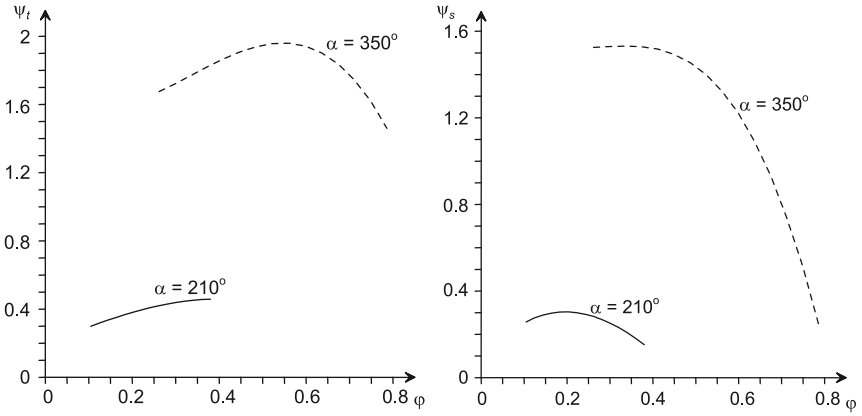

Fig. 2. Comparison between performances at angular position of internal vane: $\alpha = 210^o$ and $\alpha = 350^o$

Rys. 2. Porównanie charakterystyk dla położenia kątowego łopatki: $\alpha = 210^o$ i $\alpha = 350^o$

In table 2 the results of flow rate coefficients selected for similar values of static pressure coefficient during are presented.

It is worth to notice, that for almost the same values of static pressure coefficient (3.6% variation) the flow rate coefficients have increased about 648%. This case shows possibility of volumetric flow stream regulation.

Table 2

Selected values of ψ_s and φ for different angular position of internal vane

α	ψ_s	φ
210	0.257	0,105
350	0.248	0.786

5. Numerical simulation of flow inside the cross flow fan incorporating a flat vane

To numerical simulation of flow in cross flow fan program Flo^{++} based on finite volume method (FVM) has been used. The results of numerical calculation were verified by experimental data obtained for model of fan having the same geometry and basic impeller dimension: outer diameter $D_2 = 100$ mm, length $L = 450$ mm. Construction of numerical model of flow as well as Flo^{++} program used to solve the unsteady, two-dimensional, incompressible flow with small velocities (Ma < 0.3) are in details described in [5].

Cross section of the fan model (Fig. 3) with circle being a sliding edge between unmoving casing and moving impeller (use of the sliding mesh technique for interaction relying upon the interpolation of the calculated values at contact cells in following time step) divided into 19 casing blocks (a) and impeller block with an internal rotated flat vane (b) is shown in Fig. 3 [6].

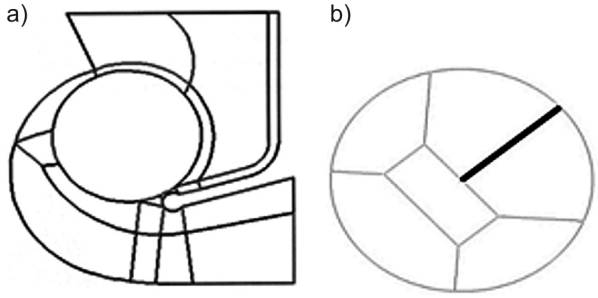

Fig. 3. Cross section of fan model with internal flat vane

Rys. 3. Przekrój poprzeczny modelu wentylatora z wewnętrzną płaską łopatką

The influence of the angular position of internal vane on the flow structure at the same rotational speed could be observed in Fig. 4 where some selected numerical results in form of the vector velocity graphs for different angles $\alpha = 0^o$; 50^o ;120^o at $n = 24.16$ s^{-1}. For the angular position $\alpha = 0^o$ on the both sides of the vane the dead zones are observed.

The throughflow velocity has rather low values and at inlet region (suction) as well as on a greater part of inlet arc of blading flow with small velocities has been realized (Fig. 4a). Different flow structure is shown in Fig. 4b where for the vane angular position $\alpha = 50^o$ the eccentric vortex with the center near blading close to stabilizer appears and only on

one side of vane the dead zone exists. The fluid stream flows with higher velocities which values have significant increased at the angular vane position described by $\alpha = 120^{o}$ (Fig. 4c). For this vane position the vortex center has moved towards rear wall (opposite direction as during throttling) and let the fluid stream occupy a larger part of outlet arc of blading giving possibility to generate a greater volumetric flow.

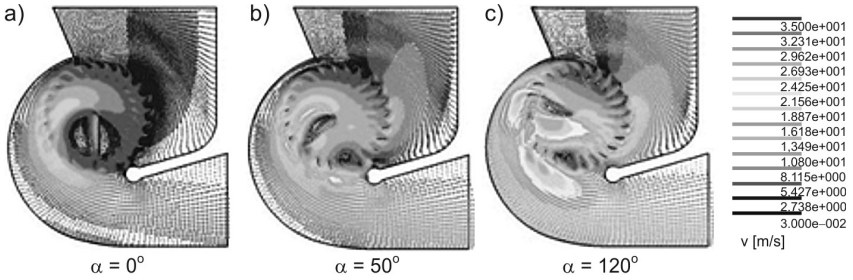

Fig. 4. Vector velocity field for different angular position of internal vane

Rys. 4. Pole wektorowe prędkości dla różnych kątowych położeń łopatki wewnętrznej

Some selected theoretically determined dimensionless aerodynamic performances for the cross flow fan for different α mentioned above at $n = 37.5\ s^{-1}$, are presented in Fig. 5.

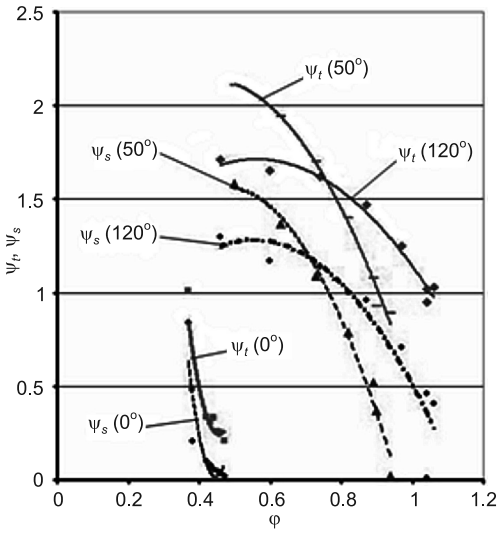

Fig. 5. Total ψ_t and static ψ_s pressure coefficient versus flow coefficient φ [6]

Rys. 5. Wskaźnik spiętrzenia całkowitego ψ_s i statycznego ψ_s w funkcji wskaźnika przepływu φ [6]

The shape of curves $\psi_t = f(\varphi)$, $\psi_s = f(\varphi)$ obtained for different angular position α of internal flat vane are comparable to results of experiments carried out for cross flow fans with different ratios of impeller length to diameter: $L/D_2 = 4.5$ and $L/D_2 = 3$ (see Fig. 1).

Analyzing the curves shown in Fig. 5 obtained numerically for two angular position of rotated vane ($\alpha = 0^o$ and $\alpha = 120^o$) one can observe almost threefold increase of flow rate coefficients for the same value of pressure coefficient.

6. Conclusions

Some selected results of experimental and numerical calculations show that the vane mounted axially inside of the cross flow fan impeller can be a controllable element used for changing the volumetric flow rate. Using for analysis the experimental curves: static pressure versus volumetric flow rate obtained at the different rotational speeds in range $n = 12.5–27.3\ s^{-1}$ published in [4] for CFF ($L/D_2 = 4.5$) the sentence mentioned above can find a confirmation. The results indicate that the lowest value of volumetric flow rate obtained at $n = 12.5\ s^{-1}$ has been tenfold less than the highest one obtained at $n = 27.3\ s^{-1}$. For such increase of rotational speed the required power (energy) consumption is equal to $[27.3/12.5]^3 = 10.36$.

It's worth to notice that the same increase in volumetric flow rate (about tenfold) has been obtained by changing the angular position of internal flat vane from $\alpha = 140^o$ to $\alpha = 220^o$.

This show that a method of volumetric flow rate control with use of internal vane instead of frequency converter seems to be more simple and more economic proposal.

References

[1] Stacharska-Targosz J., Chmielowiec M., *The influence of internal vane on uniform velocity distribution in the cross-flow fan*, The Archive of Mechanical Engineering, Vol. LVI, No. 1, 2009, 61-72.

[2] Korowkin A.G., *Isslledowanije regulacjonnych elementow diametralnych wentilatorow*, Promyszlennaja Aerodynamika, Wyp. 33, 1986.

[3] Gołogorski J., Stacharska-Targosz J., *Wentylatory poprzeczne o sterowalnej charakterystyce – metoda oceny działania*, Chłodnictwo, t. XXVI, Nr 11 ,10-13.

[4] Stacharska-Targosz J., *Wentylatory poprzeczne*, Politechnika Krakowska, Kraków 2006.

[5] Sowa A., *Flow simulation in cross flow fans using finite element and finite volume methods*, TASK Quarterly, 1/2004.

[6] Stacharska-Targosz J., Chmielowiec M., *Application of finite volume method for numerical calculations of cross flow fan performance curves*, Archive of Thermodynamics, Vol. 29, No. 2, 2008, 3-20.

TECHNICAL TRANSACTIONS | **CZASOPISMO TECHNICZNE**
MECHANICS | MECHANIKA
1-M/2013

PAWEŁ WOJAKOWSKI*

SOME ASPECTS OF VISUAL MANAGEMENT SYSTEMS APPLIED IN MODERN INDUSTRIAL PLANT

ASPEKTY STOSOWANIA SYSTEMÓW KONTROLI WIZUALNEJ W NOWOCZESNYCH ZAKŁADACH PRZEMYSŁOWYCH

A b s t r a c t

The paper describes the main features of visual management systems applied to track production state inside manufacturing cells. The description is restricted to the class of the systems called electronic andon system. The way of gathering data from manufacturing cell about process performance is depicted. Integration of electronic andon with ERP systems is presented.

Keywords: *visual management*, *andon*, *shop floor control*

S t r e s z c z e n i e

W artykule opisano główne cechy systemów kontroli wizualnej stosowanych do śledzenia produkcji w gniazdach przedmiotowych. Ograniczono się do opisu klasy systemów kontroli wizualnej zwanej elektronicznym systemem andon. Zobrazowano sposoby gromadzenia danych w takich systemach. Przedstawiono sposoby integracji tych systemów z systemami zewnętrznymi na przykładzie komunikacji z ERP.

Słowa kluczowe: *kontrola wizualna*, *andon*, *system kontroli produkcji*

* PhD. Eng. Paweł Wojakowski, Institute of Production Engineering, Faculty of Mechanical Engineering, Cracow University of Technology.

1. Introduction

Effective functionality of an industrial enterprise requires a real effort to control production activities. Effective management of the production systems requires receiving valuable and adequate information from the area where operations are processed. It can be noticed recently that manufacturing plants need a revolution in communication between operative units within a company. Traditional methods such as e-mail, reports, telephones or computers – are not enough. These channels are overloaded, information is illegible, the working environment is becoming crowded, and operating expenses get out of control [1].

It means that information should be simple, clear and suitable for immediate interpretation in order to still improve manufacturing productivity. This information should inform, warn and motivate for every employee responsible for the production process on the shopfloor. Moreover, the information should be gathered as fast as possible to have instant performance feedback about how the system is utilized. The answer to this is the concept of visual management.

According to ref. [2], the concept of visual management was created to highlight the problems associated with the production directly to the workstation. Production problems, in particular reasons of their occurrence, result in production losses, classified into Six Big Losses [3]. It can be categorized into the availability losses, which include losses caused by unplanned downtime related to equipment failures or lack of material and losses caused by workstations stopping due to changeover of machines. The next two categories of production losses concerns the case in which workstations performance declines. These contain any reduced speed of ideal production run rate or small stops. These are extremely dangerous categories of production losses in the case of low production cycle times (approximately 10 seconds), because, from the point of view of production of individual pieces, these losses are almost "invisible", and the accumulation of their value, e.g. per shift, may exceed losses due to machine breakdown. The latter two categories are associated with the generation of quality defects. These include loss of quality in steady-state production as well as quality losses emerging at the start of production of a new batch (for example, after the changeover, it can also be rejects during warm-up, startup or other early production state).

Decision makers of production system are required to manage in five areas known as 5M [4]. These management areas include: employees, machines, materials flow, methods or procedures, and measurements. Due to the wide range of activities of visual management, the rest of the article is limited to the analysis of visual controls considering first two areas 5M used inside production cells, namely, employees and machines. Article focuses on issues concerning the measurement of key performance indicators KPIs and their presentation in the form of messages by visual control systems. Hence the article is prepared as follows. Section 2 gives the description of widely utilized visual control systems which can be applied into manufacturing cell. Among this, the definition of andon systems as foundation of visual control systems is quoted. Section 3 describes how to gather data directly from the manufacturing cell by the use of electronic visual control systems. In Section 4 the communication between visual control system and other resources like enterprise resource planning ERP is explained. Chapter 5 provides a summary of the article.

2. A note on visual control systems

A visual control system is the system which gathers data from real process, transforms these data into more valuable information in the form of KPIs and displays critical information so that anyone entering a work place, even those who are unfamiliar with the details of the process, can very rapidly see what is going on, understand it and see what is under control and what isn't. Essentially, the current status of the process execution can be assessed immediately.

A visual control system derives from traditional andon system which has been exploited for many years before. Based on the foundation of , Andon refers to any visual display that shows status information on the shopfloor. Its origin is in the Japanese word for "paper lantern" using electric light board or other signal devices [5] which can be hung in the factory like depicted on Fig. 1. The first andon systems in manufacturing were simple lights that enabled operators to signal line status based on color: green for normal operation, yellow when assistance was needed and red when the line was down. Today, more sophisticated visual displays are often used for andon systems, but their purpose – efficient, real-time communication of shopfloor status – remains the same [6].

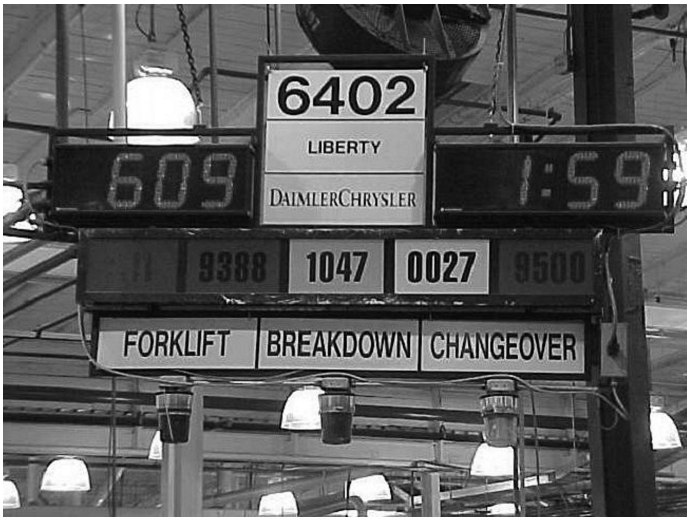

Rys. 1. Przykład systemu andon [7]

Fig. 1. An example of andon system [7]

One of the earliest descriptions of andon system can be found in the book which explains in detail Toyota Production System [3]. In that book the andon system is presented as a set of line stop boards that show the location and nature of trouble situations at a glance. It is outlined a three-color system of lights controlled by the operator, where green indicates normal operation, yellow indicates a call for an adjustment and red alerts that the line is stopped. Over time, the nature and role of andon systems has evolved. Visual cues are

sometimes reinforced with audible cues, and basic stack lights are sometimes replaced with more sophisticated message boards creating modern electronic andon systems. Nonetheless, the basic principles remain the same: firstly show line status at a glance (e.g. running, stopped, changeover or standby), secondly enable operators to call for help as needed (e.g. from maintenance or supervisors) [8].

One of the key principles underlying electronic andon systems is the possibility to control the process by giving information about KPIs. KPIs are measurements and metrics that support and facilitate achieving critical goals of the organization. KPIs are very important for understanding and improving manufacturing performance both from the lean manufacturing perspective of eliminating waste and from the corporate perspective of achieving strategic goals. As an example, one of the most valuable KPIs is OEE factor which presents every kind of production losses in the form of percentage value. It is very important factor when higher machine effectiveness is required to perform products quickly and more reliable [9]. Proper gathering data from manufacturing cells allow to calculate OEE factor in the on-line mode.

3. How to gather data for electronic andon system

An electronic andon system is equipped with standard I/O modules which allows to connect this system to accessories located on production asset. A production asset is the place in manufacturing system which is embraced of monitoring by andon system. It can be production line as well as manufacturing cell. It is valid that batch production should be performed inside a production asset in order to fully gain advantages of andon system. The reason is the adaptation of andon system to track production according to cycle time between two consecutive parts leaving the production asset [10].

There are two kinds of andon systems: open architecture andon system and closed architecture andon system. The first one uses external database to manage data from production asset. The second one is built as a firmware which contains database as well as management tools to make primary settings inside a box integrated with visual display. An example of closed architecture andon system is depicted on Fig. 2. The latter case is explained in more details below.

Fig. 2. An example of closed architecture andon system [8]

Rys. 2. Przykład systemu andon z architekturą zamkniętą [8]

A closed architecture andon system can be used to instantly track process in production asset by one andon unit. The installation of that system is very simple because there is no need to implement specification of production asset. Integration with production asset is

based on set a specific standard configuration in order to get data from asset in appropriate manner. All data gathered from production asset are stored in two dependent databases. The first database is connected to control module which tracks production on-line. This database stores real-time data and metrics generated by control modules in the form of registers which can be displayed on monitor. Registers store information about current production state, therefore the size of database is limited to set of parameters defined by the user.

The second database is used as a warehouse of historical data about production states as well as shifts or jobs performance. This database stores archived data in the form of production records named streams. Historical data can be exported to external information systems such as ERP system or manufacturing execution system MES.

Communication between closed architecture andon system and production asset can be devised regarding many options. Data from production asset can be gathered by traditional electrical devices such as sensors, buttons, encoders or relays. In this case, andon system is equipped with I/O module which watches on electrical signals from devices. Based on this signals, andon system reacts on production behaviour of the asset. This way of communication is presented on Fig. 3.

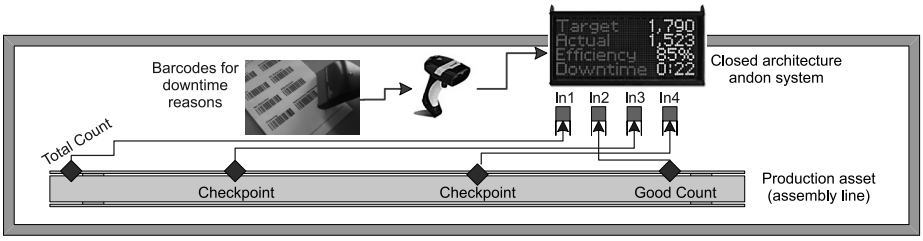

Fig. 3. An example of communication between andon system and production asset

Rys. 3. Przykład komunikacji komórki produkcyjnej z systemem andon

Other examples of communication establishments concern transferring signal by standard communication protocols. It is allowed to transfer signals by RS-232/RS-485 standard and 10/100 Ethernet standard as well. The first case is used, e.g. to set a communication serially between andon system and operator panels installed on machines. Features include installing multiple panels and addressing multiple andon units as a group, and verifying transmissions through different protocol packages. The way is to send specific frame of data between transmitter (operator panel) and receiver (andon system). The second case is used in order to establish connection between andon system and PLCs integrated with machines. That communication allows to send automatically data from PLC to andon system. Inverse direction of data transferring is not permitted because andon system cannot be the unit which controls manufacturing process. Data are transmitted with the usage of OPC standard in order to read and write registers values in the form of traditional data types.

The aforementioned description introduces the communication of andon system and other devices installed on production asset to track process performance inside this asset. Further, integration of multiple closed architecture andon systems with other systems inside manufacturing plant will be explained.

4. Integration of andon systems in an industrial plant

One andon unit can be installed to track process inside individual production asset. The challenge is to integrate many andon units into one consistent system which can cooperate with other systems such as ERP or MES implemented into manufacturing plant. It is a challenge for engineers in terms of talking the same production language as well as interpreting factors and metrics generated by andon systems in the same way.

This problem generally concerns closed architecture andon systems, because data and information stored in the unit are isolated and unavailable for other systems. While communication and transferring data between andon systems carried out by the same supplier can be done, these functionality is impossible without additional system integrators.

Possessing tools for transfer data between andon systems and other applications enable managers be more flexible in terms of possibility of systems integration from different suppliers. Production data can be modified and sent to workers in order to improve process based on the clues prepared by lean managers. An example of real integration of andon systems in manufacturing corporation is showed on Fig. 4.

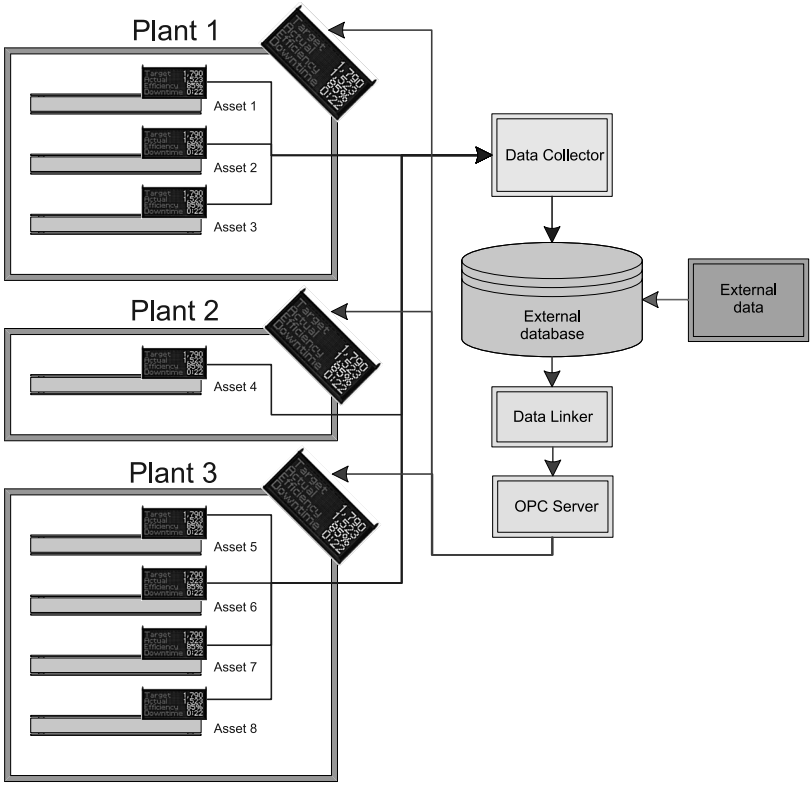

Fig. 4. An example of integration of andon systems in manufacturing corporation

Rys. 4. Przykład integracji systemów andon wewnątrz korporacji produkcyjnej

This integration includes three manufacturing plants producing ceramic products such as tiles, toilets, shower cabs, etc. Each manufacturing plant consists of several production lines. Each production line is able to fabricate selected products family, thus production lines have individual effectiveness which should be monitored. The general requirement is to control process performance and effectiveness for every shift per production line as well as aggregate separated values of process performance in order to obtain one value of performance which represents separated manufacturing plants and also whole company. By the use of additional andon systems which display aggregated factors, the company is able to instil motivation elements into workers who try to improve process to be more efficient.

5. Conclusions

Each production company, whether or not they practice continuous improvement, strives to achieve process flow uninterrupted. The only way to know the level of plant effectiveness is to adopt some form of visual management system called andon system. This is a term that refers to a system used to notify management, maintenance and other personnel of a process or quality issue. The green, yellow and red lights displayed by andon systems facilitate communication on the shopfloor by messaging in action. Mounted up high, these simple andon systems enable everyone to see the status of every production asset. A green light means the asset is running well, while a yellow light usually indicates the asset is running but requires attention. A red light almost always means that the process has stopped and requires immediate attention to repair a breakdown of the asset. This kind of alert is convenient and it provides a lot of other information which in detail describe production status of the asset.

The amount of increased profit a given company achieves by the use of andon system depends on the company, and its existing processes. It should be considered that the greatest productivity improvement can be gained if downtime of production assets could be reduced by as much as possible. Companies considering implementing andon systems should combine andon with others tolls for process improvement. However, just how little improvement is necessary to realize an attractive return of investment may be surprising. Further, since some solutions cost only a few thousand dollars, there is very little risk involved for what is a potentially large return.

References

[1] Greif M., *The Visual Factory. Building Participation Through Shared Information*, Productivity Press, New York 1991.

[2] Imai M., *Gemba Kaizen: A commonsense, low-cost approach to management*, McGraw-Hill Inc., 1997.

[3] Ohno T., *Toyota Production System: Beyond large scale production*, Productivity Press, New York 1988.

[4] Imai M., *Kaizen: The key to Japan's competitive success*, McGraw-Hill Inc., 1986.

[5] Li J., Blumenfeld E., *Analysis of andon type transfer production lines: A quantitative approach*, Proceedings of the 2005 IEEE International Conference on Robotics and Automation, Barcelona, Spain 2005, 278-283.

[6] Liker J.K., *The Toyota way: 14 management principles from the World's greatest manufacturer*, McGraw-Hill Inc., 2003.
[7] Learning centre of The Lean Assessment Inc. (Theleanassessment.co.uk).
[8] Learning centre of Vorne Industries Inc. (www.vorne.com).
[9] Relkar A.S., Nandurkar K.N., *Optimizing and analysing overall equipment effectiveness (OEE) through design of experiments (DOE)*, Procedia Engineering, Vol. 38, 2012, 2973-2980.
[10] Riezebos J., Klingenberg W., Hicks Ch., *Lean Production and information technology: Connection and contradiction*, Computers in Industry, Vol. 60, 2009, 237-247.

TECHNICAL TRANSACTIONS | **CZASOPISMO TECHNICZNE**
MECHANICS | MECHANIKA
1-M/2013

PAWEŁ WOJAKOWSKI*, DOROTA WARŻOŁEK*

RESEARCH STUDY OF STATE-OF-THE-ART ALGORITHMS FOR FLEXIBLE JOB-SHOP SCHEDULING PROBLEM

PRZEGLĄD WSPÓŁCZESNYCH ALGORYTMÓW HARMONOGRAMOWANIA ZADAŃ Z MASZYNAMI ALTERNATYWNYMI

Abstract

The paper discusses various approaches used to solve flexible job-shop scheduling problem concentrating on formulations proposed in the last ten years. It mainly refers to the applied metaheuristic techniques which have been exploited in this research area. A comparison of presented approaches is attempted, some concluding insights are highlighted. Finally future research directions are suggested.

Keywords: *flexible job-shop scheduling*, *multi-objective optimization*, *review*

Streszczenie

W artykule opisano różne podejścia stosowane do rozwiązania problemu harmonogramowania zadań z maszynami alternatywnymi. Skoncentrowano się na opracowaniach opublikowanych w ostatnich dziesięciu latach. Głównie skupiono uwagę na podejściach wykorzystujących algorytmy metaheurystyczne. Dokonano próby porównania merytorycznego dostępnych w literaturze rozwiązań oraz wskazano kierunki dalszych prac.

Słowa kluczowe: *harmonogramowanie zadań z maszynami alternatywnymi*, *optymalizacja wielokryterialna*, *przegląd literatury*

* PhD. Eng. Paweł Wojakowski, MSc. Eng. Dorota Warżołek, Institute of Production Engineering, Faculty of Mechanical Engineering, Cracow University of Technology.

1. Introduction

One of the most popular research problem that is exploited in recent years by international research centres is job-shop scheduling problem. Because of its combinatorial complex nature of sequencing operations on available machines, it is quite difficult to obtain optimal solution directed to specific criterion. Therefore, many evolutionary approaches emerged in order to cope with this problem. These approaches provide sub-optimal satisfactory solutions with the emphasis on, in the most cases, one chosen criterion achieved in deterministic conditions [1]. It is worth noticing that optimization process runs with considering many constraints. One of them is that an operation can be processed only on one machine.

As an extension of this problem, flexible job-shop scheduling (FJS) problem has increasingly focused research attention over last ten years. This is because of eliminating explicitly onerous constraint which does not permit doing operations on alternative machines. However, by the evolution to FJS problem, the level of computational complexity has been deepened significantly. The main reason is concerned to necessity of combining several optimization criteria such as minimizing the overall completion time (makespan), total workload of machines and the workload of the most loaded machine [2]. The need for developing new approaches in the domain of multi-objective optimization FJS problem has been intensified.

This paper is prepared for the investigation how modern research solve FJS problem. It is organized as follows. In section 2 the definition of flexibility of manufacturing systems is described. In section 3 problem definition and formulation is discussed. Section 4 presents solution methodologies for FJS problem and literature review based on the articles which were published over last ten years. Finally, summary and directions for future work is covered in section 5.

2. The definition of flexibility of manufacturing systems

The flexibility of manufacturing system can be defined as the ability of this system to adapt quickly to both the changeable demands of a market (demand uncertainty) or resources failures on the shopfloor (production uncertainty). This changeable conditions can be expressed by disturbances which result in lower efficiency of the manufacturing system. To cope with disturbances, management should identify and decide on the type and scope of flexibility corresponding to the manufacturing system. This can gain benefits in terms of increasing the value of total efficiency factor [3].

From the point of view of manufacturing systems, there is many kinds of flexibility which can be considered. Two of them are crucial, namely, a) the flexibility expressed by the possibility of machines rearrangement to produce part families according to group technology concept [4], b) the flexibility expressed by the possibility of machines to produce different parts without necessity to loss much time for reconfiguring machines [5]. Regarding the FJS problem, the second one is more interesting one.

In the study of ref. [6], two types of the second kind of flexibility have been investigated. Machine flexibility and routing flexibility have been selected and compared. According to the description from ref [6], machine flexibility is the capability of a machine to perform different

operations required by a given set of part types and includes quick machine setup and jig changing. This type of flexibility can be achieved by the use of high-tech automatic tool--changing or jig-changing devices in conjunction with sufficient tools and fixtures magazines as well as reconfigurable machines which allow to replace whole machine modules to perform other operations [7]. Machine flexibility allows smaller batch sizes, causing shorter lead times, higher machines utilization and reduced work-in-progress inventory level. Routing flexibility, in turn, is the capability of processing a given set of part types using more than one route (alternative routings) [8]. Routing flexibility assumes existence of alternative paths which can be followed through the manufacturing system for a given process plan [9].

Routing flexibility leads directly to the problem of FJS. This problem concerns two major steps: a) assignment of each operation to one of the alternative machines (as an assignment sub-problem), and b) sequencing the set of operations on each machine which has been previously assigned to perform these operations (as sequencing sub-problem) [10]. Routing flexibility can be improved by having identical machines or multipurpose machines. It can help to handle unplanned events such as machine breakdowns or rush orders [6].

FJS problem is strongly NP-hard. That's why it focus great attention by very large number of researchers. This paper describes only a handful of available research approaches which are available in literature. This approaches are mainly directed towards FJS problem with routing flexibility. The investigation has been conducted to find out the optimization methods used for solving multiobjective FJS problem, what is presented in the section 4.

3. Problem definition and formulation

FJS problem is an extension of the classical job-shop scheduling (JS) problem. In turn, job-shop scheduling is, next to single-machine scheduling, flow-shop scheduling and open-shop scheduling, one of the four basic problems, which have been classified as the challenging scheduling problems [11].

The classical JS problem considers N jobs to be processed on M machines assuming that they have pre-determined sequences of operations and each operation is performed on a predefined machine. It means that for each job, distinct routing is fixed and known in advance. In general, this problem is to determine optimal schedule of jobs so that one or more performance criteria could be achieved.

FJS problem is associated with two difficulties. The first one is to assign all operations to relevant machines (selected from $M_k \in M_{i,j}$). The second one is to calculate of the starting times of operations in order to determine appropriate (optimal) sequence of their execution on each machine so that technological constraints were not violated and predefined objectives could be obtained [12].

FJS problem belongs to class of NP-hard problems just as mentioned JS problem. This means that along with the growth of problem size, the number of calculations which must be done increase in an exponential manner, where N denotes problem size. It also is worth noticing that it has more complex nature than JS problem because of enlarged searching scope of potential solutions through reduce machine constraints. Bruker nad Schlie (1990) were among the first who took up solution of this problem [13].

FJS problem can be defined as follows [14]:
- there are N jobs independent from other jobs, indexed by i, $i = 1, \ldots, N$, where N denotes total number of jobs;
- each job consists of a sequence of operations, denotes by J_i (precedence constraints);
- there is the set of machines, indexed by M, $M = M_1, \ldots, M_k$, where M_k means total number machines in the set and k denotes k-th machine;
- each operation is indexed by $O_{i,j}$, $j = 1, \ldots, J_i$, where $O_{i,j}$ and J_i denote that J_i-th operation of job i and number of operations required for job i, respectively;
- each operation $O_{i,j}$ can be processed on only one machine out of a set of given machines which are able to perform it. The set of eligible machines is denoted by $M_{i,j}$ and $M_{i,j} \subseteq M$ (routing constraints);
- there is a predefined set of processing times. For a given operation $O_{i,j}$ and a given machine, the processing time is denoted by $t_{i,j,k}$;

moreover [14]:
- if each operation $O_{i,j}$ can be assigned to each machine from the set of available machines M, that is $M_{i,j} = M$, then it is called total flexibility FJS problem (T-FJS problem);
- if certain operations can be executed only by some machines from the set of available machines, that is $M_{i,j} \subset M$, then it is called partial flexibility FJS problem (P-FJS problem);

Additionally, the following assumptions are made during the process of solving this problem[14]:
- none of operation $O_{i,j}$ cannot be interrupted during its processing (non-preemption condition);
- each machine M_k can perform no more than one operation at any time (resource constraints);
- each machine is available to other operations immediately after operation which is assigned as the last to be completed;
- all machines are available at $t = 0$;
- all jobs can be started at $t = 0$;
- machines are independent from each other;
- there are no precedence constraints among operations of different jobs;
- setting up times of machines and transportation times between work stations (operations) are neglected;
- breakdowns are not considers;
- neither release times nor due dates are specified.

In the literature, the following performance criteria for FJS problem are often to be minimized [11]:
- maximal completion time, i.e. makespan $C_{\max}$;
- weight or mean completion time;
- maximal machine workload, i.e. sum of processing times of operations on a critical machine;
- total workload of machines, i.e. sum of working times over all machines;
- maximal tardiness;
- maximal lateness;

– maximum earliness;
– (weight) number of tardy jobs;
– maximal cost.

The most popular optimization criterion in the case of both single objective and multi-objective optimization of FJS problem is to minimize the makespan.

4. Solution methodologies for FJS problem

Due to the high complexity of FJS problem, we distinguish two classes of optimization approaches used to solve this problem. The first one is mathematical modeling while the second one is metaheuristic approach.

Mathematical modeling allows to obtain optimal solution for small size problems, in turn metaheuristic approach is used to solve medium and large size problems. Metaheuristic approaches allow to achieve near-optimal solution [12].

Taking mathematical models into considerations, there are three distinct ways of formulating the sequencing problem using integer programming (IP). These three approaches differ from each other the type of binary variable what stores information about sequence of operations on individual machines. Other existing formulations are based on these three groups of variables.

The first approach is based on the sequence-position variables. It was proposed by Wagner in 1959. The second one relies on precedence variables, introduced by Manne in 1960. The latter way is based on time-indexed variables, proposed by Bowman in 1959 [15].

The second class of optimization approaches directed towards solving FJS problem is involved with the use of metaheuristics. Over the past decade, metaheuristics have been intensively exploited for the combinational optimization of FJS problem. The FJS problem is considered to be more complex and difficult to obtain optimized solution than JS problem. Thus, many researchers willingly strive for metaheuristics and try to combine them applying hybridization in the way of achieving optimal solution. Five of the most notable groups of metaheuristics approaches using to solve FJS problem are: simulated annealing, tabu search, evolutionary algorithms, ant colony optimization and particle swarm optimization as well.

Simulated annealing (SA) and tabu search (TS) metaheuristics have a common characteristics as a search process starts from one initial state which is initial solution and follows through specific trajectory of solutions in order to find optimum one according to neighbor searching. One of the oldest metaheuristics is SA. In the case of FJS problem it is usually used to schedule operations on each machine after the process of assigning operations on machines [16]. That approach has been presented by Xia and Wu [17]. Fattahi et al. in turn proposed simulated annealing approach to solve FJS problem in the case if customer demand can be released more than one for each job as an important and practical issue of FJS problem [18]. Further, Dalfard and Mohammadi developed simulated annealing approach to solve FJS problem with parallel machines and with regard of maintenance cost [19].

TS algorithm has been used as a first metaheuristic to solve FJS problem [20]. Based on this approach more effective tabu search algorithm with advanced variable neighborhood

search has been developed [21]. It can be noticed, that after publication of ref. [20], tabu search has become frequently used metaheuristics to solve FJS problem. Henceforth, it has been frequently combined with other metaheuristics thereby forming hybrid approaches. The popular way is to combine tabu search with genetic algorithm, where tabu search is used to generate initial solution [22]. In other way, it can be used to solve more developed models like this with transportation constraints and bounded processing times [23].

The most exploited metaheuristics in terms of FJS problem is definitely genetic algorithms. It was first employed by well-known study of Kacem [24]. Pezzella et al. also solved FJS problem by genetic algorithm [25]. Further, Bagheri et al. followed by Pezzella et al. and proposed artificial immune algorithm to solve FJS problem [26].

The last group of approaches employs population- based methods, which are (except of mentioned genetic algorithms) particle swarm optimization (PSO) and ant colony optimization (ACO). As an example, Xing et al. proposed ACO algorithm to solve FJS problem [27], whereas Moslehi used particle swarm optimization for the same target [28].

5. Conclusions and future work directions

In the paper, FJS problem is considered and possible methods to solve it are presented. In addition, it is worth noting that despite the strong tendency to solve much more complex and difficult variants of JS problem, so far no algorithm has been developed what gives an optimal solution for the classical JS problem regardless of its size [29].

Since FJS problem is NP – hard problem, researches around the world focus their efforts on the developing effective metaheuristics that will find a good solution for a given optimal problem in acceptable time. In other words, metaheuristics attempt to achieve trade-off between solution quality and search completeness within reasonable a time interval.

The article briefly discussed the five most commonly used group of algorithms for multi--objective optimization FJS problem and possible their hybrids. Generally speaking, the hybrid algorithms as multi-objective optimization methods used to solve FJS problem are becoming more and more popular and it can be suggested as one of directions of further research.

Furthermore, it should be taken into account that in multi-objective problems with conflicting objective functions, existing only one (optimal) solution by optimizing all objective functions is almost impossible . Hence, in recent years, more studies have also focused on Pareto – based approaches what provide a set of optimal solutions, instead of a single optimal solution.

References

[1] Lazar I., *Review on solving the job-shop scheduling problem: recent development and trends*, Transfer Inovacii, 23/2012, 55-60.

[2] Hsu T., Dupas R., Jolly D., Goncalves G., *Evaluation of mutation heuristics for the solving of multiobjective flexible job-shop by an evolutionary algorithm*, 2002 IEEE International Conference on Systems, Man and Cybernetics, Vol. 5, 2002.

[3] Das S.K., Nagendra P., *Investigations into the impact of flexibility on manufacturing performance*, International Journal of Production Research, Vol. 31, No. 10, 1993, 2337-2354.
[4] Nomden G., v.d.Zee D.J., *Virtual cellular manufacturing: Configuring routing flexibility*, International Journal of Production Economics, Vol. 112, 2008, 439-451.
[5] Pattanaik L.N., Jain P.K., Mehta N.K., *Cell formation in the presence of reconfigurable machines*, International Journal of Advanced Manufacturing Technology, Vol. 34, 2007, 335-345.
[6] Tsubone H., Horikawa M., *A comparison between machine flexibility and routing flexibility*, International Journal of Flexible Manufacturing Systems, Vol. 11, 1999, 83-101.
[7] Landers R.G., Min B.K., Koren Y., *Reconfigurable machine tools*, CIRP Annals – Manufacturing Technology, Vol. 50, 2001, 269-274.
[8] Özgüven C., Özbakir L., Yavuz Y., *Mathematical models for job-shop scheduling problems with routing and process plan flexibility*, Applied Mathematical Modelling, Vol. 34, 2010, 1539-1548.
[9] Stecke K.E., Raman N., *FMS planning decision, operating flexibilities and system performance*, IEEE Transactions on Engineering Management, Vol. 42, 1995, 82-90.
[10] Rossi A., Dini G., *Flexible job-shop scheduling with routing flexibility and separable setup times using ant colony optimization method*, Robotics and Computer-Integrated Manufacturing, Vol. 23, 2007, 503-516.
[11] Wang X.J., Zhang C.Y., Gao L., Li P.G., *A survey and future trend of study on multi-objective scheduling*, ICNC IEEE International Conference on Natural Computation, 2008, 382-391.
[12] Fattahi P., Mehrabad M S.,Jolai F., *Mathematical modeling and heuristic approaches to flexible job shop scheduling problem*, Journal of Intelligent Manufacturing, Vol. 18, 2007, 331-342.
[13] Bruker P., Schile R., *Job shop scheduling with multi-purpose machine*, Computing, Vol. 45, 1990, 369-375.
[14] Motaghedi-Iarijani A., Sabri-Iaghaie K. & Heydari M., *Solving flexible job shop scheduling with multi objective approach*, International Journal of Industry Engineering & Production Research, ISSN: 2008-4889, Vol. 21, 2010, 197-209.
[15] Demir Y., Kürnat İgleyen S., *Evaluation of mathematical models for flexible job-shop scheduling problems*, Applied Mathematical Modelling, Vol. 21, 2010, 197-209.
[16] Loukil T., Teghem J., Fortemps P., *A multi-objective production scheduling case study solved by simulated annealing*, European Journal of Operational Research, Vol. 179, 2007, 709-722.
[17] Xia W., Wu Z., *An effective hybrid optimization approach for multi-objective flexible job-shop scheduling problems*, Computers & Industrial Engineering, Vol. 48, 2005, 409-425.
[18] Fattahi P., Jolai F., Arkat J., *Flexible job shop scheduling with overlapping in operations*, Applied Mathematical Modelling, Vol. 33, 2009, 3076-3087.
[19] Dalfard V.M., Mohammadi G., *Two meta-heuristic algorithms for solving multi-objective flexible job-shop scheduling with parallel machine and maintenance constraints*, Computers and Mathematics with Applications, Vol. 64, 2012, 2111-2117.
[20] Brandimarte P., *Routing and scheduling in a flexible job-shop by tabu search*, Annals of Operations Research, Vol. 41, 1993, 157-183.
[21] Li J.Q., Pan Q., Liang Y.C., *An effective hybrid tabu search algorithm for multi-objective flexible job-shop scheduling problems*, Computers & Industrial Engineering, Vol. 59, 2010, 647-662.
[22] Vilcot G., Billaut J.C., *A tabu search and a genetic algorithm for solving a bicriteria general job shop scheduling problem*, European Journal of Operational Research, Vol. 190, 2008, 398-411.
[23] Zhang Q., Manier H., Manier M.A., *A genetic algorithm with tabu search procedure for flexible job-shop scheduling with transportation constraints and bounded processing times*, Computers & Operations Research, Vol. 39, 2012, 1713-1723.

[24] Kacem I., Hammadi S., Borne P., *Pareto-optimality approach for flexible job-shop scheduling problem: hybridization of evolutionary algorithms and fuzzy logic*, Mathematics and Computers in Simulation, Vol. 60, 2002, 245-276.
[25] Pezzella F., Morganti G., Ciaschetti G., *A genetic algorithm for the flexible job shop scheduling problem*, Computers & Operations Research, Vol. 35, 2008, 3202-3212.
[26] Bagheri A., Zandieh M., Mahdavi I., Yazdani M., *An artificial immune algorithm for the flexible job-shop scheduling problem*, Future Generation Computer Systems, Vol. 26, 2010, 533-541.
[27] Xing L.N., Chen Y.W., Wang P., Zhao S., Xiong J., *A knowledge-based ant colony optimization for flexible job-shop scheduling problems*, Applied Soft Computing, Vol. 10, 2010, 888-896.
[28] Moslehi G., Mahnam M., *A Pareto approach to multi-objective flexible job-shop scheduling problem using particle swarm optimization and local search*, International Journal of Production Economics, Vol. 129, 2011, 14-22.
[29] Baykasoglu A., Ozbakir L., Sonmez A.I., *Using multiple objective tabu search and grammars to model and solve multi-objective flexible job-shop scheduling problems*, Journal of Intelligent Manufacturing, Vol. 15(6), 2004, 777-785.

TECHNICAL TRANSACTIONS | CZASOPISMO TECHNICZNE
MECHANICS | MECHANIKA
1-M/2013

DAWID WOŹNIAK*, MIROSŁAW GŁOWACKI**, MARCIN HOJNY**

COMPUTER AIDED OF EXPERIMENTS DETERMINING THE CHARACTERISTICS OF CUTTING STEEL DEFORMED AT HIGH TEMPERATURES

KOMPUTEROWE WSPOMAGANIE EKPERYMENTÓW OKREŚLAJĄCYCH WŁAŚCIWOŚCI STALI AUTOMATOWEJ ODKSZTAŁCANEJ W WYSOKICH TEMPERATURACH

Abstract

The main goal of the paper is modelling of phenomena accompanying the steel subjected to deformation in very high temperature. Analysis of the phenomena in solid surface part and semi-solid core is necessary due to inhomogeneity of material properties in both the zones of the sample. Experimental basis of the work were TESTS done in IMZ Gliwice using Gleeble 3800 physical simulator. The interpretation of the tests was done using Def_Semi_Solid software. This program allows the numerical analysis of steel behaviour during deformation of axial-symmetrical samples at very high temperatures. The paper presents the comparison of experimental and numerical results.

Keywords: *Strain-stress curve*, *Semi-solid state of steel*, *Very-high temperature deformation*, *FEM solutions*

Streszczenie

Tematem artykułu jest modelowanie zjawisk zachodzących w stali w trakcie odkształcania w ekstra wysokich temperaturach. Ze względu na niejednorodność właściwości związanych z występowaniem w części centralnej odkształcanej próbki strefy półciekłej (*mushyzone*), zachodzi konieczność analizy zjawisk występujących zarówno w warstwie naskórka (cześć zestalona), jak również w półciekłym rdzeniu. Część eksperymentalna pracy została wykonana z wykorzystaniem symulatora Gleeble® 3800. Do przeprowadzenia części symulacyjnej wykorzystany został program Def_Semi_Solid, który umożliwia analizę zjawisk zachodzących w stali w trakcie odkształcania próbek osiowosymetrycznych w bardzo wysokich temperaturach. W artykule przedstawiono także porównanie wyników eksperymentalnych i numerycznych.

Słowa kluczowe: *krzywe umocnienia*, *ekstra wysokie temperatury*, *stan półciekły*, *MES*

* MSc. Dawid Woźniak, Faculty of Metals Engineering and Industrial Computer Science, AGH University of Science and Technology.

** Prof. Mirosław Głowacki, PhD. Marcin Hojny, Department of Applied Computer Science and Modelling, Faculty of Metals Engineering and Industrial Computer Science, AGH University of Science and Technology.

1. Introduction

In the recent years, more and more new products and technologies are designed with particular emphasis on energy preservation and environmental protection. The integrated casting and rolling technologies are modern and efficient ways of hot strip production. Currently, new technologies of steel strip manufacturing are being developed. They are called ISP (Inline Strip Production) and AST (Arvedi Steel Technologies) processes and are characterized by very high temperature at the mill entry. The main goal of the mentioned new technologies is to significantly lower the rolling forces and to reach very favourable temperature field inside the plate compared with traditional processes but this also entails certain problems specific to such metal treatment.

There are a few characteristic steel temperature values between the solidus and liquidus state. The Nil Strength Temperature (NST) is the temperature level at which material strength drops to zero while the steel is being heated above the solidus temperature. Another temperature level associated with NST is the Strength Recovery Temperature (SRT), which is specific to cooling. At this temperature the material regains strength greater than 0.5 N/mm^2. Nil Ductility Temperature (NDT) is the temperature at which the heated steel loses its ductility. The Ductility Recovery Temperature (DRT) is the temperature at which the ductility of the material (characterised by reduction of area) reaches 5% while it is being cooled. Over this temperature the plastic deformation is not allowed at any stress tensor configuration.

But the main problem concerning the simulation of semi-solid steel deformation processes is lack of appropriate strain-stress relationships. The knowledge of them is extremely important and has crucial influence on the metal flow paths. Special methods have to be applied for testing behaviour of steel being in semi-solid state.

There are also experimental problems. Keeping temperature constant during the whole experiment procedure is difficult. There are also some additional difficulties with interpretation of measurement results due to huge barrelling of central part of the sample, which is caused by strong temperature dependence of plastic resistance of mushy zone, which consist of skeleton of solid phase surrounding remaining particles of liquid phase. The solid phase may be subjected to the plastic deformation while liquid phase can flow through the porous solid phase.

The current paper presents a certain modification of previously presented methodology [1], which allows the process simulation and calculation of the stress-strain relationship for a wide ranges of temperature and strain rate. The computed yield stress functions depends now on temperature, strain and strain rate. The fact that the calculated yield stress relationship takes into consideration all the mentioned parameters makes the analysis results much more consistent with experimental data as compared to the original method.

2. The methodology

The temperature range was divided into two sub-ranges: lower – below NDT – and higher – above this temperature. A special technique of testing was developed for temperatures higher than NDT due to several serious experimental problems. The deformation process has

been divided into two main stages. The first one – a very small preliminary compression and the second one – the ultimate compression. The preliminary deformation was designed in aim to eliminate clearances in the testing equipment.

The newly developed methodology [2] allows the computation of curves depending on both temperature and strain rate. In this methodology, the temperature range was divided into exactly the same intervals as for the first variant. This approach allows to compute realistic yield stress curves depending on strain, strain rate and temperature from two different ranges. The first series of experiments was conducted between 1200°C and NDT and the second one above the NDT level. More details concerning the theoretical solution one can find in [3].

3. Computer aided experimental procedure

The computer aided experimental procedure was done at AGH-University of Science and Technology in Krakow Poland and (its experimental part) in the IMZ – Institute for Ferrous Metallurgy in Gliwice Poland. The testing material was the 11SMn30 grade steel and the testing machine the Gleeble3800 simulator. The mentioned steel grade has very poor weldability. Due to the high sulphur and phosphorus content free-cutting steel not destined to heat treatment are not generally recommended for welding. This steel grade is marked by a good machinability on machine tools and by an easy fragmentation of chips.

The following 3-stage schedule was applied for the experiments:

– stage 1: preparation of the sample (e.g. mounting thermocouples, die selection),
– stage 2: melting procedure,
– stage 3: deformation of the sample.

For the experiments were used samples shown in Fig. 1 and Fig. 2.

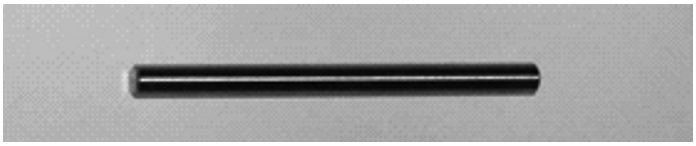

Fig. 1. Sample (6 × 82 mm) used to determine the NST temperature on the Gleeble 3800 simulator
Rys. 1. Widok próbki (6 × 82 mm) używanej do określania temperatury NDT w symulatorze Gleeble 3800

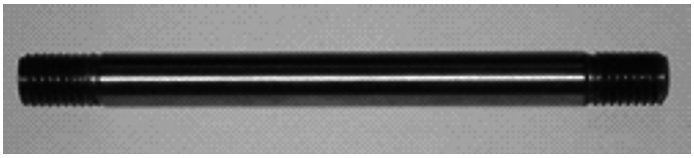

Fig. 2. Sample (10 × 125 mm) used to determine high-temperature characteristics of materials on the Gleeble 3800 simulator
Rys. 2. Widok próbki używanej do określania charakterystyk wysokotemperaturowych w symulatorze Gleeblee 3800

Die displacement, force and temperature changes in the heating zone were the main parameters recorded during experiments. Simultaneously the Def_Semi_Solid program was calculated the optimal values of coefficients having influence on material properties. The software has two main tasks. It is able to calculate the shape and size of the deformation zone together with material mechanical properties. In aim to plan right experiments one can know the right values of liquidus and solidus temperatures. For the 11SMn30 grade steel they are 1518ºC and 1439ºC, respectively.

The temperature has strong effect on remaining parameters. The non-uniform temperature distribution is the source of significant variation of microstructure and material rheological properties. The changes of these parameters can be observed mostly along the sample. They source is the temperature gradient caused by resistance heating and contact of the sample with cold cooper handles [4].

In all series of experiments samples were first heated to 1430ºC and after maintaining at constant temperature they were cooled down to the required deformation temperature. Three thermocouples were installed in each sample (Fig. 3) in order to record the temperature gradients in its central parts. The TC4 thermocouple was the control sensor of the sample heating process. The second thermo-element, marked TC2 (S-type) was placed at a distance of 7.5 mm from the TC4. The third thermocouple, i.e. TC3 (1 mm thickness – R-type) was mounted near the sample axis in a hole drilled at an angle of about 45º.

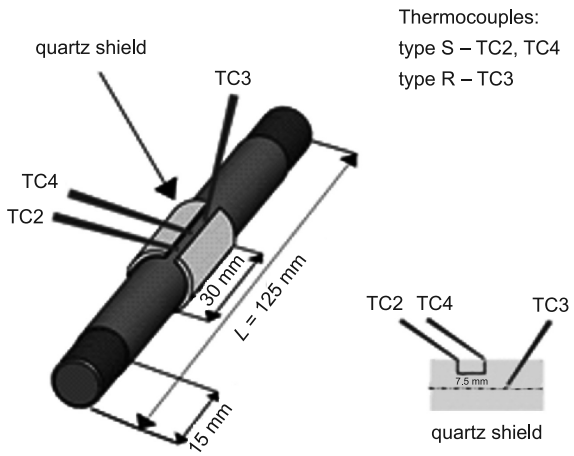

Fig. 3. Samples used for the experiments. TC2, TC3 and TC4 thermocouples

Rys. 3. Schemat próbki wraz z układem termopar

Besides the problems with maintenance of very high, constans temperature during the whole experiment there are also difficulties in the interpretation of recorded results. Due to significant inhomogeneity in deformation and stress distribution in the deformation zone the traditional methods of stress-strain curves calculation fail. Thus the application and Def_Semi_Solid software based on a sophisticated method described in details in [1] was necessary.

Figure 4 shows strain-stress curves at several strain rate levels for temperature 1400ºC and very strong strain rate dependence of the yield stress. The strain-stress curves were described by following equation:

$$\sigma_p = A\varepsilon^n \dot{\varepsilon}^m \exp(-BT) \tag{1}$$

where:

A, B, n, m – are material constant,
T – temperature,
ε – strain,
$\dot{\varepsilon}$ – strain rate.

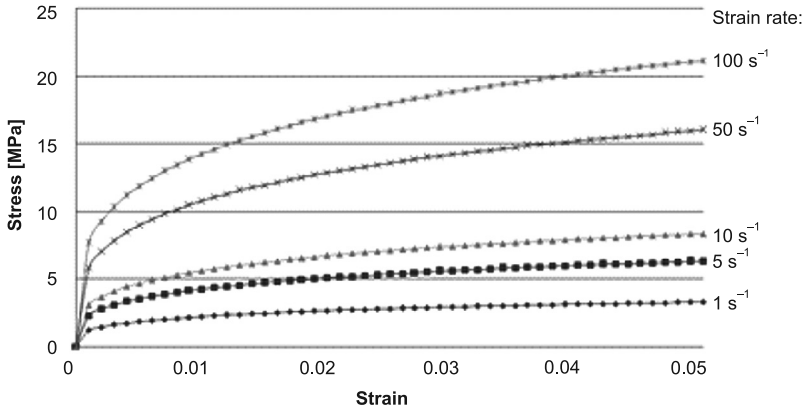

Fig. 4. Stress-strain curves at several strain rate levels for temperature 1400°C

Rys. 4. Krzywe naprężenie-odkształcenie dla różnych prędkości odkształcenia dla temp. 1400°C

Strong temperature and strain rate dependence of the yield stress require suitable experimental technique – first of all application of proper temperature program. The samples were heated to temperature of 1390°C with heat up rate of 20°C/s. Then the rate drops to 1C/s and the heating proceeds to temperature of 1460°C. Each sample is hold up in this temperature for 30 seconds and next cooled to temperature of 1430°C with rate of 10°C/s. Deformation usually starts after the sample lasts 10s in this temperature.

To eliminate disorders observed during the experiments a combination of FEM solution and inverse method was adopted. Figures 5 and 6 present a comparison of experimental and calculated forces accompanying the deformation process run at 1400°C for two different strain rate levels. The difference between both of them was the objective function of the inverse analysis.

The temperature difference between core of the sample and its surface can be as low as possible. But in fact the difference of around 30ºC exists in the final stage of the testing procedure. For the presented series of experiments the core temperature was higher than surface temperature by around 32ºC for so called cold handle (handle with long contact zone between sample and tool) and temperature of 1350ºC. The difference has grown to 35°C

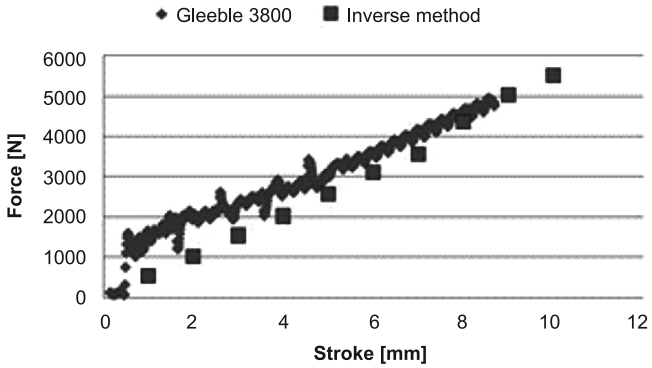

Fig. 5. Comparison between measured and calculated loads at temperature 1400°C for tool velocity 100 mm/s
Rys. 5. Porównanie zmierzonych i obliczonych dla temperatury 1400°C i prędkości narzędzia 100 mm/s

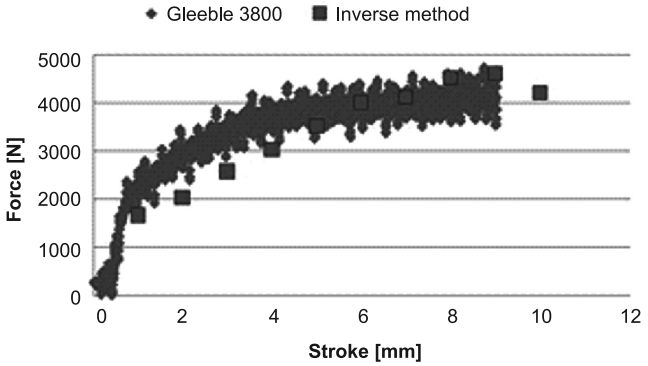

Fig. 6. Comparison between measured and computed loads at temperature 1400°C for tool velocity 20 mm/s
Rys. 6. Porównanie zmierzonych i obliczonych dla temperatury 1400°C i prędkości narzędzia 20 mm/s

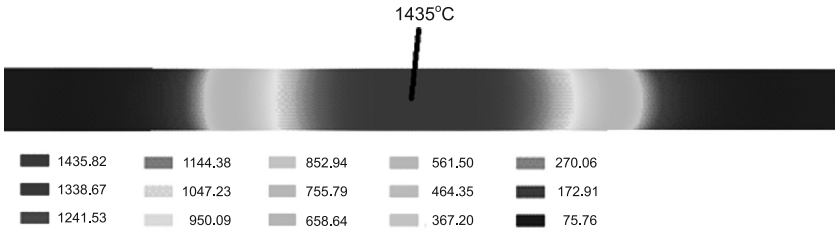

Fig. 7. Temperature distribution for simulation of heating to 1400°C – whole sample
Rys. 7. Rozkład temperatury dla symulacji nagrzewania do temperatury 1400°C – widok całej próbki

for tests conducted at 1400°C while the temperature gradient along samples is much more significant. Figures 7 and 8 show the initial temperature distribution in samples heated to the mentioned temperature levels. One can see the huge temperature difference between the sample central regions and their cold ends.

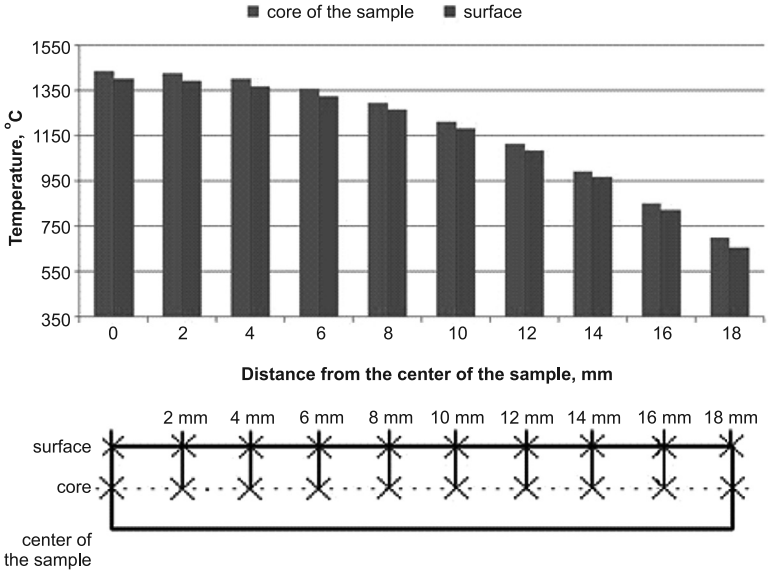

Fig. 8. The temperature difference between core of the sample and its surface for tests conducted at 1400°C – half of the sample

Rys. 8. Różnica temperatur pomiędzy rdzeniem próbki a jej powierzchnią dla prób przeprowadzonych w temperaturze 1400°C – widok połowy próbki

The numerical analysis of deformation level shows quite different results. High speed(tool speed of 100mm/s) and average speed (20mm/s) experiments are presented in Figures 9 and 10. The figures present the distribution of the effective strain for both the considered strain ranges showing similar distribution in terms of strain level and shapes of isoclines.

Metallographic investigation of samples were made as well. After deformation the samples were cooled with water. The cooling rate of the samples was variable and it changed with the temperature drop from initial level of about 20°C/s to final 5°C/s after the solid phase transformation. Macro photographical analysis leads to the conclusion that the temperature and strain rate have impact on macrostructure and the shape of deformation zone. At higher rate of deformation (tool speed 20 mm/s and 100 mm/s) one can draw a conclusion that that higher deformation temperature results in higher level of stratification of the compressed area. The deformation process itself is short, the material did not regain plasticity and the liquid phase is pushed to the outside, where it solidifies faster.

Studies of the microstructure showed that due to high deformation temperature, and relatively high cooling rate the deformation zone is dominated by acicular ferrite. The others components of the microstructure are bainite (grey phase mainly near the borders of grains)

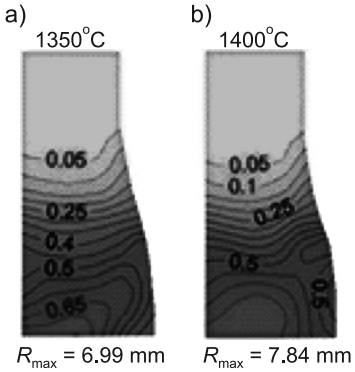

Fig. 9. The strain rate for average speed experiment (20 mm/s) – quarter of the sample (R_0 = 5 mm)
Rys. 9. Prędkość odkształcenia dla średniej prędkości (20 mms) – 1/4 próbki (R_0 = 5 mm)

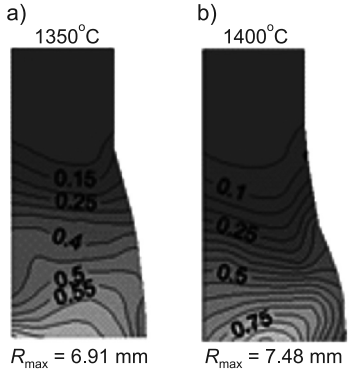

Fig. 10. The deformation intensity for high speed experiment (100 mm/s) – quarter of the sample (R_0 = 5 mm)
Rys. 10. Intensywność odkształcenia dla „dużej dynamiki" (100 mm/s) – 1/4 próbki (R_0 = 5 mm)

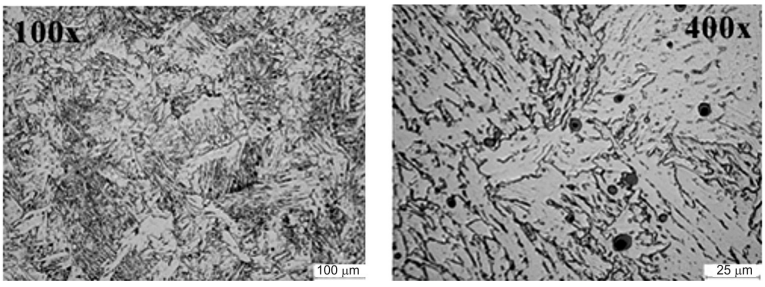

Fig. 11. Microstructure of sample deformed at 1350°C with tool velocity of 1 mm/s
Rys. 11. Mikrostruktura próbki odkształcanej w temperaturze 1350°C z prędkością narzędzia 1 mm/s

and likely martensite. Due to the large content of sulfur ($S = 0.27\%$), manganese sulphides in microstructure are demonstrated. Figures 11–13 show the microstructure of the investigated samples at different temperatures and strain rates.

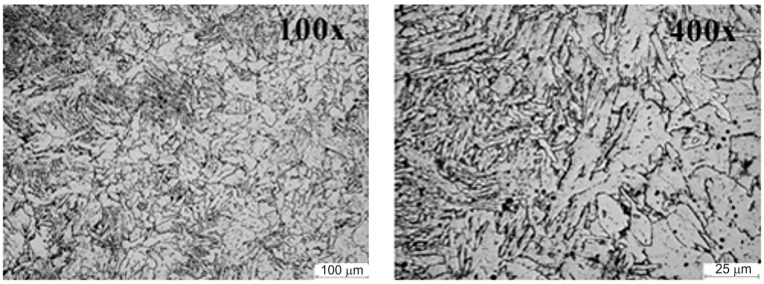

Fig. 12. Microstructure of sample deformed at 1400°C with tool velocity of 1 mm/s

Rys. 12. Mikrostruktura próbki odkształcanej w temperaturze 1400°C z prędkością narzędzia 1 mm/s

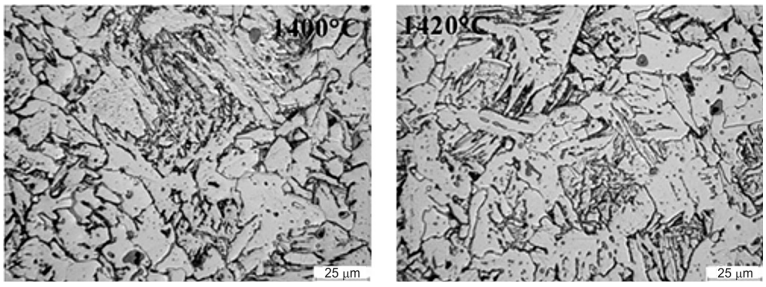

Fig. 13. Microstructure of samples deformed at 1400°C and 1420°C. Tool velocity 100 mm/s. Magnification: 400×

Rys. 13. Mikrostruktura próbek odkształcanych w temperaturze 1400°C i 1420°C. Prędkość narzędzia 1 mm/s. Powiększenie 400×

4. Conclusions

Computer aided testing of steel samples deformation at coexistence liquid and solid phase requires resolving a number of problems and the main is the interpretation of compression tests results leading to strain – stress curves. The difficulty in determination of other material thermal and mechanical properties, such as: heat transfer coefficient (and many other thermal properties) and diagrams of temperature dependent density changes are also important issues.

The presented research was focused on mechanical properties of investigated 11SMn30 steel grade. Compression tests carried out for semi-solid materials could only be interpreted using inverse analysis. The paper has thrown light on the investigation methodology and resulting temperature, shape and size of the deformation zone.

The paper has been supported by the Polish Ministry of Science and Higher Education Grant N N508 585539.

References

[1] Głowacki M., *Inverse Analysis Applied to Mushy Steel Rheological Properties Testing Using Hybrid Numerical-Analytical Model*, In: Numerical Modelling, InTech Publisher, 2012, 278-30.
[2] Hojny M., Głowacki M., *The Modified Methodology of Strain-stress Curves Investigation for Steel Deformed at Extra-high Temperatures*, Steel Research Int., spec. ed., 2012, 963-966.
[3] Hojny M., Głowacki M., *The Methodology of Strain–stress Curves Determination for Steel in Semi-solid State*, Archives of Metallurgy and Materials,54 (2), 2009, 475-483.
[4] Hojny M., Głowacki M., *Computer Modelling of Deformation of Steel Samples With Mushy Zone*, Steel Research Int., 79 (11), 2008, 868-874.

TECHNICAL TRANSACTIONS | **CZASOPISMO TECHNICZNE**
MECHANICS | MECHANIKA
1-M/2013

DAWID WOŹNIAK*, MARCIN HOJNY**, MIROSŁAW GŁOWACKI**

FROM CONCEPT TO PRODUCT – APPLICATION OF INVENTIUM SUITE SYSTEM IN THE DESIGN NEW TECHNOLOGY OF SINK STAMPING PROCESS

OD KONCEPCJI DO PRODUKTU – ZASTOSOWANIE PAKIETU INVENTIUM W PROJEKTOWANIU TECHNOLOGII PRODUKCJI ZLEWOZMYWAKA

Abstract

This paper shows example results of computer simulations supporting the production process of sink. Design and verification of deep drawing process and tools design were carried out using finite element models implemented in Inventium Suite. Wrinkling and fracture of the material were the main phenomena subjected to the investigation using numerical analysis. A number of computer simulations were carried out in order to eliminate defects and analyze the shape of the final product.

Keywords: *drawing*, *FEM modeling*

Streszczenie

W artykule przedstawiono przykładowe wyniki symulacji komputerowych wspomagających proces produkcyjny zlewozmywaka. Projekt oraz weryfikację narzędzi do procesu tłoczenia przeprowadzono z wykorzystaniem metody elementów skończonych z użyciem systemu Inventium oraz eta/Dynaform. Typowe trudności napotkane w trakcie analiz numerycznych to pofałdowanie oraz zrywanie materiału wytłoczki. Przeprowadzono szereg symulacji komputerowych mających na celu wyeliminowanie pojawiających się wad, a także analizę kształtu wyrobu.

Słowa kluczowe: *tłoczenie*, *metoda elementów skończonych*

* MSc. Dawid Woźniak, Faculty of Metals Engineering and Industrial Computer Science, AGH University of Science and Technology.

** PhD. Marcin Hojny, Prof. Mirosław Głowacki, Department of Applied Computer Science and Modelling, Faculty of Metals Engineering and Industrial Computer Science, AGH University of Science and Technology.

1. Introduction

In the last years, in the technology of sheet metal forming has undergone a number of innovative changes. The main ones are new forming techniques (e.g. rubber-pad forming [4]) and application of advanced computer technology of which the most popular is Computer Aided Engineering (CAE). The main objective of CAE systems is to reduce costs and shorten the design and production analysis time of production through the use of fast and accurate computer simulations. One of the main benefits of such systems is lowering project and production costs due to application of fast and accurate design with the help of computer systems. The systems can help not only in the development of a new technology but also in improvement of production. The process can be constantly updated according to the simulation outcome, which results in process optimization [4]. Information obtained from application of CAE helps to refine and optimize product design and manufacturing of products.

The quality requirements for sheet metal products are very high, mainly due to the technology of automatic assembly of components in the automotive industry, where the deep-drawing is the most widely used. The requirements apply to the appropriate material properties and the shape of the finished products. Wrinkles, excessive thinning and springback effects are the main disadvantages of the drawpieces. The elimination of such undesirable defects is very difficult and time-consuming. It is therefore necessary to design the appropriate technology and tools. This can be done effectively using computer simulation methods (mainly FEM).

Decisions made at the design stage of a technological process influences both its later realization and the total production costs [1]. There are a lot of commercial packages that are used to simulate metal forming. In the field of drawing the Inventium Suite system and LS-DYNA solver are the leaders. Inventium (Fig. 1) offers a streamlined product architecture, provides users access to all of the suite's software tools. Moreover it provides a high performance modeling and post-processing system. The Inventium system consists of: PreSys – excellent tool for modeling, with extensive graphics capabilities, VPG – offering a set of tools which allow engineers to create and visualize, through its modules – structure, safety, drop test and blast analyses, eta/Dynaform – the most accurate die analysis solution available today, allowing a very accurate assessment of defects in the finished product, and Nisa – a robust and comprehensive module for technical analysis using FEM.

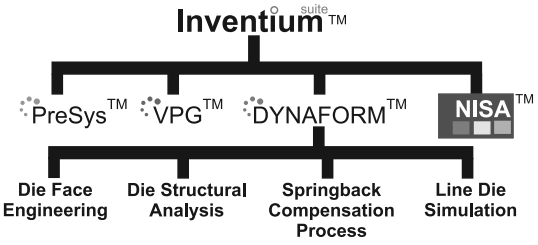

Fig. 1. The Inventium Suite

Rys. 1. Podział pakietu Inventium

Engineering Technology Associates has developed a specialized package of sheet metal forming software and additional modules such as formability module, die face engineering (DFE), blank size engineering (BSE), die structural analysis (DSA), springback compensation process (SCP) module, and line die simulation (LDS) module. [2].

Currently there are several approaches to the development of new products. The concurrent engineering, in addition to the traditional development process, are increasingly being used. They depend primarily on how the FEM simulations are used in the design and analysis of a manufacturing process, as well as tools and products. Various algorithms and procedures, ranging from explicit and implicit FEM models to one-step solvers, are develop for analysis of metal forming processes. This methods, in conjunction with new computational capabilities of current computers, provides useful tools for the implementation of parallel approach of design and manufacturing. The concurrent engineering in the development of new components stamped suggests that steps such as design of the product, process, tools, manufacture of tools and industrial tests can be carried out simultaneously [3]. The traditional process (the so-called sequential engineering) of new product development is presented in Fig 2.

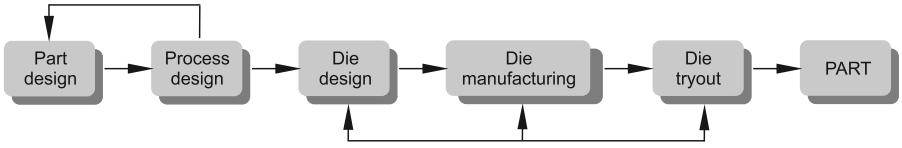

Fig. 2. The traditional process of new product development

Rys. 2. Tradycyjny process rozwoju produktu

CAD/CAE software allows for accurate analysis of the process of creating a new finished product, resulting in measurable benefits in the form of reduction in the duration the design, implementation and reduce overall costs. This behavior allows you to meet the demands of increasingly competitive and high quality products, which is especially important from a consumer perspective. CAE has another important task in the development of new products, namely one hundred percent assurance of repeatability of the product, and there by a guarantee of a modern production [4].

In order to present the expected role of the FEM simulation and CAE systems, in this paper the design process of the product (drawpiece) and design tools used in the manufacture of sink shown. Computer simulations which are using in the different phases of design, allow preliminary assessment of the correctness of the product, the number of operations needed to complete the process and finally the search for solutions in order to get a high quality product.

2. Mechanical properties of starting material

The sink is made of steel of grade SS304L of 1mm thickness. It is a steel with good weldability, corrosion-resistant, which widely used for kitchen equipments, welding elements in chemical industry, in the textile, paper, pharmaceutical and chemical industries. The main

objective of the project was to develop a production technology of sink and avoid the typical stamping defects such as wrinkling, cracking or excessive thinning. A very important aspect of the process is the precise metal flow during the forming and selection of appropriate parameters defining the process.

Some further information about material are given below:

– Young modulus: 207.0 GPa,
– Yield strength: 290.58 MPa,
– Poisson's ratio: 0.28,
– Hardening exp. *n*-value = 0.52,
– Anisotropy *r*-value = 0.905.

Stamping process parameters:

– die velocity: 5000mm/s,
– binder close velocity: 2000mm/s,
– friction coefficient: 0.125,
– thickness of drawpiece: 1 mm.

The other process parameters, such as blank holder pressure, was set differently for the different stamping conditions. The influence of pressure was analyzed to eliminate wrinkles and cracking.

3. The equivalent and geometrical drawbead model

In the analysis process, the sheet was pulled through drawbeads which are very often used in the forming technology. Their proper shape and positioning require multiple and time-consuming computer simulations. In this paper, the geometrical drawbeads was used. Drawbeads allows such forming to flow resistance of the material were distributed evenly. They meet the very important role of causing additional tensile stress, which prevents the formation of wrinkles on the surface of the drawpiece [4]. Drawbeads should be modeled as a large number of the smallest elements in order to reflect more accurately the effects of transitions metal. Simulations with geometrical drawbeads are very time consuming, so very often, in numerical analysis, effective model of drawbeads are introduce. The restraining force exerted by the actual drawbead is assigned distributely to the nodes in the regular mesh

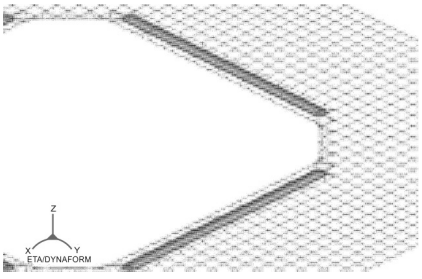

Fig. 3. The geometrical FEM drawbead model

Rys. 3. Model geometrycznego progu ciągowego

of the equivalent drawbead. The assigned restraining forces are then assumed to act on the sheet metal which moves through these nodes. Such operation allows reduction of simulation time without influence on very good calculation accuracy. In Fig. 3 and Fig. 4 are shown, respectively the geometrical drawbeads and compare of geometrical model and effective model of drawbeads.

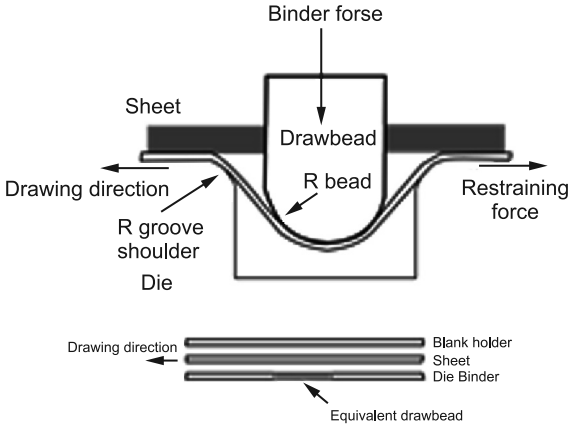

Fig. 4. Geometrical and effective drawbead models

Rys. 4. Geometryczny i efektywny próg ciągowy

4. FEM model

Main parts of the tool set: die, blank, binder and punch are presented in Fig. 5. The upper die was the moving tool.

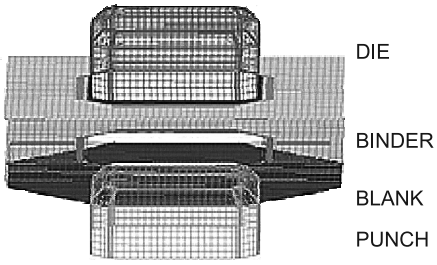

Fig. 5. FEM tools model

Rys. 5. Model MES narzędzi

FEM tools model for stamping process has been developed using DFE module, which is module of the eta/Dynaform system. An optimum sheet blank shape determined by the finite element analysis was used for all die designs by using BSE (Blank Size Estimated)

module of eta/Dynaform system. The condition contact proceeding during stamping of sink was identified by algorithms coded in eta/Dynaform system. In the present work, the four node shell element was used to construct the meshes as shown in Figure 5. The numbers of elements and nodes used for all parts of the model are listed in Table 1.

Table 1

Number of elements and nodes

Mesh	Elements	Nodes
Low Die	4929	4998
Punch	8309	8418
Binder	3380	3420
Blank	7864	7941
Total	**24482**	**24777**

5. Results of computer simulation

An sheet blank shape was determined by the finite element analysis. The BSE module is used, among others to optimize the shape of the blank (BSE – Blank Size Engineering), which is a module of the system of eta/Dynaform, was used for this purpose. The four corners of this optimum sheet blank were cut off to facilitate metal flow at the edges The shape of die cavity conforming to the geometry of the sink was also maintained as the same for all of the die face designs since the bathtub was drawn to the desired shape in one operation. A clamping force of 1.5 MPa exerted by the blank holder for the initial die design. A coefficient of friction of 0.125 was used for all analysis.The final shape that results from which design being show in Figure 6.

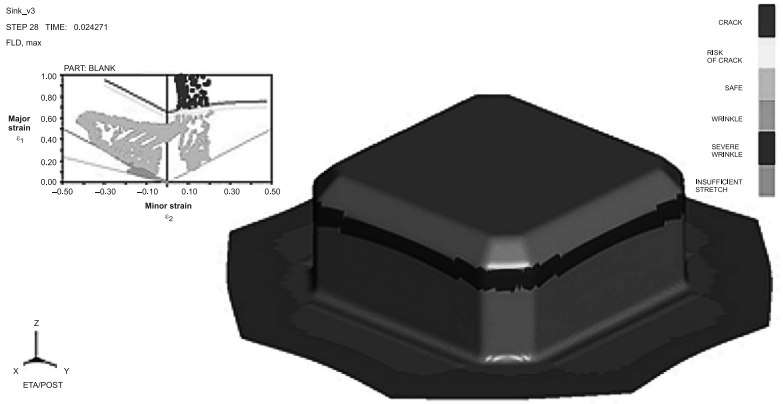

Fig. 6. Final shape of a sink and the minor and major strain and Forming Limit Diagram (FLD) for blank holder pressure 1.5 MPa

Rys. 6. Końcowy kształt umywalki oraz rozkład odkształceń głównych na tle Granicznej Krzywej Tłoczenia (GKT) dla nacisku dociskacza 1,5 MPa

The material flow is quite irregular, especially in the corners, as can be seen in Figure 6. However, the final shape of the drawpiece appeared to be cracking of the material, which is unacceptable in the finished product. The force exerted by the binder was too high and consequently led to the appearance of the typical defects of the stamping process. Cracking can be eliminated by reducing the force of binder, so in the subsequent analysis, this value was reduced to 1.4 MPa.

The major and minor strain distributions plotted on the forming limit diagram, as shown in Figure 7, indicate that the sheet metal are cracking and many of the points are above the

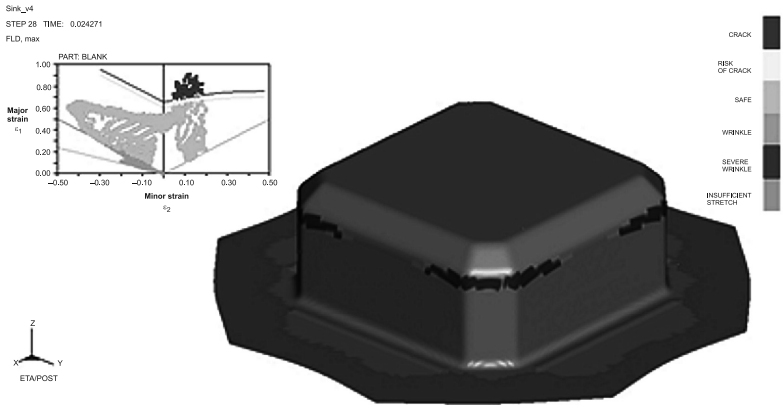

Fig. 7. Final shape of a sink and the minor and major strain and Forming Limit Diagram (FLD) for blank holder pressure 1.4 MPa

Rys. 7. Końcowy kształt umywalki oraz rozkład odkształceń głównych na tle Granicznej Krzywej Tłoczenia (GKT) dla nacisku dociskacza 1,4 MPa

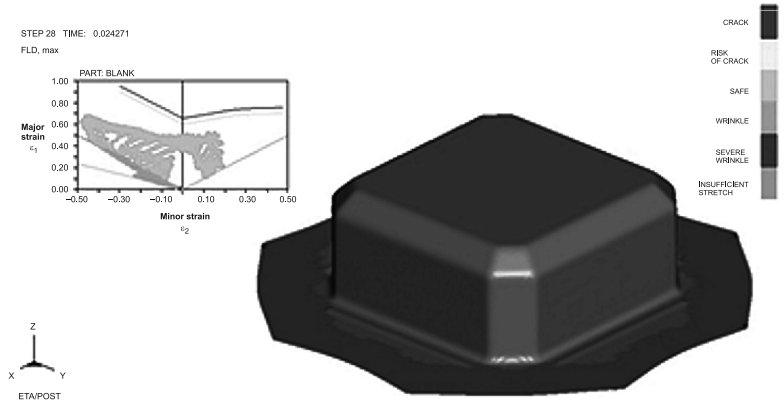

Fig. 8. Final shape of a sink and the minor and major strain and Forming Limit Diagram (FLD) for blank holder pressure 1.2 MPa

Rys. 8. Końcowy kształt umywalki oraz rozkład odkształceń głównych na tle Granicznej Krzywej Tłoczenia (GKT) dla nacisku dociskacza 1,2 MPa

risk of crack line. Reduction of binder force of 0.1 MPa allowed to obtain the final shape of the drawpiece with a limited cracking and wrinkling. However, this shape can not be accepted due to the defects in a drawpiece. The formation of wrinkles resulted from a significant metal flow at these areas.

Based on initial analysis the binder force was reduced to 1.2 MPa. This value allowed to obtain the final shape without defects such as wrinkling, excessive thinning and cracking. In the Figure 8 the final shape of a sink for the modified parameters is presented.

Appropriate modification of stamping technology parameters based on computer simulations allowed to receive the final part which is in accordance with the objectives of the technological process. Binder force reducing allowed to reduce the occurrence of wrinkling and cracking. Analysis of thinning distribution (Fig. 9) indicates that the minimum and maximum thinning was –11% and +49%, respectively. The highest values of thinning occurred spot on the corner in drawpiece.

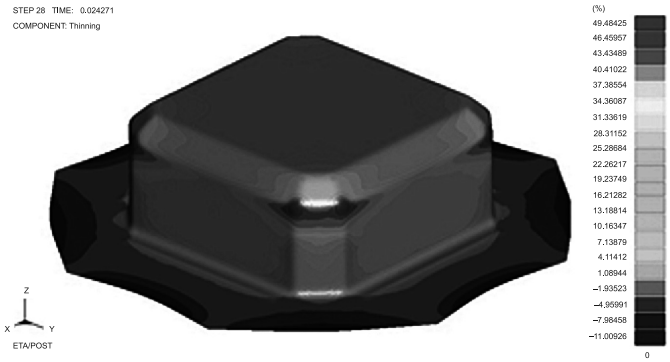

Fig. 9. Thinning distribution for the final part

Rys. 9. Rozkład pocienienia na końcowym wyrobie

6. Industrial tests

As predicted by the finite element analysis, the production part is free from defects. The Figure 10 shows the lines of final shapes from simulations and industrial tests. The final

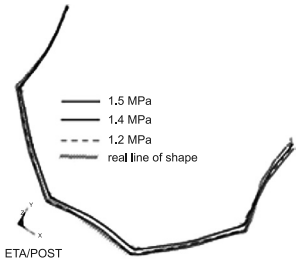

Fig. 10. Lines of final shapes from simulations and industrial tests

Rys. 10. Porównanie obrysów końcowego kształtu dla symulacji i prób przemysłowych

shape of sink is cousistent with the shape obtained by computer simulations. This confirms the benefits of using FE systems to design and verifications tools in stamping industry.

7. Conclusions

In the present work the die face design for stamping of a sink was investigated using FEM system. In the investigation the binder force on the shape and quality of drawpiece was analyzed. In the present work, an optimum tools design was performed on the basis of finite element analysis. The industrial tests have confirm achievement of defect free products. The finished product had no typical stamping process defects such as wrinkling, cracking or excessive thinning of the sheet material.

The paper was done with financial support of AGH (grant no 11.11.110.231).

References

[1] Thomas W., Altan T., *Application of computer modelling in manufacturing of automotive stampings*, Steel Res. 69 (4/5), 1998, 181-187.
[2] Engineering Technology Associates: *eta/Dynaform 5.8 User's Manual (2010)*.
[3] Liu Y., Peng X., Qin Y., *Application of FE simulations to the development of automotive sheet-metal parts – industry case study*, Proc. Of 9th International Conference on Concurrent Engineering, Cranfield, 2002.
[4] Hojny M., *Application of an integrated CAD/CAM/CAE/IBC system in the stamping process of a bathtub 1200S*, Archives of Metallurgy and Materials, 55, 713 (2010).
[5] Woźniak D., Głowacki M., Hojny M., Pieja T., *Application of CAE systems in forming of drawpieces with use rubber-pad forming processes*, Archives of Metallurgy and Materials, 57, 1180 (2012).

TECHNICAL TRANSACTIONS | **CZASOPISMO TECHNICZNE**
MECHANICS | MECHANIKA
1-M/2013

WIOLETTA WÓJTOWICZ*

BIOMETRIC WATERMARKING FOR MEDICAL IMAGES – EXAMPLE OF IRIS CODE

BIOMETRYCZNE ZNAKI WODNE W OBRAZACH MEDYCZNYCH NA PRZYKŁADZIE KODU TĘCZÓWKI

A b s t r a c t

This paper presents a preliminary investigation on medical image watermarking using biometric watermarks. The goal is to elaborate simple watermarking system based on discrete wavelet transform (DWT) decomposition and binary iris code insertion. The performance of proposed algorithm is evaluated by Hamming distance between embedded and extracted iris code.

Keywords: *watermarking technique*, *DWT decomposition*, *biometric recognition*, *Hamming distance*

S t r e s z c z e n i e

W artykule przedstawiono wstępne rezultaty badań związanych ze stosowaniem biometrycznych sygnatur jako znaków wodnych w obrazach medycznych. Przetestowano prosty algorytm oparty na przeprowadzeniu dyskretnej transformacie falkowej obrazu medycznego i umieszczenia w nim kodu tęczówki pacjenta. Wyniki związane ze skutecznością weryfikacji tożsamości pacjenta na podstawie zakodowanego i odkodowanego z obrazu kodu tęczówki oparto na analizie odległości Hamminga.

Słowa kluczowe: *technika znakowania wodnego*, *dyskretna transformacja falkowa*, *rozpoznawanie biometryczne odległość Hamminga*

* MSc. Wioletta Wójtowicz, Institute of Applied Informatics, Faculty of Mechanical Engineering, Cracow University of Technology.

1. Introduction

Today telemedicine applications play a vital role in the development of healthcare sector. The transmission, storage and sharing electronic medical data became a standard practice for many diagnosis and scientific purposes. Hospitals and health centers have huge databases including medical images and other patients' records. In the management of these databases privacy protection of medical images has always been an important issue. Security solutions should ensure that medical images cannot be accessed by unauthorized users, images are not modified during the transmission and storage and finally images are from correct sources to the claimed receivers. To achieve these objectives it is essential to provide copyright protection of medical images (e.g. [1, 2, 3, 10]). For that matter different techniques of digital watermarking have been employed. Digital watermarking is a technique of embedding a digital code into a cover image without changing the image size, quality and readability of the image. As a result usually watermark should be invisible, secret to unauthorized users, robust against attempt to tamper with it and provides data authentication ([4, 7, 12]).

In this paper, a combination of watermarking technique with biometric recognition system to increase security of medical images is proposed. As biometric data provide uniqueness and watermarking provide secrecy, some possible advantages of merging these techniques with regard to medical images will be demonstrated. The goal is to provide authentication for the patient as the owner of image by encapsulating some biometric characteristic in his medical image. Some simple watermarking algorithm based on discrete wavelet transform (DWT) decomposition, in which the watermark is embedded at different frequency bands, will be elaborated. This frequency domain were chosen as it provides better robustness against attacks and leads to less perceptibility of an embedded watermark. To assure confidentiality of patient data binary iris code is used as a watermark and system performance is evaluated by measuring the similarity between embedded and extracted iris code.

This paper is organized as follows: Section 2 describes the basic issues connected with watermarking technique and biometric recognition; in Section 3 proposed method will be described; Section 4 gives experimental results; Conclusions will be presented in section 5.

2. Review

2.1. Watermarking in DWT domain

A watermarking systems consists of two components: a watermarking embedder and a watermark detector ([2, 4, 7]). Watermark embedding is performed either in spatial domain (e.g. Last Significant Bit algorithm) or transform domain (e.g. DFT, DCT and DWT transforms). The transform domain is shown to be more robust than that is spatial domain. One of the most popular transforms operating in the frequency domain is Discrete Wavelet Transform (DWT), which provides excellent space for image watermarking ([2, 12]). DWT is a hierarchical transformation, which enables analysis of image in the spatial-frequency domain. DWT separates the image into lower resolution approximation image (LL) as well as horizontal (HL), vertical (LH) and diagonal (HH) detail components. These bands could be next decomposed recursively in the same way. Finally, the representation of the image on

many resolution levels could be obtained. In practice to get the wavelet decomposition, the highpass filter (H) and lowpass filter (L) are applied to the rows and columns of the image in the spatial domain. Then the watermark could be added to the coefficients of transformation, that are exposure and frequency functions.

Watermarking has become an important issue in medical image security, confidentiality and integrity ([1, 3, 8, 9]). Medical image watermarks are usually used to authenticate (trace the origin of an image) and /or investigate the integrity (detect whether changes have been made) of medical images. One of the key problems with medical image watermarking, is that medical images have special requirements. A hard requirement is that the image may not undergo any degradation that will affect the reading of it (see Fig. 2).

2.2. Biometric recognition

Biometric recognition refers to the automatic recognition of individuals based on their physiological and/or behavioral characteristics ([5, 6, 11]). To ensure that the rendered services are accessed only by legitimate users and no one else, personal recognition systems could be applied to either confirm or determine the identity of an individual requesting their services. Thus, biometric characteristic should be universal, discriminative and sufficient invariant. Biometric system is essentially a pattern recognition system that operates by acquiring biometric data from an individual, extracting a feature set from the acquired data, and comparing this feature set against the template set in the database. Possible applications of such systems could be: commercial (e.g. computer network logging, credit card, medical records management, etc.), government (e.g. ID card, driver's license, passport control, etc.) and forensic (e.g. criminal investigation, terrorist identification, etc.). Depending on the application context, a biometric system may operate either in the verification mode (the system validates a person's identity by comparing the captured biometric data with her own biometric templates stored in the system database) or identification mode (the system recognizes an individual by searching the templates of all users in the database for a match). In various applications a number of biometric characteristics are in use. The most popular are: DNA code, shape of ear, facial images, hand and finger geometry, fingerprint, iris code, signature and voice characteristics. Each of this feature has its strengths and weaknesses, as there is no single biometric which effectively meet the requirements of all applications.

In this paper the iris code as biometric characteristic, which could be used as watermark, is elaborated. The iris is the annular region of the eye bounded by the pupil and the sclera on either side. The visual texture of the iris is formed during fetal development and stabilizes during the first two years of life. The complex iris texture carries very distinctive information useful for personal recognition. The accuracy and speed of currently deployed iris-based recognition system is promising and point to the feasibility of large-scale identification systems based on iris information. Each iris is distinctive and, like fingerprints, even the irises of identical twins are different. In addition, it is extremely difficult to surgically tamper the texture of the iris.

In proposed approach this biometric characteristic is used as a watermark to increase the security of medical image. Instead of inserting image of iris (Fig. 1b) just iris code (Fig. 1c) is embedded. Extraction of this code will be based on the Daugman algorithm ([5, 11]).

In proposed method first segmentation of eye image must be performed to detect an iris on this image. Thus, all three parameters (r, x_c, y_c) defining the pupillary circle must be estimated separately from those of the iris. A very effective differential operator for determining these parameters is, ([11]):

$$(r, x_c, y_c) = \arg\left(\max \left| \frac{\partial}{\partial r} \oint_{r, x_c, y_c} \frac{I(x, y)}{2\pi r} ds \right| \right) \tag{1}$$

where:

$I(x, y)$ – is an image containing an eye,
(x_c, y_c) – central coordinates,
r – radius.

The operator in (1) serves to find both the papillary boundary and the outer (limbus) boundary of the iris. Then the circuit shape of detected iris is normalized and mapped to polar representation. As a result every point of iris image from Cartesian coordinates (x, y) is transformed to polar coordinates (r, θ), where r is from [0, 1] and theta is an angle form $[0, 2\pi]$. For iris feature encoding Daugman's method uses Gabor filters which are convoluted with pieces of rectangular iris image. Then obtained complex coefficients are summed and only one resulted complex number is analyzed. The sign of real and imaginary part of this number is taken into account, and for positive values binary '1' is coded, otherwise '0' (Daugman proposed code of length equal to 2048 bits). In this method only phase information is used for recognizing irises because amplitude information is not very discriminating, and it depends upon extraneous factors such as imaging contrast, illumination, and camera gain ([5]).

For identification purposes some comparison between iris codes of different people or different codes of the same person could be performed. As a measure of similarity of iris codes Daugman proposed Hamming distance, which so far is still often used in biometric identification systems. This distance for two vectors A and B of length 2048 could be defined as:

$$H(A, B) = \frac{\sum xor(A, B)}{2048} \tag{2}$$

where xor is simple Boolean Exclusive-OR operator, that detects disagreement between any corresponding pair of bits in considered vectors. Thus, the value of H can be treated as a percent of different pixels in both vectors. If we measure distance of two different person this distance should be near to 0.5, as the probability of occurring '1' or '0' in iris code is equal to 0.5. But when the patterns form the same person are analyzed Hamming distance should be equal or near to 0.

3. Proposed biometric watermarking algorithm

In this section the proposed biometric watermarking algorithm will be described with regard to two main modules: watermark encoding and watermark decoding.

3.1. Watermark encoding

The whole process starts with conversion of iris image to gray scale (see Fig. 1b) and computation of iris code using Daugman algorithm. Then obtained binary vector of length 2048 is divided to 32 vectors of length equal to 64. These vectors are then joined line by line to form binary watermark of size 32×64 (see Fig. 1c).

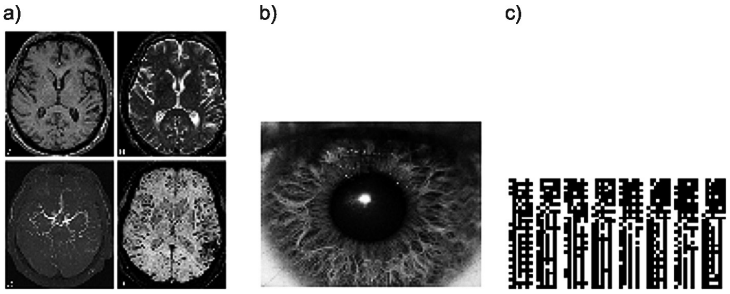

Fig. 1. Encoding: cover medical image ([15]) (a), iris image ([14]) (c), watermark – iris code (c)
Rys. 1. Kodowanie: oryginalny obraz ([15]) (a), obraz tęczówki (14) (c), znak wodny – kod tęczówki (c)

Cover image is gray scale CT image of size 1512×1304 (see Fig. 1a). First one level DWT decomposition of this medical image is computed. Then each of decomposition bands: LL, LH, HL, HH is selected to insert binary watermark. As the size of each band (756×652) is much bigger than the watermark size, it is important to note that watermark is inserted just in the top left corner of each band. The values of watermark are added to the band values and watermarked image is reconstructed using IDWT. According to watermarking of medical images requirements, for each band case watermark is imperceptible (see Fig. 2).

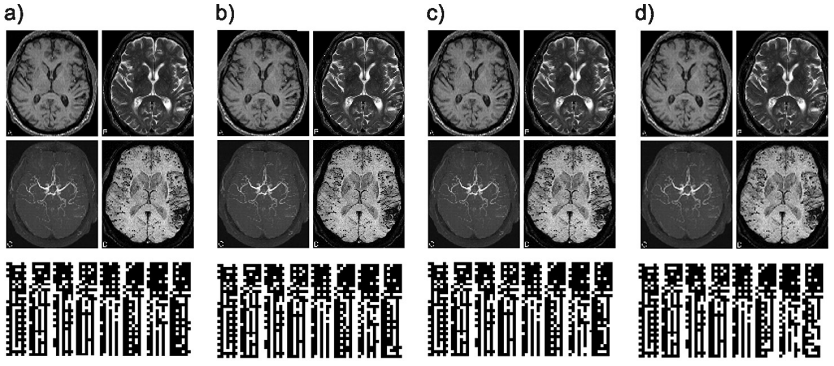

Fig. 2. Decoding: watermarked images and extracted watermarks for schemes when the watermark was inserted in LL (a), LH (b), HL (c), HH (d)
Rys. 2. Dekodowanie: obrazy ze znakami wodnym i wyeksrahowane z nich znaki wodne dla przypadków wstawiania znaku wodnego do komponentów: LL (a), LH (b), HL (c), HH (d)

3.2. Watermark decoding

During the decoding process the data encapsulated in the watermarked medical image are extracted for the authentication purposes. As in presented approach original cover image is available, first this original image is subtracted from watermarked image. Then obtained image is decomposed using DWT and region where the watermark was embedded (top left corner of each band) is selected. The chosen binary part of band should correspond to the code of inserted watermark. To measure the similarity between original iris code and the extracted one the Hamming distance could be employed (see (1), Table 1).

4. Experimental results

The performance of proposed algorithm is tested on each of DWT decomposition components. Obtained results are evaluated in terms of imperceptibility and robustness against three types of attacks: adding 'salt and pepper' noise, median filtering and rotation of watermarked image by 5º (and re-rotation before watermark extraction). The Hamming distance computed for all considered scenarios could be use to evaluate the robustness of watermarking algorithm (Table 1). Taking these values into account one can elaborate the authentication possibilities of watermarking scheme as well. As Hamming distance measures the similarity between inserted and extracted iris code of owner of medical image one can determine in which case the recognition (verification) will be possible. As most of the biometric features of the same individual taken at different times are almost never identical, the threshold t of acceptable difference between iris codes should be introduced. If one set $t = 0.2$, it means that if Hamming distance between two codes is less that t they come from the same person.

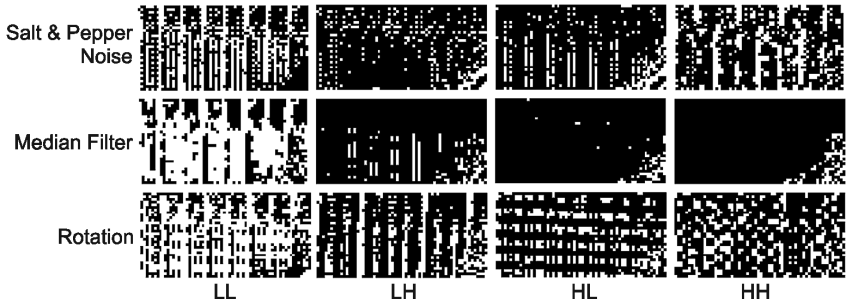

Fig. 3. Extracted watermarks for particular bands LL, LH, HL, HH and considered attacks
Rys. 3. Wyekstrahowane znaki wodne dla poszczególnych komponentów: LL, LH, HL, HH i rozpatrywanych typów ataków na obrazy

In the Figure 1 and Figure 2 all extracted watermarks are presented. In no attack case extracted iris codes are very similar to each other and to the inserted watermark as well, as the Hamming distance for all bands cases is almost equal to 0 (Table 1). But when watermarked image is subjected to different attacks this distance significantly increased, especially for

median filter attack, when for HL, LH, HH Hamming distance is not only much higher than threshold *t,* but it is almost equal to 0.5, what means that analyzed iris codes are from two different people. However obtained results demonstrate that the best verification could be obtained inserting watermark into LL component, which contains details of the original image.

Table 1

Experimental results – Hamming distance between inserted and extracted watermarks

DWT decomposition bands	No attack	Salt & pepper attack	Median filter attack	Rotation (5º → 5º)
LL	0.0059	0.0376	0.2725	0.2090
LH	0.0039	0.3496	0.4897	0.3018
HL	0.0044	0.3477	0.4458	0.2866
HH	0.0122	0.2617	0.4438	0.3286

5. Conclusions

In this paper biometric watermarking scheme for medical images has been elaborated. The proposed scheme satisfies the security and imperceptibility requirements and allow to authenticate medical images using iris code as biometric feature. The confidentiality of patient data is improved by hiding this biometric data as a watermark. The experimental results shows that some simple types of attack can make difficult or even impossible to find the data belongs to particular patient or not. Also it has been noticed that LL component of DWT of image is the most robust against performed attacks.

In a further work, the algorithm will be enhanced in order to obtain watermarked medical images with better robustness and to have recovered watermark with better accuracy.

References

[1] Abdelkader F.M., Elhindy H.M., El-sheimy N., Mostafa S.A., *Wavelet pac ket-based blin watermarking for medical image management*, Open Biomed Eng J, vol. 4, 2010, 93-98.

[2] Arnold M., Schmucker M., Wolthusen S.D., *Techniques and applications of digital watermarking and content protection*, Artech House, Boston, 2003.

[3] Coatrieux G., Maitre H., Sankur B., Rolland Y., Collorec R., *Relevance of watermarking in medical imaging*, 2000 IEEE EMBS Conference on Information Technology Applications in Biomedicine, Arlington, USA, 2000, 250-5.

[4] Cox I.J., Miller M.L., Bloom J.A., Fridrich J., Kalker T., *Digital watermarking and steganography*, San Francisco: Morgan Kaufmann Publishers, 2008.

[5] Daugman J., *How iris recognition works*, IEEE Trans. CSVT, vol. 14, no. 1, 2004, 21-30.

[6] Jain A.K., Ross A., Prabhakar S., *An Introduction to Biometric Recognition*, IEEE Transactions on Circuits and Systems for Video Technology, vol. 14, no. 1, 2004.

[7] Katzenbeisser S., Petitcolas F.A., *Information hiding techniques for steganography and digital watermarking*, Artech House, Norwood, MA, 2000.

[8] Maeder A., Planitz B., *Medical image watermarking: a study on image degradation*, Australian Pattern Recognition Society (APRS) Workshop on Digital Image Computing (WDIC 2005), 2005, 3-8.
[9] Li M., Narayanan S., Poovendran R., *Engineering in Medicine and Biology Society*, 26th Annual International Conference of the IEEE,vol. 2, 2004, 3233-3236.
[10] Ogiela M.R., *Systemy utajania informacji – od algorytmów do kryptosystemów szyfrujących*, Wydawnictwa AGH, Kraków 2003.
[11] Ślot K., *Wybrane zagadnienia biometrii*, Wydawnictwa Komunikacji i Łączności, Warszawa 2008.
[12] Vatsa M., Singh R., Noore A., *Feature based RDWT watermarking for multimodal biometric system*, Image and Vision Computing, vol. 27, no. 3, 2009, 293-304.
[13] Zieliński T.P., *Cyfrowe przetwarzanie sygnałów*, Wydawnictwa Komunikacji i Łączności, Warszawa 2005.
[14] Bolwidt E., *In my eyes*, 2008 (http://www.nowpublic.com/health/my-eyes – accessed 1 March 2013).
[15] Mittala S., Wue Z., Neelavallib J., Haacke E.M., *Susceptibility-Weighted Imaging: Technical Aspects and Clinical Applications*, American Journal of neuroradiology, 2009, doi: 10.3174/ajnr. A1461 (http://www.ajnr.org/content/30/2/232/F6.expansion.html – accessed 1 March 2013).

TECHNICAL TRANSACTIONS | CZASOPISMO TECHNICZNE
MECHANICS | MECHANIKA
1-M/2013

MIROSLAV ŽILKA*

STRATEGY OF MAINTENANCE SYSTEM IN INDUSTRIAL COMPANY

STRATEGIA SYSTEMU UTRZYMANIA RUCHU W ZAKŁADACH PRZEMYSŁOWYCH

A b s t r a c t

This paper introduces the main conclusions of the doctoral thesis "Strategy of maintenance system in industrial company", which focuses on improving of economic efficiency of the maintenance system by selecting the appropriate maintenance strategy for production machines. In the paper I characterise outputs of the survey, which focuses on characterization of maintenance management level, maintenance cost control and allocation level and range of modern maintenance management tools (Computerized Maintenance Management Systems = CMMS) utilization in industrial enterprises in Czech Republic. This article also deals with proposed methodology for selecting the appropriate maintenance strategy and with the brief characteristic of the model MAM (Maintenance Analytical Module), which was developed as a decision support tool for maintenance managers.

Keywords: *maintenance*, *maintenance strategy*, *maintenance management*, *maintenance planning*, *CMMS*, *Computerised Maintenance Management Systems*

S t r e s z c z e n i e

Artykuł prezentuje główne wnioski z pracy doktorskiej „Strategia systemu utrzymania ruchu w zakładzie przemysłowym", która skoncentrowała się na ulepszeniu ekonomicznej wydajności systemu utrzymania ruchu poprzez wybór właściwej strategii konserwacji maszyn produkcyjnych. W artykule została zaprezentowana charakterystyka przeglądów, które skupiają się na charakterystyce poziomu zarządzania obsługą, kontrolą kosztów utrzymania i poziomu alokacji, zakresu wykorzystania nowoczesnych narzędzi do zarządzania remontami w zakładach przemysłowych w Czechach. W artykule opisano proponowaną metodę wyboru właściwej strategii zarządzania remontami, scharakteryzowano model MAM (Maintenance Analytical Module), który pełni rolę narzędzia wspomagającego decyzję personelu zarządzającego konserwację.

Słowa kluczowe: *konserwacja*, *strategia konserwacji utrzymanie ruchu*, *CMMS*

* Eng. Miroslav Žilka, Department of Management and Economics, Faculty of Mechanical Engineering, Czech Technical University in Prague.

Abbreviations

CMMS – Computerised Maintenance Management Systems
ERP – Enterprise Resource Planning
HCT – Hourly Cost Tariff [EUR/hour]
MAM – Maintenance Analytical Module = decision support model

1. Main objectives of the thesis

Maintenance is an integral part of any production system, plays an important role in ensuring the operability of the company and significantly influences its productivity. Appropriately chosen maintenance strategy contributes to the fact that customers receive their products in the required time and required quality, which is involved in maintaining business competitiveness. It is therefore obvious that the level of maintenance management can significantly influence the success of business. For this reason I chose maintenance as a target area for my doctoral thesis Strategy of maintenance system in industrial company, which focuses on improving of maintenance system economic effectiveness.

The main task of the thesis is to provide maintenance managers with the information necessary for selecting the appropriate maintenance strategy in the enterprise. This strategy should ensure that the resources allocated to maintenance are used effectively. For fulfilling this task, the following objectives were identified:

A. Des cription of current state in the field of maintenance management and planning
Using research of information sources and survey among target companies I described current state in this field and identified requirements of target industrial enterprises, weaknesses in their maintenance management systems and potential areas for future development.

B. Proposal of the methodology for selecting the appropriate maintenance strategy
I proposed and characterised steps of the methodology for selecting appropriate maintenance strategy which effectively uses allocated resources.

C. Design of the decision support model for selecting of the appropriate maintenance strategy
I designed the decision support model MAM (Maintenance Analytical Module) as a key tool integrated in the proposed methodology. This model provides managers with important information for the selection of maintenance strategy.

D. Characteristics of the links between the model and other information systems and sources
Because the methodology and the MAM model are demanding on input data an essential part of the thesis represents description of the links and information flows between information systems and other information sources.

E. Evaluation of the maintenance efficiency
As the last step of the methodology I proposed a system of evaluation indicators that helps maintenance managers to verify if the appropriate maintenance strategy was chosen.

In the following parts of article I will deal with a brief description of the three main outputs of the dissertation: survey of the maintenance management level in industrial enterprises in Czech Republic, methodology for selecting of appropriate maintenance strategy and decision support model MAM.

2. Survey of the maintenance management level in industrial enterprises in Czech Republic

Determining the level of maintenance management in Czech engineering enterprises was the main objective of the survey. I chose an electronic questionnaire in combination with structural interviews to meet this objective. The questionnaire consists of five main parts, which represent key characterization areas of maintenance management level.

A. Definition of the role of maintenance in the enterprise
Respondent defines the scope of maintenance and characterizes the importance of maintenance to ensure the operability of the company.

B. Maintenance strategy
Respondent defines which approaches and strategies are applied in the management and maintenance planning in the company.

C. Causes of failure
Respondent characterizes the typical causes of failure (if they are monitored and set by the company).

D. Use of IT tools in the management and maintenance planning
Respondent defines what tools and IT support uses for planning and managing maintenance. When the company uses Computerized Maintenance Management Systems, in which way this system is used, which are the main benefits of the implemented systems.

E. Costs associated with maintenance
Respondent characterizes the amount of the cost of maintenance and explains what kinds of cost are monitored in the company and to what level they are allocated. This part of questionnaire should be answered by maintenance manager or in consultation with controlling manager.

Brief characteristic of the survey is in the Table 1.

2.1. Results of the survey

Most of the respondents define their maintenance strategy as a combination of reactive and preventive approach. They differ only in the ratio between these parts. Average share of machines on which preventive maintenance is performed is approximately 75%. This share is lower for companies with smaller number of machines and younger machines.

Results show that a large portion of failures can be directly influenced by maintenance (normal wear, lack of lubrication or cleaning, poorly performed maintenance).

Only 25% of respondents have implemented specialized CMMS systems. The wider application of these modern tools can be seen as a potential way for improving maintenance management level in target enterprises.

Mostly only direct maintenance costs are closely monitored and calculated, allocation level of costs is insufficient for proper choice of maintenance strategy.

Maintenance management level in target companies cannot be considered as low, but maintenance managers often have not enough information for choosing appropriate maintenance strategy.

More detailed information about the survey was published in articles [1, 2].

Table 1

Survey characteristic

Survey characteristic
Goal
Characterization of the maintenance management level, maintenance cost control and allocation level and range of modern maintenance management tools (Computerized Maintenance Management Systems=CMMS) utilization in industrial enterprises in Czech Republic.
Method of data collection
Questionnaires created in Adobe Acrobat Professional in combination with structured interviews
Target person
Head of Maintenance Department, the last part of the survey focused on costs is determined by staff responsible for monitoring and analysing costs (e.g. staff of controlling or economic department)
Target respondents
▫ **Midsized and larger engineering enterprises with mostly small-lot production:** These companies already have such a number of machines, which requires a systematic approach to maintenance management. On the other hand, sophisticated maintenance management systems are often not implemented and maintenance processes are not precisely defined as it could be seen in automated mass production. ▫ **Number of complete questionnaires - 12 pcs** ▫ **Return rate of questionnaires - 15%**

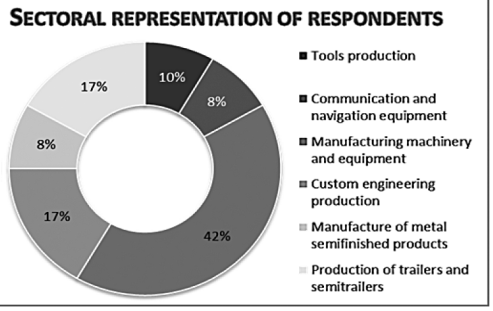

3. Methodology for selecting the appropriate maintenance strategy

This part of the paper deals with a brief description of the methodology for selecting of the appropriate maintenance strategy for defined system of machines. The methodology focuses primarily on the economic benefits of implemented strategies and is primarily based on the Reliability Centred Maintenance (RCM) approach [3–5].

The main goal of the methodology is to prepare and provide information needed for the selection of the maintenance strategy for individual system element (machine), which effectively uses resources allocated to the maintenance and has maximum benefits for the whole system. The final decision about maintenance strategy makes maintenance manager. However, he can rely not only on his experience, but also on relevant information obtained through the proposed methodology and by using the developed MAM decision support model.

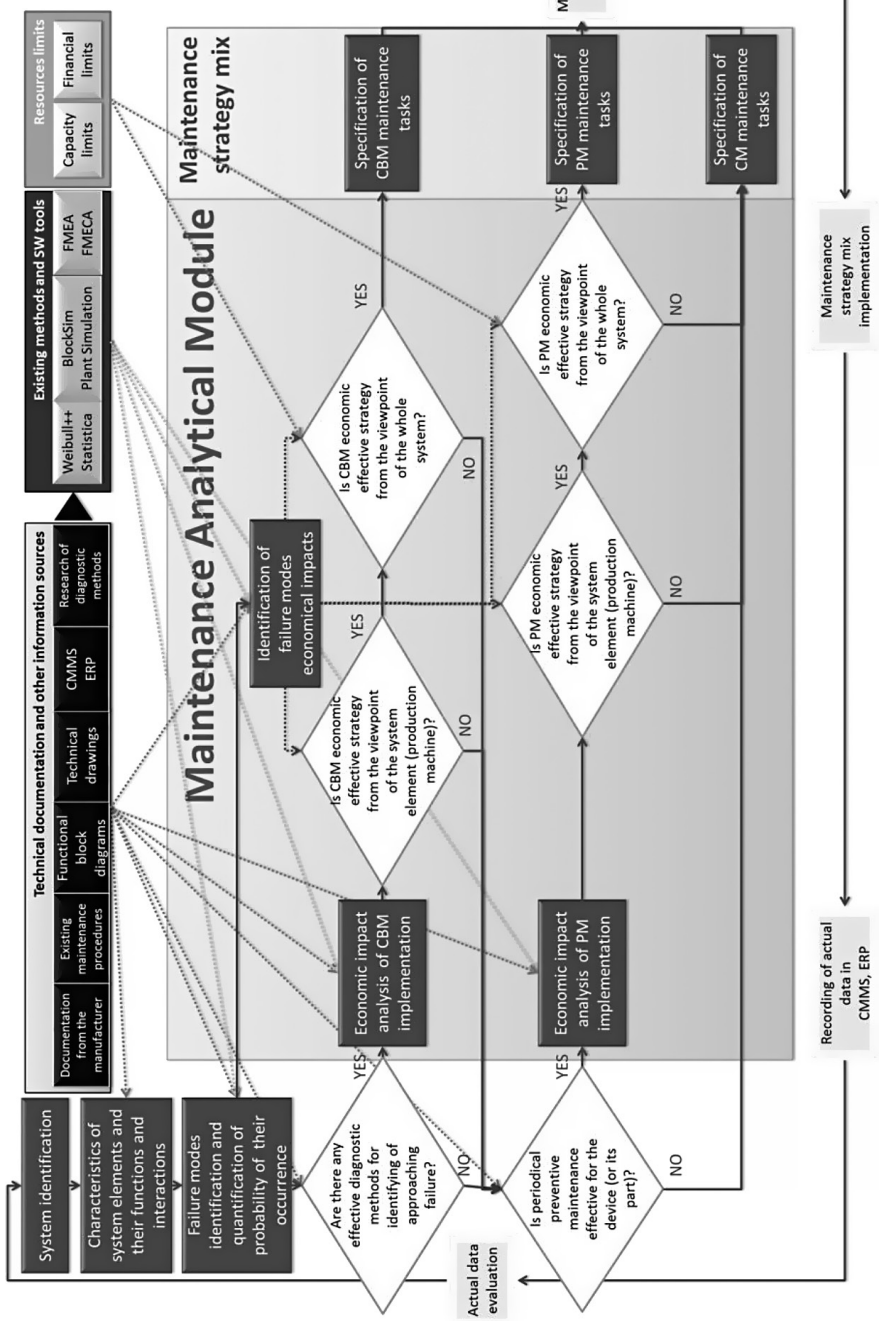

Fig. 1. Process map of the methodology for selecting appropriate maintenance strategy

Rys. 1. Mapa procesu metodyki wyboru właściwej strategii remontu

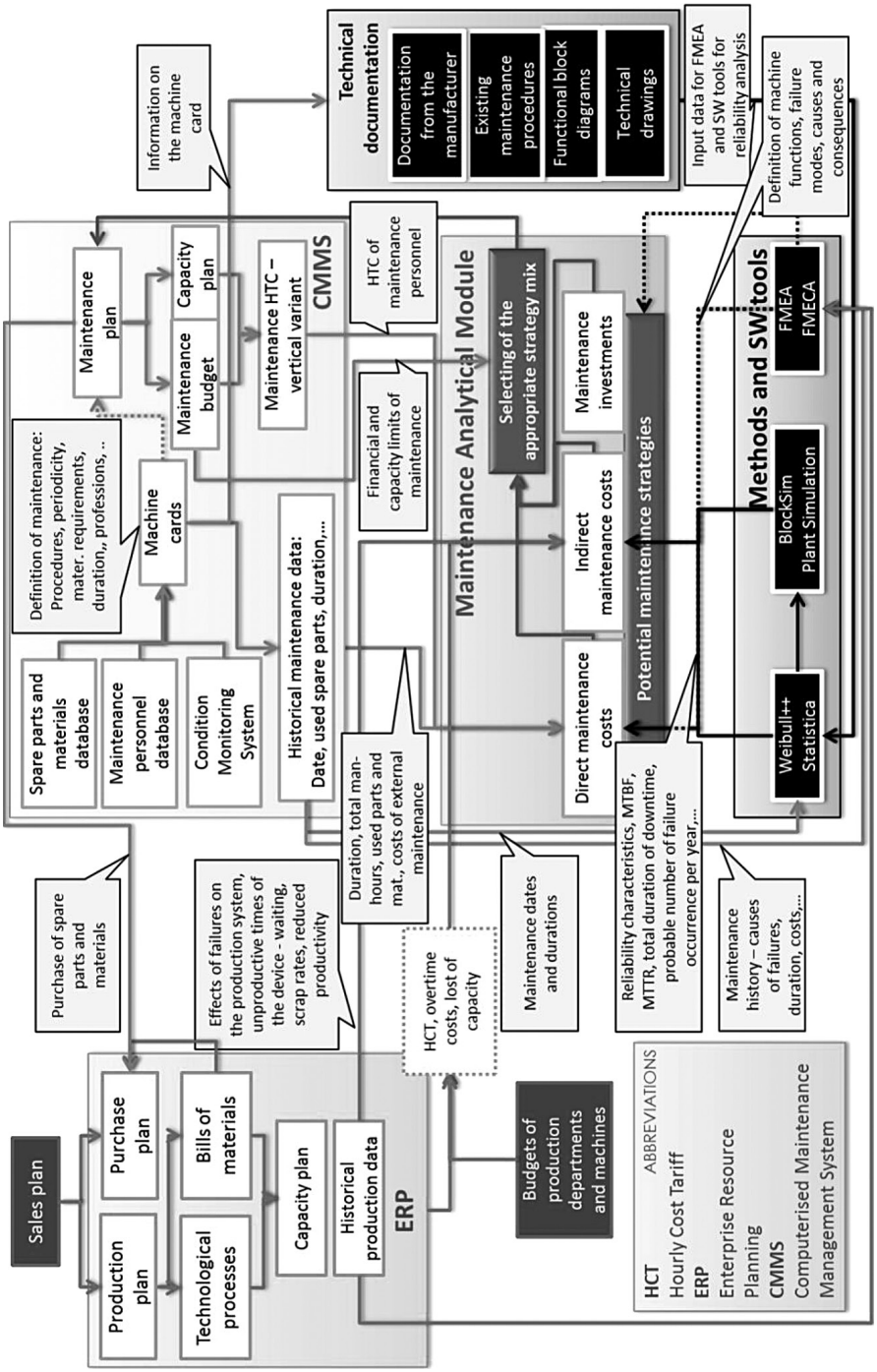

Fig. 2. Information flows between information systems used within proposed methodology

Rys. 2. Przepływ informacji pomiędzy systemami wykorzystanymi w proponowanej metodyce

Individual steps of the methodology are shown in the Figure 1. Information flows and links between information systems and sources within the methodology are shown in the Figure 2.

Because the methodology is very demanding on input data the possibility of its application without using advanced software tools (CMMS, SW for reliability data analysis) is very limited. It is also very important to ensure the linkages between information systems, as shown in Figure 2.

4. Decision support model MAM (Maintenance Analytical Module)

Model MAM was developed as an integral part of the methodology (the field of application of the model within the methodology is marked in the Fig. 1 and 2). It is decision support model (not optimization model), which represents specialized module for complex analysis of the maintenance system. Model uses big amount of input data from different information sources for generating outputs needed for decision making on maintenance strategies (see Fig. 2).

The main objective of the model MAM is an information support for maintenance managers in choosing the appropriate maintenance strategy. With this main objective are connected these benefits of the model:

- Simplifies the quantification of the direct and indirect maintenance costs
- Organizes the data about individual system elements (machines) as well as the entire system and thus provides decision support for maintenance managers at three different levels:
  - Mutual comparison of different maintenance strategies on one machine,
  - Mutual comparison of system elements (machines) within the whole system,
  - Mutual comparison of the strategic mixes,
- Provides sensitivity analysis and simulations of the impact of changes in various inputs on the overall costs of maintenance, production capacity and other characteristics (e.g. in case of lack of empirical data),
- Provides financial arguments to maintenance managers for negotiations with top management on investments in the maintenance system development.

Model MAM represents prototype of the information system programmed in MS Excel, which is used for presentation of basic structure, verification of the model functionality and illustration of the links between individual model parts. For demonstration of the model functionality the case study for system of ten machines was defined.

The model structure is hierarchical and is shown in the Fig. 3.

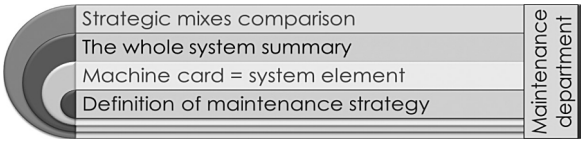

Fig. 3. Structure of the MAM model

Rys. 3. Struktura modelu MAM

Model MAM provides output characteristics, which can be used by maintenance managers for selecting of maintenance strategy mix suitable for individual system element (machines). This strategy mix brings maximal benefits for the whole system. Selected outputs characteristics provided by the MAM model are shown in the Table 2.

Table 2

Output characteristics for different maintenance strategies provided by the MAM model		
✓ Purchasing price of the machine	✓ Total maintenance costs (direct and indirect)	✓ Work hours of the maintenance department
✓ Age of the machine /planned durability	✓ Savings in the implementation of the chosen maintenance strategy	✓ Increase of the real production capacity of the machine
✓ Hourly costs of overtime and lost production capacity	✓ CAPEX associated with maintenance strategy, ROI, payback period	✓ Downtime/Uptime rate

5. Conclusions

This article deals with brief description of three main outputs of the doctoral thesis Strategy of maintenance system in industrial company. At first it describes survey of the maintenance management level in industrial enterprises that was used for definition of current state, needs of target companies and together with research of information sources for identification of potential ways of development in field of maintenance management. Second part of the article describes methodology for selecting appropriate maintenance and developed SW tool – MAM decision support model. Dissertation as a whole is beneficial mostly for maintenance managers, whom provides information and methodological support.

References

[1] Žilka M., *Úroveň managementu údržby v průmyslových podnicích v ČR*, In: Trendy a inovatívne prístupy v podnikových procesoch 2012, Košice, TU Košice, 2012, ISBN 978-80-553-1126-5.

[2] Žilka,, M., *Survey of the maintenance management level in industral enterprises in Czech Republic*, In: MAINTENANCE 2012. Zenica: University of Zenica, 2012, vol. 1, 136-142, ISSN 1986-583X.

[3] Moore R., *Selecting the right manufacturing improvement tools: What tool? When?*, Burlington: Butterworth-Heinemann, 2007, xxii, 390 s., ISBN 07-506-7916-6.

[4] Rausand M., *Reliability centered maintenance*, Reliability engineering [online], 1998, 60/2, s. 121-132 [cit. 2012-08-03], ISSN 09518320. DOI: 10.1016/S0951-8320(98)83005-6 (http: //linkinghub.elsevier.com/retrieve/pii/S0951832098830056).

[5] Zhou X., Xi L., Lee J., *Reliability-centered predictive maintenance scheduling for a continuously monitored system subject to degradation*, Reliability engineering [online], 2007, 92/4, s. 530--534 [cit. 2012-10-07], ISSN 09518320. DOI: 10.1016/j.ress.2006.01.006 (http://linkinghub. elsevier.com/retrieve/pii/S0951832006000305).

CONTENTS

TREŚĆ